SPECIALIZED DATA ANALYSIS OF SSME AND ADVANCED PROPULSION SYSTEM VIBRATION MEASUREMENTS

Engineering Report: ER-60900-93-F

by

Thomas Coffin
Wayne L. Swanson
Jen-Yi Jong

Wyle Laboratories
Engineering Division
October 1993

A Final Report of Work Performed Under Contract NAS8-38156

for

NATIONAL AERONAUTICS AND SPACE ADMINISTRATION
George C. Marshall Space Flight Center
Marshall Space Flight Center, Alabama 35812

FOREWORD

This report was prepared by Wyle Laboratories, Scientific Services & Systems Group, for the George C. Marshall Space Flight Center, National Aeronautics and Space Administration. The work was performed under contract NAS8-38156, entitled "Data Analysis and Diagnostic Evaluation of Space Shuttle Main Engine Dynamic Measurements" over the time period from June 1989 through October 1993.

The investigation was carried out by the Systems Analysis Department, with Mr. T. Coffin serving as Program Manager. Mr. W. L. Swanson was Project Engineer for SSME data analysis and bearing element dynamic modeling, in particular. Dr. J. Jong was responsible for the development of diagnostic signal processing techniques, and application of these methods to SSME anomaly investigations. In addition, he conducted several seminars at MSFC concerning advanced signal processing methods and applications. This report documents the diagnostic analysis effort performed under the above contract. A secondary objective of the authors was to provide an overview of the SSME diagnostic evaluation process, and the computational tools available to support this task.

Messrs. J. E. McBride and C. P. Jones, MSFC/ED23, provided valuable guidance through coordination of test evaluation activities and definition of task requirements and priorities. Mr. J. H. Jones, MSFC/ED33, provided valuable technical advice and encouragement to the diagnostic technique development effort.

TABLE OF CONTENTS

		Page
Foreword		i
Section I - Executive Summary		I-1
Section II - Program Overview and Summary of Tasks		II-1
2.1	Introduction	II-1
2.2	The Space Shuttle Vehicle System	II-2
2.3	The Space Shuttle Main Engines	II-2
2.4	SSME Development and Certification Testing	II-3
2.5	Data Analysis and Evaluation Considerations	II-9
	2.5.1 Quick-Look Data Assessment	II-9
	2.5.2 SSME Data Base Application and Refinement	II-13
	2.5.3 Diagnostic Methods and Applications	II-19
	2.5.4 Statistical Characterization of SSME Data	II-26
2.6	Task Requirement and Accomplishments	II-33

APPENDIX A
Reports/Publications in Support of SSME Tasks

Some Non-Linear Spectral Methods and Their Application to Rocket Engine Diagnostic Evaluation	A-1
The TOPO Plot: A Data Reduction / Graphics Routine for Tracking Spectral Trends in Data	A-10
An Algorithm for Periodic Waveform Recovery from Space Shuttle Main Engine Vibration Measurements	A-13
Correlation Identification Between Spectral Components in Turbomachinery Measurements by Generalized Hypercoherence	A-17
Time-Frequency Representation of Nonstationery Signals	A-24
Some Recent Developments in Turbomachinery Diagnostic Monitoring	A-56
Cavitation Detection and Monitoring Using Wide-Band Demodulation	A-67
Anomaly Identification for Space Shuttle Main Engine Diagnostics	A-93
Statistical Analysis of SSME Turbopump Vibration Levels	A-95

TABLE OF CONTENTS (Continued)

	Page
Statistical Summary (Update) of SSME Turbopump Vibration Levels	A-109
Synchronous Frequencies of the ATD High Pressure Oxidizer Turbopump	A-176
Comparison of Gamma, Weibull and Normal Distributions with ATD High Pressure Oxidizer Turbopump Vibration Data	A-184

APPENDIX B
Seminar Notes on Signal Processing/Diagnostics

Theory and Application of Bi-Spectrum Analysis	B-1
Nonlinear Spectral Analysis Methods for SSME Diagnostics	B-39
MEM Spectrum Analysis and Adaptive Filtering	B-93
Cepstrum, Rotary Spectrum, Wavenumber Spectrum, P.D.A. Coherence and the TOPO Plot	B-127

LIST OF FIGURES AND TABLE

		Page
Figure 2-1	Space Shuttle Main Engine	II-4
Figure 2-2	Space Shuttle Main Engine Power Head	II-5
Figure 2-3	SSME Propellant Flow Schematic	II-6
Figure 2-4	High Pressure Oxygen Turbopump	II-7
Figure 2-5	ATD Oxidizer Turbopump	II-8
Figure 2-6	Standard SSME Ground Test Instrumentation Location Schematic	II-10
Figure 2-7	SSME Hot Firing Profiles	II-11
Figure 2-8	Power Spectral Density of Two High Pressure Fuel Turbopump Measurements	II-15
Figure 2-9	Illustration of Isoplot and TOPO Plot Routines	II-17
Figure 2-10	Turbopump RMS Time Histories and Statistical Ranges	II-18
Figure 2-11	Signal Detection by Hypercoherence Filtering	II-20
Figure 2-12	Frequency Translation by Wide-Band Demodulation	II-21
Figure 2-13	Algorithms for Wide-Band Demodulation (WBD)	II-22
Figure 2-14	FFT Isoplot of Two Modulated Sine Waves	II-23
Figure 2-15	WD Isoplot of Two Modulated Sine Waves	II-24
Figure 2-16	MWD Isoplot of Two Modulated Sine Waves	II-25
Figure 2-17	ADORE Output - Misalignment	II-27
Figure 2-18	ADORE Output - Axial Loading	II-28
Figure 2-19	ADORE Output - Radial and Axial Loading and Ball Wear	II-29
Figure 2-20	ADORE Output - Ball Wear	II-30
Figure 2-21	Histogram Synchronous Frequency @ 100% PWL ATD High Pressure Oxidizer Turbopump (HPOTP)	II-32
Figure 2-22	Histogram Synchronous Frequency @ 104% PWL ATD High Pressure Oxidizer Turbopump (HPOTP)	II-32
Figure 2-23	ATD Cumulative Histogram Composite @ 100% PWL	II-34
Figure 2-24	ATD Density Histogram Composite @ 100% PWL	II-34
Table 2-1	Log of SSME Hot Firings (Test and Flight) Through October 1993	II-39

SECTION I
EXECUTIVE SUMMARY

The Marshall Space Flight Center is responsible for the development and management of advanced launch vehicle propulsion systems, including the Space Shuttle Main Engine (SSME), which is presently operational, and the Alternate Turbopump Development (ATD) concept presently under test. Advanced turbomachinery bearing, blade material, and instrumentation concepts are also under evaluation at the MSFC Technology Test Bed (TTB). The SSMEs provide high performance within stringent constraints on size, weight, and reliability. Based on operational experience, continuous design improvement is in progress to enhance system durability and reliability. Specialized data analysis and interpretation was provided by Wyle Laboratories in support of SSME and advanced propulsion system diagnostic evaluations, under NASA Contract NAS8-38156.

Under the extreme temperature, pressure, and dynamic load environments sustained during operation, engine systems and components, such as pumps, turbines, and associated hardware, are subjected to severe pressure oscillations and damaging mechanical vibrations. Through extensive data evaluation and analytical effort, turbomachinery and related component vibrations have been implicated as a primary source of equipment degradation and even several catastrophic failures. Measured vibration signatures have varied from stationary random in nature to highly transient functions and even pure tones in some cases.

Most mechanical failures are preceded by growing tolerances, imbalance, bearing element wear and the like, which may manifest themselves through subtle changes in the waveform observed by dynamic measurements. Diagnostic vibration analysis is based on observing and discriminating between measurable vibration patterns that occur as a result of nominal system operation and those associated with component degradation. The techniques are analytical, but their application is necessarily empirical, relying heavily on a data base of engine measurements permitting correlation between derived signature characteristics and observed mechanical condition. The diagnostic evaluation of complex vibration signatures requires the use of sophisticated statistical/signal processing techniques and highly experienced analysts for efficient interpretation.

Comprehensive evaluation of the dynamic measurements obtained from test and flight operations is necessary to provide timely assessment of the vibrational characteristics indicating the operational status of the turbomachinery and other critical engine components. Efficient

performance of this effort is critical due to the significant impact of dynamic evaluation results on ground test and launch schedules and requires direct familiarity with SSME and derivative systems, test data acquisition, and diagnostic software.

The basic objectives of this contract were to perform detailed analysis and evaluation of dynamic data obtained during SSME test and flight operations, including analytical/statistical assessment of component dynamic performance, and to continue the development and implementation of analytical/statistical models to effectively define nominal component dynamic characteristics, detect anomalous behavior, and assess machinery operational condition. This study was to provide timely assessment of engine component operational status, identify probable causes of malfunction, and define feasible engineering solutions. The work was performed under three broad tasks which are summarized as follows.

TASK I: Analysis, Evaluation, and Documentation of SSME Dynamic Test Results

Under this task, Wyle performed analysis, evaluation, and documentation of SSME dynamic test results. This task represented the mainstream of the contract effort and included data verification, analysis, evaluation, and documentation for each SSME ground test and, additionally, for SSV flight measurements. Results were provided immediately and informally for SSME Program Management Review. Over the course of this study, 456 SSME hot firings, including 372 single engine tests and 28 STS flights were evaluated. Of the single engine tests, 38 included instrumented ATD turbopump configurations. Additional data analysis was provided for component tests at the MSFC Technology Test Bed, water flow facility and various contractor locations.

TASK II: Data Base and Analytical Model Development and Application

The Automated Data Base and associated statistical models of the SSME component dynamic response were updated and applied to generate characterizing profiles of observed parameter ranges, distributions, etc. under nominal and abnormal operating conditions at all power levels. Statistical and graphical routines were incorporated to aid in data evaluation and interpretation.

TASK III: Development and Application of Vibration Signature Analysis Techniques

Signature analysis techniques were developed, updated, and applied for detailed SSME diagnostic evaluation. Under this phase, Wyle developed a number of advanced time domain and spectral evaluation algorithms and implemented them on the OISPS.

The above tasks are seen to be intimately related since promising fault detection schemes were immediately integrated into the SSME evaluation process. These efforts were directed to a number of specific SSME engineering applications, including:

- Analysis, evaluation, and documentation of SSME test/flight measurements.
- Support of abnormal SSME operation or component failure investigations.
- Development of analytical/statistical models of component dynamic behavior and application to SSME component evaluations.
- Analysis, modeling, and simulation to refine test and flight vibration redlines and flight certification ("green-run") specifications.
- Data base development and implementation to support SSME data classification and evaluation.
- Development/implementation of advanced vibration signature analysis techniques for monitoring SSME operational condition and diagnostic assessment of component degradation.

This report provides an overview of study objectives and approaches applied by Wyle in the performance of Contract NAS8-38156. As a test/evaluation program, rigid, long term task planning was neither feasible nor desirable. On the contrary, most tasks performed under this contract were initiated on an ad hoc basis, motivated by observed or suspected SSME component failure modes. Continued coordination with the MSFC COTR was, therefore, maintained to revise task priorities based on SSME test results and Project Office requirements. Consistent with stringent SSME test and flight certification schedules, evaluation results were immediately provided the COTR in the form of presentations and informal data packages. To illustrate the diversity of tasks accomplished under this contract, some reports and presentations prepared by Wyle in support of propulsion system dynamic evaluations are summarized in Appendix A at the end of this report. Appendix B includes the course notes for a seminar series on Advanced Diagnostic Techniques, provided under this contract. A detailed chronology of these evaluations is given in the technical progress reports provided under this contract.

The primary purpose of this report is to document the work performed under NASA Contract NAS8-38156. A secondary objective of the authors was to provide an introductory overview of the data analysis/diagnostic evaluation process. In particular, the investigations discussed in Appendix A and the analytical techniques described in Appendix B should prove a valuable guide for orientation regarding data analysis procedures and the tools available for component diagnostic assessment.

SECTION II
PROGRAM OVERVIEW AND SUMMARY OF TASKS

2.1 Introduction

The Marshall Space Flight Center is responsible for the development and management of advanced launch vehicle propulsion systems, including the Space Shuttle Main Engine (SSME), which is presently operational, and the Alternate Turbopump Development (ATD) concept presently under test. Advanced turbomachinery bearing, blade material, and instrumentation concepts are also under evaluation at the MSFC Technology Test Bed (TTB). The SSMEs provide high performance within stringent constraints on size, weight, and reliability. Based on operational experience, continuous design improvement is in progress to enhance system durability and reliability.

During development of the propulsion system for the Space Shuttle, the state-of-the-art in rocket engines has seen significant advances. The performance of such engine components as pumps, turbines, and bearings in the presence of high rotational and fluid velocities at high dynamic pressures has resulted in severe fluid pressure fluctuations and destructive vibrations. The character of these vibration signatures varies from random in nature to that of complex periodic functions and even pure tones in some cases. To quantify and analyze these complex signatures, in many cases, requires the utilization of sophisticated analysis techniques and highly experienced analysts for interpretation. Under NASA Contract NAS8-38156, Wyle Laboratories has provided specialized data analysis and interpretation in support of SSME diagnostic evaluations. This report summarizes the effort performed under that contract.

Under the severe temperature, pressure, and dynamic environments sustained during operation, engine systems and components have been subject to malfunction and failure. Over the past 17 years of SSME development, over 28 major component failures have occurred, causing extensive damage to engine hardware and test facilities, at considerable expense in cost and schedules. In addition, numerous off normal operations of a less severe nature have occurred, including turbine blade cracks and bearing element failure. Through extensive test and data evaluation effort, turbomachinery and related component vibrations have been implicated as the source of many high cycle fatigue problems and some catastrophic failures. These events underline the need for comprehensive evaluation of the dynamic measurements obtained from test and flight operations, to provide timely assessment of the vibrational characteristics indicating the operational status of turbomachinery and other critical engine components.

Efficient performance of this effort is critical due to the significant impact of dynamic evaluation results on ground test and launch schedules and requires direct familiarity with SSME and derivative systems, test data acquisition, and diagnostic software.

This section presents an overview of program objectives and task accomplishments. The Space Shuttle system is briefly described, with particular attention to SSME operational characteristics. Summarized also are some technical considerations in the analysis and evaluation of SSME dynamic data. SSME development/certification test procedures are briefly reviewed and a typical test data review cycle is summarized. Contract task requirements are reviewed, along with engineering approaches applied to their accomplishment. A summary of reports generated in the conduct of this contract is included at the end of this section, which illustrates the diversity of investigations performed. Analytical/statistical modeling studies, to characterize SSME component dynamic behavior, are included in the Appendix.

2.2 The Space Shuttle Vehicle System

The SSV is composed of the Orbiter, an External Tank (ET), which contains fuel for the Orbiter's three SSMEs, and two Solid Rocket Boosters (SRB). The Orbiter and SRBs are reusable; the ET is expended on each launch.

A Space Shuttle mission begins with installation of the mission payload into the Orbiter cargo bay. The SRBs and the SSMEs fire together at liftoff. The two SRBs are jettisoned after burnout—about 45 kilometers (28 miles) high—and recovered for reuse by means of a parachute recovery system. The SSMEs continue to burn until the Orbiter is just short of orbital velocity, at which time the engines are shut down and the ET jettisoned. During its return through the atmosphere, the tank will tumble, break up and be destroyed.

The orbital maneuvering system is used to attain the desired orbit and to make any subsequent maneuvers that may be needed during a mission. After orbital operations are completed, normally about seven days, deorbiting maneuvers are initiated. The Orbiter reenters the Earth's atmosphere at a high angle of attack. It then levels into horizontal flight at low altitude for an unpowered aircraft-type approach, landing at a speed of about 335 kilometers per hour (208 miles per hour).

2.3 The Space Shuttle Main Engines

The Orbiter vehicle main propulsion system consists of three SSMEs. The SSMEs are reusable, high-performance, liquid-propellant rocket engines with variable thrust. All three engines are

ignited on the ground at launch and operate for approximately 500 seconds total firing duration. Each engine operates at a mixture ratio (liquid oxygen/liquid hydrogen) of 6:1 and a chamber pressure of approximately 3000 psia to produce a sea-level thrust of 375,000 pounds and a vacuum thrust of 470,000 pounds. The engines are presently throttleable over a thrust range of 60 to 109 percent of the design thrust level. This provides a higher thrust level during liftoff and the initial ascent phase, and allows Orbiter acceleration to be limited to 3 g's during the final ascent phase. The engines are gimbaled (±10.5 degrees for pitch and ±8.5 degrees yaw) to provide pitch, yaw, and roll control during the Orbiter boost phase.

Significant to meeting performance requirements is the use of a staged combustion power cycle coupled with high combustion chamber pressures. In the SSME-staged combustion cycle, the propellants are partially burned at high pressure and relatively low temperature in the preburners, then completely combusted at high temperature and pressure in the main chamber before expanding through the high-area-ratio nozzle. Hydrogen fuel is used to cool all combustion devices in contact with high-temperature combustion products. An electronic engine controller automatically performs checkout, start, mainstage, and engine shutdown functions. Major components of the SSME are illustrated in Figure 2-1. A more detailed view of the SSME power head is shown in Figure 2-2. This figure provides an indication of the complexity of the SSME turbomachinery. The propellant flow schematic, Figure 2-3, illustrates the staged combustion cycle discussed above.

2.4 SSME Development and Certification Testing

To validate system performance and ensure equipment reliability, the SSME and components have been and are presently undergoing extensive development and qualification tests. For example, testing of a candidate replacement (the A.T.D. unit) for the operational High Pressure Oxygen Turbopump, Figure 2-4, is in progress. The A.T.D., Figure 2-5, incorporates advanced manufacturing (forging/welding) techniques and alternate bearing/rotor technology . Testing of the engine and components is conducted at several NASA and contractor locations. Full scale engine test firings for development and flight acceptance are performed on single-engine test stands at Stennis Space Center, Bay St. Louis, Mississippi. In addition, propulsion system testing is in progress at the NASA Engine Technology Test Bed and gas/liquid flow facilities, Marshall Space Flight Center, Alabama.

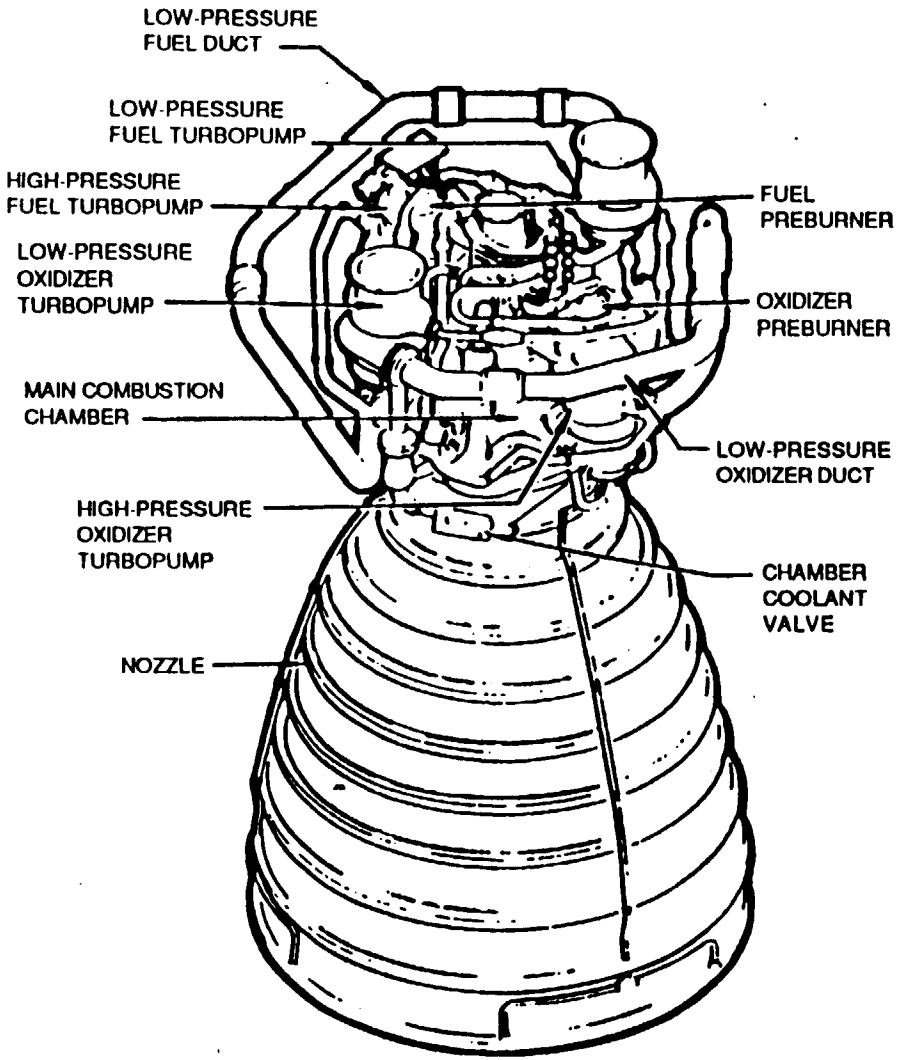

FIGURE 2-1. SPACE SHUTTLE MAIN ENGINE

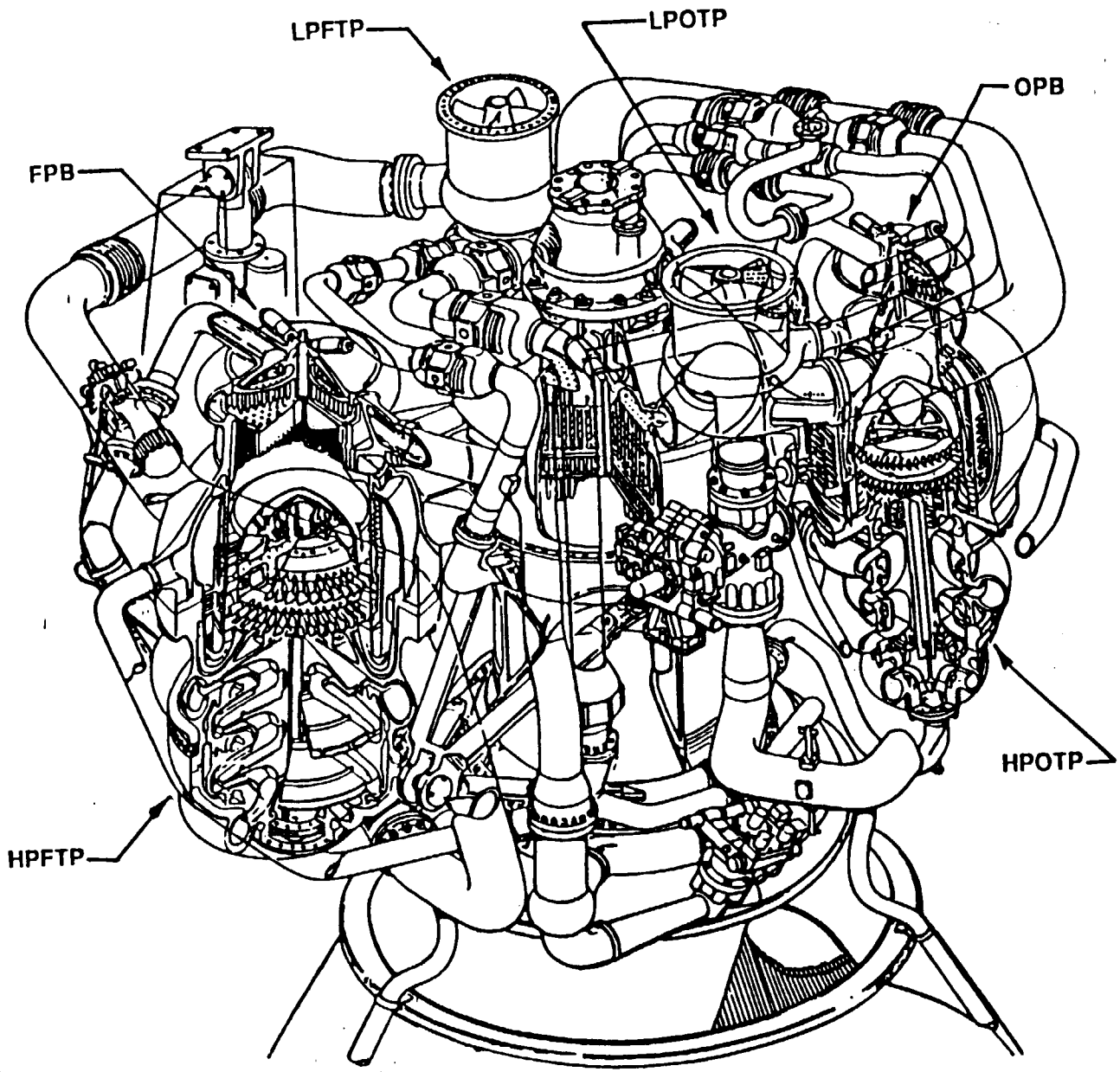

FIGURE 2-2. SPACE SHUTTLE MAIN ENGINE POWER HEAD

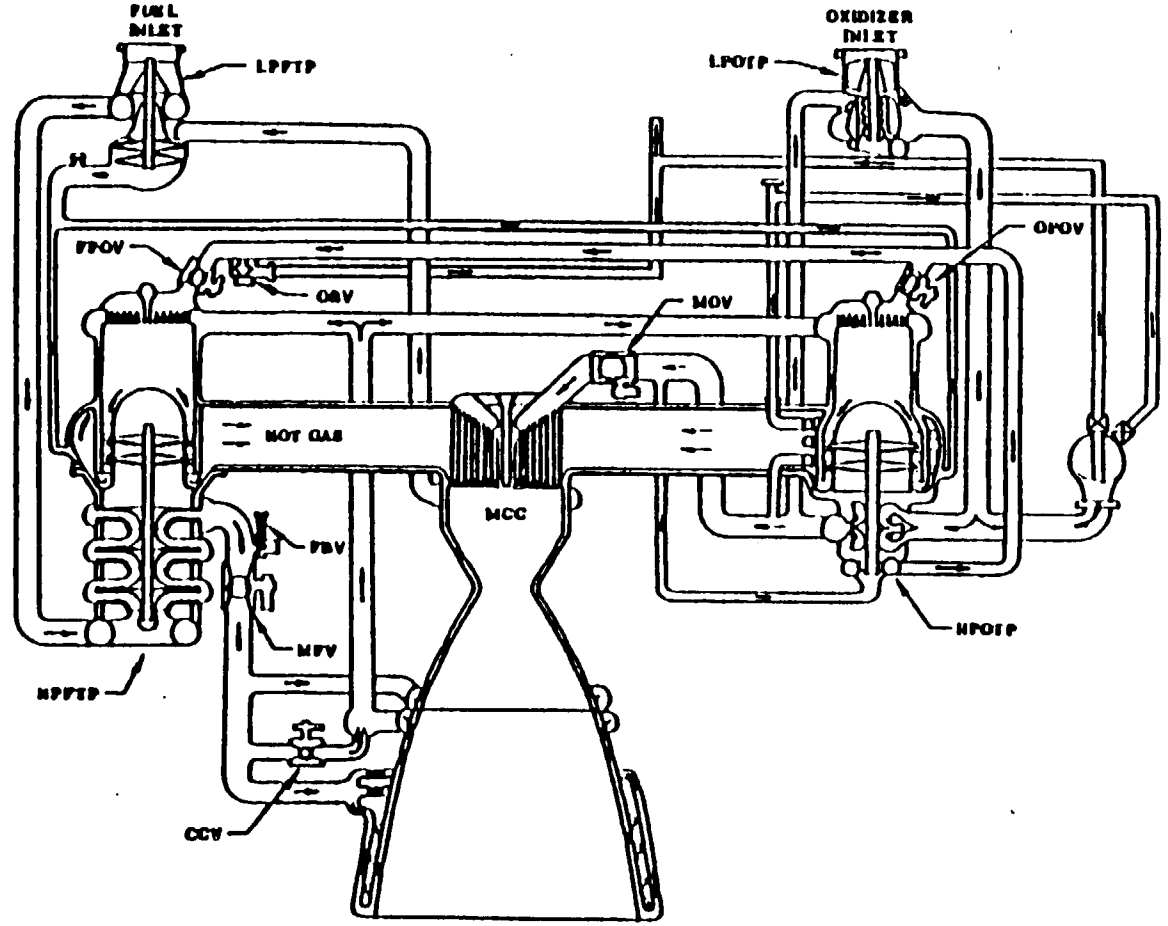

LEGEND:

CCV	-	CHAMBER COOLANT VALVE	FPOV	-	FUEL PREBURNER OXIDIZER VALVE
MCC	-	MAIN COMBUSTION CHAMBER	OPOV	-	OXIDIZER PREBURNER OXIDIZER VALVE
FBV	-	FUEL BLEED VALVE	HPFTP	-	HIGH PRESSURE FUEL TURBOPUMP
OBV	-	OXIDIZER BLEED VALVE	HPOTP	-	HIGH PRESSURE OXIDIZER TURBOPUMP
MFV	-	MAIN FUEL VALVE	LPFTP	-	LOW PRESSURE FUEL TURBOPUMP
MOV	-	MAIN OXIDIZER VALVE	LPOTP	-	LOW PRESSURE OXIDIZER TURBOPUMP

FIGURE 2-3. SSME PROPELLANT FLOW SCHEMATIC

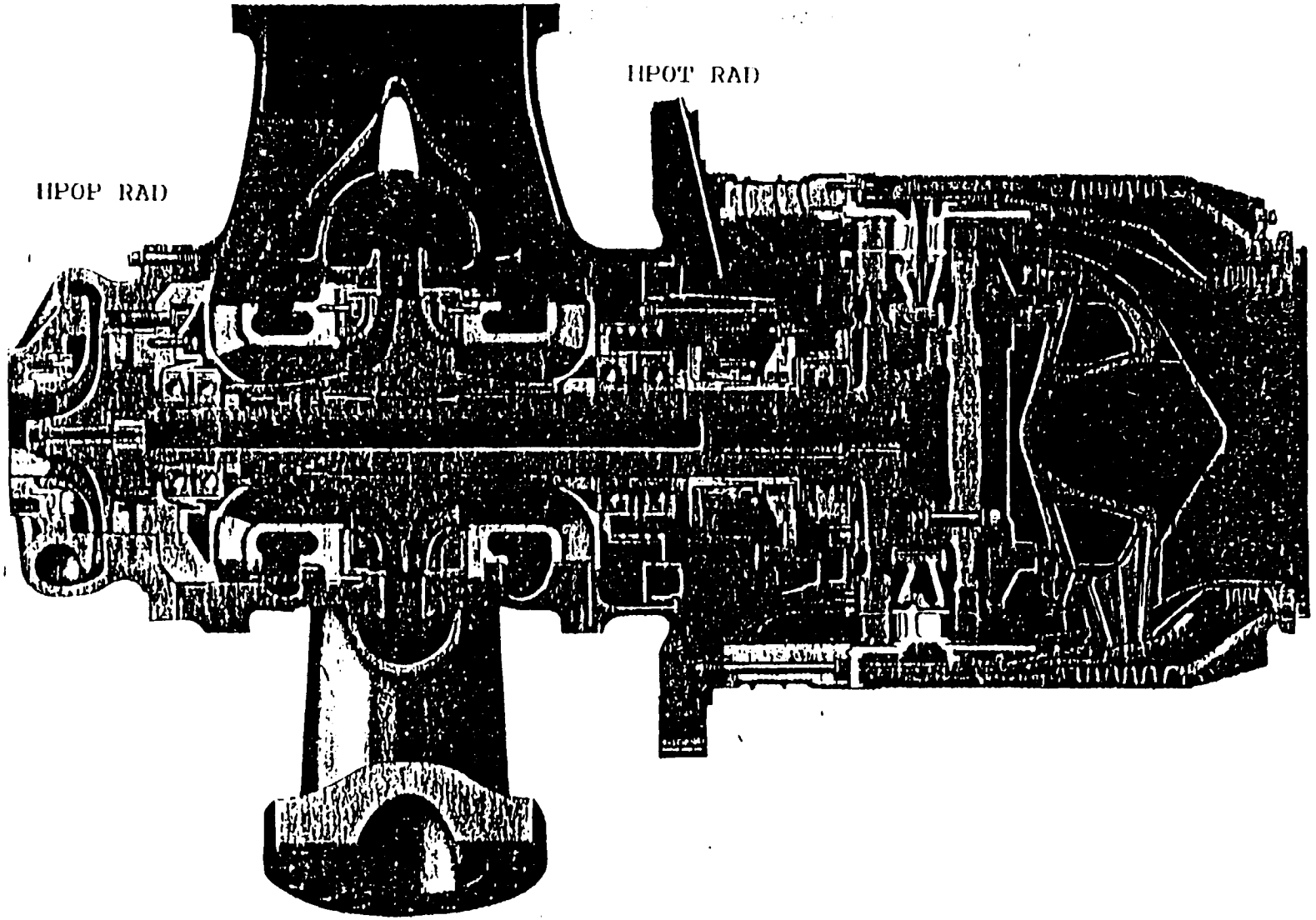

FIGURE 2-4. HIGH PRESSURE OXYGEN TURBOPUMP

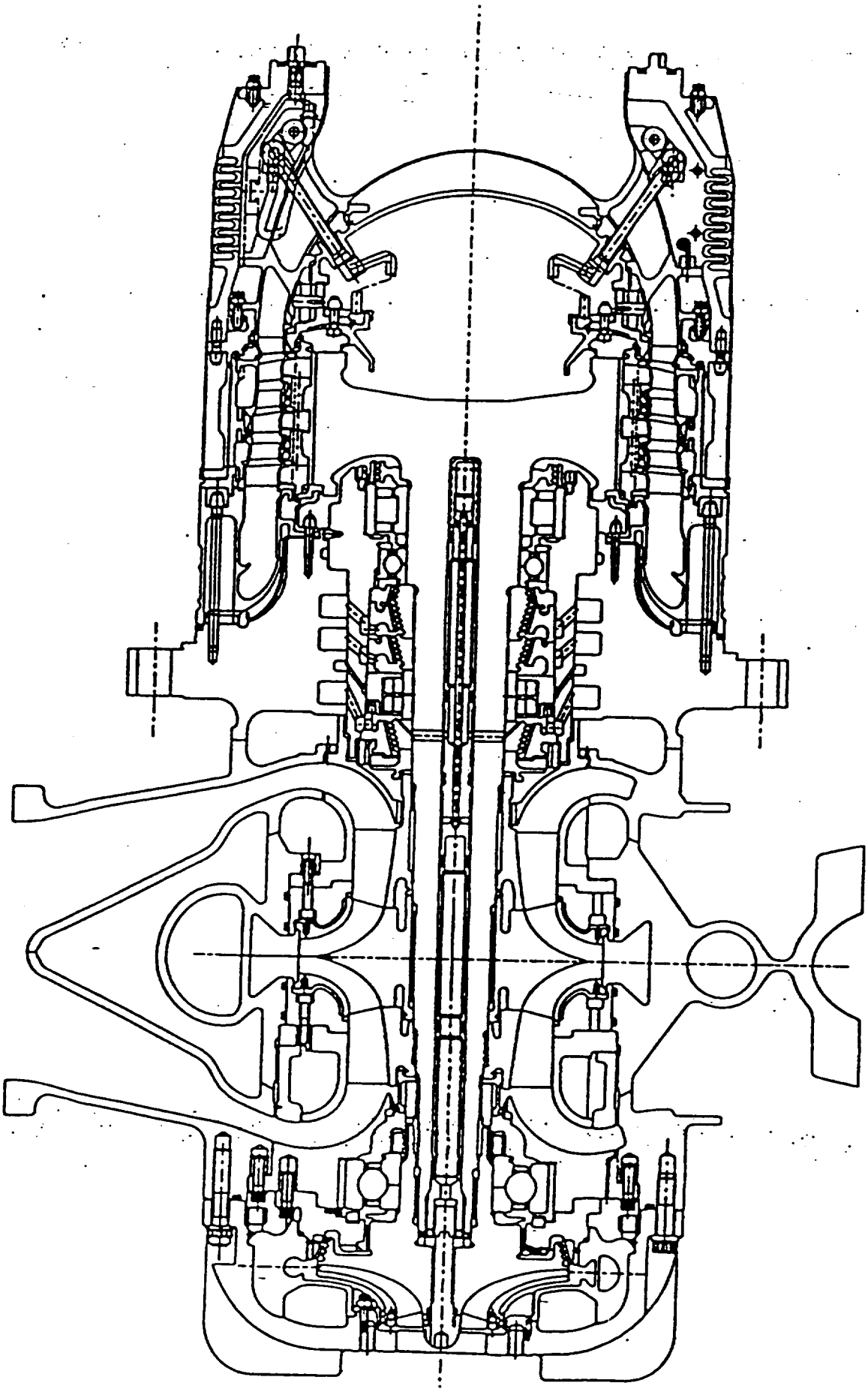

FIGURE 2-5. ATD OXIDIZER TURBOPUMP

Testing is performed on a continuing basis. The length of a given test is dependent on specific test objectives and may run from several seconds to over 800 seconds. Tests are generally designed to satisfy multiple specific objectives, which fall into two broad categories: (1) Acceptance/certification firing of flight hardware and (2) Development testing directed toward design verification, performance, and reliability improvement. Test operations are controlled by a computer called the Command and Data Simulator (CADS) which communicates with the engine, displays vital measurements for on-line observation/control and initiates pre- and post-procedures.

Approximately 250 measurements are recorded on a given test, including wide band vibration, dynamic pressure and strain at critical engine locations. Some of these measurements are utilized on-line as emergency cut-off indicators and all are recorded on magnetic tape or stored digitally for subsequent analysis and evaluation. Limited SSME vibration measurements are recorded on magnetic tape during SSV flights for evaluation after orbiter landing. Figure 2-6 illustrates a schematic of the standard SSME ground test instrumentation. In addition to the above engine tests, dynamic data are also acquired from component testing at government and contractor facilities.

2.5 Data Analysis and Evaluation Considerations

2.5.1 Quick-Look Data Assessment

Acceleration measurements are obtained at fuel and oxidizer turbopump locations during all test firings, providing an extensive vibration data base representing various turbopump builds under widely differing operating conditions. Additional measurements are obtained on a test-specific basis, depending on performance, structural integrity, or rotor dynamic characteristics under evaluation. For example, test series have been performed with some 80 strain measurements to support engine nozzle and injector dynamic stress evaluations. Recent firings have also been conducted with internally instrumented turbopumps to define component dynamic load and signature characteristics. Figure 2-7 illustrates the standard SSME hot firing test profiles and associated mission phase/test objectives, indicating the wide range of engine operating conditions to be assessed. Thus, it is seen that the extent of the evaluation process varies widely from test to test, even though engine performance is nominal. In the event of anomalous performance or component malfunction, the extent of this process is increased significantly. Limited turbopump measurements are also obtained from the three SSMEs on each SSV flight. Data bandwidths available from SSV flight instrumentation differ from the wide-band capability used during ground testing, thus, the need for generating a data base of filtered ground test

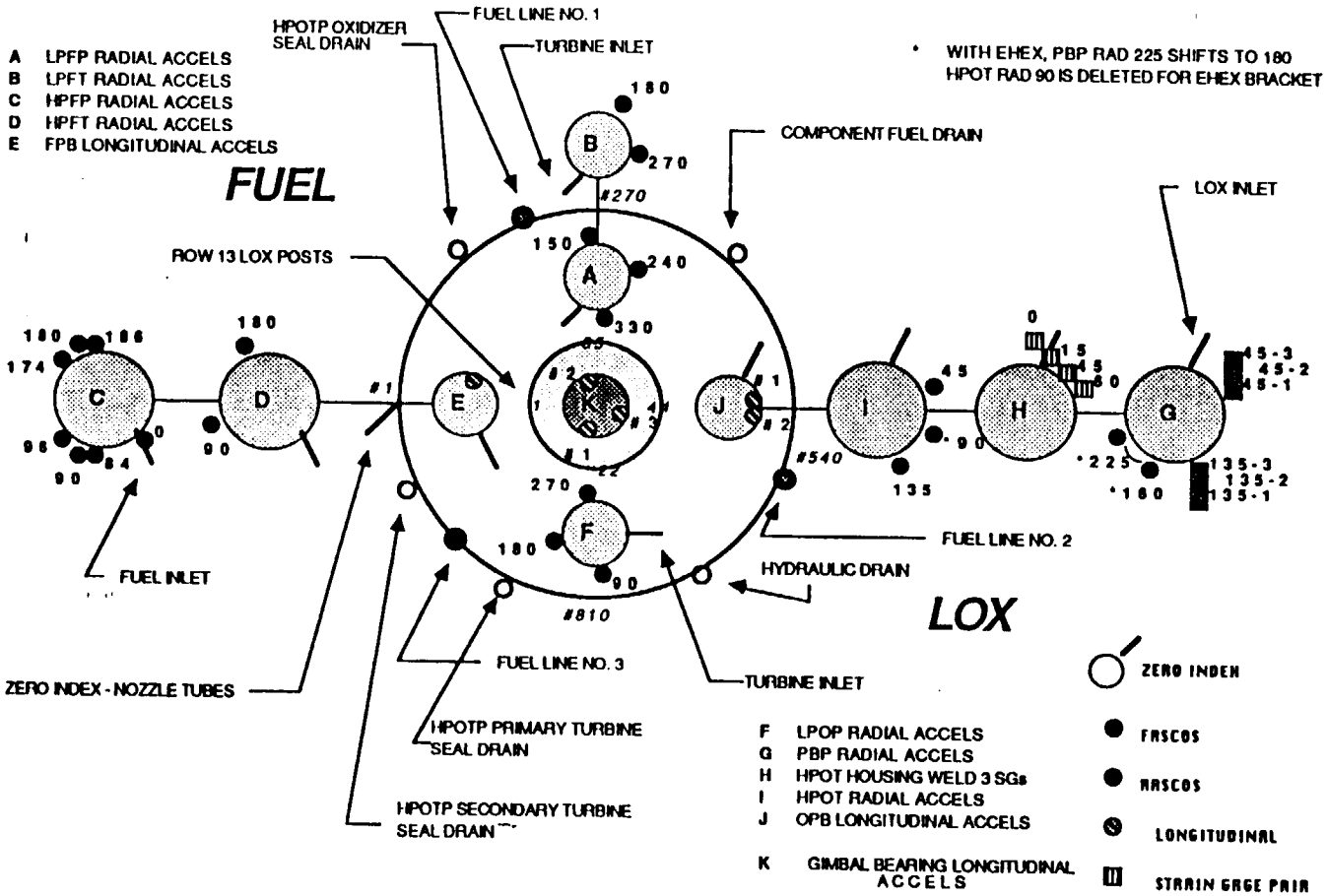

FIGURE 2-6. STANDARD SSME GROUND TEST INSTRUMENTATION LOCATION SCHEMATIC

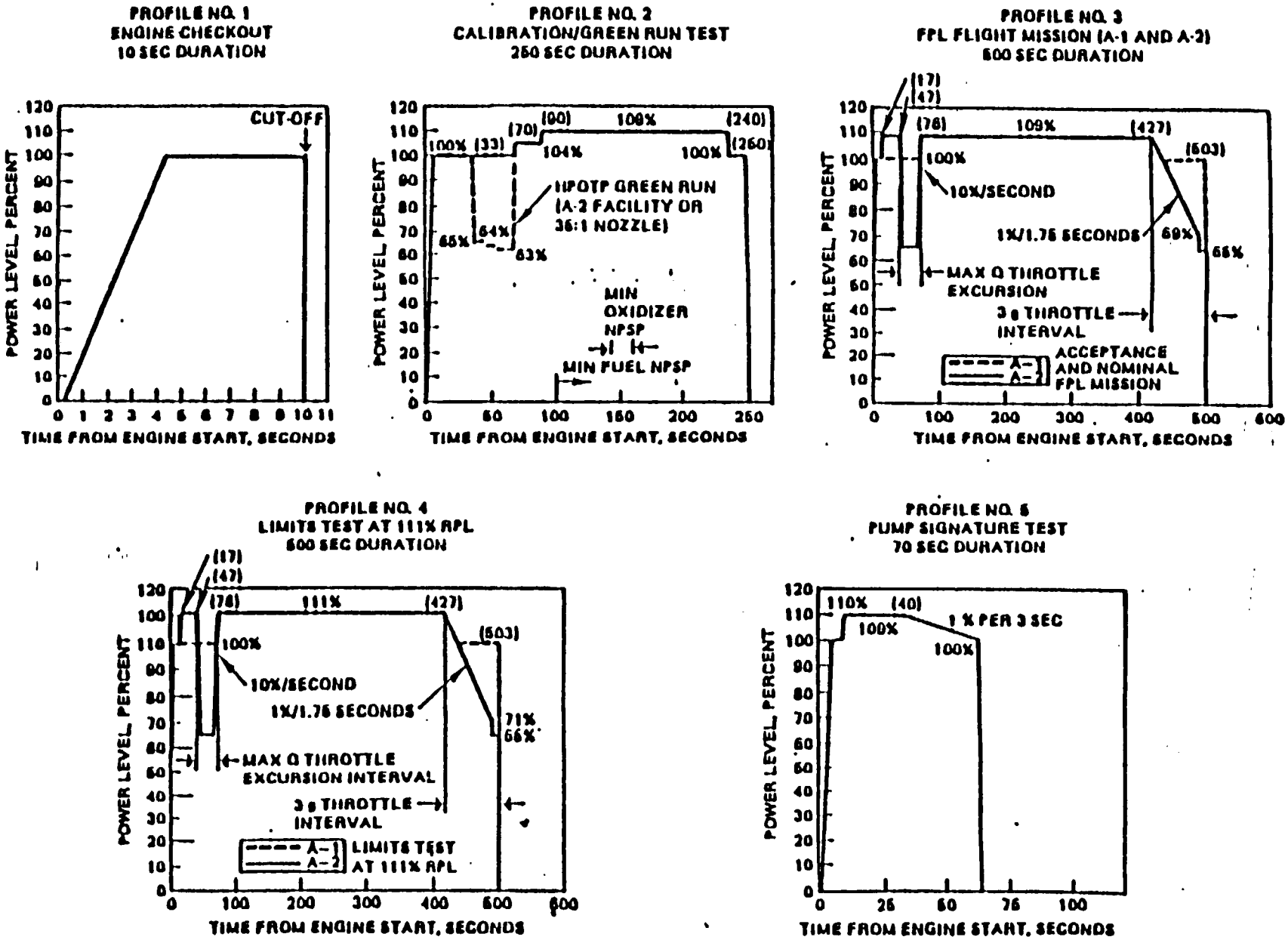

FIGURE 2-7. SSME HOT FIRING PROFILES

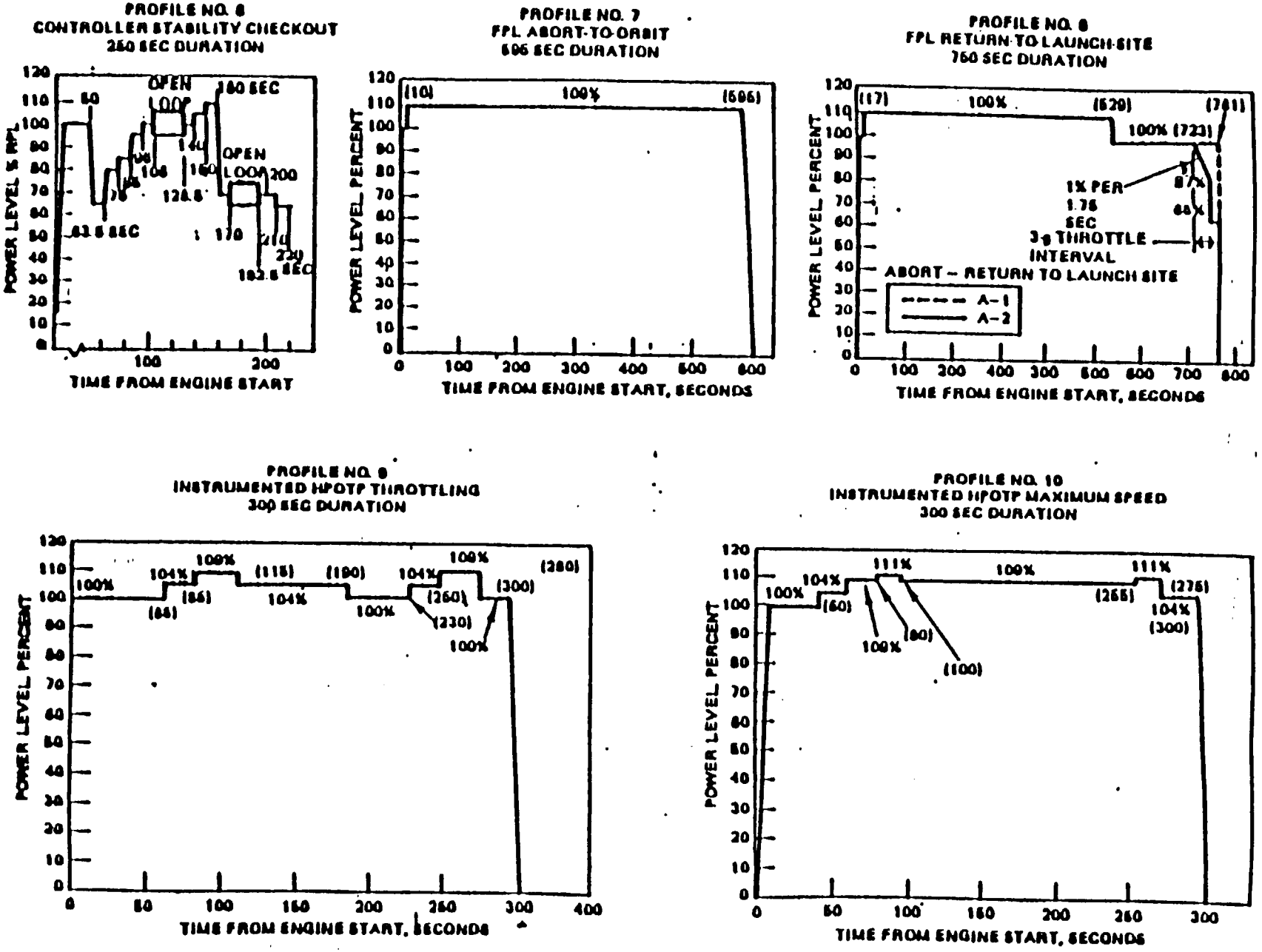

FIGURE 2-7. SSME HOT FIRING PROFILES (Continued)

measurements to permit direct comparison with flight results. Typical activities involved in an SSME test evaluation cycle are summarized as follows.

Data Evaluation and Documentation:

- Data verification and validation
- Events analysis
- Temporal and spectral correlation with operating profile, machine dynamic characteristics, and previous measurements
- Test/flight data summary, including conclusions concerning component condition and operability

Analytical/Statistical Modeling and Classification:

- Update statistical models characterizing normal and abnormal behavior
- Update SSME diagnostic data base and redlines
- Develop and apply computer programs to define SSME component dynamic behavior

Failure/Anomaly Investigation:

- Time/event correlations with other test parameters/observations
- Temporal and spectral comparison with structural dynamic and statistical models and associated failure modes
- Detail signal analysis with fault detection/identification algorithms
- Evaluation and recommendations of probable cause/effect scenarios, and means of resolution

It should be noted that the above evaluations must be performed under extremely limited time constraints consistent with test and flight schedules. Also, the extent of a given evaluation will vary significantly, depending on the specific measurements acquired and whether or not observed engine operation is nominal.

2.5.2 SSME Data Base Application and Refinement

Efficient performance of the above evaluation relies strongly on historical data representing SSME component operating characteristics under varying conditions. Significant effort was directed to the development, modification, and application of MSFC Diagnostic and Statistical data base programs. These programs are used extensively in routine test evaluation and also in diagnostic investigations. The SSME diagnostic data base and software have greatly facilitated the generation of quick-look performance summaries and comparisons for input to the SSME data reviews conducted immediately after each test, as well as the maintenance and update of historic statistical profiles.

A number of sophisticated diagnostic algorithms have been integrated into the "Operator Interactive Signal Processing System (OISPS)," and are operational on the MSFC/Structures and Dynamics Laboratory computers. These include non-linear and non-stationary spectrum analysis, adaptive filtering, cavitation detection and other analytical methods applicable to specific SSME mechanical symptom detection and identification investigations. These techniques and their application are discussed in detail in Appendix A of this report. For quick-look data assessment, the (linear) power spectral density (PSD), 'Isoplot,' Topo Plot, and Root-Mean-Square (R.M.S.) time history of a measurement are the most basic and valuable computational tools. When viewed in the context of empirical statistical data representing SSME component measurements obtained under similar operating conditions, these analyses can provide a quick, qualitative indication of component "health" (from a dynamics standpoint) and signal any gross deviations from nominal operation.

The most fundamental "Signature" utilized to characterize an SSME vibration (acceleration, pressure, strain, etc.) measurement is the mean-square density spectrum, or power spectral density (PSD). Figure 2-8 illustrates a PSD from two high pressure fuel pump acceleration measurements obtained during constant operation at 109 percent power level. Pump shaft (synchronous) speed and related spectral peaks are clearly indicated, as well as an anomalous spike, requiring further investigation.

Interpretation of these results clearly requires knowledge of the mechanical system and reference to nominal data base statistical values, as noted above. In addition to the PSD, these figures include descriptive information to aid in data identification and evaluation, including

- SSME Test Number
- Measurement Location
- Test Time of Analysis
- Engine Power Level (at time of analysis)
- A Summary of Predominant Spectral Peaks and Associated Frequencies
- Composite Vibration Level (RMS)
- Band-Pass Level (RMS) at the Synchronous Frequency
- Sample Size (No. of Averages) Used in the Analysis
- Spectral Resolution (Bandwidth) of the Analysis.

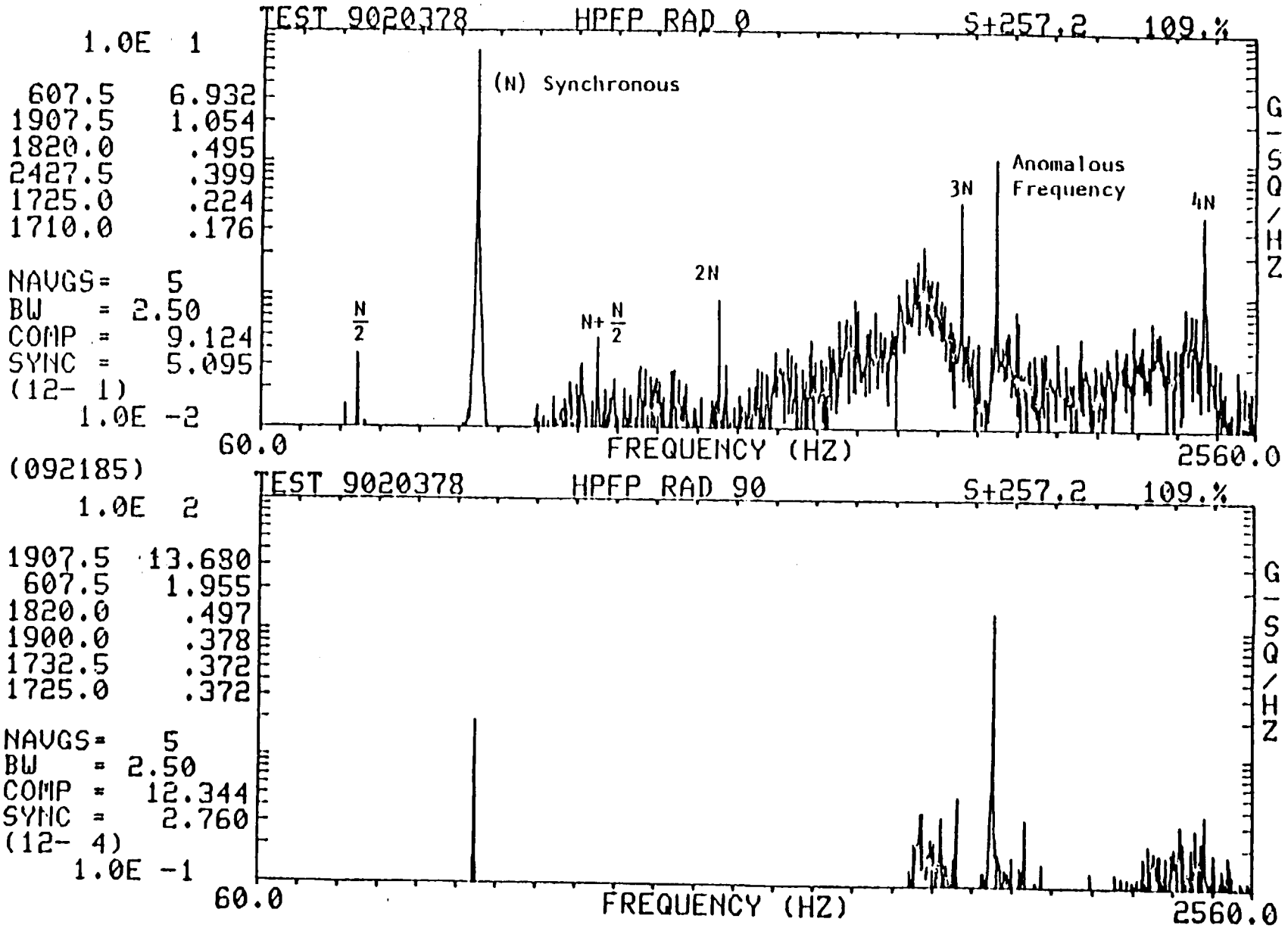

FIGURE 2-8. POWER SPECTRAL DENSITY OF TWO HIGH PRESSURE FUEL TURBOPUMP MEASUREMENTS

Figure 2-9 illustrates an isoplot of a strain gauge measurement representing 450 seconds during a hot-firing test and also a fuel pump acceleration measurement. The PSD provides a detailed 'snap-shot' of conditions over an interval of (usually) constant power operation. In contrast, the isoplot yields a more qualitative indication of amplitude/frequency trends over a complete hot-firing test or powered flight. These plots are particularly useful for detecting the time of any significant deviations in the vibration signature and correlation with engine operating parameters (power profile, programmed venting, etc.). To provide improved tracking of spectral trends, a method called "TOPO" (for Topographic Plot) was developed and programmed. The method uses a novel peak-identifying routine to pick out all meaningful peaks in each PSD and assign a "peakyness" parameter for each identified peak. Each peak is then plotted on a TOPO plot as a dot whose width is proportional to the "peakyness" parameter associated with the peak. Figure 2-9 includes an example of bearing test data during ramp-up. Four hundred PSD's are plotted in this figure, and the non-stationary and crossover behavior can be clearly visualized.

To generate quick-look analyses, the SSME Isospectral Data Base System has been applied extensively. With this system, spectra are extracted at the test site (typically, every 0.4 seconds) for each measurement throughout each test and stored. On command, the spectral data is telemetered to MSFC via satellite. Based on MSFC-developed software, these preprocessed data are then manipulated and printed to display isoplots, bandpass trends, engine speed, etc., on user command. In computing the above isoplot, a frequency band of 3 KHz to 5 KHz was selected and a spectrum plotted every 5 seconds. The displayed amplitude range is selectable, permitting clear representation of major spectral peaks or identification of low level spectral components. Interpretation obviously requires correlation with engine speed and other parameters. Figure 2-10 illustrates the root-mean-square acceleration time history composite and synchronous levels for two selected measurements. These time histories were synthesized from the stored isospectral data by integrating over the PSDs obtained at 0.4-second intervals during the test.

Figure 2-10 also illustrates a highly useful aid to data evaluation, developed under previous contract. Superimposed on the measurement time histories are characterizing statistical levels derived from analysis of extensive previous tests, representing nominal SSME operation. As far as these two condition indicators are concerned, brief inspection indicates a very smooth running machine. It should be noted that these 'overlay plots' represent a separate statistical analysis of each measurement, for each constant power level, extracted from the SSME vibration data base. Several diagnostic algorithms, to enhance data base application, have been incorporated in the menu driven system.

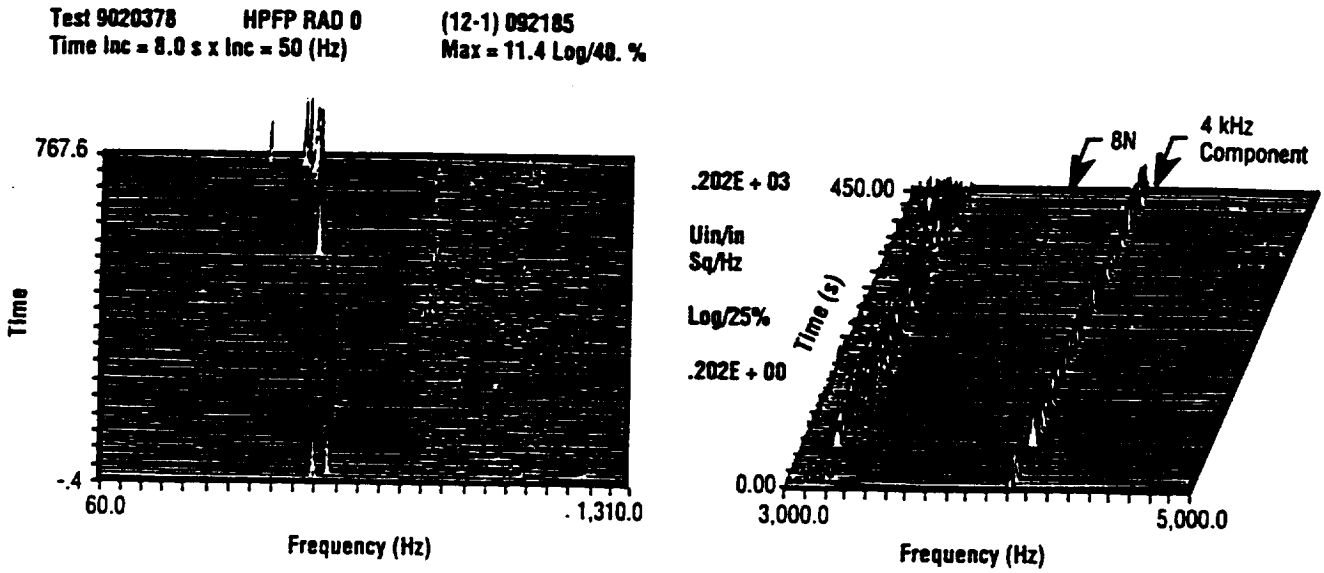

Illustration Isoplot Format

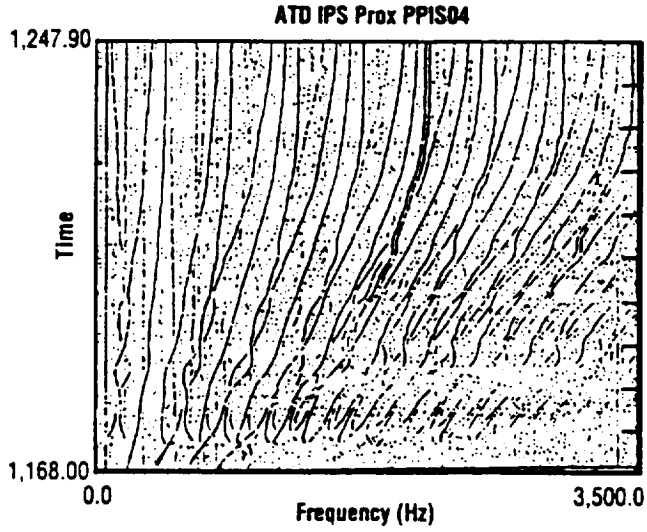

npk = 80
isp = 1
neigh= 5
ipara = 5
mx = 1
my = 1

#PSU = 400
#AVGS= 1
BW = 5.00

TOPO Plot of Bearing Displacement During Speed Change

FIGURE 2-9. ILLUSTRATION OF ISOPLOT AND TOPO PLOT ROUTINES

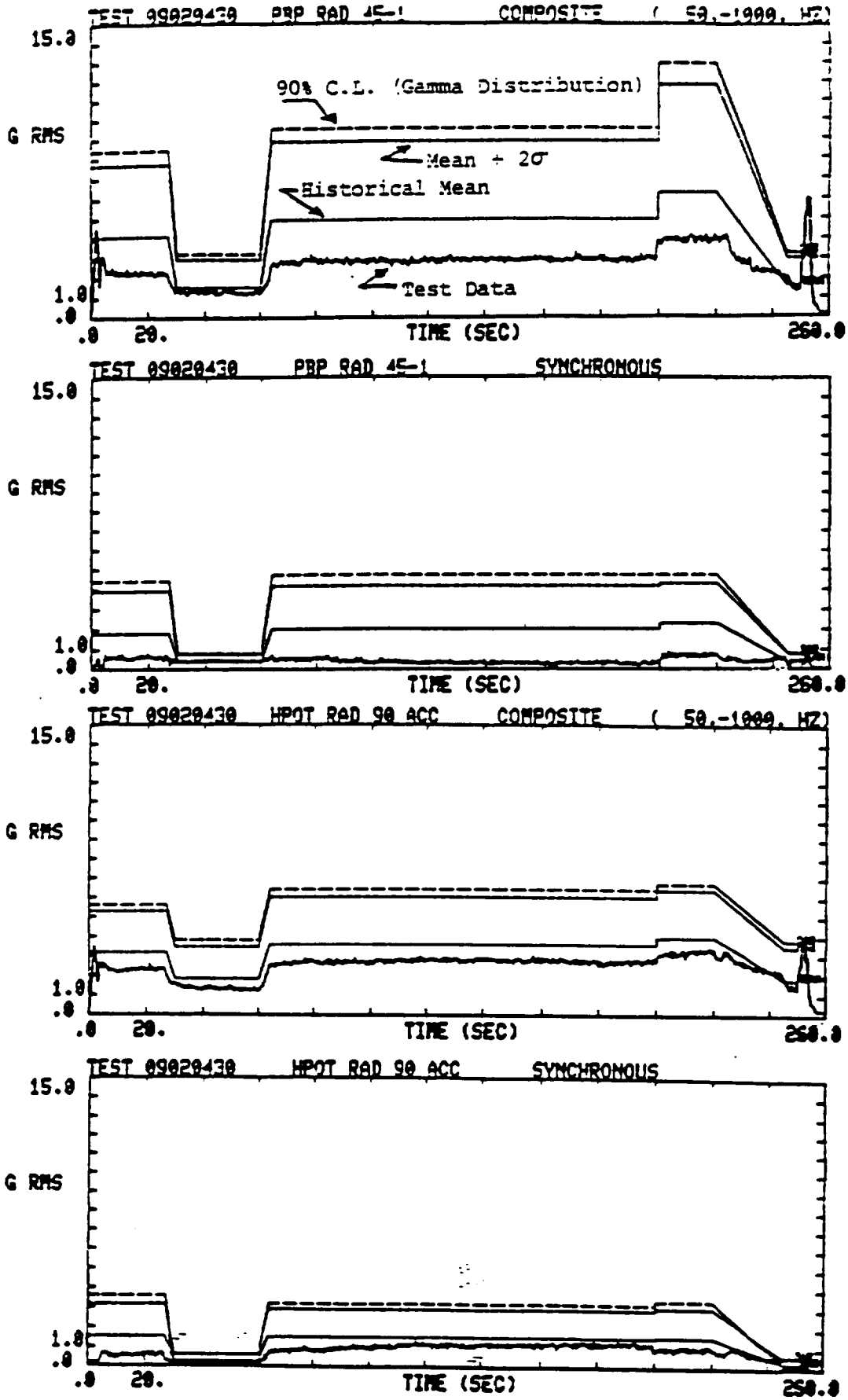

FIGURE 2-10. TURBOPUMP RMS TIME HISTORIES AND STATISTICAL RANGES

2.5.3 Diagnostic Methods and Applications

The hypercoherence method was extended to a time-domain filtering algorithm for the extraction of periodic vibration signals in noisy SSME data. The procedure is best illustrated by example. Figure 2-11a illustrates the orbit plot for two jointly periodic signals, each containing three harmonic components. Figure 2-11b represents the same plot when uncorrelated noise and independent, coincident periodic components have been added to each signal. This chaotic pattern is highly representative of hot firing data. Figures 2-11c and 2-11d are the recovered orbital diagrams by hypercoherence filtering and comb filtering, respectively. The superior performance of hypercoherence filtering is clearly indicated.

The Wide Band Demodulation (WBD) technique was applied to the detection of cavitation in turbopump systems. When cavitation occurs, the periodic shaft rotational components will amplitude modulate the wide-band noise generated from collapsing cavitation bubbles. This wide-band modulation will make the periodic component become undetectable in the raw PSD of its dynamic measurement signal. However, this special phenomenon provides a unique signature for cavitation detection and monitoring. By using the WBD technique, the hidden periodicity can be recovered from a wide-band high frequency noise signal. The resulting WBD PSD can better indicate cavitation condition changes as compared to an ordinary raw data PSD. The application of WBD to cavitation detection is illustrated in Figure 2-12. Figure 2-13 indicates several analytical approaches to perform the transformation. The WBD method has aided the identification of hidden periodicities in MSFC turbopump inducer flow test data and correctly indicated changes in the cavitation level during test.

A novel technique, the Modified Wigner Distribution (MWD) was developed for resolving time-frequency trends in highly non-stationary vibration data. Standard Fourier-based routines (e.g. FFT) imply the assumption of a stationary time series. However, turbomachinery operation includes highly nonstationary periods associated with engine startup, shutdown, and throttling. The Wigner Distribution (WD) is capable of high resolution estimates for nonstationary signals, but suffers from aliasing resulting in false peaks, for series with multiple spectral peaks. A demonstration of the MWD method in the evaluation of multiple components signals is shown in Figures 2-14, 2-15, and 2-16. Figure 2-14 shows the short-time FFT isoplot of a simulated signal composed of two sine waves. The frequencies and amplitudes of the discrete components are changing rapidly, and the corresponding spectral peaks are smeared. The WD spectrum for the same signal is shown in Figure 2-15. With the multicomponent signal, the WD introduces erroneous cross coupling component between the two simulated sine waves. This "phantom" peak train distorts the resulting time-frequency spectrum. Figure 2-16 is the corresponding

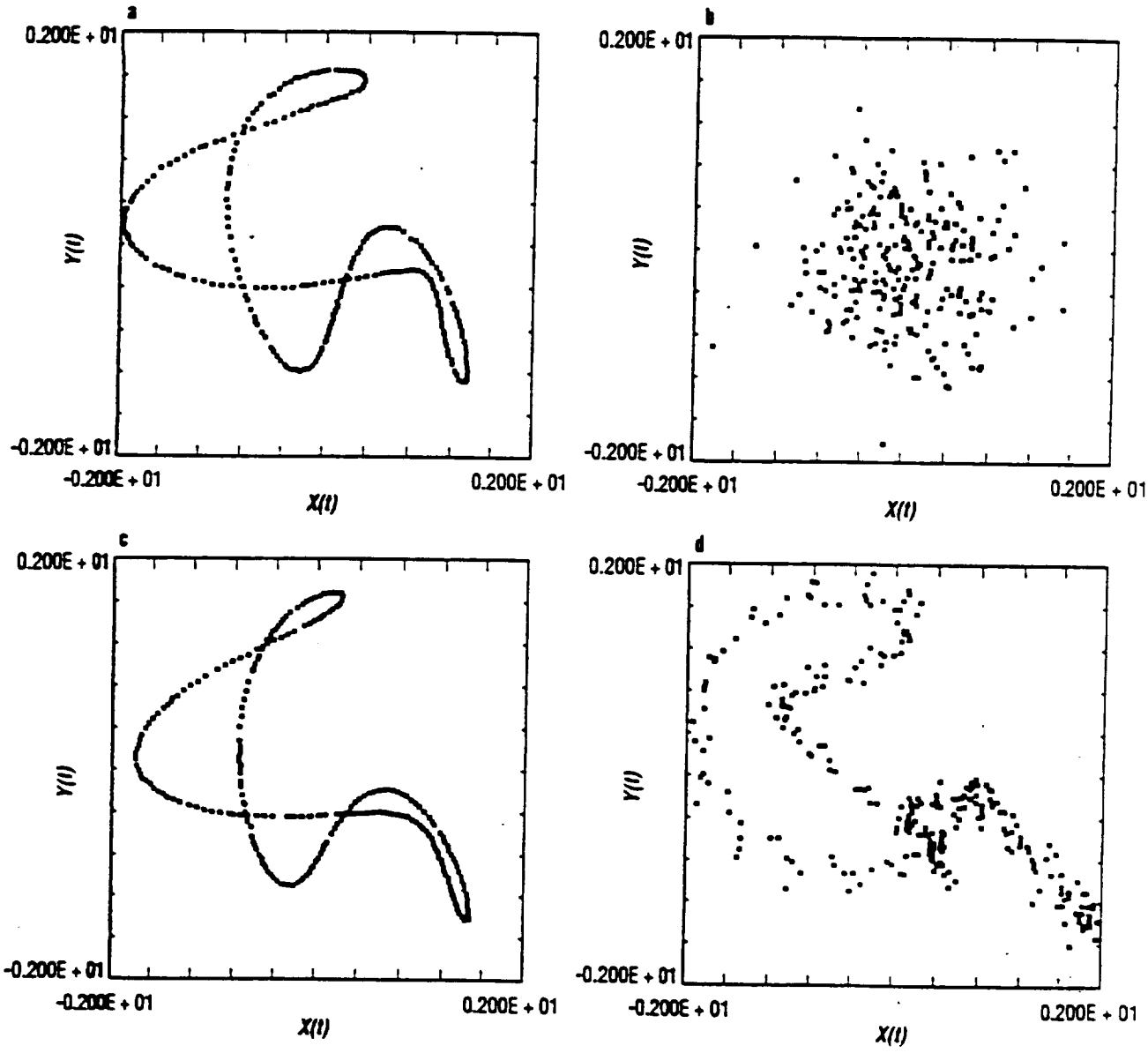

(a) Orbital Diagram of Noise-Free Simulation, (b). Orbital Diagram of Simulation With Additive Gassian White Noise. (c). Recovered Orbital Diagram by Using Hypercoherence Filtering. (d). Recovered Orbital Diagram by Using Comb Filtering

FIGURE 2-11. SIGNAL DETECTION BY HYPERCOHERENCE FILTERING

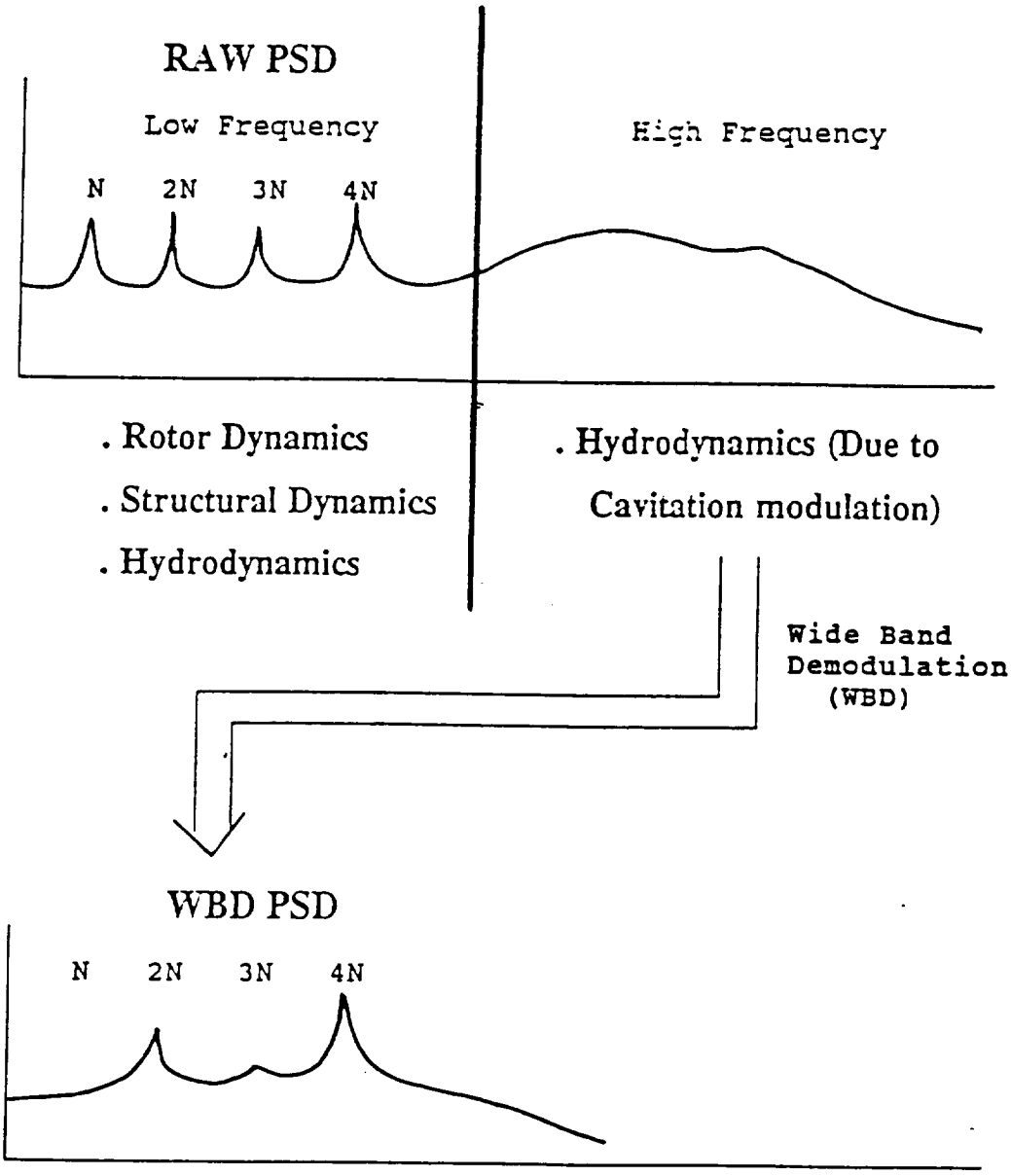

. If no cavitation, PSD of WBD will be broadband noise

. If cavitation occur, PSD of WBD will show discrete peaks corresponding to the low frequency periodic pressure fluctuation due to rotational process.

FIGURE 2-12. FREQUENCY TRANSLATION BY WIDE-BAND DEMODULATION

(1) Tri-spectra Method:

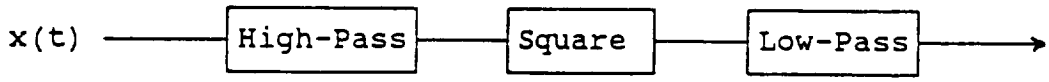

(2) Rectify Method (Envelope Detection):

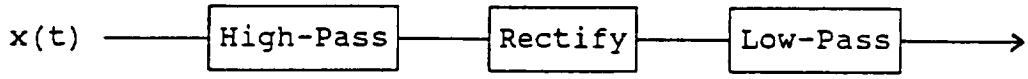

(3) Hilbert Transform Method (Envelope Detection):

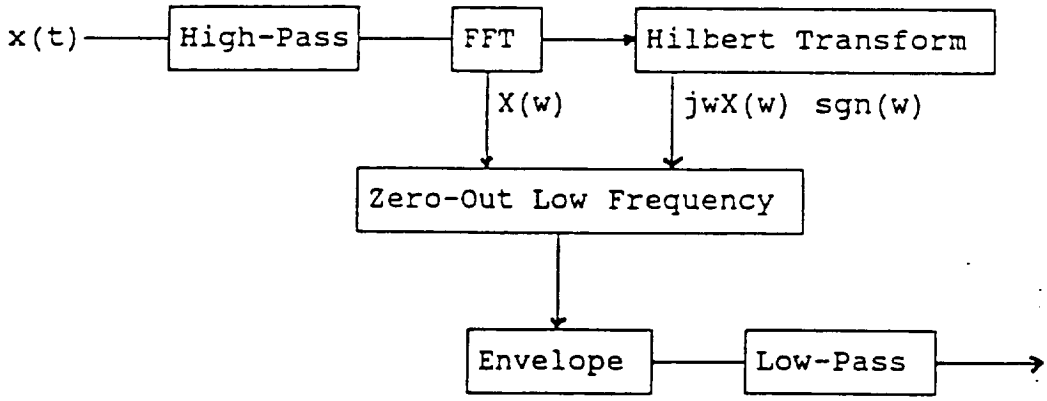

FIGURE 2-13. ALGORITHMS FOR WIDE-BAND DEMODULATION (WBD)

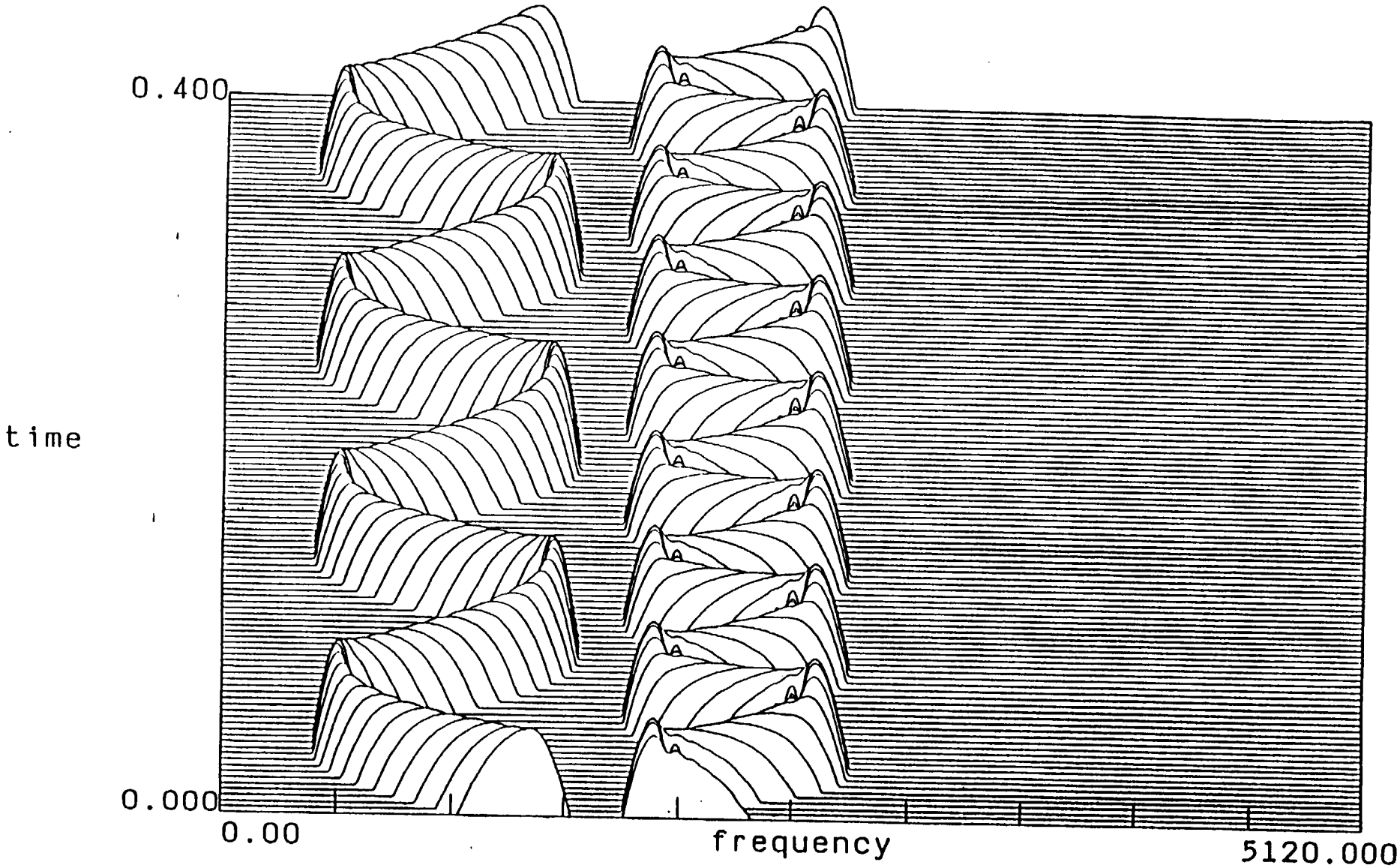

FIGURE 2-14. FFT ISOPLOT OF TWO MODULATED SINE WAVES

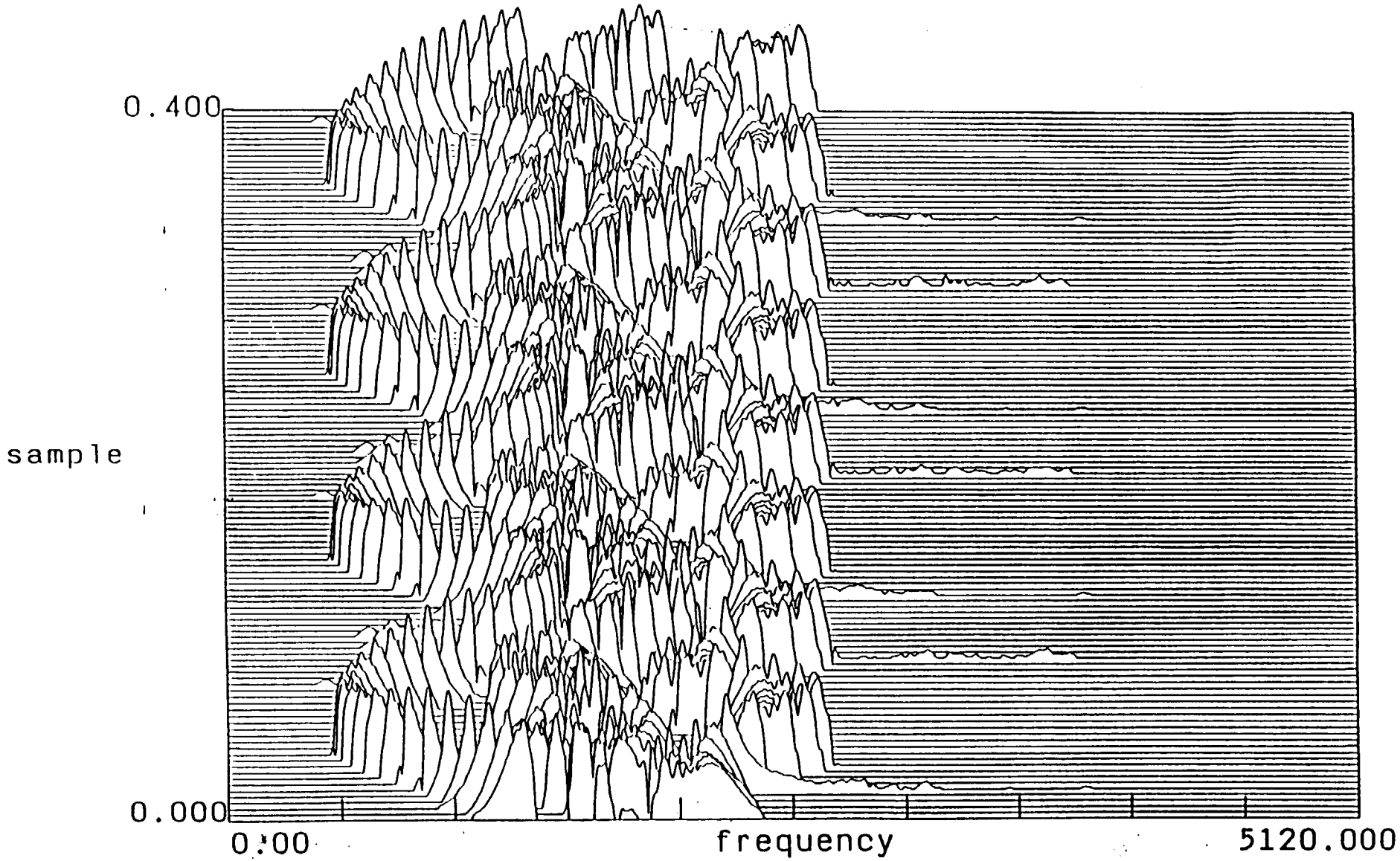

FIGURE 2-15. WD ISOPLOT OF TWO MODULATED SINE WAVES

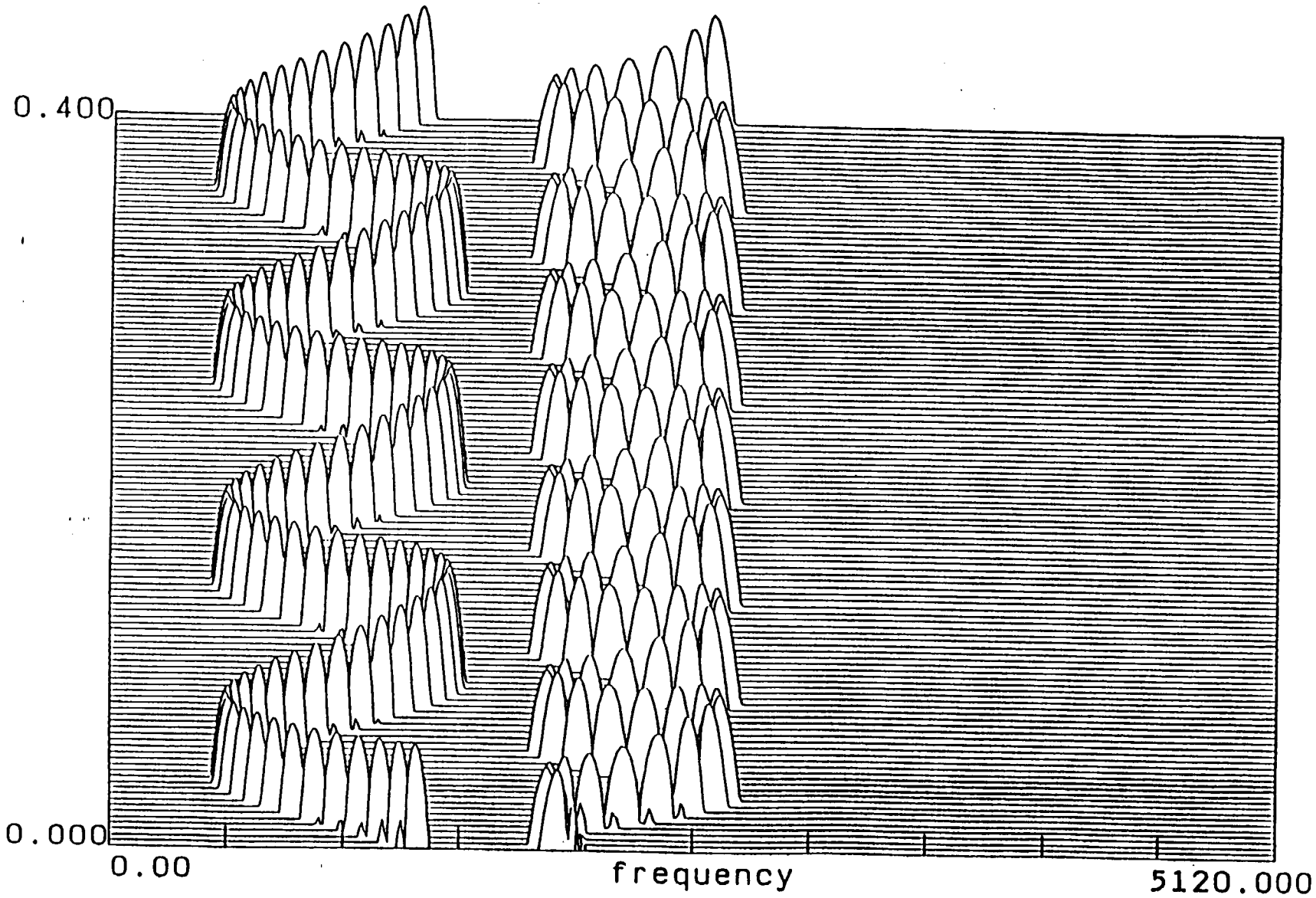

FIGURE 2-16. MWD ISOPLOT OF TWO MODULATED SINE WAVES

MWD spectrum for the SSME signal. As can be seen in the figure, an improved resolution is attained over that of the STFT, without unwanted cross coupling terms.

The SSME static firing and flight vibration data contains many frequency components that can be confused with incipient bearing deterioration signatures if not carefully analyzed. This can lead to rejection of turbopumps with good bearings and the extremely high cost associated with teardown, inspection, and recertification, not to mention the impact on schedules. In an effort to define the rotational frequencies and detect signature of ball bearings operating at high speeds from the geometrical bearing configuration, a number of analytical and computer simulation routines were developed and implemented. The ADORE (Advanced Dynamics of Rolling Element bearings) program has been extensively applied over the last two years. With this program, any arbitrary variation in bearing geometry (ball wear, etc.) or manufacturing tolerances, can be modeled and the influence of time varying operating condition on each bearing element calculated. The bearing elements include the inner and outer race, ball or roller, and the cage. For each rolling element the orbital position, velocity, relative angular position, spin/roll ratio and slip velocity are available for studying the vibration signature. This program has basically replaced the previously developed methods, which only considered the geometrical bearing configuration. Some of the imperfections, operational conditions and manufacturing tolerances investigated recently with the ADORE program include:

- Imperfections in rolling elements (wear)
- Combined loading
- Outer/inner race curvature factors
- Variation in cage pocket shape

A sensitivity analysis of bearing behavior is illustrated in Figures 2-17 through 2-20. The study of bearing dynamics represents a continuing effort to define with greater accuracy ball bearing signatures for prediction of wear and/or incipient bearing failure. Application of the techniques, summarized in this section, are discussed more fully in the Appendices to this report.

2.5.4 Statistical Characterization of SSME Data

A comprehensive statistical data base of vibration spectra, representing SSME-component response over a wide range of engine operating conditions, has been developed. These data are invaluable in the efficient assessment of hot firing test results. Measurements from over 2000 hot firing tests, with an average of 19 vibration measurements per test, are presently stored. Table 2-1, at the end of this report, is a log of all SSME hot firings, including flights. Extensive statistical analyses have been applied utilizing this data base, primarily to

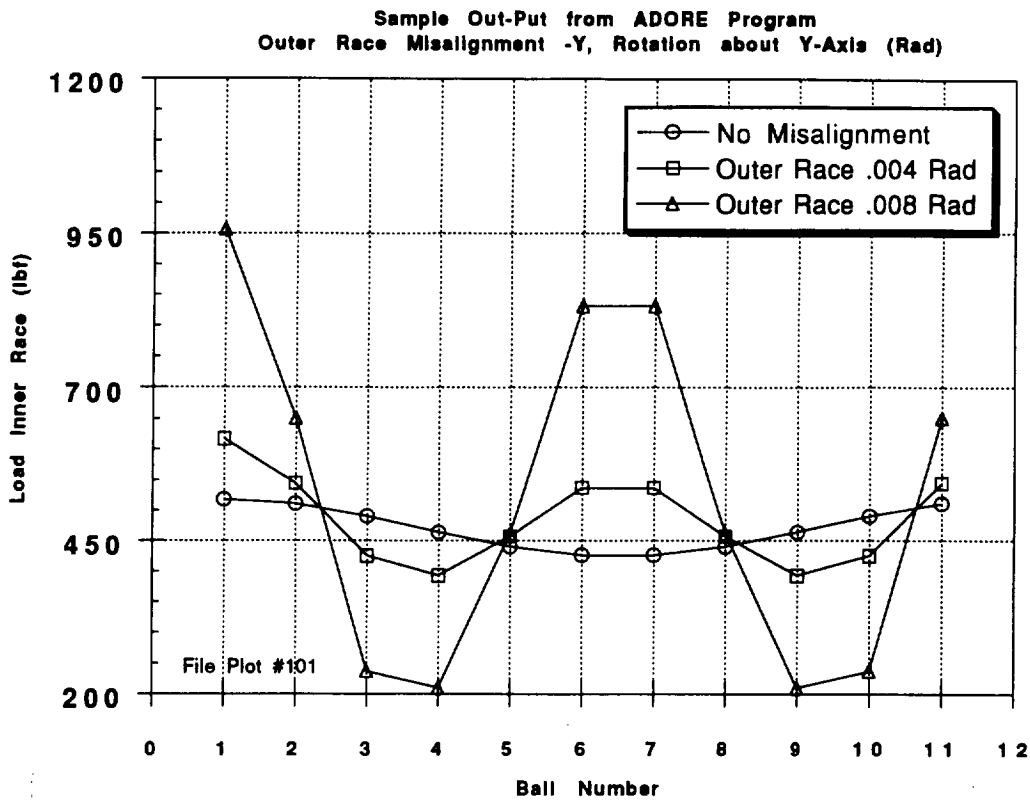

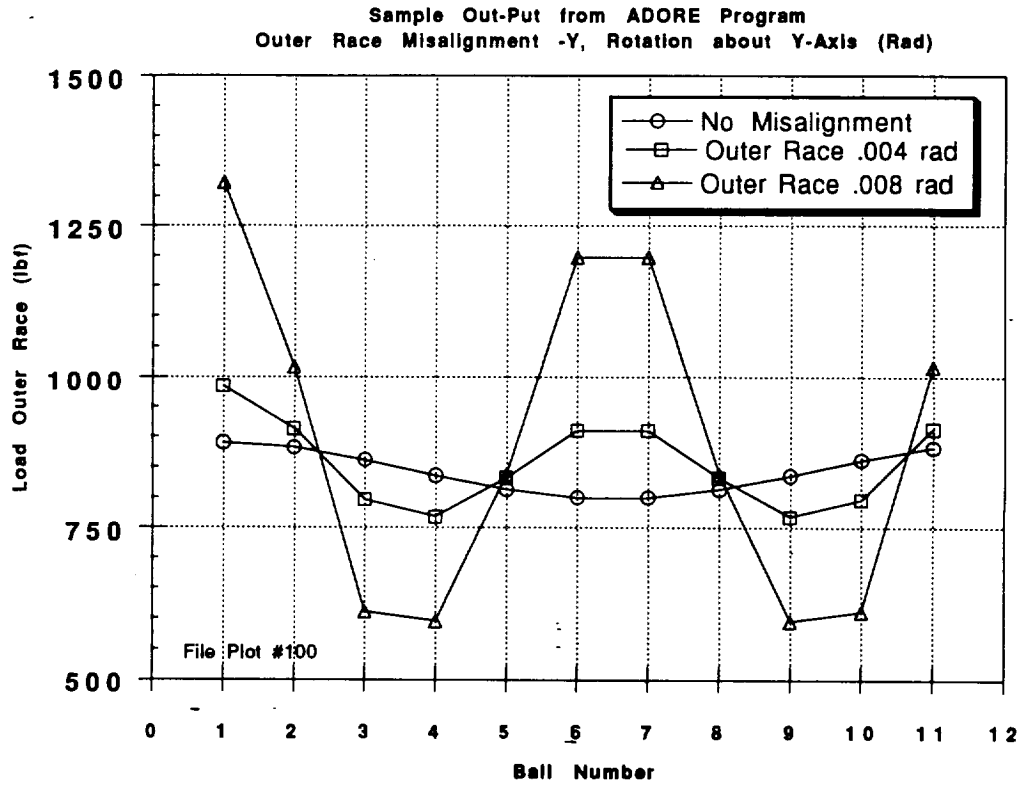

FIGURE 2-17. ADORE OUTPUT - MISALIGNMENT

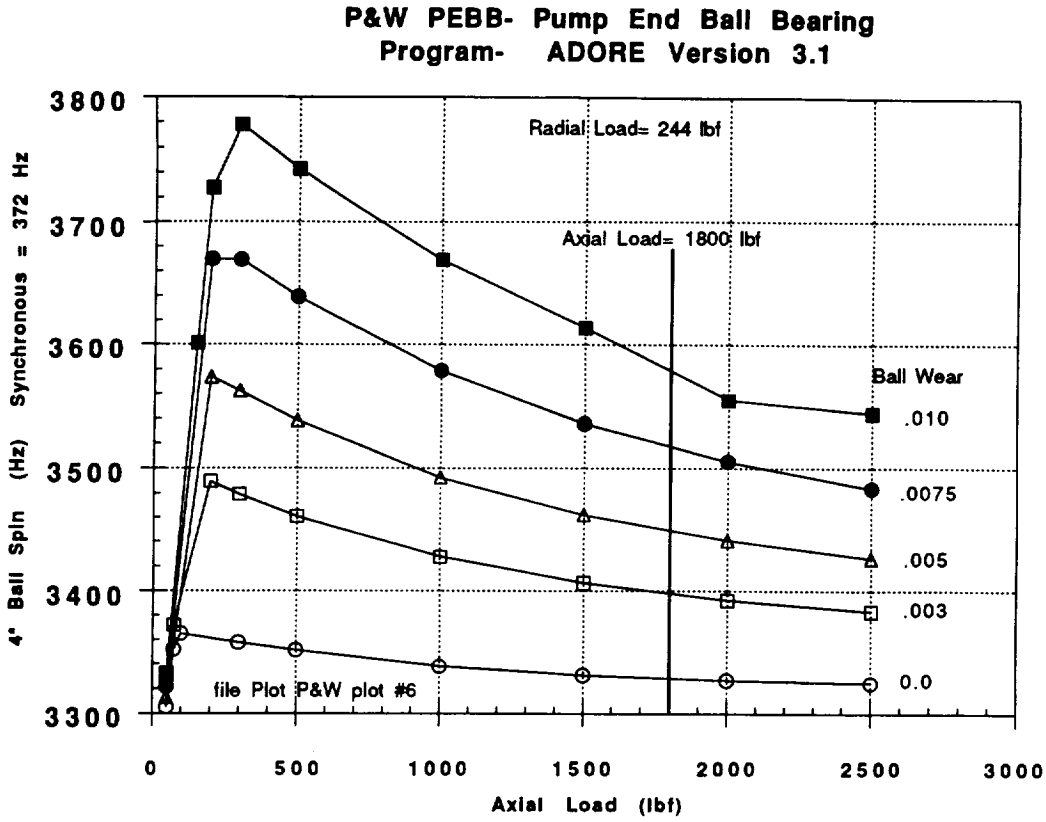

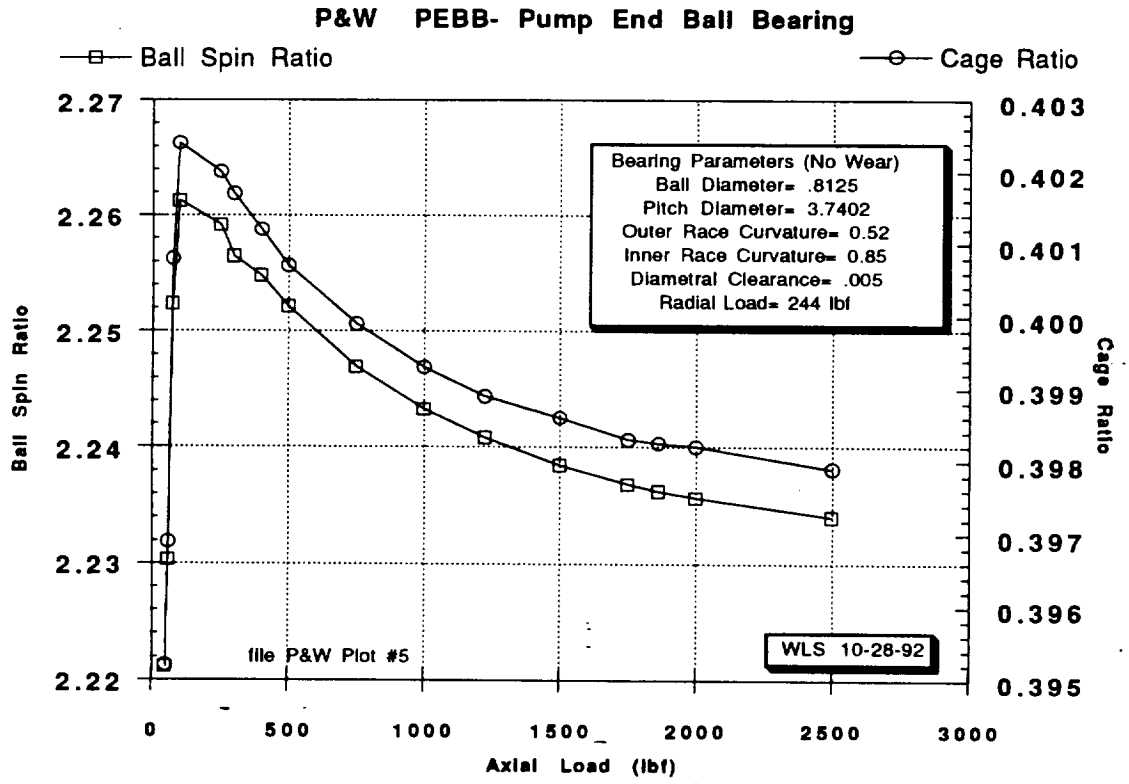

FIGURE 2-18. ADORE OUTPUT - AXIAL LOADING

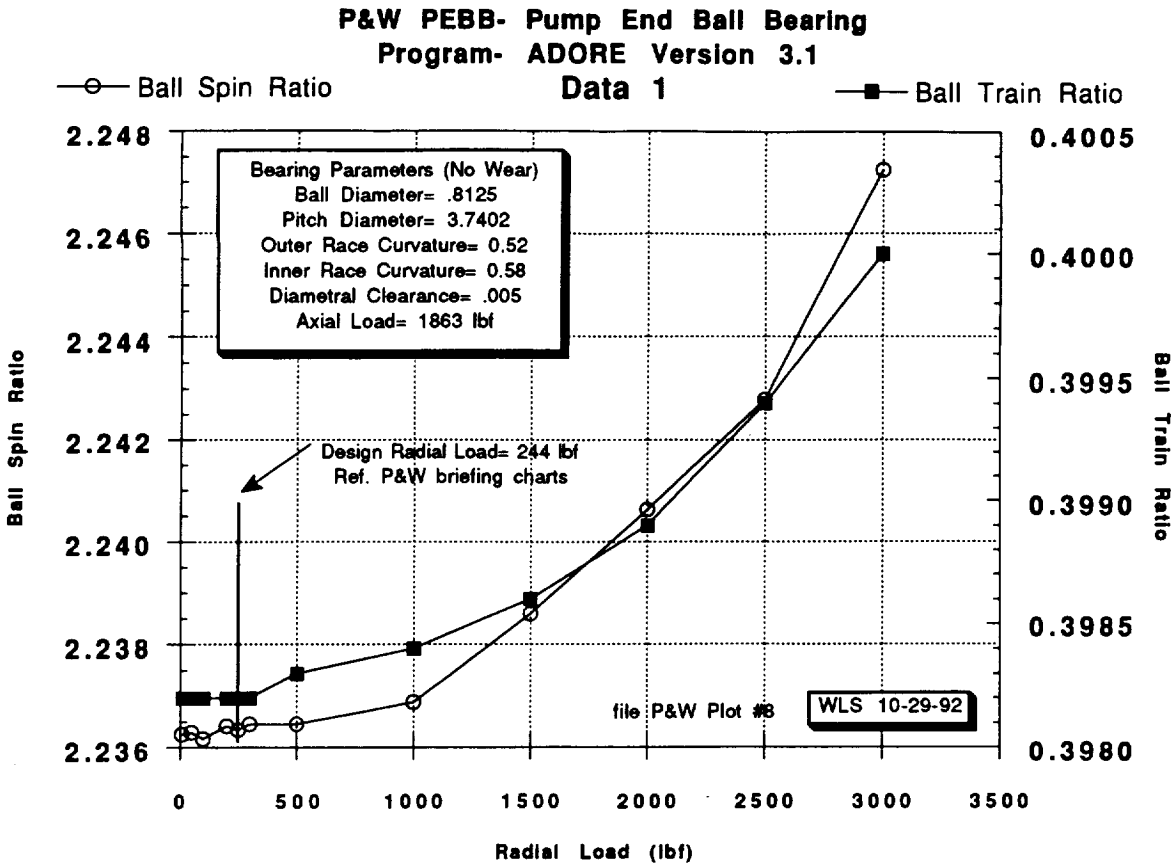

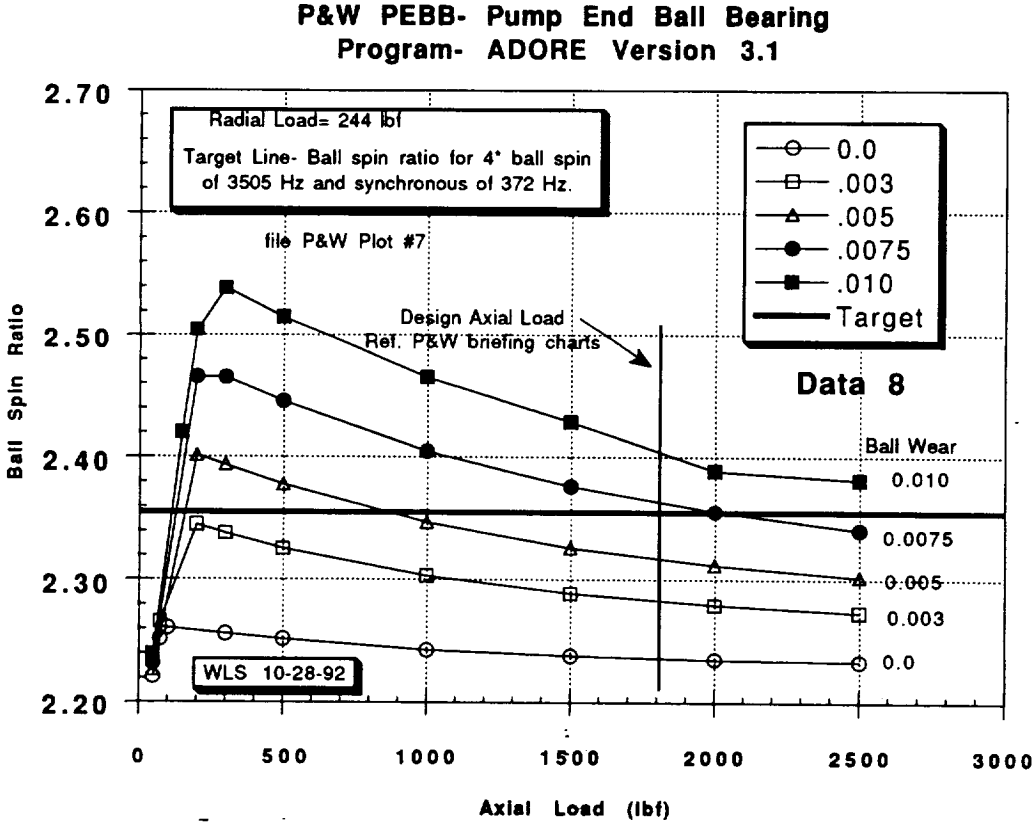

FIGURE 2-19. ADORE OUTPUT - RADIAL AND AXIAL LOADING AND BALL WEAR

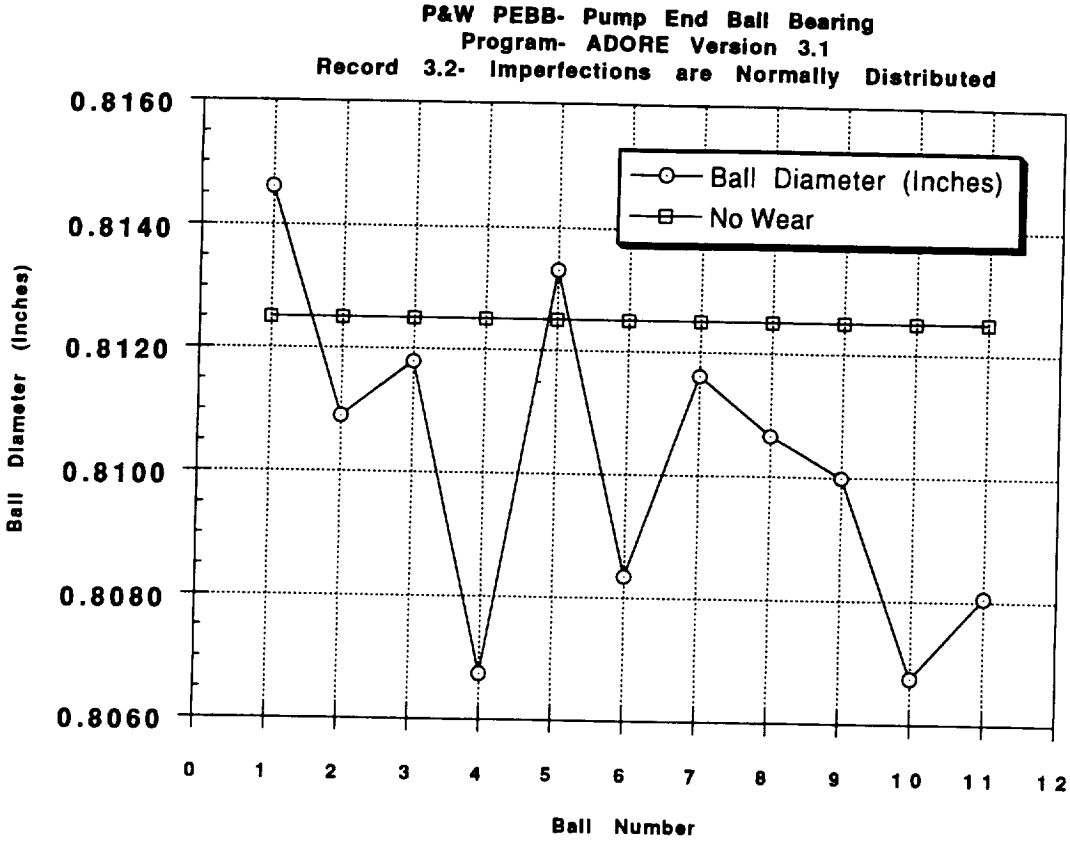

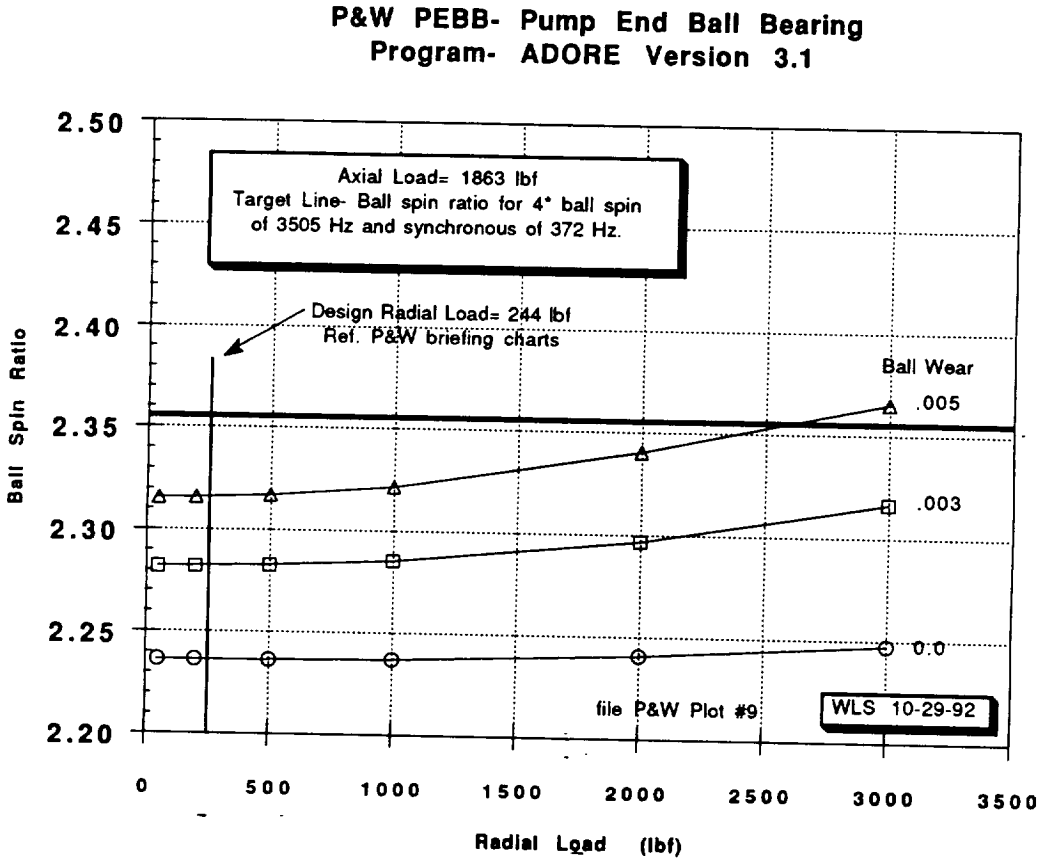

FIGURE 2-20. ADORE OUTPUT - BALL WEAR

- Classify (statistically) measurements by location, engine operating conditions, and component condition.
- Discriminate between nominal and abnormal component operation.
- Establish vibration redlines and flight certification acceptance criteria.

Figures 2-21 and 2-22 illustrate the statistical variation in shaft speed for the ATD turbopump, during nominally constant power level operation. Such results are useful in the interpretation of component response measurements since rotational component frequencies (turbine blades, bearing elements, etc.) of interest will vary with shaft speed.

Operating redlines (vibration, pressure, temperature, etc.) are utilized to terminate, or otherwise alert, SSME test operations in order to minimize the possibility of damage to equipment or personnel. Turbopump vibration measurements provide a significant input to test operation decisions. Detailed statistical analyses are required to establish these criteria. During Space Shuttle flight, a Flight Accelerometer Safety Cut-off System (FASCOS) is utilized to monitor SSME turbopump vibrations. (This system is not yet active in the loop.) Similar analyses are required to assess flight certification (green run) acceptance levels. Vibration acceptance criteria for the operational SSME turbopumps are summarized as follows:

- HPFTP Acceptance Criteria @ 104%-109% RPL
  Synchronous (1N) - pump end/turbine end grms: 7.5 max/7.5 max
  3X synchronous (3N) - pump end/turbine end grms: 7.5 max/11.0 max
  Any subsynchronous on HPFTP shall be addressed during acceptance review

  LPFTP Acceptance Criteria @ 105% - 109% RPL
  Synchronous (1N) - pump end/turbine end grms: 3.0 max/4.5 max

- HPOTP Acceptance Criteria @ 104% - 109% RPL
  Synchronous (1N) - pump end/turbine end grms: 3.0 max/3.0 max
  Cage Frequency Harmonic Amplitude: any sustained (two or three consecutive data samples) amplitude strain placed on the ball cage frequency harmonics is not acceptable
  Any subsynchronous on HPOTP shall be addressed during acceptance review

  LPOTP Acceptance Criteria @ 104%/109% RPL
  Synchronous (1N) - pump end/turbine end grms: 1.0 max/1.0 max

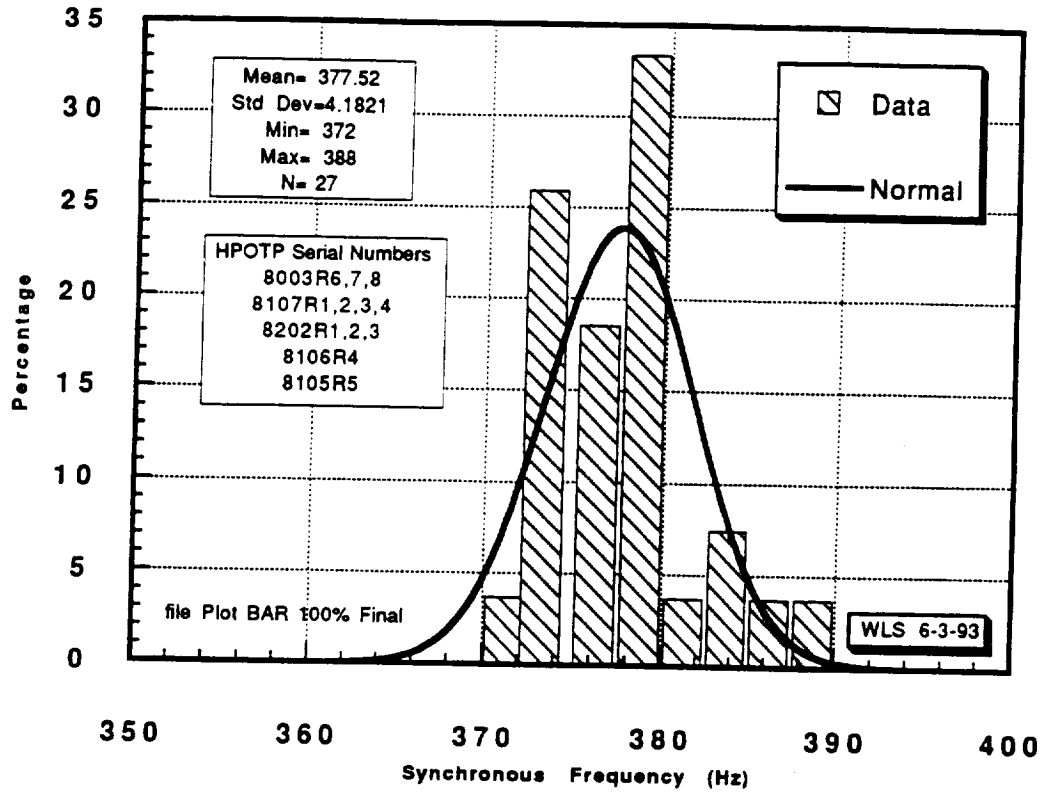

FIGURE 2-21. HISTOGRAM SYNCHRONOUS FREQUENCY @ 100% PWL ATD HIGH PRESSURE OXIDIZER TURBOPUMP (HPOTP)

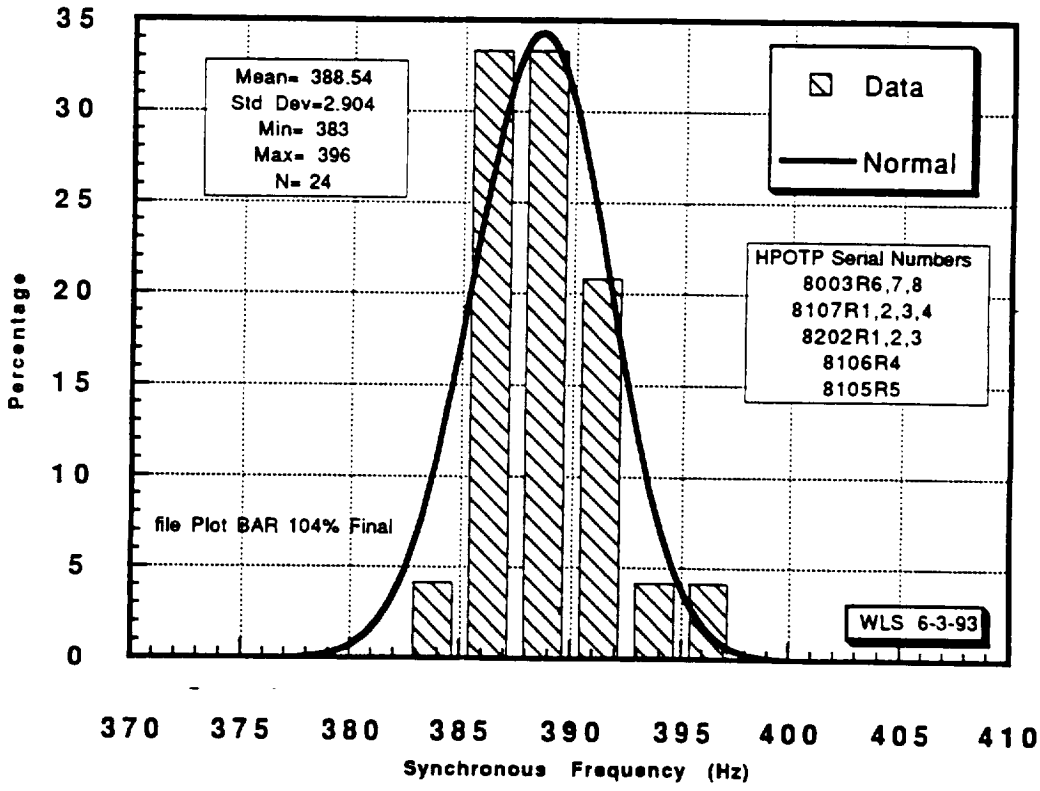

FIGURE 2-22. HISTOGRAM SYNCHRONOUS FREQUENCY @ 104% PWL ATD HIGH PRESSURE OXIDIZER TURBOPUMP (HPOTP)

The sample mean and standard deviation of a collection of measurements provide a simple and useful measure of the 'center of gravity' and dispersion of the data. In addition, such statistics can be used to estimate the probability distribution for representing the data set. Classical distributions provide a useful tool for modeling empirical measurements. This permits direct comparison of newly observed results, with previous trends. Fundamental steps in the assignment of analytical distributions to represent a collection of data, include the selection of reasonable analytical models, and performance of tests to gauge how well a selected model fits the empirical data set. Figures 2-23 and 2-24 illustrate the 'fit' of three theoretical distributions to the empirical distribution of recent ATD turbopump vibration measurements. The mean-square error noted on the figures indicates the relative goodness-of-fit between each theoretical distribution and the observed measurements. Application of statistical techniques to SSME evaluations are discussed further in Appendix A. Specific tasks performed under the subject contract are summarized in the next section.

2.6 Task Requirements and Accomplishments

The basic objectives of this study were to perform detailed analysis and evaluation of dynamic data obtained during SSME test and flight operations, including analytical/statistical assessment of component dynamic performance, and to continue the development and implementation of analytical/statistical models to effectively define nominal component dynamic characteristics, detect anomalous behavior, and assess machinery operational condition. Our overall goal was to provide timely assessment of engine component operational status, identify probable causes of malfunction, and define feasible engineering solutions. The work performed under this contract may be summarized by the three broad task areas outlined below. Consistent with stringent SSME test and flight certification schedules, test evaluation and the resolution of discrepancies were given priority throughout the study.

Data Analysis, Evaluation and Documentation. This task represented the major contract effort and included data verification, analysis, and documentation for each SSME ground test and, additionally, for all SSME flight measurements. Advanced component tests performed at NASA and contractor facilities were also supported. This included ATD and TTB data analysis, as required. Results included definition of temporal and spectral characteristics observed. Spectral values associated with rotor/shaft dynamics, bearing elements, and the like were identified and summarized for engine components under all operating conditions, permitting comparison with previous test and flight results. Extensive utilization of the SSME automated data base system was made to provide timely, informative data summaries. Informal oral and/or written summaries to support

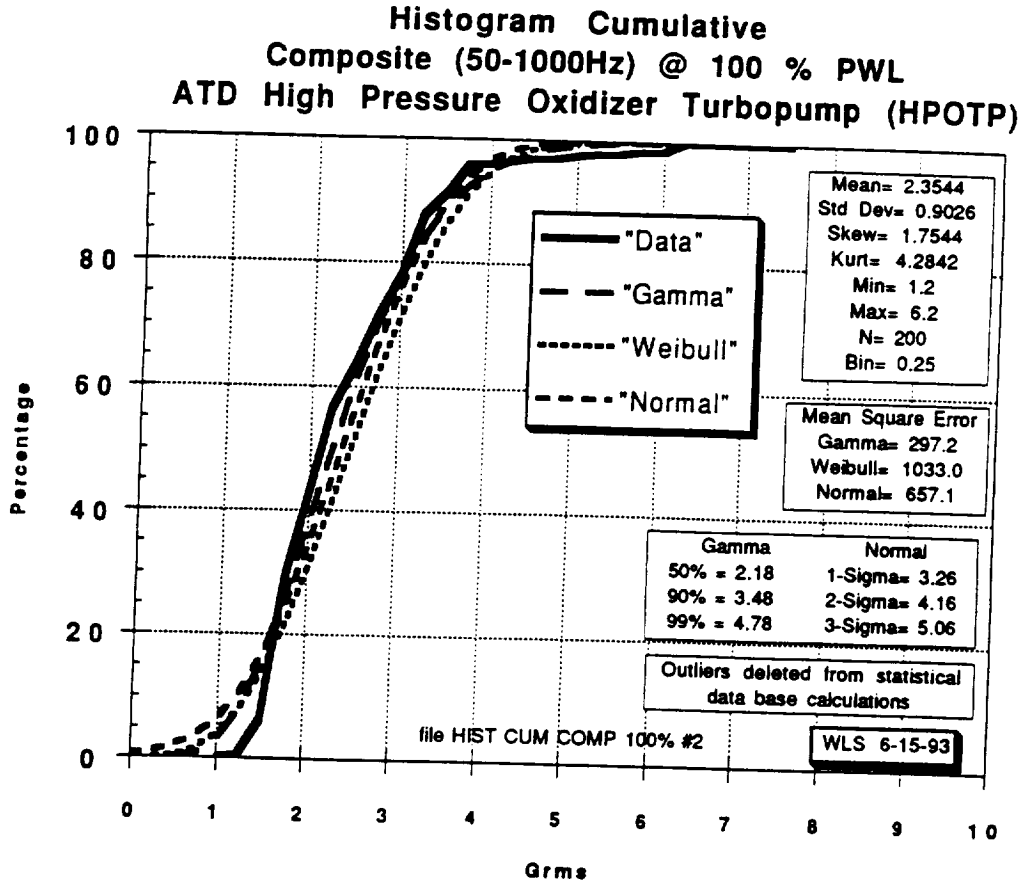

FIGURE 2-23. ATD CUMULATIVE HISTOGRAM COMPOSITE @ 100 % PWL

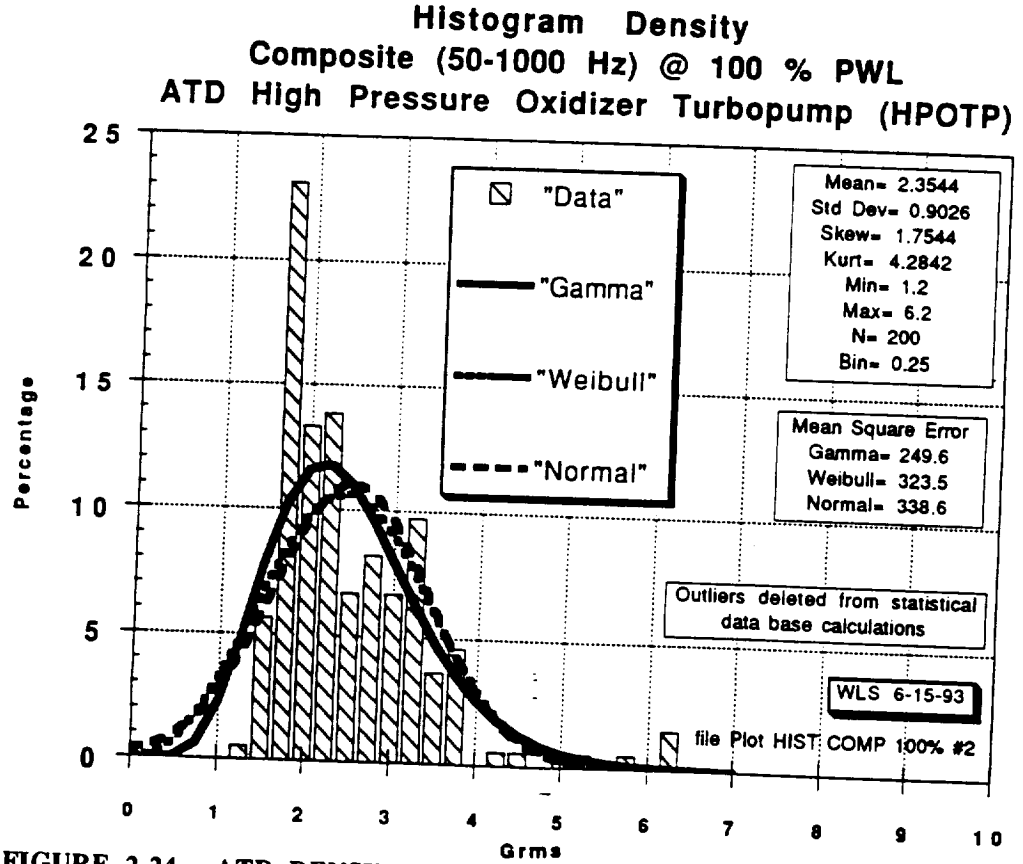

FIGURE 2-24. ATD DENSITY HISTOGRAM COMPOSITE @ 100% PWL

assessment of each test and to document the results was provided, including recommendations as to the integrity of the engine system and components.

Discrepancy investigations were conducted on tests or flights exhibiting abnormal system operation or anomalous dynamic behavior. This effort made use of the automated data base and Operator Interactive Signal Processing System (OISPS) analytical capabilities and included time/event correlations and spectral and temporal trend comparisons with previous component heritage and available models and correlations with operational performance data. These results were applied to identify probable causes of malfunction and approaches to their resolution. Failure analyses required routine application of the advanced software operational on the OISPS, including hypercoherence, phase-domain averaging, and nonstationary (modified Wigner) spectral methods. Close coordination of these efforts with MSFC was maintained.

Data Base Development and Applications. Wyle engineers utilized the automated data base and associated statistical models of SSME component dynamic response to generate characterizing profiles of observed parametric ranges, distributions, etc., under nominal and abnormal engine operating conditions at all power levels. These statistics were applied directly to support the above data analysis effort. Parametric and nonparametric tests were applied to test for homogeneity between measurement location and operating condition. Similar analyses were performed to refine and update Redline Accelerometer Safety Cut-off System (RASCOS) and turbopump flight certification ("green-run") vibration levels, most recently for the ATD turbopump design. Algorithms were implemented to increase the efficiency of quick-look data assessment/component evaluation.

Application and Refinement of Vibration Diagnostic Techniques. Under this task, Wyle continued the development, update, and application of signature analysis techniques for detailed SSME and advanced system diagnostic evaluation. A number of advanced time domain and spectral evaluation algorithms were developed and implemented on the OISPS. These algorithms include nonstationary spectral techniques, nonlinear coherence methods, and advanced adaptive filtering techniques. Application of these methods was provided for efficient and immediate assessment of machinery condition. In addition, analytical models were developed and applied to provide improved identification of bearing element wear, whirl onset, squeal, rubbing, and other types of component degradation. Analyses were conducted to identify component failure signatures and

other anomalous indications that can be used to indicate component health. All software developed under this contract was implemented on the OISPS, resident at MSFC. A series of tutorial seminars was conducted to describe application of the advanced algorithms implemented on MSFC computers.

A log of SSME hot firings, including flights, is included in Table 2-1. Over the course of this study, data analysis support was provided for 456 SSME hot firings, including 372 single engine tests and 28 STS flights. Of the single engine tests, 38 included instrumented ATD turbopump configurations. Additional data analysis was provided for component tests at the MSFC Technology Test Bed, water flow facility and various contractor locations. As a test/evaluation program,. rigid, long term task planning was neither feasible nor desirable. On the contrary, most tasks performed under this contract were initiated on an ad hoc basis, motivated by observed or suspected SSME component failure modes. Continued coordination with the MSFC COTR was, therefore, mandatory to revise task priorities based on SSME test results and Project Office requirements. To support SSME test and flight requirements, evaluation results were immediately provided the COTR in the form of presentations and informal data packages. To illustrate the diversity of tasks accomplished under this contract, some reports and presentations prepared by Wyle in support of SSME dynamic evaluations are summarized below. *It should be emphasized that most of these reports represent a collaborative engineering effort* between Wyle and MSFC personnel.

Some Non-Linear Spectral Methods and Their Application to Rocket Engine Diagnostic Evaluation

First International
Machinery Monitoring and Diagnostics Conference
Las Vegas, Nevada; September 1989

Statistical Analysis of SSME Turbopump Vibration Levels
Part I: High Pressure Oxidizer Turbopump
Part II: High Pressure Fuel Turbopump
Part III: Low Pressure Oxidizer Turbopump
Part IV: Low Pressure Fuel Turbopump

Wyle Laboratories Technical Note
TN 60900-90-611, June 1990

The TOPO Plot: A Data Reduction / Graphics Routine for Tracking Spectral Trends in Data

1990 Annual Report of the Marshall Space Flight Center
NASA TM-103510, December 1990

An Algorithm for Periodic Waveform Recovery from Space Shuttle Main Engine Vibration Measurements

1990 Annual Report of the Marshall Space Flight Center
NASA TM-103510, December 1990

Correlation Identification Between Spectral Components in turbomachinery Measurements by Generalized Hypercoherence

Third International
Machinery Monitoring and Diagnostics Conference
Las Vegas, Nevada,; December 1991

Time-Frequency Representation of Nonstationery Signals

Wyle Technical Progress Report
TR-60900-91-12, December 1991

Some Recent Developments in Turbomachinery Diagnostic Monitoring

Advanced Earth-to-Orbit Propulsion Technology 1992
NASA Conference Publication 3174, May 1992

Statistical Summary (Update) of SSME Turbopump Vibration Levels
Part I: High Pressure Oxidizer Turbopump
Part II: High Pressure Fuel Turbopump
Part III: Low Pressure Oxidizer Turbopump
Part IV: Low Pressure Fuel Turbopump

Wyle Laboratories Technical Note
TN 60900-92-01, June 1992

Cavitation Detection and Monitoring Using Wide-Band Demodulation

Wyle Laboratories Technical Progress Report
TR-60900-93-01, January 1993

Synchronous Frequencies of the ATD High Pressure Oxidizer Turbopump

Wyle Laboratories Technical Memorandum
TM 62200-93-11, June 1993

Comparison of Gamma, Weibull and Normal Distributions with ATD High Pressure Oxidizer Turbopump Vibration Data

Wyle Laboratories Technical Memorandum
62200-93-12, June 1993

Anomaly Identification for Space Shuttle Main Engine Diagnostics

Proceedings of the 49th Meeting of the
Mechanical Failures Prevention Group
(to be published April 1994)

Selected reports, or their abstracts, from the above list are included in Appendix A. These reports provide detailed discussion of specific data analysis and modeling efforts performed and the signal processing techniques developed and applied to SSME diagnostic evaluations. The Technical Progress Reports, generated in the course of this study, give a monthly chonology of investigations performed, techniques applied and interim results obtained. Appendix B includes the course notes for a MSFC seminar series on Advanced Signal Processing Techniques, prepared by Dr. J. Jong of Wyle, under this contract. In addition to documenting the efforts of this study, these two appendices provide a comprehensive overview of the SSME data analysis and diagnostic evaluation process, and computational methods, which should prove useful as an orientation guide for analysts new to the field.

TABLE 2-1. LOG OF SSME HOT FIRINGS (TEST AND FLIGHT) THROUGH OCTOBER 1993

SSME DIAGNOSTIC DATA BASE DIRECTORY
A1 TEST STAND
POWER LEVEL KEY: 1=65%; 2=90%; 3=100%; 4=104%; 5=109%; 6=111%

TEST #	DATE	DUR	ENG #	HPOTP	HPFTP	LPOTP	LPFTP	123456
A10183	06/05/78	51.0	0005	0005	0102R8	9201	9003	X
A10194	09/06/78	310.1	0005	0105	9003R2	0103	9103R1	X
A10203	09/28/78	300.0	0005	2202	2102	2003	9404	X
A10225	12/27/78	255.6	2001	2003	2003	92101	2103	XX
A10228	03/07/79	15.4	2003	0103	2101	92102	9203	X
A10230	03/12/79	18.3	2003	0103	2101	92102	9203	X
A10231	03/14/79	60.0	2003	0103	2101	92102	9203	X
A10232	03/17/79	520.0	2003	0103	2101	92102	9203	XX
A10234	04/04/79	60.0	0006	2402	2006	0007	0205R1	X
A10237	05/02/79	100.0	2007	2005	2006	2006	2006	X
A10238	05/05/79	61.8	2007	2005	2006	2006	2006	XX
A10239	05/10/79	285.3	2007	2005	2006	2006	2006	XX
A10240	05/12/79	520.0	2007	2005	2006	2006	2006	XX
A10244	06/12/79	100.0	2006	0006	0106	0008	2004R2	X
A10245	06/16/79	520.0	2006	0006	0106	0008	2007	XX
A10247	07/16/79	100.0	2007	2104	9006	2006	2006	X
A10249	08/04/79	50.0	0007	9005	2006R1	2007	9604	X
A10251	08/18/79	10.0	0007	2006R1	0404	2007	9220	X
A10252	08/21/79	10.0	0007	2006R1	0404	2007	92201	X
A10254	08/27/79	100.0	0007	2006R1	0007R2	2007	92201	X
A10256	09/18/79	100.0	0007	9105	2006R1	92202	0206	X X
A10259	10/12/79	100.0	0008	9006	2007	0009	0008	X
A10260	10/18/79	520.0	0008	9006	2007	0009	0008	XX
A10261	10/26/79	520.0	0008	9006	2007R1	0009	0008	XX
A10262	11/24/79	100.0	0008	9006	2007R1	0009	0008	X X
A10267	02/02/80	39.6	0009	2007	9007R1	92202	0009	X
A10268	02/09/80	520.0	0009	2007	9007R1	92202	92201	XX
A10270	02/29/80	520.0	0009	2007	9007R2	92202	92201	XX
A10271	03/05/80	823.0	0009	2007	9007R2	92202	92201	XX
A10272	03/15/80	665.0	0009	2007	9007R2	92202	92201	XX
A10273	03/22/80	520.0	0009	2007	9007R2	92202	92201	XX
A10274	03/28/80	520.0	0009	2007	9007R2	92202	92201	XX
A10275	04/08/80	520.0	0009	2007	9007R2	92202	92201	XX
A10276	04/12/80	520.0	0009	2007	9007R2	92202	92201	XX
A10277	04/18/80	10.0	0009	2007	9007R2	92202	92201	X
A10278	04/21/80	10.0	0009	2007	9007R2	92202	92201	X
A10279	04/25/80	300.0	0009	2007	9007R2	92202	92201	XX
A10280	04/28/80	520.0	0009	2007	9007R2	92202	92201	XXX
A10282	06/16/80	520.0	2007	0007R1	9006R1	2006	2006	XX
A10284	07/30/80	9.8	0010	9106	0010	0010	0010	X
A10286	08/29/80	10.0	0009	9108	9107	90303	92201	X
A10287	09/02/80	100.0	0009	9108	9107	90303	92201	X
A10288	09/11/80	392.6	0009	9108	0010R1	90303	92201	XX
A10289	09/18/80	520.0	0009	0305R1	0010R1	90303	92201	XX
A10290	10/07/80	520.0	0009	0009	0010R1	90303	92201	XX
A10291	10/10/80	520.0	0009	0009	0010R1	90303	92201	XXX
A10292	10/15/80	520.0	0009	0009	0010R1	90303	92201	XX
A10293	10/22/80	823.0	0009	0009	0010R1	90303	92201	XX
A10294	10/24/80	665.0	0009	0009	0010R1	90303	92201	XX
A10295	11/07/80	520.0	0009	9208	9008R1	90303	92201	X
A10296	11/11/80	519.3	0009	9208	9008R1	90303	92201	X
A10297	11/13/80	10.0	0009	9208	9008R1	90303	92201	X

TABLE 2-1. LOG OF SSME HOT FIRINGS (TEST AND FLIGHT) THROUGH OCTOBER 1993 (Continued)

POWER LEVEL KEY: 1=65%; 2=90%; 3=100%; 4=104%; 5=109%; 6=111%

TEST #	DATE	DUR	ENG #	HPOTP	HPFTP	LPOTP	LPFTP	123456
A10298	11/19/80	10.0	0009	9208	9008R1	90303	92201	
A10299	11/24/80	10.0	0009	9208	9008R1	90303	92201	
A10300	12/02/80	10.0	0009	9208	9008R1	90303	92201	
A10301	12/15/80	823.0	0009	2206	9008R2	90303	92201	XX
A10303	01/19/81	53.0	0009	9208	90201R	0106	90301	X X
A10304	01/21/81	81.7	0009	9208	90201R	0106	90301	X X
A10305	01/23/81	79.0	0009	9208	90201R	0106	90301	X X
A10306	01/26/81	80.3	0009	9208	90201R	0106	90301	X X
A10307	01/28/81	75.0	0009	9208	90201R	0106	90301	X X
A10308	02/26/81	3.9	0006	2107	0007R5	0106	2104	
A10309	02/28/81	67.3	0006	2107	0007R5	0106	2104	X X
A10310	03/03/81	67.4	0006	2107	0007R5	0106	2104	X X
A10311	03/05/81	64.3	0006	2107	0007R5	0106	2104	X X
A10312	03/14/81	60.1	0006	2107	0007R5	0106	2104	X X
A10313	03/18/81	63.7	0006	2107	0007R5	0106	2104	X X
A10314	03/20/81	47.6	0006	2107	0007R5	0106	2104	X
A10315	03/26/81	66.8	0006	2107	0007R5	0106	2104	X X
A10316	04/14/81	15.0	0006	2602	0007R5	90401R2	2104	X
A10317	04/20/81	15.0	0006	2602	0007R5	90401R2	2104	XX
A10319	04/23/81	100.0	0006	2602	0007R5	90401R2	2104	XX
A10321	05/13/81	300.0	2108	2306	0210R1	2108	2110	X
A10322	05/21/81	290.0	2108	2306	0210R1	2205	2110	XXXX
A10323	05/26/81	260.0	2108	2306	0210R1	2205	2110	XXXX
A10324	05/28/81	520.0	2108	2306	0210R1	2205	82502R2	X X
A10325	05/30/81	520.0	2108	2306	0210R1	2205	82502R2	X X
A10326	06/06/81	300.0	2108	2306	2007R4	90403	82502R2	X
A10327	06/11/81	520.0	2108	2306	0210R2	90403	80306R1	X X
A10328	06/16/81	520.0	2108	2306	2010	90403	2108R2	X X
A10329	06/23/81	500.0	2108	2306	2010	90403	2108R2	XX X
A10330	07/10/81	170.0	2108	2306	2010	90403	2108R2	XXX
A10331	07/15/81	233.1	2108	2306	2010	90403	2108R2	XX X
A10333	08/11/81	81.8	0008	9303R2	2007R4	0110	9203	X X
A10334	08/14/81	84.2	0008	9303R2	2007R4	0110	9203	X X
A10335	08/17/81	57.7	0008	9303R2	2007R4	0110	9203	X
A10336	08/19/81	54.4	0008	9303R2	2007R4	0110	9203	X
A10338	10/09/81	15.2	0107	0209	0210R4	2110	2012	X
A10339	10/13/81	300.0	0107	0209	0210R4	2110	2012	X X X
A10340	10/15/81	405.5	0107	0209	0210R4	2110	2012	X X
A10341	10/30/81	100.0	0107	0209	2308	2110	2012	XX X
A10342	11/05/81	200.0	0107	0209	2308	2110	2012	XX X
A10343	11/08/81	500.0	0107	0209	2308	2110	2012	XX X
A10344	11/14/81	500.0	0107	2109	2110	2110	82602	XX X
A10345	11/18/81	270.0	0107	2109	2110	2110	2012	XX X
A10346	11/19/81	500.0	0107	2109	2110	2110	2012	XX X
A10347	11/30/81	95.4	0107	2109	2110R2	2110	2012	X X
A10348	12/02/81	750.0	0107	2109	2110R2	2110	2012	XX X
A10349	12/04/81	463.6	0107	2109	2110R2	2110	2012	X X
A10350	12/16/81	300.0	0107	2105R1	9009	2110	2012	XX
A10351	12/28/81	500.0	0107	0209R1	2210	2403	2012	XX X
A10352	12/30/81	500.0	0107	0209R1	2210	2403	2012	XX X
A10353	01/14/82	424.1	0107	2011R1	2111	2403	2012	X X
A10354	01/18/82	270.0	0107	2011R1	2111	2403	2012	X X
A10355	01/20/82	500.0	0107	2011R1	2111	2403	2012	X XX

TABLE 2-1. LOG OF SSME HOT FIRINGS (TEST AND FLIGHT) THROUGH OCTOBER 1993 (Continued)

POWER LEVEL KEY: 1=65%; 2=90%; 3=100%; 4=104%; 5=109%; 6=111%

TEST #	DATE	DUR	ENG #	HPOTP	HPFTP	LPOTP	LPFTP	123456
A10356	01/25/82	37.2	0107	2011R1	2111	2403	2012	X X
A10357	02/01/82	500.0	0107	2108	2111R1	2403	2012	X XX
A10358	02/08/82	500.0	0107	2108	2111R2	2403	2012	X X
A10360	03/10/82	100.0	2013	9308	9109	2208	2013	X
A10361	03/22/82	500.0	2013	2210	2211	2208	2013R1	XX X
A10362	03/27/82	500.0	2013	2210	2211R1	2208	2013R1	XX X
A10363	03/30/82	250.0	2013	2210	2211R1	2208	2013R1	X X X
A10364	04/07/82	392.2	2013	2014	2211R2	2208	2013R1	XX X
A10366	05/19/82	100.0	2014	2211	2113	2014	2011R1	X
A10367	05/25/82	500.0	2014	2113	2113	2014	2011R1	XX X
A10368	06/03/82	60.0	2014	2113	2212	2014	9005	X X
A10369	06/05/82	500.0	2014	2113	2212	2014	9005	XX X
A10370	06/07/82	750.0	2014	2113	2212	2014	9005	XX X
A10371	06/15/82	250.0	2014	2113	2113R1	2014	2114R1	XX X
A10372	06/17/82	250.0	2014	2113	2113R1	2014	2114R1	XX X
A10373	06/22/82	50.0	2014	9408	2113R1	2014	2114R1	XX
A10374	06/30/82	500.0	2014	2212	2113R1	2014	2114R1	XX X
A10375	07/03/82	50.0	2014	2212	2113R1	2014	2114R1	XX
A10376	07/10/82	5.1	2014	2212	9006R2	0108	2210	X
A10377	07/14/82	300.0	2014	2212	9006R2	0108	2210	X
A10379	07/25/82	50.0	2014	2212	2113R2	2014	2012R1	XX X
A10380	07/27/82	500.0	2014	2212	2113R2	2014	2012R1	XX X
A10381	07/30/82	500.0	2014	2212	2113R2	2014	2012R1	X X
A10382	08/02/82	500.0	2014	2212	2113R2	2014	2012R1	XX X
A10383	08/15/82	300.0	2014	0007R2	2113R3	2014	2012R1	X
A10384	08/24/82	595.0	2014	9508	2113R3	2014	2012R1	X X
A10385	08/27/82	250.0	2014	9508	2113R3	2014	2012R1	X X
A10389	09/25/82	120.0	2011	0110R1	2214R1	9005	2111	XX
A10390	10/04/82	175.0	2011	9010	2214R1	9005	9106	XXXX
A10391	10/07/82	500.0	2011	9010	2214R1	9005	9106	XXX
A10393	10/21/82	51.0	2012	2312	2213	2012	2016	X
A10394	10/26/82	210.0	2012	2410	2213	2012	2016	XXXX
A10395	10/30/82	500.0	2012	2410	2213R1	2012	2016	X X
A10397	12/07/82	100.0	2014	2311	9409	2014	2214	XX
A10398	12/14/82	500.0	2014	2311	9409	2014	2012R1	XX X
A10399	12/18/82	500.0	2014	2311	9409	2014	2012R1	XX X
A10400	12/23/82	500.0	2014	2311	9409	2014	2012R1	XX X
A10401	01/05/83	500.0	2014	9111	9409	2014	2012R1	XX X
A10402	01/08/83	250.0	2014	9111	9409	2014	2012R1	X X
A10403	01/22/83	50.0	2014	2311R1	9111	2014	2314	XX
A10404	01/28/83	250.0	2014	2311R1	9111	2014	2314	XX X
A10405	02/04/83	500.0	2014	2311R1	9509	2014	2314	XX X
A10406	02/17/83	60.0	2014	9608	9509	2014	2314	XXX
A10407	03/13/83	500.0	2014	2410	9509	2014	2314	XXX
A10408	04/06/83	520.6	2014	2410R1	9509	2014	2314	XXX
A10409	04/20/83	750.0	2014	2410R1	9509	2014	2314	XXX
A10410	04/23/83	595.0	2014	2410R1	9509	2014	2314	XX
A10413	05/25/83	190.0	2018	9211	0209	2016	4001	XXX
A10414	06/06/83	500.0	2018	9211	2314R1	2016	4001R1	XXX
A10416	07/11/83	190.0	2010	2410R1	Q209R1	2014	2314	XXX
A10417	07/15/83	510.0	2010	2410R1	0209R1	2014	2314	XXX
A10418	07/20/83	510.0	2010	2410R1	0209R1	2014	2314	XXX
A10419	08/12/83	510.0	2010	2410R2	2414	2014	2314	XXX

TABLE 2-1. LOG OF SSME HOT FIRINGS (TEST AND FLIGHT) THROUGH OCTOBER 1993 (Continued)

PAGE 4

POWER LEVEL KEY: 1=65%; 2=90%; 3=100%; 4=104%; 5=109%; 6=111%

TEST #	DATE	DUR	ENG #	HPOTP	HPFTP	LPOTP	LPFTP	123456
A10420	08/30/83	750.0	2010	2410R2	2414	2014	2314	XXX
A10421	09/25/83	148.5	2010	2410R2	2414R1	2014	80506R2	XX
A10422	09/29/83	50.0	2010	2410R2	2414R1	2014	80506R2	X
A10423	10/01/83	50.0	2010	2410R2	2414R1	2014	80506R2	XX
A10424	10/13/83	50.0	2010	0310	2109	2014	2314	XX
A10425	10/17/83	510.0	2010	0310	2109	2014	2314	XXX
A10426	10/24/83	6.6	2010	0310	2109	2110	2314	X
A10427	11/02/83	510.0	2010	0310	5101R1	2110	2117	XXX
A10428	11/18/83	510.0	2010	0310	2410	2110	2314	XXX
A10429	11/23/83	595.0	2010	0310	2410	2110	2314	XX
A10430	12/07/83	510.0	2017	9010R1	2415	2211	9206	XXX
A10432	01/04/84	190.0	0108	2208R1	0506	99601	2112	XXX
A10433	01/21/84	700.0	0108	2512	0107	99601	2112	XXXX
A10434	01/24/84	700.0	0108	2512	0107	99601	2112	XX X
A10435	02/08/84	60.0	0108	2512	0107	99601	2112	XX X
A10436	02/14/84	611.1	0108	2512	0606	99601	2112	X X
A10437	03/22/84	60.0	2019	2019	9210	2017	2118	XXX
A10438	03/27/84	510.0	2019	2019	9210	2017	2118	XXX
A10440	04/11/84	250.0	2019	2022	4002	2017	2118	XXX
A10442	05/08/84	100.0	0207	0207	2109R1	0206	80606	XXX
A10443	05/14/84	110.0	0207	0207	2109R1	0206	80606	XXXX
A10444	05/18/84	160.0	0207	0207	2109R1	0206	80606	XXXX
A10445	06/09/84	100.0	0207	2308R1	2109R1	0206	80606	XX X
A10446	06/15/84	91.3	0207	2308R1	2109R1	0206	80606	XXX
A10447	06/27/84	100.0	0207	2308R1	2608	0206	80606	XX X
A10448	07/10/84	500.0	0207	2308R1	2608	0206	80606	XX X
A10449	07/14/84	500.0	0207	2308R1	2608	0206	80606	XX X
A10450	07/26/84	124.3	0207	2308R1	0309R1	2110	80606	X X
A10451	08/09/84	10.7	0207	2308R1	0309R2	2110	80606	X X
A10452	08/21/84	100.0	0207	2606R2	90701R1	2110	80606	XX X
A10453	08/31/84	300.0	0207	2606R2	90701R1	2110	80606	XXXX
A10454	09/12/84	100.0	0207	2606R2	90701R1	2110	80606	XX X
A10455	09/21/84	500.0	0207	2606R3	90701R2	2110	80606	X X
A10456	09/25/84	595.0	0207	2606R3	90701R2	2110	80606	X X
A10457	09/29/84	500.0	0207	2606R3	90701R2	2110	80606	X X
A10458	10/05/84	500.0	0207	2606R3	90701R2	2110	80606	X X
A10459	10/26/84	193.4	0207	2606R3	0309R3	2110	80606	X X
A10460	11/12/84	500.0	0207	9505	0309R3	2110	80606	X X
A10461	12/28/84	90.0	0207	9505R1	2209	2110	80606	X X
A10462	01/05/85	90.0	0207	9505R1	2209R1	2110	80606	X X
A10463	01/14/85	250.0	0207	9505R1	2209R1	2110	80606	X X
A10464	01/17/85	283.8	0207	9505R1	2209R1	2110	80606	X X
A10465	01/19/85	34.0	0207	9505R1	2209R1	2110	80606	X X
A10466	01/24/85	500.0	0207	9505R1	2209R1	2110	80606	X X
A10467	01/30/85	586.8	0207	9505R1	2209R1	2110	80606	X X
A10468	02/04/85	203.9	0207	9505R1	2209R2	2110	80606	X X
A10470	02/25/85	250.0	2105	2217	4004	4004	9105R1	XXX
A10471	02/27/85	503.0	2105	2217	4004	4004	9105R1	X X
A10472	03/04/85	520.0	2105	2217	4004R1	4004	9105R1	XX
A10473	03/06/85	503.0	2105	2217	4004R1	4004	9105R1	X X
A10474	03/22/85	503.0	2105	9808	4004R1	2022	9105R1	X X
A10475	04/17/85	520.0	2105	9808	4004R2	2022	9105R1	XX
A10476	05/21/85	70.0	2105	9505R2	5102R1	2022	9105R1	X X

TABLE 2-1. LOG OF SSME HOT FIRINGS (TEST AND FLIGHT) THROUGH OCTOBER 1993 (Continued)

POWER LEVEL KEY: 1=65%; 2=90%; 3=100%; 4=104%; 5=109%; 6=111%

TEST #	DATE	DUR	ENG #	HPOTP	HPFTP	LPOTP	LPFTP	123456
A10477	05/24/85	250.0	2105	9505R2	5102R1	2022	9105R1	XXX
A10478	06/01/85	503.0	2105	9505R2	5102R1	2022	9105R1	X X
A10479	06/05/85	503.0	2105	9505R2	5102R1	2022	9105R1	X X
A10480	06/07/85	503.0	2105	9505R2	5102R1	2022	9105R1	X X
A10481	06/10/85	520.0	2105	9505R2	5102R1	2022	9105R1	XX
A10482	07/09/85	520.0	2105	4004	5102R1	2022	9105R1	XX
A10483	07/13/85	520.0	2105	4004	5102R2	2022	9105R1	XX
A10484	07/19/85	603.0	2105	4004	5102R2	2022	9105R1	X X
A10485	07/24/85	29.0	2105	4004	4104	2113	9105R1	X X
A10486	07/30/85	520.0	2105	4004	5102R2	2113	9105R1	XX
A10487	08/04/85	503.0	2105	4004	5102R2	2113	9105R1	XXX
A10488	08/07/85	503.0	2105	4004	5102R2	2022	9505R1	X X
A10489	08/12/85	302.0	2105	4004	0307	2113	4003R1	XX
A10490	08/31/85	503.0	2105	4004R1	0307	2022	9105R1	X X
A10491	09/07/85	503.0	2105	4004R1	0307	2022	9105R1	X X
A10492	09/19/85	503.0	2105	4004R1	0307	2022	9105R1	X X
A10493	09/24/85	350.0	2105	4004R1	0307R2	2022	9105R1	XXX
A10495	10/22/85	250.0	2026	2504	2614	4005	4004	XX
A10497	10/04/86	520.0	2105	4104R1	5202R3	2026	4003R1	XX
A10498	10/14/86	520.0	2105	4104R1	5202R3	2026	4003R1	XX
A10499	10/18/86	520.0	2105	4104R1	5202R3	2026	4003R1	XX
A10500	10/25/86	520.0	2105	4104R1	5202R3	9005	4003R1	XX
A10501	11/06/86	520.0	2105	0307R3	4005R1	9005	4003R1	XX
A10502	11/26/86	520.0	2105	0307R3	4005R1	9005	4003R1	XX
A10503	12/02/86	520.0	2105	0307R3	4005R1	9005	4003R1	XX
A10504	12/06/86	520.0	2105	0307R3	4005R1	9005	4003R1	XX
A10505	12/09/86	520.0	2105	0307R3	4005R1	9005	4003R1	XX
A10506	12/12/86	520.0	2105	0307R3	4005R1	9005	4003R1	XX
A10507	12/16/86	590.0	2105	0307R3	4005R1	9005	4003R1	XX
A10508	12/30/86	520.0	2105	2024	2024R1	9005	4003R1	XX
A10509	01/05/87	520.0	2105	2024	2024R1	9005	4003R1	XX
A10510	01/12/87	520.0	2105	2024	2024R1	9005	4003R1	XX
A10511	01/15/87	520.0	2105	2024	2024R1	9005	4003R1	XX
A10513	01/30/87	520.0	2105	4204	6001	9005	4003R1	XX
A10514	02/11/87	520.0	2105	4204	6001	9005	4003R1	XX
A10515	02/14/87	503.0	2105	4204	6001	9005	4003R1	X X
A10516	02/17/87	761.0	2105	4204	6001	9005	4003R1	X X
A10517	02/24/87	603.0	2105	4204	6001	9005	4003R1	X X
A10518	03/02/87	520.0	2105	4204	6001	9005	4003R1	XX
A10520	03/19/87	200.0	2011	2021R1	2614R1	2211	2411R1	XXX
A10521	04/04/87	320.0	2011	9311	2614R1	2211	2411R1	XXX
A10522	04/24/87	520.0	2105	9311	5302	9005	4003R1	XX
A10523	04/30/87	520.0	2105	9311	5302R1	9005	4003R1	XX
A10524	05/09/87	850.0	2105	9311	5302R1	90402	4003R1	XX
A10525	05/14/87	250.0	2105	9311	5302R1	90402	4003R1	XX
A10526	05/20/87	520.0	2105	9908	5302R1	90402	4003R1	XX
A10527	05/30/87	700.0	2105	9908	4105	90402	4003R1	XX
A10528	06/04/87	503.0	2105	9908	4105	90402	4003R1	X X
A10529	06/08/87	603.0	2105	9908	4105	90402	4003R1	X X
A10530	06/11/87	503.0	2105	9908	4105	90402	4003R1	X X
A10531	06/13/87	520.0	2105	9908	4105	90402	4003R1	XX
A10532	06/17/87	520.0	2105	9908	4105	90402	4003R1	XX
A10533	06/25/87	520.0	2105	9908	4105	2211	4003R1	XX

TABLE 2-1. LOG OF SSME HOT FIRINGS (TEST AND FLIGHT) THROUGH OCTOBER 1993 (Continued)

POWER LEVEL KEY: 1=65%; 2=90%; 3=100%; 4=104%; 5=109%; 6=111%

TEST #	DATE	DUR	ENG #	HPOTP	HPFTP	LPOTP	LPFTP	123456
A10534	07/06/87	520.0	2105	9908	4105	2211	4003R1	XX
A10535	07/18/87	761.0	2105	9908	4106	2211	4003R1	XXX
A10536	08/06/87	520.0	2105	4204R2	5302R1	2122R1	4003R1	XX
A10537	08/12/87	656.0	2105	2604	2614R1	2122R1	4003R1	XX
A10539	09/12/87	300.0	0211	2604	6201	2122R1	4003R1	XX
A10540	09/15/87	300.0	0211	2604	6201	2122R1	4003R1	XX
A10541	09/17/87	300.0	0211	2604	6201	2122R1	4003R1	XX
A10542	09/19/87	300.0	0211	2604	6201	2122R1	4003R1	XX
A10543	09/21/87	300.0	0211	2604	6201	2122R1	4003R1	XX
A10544	09/23/87	300.0	0211	2604	6201	2122R1	4003R1	XX
A10545	09/26/87	210.0	0211	2604	2808	2122R1	4003R1	XX
A10546	09/30/87	250.0	0211	2604	2808	2122R1	2024	XXX
A10547	10/03/87	135.0	0211	2604	2808	2122R1	2218R1	XX
A10548	10/05/87	250.0	0211	2604	2808	2122R1	2218R1	XX
A10550	11/22/87	250.0	2019	0510	6002	2025R1	2022	XXX
A10551	11/28/87	520.0	2019	0510	6002	2025R1	2025R1	XXX
A10552	12/29/87	754.0	2027	0510	4204	2211	2022	XX
A10553	01/22/88	520.0	0211	0510	4204	2106R1	2218R1	XXX
A10554	01/27/88	520.0	0211	0510	4204	90501	2218R1	XX
A10555	02/02/88	520.0	0211	0510	4204	90501	2218R1	XX
A10556	02/10/88	520.0	0211	0510	4205	4103	2218R1	XX
A10557	02/14/88	503.0	0211	0510	4204	4103	2218R1	X X
A10558	02/18/88	503.0	0211	0510	4205	4103	2218R1	X X
A10559	02/21/88	603.0	0211	0510	4205	4103	2218R1	X X
A10560	02/25/88	573.0	0211	0510	4204	4103	2218R1	XX
A10561	03/05/88	520.0	0211	0510	4205	4104R1	2218R1	XX
A10562	03/10/88	520.0	0211	0510	4204R1	4104R1	2218R1	XX
A10563	03/21/88	20.0	0211	9311R2	4204R1	4104R1	2218R1	XX
A10564	03/29/88	520.0	0211	9311R2	4205	4104R1	2218R1	XX
A10565	04/05/88	623.0	0211	9311R2	4205	4104R1	2218R1	XX
A10566	04/08/88	520.0	0211	9311R2	4205	4104R1	2218R1	XX
A10567	04/16/88	520.0	0211	9311R2	4204R1	9105	2218R1	XX
A10568	04/19/88	503.0	0211	9311R2	4204R1	9105	2218R1	X X
A10569	04/29/88	520.0	0211	9908R2	4205	9105	2218R1	XX
A10570	05/03/88	761.0	0211	9908R2	4205	9105	2218R1	X X
A10571	06/03/88	520.0	0211	2215	0607	9105	4001R1	XX
A10572	06/08/88	503.0	0211	2215	0607	9105	4001R1	X X
A10573	06/13/88	1040.0	0211	2215	0607	9105	4001R1	XX
A10574	06/20/88	1040.0	0211	2215	0607	90503	4001R1	XX
A10575	06/27/88	1040.0	0211	2215	9511	90503	4001R1	XX
A10576	07/08/88	1040.0	0211	2215	9511	90503	4001R1	XX
A10577	07/21/88	87.1	0211	2118R1	9511R1	90503	4001R1	X X
A10578	07/28/88	596.4	0211	2118R1	9511R1	90503	4001R1	XXX
A10579	08/10/88	600.0	0211	2118R1	9511R1	90503	4001R1	XX
A10580	08/29/88	1040.0	0211	0407R3	4305	90503	9205R1	XX
A10581	09/12/88	50.0	0211	4204R3	4305	90503	4001R1	XX
A10582	09/15/88	50.0	0211	4204R3	4305	90503	4001R1	XX
A10583	10/06/88	300.0	0211	2118R2	6301	90503	4001R1	XX
A10588	10/28/88	50.0	0211	2118R2	6301	90503	2218R1	XX
A10590	11/18/88	50.0	0211	2118R3	6301	90503	9205R1	XX
A10591	12/07/88	761.0	0211	2118R3	6301R1	90503	9205R1	X X
A10592	12/12/88	623.0	0211	2118R3	6301R1	90503	9205R1	XX
A10593	12/20/88	456.0	0211	2118R3	6301R1	90502R1	9205R1	X X

TABLE 2-1. LOG OF SSME HOT FIRINGS (TEST AND FLIGHT) THROUGH OCTOBER 1993 (Continued)

PAGE 7

POWER LEVEL KEY: 1=65%; 2=90%; 3=100%; 4=104%; 5=109%; 6=111%

TEST #	DATE	DUR	ENG #	HPOTP	HPFTP	LPOTP	LPFTP	123456
A10594	01/16/89	520.0	0211	2118R3	5502	90502R1	9205R1	XX
A10595	02/11/89	530.0	0211	2224	5502	90502R1	2218R1	XXX
A10596	02/21/89	795.0	0211	2216R1	5502	90503	2218R1	XX
A10597	03/08/89	300.0	2015	0407R4	4404	2029	2031	XXX
A10599	05/16/89	10.0	0209	2215R2	4206R2	90503	4001R1	X
A10600	06/03/89	288.6	0209	2215R2	12008	90503	4001R1	XX
A10601	06/10/89	1040.0	0209	2215R2	12008	90503	4001R1	XX
A10602	06/20/89	1040.0	0209	2215	12008	90503	4001R1	XX
A10603	07/12/89	10.0	0209	9311R6	9611	90503	4001R1	X
A10604	07/29/89	754.0	0209	4201	0707	90503	4001R1	XX
A10605	08/23/89	1075.0	0209	4201	0707	90503	4001R1	XXXX
A10606	08/25/89	300.0	0209	4201	0707	90503	4001R1	XXXX
A10607	08/31/89	1040.0	0209	4201	0707	90503	4001R1	XXX
A10608	10/19/89	27.0	0209	2417	12008R1	90503	4001R1	XX
A10609	10/25/89	216.8	0209	2417	12008R1	90503	4001R1	XXXX
A10610	11/10/89	530.0	0209	2417	12008R1	90503	4001R1	XXXX
A10611	11/29/89	9.1	0209	2417	12008R1	90503	4001R1	X
A10612	12/02/89	520.0	0209	2417	12008R1	90503	4001R1	XXXX
A10613	12/08/89	520.0	0209	2417	12008R1	90503	4001R1	XXXX
A10614	12/15/89	520.0	0209	2417	0707R1	90503	4001R1	XXXX
A10615	12/19/89	520.0	0209	2417	0707R1	90503	4001R1	XXX
A10616	01/05/90	520.0	0209	2417	0707R1	90503	4001R1	XXX
A10617	01/17/90	80.0	0209	2417	0707R1	90503	4001R1	XX
A10618	01/27/90	520.0	0209	2417	0707R1	90503	4001R1	XXX
A10619	01/31/90	503.0	0209	2417	0707R1	90503	4001R1	XXX
A10620	02/05/90	503.0	0209	2417	0707R1	90503	4001R1	XXX
A10622	03/08/90	530.0	0214	19008	2424	4104R2	4001R1	XX
A10623	04/10/90	265.0	0214	4301	2424	2312	4001R1	XX
A10624	04/19/90	530.0	0214	4301	2424	2312	4001R1	XX
A10625	04/26/90	530.0	0214	4301	2424	2312	4001R1	XX
A10626	05/03/90	518.0	0214	4301	2424	2312	4001R1	X X
A10627	05/10/90	530.0	0214	4301	2424	2312	4001R1	XX
A10628	05/14/90	513.0	0214	4301	2424	2312	4001R1	X X
A10629	05/17/90	754.0	0214	4301	2424	2312	4001R1	XX
A10630	05/23/90	771.0	0214	4301	2424	2312	4001R1	X X
A10631	06/01/90	300.0	0214	4301	2424	2312	4001R1	XXXX
A10632	06/07/90	530.0	0214	4301	2424	2312	4001R1	XX
A10633	06/12/90	530.0	0214	4301	2424	2312	4001R1	XX
A10634	07/02/90	513.0	0214	2417R3	2424	2312	4001R1	X X
A10635	07/06/90	771.0	0214	2417R3	2424	2312	4001R1	X X
A10636	07/11/90	175.0	0214	2417R3	2424	2312	4001R1	XXXX
A10637	07/18/90	513.0	0214	2417R3	2424	2312	4001R1	X X
A10638	07/20/90	530.0	0214	2417R3	2424	2312	4001R1	XX
A10639	07/25/90	530.0	0214	2417R3	2424	2312	4001R1	XX
A10640	08/02/90	754.0	0214	2417R3	2424	2312	4001R1	XX
A10641	08/09/90	140.0	0214	2417R3	2424	2312	2023R1	XX
A10643	09/27/90	300.0	0214	0507	12108	2405	2023R1	XXX
A10644	10/09/90	530.0	0214	4301R2	12108	2405	82207R1	XXX
A10645	10/22/90	530.0	0214	4301R2	12108	2405	2023R1	XX
A10646	11/28/90	530.0	0214	4301R2	12108	2405	2023R1	XX
A10647	12/03/90	754.0	0214	4301R2	12108	2405	2023R1	XX
A10648	12/07/90	530.0	0214	4301R2	12108	2405	2023R1	XX
A10649	12/12/90	530.0	0214	4301R2	12108	2405	2023R1	XXX

TABLE 2-1. LOG OF SSME HOT FIRINGS (TEST AND FLIGHT) THROUGH OCTOBER 1993 (Continued)

PAGE 8

POWER LEVEL KEY: 1=65%; 2=90%; 3=100%; 4=104%; 5=109%; 6=111%

TEST #	DATE	DUR	ENG #	HPOTP	HPFTP	LPOTP	LPFTP	123456
A10650	01/03/91	513.0	0214	4301R2	12108	2405	2023R1	X X
A10651	02/08/91	530.0	0215	0607	0807	2405	2023R1	XX
A10652	02/16/91	150.0	0215	0607	0807	2405	2023R1	XX
A10653	02/21/91	530.0	0215	0607	0807	2405	2023R1	XX
A10654	03/01/91	100.0	0215	0607	0807	2405	2023R1	XX
A10655	03/07/91	640.0	0215	0607	0807	2405	2023R1	X X
A10656	03/14/91	594.0	0215	0607	5602	2405	2023R1	XX
A10657	03/20/91	754.0	0215	0607	5602	2405	2023R1	XX
A10658	03/28/91	771.0	0215	0607	6401	2405	2023R1	XXX
A10660	05/13/91	75.0	0215	4304R2	2814	2405	4004R2	XXX
A10661	05/16/91	100.0	0215	4304R2	2814	2405	4004R2	XXX
A10662	06/18/91	75.0	0215	0607R2	0807	2405	2023R1	XXX
A10663	06/24/91	100.0	0215	0607R2	5602R1	2405	2023R1	XXX
A10664	06/27/91	300.0	0215	0607R2	5602R1	2405	2023R1	XXXX
A10665	07/12/91	530.0	0215	0607R2	5602R1	2405	2023R1	XXXX
A10667	08/23/91	300.0	2011	2521R2	4014	2126	2030	XXXX
A10668	08/29/91	550.0	2011	2521R2	4109R1	4008	2023R1	XXXX
A10669	09/19/91	513.0	2206	0810	4406R1	4008	2023R1	X X
A10670	09/23/91	771.0	2206	0810	4406R1	4008	2023R1	XXXX
A10671	10/03/91	754.0	2206	0810	4406R1	4008	2023R1	XX
A10672	10/10/91	300.0	2206	2315R1	4406R1	2106R1	2023R1	XX
A10673	10/14/91	771.0	2206	2315R1	4406R1	2106R1	2023R1	XX X
A10675	11/20/91	400.0	2032	4009R3	4110	2035	2124	XXX
A10676	12/12/91	75.0	0219	2315R2	12208	2311	9306R1	XXX
A10677	12/19/91	530.0	0219	2315R2	12208	2311	2411	XX
A10678	01/04/92	754.0	0219	2315R2	12208	2311	2109R5	XXX
A10679	01/09/92	530.0	0219	2315R2	12208	2311	2218R2	XXX
A10680	01/15/92	513.0	0219	2315R2	12208	2311	2218R2	X X
A10681	01/28/92	530.0	0219	0810R1	2624	2311	2218R2	XX
A10682	02/05/92	513.0	0219	0810R1	4604	2311	2218R2	X X
A10683	02/10/92	530.0	0219	0810R1	4604	2311	2218R2	XX
A10684	02/13/92	530.0	0219	0810R1	4604	2311	2218R2	XX
A10685	02/21/92	530.0	0219	2129	5004	2311	2218R2	XX
A10686	02/25/92	300.0	0219	2129	5004	2311	2218R2	XXX
A10687	02/28/92	530.0	0219	2129	5004	2311	2218R2	XXX
A10688	03/03/92	50.0	0219	2129	5004	2311	2218R2	X
A10689	03/07/92	50.0	0219	2129	5004	2311	2218R2	X
A10690	03/12/92	530.0	0219	2129	5004	2118	2218R2	XXX
A10691	03/17/92	513.0	0219	2129	5004	2118	2218R2	X X
A10692	03/24/92	530.0	0219	2129	5004	2118	2218R2	XX
A10693	03/26/92	530.0	0219	2129	5004	2118	2218R2	XX
A10694	04/10/92	370.0	0219	0810R2	5004	2113	2218R2	XXX
A10695	04/22/92	530.0	0219	0810R2	5004	9104	2218R2	XX
A10696	04/28/92	530.0	0219	0810R2	6501	9104	2218R2	XX
A10697	05/01/92	754.0	0219	0810R2	6501	9104	2218R2	XX
A10698	05/14/92	530.0	0219	0810R2	6501	9104	2218R2	XX
A10699	05/19/92	771.0	0219	0810R2	6501	9104	2218R2	XXX
A10700	05/26/92	530.0	0219	0810R2	2724	9104	2218R2	XXX
A10701	05/29/92	513.0	0219	0810R2	2724	9104	2218R2	X X
A10702	06/09/92	513.0	0219	0810R2	6501	9104	2218R2	X X
A10703	06/11/92	530.0	0219	0810R2	6501	9104	2218R2	XX
A10704	06/16/92	200.0	0219	0810R2	6501	9104	2218R2	XX
A10705	06/19/92	- 80.0	0219	0810R2	6501	9104	2218R2	XX

TABLE 2-1. LOG OF SSME HOT FIRINGS (TEST AND FLIGHT) THROUGH OCTOBER 1993 (Continued)

PAGE 9

POWER LEVEL KEY: 1=65%; 2=90%; 3=100%; 4=104%; 5=109%; 6=111%

TEST #	DATE	DUR	ENG #	HPOTP	HPFTP	LPOTP	LPFTP	123456
A10706	06/29/92	530.0	0219	6802	6501	9104	2218R2	XXXX
A10707	07/01/92	530.0	0219	6802	6501	9104	4101	XXXX
A10708	07/16/92	80.0	0219	4111R3	2227R1	9104	2218R3	XXX
A10709	07/28/92	520.0	0219	6802	2227R1	2117R1	2209	XXXX
A10710	08/04/92	600.0	0219	6802	2227R1	2117R1	2209	XXXX
A10711	08/12/92	600.0	0219	6802	2227R1	9104	2209	XXXX
A10712	08/18/92	250.0	0219	6802	2227R1	9104	2209	XXXX
A10713	08/20/92	50.0	0219	6802	2227R1	9104	2209	XXX
A10714	08/27/92	350.0	0219	6802	2227R1	2117R1	2209	XX X
A10715	09/03/92	600.0	0219	6802	2227R1	2117R1	2209	XXX
A10716	09/23/92	520.0	0220	4013	5303	9104	4101	XXXX
A10717	10/05/92	520.0	0220	8105R2 A	5303	9104	4101	XX
A10718	10/09/92	520.0	0220	8105R2 A	5303	9104	4101	XXX
A10719	10/20/92	520.0	0220	8106 A	5303	9104	4101	XX
A10720	11/03/92	520.0	0220	8105R3 A	5303	9104	4101	XXX
A10721	11/19/92	26.0	2035	6109R1	2031	2034	2035	XXXX
A10722	12/22/92	520.0	0220	8107 A	2227R1	9104	2217	XXX
A10723	01/18/93	754.0	0220	2229	2227R1	9104	2209	XXX
A10724	01/25/93	10.0	0220	2229	2227R1	9104	2209	X
A10725	01/27/93	10.0	0220	2229	2227R1	9104	2209	X
A10726	01/29/93	10.0	0220	2229	2227R1	9104	2209	X
A10728	02/11/93	71.8	2107	8003R6 A	5104	2210	2123	XXX
A10729	02/24/93	100.6	2107	8202R1 A	5104	2210	2123	XXX
A10730	03/05/93	195.0	2107	8106R3 A	5104	4401	2123	XXX
A10731	03/19/93	850.0	2107	8008R1 A	5104	4401	2123	XXXX
A10732	03/29/93	136.0	2107	8003R8 A	5104	4401	2123	XXX
A10733	04/02/93	520.0	2107	8003R8 A	5104	4401	2123	XXXX
A10734	04/06/93	850.0	2107	8003R8 A	5104	4401	2123	XXXX
A10735	04/14/93	520.0	2107	8003R8 A	2322	4401	2123	XXXX
A10736	04/19/93	850.0	2107	8003R8 A	2322	4401	2123	XXXX
A10737	04/23/93	850.0	2107	8003R8 A	2031	4401	2123	XXX
A10738	05/03/93	15.0	2107	8106R4 A	2604R1	4401	2123	XX
A10739	05/06/93	15.0	2107	8106R4 A	2604R1	4401	2123	XX
A10740	05/20/93	318.0	2107	8107R4 A	2604R1	4401	2123	XXX
A10741	05/27/93	475.8	2107	8107R4 A	2423	4401	2123	XXX
A10742	06/07/93	850.0	2107	8107R4 A	2423	4401	2123	XXXX
A10743	06/15/93	850.0	2107	8107R4 A	4110R1	4401	2123	XXX
A10744	06/23/93	761.0	2107	8105R6 A	4110R1	4401	2123	XX X
A10745	06/26/93	761.0	2107	8105R6 A	4110R1	4401	2123	XX X
A10746	07/13/93	150.3	2107	8107R5 A	5104R2	4401	2123	XX X

TABLE 2-1. LOG OF SSME HOT FIRINGS (TEST AND FLIGHT) THROUGH OCTOBER 1993 (Continued)

SSME DIAGNOSTIC DATA BASE DIRECTORY
A2 TEST STAND
POWER LEVEL KEY: 1=65%; 2=90%; 3=100%; 4=104%; 5=109%; 6=111%

TEST #	DATE	DUR	ENG #	HPOTP	HPFTP	LPOTP	LPFTP	123456
A20145	12/08/78	68.6	2002	0205	2103R1	0006	2202	XX
A20150	03/24/79	50.0	2004	9004	2004R1	2005	2005	X
A20151	03/27/79	520.0	2004	9004	2004R1	2005	2005	X X
A20152	04/02/79	520.0	2004	9004	2004R1	2005	2005	X X
A20156	05/07/79	10.0	2004	9004R1	2104	2005	2005	X
A20157	05/10/79	90.5	2004	9004R1	2104	2005	2005	X X
A20158	05/22/79	27.7	2004	9004R1	2104	2005	2005	X
A20160	06/02/79	520.0	2004	9004R1	2104	2005	2005	X X
A20161	06/08/79	665.0	2004	9004R1	9006	2005	2005	X X
A20163	06/21/79	520.0	2004	9004R1	2104R1	2005	2005	X X
A20164	06/25/79	520.0	2004	9004R1	2104R1	2005	2005	X X
A20165	06/27/79	823.0	2004	9004R1	2104R1	2005	2105	X X
A20167	07/24/79	10.0	2004	2006	0007R1	90203	2105	X
A20171	08/14/79	56.0	2004	9004R2	2204	2105	2105	X X
A20174	09/17/79	135.9	2004	9004R3	2204	2105	2105	X X
A20176	09/22/79	520.0	2004	9004R3	2204	2105	2105	X X
A20177	10/01/79	520.0	2004	9004R3	2204	2105	2105	X X
A20179	10/12/79	823.0	2004	9004R3	2202R1	2105	2105	X X
A20189	03/13/80	125.0	2004	9008	2304	99401	92403	XX X
A20190	03/24/80	241.0	2004	9008	2304	99401	92403	X
A20191	03/31/80	610.0	2004	9008	2304	99401	2205	XX X
A20192	04/14/80	610.0	2004	9008	2304R1	99401	2205	XX X
A20193	04/19/80	610.0	2004	9008	2304R1	99401	2205	XX X
A20195	06/20/80	250.0	2004	9104R1	2404	2205	2205	X
A20196	06/24/80	520.0	2004	9104R1	2404	2205	2205	X
A20197	07/02/80	520.0	2004	9104R1	2404	2205	2205	X
A20200	09/13/80	100.0	2008	0106R3	9008	99501	2008	X
A20201	09/16/80	250.0	2008	0106R3	9008	99501	2008	X XX
A20202	09/23/80	50.0	2008	0106R3	9008	99501	2008	X
A20204	10/13/80	260.0	0006	2107	0007R5	0007	2104	XX
A20206	10/30/80	100.0	2008	0106R4	9008R1	2010	2008	X
A20207	11/05/80	520.0	2008	0106R4	2008	2010	2008	X X
A20208	11/11/80	520.0	2008	0106R4	2008	2010	2008	X
A20209	11/15/80	823.0	2008	0106R4	2008	2010	2008	X X
A20210	11/21/80	665.0	2008	0106R4	9207	2010	2008	X
A20211	12/05/80	250.0	2008	0009R2	0110	2010	2008	X
A20212	12/10/80	520.0	2008	0009R2	0110	2010	2008	X XX
A20213	12/18/80	520.0	2008	0009R2	0110R1	2010	2008	X XX
A20214	12/23/80	520.0	2008	0009R2	0110R1	2010	2008	X X
A20215	12/30/80	520.0	2008	0009R2	0110R1	2010	2008	X X
A20216	01/05/81	520.0	2008	0009R2	0110R1	2010	2008	X X
A20218	02/03/81	100.0	2009	0010	2009	2009	2009	X
A20219	02/09/81	520.0	2009	0010	2009	2009	2009	X X
A20220	03/07/81	100.0	0008	0109	90301	99501	0008	X X
A20221	03/10/81	610.0	0008	0109	90301	99501	0008	X X
A20222	03/12/81	610.0	0008	0109	90301	99501	0008	X X
A20223	03/17/81	610.0	0008	0109	90301	0110	0008	X X X
A20228	04/21/81	100.0	0204	0405	2108	90202	80306	X
A20229	04/24/81	100.0	0204	0405	2108	90202	82502R2	X
A20230	04/27/81	270.0	0204	0405	2108	90202	82502R2	X X X
A20231	05/05/81	268.0	0204	0405	2108R1	90202	82502R2	X X X
A20232	05/07/81	-520.0	0204	0405	2108R1	90202	82502R2	X X X

TABLE 2-1. LOG OF SSME HOT FIRINGS (TEST AND FLIGHT) THROUGH OCTOBER 1993 (Continued)

POWER LEVEL KEY: 1=65%; 2=90%; 3=100%; 4=104%; 5=109%; 6=111%

TEST #	DATE	DUR	ENG #	HPOTP	HPFTP	LPOTP	LPFTP	123456
A20233	05/09/81	520.0	0204	0405	2108R1	90202	82502R2	X X X
A20234	05/14/81	500.0	0204	0405	2108R1	90202	82502R2	XXX X
A20235	05/19/81	500.0	0204	0405	2108R1	0106	82502R2	XXX X
A20236	05/23/81	500.0	0204	0405	2108R1	0106	82502R2	X X X
A20237	06/05/81	50.0	0204	0010R1	9108	90401R2	2108R1	XXX X
A20238	06/09/81	475.0	0204	0010R1	9108	0106	82502R2	X X X
A20239	06/19/81	25.0	0204	2602R1	9108	0106	82502R2	X X X
A20240	06/22/81	10.0	0204	2602R1	9108	0106	82502R2	X
A20241	06/24/81	15.0	0204	2602R1	9108	0106	82502R2	X X
A20242	07/02/81	300.0	0204	0108	9108	0106	82502R2	X X X
A20243	07/08/81	100.0	0204	0108	9108	0106	82502R2	X X
A20244	07/14/81	450.0	0204	0108	9108	0109	82502R2	X X
A20245	08/12/81	25.0	0204	2009	0210R3	0109	82502R2	X X X
A20246	08/22/81	25.0	0204	0203	0210R3	0109	82502R2	X X X
A20247	08/31/81	200.0	0204	0203	9108	0109	82502R2	X X X
A20248	09/14/81	500.0	0204	9204	9108	99601	82502R2	X X X
A20249	09/21/81	450.5	0204	9204	99202	99601	82502R2	XXX
A20251	12/11/81	100.0	2010	2010	2012	2011	2110R1	X
A20252	12/14/81	500.0	2010	2010	2012	2011	2110R1	X X X
A20253	12/18/81	500.0	2010	2010	2012	2011	2110R1	X XXX
A20254	12/21/81	250.0	2010	2010	2012	2011	2110R1	X X
A20255	01/02/82	750.0	2010	2406	2012R1	2011	2110R1	X X X
A20256	01/05/82	500.0	2010	2406	2012R1	2011	2110R1	X X X
A20257	01/07/82	595.0	2010	2406	2012R1	2011	2110R1	X X
A20258	01/16/82	10.0	2010	2406	2012R2	2011	2110R1	X
A20259	01/18/82	60.0	2010	2406	2012R2	2011	2110R1	X X
A20260	01/27/82	250.0	2010	2110	9009R1	2011	2110R1	X X
A20261	01/29/82	500.0	2010	2110	9009R1	2011	2110R1	X X X
A20262	02/02/82	500.0	2010	2110	9009R1	2011	2110R1	X X
A20263	02/06/82	500.0	2010	2110	9009R2	2011	2110R1	X X X
A20264	02/09/82	10.0	2010	2110	9009R2	2011	2110R1	X
A20265	02/19/82	100.0	2010	2108R1	2112	2011	2110R1	X
A20266	02/22/82	500.0	2010	2108R1	2112	0109	2110R1	X X X
A20267	03/08/82	500.0	2010	2013	2112R1	0109	2110R1	X X X
A20268	03/16/82	500.0	2010	2111	2112R1	0109	2110R1	X X X
A20269	03/23/82	500.0	2010	2111	2112R2	0109	2110R1	X X X
A20270	03/29/82	250.0	2010	2111	2112R2	0109	2110R1	X X
A20271	04/30/82	300.0	2010	2310	0306R2	0109	2110R1	X
A20272	05/05/82	500.0	2010	2310	2112R4	0109	2110R1	X X X
A20273	05/08/82	500.0	2010	2310	2115	0109	2014	X X X
A20274	05/11/82	60.0	2010	2310	2115	0109	2014	X X
A20275	05/13/82	750.0	2010	2310	2115	0109	2012R1	X X X
A20276	05/29/82	595.0	2010	2310R1	2115R1	0109	2012R1	X X X
A20277	06/06/82	250.0	2010	0110	2114	0109	2012R1	X X X
A20279	06/20/82	50.0	2010	2108R2	9208R2	0109	2012R1	X X
A20283	07/04/82	50.0	2010	2108R2	9208R2	0109	2012R1	X X X
A20284	07/09/82	500.0	2010	2108R2	2310R1	0109	2012R1	X X X
A20285	07/13/82	10.0	2010	2108R2	9208R3	0109	2012R1	X
A20286	07/19/82	250.0	2010	2209	9209	0109	2012R1	X X
A20287	07/21/82	500.0	2010	2209	9209	0109	2208	X
A20288	07/27/82	250.0	2010	2209	2214	0109	2208	X X
A20289	08/01/82	250.0	2010	2209	9010	0109	2208	X X X
A20290	08/05/82	750.0	2010	2209	9309	0109	2208	X X X

TABLE 2-1. LOG OF SSME HOT FIRINGS (TEST AND FLIGHT) THROUGH OCTOBER 1993 (Continued)

PAGE 3

POWER LEVEL KEY: 1=65%; 2=90%; 3=100%; 4=104%; 5=109%; 6=111%

TEST #	DATE	DUR	ENG #	HPOTP	HPFTP	LPOTP	LPFTP	123456
A20291	08/07/82	250.0	2010	2209	9309	0109	2208	X XXX
A20292	08/09/82	146.0	2010	2209	9309	0109	2208	X XX
A20294	09/10/82	120.0	2012	9010	2214R1	2012	9005R1	X XX
A20296	09/25/82	120.0	2015	2015	2215	2113	2015R1	X XX
A20297	09/30/82	23.5	2015	2015	2215	2113	2111	X X X
A20298	10/06/82	185.0	2015	2015	9010R2	2113	2012R1	XXX
A20299	10/08/82	500.0	2015	2015	9010R2	2113	2012R1	X X X
A20302	11/15/82	215.0	2016	2016	9011	2015	9005R2	XX
A20303	12/05/82	210.0	2016	2410	9110	2015	9005R3	XXX
A20304	12/07/82	500.0	2016	2410	9110	2015	9005R3	X X X
A20306	01/13/83	86.4	2017	0210R1	2016R1	2211	2115	XX
A20307	02/15/83	500.0	2017	9010	2016R1	2211	9106	XXXX
A20309	04/14/83	5.0	2011	2208	2017	9005	9005R3	X
A20310	04/18/83	190.0	2011	2208	2017	9005	9005R3	XXX
A20311	04/27/83	500.0	2011	2018	2017R1	9005	9005R3	XXXX
A20313	06/09/83	190.0	2019	2019	9210	2017	2118	XXX
A20314	06/20/83	500.0	2019	2019	9210	2017	2118	XXXX
A20316	08/31/83	4.3	2109	2020	5101	2018	2109	X
A20318	10/15/83	190.0	2109	2020	5101	2018	9105	XXX
A20319	10/18/83	510.0	2109	2020	5101	2018	9105	XXXX
A20322	11/11/83	190.0	2020	0107	2018	0208	2019	XXX
A20323	11/19/83	510.0	2020	2021	2018	0208	2019	XXXX
A20325	12/05/83	190.0	2021	4001	2109	2019	9105R1	XXX
A20326	12/10/83	510.0	2021	4001	2109	2019	9105R1	XXXX
A20327	01/10/84	6.4	2010	4002	2410	2010	2314	X
A20328	01/15/84	510.0	2010	4002	2410	2010	2314	XXXX
A20329	01/25/84	510.0	2010	9110	2410	2010	2314	XXXX
A20331	02/13/84	510.0	2010	0310	2514	2010	2314	XXXX
A20332	03/13/84	60.0	2010	0310	9211	2010	2314	XXXX
A20333	03/21/84	60.0	2010	0310	9211	2010	2314	XX
A20335	04/12/84	250.0	2022	2015R1	4001	2020	2020	XXX
A20336	05/10/84	250.0	2022	2022	2020R1	4002	2020	XXX
A20337	05/22/84	510.0	2022	2022	2020R1	4002	2020	XXXX
A20339	06/13/84	250.0	2023	2019R1	2021	2015	4002	XXXX
A20340	06/21/84	250.0	2023	2019R1	2515	2015	2118	XXX
A20341	06/30/84	510.0	2023	2019R1	2515	2015	2118	XXXX
A20343	07/21/84	250.0	2014	2016R1	9310	4003	2118	XXXX
A20344	08/07/84	250.0	2014	2117	9311	2021	2314	XXXX
A20345	08/12/84	250.0	2014	2117	4102	2021	2314	XXX
A20346	08/20/84	250.0	2014	2117	2313	2021	2021R1	XXX
A20347	09/13/84	250.0	2014	2115	2118	2021	4002R1	XXXX
A20348	09/28/84	250.0	2014	2016R2	2118	2021	2314	X XX
A20349	10/10/84	250.0	2014	2018R1	9310R1	90403	2314	X XX
A20350	10/16/84	250.0	2014	2018R1	2216	4004	2314	X XX
A20351	10/24/84	250.0	2014	2022R1	4202	2022	2314	X XX
A20352	11/02/84	250.0	2014	4102	4003	2022	2311	X XX
A20354	12/01/84	250.0	2014	2016R3	2121	2022	2314	X XX
A20356	02/11/85	250.0	2015	0310R2	4101	2113	2022	XX
A20357	02/19/85	510.0	2015	4003	2413R1	2113	2022	X XX
A20358	03/05/85	250.0	2014	4003	5301	2022	2314	XX
A20359	03/13/85	250.0	2014	4003	9410	2021	2314	XX
A20360	03/16/85	250.0	2014	4003	2120	2021	2314	XX
A20361	03/27/85	-250.0	2014	9211R1	2218	2021	2109R3	X XX

TABLE 2-1. LOG OF SSME HOT FIRINGS (TEST AND FLIGHT) THROUGH OCTOBER 1993 (Continued)

POWER LEVEL KEY: 1=65%; 2=90%; 3=100%; 4=104%; 5=109%; 6=111%

TEST #	DATE	DUR	ENG #	HPOTP	HPFTP	LPOTP	LPFTP	123456
A20363	04/25/85	250.0	2024	2020R2	4201	4003	2116	X XX
A20364	05/03/85	250.0	2024	2020R2	4202R1	4003	2411	X XX
A20365	05/13/85	380.4	2024	4003R1	2218R1	4003	4003R1	X XX
A20366	06/17/85	250.0	2024	2504	2413R2	4101R1	2109R4	X XX
A20367	06/29/85	250.0	2024	2018R2	2413R2	4101R1	2109R4	X XX
A20368	07/02/85	60.0	2024	2018R2	2413R2	4101R1	2109R4	X X
A20369	07/17/85	250.0	2024	2020R3	9510	2123	2109R4	X XX
A20371	08/03/85	250.0	2116	2317	4104	2109	2218	X XXX
A20372	08/08/85	503.0	2116	2317	4104	2109	2218	X X X
A20373	08/13/85	520.0	2116	2317	4104	2109	2218	X XX
A20374	08/17/85	226.0	2116	2317	4104	2109	4003R1	X XX
A20375	09/07/85	461.3	2116	0307	4104	2109	4003R1	X XXX
A20376	09/13/85	466.0	2116	0307	4104	2109	4003R1	X XXX
A20377	09/17/85	503.0	2116	2317R1	4104	2109	4003R1	X X X
A20378	09/20/85	761.0	2116	2317R1	4104R1	2109	4003R1	X X X
A20379	09/25/85	503.0	2116	2317R1	4104R1	2109	4003R1	X X X
A20380	10/07/85	503.0	2116	9808R1	0409R1	2109	4003R1	X X X
A20381	10/14/85	603.0	2116	9808R1	0409R1	2109	4003R1	X X
A20382	10/19/85	503.0	2116	9808R1	0409R1	2109	4003R1	X X X
A20383	10/26/85	275.0	2116	9110R1	5301R1	2109	4003R1	X XX
A20384	11/05/85	250.0	2116	4001R2	2117	2109	4003R1	X XX
A20385	11/20/85	250.0	2116	0307R1	0409R1	2109	4003R1	X XXX
A20386	12/11/85	18.2	2026	4005	2022	4005	4004	X X
A20387	12/20/85	503.0	2026	4005	2022	4005	4004	X XXX
A20388	12/23/85	200.0	2026	4005	2022	4005	4004	X X
A20389	01/17/86	250.0	2022	9110R1	9510	4002	2411	X XXX
A20391	07/16/86	250.0	2106	0307R2	4005	2026	82106	XX
A20392	07/25/86	520.0	2106	0307R2	4005	2026	82106	X XX
A20393	08/23/86	520.0	2106	0307R2	2117	2026	82106	X XX
A20397	12/07/86	520.0	2106	2023	9411	2109	82106	X XX
A20398	12/11/86	520.0	2106	2023	2023R1	2109	82106	XX
A20399	12/15/86	600.0	2106	2023	2023R2	2109	82106	XX
A20400	12/18/86	520.0	2106	2023	2023R3	2109	82106	XX
A20401	01/02/87	520.0	2106	6002R1	2023R3	2109	82106	XX
A20402	01/10/87	520.0	2106	6002R1	2218R1	2109	82106	XX
A20403	01/14/87	520.0	2106	6002R1	2218R1	2109	82106	XX
A20404	01/16/87	520.0	2106	6002R1	2218R1	2109	82106	XX
A20405	01/31/87	200.0	2106	0307R4	4006R2	2109	82106	X XX
A20406	02/03/87	200.0	2106	0307R4	4006R2	2109	82106	X XX
A20407	02/06/87	200.0	2106	0307R4	4006R2	2109	82106	X XX
A20408	02/12/87	200.0	2106	0307R4	4006R2	2109	82106	X XX
A20409	02/19/87	200.0	2106	0307R4	4006R2	2109	82106	X XX
A20410	03/02/87	520.0	2106	0307R4	0407	2109	82106	X XX
A20411	03/11/87	520.0	2106	4101	0407	2109	82106	X XX
A20412	03/13/87	520.0	2106	4101	0407	2109	82106	X XX
A20413	03/17/87	503.0	2106	4101	0407	2109	82106	X X X
A20414	03/23/87	567.6	2106	4101	0407	2109	82106	X X
A20415	03/31/87	520.0	2106	4101	0407	2109	92603	X XX
A20416	04/09/87	520.0	2106	4101	0407	2122	92603	X XX
A20417	04/20/87	797.0	2106	4101	0407	2122	82106	X X X
A20418	04/28/87	750.0	2106	4101	0407	2122	82106	X XX
A20419	05/01/87	90.0	2106	4101	0407	2122	82106	X XX
A20420	05/18/87	520.0	2106	4204R1	6101	2109	82106	X XX

TABLE 2-1. LOG OF SSME HOT FIRINGS (TEST AND FLIGHT) THROUGH OCTOBER 1993 (Continued)

POWER LEVEL KEY: 1=65%; 2=90%; 3=100%; 4=104%; 5=109%; 6=111%

TEST #	DATE	DUR	ENG #	HPOTP	HPFTP	LPOTP	LPFTP	123456
A20421	05/27/87	680.0	2106	4204R1	6101	2109	82106	XX
A20422	05/29/87	503.0	2106	4204R1	6101	2109	82106	X X X
A20423	06/03/87	520.0	2106	4204R1	6101	2122R1	82106	X XX
A20424	06/06/87	275.0	2106	4204R1	6101	2122R1	82106	XX
A20425	06/11/87	520.0	2106	4204R1	6101	2122R1	82106	X XX
A20426	06/22/87	1000.0	2106	9311	5302	2122R1	82106	X XX
A20427	06/26/87	139.0	2106	9311	5302	2122R1	82106	XX
A20428	07/01/87	204.0	2106	9311	5302	2122R1	82106	XX
A20431	10/10/87	520.0	2027	4106	2122	2027R1	2026	X XXX
A20433	11/06/87	250.0	2022	6102	4106	4201	2027	X XXX
A20434	11/21/87	520.0	2022	2025	2025	2104R1	2024	X XXX
A20436	12/15/87	250.0	2028	2121	2223	2027R1	4001R1	X XXX
A20437	12/23/87	520.0	2028	2121	2124	2027R1	2026R2	X XXX
A20439	02/09/88	250.0	2029	9109	2025R2	4106	2027	X XXX
A20440	02/19/88	520.0	2029	9109	2026	4106	2027	X XXX
A20441	03/04/88	250.0	2029	9109	5203	4106	2027	X XXX
A20443	03/28/88	300.0	2030	6102	4007	4201	2027	X XXX
A20444	04/10/88	520.0	2030	6102	2223R1	4201	2027	X XXX
A20446	05/10/88	250.0	2027	2124R1	2122R1	2124	2028	X XXX
A20447	05/20/88	520.0	2027	2124R1	6102	2124	2029	X XXX
A20449	06/15/88	252.0	2029	2118R1	4206	4106	4005	X XXX
A20450	06/23/88	520.0	2029	2118R1	2224	4106	2029	X XXX
A20452	07/29/88	300.0	2107	4202	4206	4102	2022R1	X XXX
A20454	08/31/88	300.0	2015	2122	2323	2216	2117R1	X XXX
A20455	09/16/88	520.0	2015	2123R1	2224R1	2120	2022R1	X XXX
A20457	11/01/88	300.0	2031	2026	4206R2	4105	82107R1	X XXX
A20458	11/08/88	530.0	2031	2026	2125	4105	82107R1	X XXX
A20460	01/14/89	300.0	2019	2221	2026R1	2025R1	2025R1	X XXX
A20461	01/23/89	550.0	2019	4206	2324	2025R1	2025R1	X XXX
A20462	02/08/89	530.0	2019	4105	4206R2	2025R1	2025R1	X XXX
A20463	02/12/89	530.0	2019	2222	4206R2	2025R1	2025R1	X XXX
A20465	03/02/89	446.0	2107	4306	4009	2028	2120	X XXX
A20466	03/15/89	550.0	2107	4302	4009R1	2213	2120	X XXX
A20467	03/25/89	530.0	2107	2126R1	4010	2213	2120	X XXX
A20468	04/15/89	530.0	2206	4406	5502	0209	2028	X XXX
A20469	04/29/89	483.0	2206	6003	4404R1	0209	2028	X XXX
A20470	05/22/89	530.0	2206	2321R1	4404R1	0209	2028	X XXX
A20471	06/02/89	147.6	2206	9311R6	4305	0209	2028	XX
A20473	06/27/89	530.0	2011	2322	4011	4301	4006	X XXX
A20474	07/08/89	50.0	2011	4205	4009R1	4301	82207	XX
A20475	07/13/89	550.0	2011	4205	4012	2126	82207	X XXX
A20477	08/30/89	530.0	2024	2323	2126	4206	4007	X XXX
A20478	09/08/89	550.0	2024	4107	6007	4206	2131	X XXX
A20479	09/26/89	314.7	2206	2422	4404R2	4302	2109R5	X XXX
A20480	10/09/89	300.0	2206	2305	4404R2	4103R1	2109R5	X XXX
A20481	10/28/89	300.0	2206	4406R2	6008	4103R1	2109R5	X XXX
A20482	11/04/89	300.0	2206	2324R3	4007R1	4103R1	2109R5	X XXX
A20483	11/11/89	300.0	2206	2027	5203R1	4103R1	2109R5	X XXX
A20484	11/19/89	300.0	2206	4008	4404R2	4103R1	2109R5	X XXX
A20485	11/28/89	80.0	2206	2321R2	4404R2	4103R1	2109R5	XX
A20486	12/05/89	200.0	2206	6003R2	4404R2	4103R1	2109R5	XX
A20487	12/14/89	300.0	2206	2226	2222	4103R1	2109R5	X XXX
A20488	01/09/90	300.0	2206	4502	4109	4103R1	2109R5	X XXX

TABLE 2-1. LOG OF SSME HOT FIRINGS (TEST AND FLIGHT) THROUGH OCTOBER 1993 (Continued)

PAGE 6

POWER LEVEL KEY: 1=65%; 2=90%; 3=100%; 4=104%; 5=109%; 6=111%

TEST #	DATE	DUR	ENG #	HPOTP	HPFTP	LPOTP	LPFTP	123456
A20489	01/18/90	80.0	2206	6402R2	6401	4103R1	2109R5	XX
A20490	01/24/90	80.0	2206	4205R2	6401	4103R1	2109R5	XX
A20492	02/13/90	300.0	2012	2421	2323R1	4306	4006	X XXX
A20493	02/20/90	550.0	2012	4304	2222R1	4306	4006	X XXX
A20495	03/17/90	300.0	2026	9309	6401	2224	2025R2	X XXX
A20496	03/23/90	300.0	2026	9309	6401	2224	2025R2	X XXX
A20497	03/30/90	550.0	2026	2522	4109R1	2224	2025R2	X XXX
A20498	04/23/90	300.0	2022	4009	6401	2104R1	2024R1	X XXX
A20499	05/15/90	400.0	2026	2522R1	4012R2	2224	2025R2	X XXX
A20501	05/31/90	300.0	2029	2305R2	6003R1	2121	2128	X XXX
A20502	06/05/90	530.0	2029	2521R1	4010R3	2121	2128	X XXX
A20503	06/22/90	80.0	2206	4008R2	6401	4104R2	2218R2	XX
A20504	06/30/90	80.0	2206	2226R2	6401	4104R2	2218R2	XX
A20506	08/03/90	300.0	2030	6502	4011R2	2030	2027	X XXX
A20507	08/10/90	530.0	2030	4010	6102R2	2030	2027	X XXX
A20508	08/22/90	300.0	2206	2424	2225	4104R2	2218R2	X XXX
A20510	09/20/90	420.0	2032	2325R1	2323R2	4007	2032	X XXX
A20511	10/02/90	550.0	2032	6007	2028	4007	2033	X XXX
A20512	10/19/90	300.0	0208	2408	2318	2117R1	9306R1	XXX
A20513	10/30/90	310.0	0208	2408	2318	2117R1	9306R1	XXXX
A20514	11/05/90	520.0	0208	2408	2318	2117R1	9306R1	X XXX
A20515	11/08/90	520.0	0208	2408	2318	2117R1	9306R1	X XXX
A20516	11/30/90	300.0	2206	2622	2029	2129	2218R2	X XXX
A20518	12/19/90	310.0	2015	6008	4013R1	4205	2216	X XXX
A20519	01/11/91	550.0	2015	6602R1	2322	4401	2216	X XXX
A20521	02/06/91	310.0	2033	4010R2	2322	2032	2034	X XXX
A20522	02/15/91	550.0	2033	4011	2030	2032	2034	X XXX
A20523	03/01/91	80.0	2206	4009R2	6401R1	2118	2218R2	XXX
A20524	03/05/91	100.0	2206	2424R2	6401R1	2118	2218R2	XXX
A20525	03/23/91	208.8	2034	2028	2031	2033	2032R1	X XXX
A20526	03/29/91	226.0	2034	2028	2031	2033	2032R1	X XXX
A20527	04/06/91	550.0	2034	2425	2127	2033	2032R1	X XXX
A20528	04/17/91	300.0	2206	4111	2127	2118	2228	X XXX
A20529	04/23/91	300.0	2206	2405	2127	2118	2228	X XXX
A20530	04/29/91	300.0	2206	2028R1	2127	2118	2228	X XXX
A20531	05/09/91	300.0	2035	2424R3	2127	2034	2035	X XXX
A20532	05/17/91	550.0	2035	6702	2127	2034	2035	X XXX
A20533	06/05/91	300.0	2206	4305	2127	2118	2218R2	X XXX
A20534	06/17/91	300.0	2206	6103	4504	2118	2218R2	X XXX
A20535	07/02/91	300.0	2206	6109	4504	2118	4008	X XXX
A20536	07/16/91	300.0	2206	2029	4504	2118	2026R2	X XXX
A20537	08/02/91	300.0	2035	4207	4108	2034	2035	X XXX
A20538	08/15/91	310.0	0216	2315	4504	2117R1	9306R1	XXXX
A20539	08/21/91	530.0	0216	2315	4504	2117R1	9306R1	X XXX
A20540	08/27/91	530.0	0216	2315	2127R1	2117R1	9306R1	X XXX
A20541	09/03/91	65.4	0216	2315	2127R1	2117R1	9306R1	X XX
A20542	09/06/91	460.0	0216	2315	2127R1	2117R1	9306R1	X XXX
A20543	09/16/91	300.0	0216	2423	4109R1	2117R1	9306R1	X XXX
A20544	10/07/91	300.0	0217	2521R2	4604	4203	9306R1	XXX
A20545	10/21/91	530.0	0217	4009R3	4604	2521R1	4306R1	X XXX
A20546	11/01/91	300.0	2011	2127	4016	4406	4009	X XXX
A20547	11/15/91	420.0	2011	2129	4015	4016	4009	X XXX
A20548	12/06/91	300.0	2206	9409	4604	2106R1	2218R2	X XXX

TABLE 2-1. LOG OF SSME HOT FIRINGS (TEST AND FLIGHT) THROUGH OCTOBER 1993 (Continued)

PAGE 7

POWER LEVEL KEY: 1=65%; 2=90%; 3=100%; 4=104%; 5=109%; 6=111%

TEST #	DATE	DUR	ENG #	HPOTP	HPFTP	LPOTP	LPFTP	123456
A20549	12/16/91	300.0	2206	2030	4604	2106R1	2218R2	X XXX
A20550	01/14/92	300.0	2206	4108	6108	2106R1	2109R5	X XXX
A20551	02/04/92	300.0	2017	9210	2032	4009	2215	X XXX
A20552	02/18/92	550.0	2017	2031	4107	4009	2215R1	X XXX
A20553	03/11/92	300.0	2107	2621	2227	4203	4101	X XXX
A20554	03/24/92	300.0	2107	4109	6108	4203	4101	X XXX
A20555	04/08/92	260.0	2035	2218	2033	4203	9305	XXX
A20556	04/22/92	300.0	2107	4012	4209	2128	9305	X XXX
A20557	05/05/92	300.0	2107	2218	2034	2125	9305	X XXX
A20558	05/15/92	300.0	2107	2218	4406R2	4203	9305	X XXX
A20559	05/20/92	80.0	2107	4108	4406R2	4203	9305	XX
A20561	06/10/92	300.0	2107	2326	2326	4203	2125	X XXX
A20564	07/14/92	300.0	0218	4110	4107R1	2130	9305	X XXX
A20565	07/24/92	135.0	0218	4207R1	4406R2	2130	9305	XXX
A20566	08/07/92	80.0	0218	6109R1	4406R2	2312	9305	XXX
A20567	09/01/92	300.0	2018	4013	2035	2206	4105	X XXX
A20568	09/12/92	550.0	2018	2405R2	2323R3	2206	5001	X XXX
A20569	10/03/92	300.0	2107	4602	6107	2034	2123	X XXX
A20570	10/15/92	80.0	2107	2028R3	2323R3	2210	2123	XXX
A20571	10/28/92	300.0	2107	2032	6103R1	2210	2126	X XXX
A20572	11/09/92	300.0	2107	2033	4213	2210	2123	X XXX
A20573	12/02/92	550.0	2109	2405R3	2323R3	2031	2034R1	X XXX
A20574	12/12/92	300.0	2109	2525	4111	2031	2034R1	X XXX
A20575	02/19/93	300.0	2015	4405	6109	4401	4110	X XXX
A20576	03/11/93	300.0	2015	2426	2322	2306	2217	X XXX
A20577	03/25/93	80.0	2015	4108R2	2322	2306	2217	XX
A20578	05/25/93	300.0	2015	4606	2036	2210R1	2217	X XXX
A20579	06/15/93	300.0	2015	2034	4309	2210R1	2217	X XXX
A20580	07/14/93	300.0	2015	2032R2	4211	2210R1	2217	X XXX
A20581	07/24/93	300.0	2015	2405R3	4112R1	2210R1	2217	X XXX

TABLE 2-1. LOG OF SSME HOT FIRINGS (TEST AND FLIGHT) THROUGH OCTOBER 1993 (Continued)

SSME DIAGNOSTIC DATA BASE DIRECTORY

A4 TEST STAND

POWER LEVEL KEY: 1=65%; 2=90%; 3=100%; 4=104%; 5=109%; 6=111%

TEST #	DATE	DUR	ENG #	HPOTP	HPFTP	LPOTP	LPFTP	123456
A40002	04/09/88	25.0	2206	2118	2908	4103R1	82106	X
A40003	04/20/88	220.0	2206	2118	2908	4103R1	82106	XX
A40004	04/30/88	350.0	2206	2118	4206	4103R1	82106	X XXX
A40005	05/09/88	520.0	2206	2118	4205	4103R1	82106	X XX
A40006	05/13/88	520.0	2206	2118	4206	4103R1	82106	X XX
A40007	05/20/88	520.0	2206	2118	0509	4103R1	82106	X XX
A40008	06/01/88	503.0	2206	0407	4206	4103R1	82106	X X X
A40009	06/04/88	754.0	2206	0407	4206	4103R1	82106	XX
A40010	06/13/88	520.0	2206	0407	2908R1	4103R1	82106	X XX
A40011	06/17/88	603.0	2206	0407	2908R1	4103R1	82106	X X X
A40012	06/24/88	503.0	2206	0407	2908R1	4103R1	82106	X X X
A40013	06/28/88	520.0	2206	0407	2908R1	4103R1	82106	X XX
A40014	07/05/88	520.0	2206	0407	4206	4103R1	82106	X XX
A40015	07/26/88	1078.0	2206	0407R2	0509R1	90502	82106	XXXX
A40016	07/30/88	1078.0	2206	0407R2	0509R1	90502	82106	XXXX
A40017	08/03/88	2017.0	2206	0407R2	0509R1	90502	82106	XXX
A40018	08/15/88	2016.9	2206	9311R3	0509R1	90502	82106	XXX
A40019	08/20/88	1692.0	2206	9311R3	6301	90502	82106	XXX X
A40020	08/29/88	332.0	2206	9311R3	6301	90502	82106	X X X
A40021	09/10/88	220.0	2206	9311R3	6301	90502	82106	X XX
A40022	09/15/88	50.0	2206	9311R3	6301	90502	82106	X XX
A40023	09/21/88	220.0	2206	9311R3	6301	0209	82106	X XX
A40024	10/06/88	220.0	2206	0407R4	4305	0209	82106	X X X
A40025	10/19/88	350.0	2206	4202	6003	0209	82106	X XXX
A40026	11/22/88	15.0	0212	2216R1	4304	2117	4001R1	X
A40027	12/17/88	550.0	0212	6202	4008	0209	4001R1	X XXX
A40028	01/10/89	550.0	0212	2125	2027	2126	2030	X XXX
A40029	01/26/89	14.0	0212	2216R1	4305	90501	9205R1	X
A40030	02/10/89	530.0	0212	9209R1	4305	90501	9205R1	X XXX
A40031	02/27/89	550.0	0212	6302	4305	90501	9205R1	X XXX
A40032	03/11/89	530.0	0212	2126	5502	90501	9205R1	X XXX
A40033	03/18/89	530.0	0212	2205	5502	90501	82106	X XXX
A40034	03/25/89	530.0	0212	2223	5502	4103R1	9205R1	X XXX
A40035	03/31/89	530.0	0212	2324	4305	4103R1	9205R1	X XXX
A40036	04/11/89	170.0	0212	4406	4010	4103R1	9205R1	X XXX
A40037	04/19/89	170.0	0212	2126R3	4305	90502R2	9205R1	XXX
A40038	05/04/89	550.0	0212	2225	4305	90502R2	9205R1	X XXX
A40039	05/18/89	530.0	0212	2216R1	12008	90502R2	9205R1	XXXXX
A40040	05/25/89	19.0	0212	2216R1	4206R2	90502R2	9205R1	XX
A40041	06/09/89	1022.0	0212	2216R1	4206R2	90502R2	9205R1	X XXX
A40042	06/13/89	1022.0	0212	2216R1	4404R1	90502R2	9205R1	X XXX
A40043	06/17/89	390.0	0212	2216R1	5502R1	90502R2	9205R1	X X X
A40044	06/23/89	1270.7	0212	2216R1	5502R1	90502R2	9205R1	X XXX
A40045	07/11/89	550.0	2031	4007	6102R1	2120	2120R1	X XXX
A40046	08/01/89	530.0	2031	4402	2027	2120	2120R1	X XXX
A40047	08/11/89	550.0	2031	6402	2027	2120	2120R1	X XXX
A40049	09/16/89	530.0	0213	4402R2	2027	2311	2411R1	X XXX
A40050	09/28/89	220.0	0213	9209R2	2027	2305	2411R1	XX
A40051	10/03/89	530.0	0213	9209R2	2027	2305	2411R1	X XX
A40052	10/07/89	754.0	0213	9209R2	2027	2305	2411R1	XX
A40054	10/21/89	754.0	0213	9209R2	2027	2305	2411R1	XX
A40055	10/25/89	206.0	2027	9209R2	2027	2305	2411R1	X XX

TABLE 2-1. LOG OF SSME HOT FIRINGS (TEST AND FLIGHT) THROUGH OCTOBER 1993 (Continued)

POWER LEVEL KEY: 1=65%; 2=90%; 3=100%; 4=104%; 5=109%; 6=111%

TEST #	DATE	DUR	ENG #	HPOTP	HPFTP	LPOTP	LPFTP	123456
A40114	04/15/91	754.0	0213	2510R1	0807	2222	2411R1	X XX
A40115	04/24/91	400.0	0213	2510R1	0807	2222	2411R1	XXXXX
A40116	05/01/91	513.0	0213	2510R1	0807	2222	2411R1	X X X
A40117	05/06/91	771.0	0213	2510R1	0807	2222	2411R1	X X X
A40118	05/14/91	195.0	0213	2510R1	5602R1	4104R2	2411R1	X XX
A40121	06/11/91	13.0	0213	2408	8104 A	4104R2	2411R1	X
A40122	06/19/91	210.0	0213	2408	8104 A	4104R2	2411R1	X
A40123	06/25/91	310.0	0213	2408	8104 A	4104R2	2411R1	XXX
A40124	07/08/91	105.0	0213	2408	8104 A	4104R2	2411R1	X
A40126	08/03/91	221.0	0213	2408	8005 A	4104R2	2411R1	X X
A40127	08/13/91	125.0	0213	2408	8005 A	4104R2	2411R1	XX
A40128	08/22/91	175.0	0213	2408	8005 A	4104R2	2411R1	XX
A40129	08/28/91	358.0	0213	2408	8005 A	4104R2	2411R1	X XX
A40133	10/15/91	45.0	0213	2408	8005 A	4104R2	2411R1	X
A40134	10/23/91	45.0	0213	2408	8005 A	4104R2	2411R1	XX
A40135	10/31/91	45.0	0213	2408	8005 A	4104R2	2411R1	XX
A40136	11/07/91	45.0	0213	2408	8005 A	4104R2	2411R1	XX
A40137	12/02/91	25.0	0213	0810R1	8005 A	4104R2	2411R1	X X
A40139	12/21/91	13.0	0213	8006 A	8006R1 A	4104R2	4101	X
A40140	01/07/92	222.0	0213	8006 A	8006R1 A	4104R2	4101	X X
A40141	02/08/92	158.0	2206	8006R2 A	8006R1 A	4104R2	4101	X X
A40160	02/16/92	520.0	0218	8106R1 A	5303	2312		X XXX
A40142	04/07/92	67.3	2206	8007R3 A	4406R2	4104R2	4101	X X
A40143	04/28/92	150.0	2206	8007R3 A	5004	4104R2	4101	XX
A40144	05/07/92	99.4	2206	8102R1 A	5004	4104R2	4101	X
A40145	06/03/92	240.2	2206	8007R5 A	5004	4104R2	4101	X
A40146	07/21/92	46.0	2206	8007R6 A	5004	4104R2	4101	X X
A40147	07/23/92	520.0	2206	8007R6 A	5004	4104R2	4101	X X
A40148	07/31/92	520.0	2206	8007R6 A	5004	4104R2	4101	X X
A40149	08/11/92	109.8	2206	8007R6 A	5004	4104R2	4101	X X
A40150	08/31/92	520.0	0218	8003R1 A	5004	2312	9305	X X
A40151	09/04/92	520.0	0218	8003R1 A	5004	2312	9305	X XX
A40152	09/19/92	520.0	0218	8105R2 A	6202	2312	9305	X X
A40153	09/25/92	520.0	0218	8105R2 A	6202	2312	9305	X XX
A40154	10/01/92	520.0	0218	8003R3 A	6202	2312	9305	X X
A40155	10/26/92	79.8	0218	8202 A	6202	2312	9305	X X
A40156	10/29/92	210.2	0218	8202 A	6202	2312	9305	X XX
A40157	11/11/92	166.0	0218	8105R3 A	6202	2312	9305	XX
A40158	11/23/92	520.0	0218	8003R4 A	6202	2312	9305	X XX
A40159	12/03/92	187.8	0218	8003R4 A	6202	2312	9305	XX
A40161	12/22/92	293.7	0218	8003R5 A	6202	2312	9305	X XX
A40162	01/13/93	520.0	0218	8107 A	6202	2312	2022R1	X XX
A40163	02/01/93	520.0	0218	8107R1 A	6202	2312	2022R1	X XXX
A40164	02/03/93	754.0	0218	8107R1 A	6202	2312	2022R1	XXXX
A40165	02/05/93	503.0	0218	8107R1 A	6202	2312	2022R1	X X X
A40166	02/18/93	258.6	0218	8008 A	6202	9104	2022R1	X X
A40167	03/01/93	754.0	0218	8107R2 A	6202	2217	2022R1	XXXX
A40168	03/08/93	40.0	0218	8003R7 A	6202	2217	2022R1	XXX
A40169	03/10/93	754.0	0218	8003R7 A	6202	2217	2022R1	XXXX
A40170	03/12/93	850.0	0218	8003R7 A	6202	2217	2022R1	X XXX
A40171	03/17/93	860.0	0218	8003R7 A	5303	2217	2022R1	X XXX
A40172	03/30/93	850.0	0218	8107R3 A	5303	2217	2022R1	X XXX
A40173	04/01/93	850.0	0218	8107R3 A	5303	2217	2022R1	X XX

TABLE 2-1. LOG OF SSME HOT FIRINGS (TEST AND FLIGHT) THROUGH OCTOBER 1993 (Continued)

PAGE 4

POWER LEVEL KEY: 1=65%; 2=90%; 3=100%; 4=104%; 5=109%; 6=111%

TEST #	DATE	DUR	ENG #	HPOTP	HPFTP	LPOTP	LPFTP	123456
A40174	04/13/93	219.0	0218	8008R2 A	2227R1	2217	2022 R1	X X
A40175	04/27/93	520.0	0218	8202R3 A	2031	2217	2022 R1	X X
A40176	04/30/93	73.5	0218	8202R3 A	2031	2217	2022R1	X XX
A40177	05/10/93	520.0	0218	8202R3 A	2031	2217	2022R1	X XXX
A40178	05/14/93	265.0	0218	8202R3 A	2031	2217	2022R1	X X
A40179	05/19/93	520.0	0218	8202R3 A	2031	2217	2022R1	X XX
A40180	05/26/93	850.0	0218	8202R3 A	2031	2217	2022R1	X XXX
A40181	06/16/93	520.0	0218	8105R6 A	5104R1	2217	2022R1	X XXX

TABLE 2-1. LOG OF SSME HOT FIRINGS (TEST AND FLIGHT) THROUGH OCTOBER 1993 (Continued)

SSME DIAGNOSTIC DATA BASE DIRECTORY
STS TEST STAND

POWER LEVEL KEY: 1=65%; 2=90%; 3=100%; 4=104%; 5=109%; 6=111%

TEST #	DATE	DUR	ENG #	HPOTP	HPFTP	LPOTP	LPFTP	123456
STS001E1	04/12/81	520.0	2007	0007R1	9006R1	2006	2006	X X
STS01E2	04/12/81	514.0	2006	2404	0306R2	0008	2007	X X
STS001E3	04/12/81	520.0	2005	2105	0009R1	2004	0007	X X
STS02E1	11/12/81	520.0	2007	0007R1	9006R1	2006	2006	X X
STS002E2	11/12/81	520.0	2006	2404	0306R1	0008	2007	X X
STS002E3	11/12/81	520.0	2005	2105	0009R1	2004	0007	X X
STS003E1	03/22/82	520.0	2007	0007R1	9006R1	2006	2006	X X
STS003E2	03/22/82	520.0	2006	2404	0306R2	0008	2007	X X
STS003E3	03/22/82	520.0	2005	2105R1	0009R1	2004	0007	X X
STS004E1	06/27/82	514.0	2007	0007R1	2009	2006	2006	X X
STS004E2	06/27/82	514.0	2006	2404	0306R2	2009	2007	X X
STS004E3	06/27/82	514.0	2005	2105R1	0009R2	2004	0007	X X
STS05E1	11/11/82	514.0	2007	9009R3	2009	2006	2006	X X
STS005E2	11/11/82	518.0	2006	2404	0306R2	2009	2007	X X
STS005E3	11/11/82	518.0	2005	2105R1	9006R2	2004	0007	X X
STS06E1	04/03/83	505.0	2017	9010	9110	2211	9106	X XX
STS06E2	04/03/83	505.0	2015	2015	2315	2113	2211	X XX
STS06E3	04/03/83	505.0	2012	2016	2213R1	2012	2016	X XX
STS07E1	06/18/83	505.0	2017	9010	2315	2211	9106	X XX
STS07E2	06/18/83	505.0	2015	2015	9211	2113	2211	X XX
STS07E3	06/18/83	505.0	2012	2016	2213R1	2012	2016	X XX
STS08E1	08/30/83	528.0	2017	9010	2315	2211	9106	X X
STS08E2	08/30/83	528.0	2015	2015	9211	2113	2211	X X
STS08E3	08/30/83	528.0	2012	2016	2116R2	2012	2016	X X
STS11E1	02/03/84	520.9	2109	2020	5101R1	2018	2117	X X
STS11E2	02/03/84	520.9	2015	2015	9211	2113	2211	X X
STS11E3	02/03/84	520.9	2012	2016	2116R2	2012	2016	X X
STS13E1	04/06/84	510.0	2109	2020	5101R1	2018	2117	X XX
STS13E2	04/06/84	510.0	2020	2021	2018	0208	2019	X XX
STS13E3	04/06/84	510.0	2012	2016	2116R2	2012	2016	X XX
STS41DE1	08/30/84	521.0	2109	2020	2020R1	2018	2117	X XX
STS41DE2	08/30/84	521.0	2018	9211	2017R2	2020	4001R1	X XX
STS41DE3	08/30/84	521.0	2021	4001	4001R1	2019	9105R1	X XX
STS41GE1	10/05/84	536.0	2023	2019R1	2515R1	2015	2020	X X
STS41GE2	10/05/84	536.0	2020	2021	9311R1	0208	2019	X X
STS41GE3	10/05/84	536.0	2021	4001	4001R1	2019	2021R1	X X
STS51AE1	11/08/84	520.0	2109	2020	2020R2	2018	2117	X XX
STS51AE2	11/08/84	519.8	2018	9211	2017R2	2020	4001R1	X XX
STS51AE3	11/08/84	519.8	2012	9110	2118	2012	9206	X XX
STS51CE1	01/24/85	518.0	2109	2020	4202	2018	2117	X XX
STS51CE2	01/24/85	518.0	2018	2018R1	2017R2	2020	4001R1	X XX
STS51CE3	01/24/85	518.0	2012	9110	4003	2012	9206	X XX
STS51DE1	04/13/85	538.0	2109	2115	4202	2018	2117	XXX
STS51DE2	04/13/85	538.0	2018	2018R1	2017R2	2020	4001R1	XXX
STS51DE3	04/13/85	538.0	2012	9110	4003	2012	9206	XXX
STS51BE1	04/30/85	521.0	2023	2019R1	2515R1	2015	4002R1	X XX
STS51BE2	04/30/85	521.0	2020	2021	9311R1	0208	2019	X XX
STS51BE3	04/30/85	521.0	2021	4001	2216	2019	2021R1	X XX
STS51GE1	06/17/85	523.0	2109	2115	2121	2018	2117	X XX
STS51GE2	06/17/85	523.0	2018	2016R3	4201	2020	4001R1	X XX
STS51GE3	06/17/85	523.0	2012	9110	4003R1	2012	9206	X XX
STS51FE1	07/29/85	-349.7	2023	2019R2	2515R1	2015	4002R1	X XX

TABLE 2-1. LOG OF SSME HOT FIRINGS (TEST AND FLIGHT) THROUGH OCTOBER 1993 (Continued)

POWER LEVEL KEY: 1=65%; 2=90%; 3=100%; 4=104%; 5=109%; 6=111%

TEST #	DATE	DUR	ENG #	HPOTP	HPFTP	LPOTP	LPFTP	123456
STS51FE2	07/29/85	588.0	2020	4003R2	4202R1	0208	2019	X XX
STS51FE3	07/29/85	588.0	2021	4001R1	2216	2019	2021R1	X XX
STS51IE1	08/27/85	514.0	2109	2115	2121R1	2018	2117	XX
STS51IE2	08/27/85	514.0	2018	2016R3	4201	2020	4001R1	XX
STS51IE3	08/27/85	514.0	2012	2018R2	4003R1	2012	9206	XX
STS51JE1	10/03/85	518.0	2011	2022R2	5301	9005	2115	X XX
STS51JE2	10/03/85	518.0	2019	9211R2	2120	2017	2022	X XX
STS51JE3	10/03/85	518.0	2017	4102R1	2218R1	2211	2020	X XX
STS61AE1	10/30/85	521.0	2023	2019R2	2515R1	2015	4002R1	X XX
STS61AE2	10/30/85	521.0	2020	4003R2	4202R1	0208	2019	X XX
STS61AE3	10/30/85	521.0	2021	2020R3	2216	2019	2021R1	X XX
STS61BE1	11/27/85	517.0	2011	2022R2	2413R2	9005	2115	X XX
STS61BE2	11/27/85	517.0	2019	9211R2	2120	2017	2022	X XX
STS61BE3	11/27/85	517.0	2017	4102R1	2218R1	2211	2020	X XX
STS61CE1	01/12/86	508.0	2015	2018R2	4003R1	4101R1	2116	XX
STS61CE2	01/12/86	508.0	2018	2504	4201R1	2020	4001R1	XX
STS61CE3	01/12/86	508.0	2109	2115	2121R1	2018	2117	XX
STS51LE1	01/28/86	81.0	2023	2019R2	2515R1	2015	4002R1	X XX
STS51LE2	01/28/86	81.0	2020	4003R2	4202R1	0208	2019	X XX
STS51LE3	01/28/86	81.0	2021	2020R3	2216	2019	2021R1	X XX
STS026E1	09/29/88	519.0	2019	4106R1	2026R1	2025R1	2025R1	X XX
STS026E2	09/29/88	519.0	2022	2025R1	5203	2104R1	2024R1	X XX
STS026E3	09/29/88	519.0	2028	2121R1	4007	2027R1	2026R2	X XX
STS027E2	12/02/88	520.0	2030	2122R2	2323	2216	2027	X XX
STS027E3	12/02/88	520.0	2029	9109R1	2112R2	2106R1	2029	X XX
STS027E1	12/02/88	520.0	2027	2124R2	6102	2124	4005	X XX
STS029E1	03/13/89	515.0	2031	9209R1	2125	4105	2022R1	X XX
STS029E2	03/13/89	515.0	2022	2222	5203	2104R1	2024R1	X XX
STS029E3	03/13/89	515.0	2028	4105	4007	2027R1	2026R2	X XX
STS030E1	05/04/89	516.0	2027	6302	6102	2124	4005	X XX
STS030E2	05/04/89	516.0	2030	2223R1	2323	2216	2027	X XX
STS030E3	05/04/89	516.0	2029	4302	6003	2106R1	2029	X XX
STS028E1	08/08/89	521.0	2019	2126R4	2125	2025R1	2025R1	X XX
STS028E2	08/08/89	521.0	2022	4406R1	5203	2104R1	2024R1	X XX
STS028E3	08/08/89	521.0	2028	2324R2	4007	2027R1	2026R2	X XX
STS034E1	10/18/89	519.0	2027	2225R1	4008	2124	4005	X XX
STS034E3	10/18/89	519.0	2029	6003R1	6003	2106R1	2029	X XX
STS034E2	10/18/89	519.0	2030	2321R1	2323	2216	2027	X XX
STS033E1	11/23/89	513.0	2011	4205R1	4012R1	2126	82207	X XX
STS033E2	11/23/89	513.0	2031	6402R1	6102R1	2120	2120R1	X XX
STS033E3	11/23/89	513.0	2107	2422R1	4011	4105	2117R1	X XX
STS032E2	01/09/90	519.0	2022	2305R1	4010R2	2104R1	2024R1	X XX
STS032E1	01/09/90	519.0	2024	4107R1	6007	2029	2131	X XX
STS032E3	01/09/90	519.0	2028	2323R1	2126	2027R1	2026R2	X XX
STS036E1	02/28/90	516.0	2019	4406R3	6008	2025R1	2022R1	X XX
STS036E2	02/28/90	516.0	2030	2324R5	6003	2216	2027	X XX
STS036E3	02/28/90	516.0	2027	2225R3	4010R2	2124	4005	X XX
STS031E1	04/24/90	518.0	2011	2027R1	5203R1	2126	2030	X XX
STS031E2	04/24/90	518.0	2031	4008R1	6102R1	2120	2120R1	X XX
STS031E3	04/24/90	518.0	2107	2226R1	4011R1	4105	4007	X XX
STS041E1	10/06/90	517.0	2011	2027R2	5203R1	2126	2030	X XX
STS041E2	10/06/90	517.0	2031	2521R1	4010R3	2120	2120R1	X XX
STS041E3	10/06/90	517.0	2107	2305R3	6003R1	2216	4007	X XX

TABLE 2-1. LOG OF SSME HOT FIRINGS (TEST AND FLIGHT) THROUGH OCTOBER 1993 (Continued)

POWER LEVEL KEY: 1=65%; 2=90%; 3=100%; 4=104%; 5=109%; 6=111%

TEST #	DATE	DUR	ENG #	HPOTP	HPFTP	LPOTP	LPFTP	123456
STS038E1	11/15/90	517.0	2019	2323R4	6008	2025R1	2022R1	X XX
STS038E2	11/15/90	517.0	2022	4107R3	6007R1	2104R1	2024R1	X XX
STS038E3	11/15/90	517.0	2027	9309R1	4109R1	4302	4005	X XX
STS035E1	12/02/90	519.0	2024	4205R3	4008	2106R1	2131	X XX
STS035E2	12/02/90	519.0	2012	6003R3	4007R3	4306	4006	X XX
STS035E3	12/02/90	519.0	2028	4502R1	6009	2027R1	2026R2	X XX
STS037E1	04/05/91	520.0	2019	9309R2	6008	2025R1	2022R1	X XX
STS037E2	04/05/91	520.0	2031	2027R3	4010R3	2120	2120R1	X XX
STS037E3	04/05/91	520.0	2107	2521R2	6003R1	2216	4007	X XX
STS039E1	04/28/91	520.0	2026	2226R3	4012R2	2224	2025R2	XX
STS039E2	04/28/91	520.0	2030	4506R1	4011R2	2030	2027	XX
STS039E3	04/28/91	520.0	2029	4008R3	2126R1	2121	2029	XX
STS040E1	06/05/91	517.0	2015	4010R3	4013R1	4401	2216	XX
STS040E2	06/05/91	517.0	2022	4502R2	6007R1	2104R1	82207R1	XX
STS040E3	06/05/91	517.0	2027	6008R1	4109R1	4302	4005	XX
STS043E1	08/02/91	514.0	2024	4009R3	6102R3	2028	2131	XX
STS043E2	08/02/91	514.0	2012	2425R1	4007R3	2213	4006	XX
STS043E3	08/02/91	514.0	2028	2405R1	6009	2027R1	2228	XX
STS048E1	09/12/91	523.0	2019	2424R4	5203R1	2025R1	2022R1	XX
STS048E2	09/12/91	523.0	2031	2226R4	2323R2	2120	2120R1	XX
STS048E3	09/12/91	523.0	2107	4305R1	6003R1	2216	4007	XX
STS044E1	11/24/91	516.0	2015	4010R4	4013R1	4401	2216	XX
STS044E2	11/24/91	516.0	2030	4506R2	4011R2	2030	2027	XX
STS044E3	11/24/91	516.0	2029	6103R1	2322	2121	2029	XX
STS042E1	01/22/92	516.0	2026	2425R2	4012R2	2224	4008	XX
STS042E2	01/22/92	516.0	2022	4502R3	6007R2	2129	82207R1	XX
STS042E3	01/22/92	516.0	2027	6008R2	2225	4302	2026R2	XX
STS045E1	03/24/92	517.0	2024	4305R2	2323R3	4205	2131	XX
STS045E2	03/24/92	517.0	2012	4207	4108	2213	4006	XX
STS045E3	03/24/92	517.0	2028	2405R2	6009R1	2027R1	2228	XX
STS049E1	05/16/92	516.0	2030	4506R3	4011R2	4008	2027	XX
STS049E2	05/16/92	516.0	2015	2030	4015	4401	2216	XX
STS049E3	05/16/92	516.0	2017	2031	2032	4009	4009	XX
STS050E1	06/25/92	514.0	2019	9409	4110R1	2126	2022R1	XX
STS050E2	06/25/92	514.0	2031	2423R1	4014	2120	2120R1	XX
STS050E3	06/25/92	514.0	2011	2127	4016	4406	2030	XX
STS046E1	07/31/92	516.0	2032	6007R1	2028	2035	2033	XX
STS046E3	07/31/92	516.0	2027	6008R3	2225	4302	4007	XX
STS046E2	07/31/92	516.0	2033	9210	2029	2032	2215R1	XX
STS047E1	09/12/92	520.0	2026	4109	4012R2	2224	4008	XX
STS047E2	09/12/92	520.0	2022	4012	2033	2129	82207R1	XX
STS047E3	09/12/92	520.0	2029	6103R2	2322	2121	2029	XX
STS052E1	10/22/92	519.0	2030	4111R3	2326	4008	2124	XX
STS052E2	10/22/92	519.0	2015	2030R1	4107R1	4401R1	2216	XX
STS052E3	10/22/92	519.0	2034	4207R1	2030	2033	2032R1	XX
STS054E1	01/13/93	517.0	2019	9409	4110R1	2126	2125	XX
STS054E2	01/13/93	517.0	2033	9210	2029	2032	2215R1	XX
STS054E3	01/13/93	517.0	2018	4602	2035	2130	4105	XX
STS056E1	04/08/93	520.0	2024	4111R4	6108R1	4205	2131	XXX
STS056E2	04/08/93	520.0	2033	6109R2	6107	2032	2215R2	XXX
STS056E3	04/08/93	520.0	2018	4602R1	2035	2130	4105	XXX
STS055E1	04/26/93	517.0	2031	2423R1	4014	2120	2120R1	XX
STS055E2	04/26/93	517.0	2109	2525R1	6103R1	2031	2035	XX

TABLE 2-1. LOG OF SSME HOT FIRINGS (TEST AND FLIGHT) THROUGH OCTOBER 1993 (Continued)

POWER LEVEL KEY: 1=65%; 2=90%; 3=100%; 4=104%; 5=109%; 6=111%

TEST #	DATE	DUR	ENG #	HPOTP	HPFTP	LPOTP	LPFTP	123456
STS055E3	04/26/93	517.0	2029	4405R1	4015	2121	2029	XX
STS057E1	06/21/93	518.0	2019	2426R2	2033	2126	2125	XX
STS057E2	06/21/93	518.0	2034	4602R1	2030	2033	2032R1	XX
STS057E3	06/21/93	518.0	2017	4109R1	2029	4007	4009	XX

TABLE 2-1. LOG OF SSME HOT FIRINGS (TEST AND FLIGHT) THROUGH OCTOBER 1993 (Continued)

SSME DIAGNOSTIC DATA BASE DIRECTORY
TTB TEST STAND

POWER LEVEL KEY: 1=65%; 2=90%; 3=100%; 4=104%; 5=109%; 6=111%

TEST #	DATE	DUR	ENG #	HPOTP	HPFTP	LPOTP	LPFTP	123456
TTB004	02/25/89	45.0	0208	2704	2714	2112R1	9306R1	X
TTB005	04/06/89	120.0	0208	2704	2714	2112R1	9306R1	X
TTB006	04/26/89	140.0	0208	2704	2714	2117	9306R1	XX
TTB008	06/22/89	40.8	0208	2704	2714	2117	9306R1	XX
TTB009	07/15/89	120.0	0208	2704	2714	2117	9306R1	XX
TTB010	08/03/89	160.0	0208	2704	2714	2117	9306R1	XXXX
TTB011	08/17/89	145.0	0208	2704	2714	2117	9306R1	XXXX
TTB012	11/08/89	160.0	0208	2408	2318	2117	9306R1	XXXX
TTB013	12/07/89	160.0	0208	2408	2318	2117	9306R1	XXXX
TTB015	02/15/90	150.0	0208	2408	2318	2117	9306R1	XXX
TTB016	02/22/90	165.0	0208	2408	2318	2117	9306R1	XXX
TTB017	03/20/90	160.0	0208	2408	2318	2117	9306R1	XXXX
TTB018	03/26/90	160.0	0208	2408	2318	2117	9306R1	XXXX
TTB019	04/12/90	160.0	0208	2408	2318	2117	9306R1	XXXX
TTB021	03/15/91	170.0	3001	4304R3	2814	2210	4004R2	XXX
TTB023	09/18/91	112.9	3001	9705	2604R1	2210	4004R2	XX
TTB024	10/22/91	20.5	3001	9705	2604R1	2210	4004R1	XX
TTB025	11/26/91	205.0	3001	9705	2604R1	2210	4004R2	XX
TTB026	12/10/91	170.0	3001	9705	2604R1	2210	4004R1	XX
TTB027	12/19/91	41.9	3001	9705	2604R1	2210	4004R1	XX
TTB028	01/24/92	210.0	3001	9705	2604R1	2210	4004R1	XXXX
TTB031	04/15/92	85.0	3001	4404	2814R2	2210	4004R2	XXX
TTB032	04/28/92	205.0	3001	4404	2814R2	2210	4004R2	XXX
TTB033	05/14/92	17.8	3001	4404	2814R2	2210	4004R2	XX
TTB034	05/28/92	210.0	3001	4404	2814R2	2210	4004R2	XXX
TTB035	06/11/92	200.0	3001	4404	2814R2	2210	4004R2	XXX
TTB036	09/04/92	51.0	3001	9705	8301 A	2210	4004R2	XX
TTB037	09/17/92	114.0	3001	9705	8301 A	2210	4004R2	XX
TTB038	09/29/92	138.0	3001	9705	8301 A	2210	4004R2	XXX
TTB039	01/14/93	210.0	3001	2722	4406R2	2218	4004R2	XXXX
TTB040	02/11/93	180.0	3001	2722	4406R2	2218	4004R2	XXXX
TTB041	04/08/93	202.0	3001	8105R5 A	4406R2	2218	4004R2	XXX
TTB042	04/30/93	203.0	3001	8105R5 A	8006R1 A	2218	4004R2	XXXX
TTB043	07/08/93	190.0	3001	8202R3 A	4406R2	2218	4004R2	XXXX

APPENDIX A

REPORTS AND PRESENTATIONS PREPARED BY WYLE IN SUPPORT OF SSME DYNAMIC EVALUATIONS

WYLE
LABORATORIES

SOME NON-LINEAR SPECTRAL METHODS AND THEIR APPLICATION TO ROCKET ENGINE DIAGNOSTIC EVALUATION

BY

THOMAS COFFIN & JEN-YI JONG

WYLE LABORATORIES

1ST INTERNATIONAL
MACHINERY MONITORING AND DIAGNOSTICS CONFERENCE
LAS VEGAS, NEVADA
SEPTEMBER 11-14, 1989

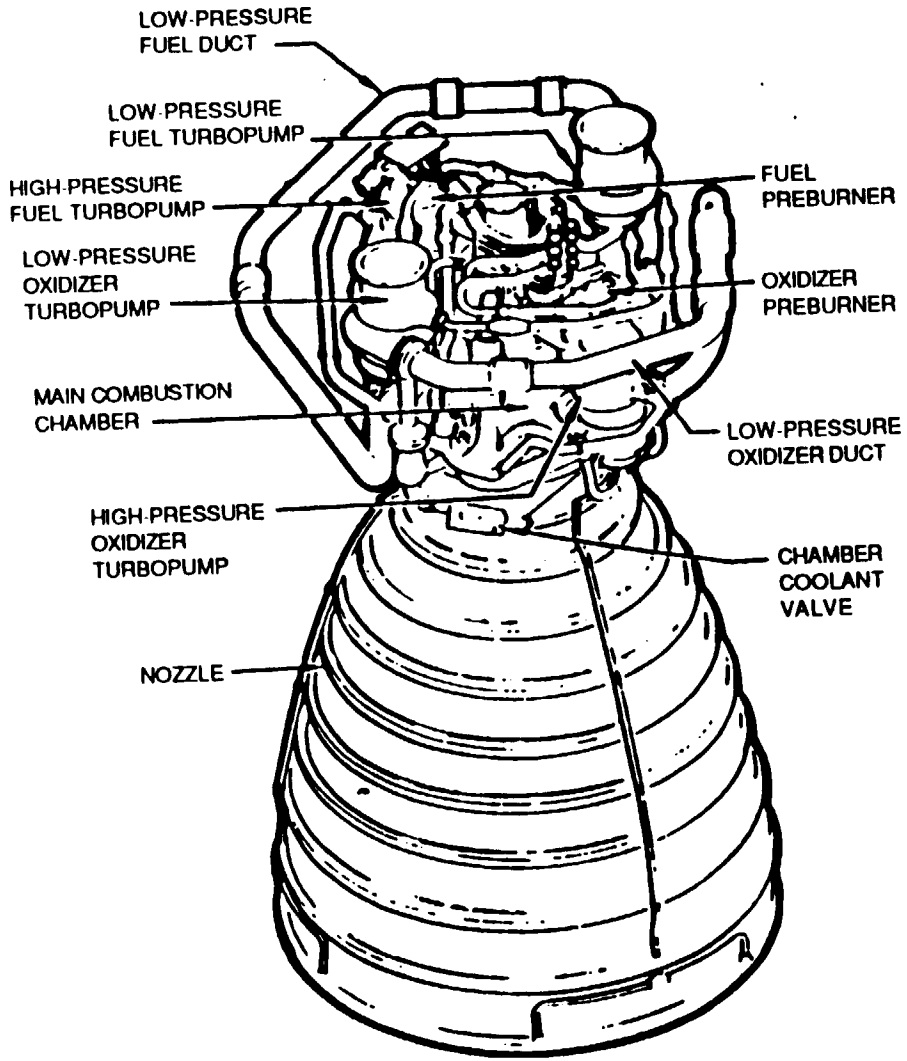

SPACE SHUTTLE MAIN ENGINE

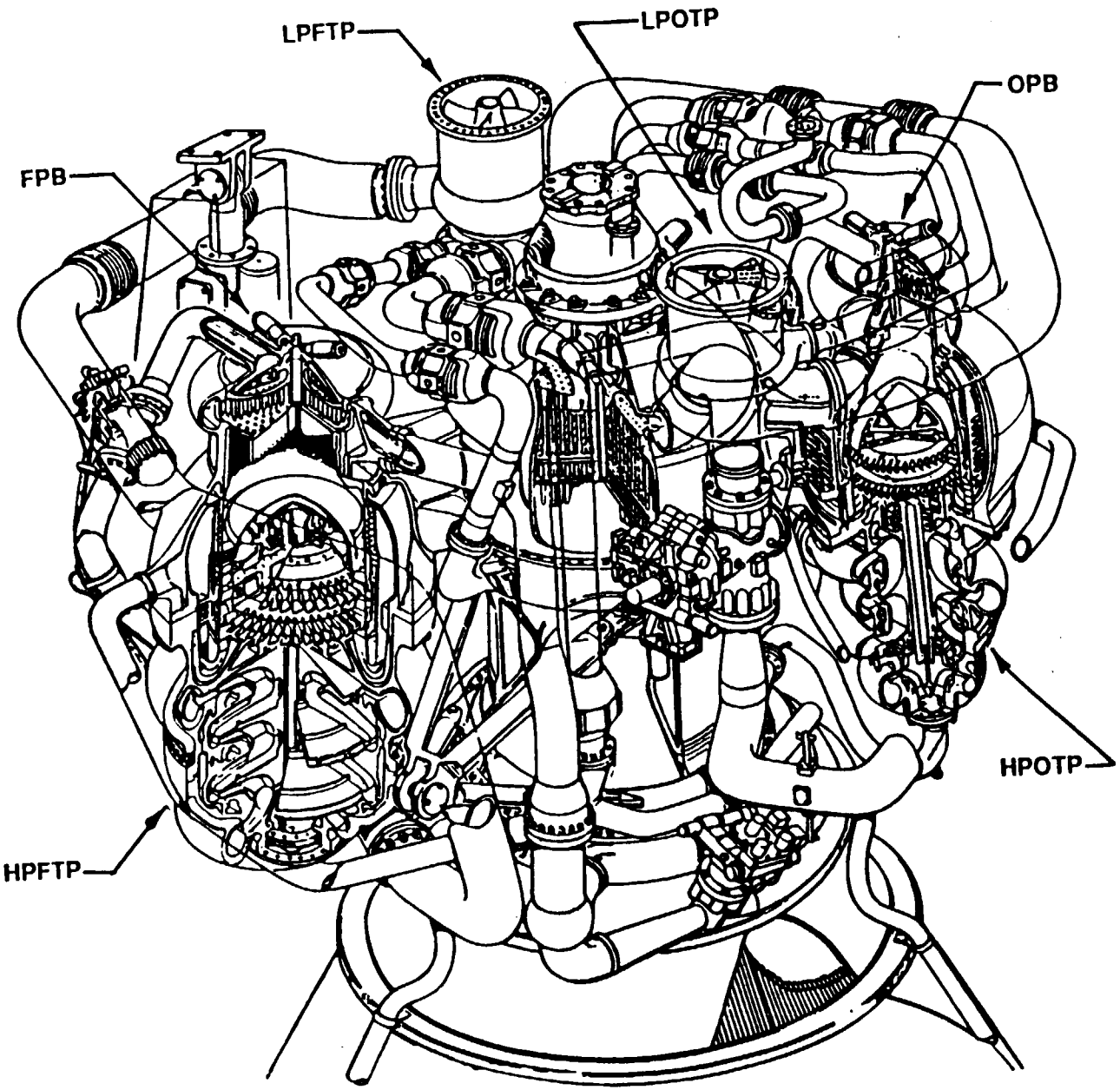

SPACE SHUTTLE MAIN ENGINE POWER HEAD

WYLE LABORATORIES

HIGHER ORDER POWER SPECTRA

- **MEAN VALUE:**

$M_x(f) = E[X(f)] = 0$ (ZERO MEAN STATIONARY PROCESS)

- **LINEAR (ORDINARY) SPECTRUM:**

$S_{xx}(f) = E[X(f_1)\, X(f_2)], \quad f_1 + f_2 = 0$

$= E[X(f)\, X^*(f)]$

- **BISPECTRUM:**

$B_{xxx}(f_1, f_2) = E[X(f_1)\, X(f_2)\, X(f_3)], \quad f_1 + f_2 + f_3 = 0$

$= E[X(f_1)\, X(f_2)\, X^*(f_1 + f_2)]$

- **TRISPECTRUM:**

$T_{xxxx}(f_1, f_2, f_3) = E[X(f_1)\, X(f_2)\, X(f_3)\, X(f_4)] - E[X(f_1)\, X(f_2)]\; E[X(f_3)\, X(f_4)]$

$- E[X(f_1)\, X(f_3)]\; E[X(f_2)\, X(f_4) - E[X(f_1)\, X(f_4)]\, E[X(f_2) X(f_3)],$

$f_1 + f_2 + f_3 + f_4 = 0$

WYLE LABORATORIES

THE HYPER-SPECTRUM AND HYPER-COHERENCE

- **DEFINE THE HYPER-SPECTRUM**

$$H(n; f_1) = E[X(f_1)\, X(f_2) \ldots X(f_n)\, X^*(f_1 + f_1 + \ldots + f_n)], \qquad f_1 = f_2 \ldots f_n$$

OR,

$$H(n; f_1) = E[X^n(f_1)\, X^*(nf_1)], \qquad n = 1, 2, 3, \ldots$$

NOTE:

$$H(1; f_1) = E[X(f_1)\, X^*(f_1)] = S_{xx}(f_1)$$

$$H(2; f_1) = E[X(f_1)\, X(f_2)\, X^*(f_1 + f_2)], \qquad f_1 = f_2$$

$$= B_{xxx}(f_1, f_1)$$

ETC.

- **THE NORMALIZED HYPER-SPECTRUM (HYPER-COHERENCE)**

$$\Gamma^2(n; f_1) = \frac{\left| E[X^n(f_1)\, X^*(nf_1)] \right|^2}{E\left[\left|X^n(f_1)\right|^2\right] E\left[\left|X(nf_1)\right|^2\right]}, \qquad n = 1, 2, \ldots$$

$$0 \le \Gamma^2 \le 1$$

WYLE LABORATORIES

WAVEFORM RECOVERY

- GIVEN X(t) and Y(t) JOINTLY PERIODIC + NOISE + UNCORRELATED SIGNAL
- LET:

$$X'(t) = F^{-1}\left[\sqrt{S_{xx}(nf_1)}\,\Gamma_x(n; f_1)\right]$$

$$Y'(t) = F^{-1}\left[\sqrt{S_{yy}(nf_1)}\,\Gamma_y(n; f_1)\right]$$

$$Y''(t) = Y'(t - \tau)$$

$$\tau = \phi / 2\pi f_1$$

$$\phi = T_{an}^{-1}\left[Q_{xy}(f_1) / C_{xy}(f_1)\right]$$

Q_{xy} = QUADRATURE SPECTRUM

C_{xy} = COSPECTRUM

- FILTERED ORBIT PLOT

$X'(t)$ vs. $Y''(t)$

WYLE LABORATORIES

TEST - 471

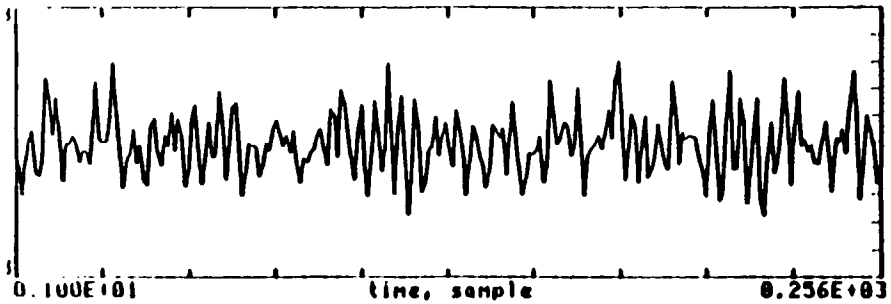

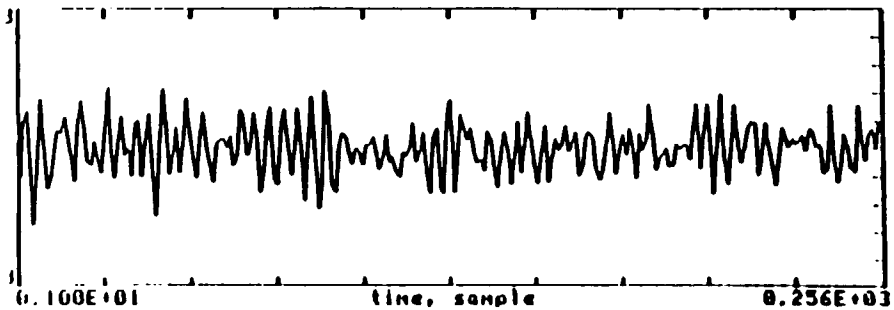

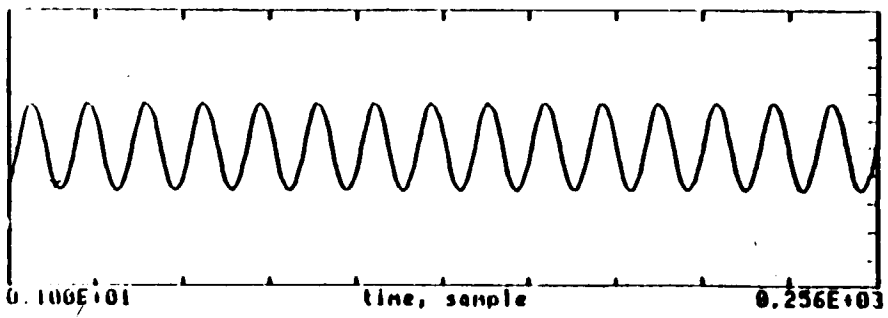

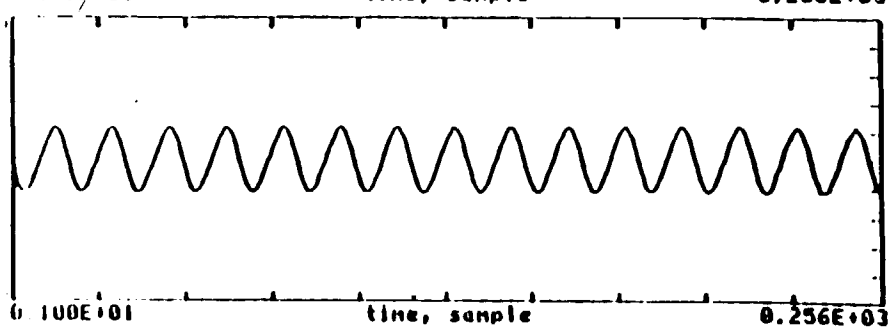

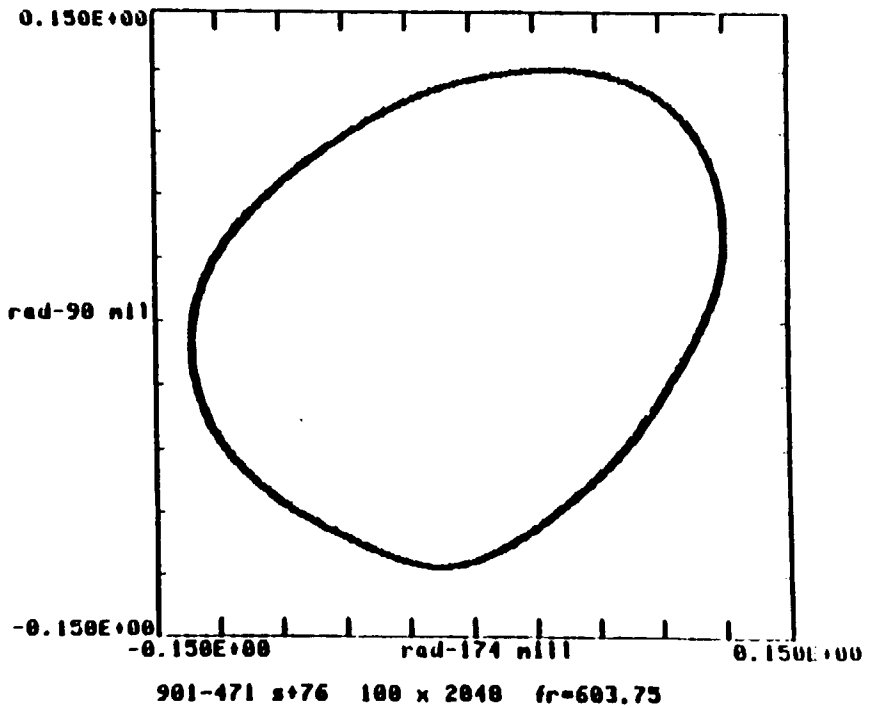

WYLE
LABORATORIES

TEST - 436

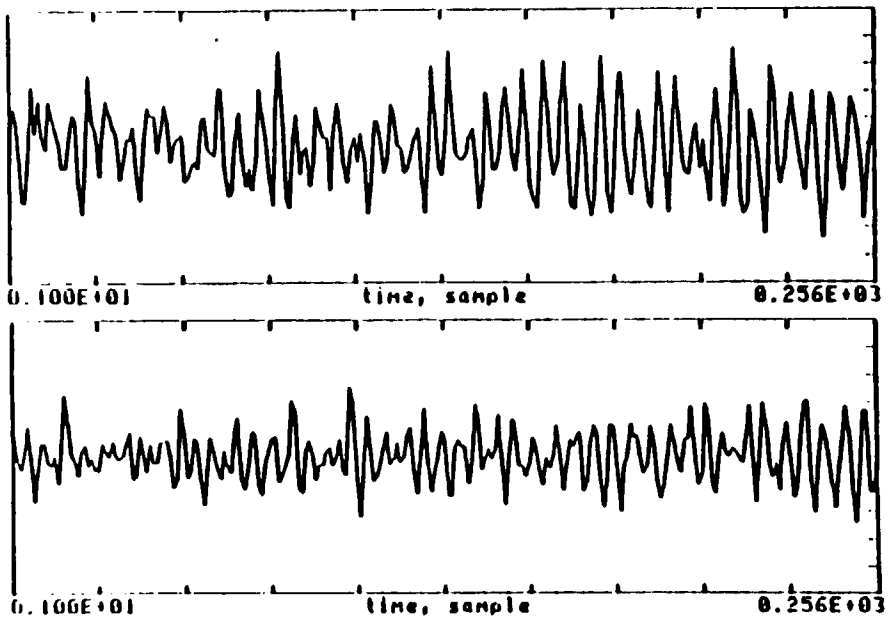

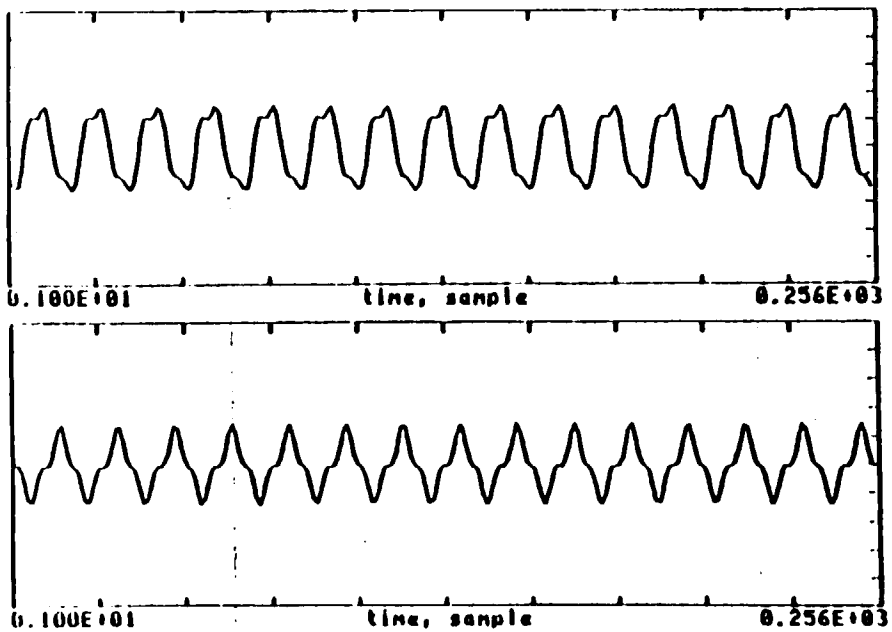

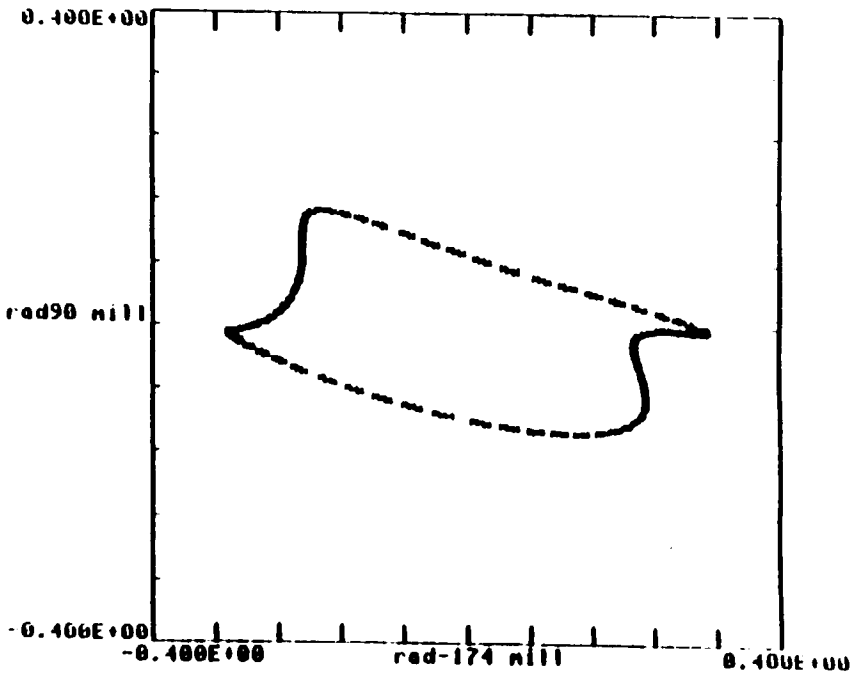

ORBITAL DIAGRAM OF 901-436 BY HYPER-COHERENCE
FILTERING 9+160 BEFORE 3N DIMINISHED

Research and Technology 1990

Annual Report of the Marshall Space Flight Center

NASA TM - 103510

NASA

National Aeronautics and
Space Administration

George C. Marshall Space Flight Center
Marshall Space Flight Center, Alabama 35812

Data Systems

The TOPO Plot: A Data Reduction/Graphics Routine for Tracking Spectral Trends in Vibration Data

(T. Coffin & J. Y. Jong)

In support of space shuttle main engine (SSME) development and advanced technology test programs, a number of sophisticated diagnostic algorithms have been integrated into the Operator Interactive Signal Processing Systems (OISPS) operational on MSFC's Structures and Dynamics Laboratory computers. These include nonlinear spectrum analysis, adaptive filtering, envelope detection, and other analytical methods applicable to specific SSME mechanical symptom detection and identification investigations. For quick-look data assessment, the (linear) **power spectral density** (PSD), isoplot, and root-mean-square (rms) time history of a measurement are the most basic and valuable computational tools. When viewed in the context of empirical statistical data representing SSME component measurements obtained under similar operating conditions, these analyses can provide a quick, qualitative indication of component "health" (from a dynamics standpoint) and signal any gross deviations from nominal operation.

The most fundamental "**signature**" used to characterize an SSME **vibration** (acceleration, pressure, strain, etc.) measurement is the mean-square density spectrum, or power spectral density. Figure 23a illustrates an isoplot, or family of spectra, from a strain gauge measurement representing 450 seconds during a hot-firing test. The **PSD** provides a detailed snapshot of conditions over an interval of (usually) constant power operation. In contrast, the isoplot yields a more qualitative indication of amplitude/frequency trends over a complete hot-firing test or powered flight. These plots are particularly useful for detecting the *time* of any significant deviations in the **vibration signature** and correlation with engine operating parameters (power profile, programmed venting, etc.). Figure 23b shows an alternate format.

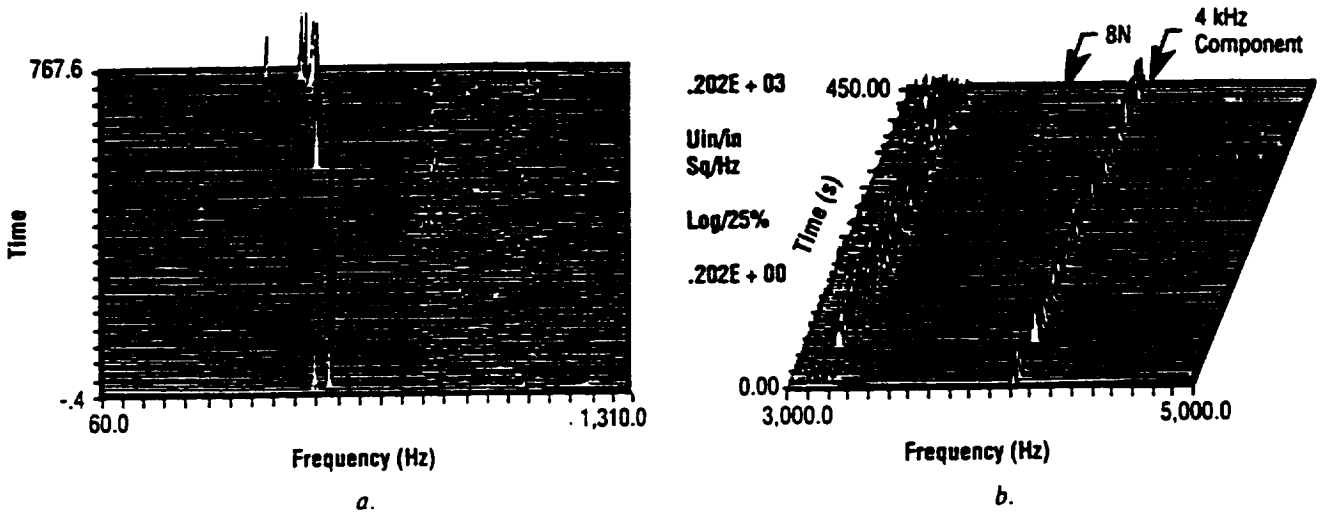

Figure 23. Illustration Isoplot Format

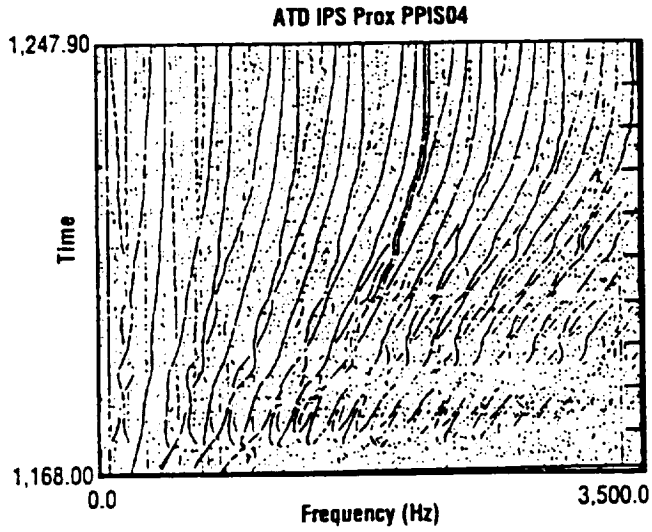

npk = 80
isp = 1
neigh= 5
ipara = 5
mx = 1
my = 1

#PSU = 400
#AVGS= 1
BW = 5.00

Figure 24. TOPO Plot of Bearing Displacement During Speed Change

The PSD isoplot has been used extensively to display spectral components in a frequency/time/amplitude format. This display is especially useful for nonstationary data, which allows one to trace any particular frequency component as a function of time. However, there are several limitations to the procedure.

- For clarity, a threshold level has to be chosen when plotting an isoplot in which some possibly significant peaks with PSD amplitude lower than the threshold are excluded.
- For a nonstationary case, when manned PSD peaks are crowded together, or crossover occurs, it is difficult to identify the trace of some peaks. Then, it is necessary to subdivide the entire frequency range into several smaller ranges and plot the results separately.
- The number of PSD's which can be legibly displayed in an isoplot is limited to approximately one hundred.

To provide improved tracking of spectral trends, a new method called "TOPO" (for Topographic Plot) was developed and programmed. The method uses a novel peak-identifying routine to pick out all meaningful peaks in each PSD and assign a "peakyness" parameter for each identified peak. Each peak is then plotted on a TOPO plot as a dot whose width is proportional to the "peakyness" parameter associated with the peak. Figure 24 is an example of bearing test data during ramp-up. Four hundred PSD's are plotted in this figure, and the non-stationary and crossover can be clearly visualized.

The TOPO plot technique has been integrated in the OISPS program and is in routine use for SSME data evaluations. For computerized data base application, the technique provides significant data compression since only spectral peak values need be stored. Enhancements in the graphic output format, to aid in data interpretation, are presently under evaluation, including color coding of amplitude ranges.

Coffin, T., Swanson, W.L., and Jong, J.Y., "Data Analysis Methods and Signal Processing Techniques for Space Shuttle Main Engine Diagnostic Evaluation," Wyle Laboratories Final Report Under Contract NAS8-36549, October 1989.

J.E. McBride/ED23
(205) 544–1523
Sponsor: Space Shuttle Main Engine Office

An Algorithm for Periodic Waveform Recovery from Space Shuttle Main Engine Vibration Measurements

(T. Coffin & J. Y. Jong)

The frequency content in dynamic measurements from rotating machinery contains much subtle information concerning equipment operating condition and component degradation. For this reason, the power spectral density (PSD) has long been employed to assess the relative magnitude of fault-related spectral contributions. Measurements on high-performance rocket engine turbomachinery suffer from severe noise contamination, from numerous extraneous sources, which impedes rotating element diagnostic evaluation. Thus, it is difficult to determine whether an apparent high-level harmonic contribution is indeed related to the fundamental rotational frequency, f_r, or possibly due to an independent source. In an effort to correlate synchronous frequency characteristics with an arbitrary harmonic component, a unique coherence spectrum was devised which we call the "**hypercoherence**" **function**. The **hypercoherence function**, $\Gamma(n;f)$, defines the nonlinear correlation between waves at a reference frequency, f, and harmonics at nf. $n = 1, 2, ...$

Application of the **hypercoherence functions** to SSME turbomachinery diagnostic data assessment was summarized in the 1986 R&T Report (NASA TM 86567). This frequency-domain analysis has since been extended to a time-domain filtering algorithm for the extraction of periodic signals in noisy data. Assume we have two turbopump vibration measurements located (approximately) 90° apart radially about the casing, say $X(t)$ and $Y(t)$. If the shaft (and inner bearing race) motion is sensed by these transducers, a plot of $X(t)$ versus $Y(t)$ should indicate the orbital motion of the shaft end measured. Each of these "signals" will clearly be corrupted with undesired noise (both random and periodic) during practice. The analytical basis for the techniques can be summarized briefly. Assume $X(t)$ and $Y(t)$ jointly periodic, with additive uncorrelated noise and (possibly coincident) period components.

Let

$$X'(t) = F^{-1}\left[\sqrt{S_{xx}(nf)_1}\,\Gamma_x(n;f_1)\right]$$
$$Y'(t) = F^{-1}\left[\sqrt{S_{yy}(nf)_1}\,\Gamma_y(n;f_1)\right]$$

where

$n = 1, 2, 3.....$

S = Ordinary power spectrum

G = **Hypercoherence function**

F^{-1} = Inverse Fourier transform

Now X' and Y' represent filtered time histories, and include only harmonics (nonlinearly) correlated with the common fundamental frequency. To generate an orbit plot, or phase-plane representation of the two quantities, let

$$Y''(t) = Y(t-\tau)$$

$$\tau = \phi/2\pi f_1$$

$$\Phi = Tan^{-1}\left[Q_{xy}(f_1/C_{xy}(f_1)\right]$$

Q_{xy} = QUADRATURE SPECTRUM

C_{xy} = COSPECTRUM

The time delay, τ, serves as a "key phasor," to initiate the relative phase angle between the two vectors. A phase-plane diagram of the filtered signals is thus obtained by plotting X' versus Y''. The procedure is best illustrated by example. Figure 122a illustrates the orbit plot for two jointly periodic signals, each containing three harmonic components. Figure 122b represents the same plot when uncorrelated noise and independent, coincident pe-

riodic components have been added to each signal. This chaotic pattern is highly representative of hot firing data. Figures 122c and 122d are the recovered orbital diagrams by **hypercoherence filtering** and comb filtering, respectively. The superior performance of **hypercoherence filtering** is clearly indicated.

When compared with available noise cancellation methods, such as time domain averaging (TDA), comb filtering, and adaptive line enhancement, the **hypercoherence filter** has the following two advantages: (1) only the **hypercoherence filter** can reject independent components at the same frequency (while the other noise cancellation methods will pass all data in the pass-band including both true harmonics and independent components); (2) a slight phase drift would be fatal for techniques, such as the TDA method, which require precise phase lock-in. For the **hypercoherence filter**, on the other hand, since only relative phase information is required, slight phase drifting is not as critical. This is significant when considering the small speed variations inherent in turbopump operation, even at a constant power level.

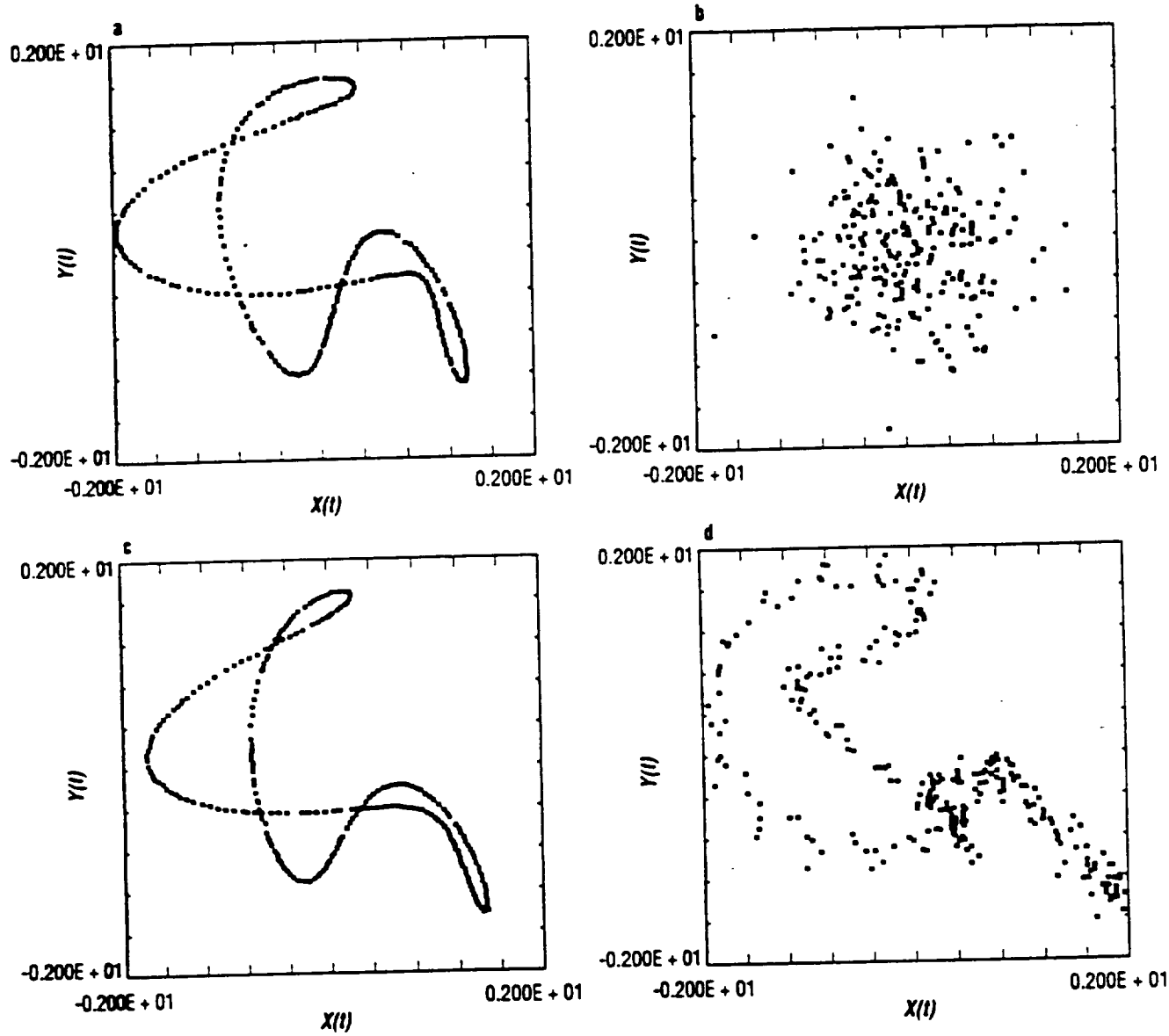

Figure 122. (a) Orbital Diagram of Noise-Free Simulation, (b). Orbital Diagram of Simulation With Additive Gassian White Noise, (c). Recovered Orbital Diagram by Using Hypercoherence Filtering, (d). Recovered Orbital Diagram by Using Comb Filtering

Figures 123a and 123b represent the filtered orbits from measurements at HPFP rad-90° and rad-170° during SSME tests 901-471 and 901-436, respectively. Figure 123a has a smooth orbital motion which represents a well behaved rotational system. Figure 123b, however, indicates a potential rubbing problem. The two locations with sharp cusps appear to indicate possible impact between stationary and rotating system components.

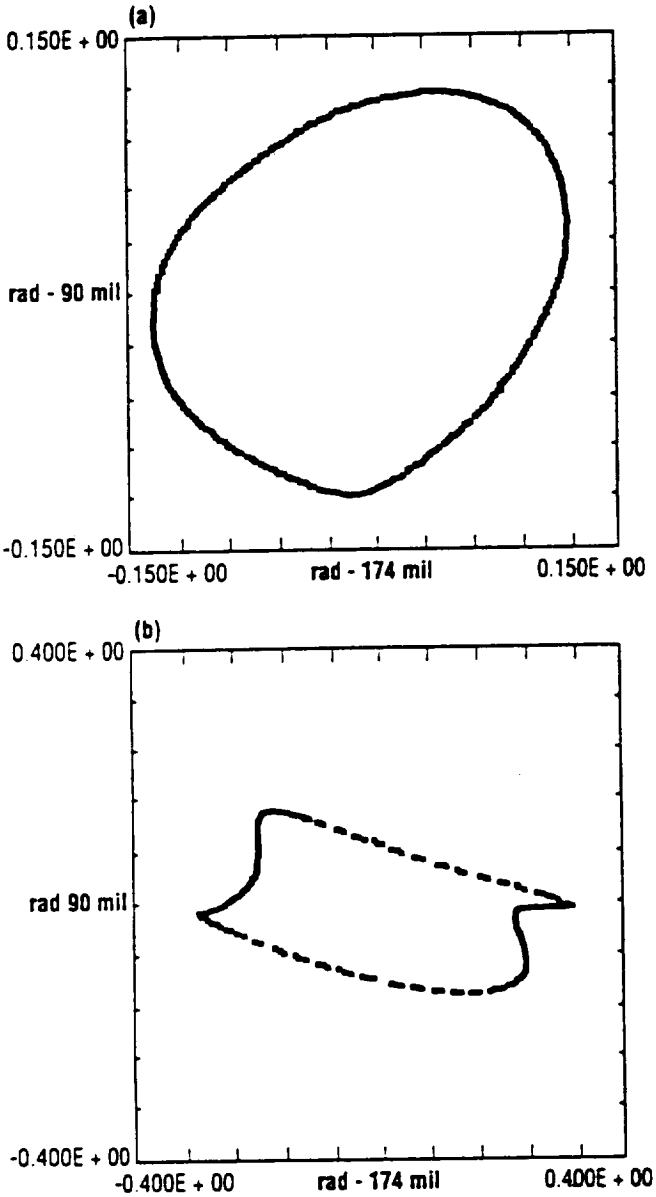

Figure 123. Orbital Plot From Test 901-4T1 by Hypercoherence Filtering, b. Orbital Diagram of 901-436 by Hypercoherence Filtering

The above algorithm is presently operational and has been integrated into the SSME Diagnostic Analysis Package developed by Structures and Dynamics Laboratory.

Coffin, T., and Jong, J.Y., "A Nonlinear Coherence Function and Its Application to Machines Diagnostics," *Journal of the Acoustical Society of America*, Supplement 1, Vol. 78, Fall, 1985.

Jong, J.Y., and Coffin, T., "Diagnostic Assessment of Turbomachinery by the Hypercoherence Method," NASA Conference on Advanced Earth-to-Orbit Propulsion Technology, Marshall Space Flight Center, May, 1986.

Coffin, T., and Jong J.Y., "Some Nonlinear Methods and Their Application To Rocket Engine Diagnostic Evaluation," 1st International Machinery Monitoring and Diagnostic Conference, September, 1989.

J.E. McBride/ED23
(205) 544–1523
Sponsor: Structures and Dynamics Laboratory

Proceedings of the 3rd International Machinery Monitoring & Diagnostics Conference

DECEMBER 9-12, 1991
Riviera Hotel and Convention Center
LAS VEGAS, NEVADA
1991

DIRECTOR:
Dominick J. DeMichele
SOCIETY FOR EXPERIMENTAL MECHANICS, INC.
Kenneth A. Galione, Managing Director
Katherine M. Ramsay, Conference Manager
UNION COLLEGE:
Arnold E.S. Gussin, Dean, Graduate and Continuing Studies

Sponsored by:
Society for Experimental Mechanics, Inc.
Bethel, CT 06801

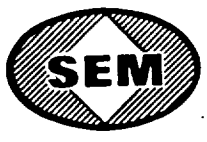

Union College
Schenectady, NY 12308

CORRELATION IDENTIFICATION BETWEEN SPECTRAL COMPONENTS IN TURBOMACHINERY MEASUREMENTS BY GENERALIZED HYPERCOHERENCE

Jen Y. Jong, Thomas Coffin

Wyle Laboratories
Huntsville, Alabama

Jess H. Jones, James E. McBride, Preston C. Jones

National Aeronautics and Space Administration
Marshall Space Flight Center, Alabama

ABSTRACT

In a rotordynamic system, the fundamental shaft rotation can be considered a source which drives other mechanisms and generates new spectral components associated with, say, gear tooth meshing or bearing element passage. The frequency content in measurements from such machinery contains much subtle information concerning system operational condition and component degradation. Measurements on high performance rocket engine turbomachinery suffer from severe noise contamination from fluid flow, combustion processes, structural resonances, etc. It is thus impossible, based on linear spectrum analysis, to determine whether a high level spectral contribution represents a rotational component frequency or an independent noise source. To detect such components, higher order spectrum analysis is required. However, the hierarchy of cumulant spectra (bispectrum, trispectrum, etc.) exist only for frequency permutations where the sum of the arguments vanishes. This does not permit direct estimation of the correlation between arbitrary frequency component pairs. The hyper-coherence function[1,2,3] was developed to detect the correlation between synchronous frequency characteristics and any *harmonic component*. The generalized hypercoherence, described in this paper, permits estimation of the nonlinear correlation between any selected reference frequency (e.g., shaft speed) and an *arbitrary* suspect frequency component. The approach is based on estimating the temporal correlation between the rate of change of instantaneous component phases. Application of the technique to extract component signature characteristics is illustrated with vibration measurements from the space shuttle main engine.

NOMENCLATURE

PSD	Power spectral density function
HC	Hypercoherence
GHC	Generalized hypercoherence
PLL	Phase lock loop
N	Synchronous (shaft rotating) frequency
C	Cage frequency
OBP	Outer ball pass frequency
SYNC	Synchronous frequency component
FM	Frequency modulation
M	Gear tooth number
R	Gear ratio
$f_i(t)$	Instantaneous frequency time signal
p(t)	Instantaneous phase
IF	Instantaneous frequency
SSME	Space shuttle main engine
HPOP	High pressure oxidizer pump

LINEAR AND HIGHER ORDER SPECTRA

Conventional linear spectral analysis[4] has long been used to identify the signal characteristics associated with machinery faults in vibration signature analysis. However, nonlinearities can play a significant role for signature identification. It has been observed that different rotational mechanisms may interact due to some nonlinear process[5,6,7]. When this occurs, coherent phase relationships may exist, which can be identified from response signals. Frequency sum and difference components are one of the commonly observed nonlinear (quadratic) phenomena. A typical example is a synchronous (shaft rotational) frequency component modulated by subsynchronous whirl[2]. Other kinds of nonlinearity include high level harmonic content of synchronous vibration due to waveform clipping from rubbing[3]. All these signals represent nonlinear phenomena since their spectral components at different frequencies are not independent of each other. Due to the lack of phase information, traditional PSD analysis cannot identify such phenomena. Therefore, higher order spectral analysis is required. This analysis includes a hierarchy of cumulant spectra such as auto/cross-bicoherence, tricoherence, etc. Each technique can identify nonlinearities of different order in a random signal and be applied to the particular type of failure mechanism to be detected.

Bispectral analysis can be used to identify the existence of amplitude modulation (quadratic correlation) among spectral components. Enrich and Eshleman[6] have described six analytical models to explain how these modulations may be physically generated. The bispectrum measures the degree of correlation by identifying phase relationship among three spectral components f_1, f_2, f_1+f_2, i.e., frequency sum or difference. It has been applied to identify the quadratic phenomenon of a synchronous frequency component modulated by the cage frequency in a ball bearing and a synchronous component modulated by a 50-percent subsynchronous whirl frequency component[2].

Trispectrum can be used to identify cubic correlation among four spectral components. A special case of its application is to determine whether an apparent PSD sideband structure is really due to modulation or not. Such a sideband structure is another commonly observed nonlinear defect signature. A typical example of this is a bearing cage frequency component periodically exciting a structure natural frequency. In this case, the envelope signal represents the periodic impact motion, and the carrier represents the structural response at a dominant natural frequency. Notice that such a sideband does not satisfy

the frequency sum or difference requirement; therefore, the bispectral analysis is not applicable. Envelope detection by using a Hilbert transform can recover the envelope signal and its PSD since the carrier frequency is shifted to zero frequency in the Hilbert transformation. But it cannot indicate whether this sideband structure is correlated or not.

The harmonic components of a vibration signal contain subtle information about machine condition. Many failure modes, such as misalignment, loose coupling, and rubbing, will generate harmonics. For example, rubbing may cause waveform clipping and generate strong odd harmonics. However, many independent sources may generate a spectral component at the same frequency and appear to be a harmonic. In this case, the hypercoherence[1,3] can identify whether an apparent spectral peak is a harmonic or independent noise. The hyperspectrum represents the joint moment between a spectral component and its harmonics. Hypercoherence (HC), which is the normalized hyperspectrum, can identify the degree of correlation between a reference component and its harmonics.

As discussed above, the spectral components to be identified by higher order spectra are required to satisfy certain frequency combinations (e.g., the sum of arguments is zero). However, in many situations, we wish to identify the correlation between two arbitrary frequency components that do not satisfy any such requirements. The generalized hypercoherence (GHC) was developed to deal with this situation. The GHC can identify the correlation between two arbitrary spectral components in the sense of frequency synchronization or lock-in.

THE GENERALIZED HYPERCOHERENCE

Consider a gear box with gear ratio R as shown in figure 1. The angular displacements (phases) at frequencies N1 and N2 will be proportional to each other, and these two spectral components are correlated in that their phase variations are synchronous. This can be seen by marking a key phasor in each of these two gears to monitor their angular displacement. If key-phasor A goes through one cycle of rotation with angular displacement a(t), then key phasor B will finish R cycle of rotation with angular displacement R•a(t). Their angular displacements will be proportional to each other by factor R. As a result, coherent phase will exist between the spectral components at frequencies N1 and N2. In general, however, the gear ratio R may be an irrational number. Such phase coherence is difficult to identify. To see this, consider the case when the gear ratio is an integer K. In this case, the HC can identify their phase correlation. This is because the ambiguity introduced by the Riemann surface phase wrapping is within an integer multiple of 2π, which does not affect the coherence estimation. However, if the ratio is not an integer, phase wrapping will introduce a noninteger multiple of 2π, which yields ambiguous phase. Therefore, phase correlation cannot be uniquely identified in the phase domain. Based on this observation, the GHC was developed to identify such phase coherence by correlating the rate of change of phase, which is also called the instantaneous frequency. By taking the time rate of change of phase, the ambiguous term is eliminated, and the phase correlation is reflected in the frequency domain as frequency synchronization.

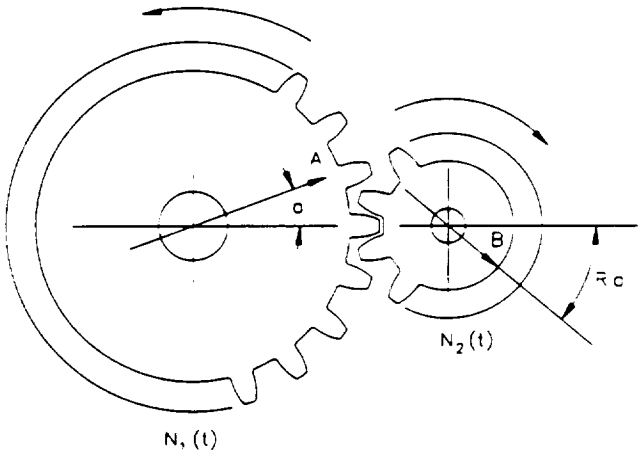

Fig. 1. Gear Box with Gear Ratio R = N_1/N_2. *The rotational frequency components are correlated to each other.*

A vibration signal may be treated as an FM signal with different spectral components at different center (carrier) frequencies. Assume that there is some intelligence being frequency modulated in the signal as the instantaneous frequency about these carriers. To recover the intelligence, we demodulate the FM signal to estimate its instantaneous frequency signal. A narrow-band random process can be modeled as a sine wave with slowly varying amplitude A(t) and phase p(t):

$$x(t) = A(t) \cos [2\pi f_c t + p(t)] \quad (1)$$

The instantaneous frequency $f_i(t)$ is defined by:

$$f_i(t) = \frac{d\, p(t)}{d\, t} \quad (2)$$

Figure 2 shows the block diagram of a FM demodulator by using the Hilbert transform method. The input signal may contain several spectral components (FM signals) at different carrier frequencies. Here, the 90-degree phase shifting is performed through multiplication by locally generated sinusoid and cosine waves (synchronous receiver) at the desired carrier frequency. This will effectively shift the spectral component from the carrier frequency to both zero and two times that frequency. A low-pass filter is then used to remove any high frequency component. The output of the low-pass filters then represent the slowly varying amplitude and phase components that have been frequency translated. The instantaneous frequency signal then can be obtained by:

$$\dot{p}(t) = [u(t)\, \dot{v}(t) - \dot{u}(t)\, v(t)] \,/\, [u^2(t) + v^2(t)] \quad (3)$$

These outputs can be represented as

$$u(t) = A(t) \cos [p(t)]$$
$$v(t) = A(t) \sin [p(t)]$$

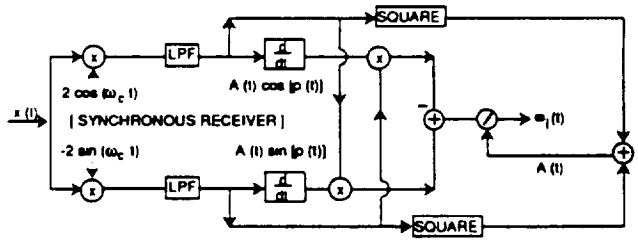

Fig. 2. Hilbert Transform Demodulation Using Synchronous Receiver

Figure 3(a) shows another FM demodulator by using the phase lock loop (PLL)[8] technique. The desired carrier frequency for FM demodulation is determined by the frequency in the Voltage Control Oscillator (VCO) in the feedback loop. The output y(t) of the PLL will be an estimation of the instantaneous frequency. To see this, the PLL can be shown as a nonlinear model in figure 3(b). It can be shown that the phase error signal e(t) tends to drive the PLL into lock. That is, any phase deviation will converge to some steady state operating point. When the PLL is operating in lock, the VCO phase, q(t), is a good estimate of the input phase, p(t). Therefore, the sinusoidal nonlinearity in figure 3(b) can be neglected, since p(t) - q(t) is small, and

$$\sin [p(t) - q(t)] = p(t) - q(t) \tag{4}$$

Therefore, the PLL becomes a typical linear feedback system with transfer function:

$$H(f) = \frac{Y(f)}{p(f)} = \frac{j2\pi f}{1+j2\pi f/K} \tag{5}$$

The loop constant K will control the frequency deviation range (lock range) for the PLL to lock. If K is large, the term $j2\pi f/K$ in equation (5) can be neglected, and the transfer function becomes

$$H(f) = j2\pi f \tag{6}$$

which is the transfer function of a differentiator, d/dt. Therefore, the output signal will be a good estimate of instantaneous frequency.

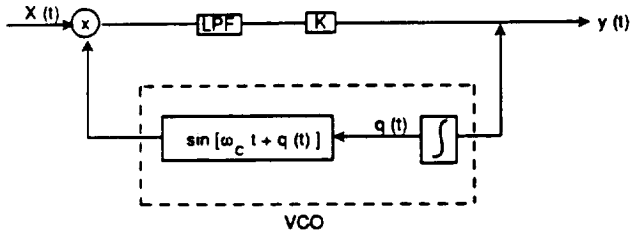

(a) Phase Lock Loop (PLL) FM Demodulator

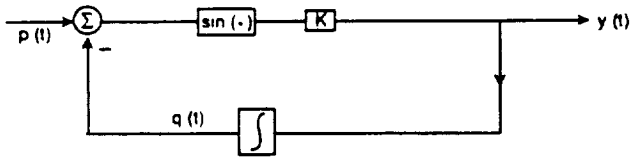

(b) Nonlinear PLL Model

Fig. 3. Schematic of an FM Demodulator

For the purpose of identifying frequency synchronization for machinery diagnostics, imagine that the vibration signal is composed of several FM signals modulated at different carrier frequencies as shown in figure 4. Each component is then passed through an FM demodulator to generate a series of new random signals. Each one represents the instantaneous frequency signal at each carrier frequency. A linear correlator is then used to correlate these signals with a specified reference carrier frequency. Their correlations are then summarized in the frequency domain to generate the GHC.

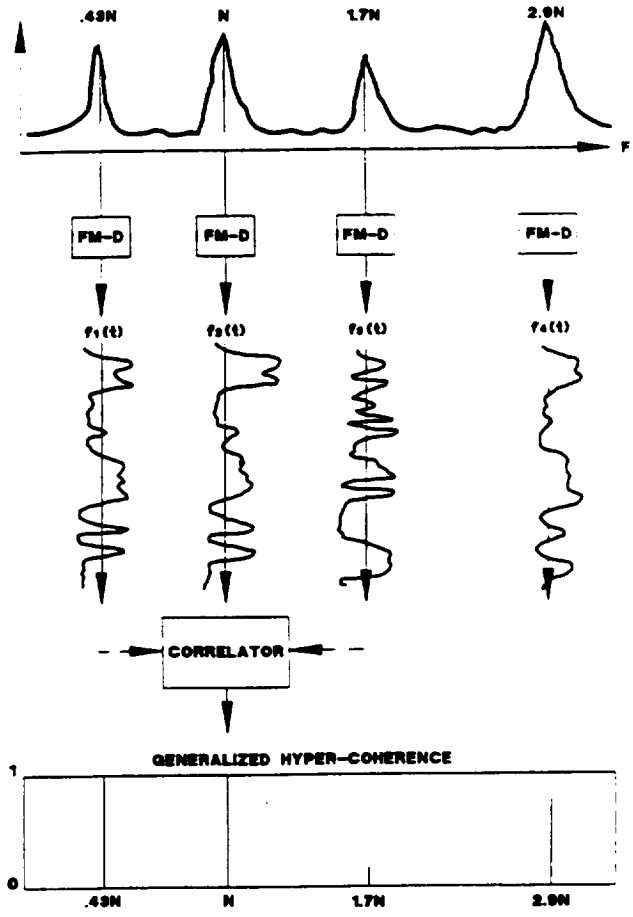

Fig. 4. GHC Through FM Demodulator

A SIMULATION MODEL

A simple simulation is used to demonstrate the GHC. Consider a gear train with 16 and 9 teeth respectively. The first gear is rotating at frequency f, with phase p(t). The angular displacement of these two gears will be proportional by a factor of 1.78. The simulation signal is composed of three spectral components. The first corresponds to the synchronous frequency component of the first gear, i.e., reference frequency. The second one is the SYNC of the second gear at center frequency 1.78 f, with proportional phase 1.78 times p(t). The third represents a component at frequency 1.36 times f with independent phase q(t). Therefore, the third component is uncorrelated with the other two. The reference frequency is at 500 Hz with a sampling rate of 10,240 Hz. A total of 20 seconds of data was generated. Figure 5(a) shows the PSD of the simulation signal with 50 averages of 4096-point FFT blocks. It is composed of three spectral components marked by R, U, and C, which represent the Reference, Uncorrelated, and Correlated component, respectively. Figures 5(c), (d), and (e) show the demodulated instantaneous frequency signal with carrier frequencies set at R, U, and C respectively. Strong correlation or synchronization can be clearly seen between the reference and correlated component while no correlation is indicated with the independent component. The linear correlation between these frequency variations is summarized in figure 5(b).

Also, notice that during this 20-second time period the instantaneous frequency variations are much smaller than the

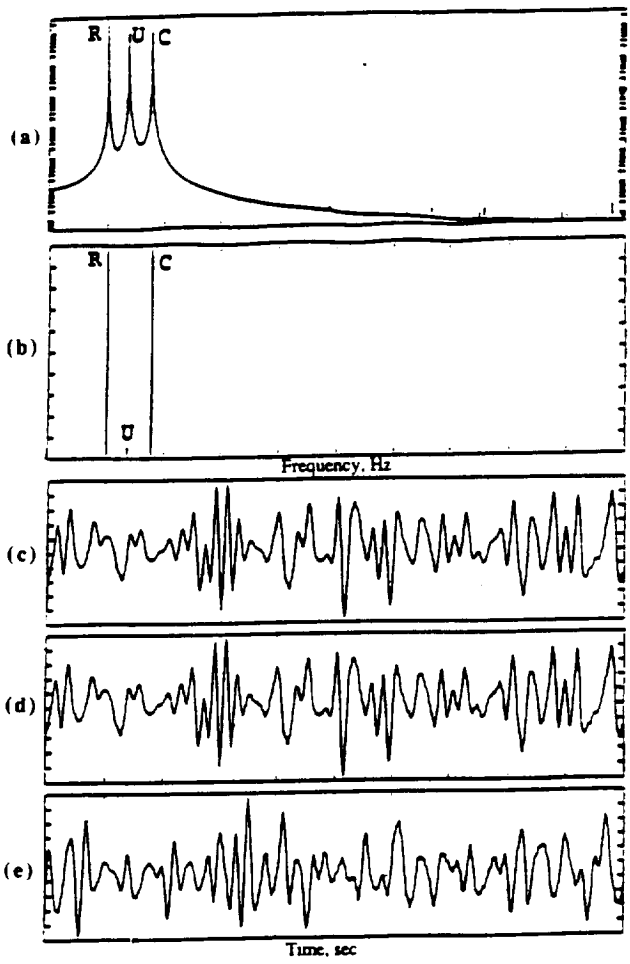

(a) PSD of the simulation signal
(b) GHC of the simulation signal with R as reference
(c) Demodulated frequency signal for R
(d) Demodulated frequency signal for C
(e) Demodulated frequency signal for U

Fig. 5. Illustration of the GHC Method

bandwidth of the PSD estimator which is 2.5 Hz. As shown in figure 5(c), the frequency variation for the reference component is only about 0.015 Hz, which is less than one percent of its PSD frequency resolution. Therefore, frequency tracking from a typical PSD isoplot or its Wigner time-frequency distribution[9] would not provide adequate frequency resolution to identify this synchronization.

APPLICATION TO MACHINE DIAGNOSIS

Synchronous/bearing signature correlation. Figure 6(a) shows the PSD of a strain gauge measurement taken from a SSME High Pressure Oxidizer Pump (HPOP) hot firing test. The peak marked 5.7N is located at 5.7 times shaft frequency N, near the predicted outer ball pass (OBP) frequency and a possible defect indication. However, many independent sources, such as a feedthrough from nearby pump units, confound signature identification. To determine whether this is indeed an outer race defect signature, the GHC analysis was performed to discover whether this 5.7N OBP component is synchronized with the SYNC component. Figures 6(b), (c), and (d) show the instantaneous frequency variation of components N, 5.7N, and an arbitrarily chosen component at 500 Hz. Strong frequency synchronization is identified between components N and 5.7N and no correlation between components N and noise at 500 Hz. This indicates that the 5.7N is a sync-related component and a potential outer race defect signature.

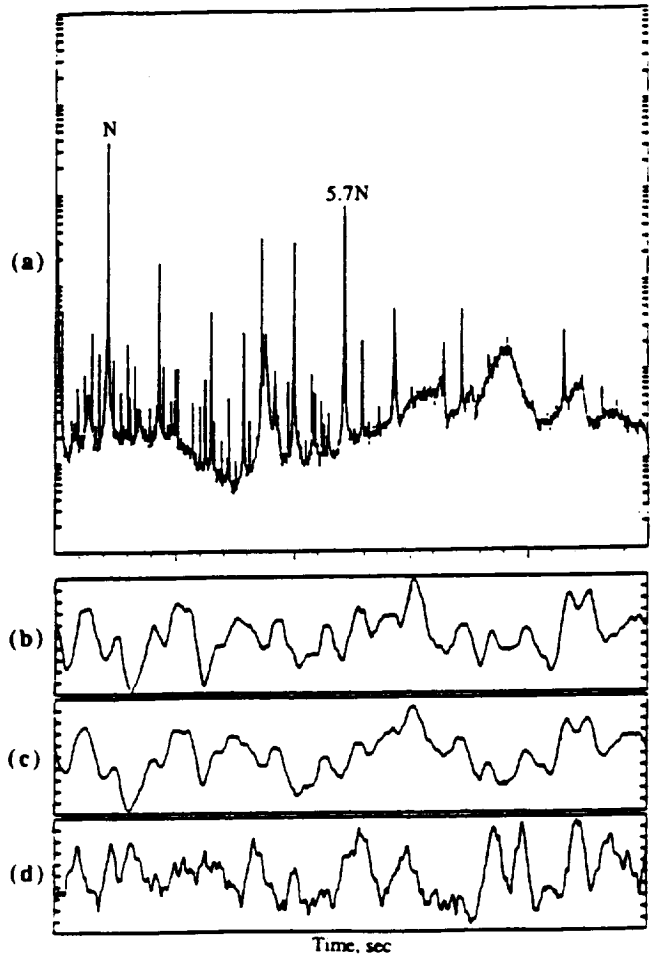

(a) PSD of SSME HPOP internal strain gauge measurement
(b) Frequency signal of N (sync)
(c) Frequency signal of 5.7N (OBP)
(d) Frequency signal of a component at 500 Hz

Figure 6. Correlation Detection by GHC

Identification of composite modulation. The GHC technique can also be applied to identify a more complicated modulation signal, the so-called "composite-modulation" phenomenon. As noted above, the bispectrum is useful for identifying the correlation between a "carrier" frequency and a modulating component signal. However, it has been observed that modulation may exist between a harmonic of the shaft speed and a harmonic of a subsystem frequency without these harmonics showing up in the linear PSD. In such cases, direct (nonlinear) spectrum analysis is impractical. This composite-modulation phenomenon was observed in SSME vibration measurements associated with a bearing element defect as shown in figure 7. This PSD is taken from the SSME HPOP internal bearing strain gauge measurement during a hot firing test. The peaks marked N, 2N, 4N, etc., are the synchronous frequency component and its harmonics. The other peaks marked C and 2C are the bearing cage frequency components and are considered normal in such internal measurements. However, a

strong anomalous component marked A is observed around frequency 8.5N. To assess this anomaly, we need to determine whether it is correlated with the cage or the sync frequency component.

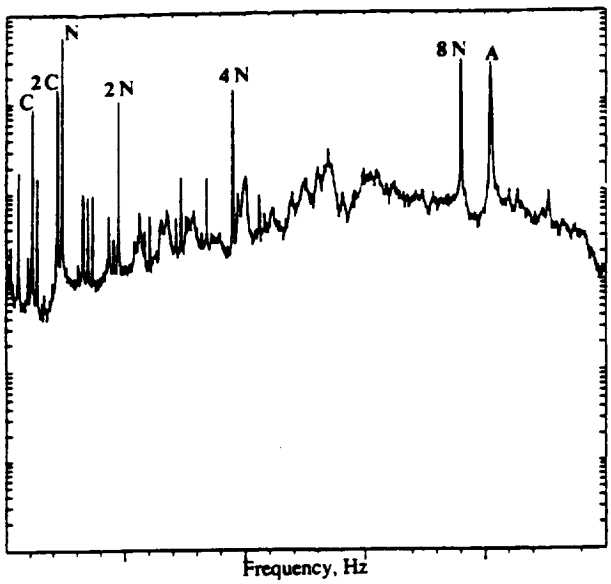

Fig. 7. Strain Gauge Measurement Showing Anomalous Component A at 8.5N

By examining the frequencies of these components, it is observed that the 8.5N is equal to 14N-12C, or 12(N-C) + 2N. This implies that the 8.5N component might be caused by the modulation between the inner ball pass component (for a 12-ball bearing set), which is at frequency 12(N-C), and the second harmonic of SYNC at 2N. In other words, this could be a composite-modulation. If the existence of such modulation can be proven, then the anomalous 8.5N component would represent a bearing-related signature. However, the spectral components at 14N, 12C, and 12(N-C) are not shown in the PSD. Therefore, the bispectrum or trispectrum cannot identify such composite-modulation. Notice that, for this particular case, the ninth order cumulant spectrum at frequencies

2N, 4N, 8N, -2C, -2C, -2C, -2C, -2C, -2C

should be able to identify this modulation since the PSD shows spectral components at frequencies 2N, 4N, 8N, and 2C. However, whenever multiple phase components are summed, the effect of noise will accumulate while that of signal will not because of the Riemann surface phase wrapping. As a result, such noise expansion effect at this high order will smear the coherent phase information and make it difficult to identify any significant coherence value.

Such noise growth in the phase domain will not exist in the instantaneous frequency domain. Thus, we can identify the composite modulation by simply matching the appropriate integer multiple of each instantaneous frequency signal corresponding to each modulating component. In this example, the carrier frequency of the FM demodulator is tuned to the cage frequency C, the SYNC frequency N, and the anomalous frequency A to generate their IF signal as shown in figures 8(a), (b), and (d). Figure 8(c) shows the summation of 12 times the IF signal of C and 14 times the IF signal of N. Theoretically, this composite IF signal should be equal to the IF signal at frequency 14N-12C due to modulation of 14N and 12C. Compare this to figure 8(d), which is IF of the anomalous component A. Strong correlation can be identified between them. Figure 9 shows the same information over a longer time period. Therefore anomaly A turns out to be SYNC- and cage-related component likely being generated from the modulation of the inner ball pass frequency at 12(N-C) and 2 times SYNC at 2N.

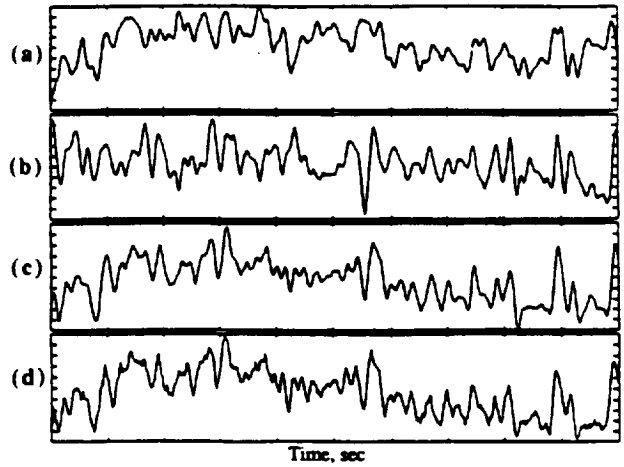

(a) Frequency signal of C (cage)
(b) Frequency signal of N (sync)
(c) Summation of 12 times the IF signal of C and 14 times the IF signal of N
(d) Instantaneous frequency signal of A (anomaly)

Fig. 8. Detection of Composite Modulation

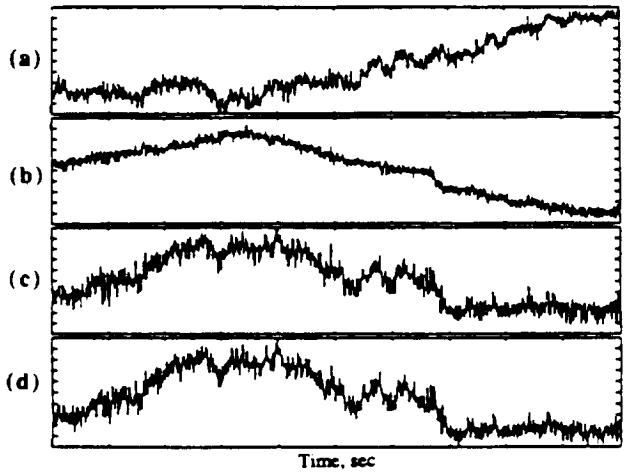

Fig. 9. Same as Fig. 8 Except for Over Long Time Period

The IF signal reflects the micromotion of a vibration spectral component. Therefore, any independent interference will disrupt such micro-information. Thus, any bearing contact angle variation or ball slippage will disrupt such frequency correlation. This can be seen in figures 8(a) and (b) where no significant correlation can be identified between the IF signal of SYNC and cage components.

CONCLUSIONS

By estimating the instantaneous frequency (IF) signal of a narrow-band spectral component, the GHC can be used to

identify the nonlinear correlation among arbitrarily chosen frequency components. This method is especially useful for machinery diagnostics, in which case a driving source generates many frequency components that may be severely contaminated with noise. In addition, the IF signal reflects the microfrequency variation for a seemingly stationary spectral component. It can identify frequency variations much smaller than the frequency resolution of a conventional PSD estimator or even that of a maximum entropy PSD estimator or obtained using the Wigner distribution. The GHC method should provide a useful addition to the tools available for the difficult task of machinery fault detection and identification.

ACKNOWLEDGEMENT

The methods presented herein were developed in support of the National Aeronautics and Space Administration, Marshall Space Flight Center, under contract NAS8-38156.

REFERENCES

1. Jong, J. Y., and Coffin, T., "A Nonlinear Coherence Function and Its Application to Machine Diagnostics," 110th Meeting of the Acoustical Society of America, Nov. 1985.

2. Coffin, T., and Jong, J. Y., "Signal Detection Techniques for Diagnostic Monitoring of Space Shuttle Main Engine Turbomachinery," Wyle Laboratories' final report under NASA contract NAS8-34961, Feb. 1986.

3. Jong, J. Y., and Coffin, T., "Diagnostic Assessment of Turbomachinery by the Hyper-coherence Method," NASA Conference Publication CP2436, May 1986.

4. Bendat, J. S., and Piersol, A. G., *Engineering Application of Correlation and Spectral Analysis.*, John Wiley & Son, 1980.

5. Collacott, R. A., *Mechanical Fault Diagnosis and Condition Monitoring*, Chapman and Hall, London, 1977.

6. Eshleman, R. L., "The role of sum and difference frequencies in rotating machinery fault diagnosis," 2nd Internat'l Conf. on Vibration in Rotating Machinery, Churchill College, 1980.

7. Bendat, J. S. *Nonlinear System Analysis and Identification*, John Wiley & Son, New York, 1990.

8. Taub, H., and Schilling, D. L., *Principles of Communication Systems*, McGraw-Hill, New York, 1971.

9. Claasen, T., and Mecklenbrauker, W., "The Wigner Distribution—A tool for time frequency analysis," *Philips J. res.*, Vol. 35, 1980, pp. 217.

TECHNICAL PROGRESS REPORT

December 1991

DATA ANALYSIS AND DIAGNOSTIC EVALUATION OF SPACE SHUTTLE MAIN ENGINE DYNAMIC MEASUREMENTS

NASA CONTRACT NO. NAS8-38156

Prepared for

NATIONAL AERONAUTICS AND SPACE ADMINISTRATION
GEORGE C. MARSHALL SPACE FLIGHT CENTER
MARSHALL SPACE FLIGHT CENTER, ALABAMA 35812

by

WYLE LABORATORIES

WYLE ENGINEERING DIVISION
7800 Governors Drive, West
Huntsville, Alabama 35807

WYLE TECHNICAL REPORT TR-60900-91-12

WYLE

Program Manager: T. Coffin
Contract Manager: J. Kelly

NASA

Contract Monitor: J. McBride
Contracting Officer: H. Amburn

TIME-FREQUENCY REPRESENTATION OF NONSTATIONARY SIGNALS VIA THE MODIFIED WIGNER DISTRIBUTION

Jen Y. Yong, Thomas Coffin
Wyle Laboratories, Huntsville, AL

Thomas F. Zoladz, Jess H. Jones
NASA, Marshall Space Flight Center, AL

ABSTRACT

This report presents a new signal analysis tecnhique called the Modified Wigner Distribution (MWD). The MWD has been developed for the Structures and Dynamics Laboratory at MSFC by Dr. Jen-Yi Jong of Wyle Laboratories. The new signal processing tool has proven very successful in resolving time-frequency representations of highly nonstationary multicomponent signals in both simulation and trials involving Space Shuttle Main Engine (SSME) high frequency data. The MWD departs from the classic Wigner Distribution (WD) in that it effectively eliminates the cross coupling among positive frequency components in a multiple component signal. This attribute of the MWD, which prevents the generation of "phantom" spectral peaks, will undoubtedly increase the utility of the Wigner Distribution for real world signal analysis applications which more often than not involve multicomponent signals.

TECHNICAL PAPER

TIME-FREQUENCY REPRESENTATION OF A HIGHLY NONSTATIONARY SIGNAL VIA THE MODIFIED WIGNER DISTRIBUTION

I. INTRODUCTION

This report describes and evaluates a new signal processing technique called the modified Wigner distribution (MWD) used for the spectral analysis of highly nonstationary multicomponent signals. The regular Wigner distribution (WD) is capable of providing high resolution time-frequency estimates of nonstationary signals which are common in many fields including the dynamic response of rotating machinery. A traditional tool for such analysis has been the short-time Fourier transform (STFT), commonly referred to as "overlap" processing, which is obtained by applying a fixed-length moving time window to nonstationary data prior to performing the fast Fourier transform (FFT). However, if spectral components within the signal vary considerably in frequency during the time window, the STFT often fails in providing enough frequency resolution to identify key time-frequency spectral characteristics.

The WD was originally introduced in 1932 by E. Wigner.[1] It received little attention until 1980 when Claasen and Mecklenbrauker[2] presented a comprehensive three-part paper describing the utility of the WD as a tool for time-frequency analysis of nonstationary signals.

Major obstacles arise in the direct use of the WD. Most notable of these problems are aliasing and the generation of artifacts or "phantom" spectral peaks in the resultant time-frequency distribution. A number of attempts, with varying degrees of success, have been employed to minimize these effects.[3–5] This paper presents yet another approach. With the introduction of the "smart window," this approach will hopefully overcome these obstacles.

The MWD will have important application in turbomachinery diagnostic analysis. It is particularly suited to those turbomachinery operations which are highly transient, i.e. during startup or ramping conditions. It can also be an important diagnostic tool in failure analysis where the dynamic signals are highly nonstationary.

II. THE WIGNER DISTRIBUTION

The WD is a powerful tool in determining the time-frequency characteristics of a highly nonstationary signal. The technique has been applied successfully in the identification of abnormal machine operating states through vibration signal analysis.[3] Other applications of the WD include the analysis of time-varying spectra in optics, speech, sonar, and seismic signal processing.

The WD of a real signal $r(t)$ is given by:

$$W(t,f) = \int z(t+\tau/2)\, z^*(t-\tau/2)\, e^{j2\pi f\tau}\, d\tau \ , \qquad (1)$$

C-2.

where $z(t)$ is the analytic signal of $r(t)$, $z(t) = r(t) + j\,i(t)$, and $i(t)$ is the Hilbert transform (HT) of $r(t)$, $i(t) = \mathrm{HT}\{r(t)\}$. Let the absence of limits on the integral symbol denote the interval $(-\infty, \infty)$. In equation (1), $z^*(t)$ represents the complex conjugate of the analytic signal $z(t)$. Therefore, the WD is the Fourier transform (FT) of the product between the original forward signal and corresponding backward signal both centered at time t. If the frequency of a subject narrowband signal is either monotonically increasing or decreasing within its time window, the product of this forward and backward signal will provide frequency cancellation, and, as a result, will estimate a frequency corresponding to the signal frequency at the center of the time window. However, the product in equation (1), which serves as the kernel of the FT, introduces a frequency summing effect. Taking a real single component signal with a discrete component at f_o as an example, the summing effect produces a peak in the WD spectrum at $2f_o$. For this reason, equation (1) scales the subject time signal by two. However, this scaling is only aesthetic and does not relax sampling constraints on the time signal. If $2f_o$ is greater than the original Nyquist frequency (determined when the subject time signal was originally sampled) aliasing within the WD spectrum will occur. For this reason, an analytic signal is used in equation (1) since it has no energy at negative frequencies. Aliasing due to the frequency summing effect can now be avoided, and, in addition, frequency difference effects (coupling between positive and negative frequency components) are eliminated. Essentially, use of the analytic signal in equation (1) returns the sampling rate constraint for a subject time signal back to its original Nyquist rate.

Prior to introducing the MWD, sample graphical illustrations of the WD for cases involving simple sinusoids will be presented. In the examples, the WD's will be processed through convolution in the frequency domain since this format conveys the frequency summing and difference effects well.

Before developing case I of the WD, equation (1) will be simplified into a convenient form representing convolution in the frequency domain. Taking the original equation and replacing $\tau/2$ with τ, gives

$$W(t,f) = \int z(t+\tau)\; z^*(t-\tau)\; e^{j2\pi f\tau}\, d\tau \;. \tag{2}$$

Note, with removal of $\tau/2$ from the WD equation, f now represents twice the actual frequency of spectral components contained in the original time signal. To simplify further evaluation, one should just consider one cross section of the WD at $t = t_o$

$$W(t_o,f) = \int z(t_o+\tau)\; z^*(t_o-\tau)\; e^{j2\pi f\tau}\, d\tau \;. \tag{3}$$

Letting

$$x(t) \equiv z(t_o+\tau)$$

$$y(t) \equiv z^*(t_o-\tau) \;.$$

Equation (3) can be viewed as the FT of the product $x(t)y(t)$

$$W(t_o,f) = FT\{x(t)y(t)\} \;. \tag{4}$$

The FT of the product $x(t)y(t)$ can also be viewed as a convolution in the frequency domain. Given that

$$x(t) \Leftrightarrow X(\alpha)$$

$$y(t) \Leftrightarrow Y(\alpha)$$

where $\Leftrightarrow$ denotes FT pair.

Equation (4) can now be written as the convolution

$$W(t_o,f) = \int X(\alpha)Y(f-\alpha)\, d\alpha \ . \qquad (5)$$

This form of the WD will be used in the following graphical evaluations.

WD CASE I: ANALYTIC SIGNAL CONTAINING SINGLE SINUSOID

For this case, the real signal is a single sinusoid at frequency f_o

$$r(t) = \cos(2\pi f_o t) \ .$$

The imaginary portion of the analytic signal, $z(t)$, is calculated through the HT of the real signal

$$i(t) = \mathrm{HT}\{\cos(2\pi f_o t)\} = \sin(2\pi f_o t) \ .$$

The analytic signal, $z(t)$, now becomes

$$z(t) = \cos(2\pi f_o t) + j \sin(2\pi f_o t) = e^{j2\pi f_o t} \ .$$

The complex conjugate of $z(t)$ is

$$z^*(t) = e^{-j2\pi f_o t}$$

and

$$z^*(-t) = e^{j2\pi f_o t}$$

Moreover, the FT of both $z(t)$ and $z^*(-t)$ is a delta function shifted by f_o.

$$\mathrm{FT}\{e^{j2\pi f_o t}\} = \delta(f-f_o)$$

This sample case is now in proper form with respect to equation (4), with

$$x(t) = z(\tau) \ ,$$

$$y(t) = z^*(-\tau) \ , \qquad (t_o = 0)$$

and

$$X(f) = \delta(f-f_o)$$

$$Y(f) = \delta(f-f_o) \ .$$

With $t_o = 0$, equation (5) can be written as a function of frequency only

$$W(f) = \int X(\alpha)\, Y(f-\alpha)\, d\alpha \ , \qquad (6)$$

and the WD for case I can now be developed graphically (fig. 1) through convolution in the frequency domain.

The left-hand side of figure 1 displays the translation of the $Y(-\alpha)$ spectrum during the convolution process defined by equation (6). The right-hand side of the figure shows successive contributions to the WD spectrum as the frequency, f, varies during the convolution. For this case involving the analytic signal of a single sinusoid, a contribution to $W(f)$ is made only when $f = 2f_o$. Remembering that f now represents twice the actual frequency of spectral components contained in the original time signal, f must be scaled by $1/2$ to yield a correct frequency value. In this case, the true frequency would be $2f_o/2$, or f_o, which is the expected result.

WD CASE II: ANALYTIC SIGNAL CONTAINING MULTIPLE SINUSOIDS

For this case, the real signal is composed of two sinusoids at frequencies of f_1 and f_2

$$r(t) = \{\cos(2\pi f_1 t) + \cos(2\pi f_2 t)\}$$

This case is identical to WD case I except that the real signal contains two discrete components. Using the same method of reduction as in the previous case yields

$$X(f) = \delta(f-f_1)+\delta(f-f_2) \ ,$$

$$Y(f) = \delta(f-f_1)+\delta(f-f_2) \ .$$

Again, using equation (6), the WD for case II can be developed graphically (fig. 2) through convolution in the frequency domain.

As in figure 1, the left-hand side of figure 2 displays the translation of the $Y(-\alpha)$ spectrum during the convolution defined by equation (6), and, the right-hand side shows successive contributions to the WD spectrum as the frequency, f, varies. Since the original time signal contains multiple discrete components, peaks in the WD spectrum are generated when $f = 2f_1$ and $f = 2f_2$. Again, scaling by $1/2$ yields the correct frequency representations of the spectral components. However, in this case, the WD spectrum also exhibits a contribution at $f = f_1+f_2$. This contribution is due to cross term coupling between the components at f_1 and f_2. This coupling is displayed in figure 2 where the peaks b and c of the $X(\alpha)$ spectrum line up with peaks c and b of the $Y([f_1+f_2] - \alpha)$ spectrum. This cross coupling effect contributes a peak to the WD spectrum at the frequency $[f_1+f_2]$. After scaling, this false peak would appear in the WD spectrum at a frequency of $[f_1+f_2]/2$.

Generation of false peaks due to cross coupling effects severely limits the practical application of the WD since few real world signals are single component. As shown in the previous

example, use of the conventional WD in developing time-frequency representations of multicomponent signals, even with the use of an analytic signal, introduces erroneous spectral components. These "phantom" peaks only confuse the resulting WD spectrum.

III. THE MODIFIED WIGNER DISTRIBUTION

In order for the WD to perform as a practical tool in the time-frequency analysis of multicomponent signals, unwanted erroneous spectral components due to cross coupling among both negative, and most notably, positive frequency components in these signals must be eliminated. The MWD accomplishes this. Thus, the superior time-frequency resolution of the WD can be attained without the generation of "phantom" spectral peaks.

For a cross section of the time-frequency representation of a real signal $r(t)$, at $t = t_o$, the MWD is introduced and is defined by:

$$M(t_o,f) = \int \mathbb{W}(\alpha - f/2)\, X(\alpha)\, Y(f-\alpha)\, d\alpha \quad , \tag{7}$$

where

$$x(t) \equiv r(t_o+t) \quad ,$$

$$y(t) \equiv r(t_o - t) \quad ,$$

and

$$X(f) \Leftrightarrow x(t) \quad ,$$

$$Y(f) \Leftrightarrow y(t) \quad .$$

As equation (7) suggests, the MWD is evaluated in the frequency domain using the FT's of a real time signal centered at t_o and its respective reversed signal also centered at t_o.The central trait of the MWD which separates the new technique from the traditional WD is its smart frequency window function, $\mathbb{W}(f)$. Use of this window function eliminates the cross coupling of positive frequency components. This in turn prevents erroneous spectral peaks from entering the MWD time-frequency representation during the evaluation of a multicomponent signal. Moreover, use of the smart window, $\mathbb{W}(f)$, eliminates cross coupling between positive and negative frequency components by preventing their interaction during the evaluation of the MWD. There are some limitations on the use of the smart window, and they will be discussed later. The MWD does not rely on the use of the analytic signal of the subject time signal; thus, the HT of the original time signal is no longer necessary. Finally, since the MWD is evaluated in the frequency domain, aliasing due to the frequency summing effect is avoided.

As with the WD, the evaluation of the MWD will also be illustrated graphically. Where the WD was reduced to a more convenient form representing convolution in the frequency domain to simplify its graphical presentation, the MWD is actually evaluated through convolution in the frequency domain. The graphical evaluations of MWD's which follow include the same two cases which were presented for the WD. MWD case I develops the spectrum for a real signal containing a single sinusoid while MWD case II evaluates a real signal containing multiple sinusoids.

Using equation (7), MWD cases I and II can be developed graphically through convolution in the frequency domain.

MWD CASE I: REAL SIGNAL CONTAINING SINGLE SINUSOID

The real signal to be evaluated is a single sinusoid at frequency f_o

$$r(t) = \cos(2\pi f_o t) \ .$$

The required time signals centered at t_o are

$$x(t) = \cos\{2\pi f_o(t_o+t)\} \ ,$$

$$y(t) = \cos\{2\pi f_o(t_o-t)\} \ .$$

To simplify the evaluation, let $t_o = 0$, yielding

$$x(t) = \cos\{2\pi f_o(+t)\} \ ,$$

$$y(t) = \cos\{2\pi f_o(-t)\} \ .$$

Fourier transformation of $x(t)$ and $y(t)$ gives $X(f)$ and $Y(f)$

$$X(f) = \delta(f-f_o)+\delta(f+f_o) \ ,$$

$$Y(f) = \delta(f+f_o)+\delta(f-f_o) \ .$$

$X(f)$ and $Y(f)$ are equivalent with both frequency representations consisting of two delta functions, one delta function being shifted along the positive frequency axis by f_o and the other shifted along the negative frequency axis by f_o. Using equation (7), the MWD for case I can be developed graphically (fig. 3).

Figure 3 is essentially the same as figure 1 which displays the development of the WD for a signal containing a single discrete component. However, since the MWD operates on real signals, the $X(\alpha)$ and $Y(\alpha)$ spectra also contain negative frequency components. Moreover, figure 3 introduces the smart window function, $W(f)$. The window function is a gate in the frequency domain of unity amplitude which translates along the dummy variable (α) axis at one half the rate of the $Y(-\alpha)$ spectrum translation during the convolution. The window, as shown in figure 3, has a width in frequency of 2m. This width parameter is almost inconsequential in the processing of single component signals such as in this case, but a proper window width is very critical in the evaluation of multicomponent signals. As previously stated, the window, $W(f)$, eliminates cross coupling between positive and negative frequency components by preventing their interaction. Moreover, it eliminates interaction between components in a multicomponent signal. The window function's influence on a multicomponent signal will be discussed in MWD case II. For a single component signal, unwanted cross coupling would have contributed a false spectral peak at zero frequency; however, the gating action provided by the window function prohibits this coupling.

For this case involving a real signal containing a single sinusoid, a contribution to the MWD spectrum, $M(f)$, is made only when $f = 2f_o$. Notice, that when the $Y(-\alpha)$ spectrum has translated

along the α axis by $2f_o$, the window function, $\mathbb{W}(f)$ has translated by a frequency of one half of $2f_o$, or, f_o. This positioning of the window function permits the desired coupling which only provides a contribution to the MWD spectrum at $f = 2f_o$. Again, this f must be scaled by 1/2 to yield a correct frequency value. This yields the expected frequency of f_o.

MWD CASE II: REAL SIGNAL CONTAINING MULTIPLE SINUSOIDS

In this case, the real signal consists of two sinusoids at frequencies of f_1 and f_2

$$r(t) = \{\cos(2\pi f_1 t) + \cos(2\pi f_2 t)\} \ .$$

This case is identical to MWD case I except that the real signal now contains two discrete components. Similar simplification as in the previous case yields the frequency representations of the time signals $x(t)$ and $y(t)$ with

$$X(f) = \delta(f-f_2) + \delta(f-f_1) + \delta(f+f_1) + \delta(f+f_2) \ ,$$

$$Y(f) = \delta(f+f_2) + \delta(f+f_1) + \delta(f-f_1) + \delta(f-f_2) \ .$$

With these frequency representations, the MWD for case II can be developed graphically (fig. 4) using equation (7).

As in the previous example, figure 4 shows how the positioning of the window function allows desired couplings which in turn make correct contributions to $M(f)$. These couplings result in peaks at the frequencies $2f_1$ and $2f_2$ in the final MWD spectrum. However, the key feature of the MWD, which separates it from the conventional WD, is its ability to eliminate the cross coupling of positive frequency components. This is shown in figure 4 when f = f_1+f_2. At this value of f, notice that the components b and c of the $X(\alpha)$ spectrum line up with peaks c and b, respectively, of the $Y([f_1+f_2]-\alpha)$ spectrum. This is a graphic representation of cross coupling between positive frequency components. This cross coupling is eliminated by the positioning of the frequency window. Notice how the smart window is positioned between the components c and b in the $Y([f_1+f_2]-\alpha)$ spectrum thereby preventing cross coupling. In this situation, the width of the frequency window is critical since too wide a window would permit cross coupling. For this reason, the frequency resolution of the MWD in differentiating spectral peaks is governed by the window function, $\mathbb{W}(f)$. In figure 4, if $[f_2-f_1]$ were less than the window width, 2m, cross coupling between positive frequency components would occur and erroneous peaks would be contributed to the MWD spectrum just as in WD case II.

IV. IMPLEMENTATION OF THE MODIFIED WIGNER DISTRIBUTION IN DIGITAL FORMAT

Before developing a digital representation of the MWD, its general form given by equation (7) will be simplified. Starting with equation (7)

$$M(t_o,f) = \int \mathbb{W}(\alpha - f/2)\, X(\alpha)\, Y(f-\alpha)\, d\alpha \ , \qquad (7)$$

where

$$x(t) \equiv r(t_o+t) \ ,$$

$$y(t) \equiv r(t_o-t) \ ,$$

and

$$X(f) \Leftrightarrow x(t) \ ,$$

$$Y(f) \Leftrightarrow y(t) \ .$$

Again, equation (7) defines a cross section of $M(t,f)$ at $t = t_o$. By defining

$$\beta = (f/2) - \alpha \ ,$$

equation (7) becomes

$$M(t_o,f) = -\int \mathbb{W}(-\beta)\, X([f/2] - \beta)\, Y([f/2] + \beta)\, d\beta \ . \tag{8}$$

Letting $f' = (f/2)$ yields

$$M(t_o,f') = -\int \mathbb{W}(-\beta)\, X(f'-\beta)\, Y(f'+\beta)\, d\beta \ . \tag{9}$$

Since the window function is symmetric, $\mathbb{W}(-\beta) = \mathbb{W}(\beta)$ and equation (9) becomes

$$M(t_o,f') = -\int \mathbb{W}(\beta)\, X(f'-\beta)\, Y(f'+\beta)\, d\beta \ . \tag{10}$$

Finally, by letting $\gamma = -\beta$, and by invoking symmetry of the frequency window once again, the MWD representation becomes

$$M(t_o,f') = \int \mathbb{W}(\gamma)\, X(f'+\gamma)\, Y(f'-\gamma)\, d\gamma \ . \tag{11}$$

Note, that in this form, the MWD represents a frequency which no longer needs scaling. Moreover, equation (11) is in a form conducive to digital implementation. The digital form of equation (11) is

$$M(k) = \sum_{i=-m}^{+m} X(k+i)\ Y(k-i) \ , \tag{12}$$

where $X(k)$ is the discrete Fourier transform (DFT) of a subject real time series, $x(n)$, centered at t_o, and $Y(k)$ is the DFT of $y(n)$, the reversal of $x(n)$, also centered at t_o. $M(k)$ represents the discrete MWD spectrum of a time signal centered at t_o, and the summation limits in equation (12) constitute the smart window function. Since $y(n)$ is the reversal of $x(n)$, it can easily be proven that,

$$Y(k) = X^*(k)\, W_N^{-k} \ . \tag{13}$$

where

$$W_N \equiv e^{-j(2\pi/N)} \ .$$

N denotes the number of discrete values in the time history used in calculation of the spectrum with n serving as a position index. Finally, by combining equation (13) and (12), the final form of the digital representation of the MWD is attained

$$M(k) = \sum_{i=-m}^{+m} X(k+i)\, X^*(k-i)\, W_N^{-(k-i)} \quad . \tag{14}$$

Equation (14) states that the evaluation of the MWD at frequency k is simply the sum of the left-hand side and right-hand side of a signal's FFT spectrum, $X(k)$, with both sides centered at frequency k, modified by a phase correction term of unity amplitude. Note, that when no window is applied ($m = 0$), the MWD reduces to a special form with an amplitude equal to the power spectral density (PSD) but modified by a phase term.

V. WIGNER AND MODIFIED WIGNER DISTRIBUTION EXAMPLES

In order to test the capability of the MWD in extreme situations, a simulated sine wave varying linearly in frequency at a rate of ~400,000 Hz/s was processed using both the traditional STFT method and the MWD. Figure 5 shows the STFT isoplot (logarithmic in amplitude) of a sine wave whose frequency first decreases then increases rapidly at this rate within 25 ms. The sampling frequency in this case is 10,240 Hz, and the length of the moving time window is 12.5 ms (corresponding to 128 discrete data points) with 20 Hanning windows applied. Use of the Hanning window makes the effective time window approximately 3 ms. As seen in figure 5, the STFT produces a very broad spectral peak since the frequency of the component varies considerably during each window. However, figure 6 shows the superior frequency resolution gained by the MWD (equation (14)) in processing the same simulated signal. Figure 7 shows the block of raw time data used in determining the first spectrum of the isoplots in figures 5 and 6. Along with this raw time signal, figure 7 also identifies the actual input simulated frequency at time 0.00625 s, the center of the first block of data. This frequency, 2,550 Hz, will serve as the benchmark in comparing the accuracy of the spectra generated by the STFT and MWD. Figure 8 shows the first spectra of figures 5 and 6 in linear format. The increased frequency resolution attained by the MWD is readily apparent. Moreover, the MWD is much more accurate in estimating the actual signal frequency at the center of the time window. While the STFT overestimated this frequency by 110 Hz, the MWD estimation was within 40 Hz. Again, this increased accuracy can be attributed to the frequency cancellation effect inherent to the MWD. Notice in figure 6 that, during the turn in frequency of the single component signal, lobing on the inside turn of the time-frequency representation becomes prominent since the frequency cancellation effect inherent to the MWD is limited during this extreme transitional period in which the signal is neither monotonically increasing or decreasing.

The isoplot of figure 9 has been developed through the STFT of a simulated sine wave whose frequency and amplitude both varied rapidly within the 400 ms of activity displayed. The length of the moving time window in the STFT is 25 ms with a sampling frequency of 10,240 Hz. Within the span of each time window, the frequency of the simulated sine wave changes approximately 300 Hz. For this reason, STFT of the signal produces a very broad spectral peak. Figure 10 shows the conventional WD spectrum for the same signal processed using the same parameters as the STFT. The increased frequency resolution relative to figure 9 is very evident. Figure 11 shows the correspond-ing MWD spectrum for the signal, which, in this case, provides just as much frequency resolution as the WD.

As shown in the previous figures, relative to traditional techniques, both the WD and MWD provide increased frequency resolution for a single component signal. However, this is not the case

in the evaluation of multiple components signals. Figure 12 shows the STFT isoplot of a simulated signal composed of two sine waves. As before, the frequencies and amplitudes of the discrete components are changing rapidly, and the corresponding spectral peaks are very broad. The WD spectrum for the same signal processed using the same parameters is shown in figure 13. With the multicomponent signal, the analysis form of the WD introduces an erroneous cross coupling component between the two simulated sine waves. This "phantom" peak train confuses the resulting time-frequency representation of the multiple component signal. Figure 14 is the corresponding MWD spectrum for the multicomponent signal. As can be seen in the figure, a high frequency resolution is attained (much improved over that of the STFT method) without unwanted cross coupling terms corrupting the time-frequency representation.

Figure 15 is a PSD isoplot showing the shutdown of an SSME alternate turbopump develop-ment (ATD) test rig following a component failure. As seen in the STFT isoplot, following the failure which occurs at 615 s into the test, the spectral distribution of the proximity probe signal becomes very noisy. In order to study the temporal and spectral characteristics of the signal just prior and following the failure, analysis focused on a very short time period around 615 s. Figure 16 shows the STFT isoplot for a 300-ms period extending from 615 to 615.3 s. No clear spectral characteristics can be identified in this time-frequency representation of the proximity probe measurement. Figure 17 is the MWD spectrum for the same period using identical processing parameters. While use of the traditional WD would introduce numerous erroneous spectral components in trying to improve upon the performance of the STFT, the MWD is successful in providing a much clearer time-frequency picture of the time signal without the "phantom" peaks.

As a final example, figure 18 is an "overlapped" (STFT) isoplot developed during the failure investigation of space shuttle main engine u/n 0215. During test 901-666, the engine experienced a premature cutoff due to a second-stage turbine-blade failure in the high pressure fuel turbopump (HPFTP) u/n 5602R1. The 0–1-kHz isoplot of figure 18 displays the time-frequency history of the fundamental shaft rotational (synchronous) frequency, N, as taken from an external pump-end accelerometer. As evidenced by the sudden increase in synchronous amplitude in the figure, the pump failure initiated at approximately 3.9 s into the test. The STFT and MWD isoplots for the pump speed transducer channel are shown in figure 19. The speed probe is a magnetic-type transducer which registers four "blips" with every revolution of the pump shaft, and, for this reason, the $4N$ component dominates both isoplots. Note the increased frequency resolution offered in the MWD plot of figure 19, especially during the ramp-down period following the failure. In order to attain more insight regarding the failure, attention was focused on the 100 ms timeframe surrounding the failure. Figure 20 shows the STFT and MWD isoplots for this extremely short period. Again, notice the increased frequency resolution offered by the MWD. Moreover, note the enhancement of the novel character of the frequency variation. The frequency separation exhibited in both plots at N, $2N$, $3N$, and $5N$ is currently interpreted as being caused by a phase discontinuity in these respective frequency components of the speed signal at the time of the failure. This phase discontinuity of the shaft precession can be attributed to the sudden turbine blade loss which instantaneously shifted the phase of the driving imbalance force. The frequency branching effect does not appear in the $4N$ component (which represents the pure shaft rotational motion, or motion other than precession) since the speed probe continues to count four "blips" per revolution regardless of the phase discontinuity at the time of the failure. It is also important to note that as a result of the branching (forking) of the frequencies, an artifact is present in the middle of the fork. This results because the difference between the upper and lower frequencies of the branch is within the bandwidth of the smart window.

REFERENCES

1. Wigner, E.: "On the Quantum Correction for Thermodynamic Equilibrium." Phys. Rev. 40, 1932, pp. 749–759.

2. Claasen, T.A.C.M., and Mecklenbrauker, W.F.G.: "The Wigner Distribution—A Tool For Time-Frequency Signal Analysis." Philips Journal of Research, vol. 35, pp. 217–250, 276–300, 372–389.

3. Boashash, B., and Black, P.: "An Efficient Real-Time Implementation of the Wigner-Ville Distribution." IEEE Transactions on Acoustics, Speech, and Signal Processing, vol. ASSP-35, No. 11, November 1987.

4. Meng, Qingfeng, and Qu, Liangsheng: "Rotating Machinery Fault Diagnosis Using Wigner Distribution." Mechanical Systems and Signal Processing, vol. 5(3), 1991, pp. 155–166.

5. Rao, P., Taylor, F., and Harrison, G.: "Real-Time Monitoring of Vibrations Using the Wigner Distribution." Sound and Vibration, May 1990.

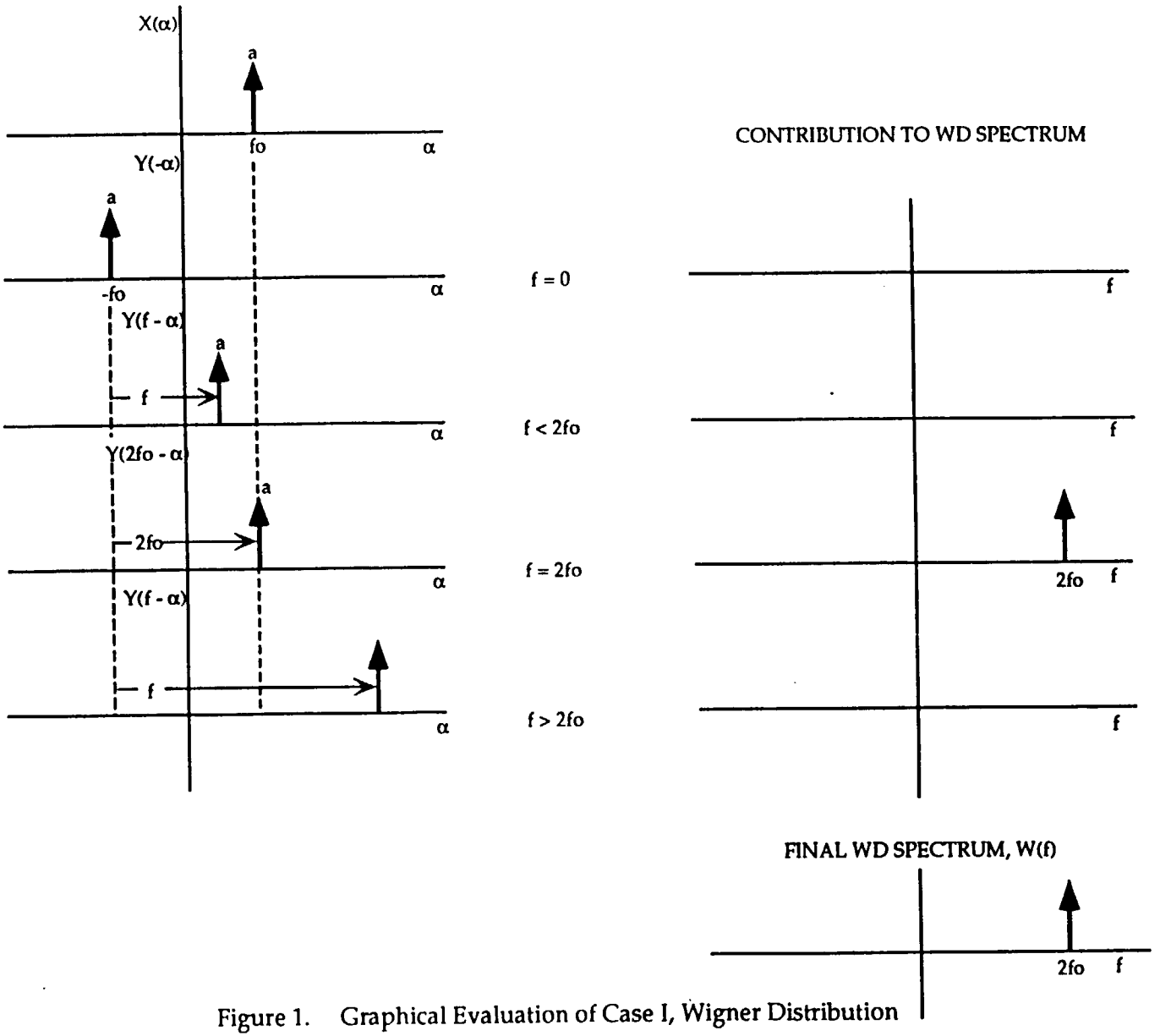

Figure 1. Graphical Evaluation of Case I, Wigner Distribution

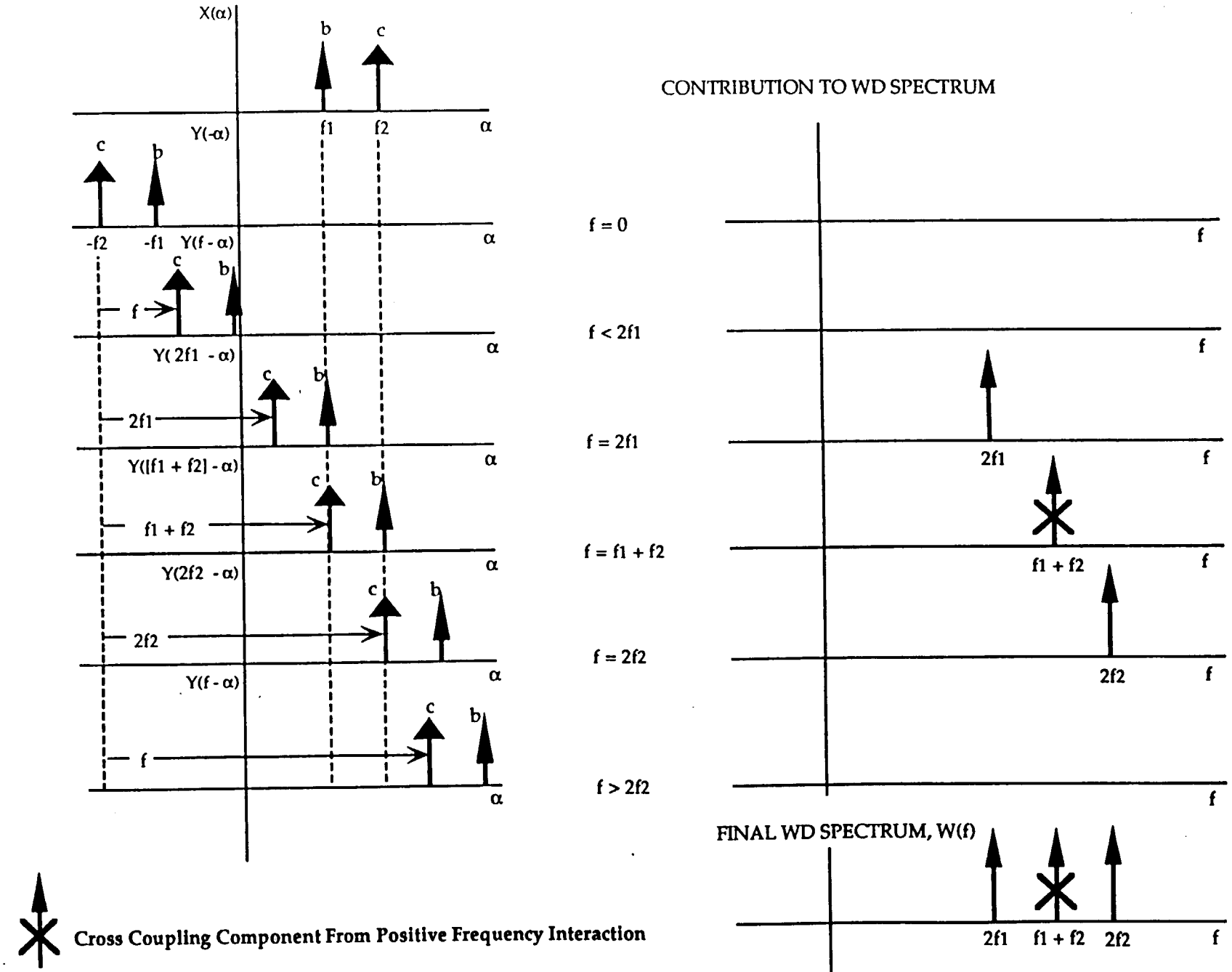

Figure 2. Graphical Evaluation of Case II, Wigner Distribution

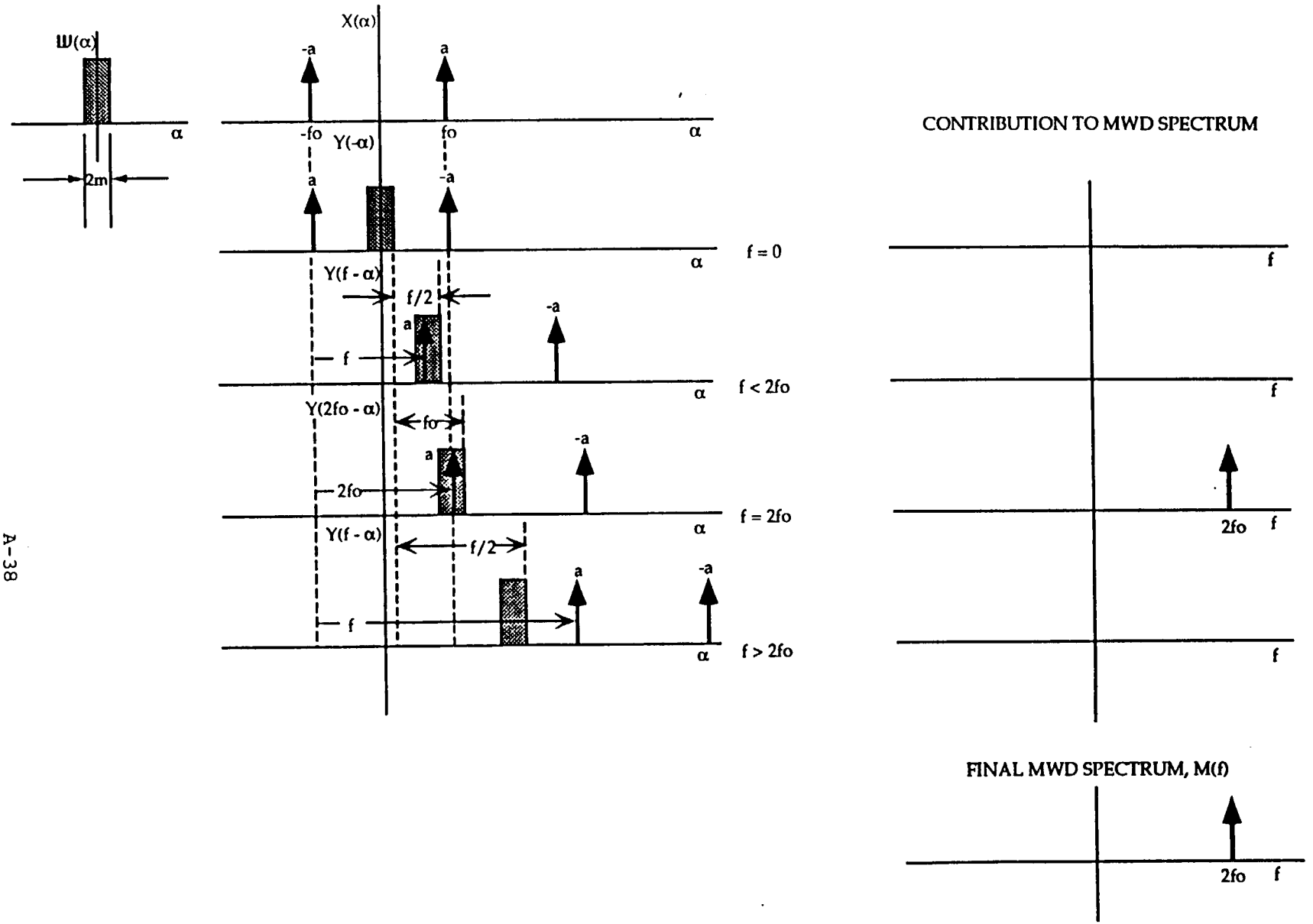

Figure 3. Graphical Evaluation of Case I, ModifiedWigner Distribution

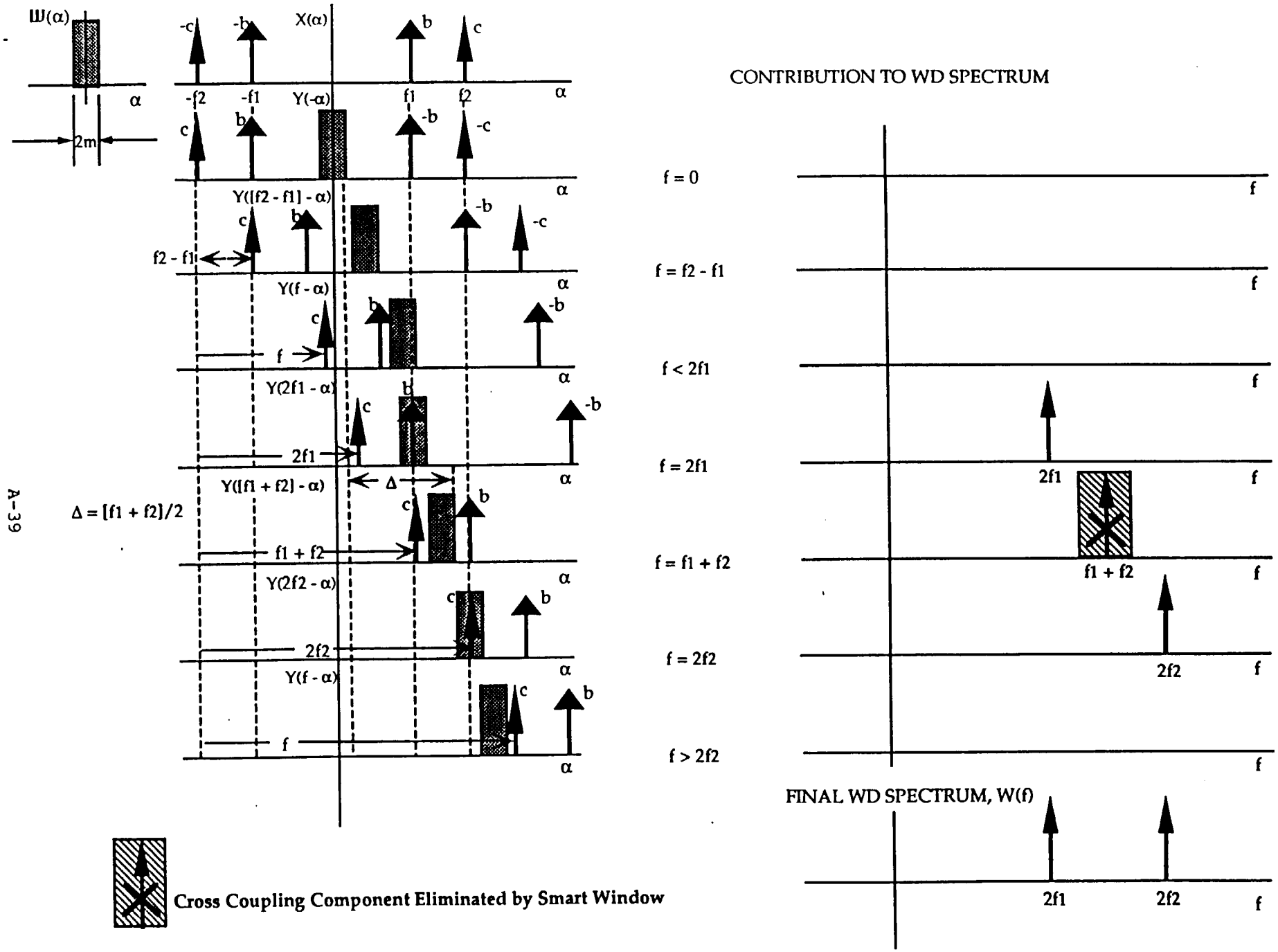

Figure 4. Graphical Evaluation of Case II, Modified Wigner Distribution

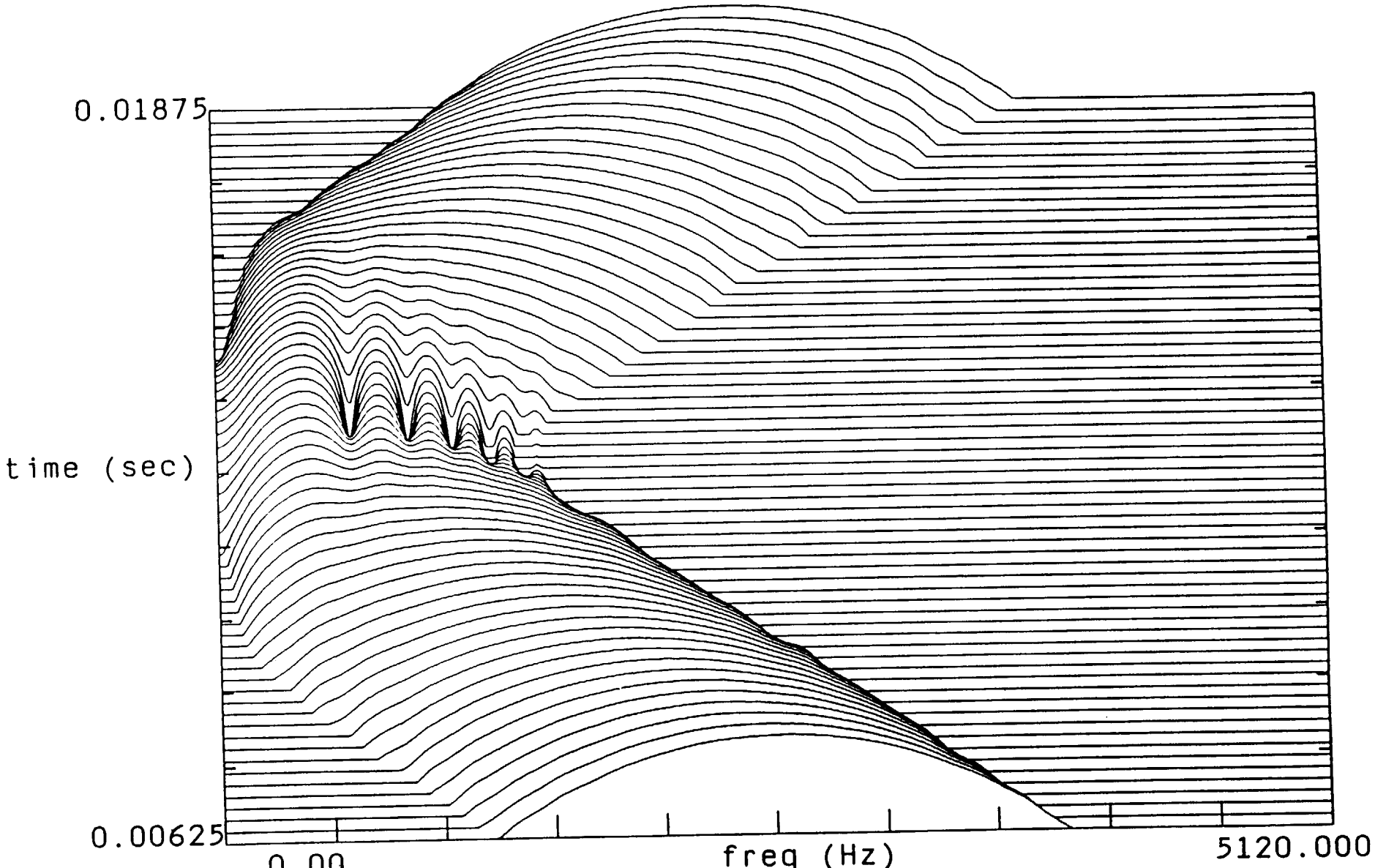

fft nn=128 nff=1024 fs=10240 novlps=64 winda=3
5000 to 100 Hz in 0.0125 seconds (with continuation into f<0

fig 5

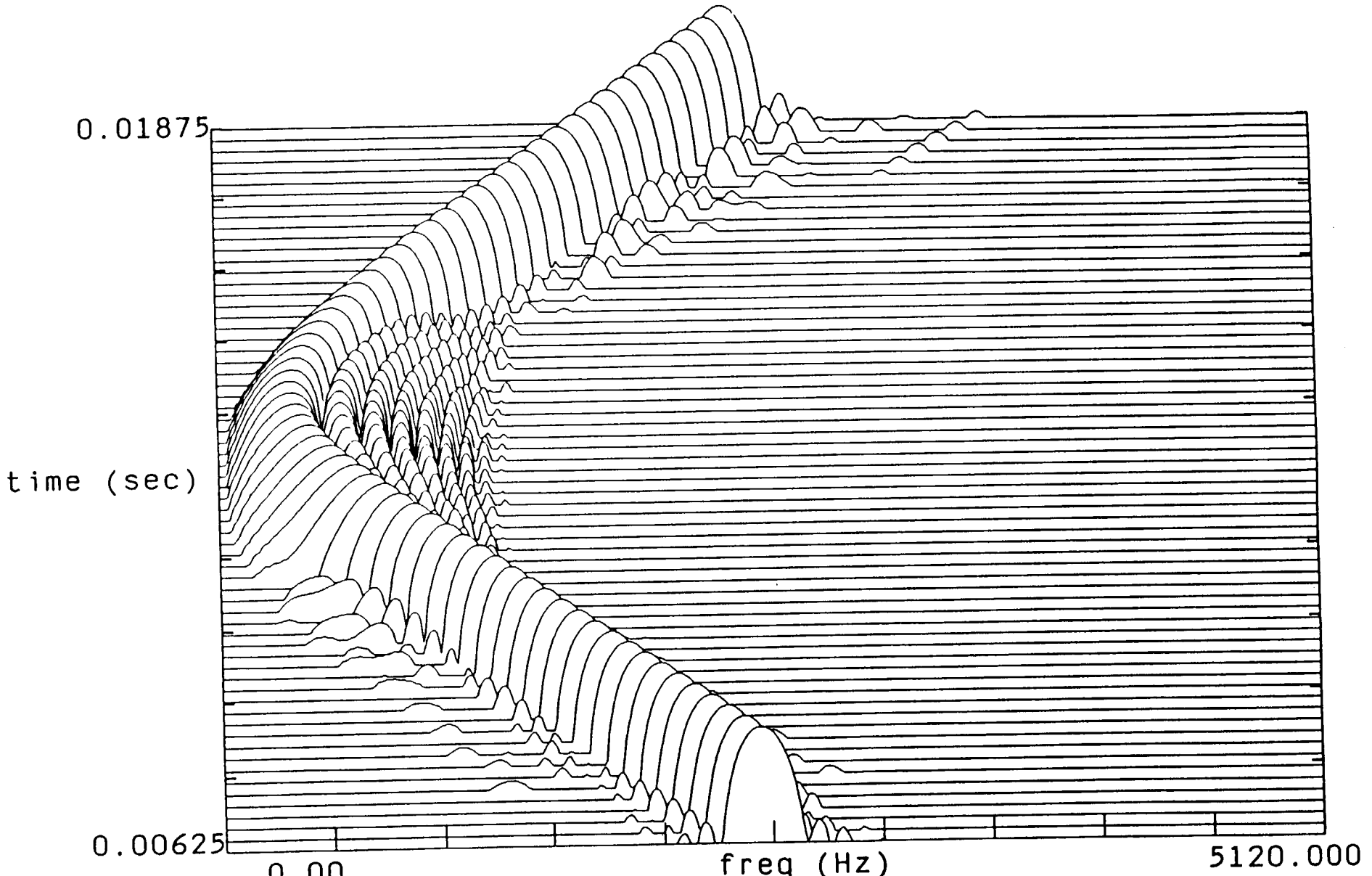
0.01875
time (sec)
0.00625
0.00
freq (Hz)
5120.000
mwd nn=128 nff=1024 fs=10240 novlps=64 winda=3 sfw=100b/s
5000 to 100 Hz in 0.0125 seconds (with continuation into f<0

Fig 6

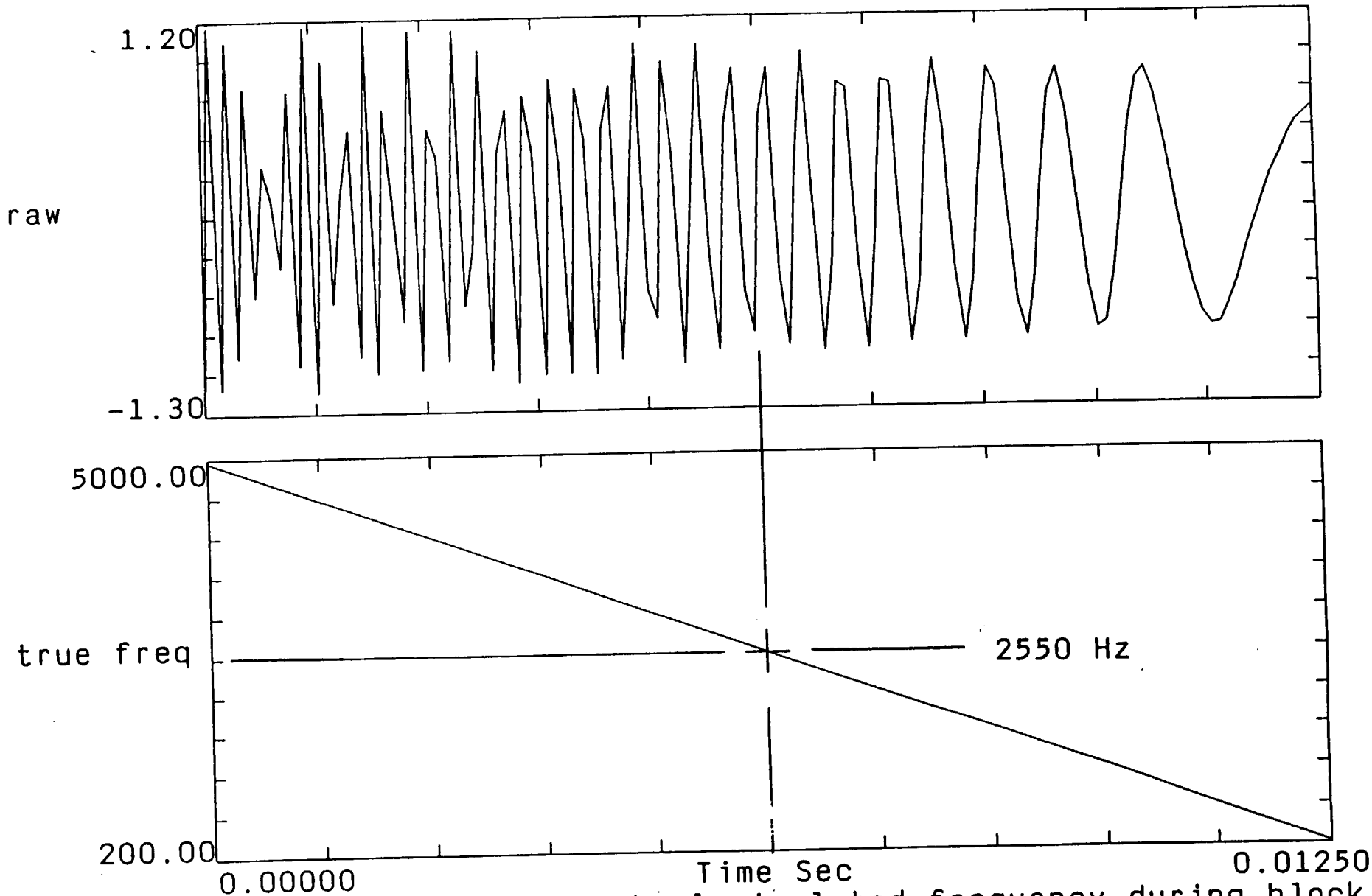

Raw time signal and actual simulated frequency during block centered at 0.00625 seconds

Fig 1

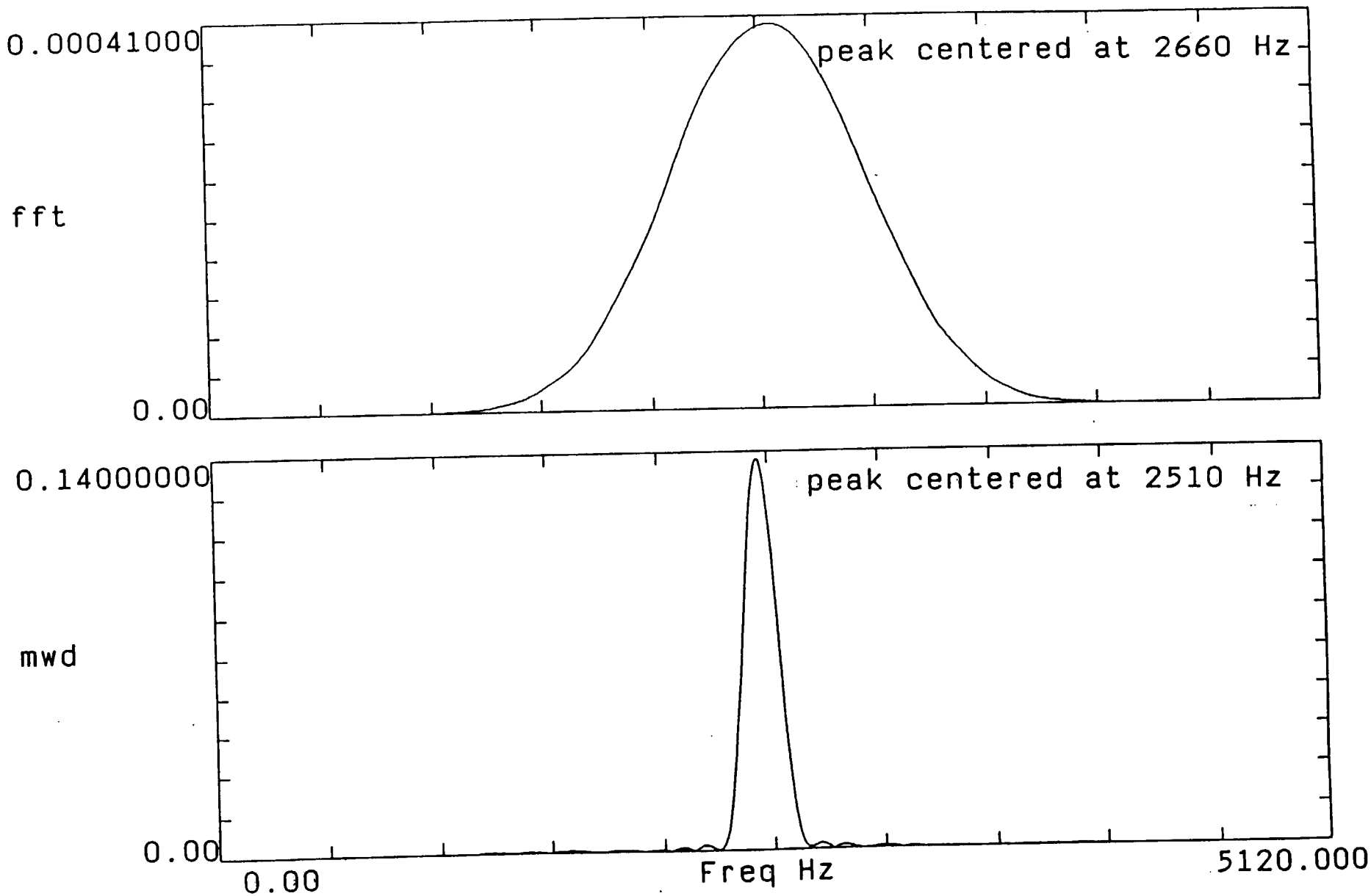

run11 nn=128 nff=1024 fs=10240 novlps=64 winda=3
Comparison of STFT to MWD at 0.00625 seconds

Fig 8

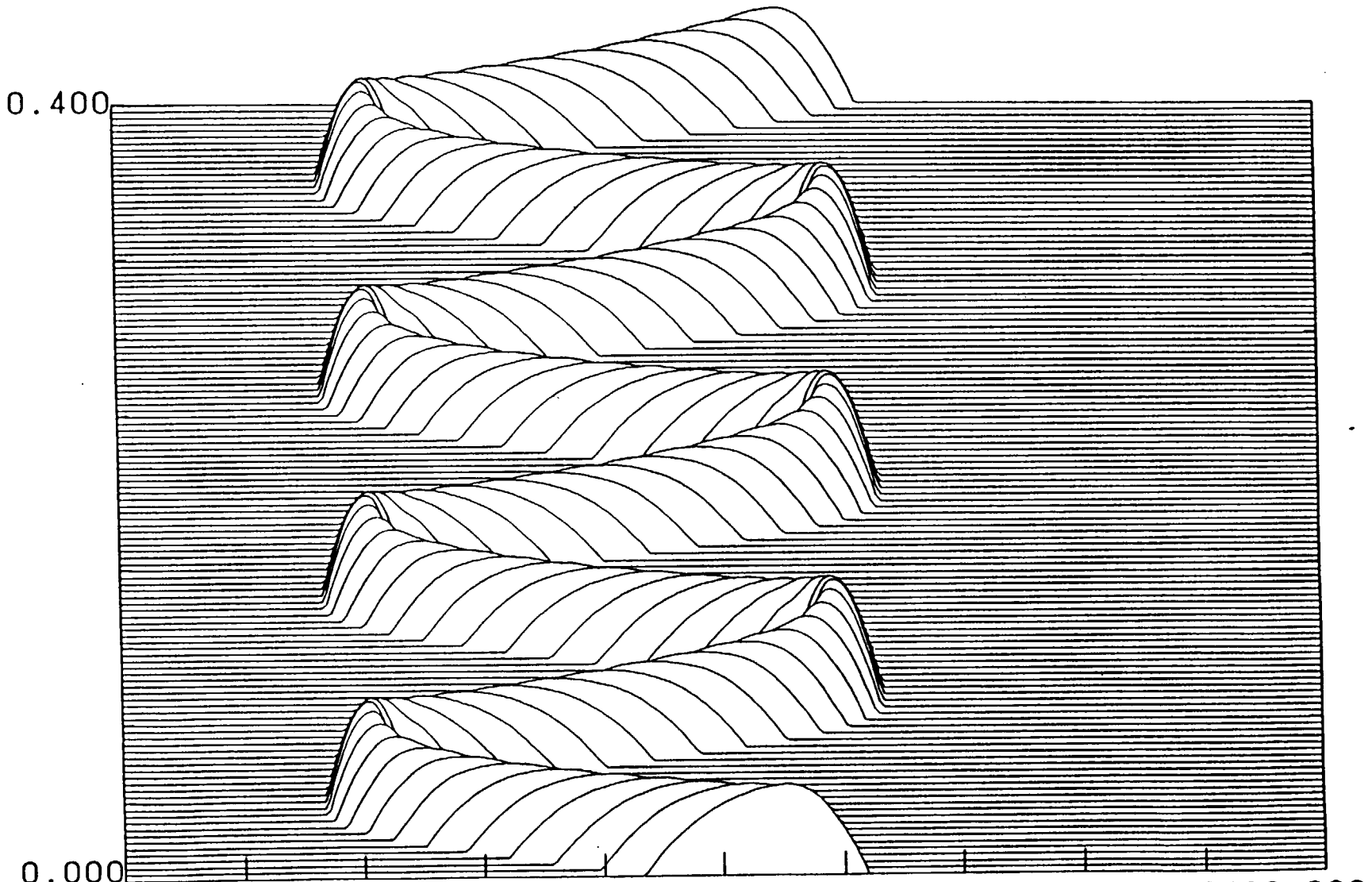
0.400
time
0.000
0.00
frequency
2500.000
FFT ISOPLOT 256x16 Novp=8 Nfft=1024
windowed

Fig-1

Fig 9

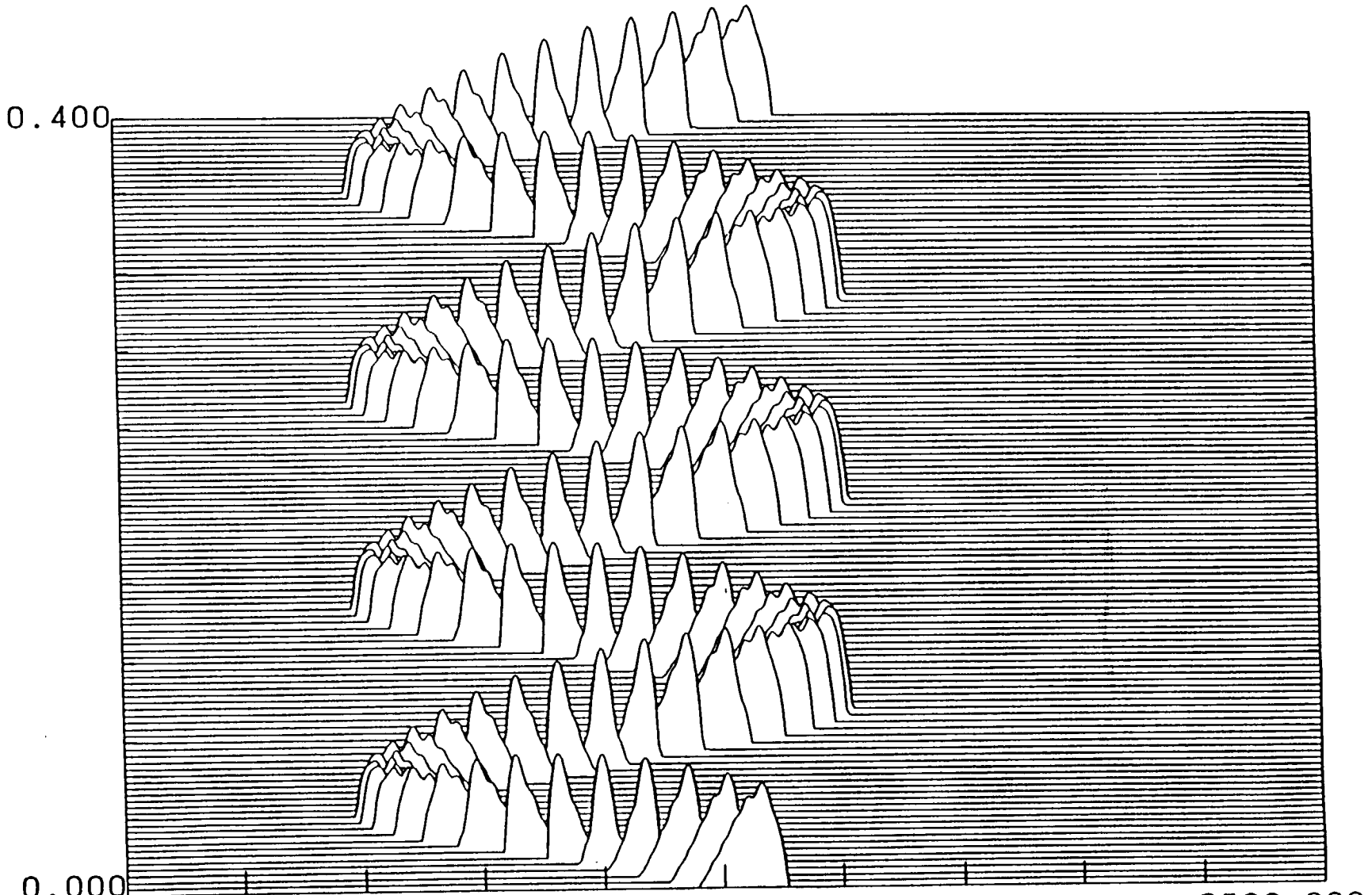
0.400
time
0.000
0.00
frequency
2500.000
WD/ANALYTICAL 256x16 Novp=8 NFFT=1024
windowed

Fig 2

Fig 10

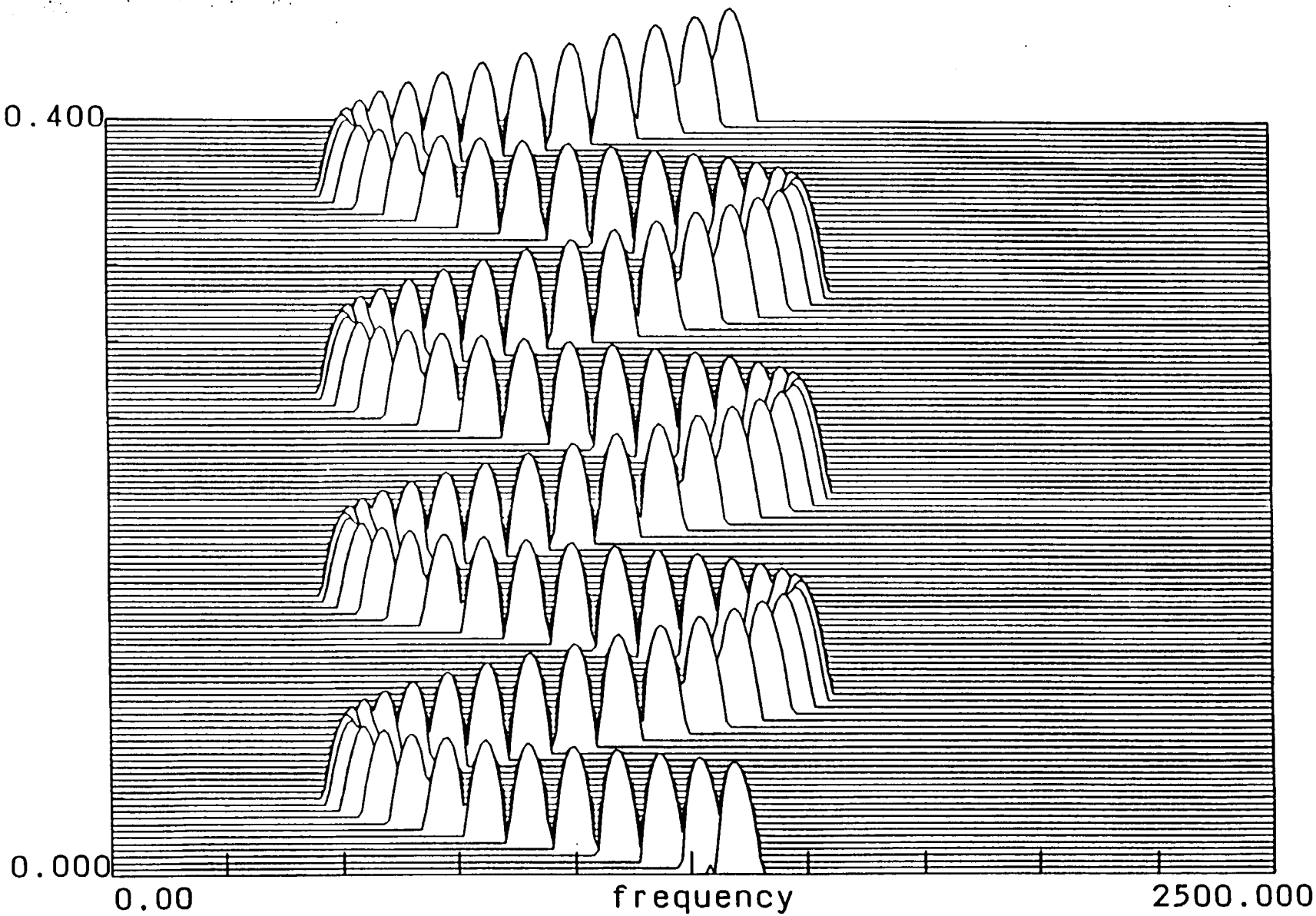

Fig 3 MWD 256x16 Novp=8 NFFT=1024
Windowed

Fig 11

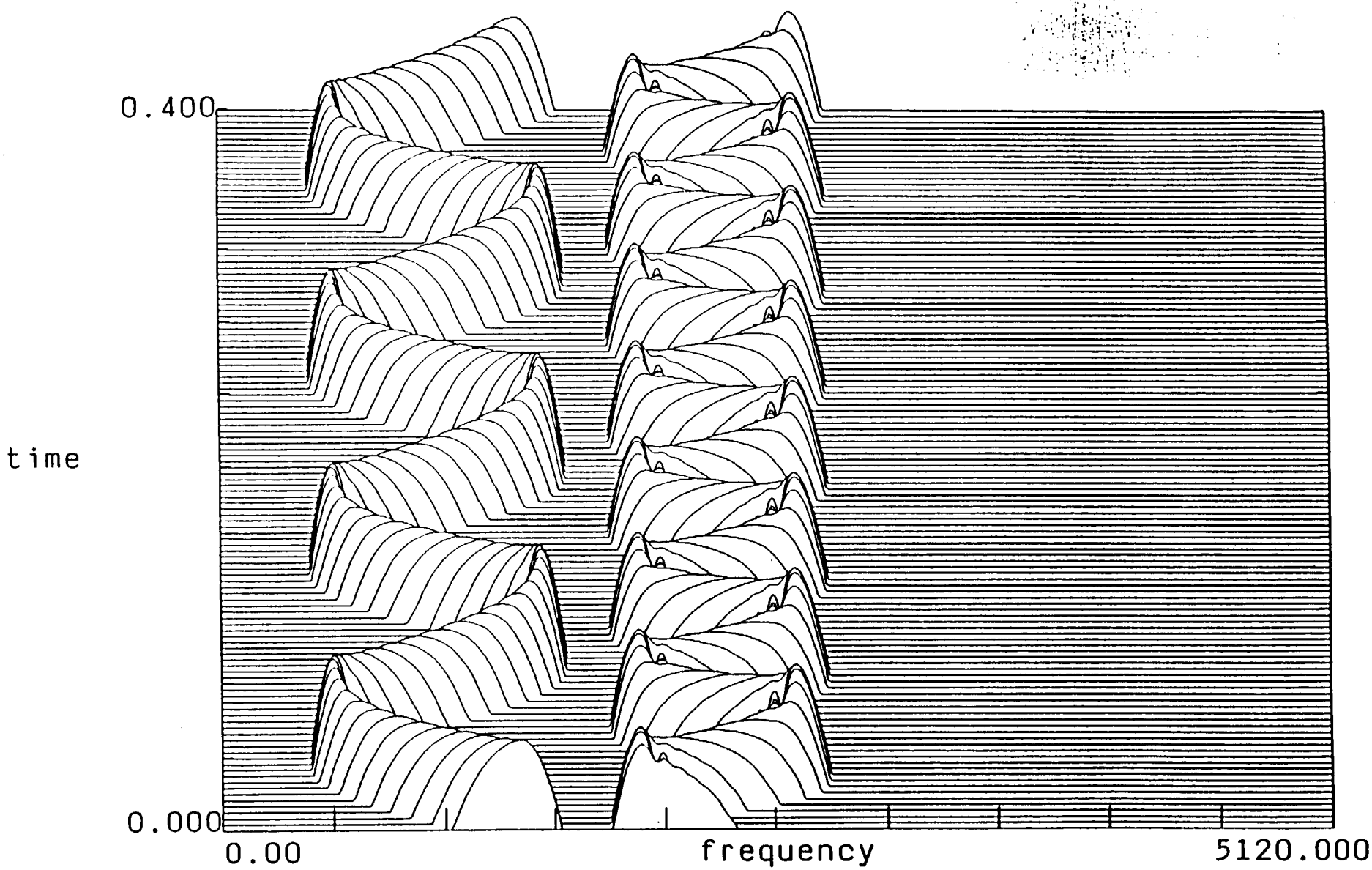

FFT ISOPLOT 256x16 Novp=8 Nfft=1024
windowed

Fig 4

Fig 12

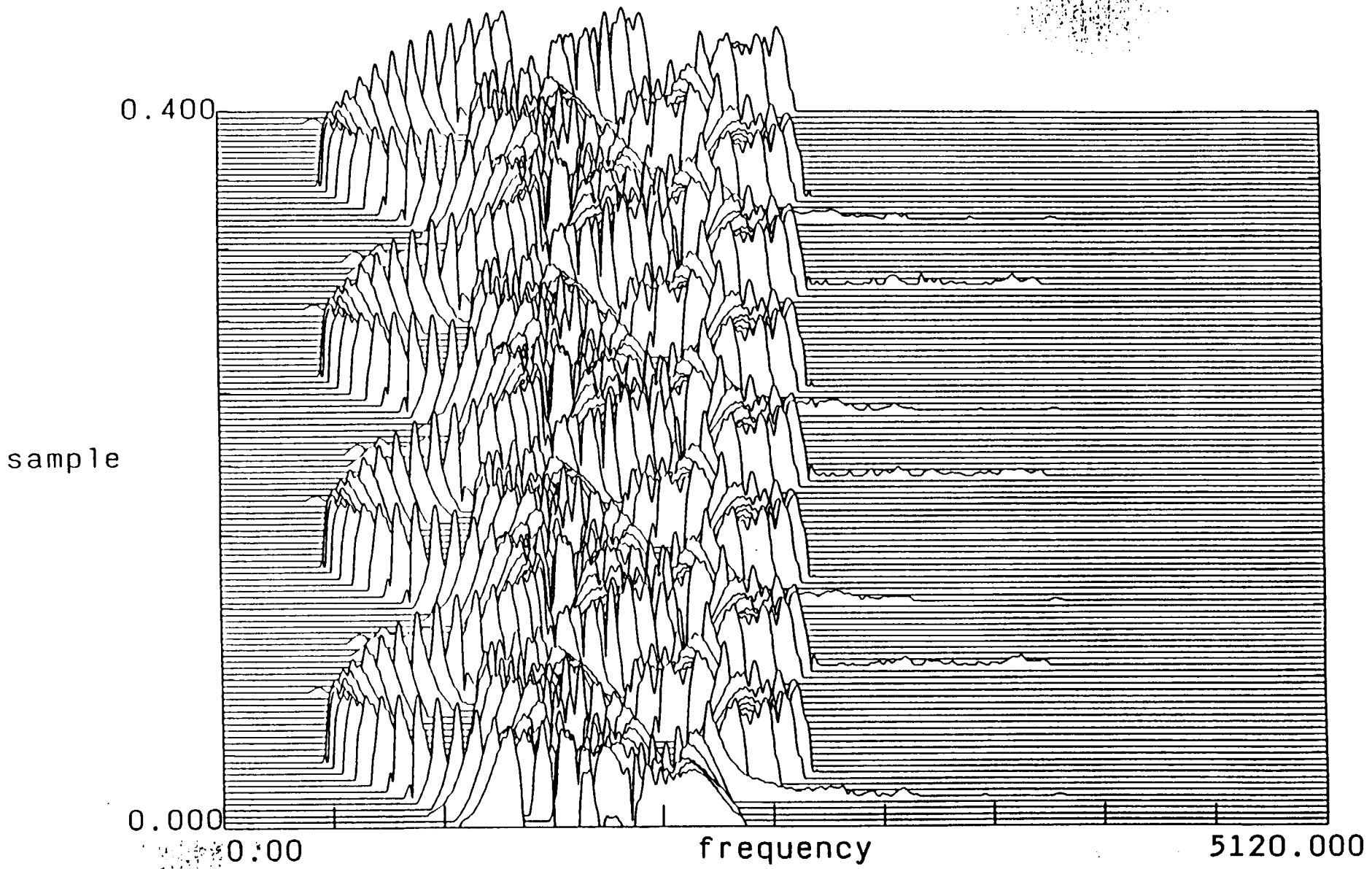

Fig 5 WD/ANALYTICAL
256x16 Novp=8 NFFT=1024

Fig 13

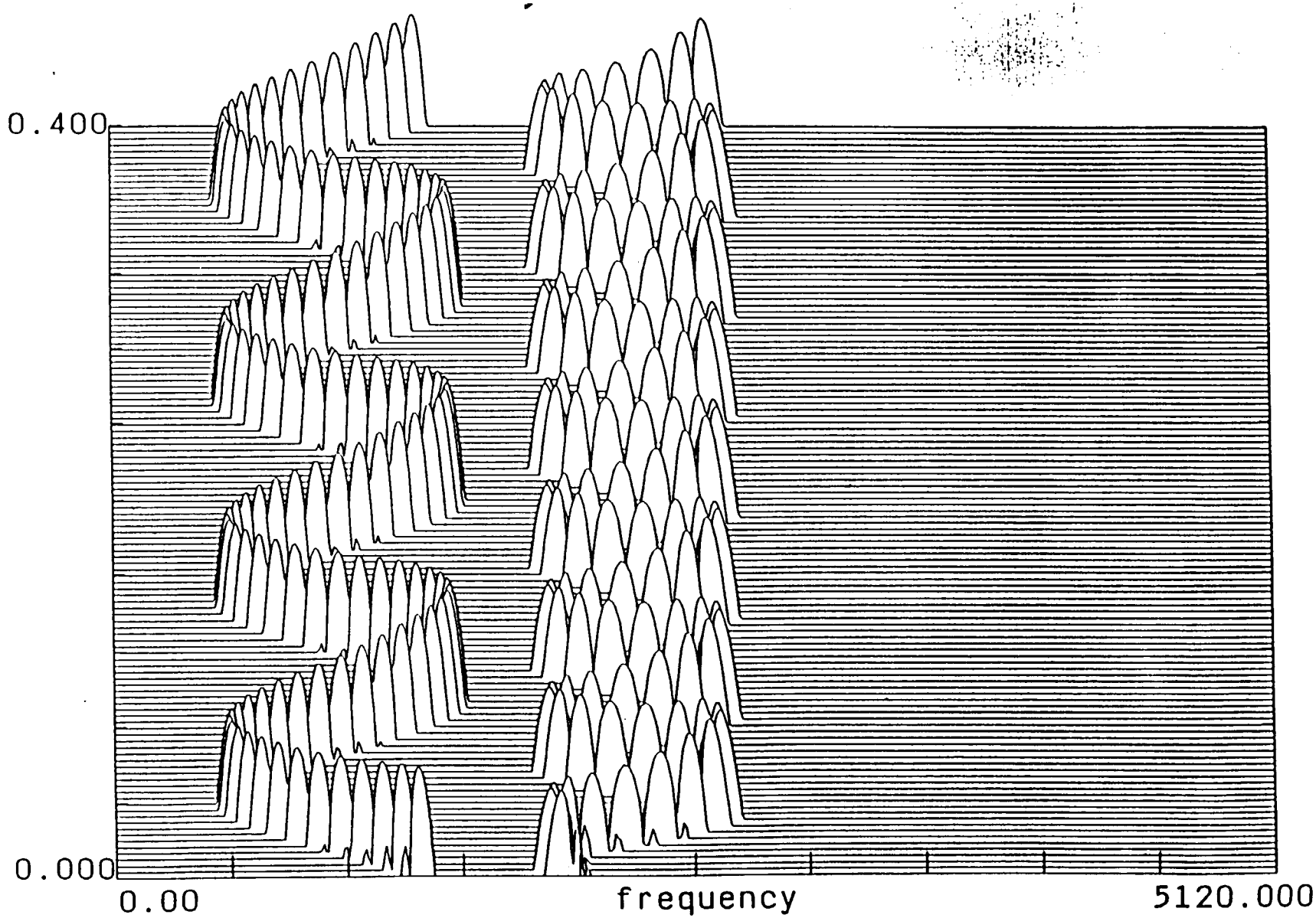

Fig-6 MWD 256x16 Novp=8 NFFT=1024
Windowed

Fig 14

BW= 2.500 ATD IPS PROX PPIS05 07/25/91
Y-INC=.200E+00 sec 2 PSDs SKIPPED <ED23>
PLOT CLIP LEVEL = .114E+02 M-SQ/Hz LOG/-40.% Freq. Range = 0.0 - 2
OVRLPS= 4
HANN/3

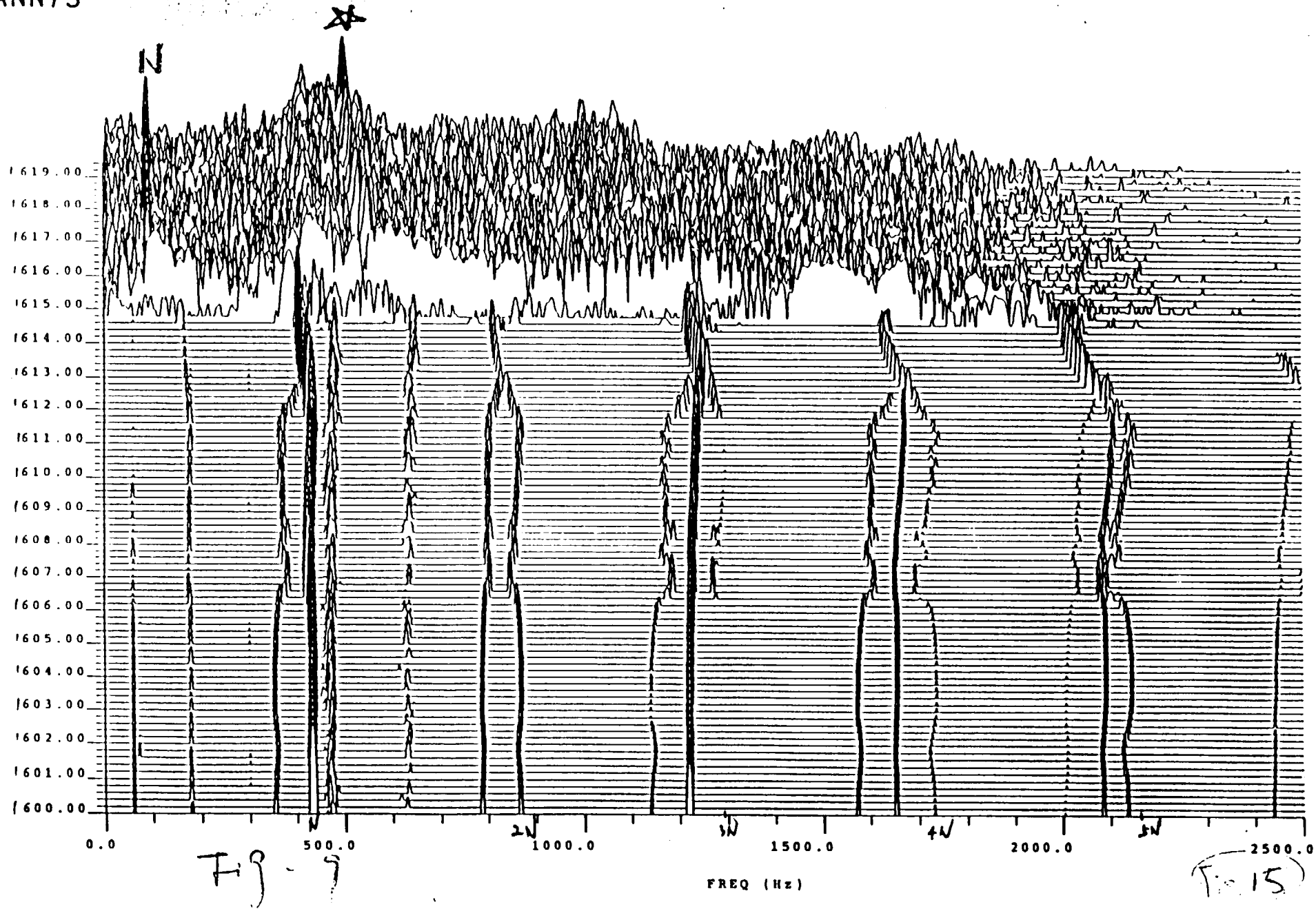

A-50

Fig - 9

Fig 15

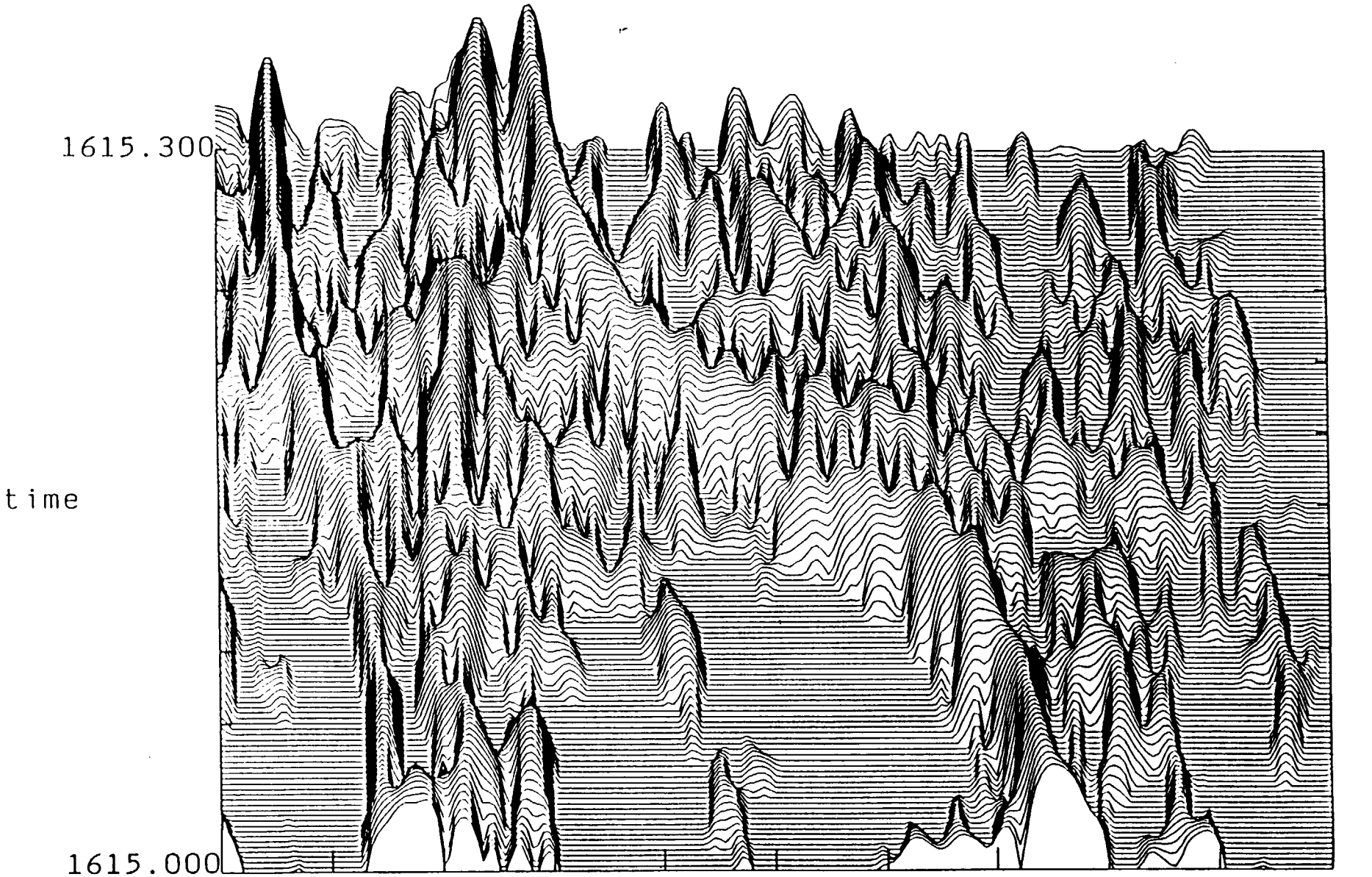
1615.300
time
1615.000
0.00
frequency
2000.000
ATD IPS PROX
NN=1024 NFFT=1024 NOVP=64 NWD=6
FFT PPIS05

Fig-1°

(F-16)

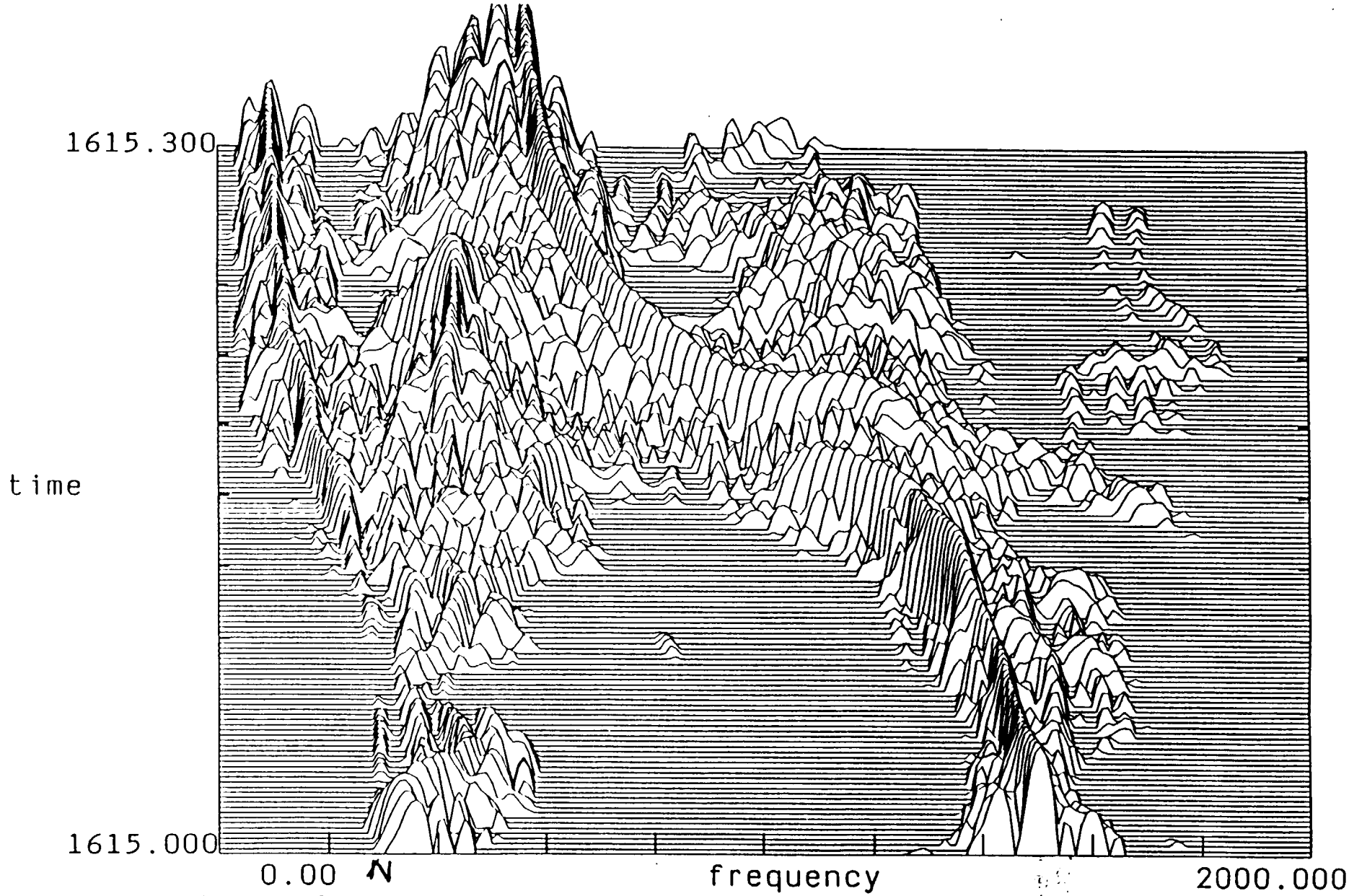
1615.300
time
1615.000
0.00
frequency
2000.000
ATD IPS PROX
NN=1024 NFFT=1024 NOVP=64 NWD=6
MWD PPISO5 NWD=10

Fig- 11

BW= 2.500 901-666 HPFP HPFP RAD 96 07/26/91
Y-INC=.500E-01 sec <ED23>
PLOT CLIP LEVEL = .500E+02 P-SQ/Hz LOG/ 0.% Freq. Range = 50.0 - 1
OVRLPS= 8 redo at 4 overlaps
HANN/3

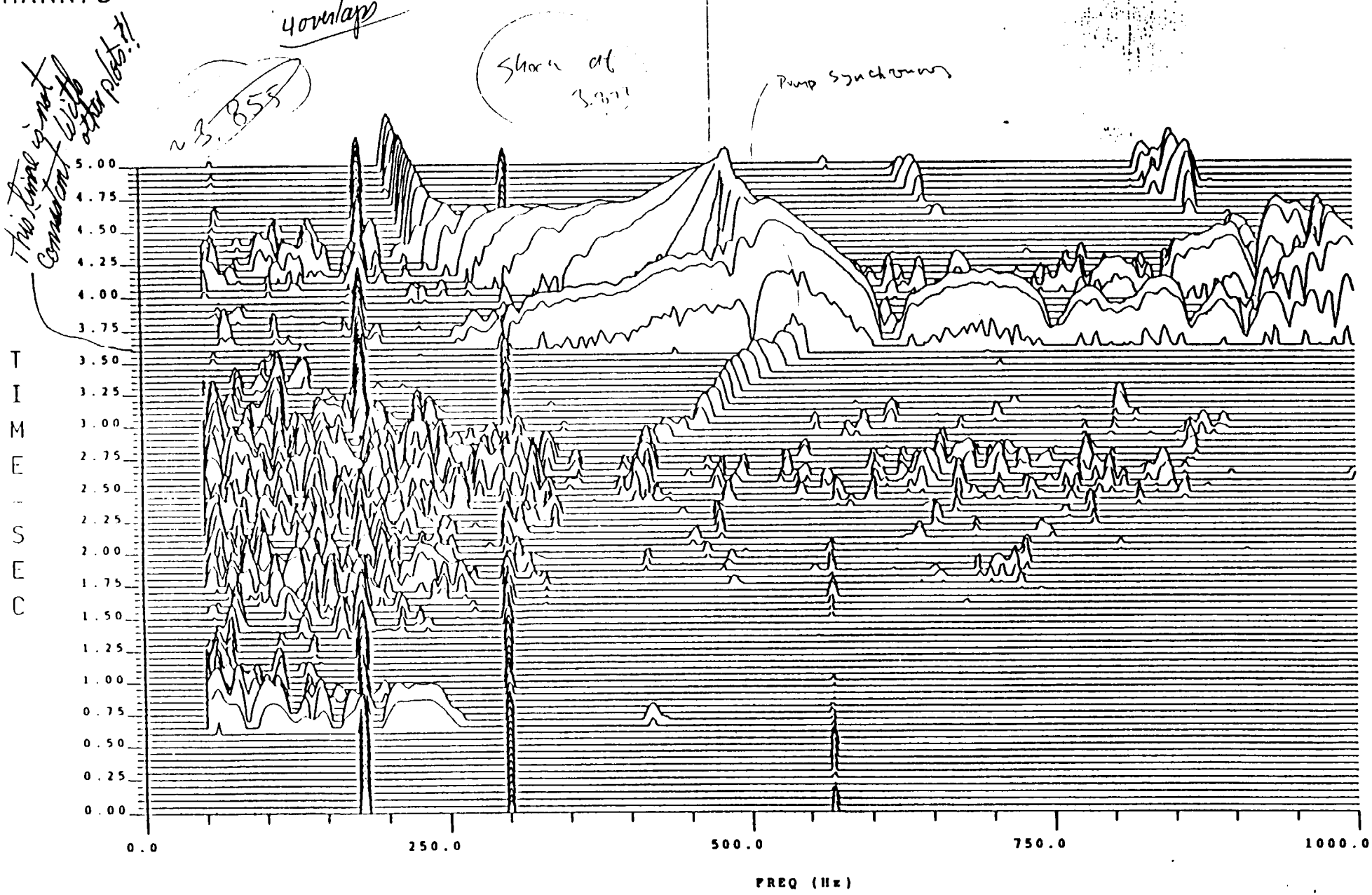

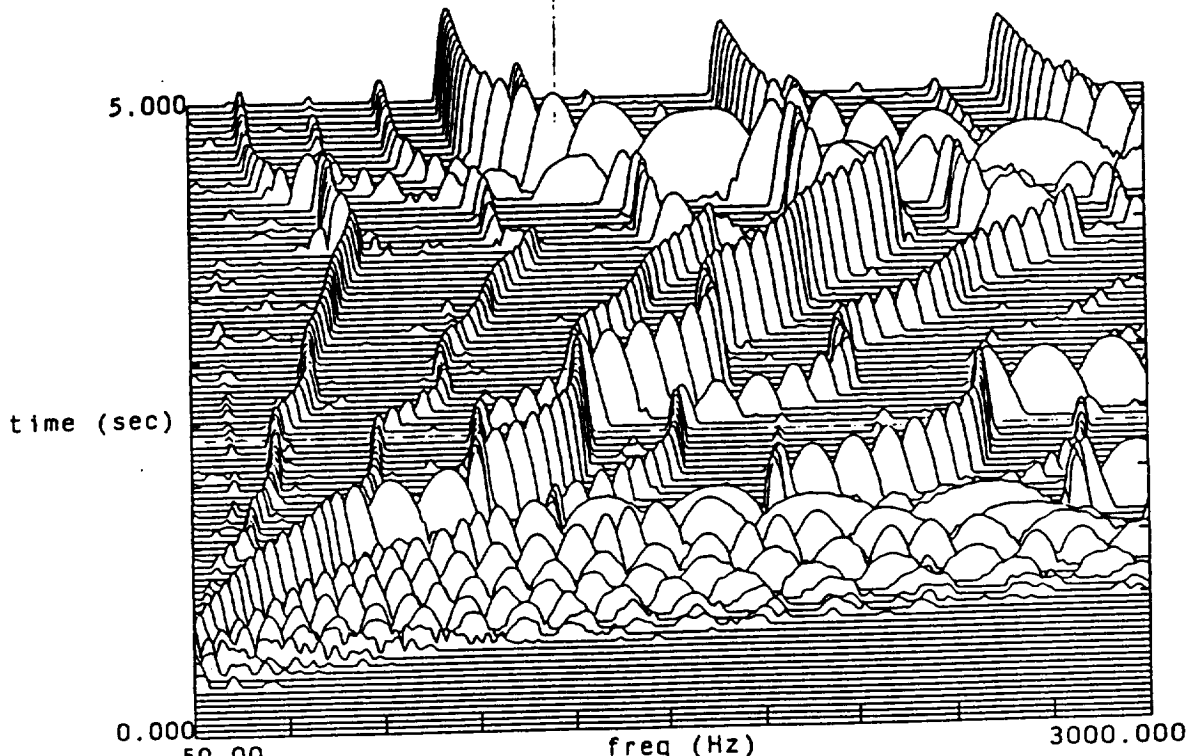

901-666 HPFP SPD NFD
NN=1024=NFFT NOVLP=4 NWD=3
FFT

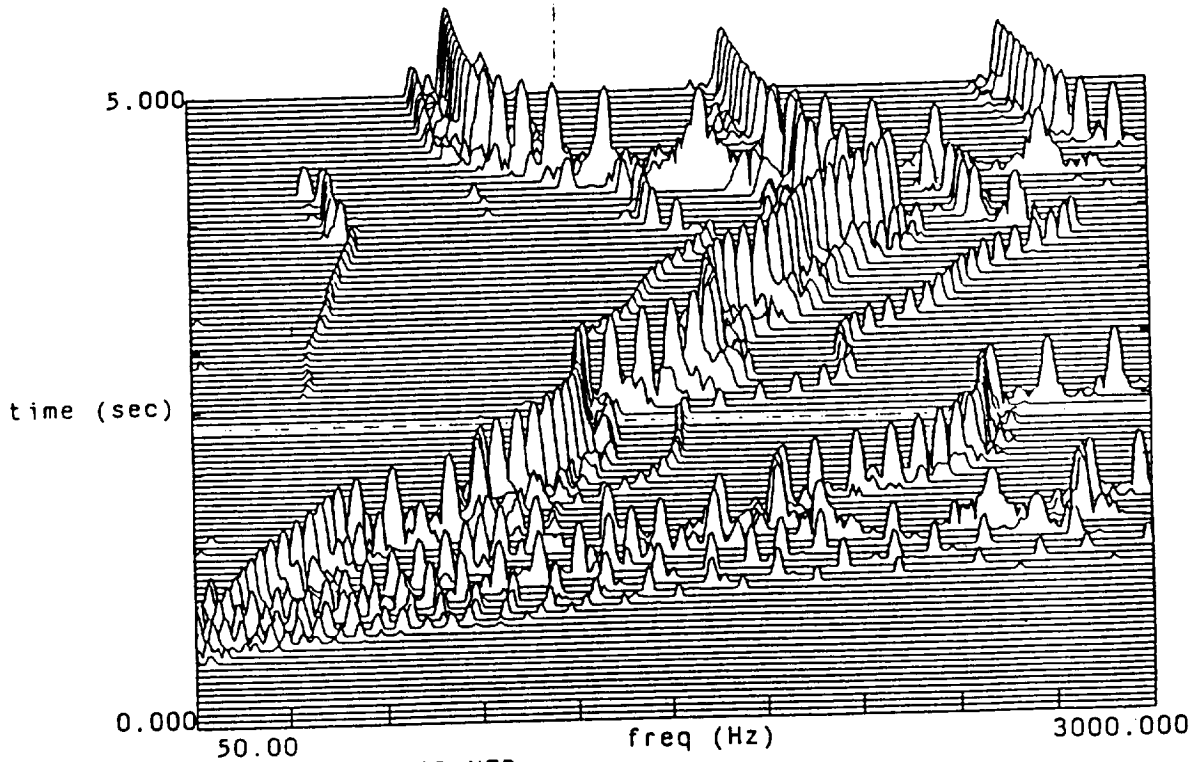

901-666 HPFP SPD NFD
NN=1024=NFFT NOVLP=4 NWD=3
MWD FWD=10

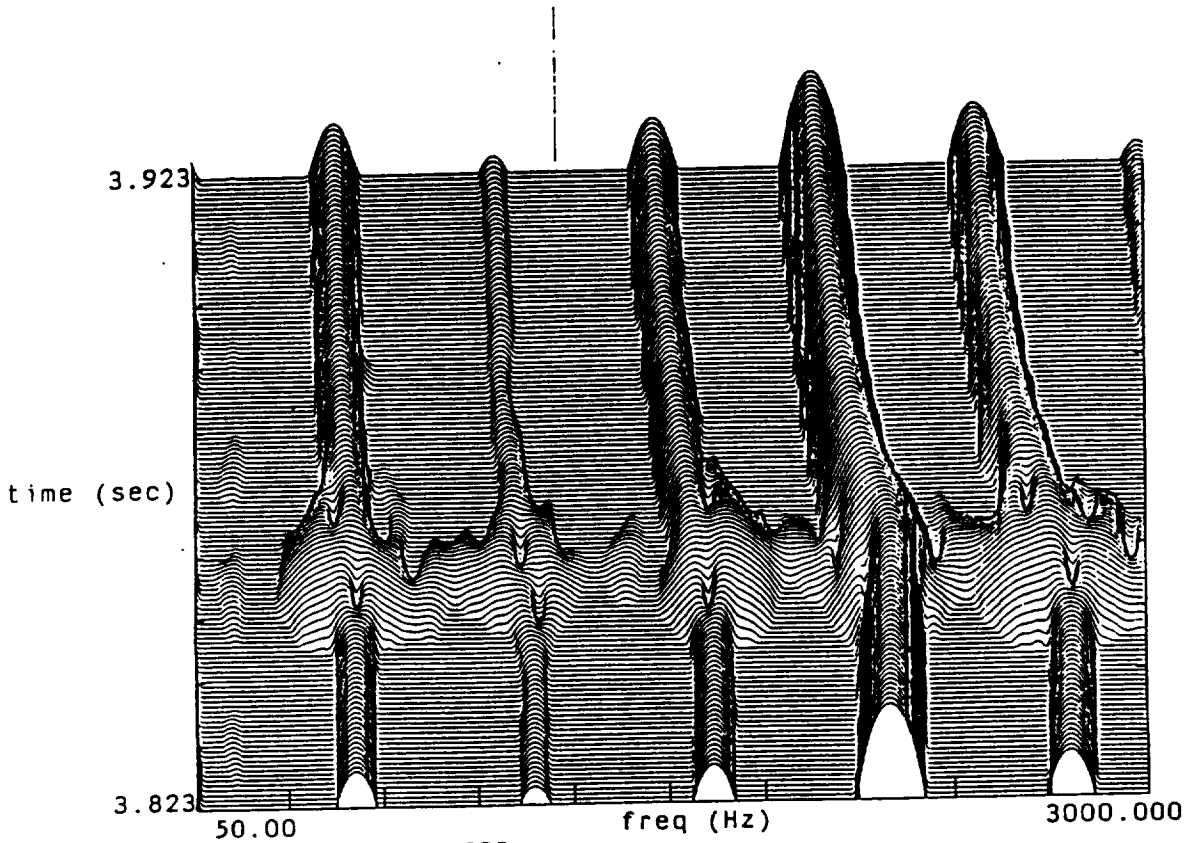

FFT 901-666 HPFP SPD
NN=NFFT=1024 NWD=20 NOVP=128

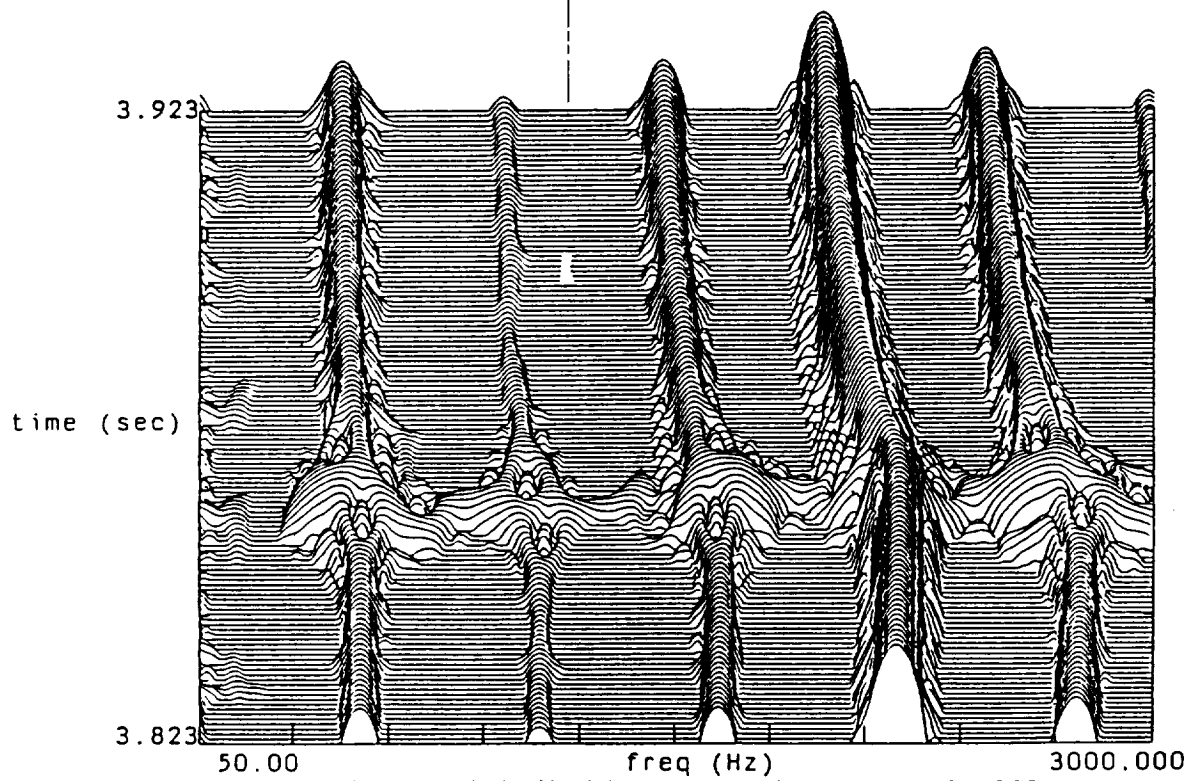

Modified Wigner Distribution (MWD) 901-666 HPFP SPD
NN=NFFT=1024 NWD=20 NOVP=128
FWD=5

NASA Conference Publication 3174, Vol. II

Advanced Earth-to-Orbit Propulsion Technology 1992

Edited by
R. J. Richmond
George C. Marshall Space Flight Center
Marshall Space Flight Center, Alabama

S. T. Wu
The University of Alabama in Huntsville
Huntsville, Alabama

Proceedings of a conference held at
NASA George C. Marshall Space Flight Center
Marshall Space Flight Center, Alabama
May 19–21, 1992

NASA
National Aeronautics and
Space Administration
Office of Management
Scientific and Technical
Information Program
1992

SOME RECENT DEVELOPMENTS IN TURBOMACHINERY DIAGNOSTIC MONITORING*

Jen Y. Jong, Thomas Coffin, Wayne L. Swanson
Wyle Laboratories

James E. McBride, Jess H. Jones, Preston C. Jones, Thomas F. Zoladz
National Aeronautics and Space Administration, Marshall Space Flight Center

ABSTRACT

Measurements on high performance rocket engine turbomachinery suffer from severe noise contamination associated with fluid flow, combustion processes, structural resonances, etc. It is thus extremely difficult to detect and discriminate between rotational system "signatures" and independent noise sources. In support of SSME development and advanced technology test programs, a number of sophisticated diagnostic algorithms have been developed and integrated into the signal processing system operational at MSFC's Structures and Dynamics Laboratory. These algorithms include higher order spectrum analysis, adaptive filtering, phase domain averaging, and other techniques applicable to specific SSME mechanical symptom detection and identification investigations.[1,2]

This presentation reviews some recent developments in mechanical system detection and identification technology. The hypercoherence function was developed to detect the correlation between synchronous frequency characteristics and any *harmonic* component.[3,4] The generalized hypercoherence,[5] more recently applied, permits estimation of the nonlinear correlation between a selected frequency (e.g., shaft speed) and *an arbitrary* frequency component. A hypercoherence filtering algorithm is also described.[6,7] A new signal processing tool (the Modified Wigner Distribution), which has proven useful in resolving time-frequency characteristics of highly nonstationary data typical of engine startup, cutoff, and throttling, is demonstrated.[8] The technique effectively suppresses the spurious spectral peaks inherent with the standard Wigner spectrum for a signal with multiple frequency components. This paper briefly summarizes the analytical basis for the above algorithms. Practical application of the methods is then demonstrated through the evaluation of vibration measurements from SSME hot firing tests.

INTRODUCTION

Equipment failures are generally preceded by growing tolerances, imbalance, bearing element wear, and the like, which may manifest themselves through subtle modifications in the waveform observed by dynamic measurements. Conventional linear spectral analysis has long been used to identify the signal characteristics associated with machinery faults in vibration signature analysis. However, nonlinearities can play a significant role for signature identification. It has been observed that different rotational mechanisms may interact due to some nonlinear process.[9,10,11] When this occurs, coherent phase relationships may exist, which can be identified from response signals. Frequency sum and difference components are one of the commonly observed nonlinear (quadratic) phenomena. A typical example is a synchronous (shaft rotational) frequency component modulated by subsynchronous whirl.[2] Other kinds of nonlinearity include high level harmonic content of synchronous vibration due to waveform clipping from rubbing.[3] All these signals represent nonlinear phenomena since their spectral components at different frequencies are not independent of each other. Due to the lack of phase information, traditional spectrum analysis cannot identify such phenomena. Therefore, higher order spectral analysis is required. This analysis includes a hierarchy of cumulant spectra such as bicoherence, tricoherence, etc. Each technique can identify nonlinearities of different order in a random signal and be applied to the particular type of failure mechanism to be detected. The following discussion summarizes some of these techniques and applications. These methods are strictly appropriate to stationary time series. Spectral analysis of transient operational periods is addressed in the final section of this paper.

HIGHER ORDER SPECTRAL METHODS

THE BISPECTRUM AND BICOHERENCE

Given a stationary, zero mean process, the ordinary (linear) spectrum $S_{XX}(f)$, may be defined by

$$S_{XX}(f) = E[X(f)\,X^*(f)]$$

where X( ) denotes the Fourier transform and E[ ] is the ensemble average.

---

* Work performed under contracts NAS8-38156/-38095 with the National Aeronautics and Space Administration, Marshall Space Flight Center.

The next higher order is called the bispectrum $B_{xxx}(f_j,f_k)$.

$$B_{xxx}(f_j,f_k) = E[X(f_j)\,X(f_k)\,X^*(f_j+f_k)]$$

Succeeding terms can be written out following the permutation rules for higher order cumulants of random variables.[12]

The bicoherence, a normalized bispectrum, $b(f_j,f_k)$, is defined as

$$b_{xxx}(f_j,f_k) = \frac{|B_{xxx}(f_j,f_k)|}{\{E[|X(f_j)\,X(f_k)|^2]\,E[|X(f_j+f_k)|^2]\}^{1/2}}$$

By Schwartz' inequality, it can be shown that the bicoherence is bounded by zero and unity. If the wave at f_j+f_k is totally correlated to the waves at f_j *and* f_k, the bicoherence will equal unity. On the other hand, if these three waves or any one of them are statistically independent, the bicoherence will be zero.

APPLICATION OF BICOHERENCE

Bispectral analysis can be used to identify the existence of amplitude modulation (quadratic correlation) among spectral components. Enrich and Eshleman[10] have described six analytical models to explain how these modulations may be physically generated. The bispectrum measures the degree of correlation by identifying phase relationship among three spectral components, i.e., frequency sum or difference. It has been applied to identify the quadratic phenomenon of a synchronous frequency component modulated by the cage frequency in a ball bearing and a synchronous component modulated by a 50-percent subsynchronous whirl frequency component.[2] As an example, Fig. 1a is the PSD of a vibration measurement taken on the turbopump on engine test 902-436. The peak marked "N" is the sync frequency component N and the peak marked "SS" is the suspected 52-percent subsynchronous whirl frequency component. There is also a component at synchronous frequency N plus SS. Notice that the level of SS component is not high enough to be of concern if it is due to independent sources. But it would be critical if it is a subsynchronous whirl component which is synchronous related. Therefore, it is important to be able to identify whether this SS component is synchronous related or not. Figure 1b shows one slice of bicoherence $b(w_1, 318.75\ \text{Hz})$ with the second frequency argument fixed at the subsynchronous frequency which is 318.75 Hz. Several peaks are detected, and the most significant peak is the one located at (N, SS; N+SS) which indicates that the SS and SS+N components are both synchronous related. Therefore, the 52-percent subsynchronous is really phase locking to the machinery rotational process and not a feedthrough from other sources.

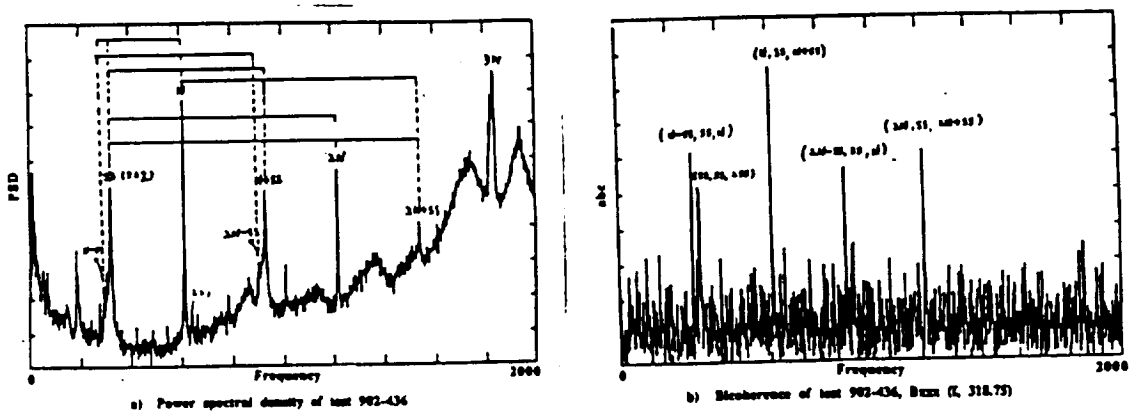

Fig. 1: Power Spectrum and Bicoherence from Engine Test 902-436

THE TRICOHERENCE

The trispectrum can be used to identify cubic correlation among four spectral components. A special case of its application is to determine whether or not an apparent sideband structure is really due to modulation or not. Such a sideband structure is another commonly observed nonlinear defect signature. Figure 2a illustrates a preburner pump radial measurement during hot firing. Notice that even though the synchronous and overall RMS levels are nominal, an apparent sideband structure consisting of three peaks marked N–120, N, and N+120 is observed, which could indicate modulation of the synchronous frequency by a lower frequency component. Figure 2b shows a slice through the tricoherence by fixing two of the three independent frequency values. If the sideband and synchronous component are truly correlated, a peak would be expected at f=N+120. Since this does not occur, it indicates the sideband components are due to an independent source and are not synchronously related. In this case, an incorrect conclusion might be made based on the ordinary spectrum.

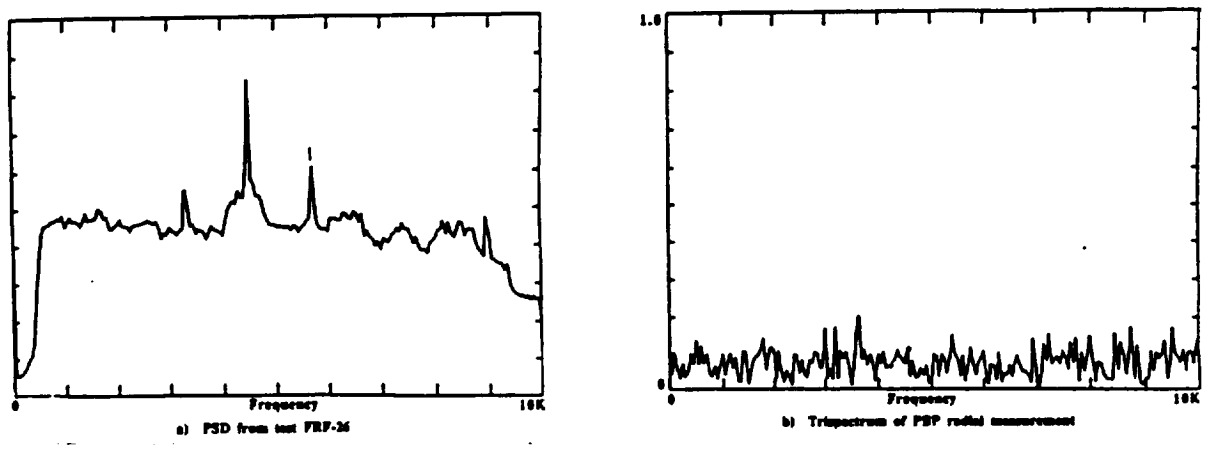

Fig. 2: Power Spectrum and Tricoherence from Engine Test FRF-26

HYPERCOHERENCE FUNCTIONS

THE HYPERSPECTRUM

To summarize the nonlinear interaction between harmonically related spectral components in a given stationary, zero mean signal, we define the *Hyperspectrum* of order n by the relation

$$H(n; f_1) = E[X^n(f_1)\, X^*(nf_1)], \qquad n = 1,2,3, \ldots$$

where f_1 is an arbitrary reference frequency, and nf_1 is an integer multiple of f_1. Thus, the ascending terms in $H(n; f_1)$ represents a single value from the linear spectrum, bispectrum, trispectrum, etc, at the specific value $f_1 = f_2 = \ldots = f_n$.

THE HYPERCOHERENCE

In anology with the ordinary coherence function, we define the hypercoherence as a normalized hyperspectrum:

$$\Gamma^2(n; f_1) = \frac{|E[X^n(f_1)\, X^*(nf_1)]|^2}{E[|X^n(f_1)|^2\; E[|X(nf_1)|^2]}, \qquad n=1, 2, \ldots$$

The hypercoherence function defines the nonlinear correlation between a reference frequency component in a vibratory signal and its harmonics. A major benefit is determination of whether an apparent harmonic in a complex vibration signal is correlated with the fundamental or caused by extraneous noise. The technique was applied to space shuttle main engine turbopump measurements. The linear spectra of two different tests appear virtually identical, other than the background noise (Figs. 3a and 3b). The PSD amplitudes at 3N frequency are very high for both tests. Figures 4a and 4b depict the hypercoherence functions computed for the same two test measurements. Figure 4a indicates that almost all the power at 3N is correlated with the rotational frequency component. On the other hand, the 3N component of the second test is due to a differing physical phenomenon not related to the rotational frequency. This indicates an improved degree of signature discrimination.

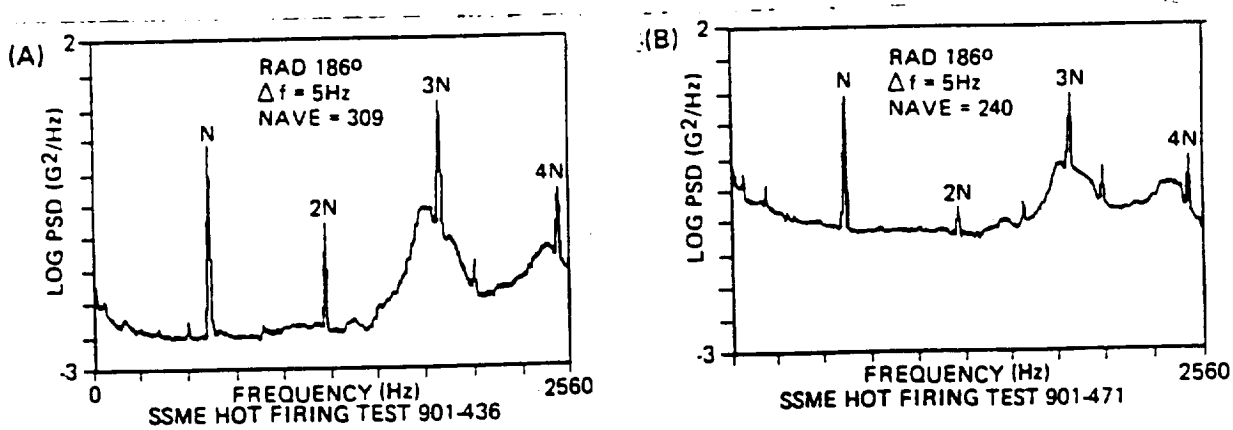

Fig. 3: Power Spectra from High Pressure Fuel Pump Measurements

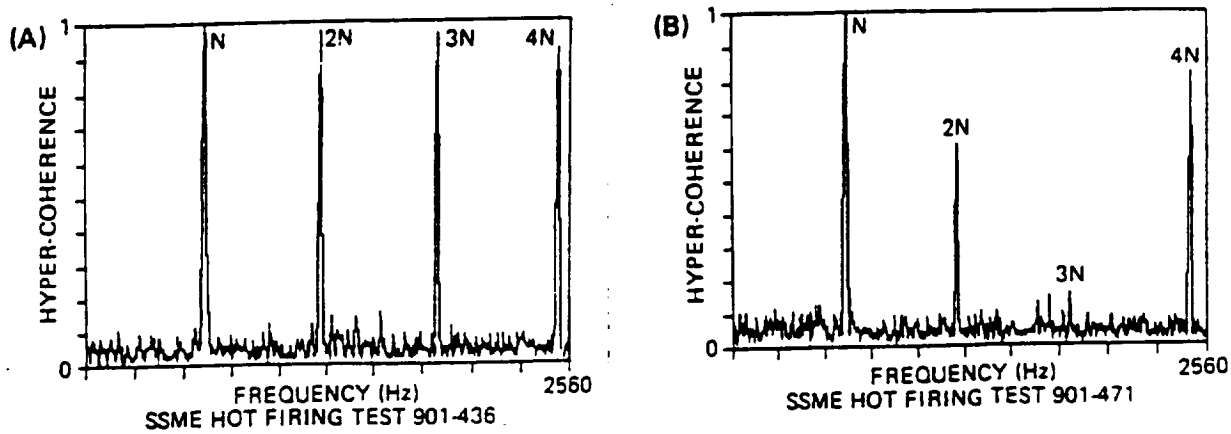

Fig. 4: Hypocoherence Spectra

THE HYPERCOHERENCE FILTER

The above frequency analysis has been extended to a time-domain algorithm for the extraction of period signals in noisy data. The analytical basis for the techniques can be summarized briefly. Assume X(t) and Y(t) jointly periodic, with additive uncorrelated noise and (possibly coincident) periodic components. Let

$$X'(t) = F^{-1}\left[\sqrt{S_{XX}(nf)_1}\,\Gamma_X\,(n;f_1)\right]$$

$$Y'(t) = F^{-1}\left[\sqrt{S_{yy}(nf)_1}\,\Gamma_y\,(n;f_1)\right]$$

n = 1, 2, 3, ...
S = Ordinary power spectrum
Γ = Hypercoherence function
F^{-1} = Inverse Fourier transform

Now X' and Y' represent filtered time histories, and include only harmonics (nonlinearly) correlated with the common fundamental frequency. To generate an orbit plot or phase-plane representation of the two quantities, let

$$Y''(t) = Y(t-\tau)$$

$\tau = \phi/2\pi f_1$
$\phi = \mathrm{Tan}^{-1}\left[Q_{xy}(f_1/C_{xy}(f_1))\right]$
Q_{xy} = Quadrature spectrum
C_{xy} = Cospectrum

The time delay, τ, serves as a "key phasor," to initiate the relative phase angle between the two vectors. A phase-plane diagram of the filtered signals is thus obtained by plotting X' versus Y''. The procedure is best illustrated by example. Figure 5a illustrates the orbit plot for two jointly periodic signals, each containing three harmonic components. Figure 5b represents the same plot when uncorrelated noise and independent, coincident periodic components have been added to each signal. This chaotic pattern is highly representative of hot firing data. Figures 5c and 5d are the recovered orbital diagrams by hypercoherence filtering and comb filtering, respectively. The superior performance of hypercoherence filtering is clearly indicated.

Figures 6a and 6b represent the filtered orbits from measurements at HPFT rad-90 degrees and rad-170 degrees during SSME tests 901-471 and 901-436, respectively. Figure 6a has a smooth orbital motion which represents a well-behaved rotational system. Figure 6b, however, indicates a potential rubbing problem. The two locations with sharp cusps appear to indicate possible impact between stationary and rotating system components.

GENERALIZED HYPERCOHERENCE

As discussed above, the spectral components to be identified by higher order spectra are required to satisfy certain frequency combinations (e.g., the sum of arguments is zero). However, in many situations, we wish to identify the correlation between two arbitrary frequency components that do not satisfy any such requirements. The generalized hypercoherence (GHC) was developed to deal with this situation. The GHC can identify the correlation between two arbitrary spectral components in the sense of frequency synchronization or lock-in.

To illustrate the approach, consider a gear train with gear ratio K. Coherent phase will exist between input and output rotational (spectral) components. When the gear ratio is an integer, the HC can identify their phase correlation. This is because the ambiguity introduced by the Riemann surface phase wrapping is within an integer multiple of 2π, which does not affect the coherence estimation. However, if the ratio is not an integer, phase wrapping will introduce a

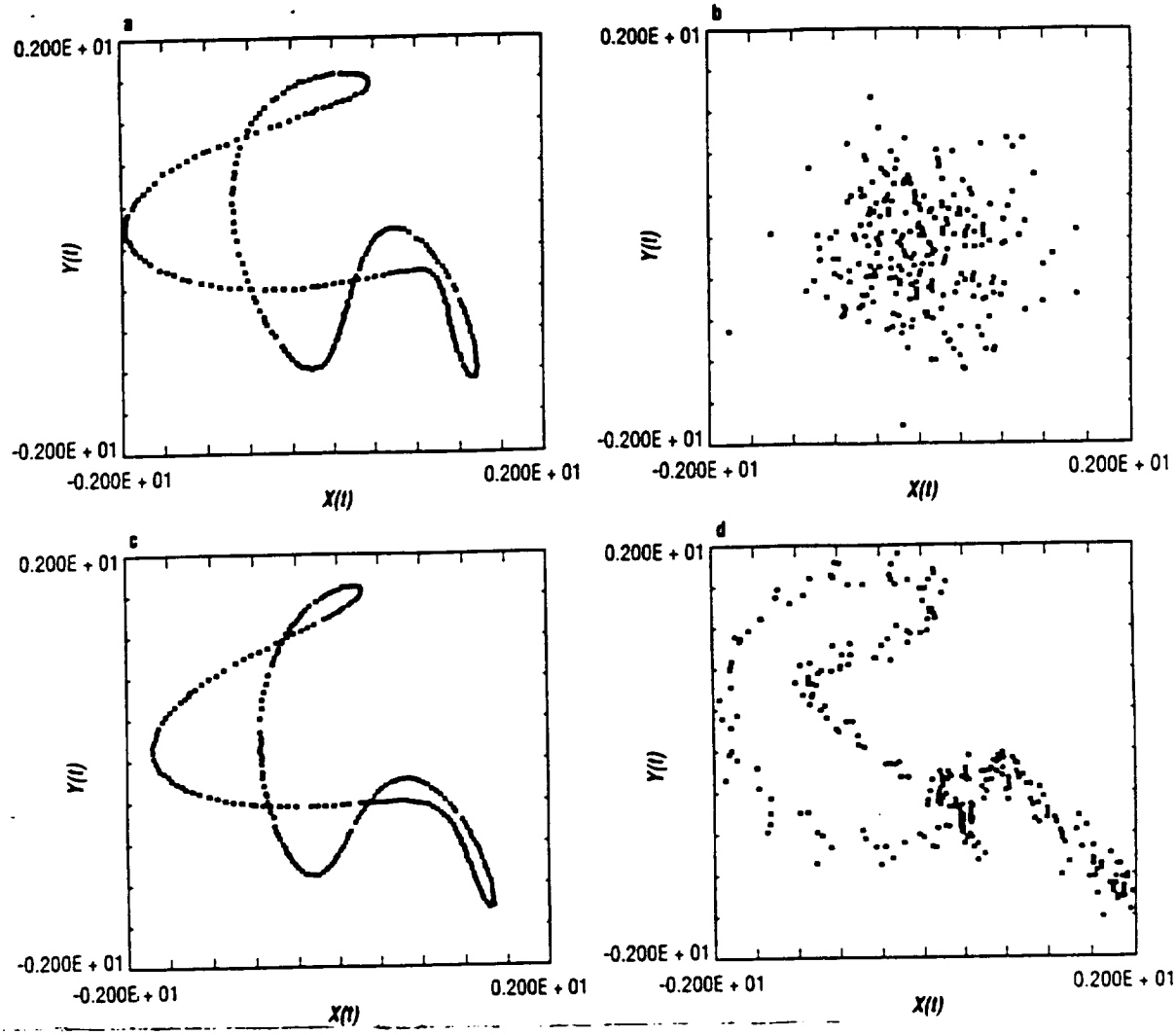

Fig. 5: (a) Orbital Diagram of Noise-free Simulation, (b) Orbital Diagram of Simulation with Additive Gassian White Noise, (c) Recovered Orbital Diagram by Hypercoherence Filtering, (d) Recovered Orbital Diagram by Using Comb

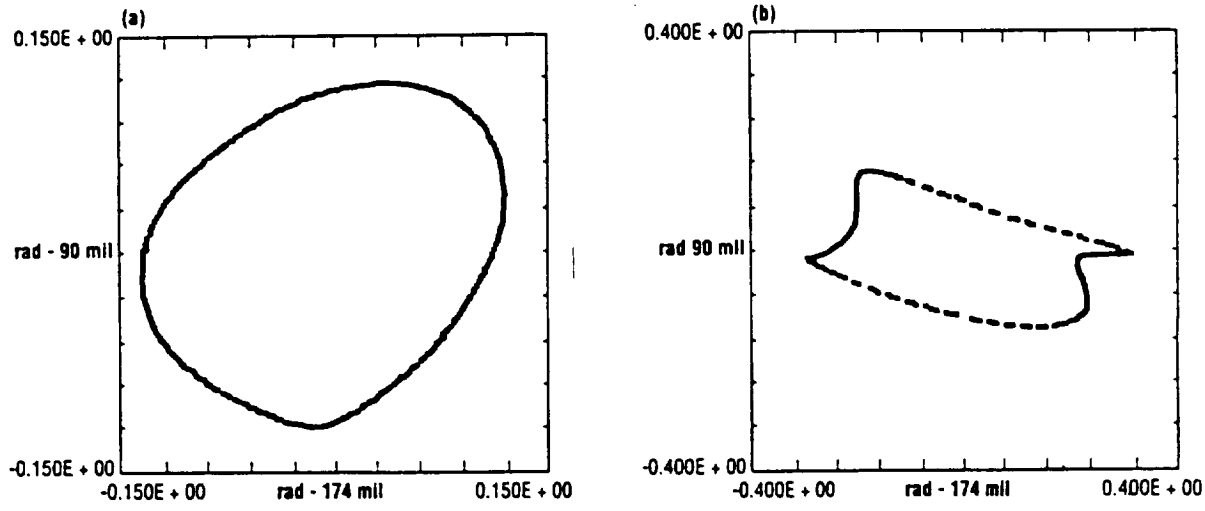

Fig. 6: a. Orbital Plot from Test 901-4T1 by Hypercoherence Filtering; b. Orbital diagram of 901-436

noninteger multiple of 2π, which yields ambiguous phase. Therefore, phase correlation cannot be uniquely identified in the phase domain. Based on this observation, the GHC was developed to identify such phase coherence by correlating the rate of change of phase, which is also called the instantaneous frequency. By taking the time rate of change of phase, the ambiguous term is eliminated, and the phase correlation is reflected in the frequency domain as frequency synchronization.

A vibration signal may be treated as an FM signal with different spectral components at different center (carrier) frequencies. Assume that there is some intelligence being frequency modulated in the signal as the instantaneous frequency about these carriers. To recover the intelligence, we demodulate the FM signal to estimate its instantaneous frequency signal. A narrow-band random process can be modeled as a sine wave with slowly varying amplitude A(t) and phase p(t):

$$x(t) = A(t) \cos [2\pi f_c t + p(t)]$$

The instantaneous frequency $f_i(t)$ is defined by:

$$f_i(t) = \frac{d\, p(t)}{d\, t}$$

A logic diagram illustrating the computational procedure is shown in Fig. 7.

Identification of composite modulation. The GHC technique was applied to identify a complicated modulation signal, the so-called "composite-modulation" phenomenon. It has been observed that modulation may exist between a harmonic of the shaft speed and a harmonic of a subsystem frequency without these harmonics showing up in the linear PSD. In such cases, direct (nonlinear) spectrum analysis is impractical. This composite-modulation phenomenon was observed in SSME vibration measurements associated with a bearing element defect as shown in Fig. 8. This PSD is taken from the SSME HPOP internal bearing strain gauge measurement during a hot firing test. The peaks marked N, 2N, 4N, etc., are the synchronous frequency component and its harmonics. The other peaks marked C and 2C are the bearing cage frequency components and are considered normal in such internal measurements. However, a strong anomalous component marked A is observed around frequency 8.5N. To assess this anomaly, we need to determine whether it is correlated with the cage or the sync frequency component.

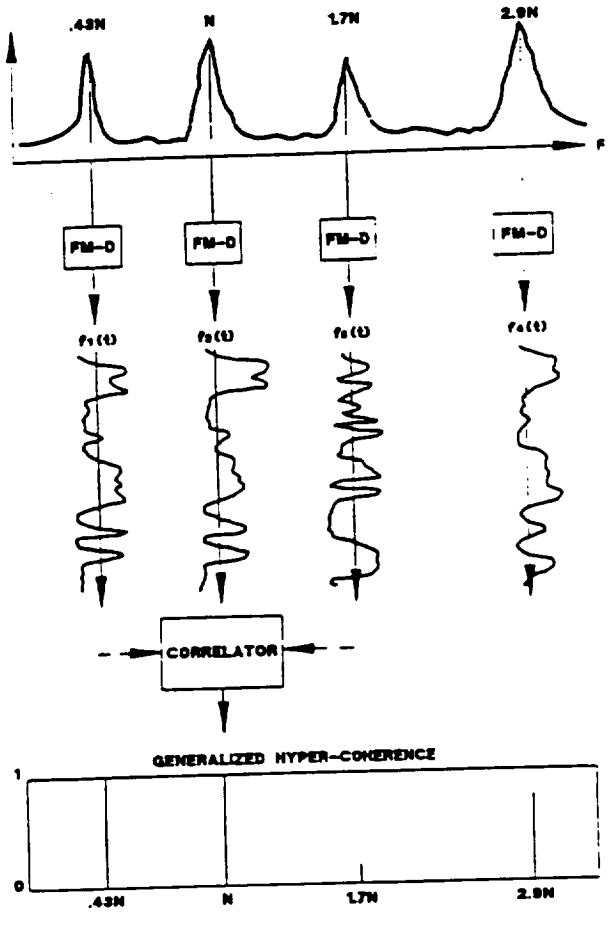

Fig. 7: GHC Through RM Demodulator

By examining the frequencies of these components, it is observed that the 8.5N is equal to 14N-12C, or 12(N-C) + 2N. This implies that the 8.5N component might be caused by the modulation between the inner ball pass component (for a 12-ball bearing set), which is at frequency 12(N-C), and the second harmonic of SYNC at 2N. If the existence of such modulation can be proven, then the anomalous 8.5N component would represent a bearing-related signature. Thus, we can identify the composite modulation by simply matching the appropriate integer multiple of each instantaneous frequency signal corresponding to each modulating component. In this example, the carrier frequency of the FM demodulator is tuned to the cage frequency C, the SYNC frequency N, and the anomalous frequency A to generate their IF signal as shown in Figs. 9(a), (b), and (d). Figure 9(c) shows the summation of 12 times the IF signal of C and 14 times the IF signal of N. Theoretically, this composite IF signal should be equal to the IF signal at frequency 14N-12C due to modulation of 14N and 12C. Compare this to figure 9(d), which is IF of the anomalous component A. Strong correlation can be identified between them. Therefore anomaly A turns out to be SYNC- and cage-related component likely being generated from the modulation of the inner ball pass frequency at 12(N-C) and 2 times SYNC at 2N.

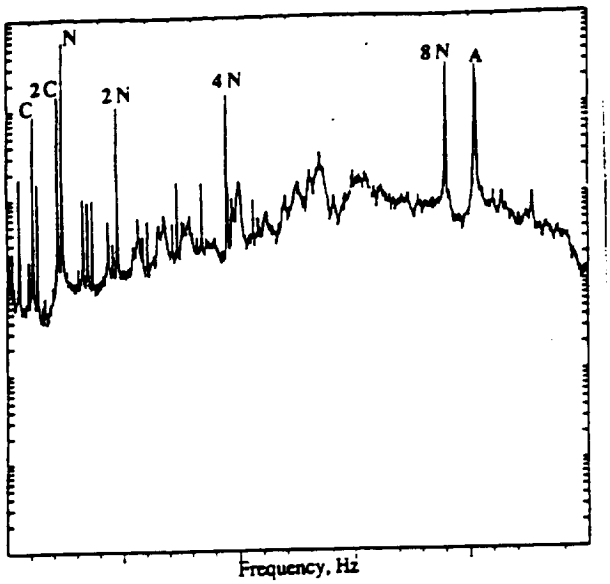

Fig. 8: Strain Gauge Measurements Showing Anomalous Component A at 8.5N

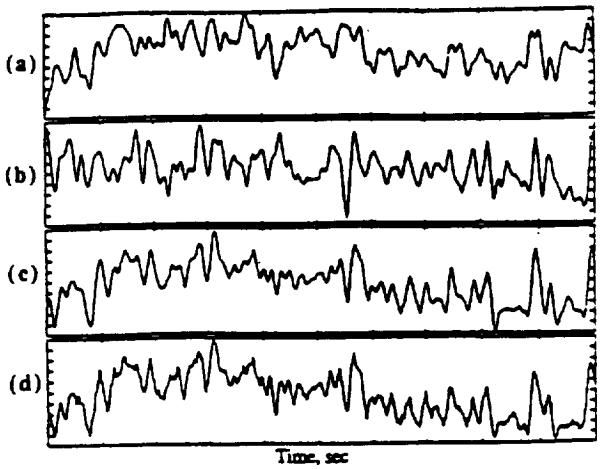

(a) Frequency signal of C (cage)
(b) Frequency signal of N (sync)
(c) Summation of 12 times the IF signal of C and 14 times the IF signal of N
(d) Instantaneous frequency signal of A (anomaly)

Fig. 9: Detection of Composite Modulation

NONSTATIONARY MODELS

Standard Fourier-based data analysis routines are based on the implicit assumption of a stationary time series. (The above techniques all require this assumption.) Turbomachinery components experience severe dynamic loads associated with highly transient operational periods of startup, shutdown, and engne throttling. A traditional tool for such analysis has been the short-time Fourier transform (STFT), which is obtained by applying a fixed-length moving time window to nonstationary data prior to performing the fast Fourier transform (FFT).[13] However, if the spectral components within the signal vary considerably during the time window, the STFT often fails in providing enough frequency resolution to identify key time-frequency spectral characteristics. It is well known in the theory of functional analysis that an arbitrary square integrable function x(t) can be decomposed into shifted and dilated versions of another square integrable function g(t) provided that g(t), called the analyzing wavelet, satisfies some additional conditions.[14] This leads to the wavelet transform (WT).[15] Having two free parameters available (a shift and a dilation), the WT offers greater flexibility than the STFT for modeling observed phenomena.

A third technique, called the Wigner distribution (WD) is capable of providing high resolution time-frequency estimates of nonstationary signals which are common in many fields, including the dynamic response of rotating machinery.[16,17] Several obstacles arise in the direct use of the WD, particularly for signals with multiple spectral peaks. Most notable of these are aliasing and the generation of "phantom" spectral peaks in the resultant time-frequency distribution. A number of attempts, with varying degrees of success, have been employed to minimize these effects.[18,19,20] The following discussion presents yet another approach. With the introduction of the "smart window," this approach will overcome these obstacles.[8]

THE MODIFIED WIGNER DISTRIBUTION

The WD is a powerful tool in determining the time-frequency characteristics of a highly nonstationary signal. The technique has been applied successfully in the identification of abnormal machine operating states through vibration signal analysis. Other applications include the analysis of time-varying spectra in optics, speech, sonar, and seismic signal processing.

The WD of a real signal r(t) is given by

$$W(t,f) = \int z(t+\tau/2)\, z^*(t-\tau/2)\, e^{j2\pi f\tau}\, d\tau ,$$

where z(t) is the analytic signal of r(t), z(t) = r(t) + ji(t), and i(t) is the Hilbert transform (HT) of r(t), i(t) = HT[r(t)]. Therefore, the WD is the Fourier transform (FT) of the product between the original forward signal and corresponding backward signal both centered at time t.

In order to serve as a practical tool in the time-frequency analysis of multicomponent signals, unwanted erroneous spectral components due to cross coupling must be eliminated. The MWD accomplishes this. Thus, the superior time-frequency resolution of the WD can be attained without the generation of erroneous spectral peaks.

For a cross section of the time-frequency representation of a real signal r(t), at $t=t_0$, the MWD is defined by

$$M(t_0,f) = \int W(\alpha - f/2)\, X(\alpha)\, Y(f-\alpha)\, d\alpha,$$

where
$$x(t) \equiv r(t_0+t)$$
$$y(t) \equiv r(t_0-t)$$
$$X(f) \Leftrightarrow x(t)$$
$$Y(f) \Leftrightarrow y(t)$$

As the above suggests, the MWD is evaluated in the frequency domain using the FTs of a real time signal centered at t_0 and its respective reversed signal also centered at t_0. The central trait of the MWD which separates the technique from the traditional WD is its smart frequency window function, $W(f)$. Use of this window function eliminates the cross coupling of positive frequency components. This in turn prevents erroneous spectral peaks from entering the MWD time-frequency representation during the evaluation of a multicomponent signal. Moreover, use of the smart window, $W(f)$, eliminates cross coupling between positive and negative frequency components by preventing their interaction during the evaluation of the MWD.

A digital recipe for extracting the MWD, given a discrete time series, is as follows:

$$M(k) = \sum_{i=-m}^{+m} X(k+i)\, X^*(k-i)\, W_N^{-(k-i)} .$$

The above states that the evaluation of the MWD at frequency k is simply the sum of the left-hand side and right-hand side of a signal's FFT spectrum, X(k), with both sides centered at frequency k, modified by a phase correction term of unity amplitude. Note that when no window is applied (m=0), the MWD reduces to a special form with an amplitude equal to the power spectral density (PSD) but modified by a phase term.

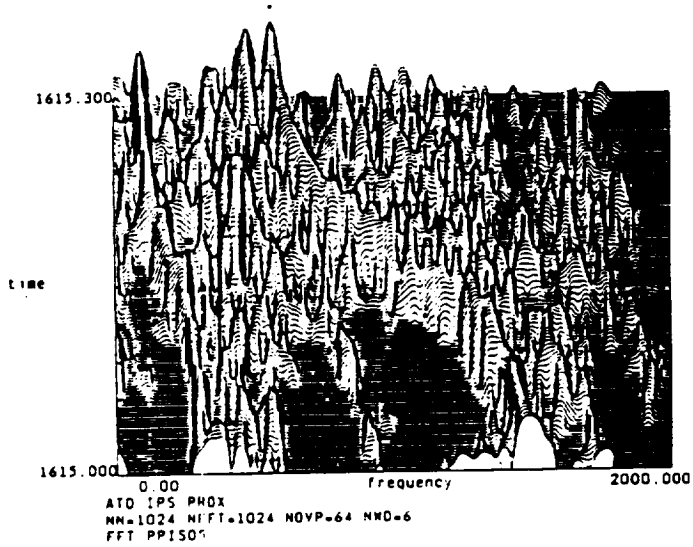

Fig. 10: Short-time Fourier Transform During Engine Shutdown

MWD APPLICATION

Figure 10 is an STFT isoplot showing the shutdown of an SSME alternate turbopump development (ATD) test following a component failure. In order to study the temporal and spectral characteristics of the signal just prior and following the failure, analysis focused on a very short time period around 615 s. Figure 10 shows the plot for a 300-ms period extending from 615 to 615.3 s. No clear spectral characteristics can be identified in this time-frequency representation of the proximity probe measurement. Figure 11 is the MWD spectrum for the same period using identical processing parameters. While use of the traditional WD would introduce numerous erroneous spectral components, the MWD is successful in providing a much clearer time-frequency picture of the signal without the "spurious" peaks.

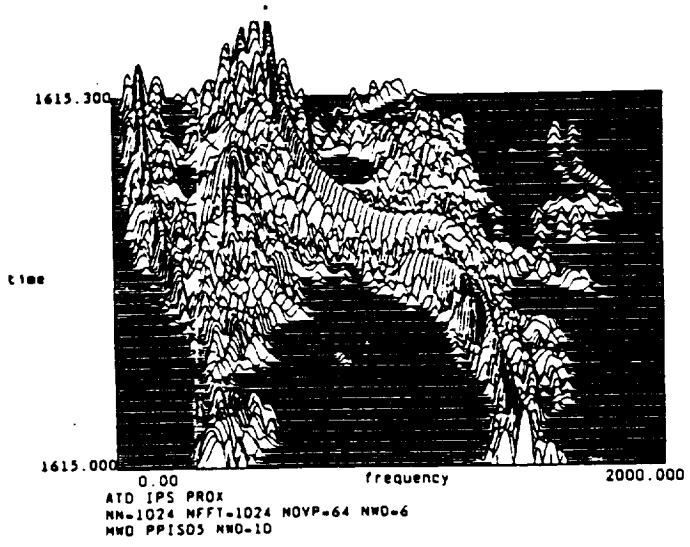

Fig. 11: Modified Wigner Distribution During Shutdown

CONCLUDING REMARKS

The above discussion provides an overview of rocket engine diagnostic efforts in progress at MSFC. The technology is seen to be highly evolutionary. The effort is strongly driven by engine test observations, but the techniques should find wide application for dynamic data analysis and system identification. In conclusion, it is well realized that dynamic data assessment is but one of many necessary elements in the MSFC engine development and reliability improvement process.

REFERENCES

1 Coffin, T., W. L. Swanson, and J. Y. Jong. "Data Analysis Methods and Signal Processing Techniques for Space Shuttle Main Engine Diagnostic Evaluation," Wyle Laboratories Final Report (NAS8-36549) Oct. 1989.

2 Jong, J. Y. "Advanced Signal Analysis Methods for SSME Diagnostic Evaluation," MSFC, S&D Lab Seminar Notes (NAS8-38156), April 1990.

3 Coffin, T., and J. Y. Jong. "A Nonlinear Coherence Function and Its Application to Machine Diagnostics," 110th Meeting of the Acoustical Society of America, Nov. 1985.

4. Jong, J. Y., and T. Coffin. "Diagnostic Assessment of Turbomachinery by the Hyper-coherence Method, " NASA Conf. Pub. CP2436, May 1986.

5. Jong, J. Y., T. Coffin, J. H. Jones, J. E. McBride, and P. C. Jones. "Correlation Identification Between Spectral Components by Generalized Hypercoherence," 3rd Internat'l Mach. Monitor. and Diag. Conf., Dec. 1991.

6 Jong, J. Y., T. Coffin, and J. H. Jones. "A Non-linear Hyper-coherence Filter for Damage Assessment in Noisy Environments," Model Determination for Large Space Systems Workshop (J. C. Chen, Ed.) JPL Doc. D-5576, vol. 3, Mar. 1988, pp. 1129-1142.

7 Coffin, T., and J. Y. Jong. "Some Nonlinear Spectral Methods and Their Application to Rocket Engine Diagnostics," First Internat'l Machinery Monitoring and Diagnostics Conf., Sept. 1989.

8 Jong, J. Y., and T. Zoladz. "Time-Frequency Representation of a Highly Nonstationary Signal Via the Modified Wigner Distribution," NASA technical paper (in publication).

9 Collacott, R. A. *Mechanical Fault Diagnosis and Condition Monitoring*, Chapman and Hall, London, 1977.

10 Eshleman, R. L. "The role of sum and difference frequencies in rotating machinery fault diagnosis," 2nd Internat'l Conf. on Vibration in Rotating Machinery, Churchill College, 1980.

11 Bendat, J. S. *Nonlinear System Analysis and Identification*, John Wiley & Son, New York, 1990.

12 Brillinger, Dr. R. "An Introduction to Polyspectra," *Annals of Mathematical Statistics*, 36, 1964.

13 Nawab, S., and T. Quatieri. "Short-Time Fourier Transform," *Advanced Topics in Signal Processing* (J. Lim and A. Oppenheim, ed.), Prentice Hall, Englewood Cliffs, N.J., 1988, pp. 289-337.

14 Grossmann, A., and J. Morlet. "Decomposition of Hardy Functions into Square Integrable Wavelets of Constant Shape," SIAM *J. Math. Anal.*, vol 15, No. 4, 1984, pp. 723-736.

15 Rioul, O., and M. Vetterli. "Wavelets and Signal Processing," IEEE *Signal Processing*, Oct. 1991, pp. 14-38.

16 Wigner, E. "On the Quantum Correction for Thermodynamic Equilibrium," Phys. Rev. 40, 1932, pp. 749-759.

17 Claasen, T. A. C. M., and W. F. G. Mecklenbrauker. "The Wigner Distribution—A Tool for Time-Frequency Signal Analysis," *Philips J. Res.*, vol. 35.

18 Boashash, B., and P. Black. "An Efficient Real-Time Implementation of the Wigner-Ville Distribution," *IEEE Transact. Acoustics, Speech, and Signal Processing*, vol. ASSP-25, No. 11, Nov. 1987.

19 Meng, Qingfeng, and Liangsheng Qu. "Rotating Machinery Fault Diagnosis Using Wigner Distribution," *Mechanical Systems and Signal Processing*, vol. 5(3), 1991, pp. 155-166.

20 Rao, P., F. Taylor, and G. Harrison. "Real-time Monitoring of Vibrations Using the Wigner Distribution," *Sound and Vibration*, May 1990.

TECHNICAL PROGRESS REPORT

January 1993

DATA ANALYSIS AND DIAGNOSTIC EVALUATION OF SPACE SHUTTLE MAIN ENGINE DYNAMIC MEASUREMENTS

NASA CONTRACT NO. NAS8-38156

Prepared for

NATIONAL AERONAUTICS AND SPACE ADMINISTRATION
GEORGE C. MARSHALL SPACE FLIGHT CENTER
MARSHALL SPACE FLIGHT CENTER, ALABAMA 35812

by

WYLE LABORATORIES

WYLE ENGINEERING DIVISION
7800 Governors Drive, West
Huntsville, Alabama 35807

WYLE TECHNICAL REPORT TR-60900-93-01

WYLE

Program Manager: T. Coffin
Contract Manager: J. Kelly

NASA

Contract Monitor: J. McBride
Contracting Officer: H. Amburn

WYLE LABORATORIES

CAVITATION DETECTION & MONITORING USING WIDE-BAND DEMODULATION SIGNAL

by: Jen-Yi Jong

[1] INTRODUCTION

A series of Inducer Test Leg (ITL) water flow tests were conducted to study cavitation phenomena in the water flow test facility at Marshall Space Flight Center (MSFC). From video taken during these tests, one can clearly visualize how cavitation develops and changes from one state to another, such as four-blade cavitation to alternate-blade cavitation. The signal from a vibration or high frequency pressure measurement also reflects such a cavitation condition change. However, in complicated operational conditions as experienced during flights or engine hot firing tests, these vibration signals will also contain elements induced by rotor-dynamics, structural dynamics, and hydrodynamics, which make it difficult to identify the failure sources when engine failure or malfunction occurs. Therefore, it is highly desirable to develop an effective method for cavitation detection and monitoring using vibration signal analysis when video information is not available.

The technique to be discussed in this section for cavitation detection and monitoring is based on a unique cavitation phenomenon reported in literature as:

> **"When cavitation occurs, the periodic rotational components (such as SYNC & its Harmonics) will amplitude modulate the wide-band high frequency noise generated from the collapse of cavitation bubbles."**

Such a wide-band modulation phenomenon thus provides a unique signature in the high frequency region conductive to cavitation detection. However, conventional PSD analysis is unable to identify the signature associated with such a modulation phenomenon. In this section, the Wide Band Demodulation (WBD) signal method for cavitation detection will be discussed. Real test data from both inducer water test leg as well as Alternate Turbopump Development (ATD) E8 test stand will be used in demonstrating this WBD technique.

[2] WIDE-BAND MODULATION (WBM) SIGNAL

The signal model for Wide-Band Modulation can be represented as a sine wave multiplied by a noise signal N(t):

$$x(t) = [\ 1 + r \cos(Wrt)]\ N(t)$$

where cos(Wrt) represents a periodic motion, and N(t) is zero-mean Gaussian White or Color Noise.

In signal processing literature, this type of signal is referred to as a "Cyclostationary signal". A special kind of periodicity exists in such a Cyclostationary signal. However, this periodic component is well hidden in the signal. An ordinary PSD will not show a discrete peak at the frequency of the periodic component. This can be easily deduced from studying its signal model. The operation between N(t) and cos(Wrt) in the time domain is multiplication, but this multiplication becomes a convolution in the frequency domain. Since the PSD of noise is flat and that of a sine wave is a delta function, the convolution of these two PSD functions remains flat without any discrete peak. For this reason, a conventional PSD is unable to identify periodic components hidden within a Wide-Band Modulation signal.

[3] WIDE-BAND DEMODULATION (WBD) SIGNAL

In this section, three different methods for demodulating a WBM signal into a WBD signal are discussed. These are the tri-spectra method, the rectification method, and the Hilbert Transform envelope detection method. Simulation examples using an analytically generated signal will be used to demonstrate these wide-band demodulation processes.

Reference: "Fourth Order Spectra of Gaussian Amplitude-Modulated Sinusoids" Roger Dwyer, Navy Underwater System Center, Journal of Acoustic Society of America, August 1991.

In this reference, Dwyer proposes a special tri-spectral method to identify the existence of cyclostationary signals in underwater sonar signal processing. This tri-spectra is based on the Fourier Transform of a special auto-tri-correlation function $R_{xxxx}(T)$, which is defined as:

$$R_{xxxx}(T) = E[\ x(t)\ x(t)\ x(t+T)\ x(t+T)\ ]$$

$$= E[\, x^2(t)\, x^2(t+T)\,] = R_{yy}(T)$$

Where $y(t) = x^2(t)$

The special tri-spectrum T(W) is defined as the Fourier Transform of $R_{xxxx}(T)$ Notice that, the function $R_{xxxx}(T)$ reduces to the ordinary auto-correlation of y(t), where y(t) is defined as the square of the original signal x(t). In other words, this special tri-spectrum is equal to the ordinary PSD of the square of the original signal. By examining the WBM signal model, it can be easily seen why such a simple square operation can recover the hidden periodicity in a WBM signal. The square of x(t) can be written as:

$$x(t)^2 = [\, 1 + r\, \mathrm{Cos}(w_r t)\,]^2\ [\, N(t)\,]^2$$

$$= [\, 1.5 + 2r\, \mathrm{Cos}(w_r t) + 0.5\, r^2\, \mathrm{Cos}(2\, w_r t)\,]\ [DC + N'(t)\,]$$

Terms Through Which Periodic Component Recovered

Where N'(t) is defined by the following relationship:

$$[\, N(t)\,]^2 = [DC + N'(t)\,]$$

When squaring a zero-mean noise signal, a DC (mean value) component is introduced, and this DC component will be multiplied by the periodic component $\mathrm{Cos}(W_r t)$. The resulting component then becomes superpositioned on the new noise component N'(t). It is this new DC-introduced superpositioned term that allows the recovery of the periodic component hidden in the original WBM signal

A simple simulation example will now be used to demonstrate this WBD process. Figure 1-a and 1-b show the respective time histories of simulated Gaussian White Noise (GWN) and a sine wave at 500 Hz. The time history x(t) in figure 1-c is generated from multiplication of the GWN and the sine wave. The time history in figure 1-d is simply generated by the squaring of x(t).

As discussed above, the ordinary PSD of x(t), as shown in figure 2-a, does not show a discrete peak at the periodic frequency of 500 Hz. However, after squaring the signal, the DC-introduced superpositioned term generates a periodic component at 1000 Hz which is twice the periodic frequency of 500 Hz. This is how such a simple squaring operation is able to recover the hidden periodicity within a WBM signal.

[4] CAVITATION GENERATED WBM SIGNAL

The signal generated by cavitation can be modelled as the multiplication of two separate components p(t) and N(t):

$$x(t) = p(t)\, N(t)$$

Here, N(t) represents the wide-band high frequency noise generated from the collapse of cavitation bubbles, while p(t) represents the low frequency periodic pressure fluctuation due to the impeller rotational process. This pressure signal p(t) contains a DC component due to its static pressure component P_{static}.

$$p(t) = [\, \underset{DC}{P_{static}} + P(t)_{dynamic} \,].$$

Therefore, a cavitation generated pressure signal is a typical WBM signal and is a good candidate for WBD processing. However, in most operational environments, the dynamic signal must be sampled at a much higher frequency than a regular dynamic analysis would require. This is because the PSD in the low frequency region always contains the fundamental Sync frequency component along with its harmonics (2N, 3N, 4N...), which are generated from the combination of all the effects of rotor dynamics, structural dynamics and hydrodynamics. These combinational effects make it difficult to isolate sources of vibration problems. However, when cavitation occurs, its signature should be contained in the noise floor of the high frequency region due to the uniqueness of wide-band modulation. The significance of this phenomenon is that the source of vibration can now be isolated to the hydrodynamic effects whose information is contained in the high frequency noise floor.

For cavitation detection, the high frequency raw signal must be high-pass filtered first to remove low-frequency discrete components while keeping the high frequency wide-

band noise data. WBD is then performed on this high-frequency noise floor data in order to recover any existing low frequency periodic component which is modulating the cavitation noise signal. As a result, a new low frequency WBD PSD is generated in addition to the original raw data PSD. However, unlike the raw data PSD which including multiple contributions from rotordynamics, structure dynamics and hydrodynamics, this new WBD PSD only reflects the hydrodynamic effect due to cavitation-generated modulation. If cavitation does not exist, the WBD PSD will reduces to regular broadband noise. However if cavitation does occur, the WBD PSD will show discrete peaks corresponding to the low frequency periodic rotational process modulating the collapsing bubble noise. This discussion is also depicted in figure 3.

Figures 4 shows three different algorithms for performing WBD. The first one shown in figure 4-(1) is the tri-spectrum method. The input raw wide-band high frequency signal is first high-pass filtered at some pre-determined cut-off frequency, then sent through a squaring operation, and then low-pass filtered. The PSD of the output signal is the special tri-spectral function T(w). The original hidden periodicity within a WBM signal will now show up at its periodic frequency in the tri-spectra function. Figure 4-(2) shows the similar algorithm using the rectification method. Again, a WBM signal is high-pass filtered, then rectified, and low-pass filtered. Figure 4-(3) shows the Hilbert Transform method. Again, the input signal is first high-pass filtered, then Hilbert Transformed into an envelope signal which is then low-pass filtered. The PSD of the output signals from both figures 4-(2) and 4-(3) should identify the original hidden periodicity within the WBM signal.

[5] WBD SIGNAL FOR REAL TEST EXAMPLE

Real test data taken from 6 different accelerometers and pressure measurements across ATD LOX pump unit 3-1A during test E8-162 can be used to successfully demonstrate the WBD process. The inducer of this unit has four blades. Figure 5 shows the ordinary raw PSD corresponding to these six different measurements up to a maximum frequency of 5 KHZ. These PSDs all show the fundamental Sync frequency component and its harmonics. Figures 6 shows the ordinary raw PSDs of these 6 measurements with the maximum frequency increased to 50 KHZ. The discrete peaks are mostly concentrated in the low frequency region with some high frequency discrete line noise peaks also in the spectra. Notice that the signal in the wide-band high frequency noise floor is the prospective information to be used for cavitation detection. These high

frequency noise floors may contain just regular noise, or may have the very unique wide-band modulation phenomenon hidden within. Using the PSDs of both figures 5 and 6, one would not be able distinguish such a subtle difference.

The high frequency signals shown in figure 6 are first high-pass filtered at 20 Khz, after which their envelope signals are calculated through Hilbert Transform. Finally the envelope signals are low-pass filtered at 5 Khz. Figure 7 shows the resulting WBD PSDs of these 6 measurements. For the first five measurements, which include four accelerometers and one inducer outlet pressure measurement, no periodic component is recovered in the WBD signal. This indicates that the original wide-band high-frequency noise components of these five measurements are just ordinary noise signals with no modulation phenomenon present. However, in the sixth plot of figure 7, corresponding to the Three Quarter Chord Inducer Inlet Kistler pressure measurement, several strong discrete components show up in the WBD PSD. This indicates that wide-band modulation phenomenon indeed exists in the high frequency noise floor. In other words, cavitation is present in this test, and the rotational periodic components modulate with collapse bubble noise generating a unique WBM high-frequency noise floor. The demodulated WBD signal thus recovers these hidden discrete components.

Moreover an interesting phenomenon is present in this wide-band demodulation result. Notice that this WBD PSD of figure 7 has a strong 2N component and relatively weaker 1N, 3N and 4N components. Would this be an indication of an alternate-blade cavitation condition in which case cavitation bubbles only attach to two diagonally opposite blades of the four-blade inducer? In the following section , a WBD signal will be used not only to detect the presence of cavitation, but it will also allow us to monitor the condition of cavitation (i.e. four-blade or alternate-blade cavitation) as a function of time during test.

[6] WBD SIGNAL FOR INDUCER TEST LEG WATER FLOW TESTING

In this section, WBD analysis for Inducer Test Leg (ITL) water flow test data is performed and cavitation condition predictions are compared to actual cavitation conditions visually monitored during the test. The actual cavitation conditions can be easily recognized in the video taken using a flow visualization device. Also in this testing, ordinary PSD already accurately reflect cavitation conditions since the testing is conducted in a laboratory environment which isolates the hydrodynamic effects. Therefore, the accuracy and effectiveness of the WBD signal for cavitation monitoring can best be verified using this water flow test data.

Figure 8 shows a regular PSD isoplot taken from a Kistler pressure measurement from Inducer Test Leg (ITL) Water Flow Test ITL-173. At the beginning of the test, one can clearly visualize from the video information that there are cavitation bubbles attached to each of the four inducer blades (four-blade cavitation). Then at a later time, around S+69s, two alternating bubbles out of the original four disappear. This indicates that the original four-blade cavitation condition has changed into alternate-blade cavitation. Later on at S+92s, the cavitation phenomenon totally disappears. This cavitation condition change is indeed accurately reflected by the raw PSD isoplot of figure 8. At the beginning of the test when the inducer is experiencing four-blade cavitation, the 4N PSD component is dominant. At S+69s, when the inducer begins experiencing alternate-blade cavitation, the 4N component diminishes while the 2N component starts to grow and dominate. Finally when all cavitation phenomenon disappears at S+92s, both the 2N and 4N components diminish. Therefore, in this particular case under isolated laboratory environment, the traditional raw PSD is already accurately monitoring the cavitation condition.

Figure 9-a and 9-b are the ordinary PSDs of the raw signal and high-pass filtered signal of the Kistler measurement with a maximum frequency 50 KHz. In this high-pass filtered version, all the low frequency discrete components under 5000 Hz are removed. WBD will be performed based on the wide-band high frequency noise floor of figure 9-b. Figure 10-a shows the 5 Khz raw data PSD at the beginning of the test, S+0s. The 4N component is dominant since the four bubble regions due to four-blade cavitation are generating a four pulse per revolution pressure fluctuation. Figure 10-b

shows the corresponding 5 Khz WBD PSD. This WBD PSD recovers several discrete components with the 4N component being the dominant one. This WBD PSD indeed correctly reflects the fact that the inducer is experiencing four-blade cavitation at the beginning of the test.

Figures 11-a and 11-b are the raw data and the WBD PSDs at S+69s when the four-blade cavitation changes into alternate-blade cavitation. The dominant peak of the WBD signal has now changed from 4N to 2N, which again correctly reflects actual cavitation condition changes the inducer experiences.

Figure 12 shows the corresponding PSD isoplot of the WBD signal. This time-frequency energy distribution agrees quite well with the regular raw data PSD isoplot and correctly monitors the cavitation condition change. However, when dealing with data from real world cases such as flight or hot firing tests rather than an isolated laboratory environment, a raw data PSD will reflect contributions from other effects (e.g. rotor and structural dynamics) other than just the hydrodynamic cavitation effects. These multiple contributions will make it difficult to identify the existence of cavitation or monitor cavitation condition changes. In this case, the WBD signal becomes an effective tool for cavitation monitoring.

[7] WBD SIGNAL FOR ATD E8 TEST

In this section, two different ATD E8 tests are discussed and analyzed using the WBD signal. In the first example (test E8-161), ATD HPOTP vibration levels are nominal. While during the test of the second example (test E8-162), an early test rig red-line cutoff occurred due to high synchronous vibration level. A WBD analysis is performed in order to determine if any significant discrepancy in the dynamic characteristics associated with cavitation condition existed between these two tests.

ATD TEST E8-161: NO HIGH SYNC VIBRATION CUTOFF

Figure 13 shows the raw PSD isoplot from Three Quarter Chord Inducer Inlet Kistler pressure measurement data taken during test E8-161. The time frame spans two different power levels, 104% and 111%. Throughout the test, the 4N component is dominant. However, immediately after the power level ramp up to 111%, the 2N

component starts to grow but remains smaller than the 4N component. Notice that, the 1N component was never really strong as compared to the 2N and 4N components.

Figure 14-a shows the composite RMS tracking time history of this Kistler measurement. The overall vibration level is getting stronger toward the end of the test. However, since the vibration level of the 1N component never exceeds the red-line level, early test rig cutoff never occurs in this test. Figure 14-b and 14-c show the raw PSD and band-pass filtered PSD of the Kistler transducer with a maximum frequency of 50 Khz. Information relating to the cavitation condition as experienced by the inducer is contained in the wide-band high frequency noise floor of figure 14-c, and will be recovered from the WBD signal.

Figure 15-a and 15-b are the 5 Khz raw and WBD PSDs of the Kistler measurement at 104% rated power level (RPL) . The raw PSD picks up moderate N, 2N, 3N responses and a strong 4N component. Since the 4N component is the dominant component, the raw PSD indicates the possible existence of four-blade cavitation. Since the WBD PSD of figure 15-b clearly shows a dominant 4N component, it verifies that cavitation does exist and is indeed four-blade cavitation.

Figure 16-a and 16-b show the raw data and WBD PSDs at 111% power level. The raw data PSD picks up a weak N, a stronger 2N, and a dominant 4N component. It now becomes more difficult to identify whether the inducer is experiencing alternate-blade or four-blade cavitation just from this raw PSD. Since the WBD PSD only picks up a strong 2N component and some weak harmonics of 2N, cavitation has changed from a four-blade cavitation condition at 104% power level into an alternate-blade cavitation at 111% power level. This cavitation condition change is not at all obvious judging from its raw PSD. This is because other sources such as the ordinary linear 4N blade-passage pressure wave are corrupting the raw data. The WBD PSD isoplot in figure 17 clearly shows this cavitation condition change. Before the power level change, 4N is weak but is still the dominating one. But right after the power level change, the 2N component immediately takes over and becomes the strongest component.

Notice that there exist some similarities between the cavitation conditions of this E8-161 test and the Inducer Test Leg (ITL) water flow test example discussed in the previous section. In both of these tests, WBD PSD all present a dominant 4N

component as an indication of four-blade cavitation, and a dominant 2N component as an indication of alternate-blade cavitation. Another significant similarity is that the 1N component of their WBD PSDs was almost non-existent. Generally speaking, the regular raw PSD of a dynamic measurement will always pick up a relatively strong sync frequency component since 1N is the fundamental driving force in the dynamic system. A 1N presence in raw PSD data is considered to be normal unless its amplitude becomes too large. However, the presence of a sync frequency component in a WBD PSD would indicate an asymmetrical or unbalanced cavitation distribution. Such an asymmetric cavitation bubble distribution might create additional shaft unbalance forces and cause a high synchronous vibration.

ATD TEST E8-162: WITH HIGH SYNC VIBRATION INDUCED EARLY CUTOFF

During the ATD HPOTP test E8-162, early red-line cutoff occurred due to high level sync vibration. Figure 18 shows the raw PSD isoplot of the HPOTP Inducer Inlet Kistler measurement. The 4N component is clearly the dominant throughout the test. Originally the 1N component is relatively weak, but at around S+25.2s, its amplitude starts to grow rapidly and turns into a strong sync vibration ultimately leading to an early test rig cutoff.

Figure 19-a shows the composite RMS tracking time history from an ATD HPOTP strain gauge measurement. Right before the cutoff, there is a small jump in RMS amplitude directly followed by a rapid amplitude growth resulting in a high vibration cutoff of the test rig. Figure 19-b shows the high-pass filtered raw data PSD in which the wide-band high frequency noise floor is used for wide-band demodulation.

Figures 20-a and 20-b are the raw data and WBD PSDs of the Kistler measurement. Unlike the previous cases, a strong 1N component starts to show up in the WBD PSD. The presence of this strong 1N component is the most distinctive feature between this high-vib test and test E8-161 along with the ITL water flow test both without high synchronous vibration. The WBD PSD isoplot in figure 21 shows more clearly this cavitation condition change. Originally, the 2N component is dominant and is an indication of alternate-blade cavitation. Later on at S+23.5s, the 1N component starts to grow rapidly and then diminishes again. About half second later, high synchronous vibration occurs and leads to test rig cutoff. The cavitation-generated WBD signature

indeed shows some peculiar condition change right before the high-vib event. Whether this peculiar WBD signature change is directly related to the follow-on high synchronous vibration acting as a precursor is yet to be determined. Further research is currently in work.

[8] CONCLUDING REMARKS

When cavitation occurs, the periodic shaft rotational components will amplitude modulate the wide-band noise generated from collapsing cavitation bubbles. This wide-band modulation will make the periodic component become undetectable in the raw PSD of its dynamic measurement signal. However, this special phenomenon provides a unique signature for cavitation detection and monitoring. By using the WBD technique, the hidden periodicity can be recovered from a wide-band high frequency noise signal. The resulting WBD PSD can better indicate cavitation condition changes as compared to an ordinary raw data PSD. Some observations are summarized below:

. Vibration data taken from Inducer Test Leg water flow tests have verified that such cavitation-generated WBM phenomenon does exist in its dynamic signal. In addition, the hidden periodicity recovered from its WBD signal correctly identifies the cavitation condition changes during the test.

. Some similarities exist between the ITL water flow test and ATD test E8-161 of which neither experienced a high vibration cutoff. During these two tests, WBD PSDs show a dominant 4N component as an indication of four-blade cavitation and a dominant 2N component as an indication of alternate-blade cavitation. Most importantly, the WBD PSD 1N components for both tests are almost non-existent. A strong sync frequency component in a WBD PSD would indicate an asymmetrical or unbalanced cavitation distribution which generates additional shaft unbalancing force.

. Unlike the cavitation conditions observed in water flow testing and the E8-161 test, a strong WBD PSD 1N component is observed during ATD test E8-162, in which strong synchronous vibrations led to an early test-rig red-line cutoff. This strong WBD 1N component is the most distinctive feature between this test with high sync vibration cutoff and those without cutoffs.

. The WBD technique discussed in this section suffers from a severe limitation. Since the hidden periodicity is recovered from the envelope signal of a high frequency wide-band noise floor, any discrete components present in this high frequency region of the raw signal will generate false discrete peaks in the WBD signal pretending to be recovered hidden periodicities. This limitation may not be so critical in an isolated environment such as during laboratory testing where no discrete component shows up in high frequency region. But it would be a critical limitation in dealing with static firing of flight data in which many other vibration sources will contribute all kinds of high frequency components that corrupt the WBD signal. Attempts to remove such high frequency interference by using bandpass and adaptive filtering have been attempted. However, only a limited degree of success was achieved for a few simple cases. This procedure is tedious and inefficient, and it is difficult to be automated. Development of an efficient and effective method for wide-band demodulation without such a discrete-interference limitation is recommended for future research.

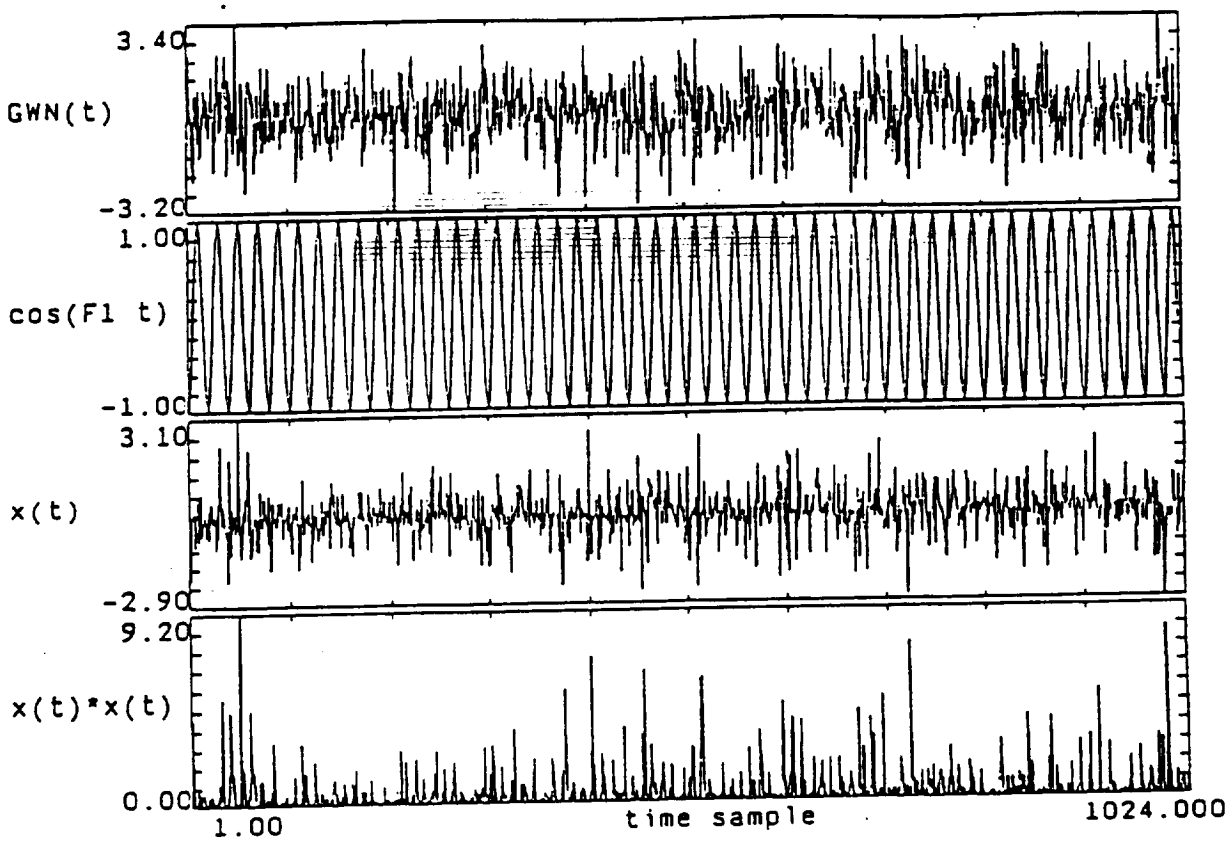

simulation signal x(t) = GWN(t) cos(F1 t) F1=500 Hz

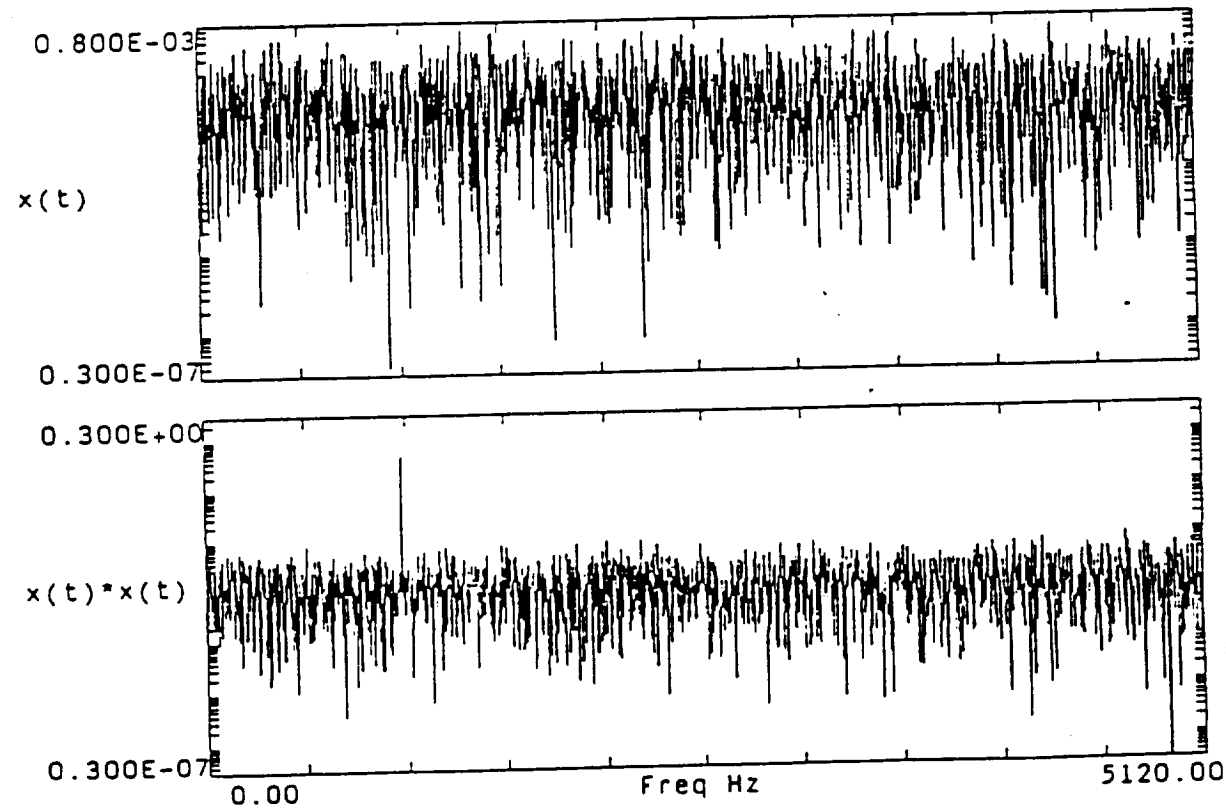

simulation signal x(t) = GWN(t) cos(F1 t) F1=500 Hz
y(t) = x(t) * x(t)

WIDE-BAND DEMODULATION

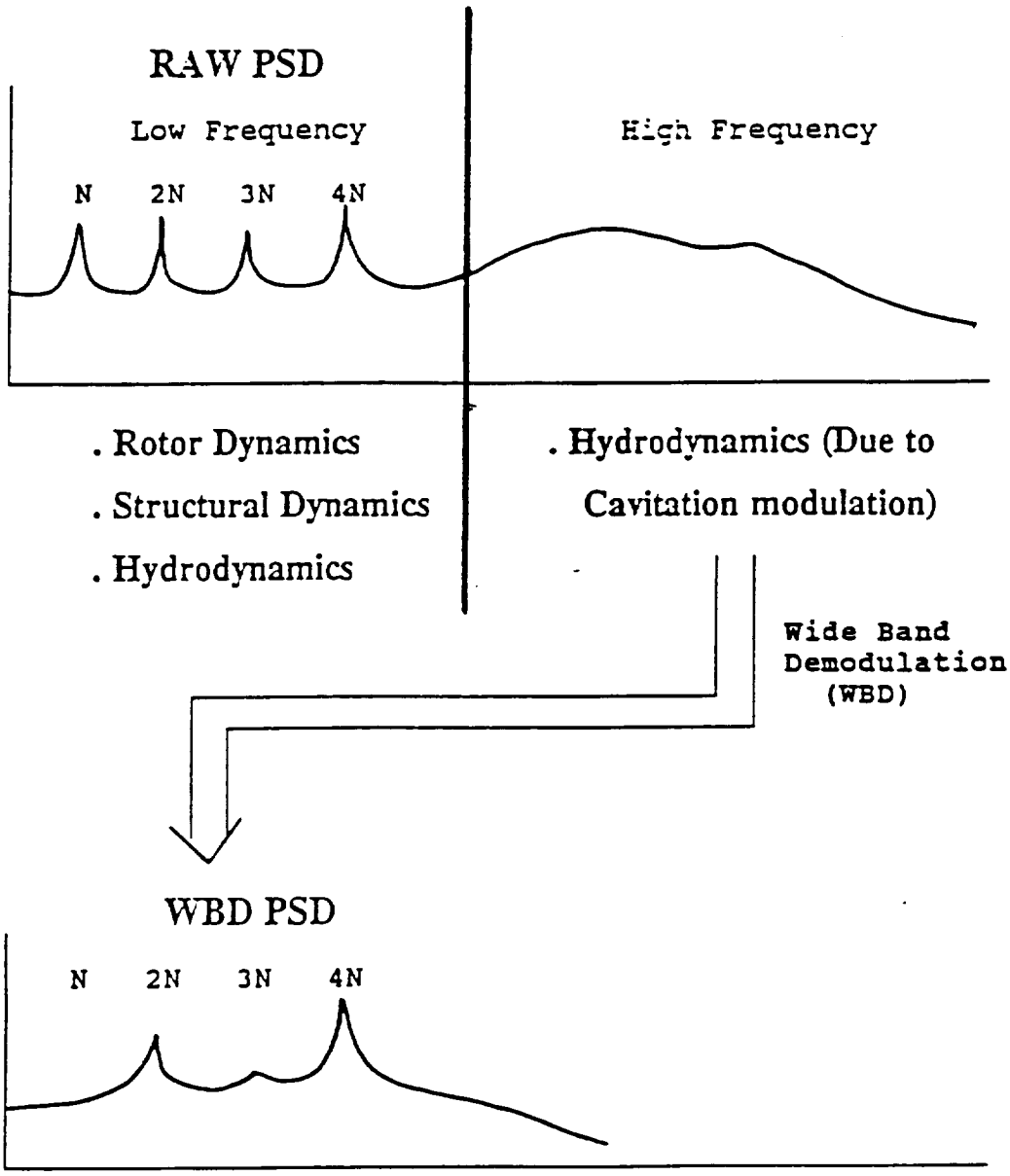

. If no cavitation, PSD of WBD will be broadband noise

. If cavitation occur, PSD of WBD will show discrete peaks corresponding to the low frequency periodic pressure fluctuation due to rotational process.

WIDE-BAND DEMODULATION (WBD)

(1) Tri-spectra Method:

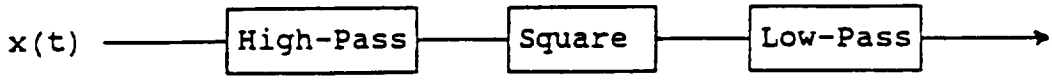

(2) Rectify Method (Envelope Detection):

(3) Hilbert Transform Method (Envelope Detection):

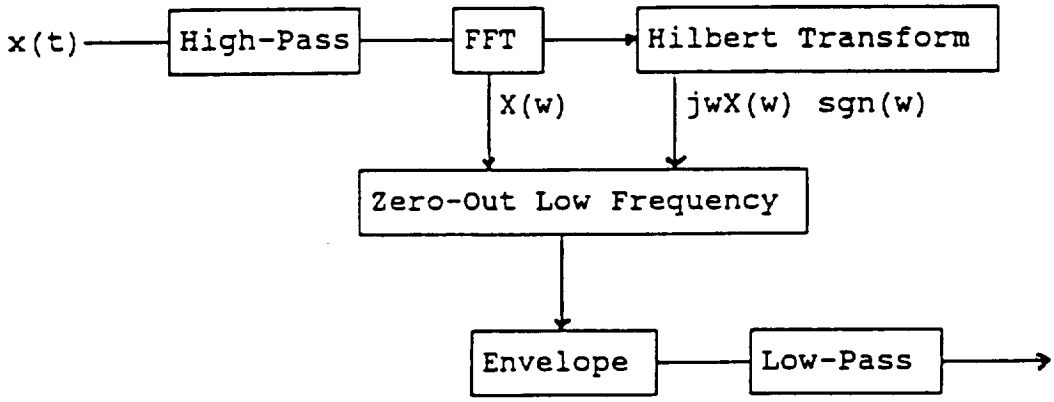

5 KHZ RAW PSD

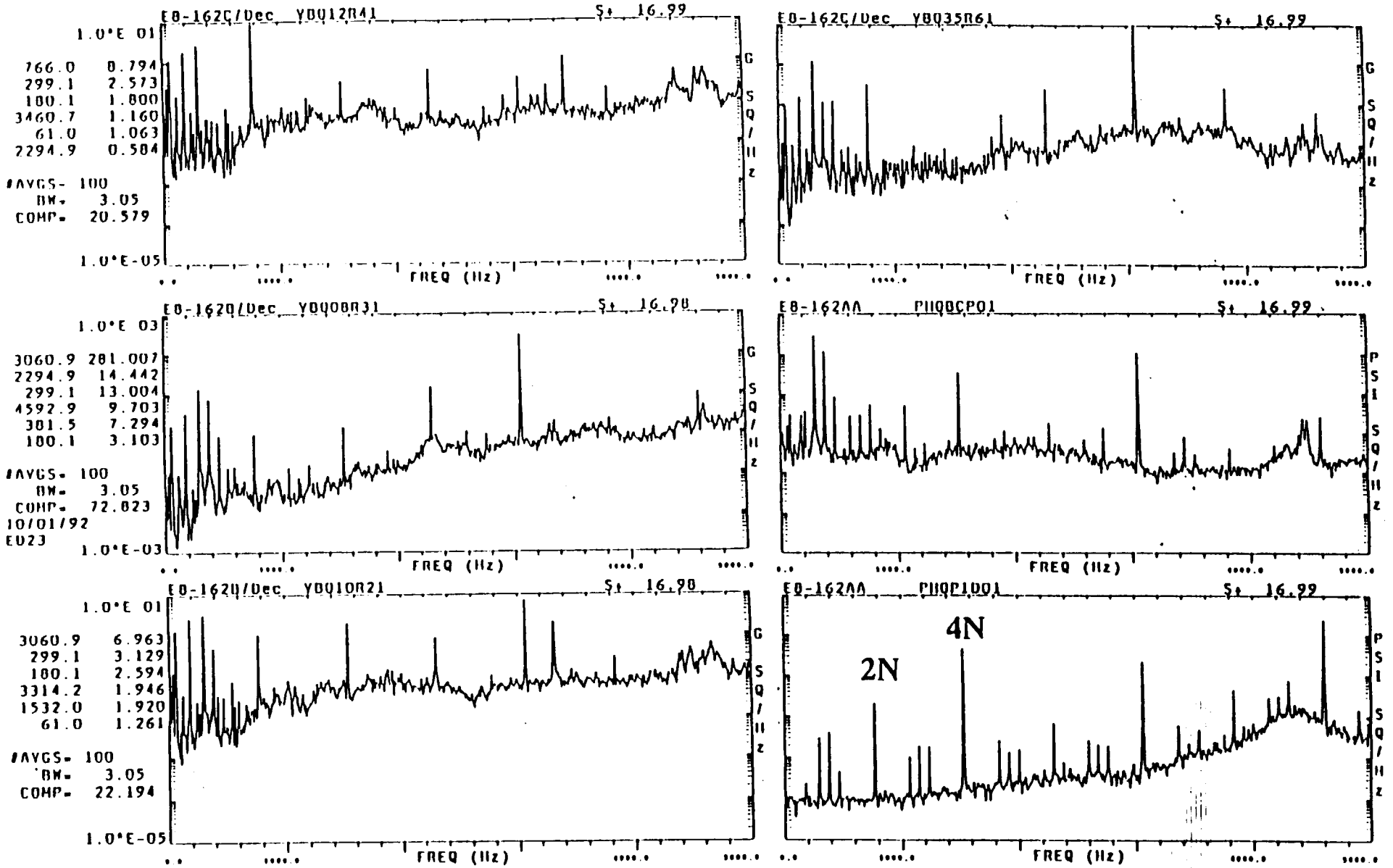
E8-162C/Dec YBQ12R41
S+ 16.99
1.0*E 01
766.0 8.794
299.1 2.573
180.1 1.800
3460.7 1.160
61.0 1.063
2294.9 0.584
#AVGS- 100
BW- 3.05
COMP- 20.579
1.0*E-05
FREQ (Hz)
G SQ/Hz
E8-162C/Dec YBQ35R61
S+ 16.99
FREQ (Hz)
G SQ/Hz
E8-162Q/Dec YBQ08R31
S+ 16.98
1.0*E 03
3060.9 281.007
2294.9 14.442
299.1 13.004
4592.9 9.703
381.5 7.294
180.1 3.103
#AVGS- 100
BW- 3.05
COMP- 72.823
10/01/92
EU23
1.0*E-03
FREQ (Hz)
G SQ/Hz
E8-162AA PHQ0CP01
S+ 16.99
FREQ (Hz)
PSI SQ/Hz
E8-162Q/Dec YBQ10R21
S+ 16.98
1.0*E 01
3060.9 6.963
299.1 3.129
180.1 2.594
3314.2 1.946
1532.0 1.920
61.0 1.261
#AVGS- 100
BW- 3.05
COMP- 22.194
1.0*E-05
FREQ (Hz)
G SQ/Hz
E8-162AA PHQP1D01
S+ 16.99
4N
2N
FREQ (Hz)
PSI SQ/Hz

50 KHZ RAW PSD

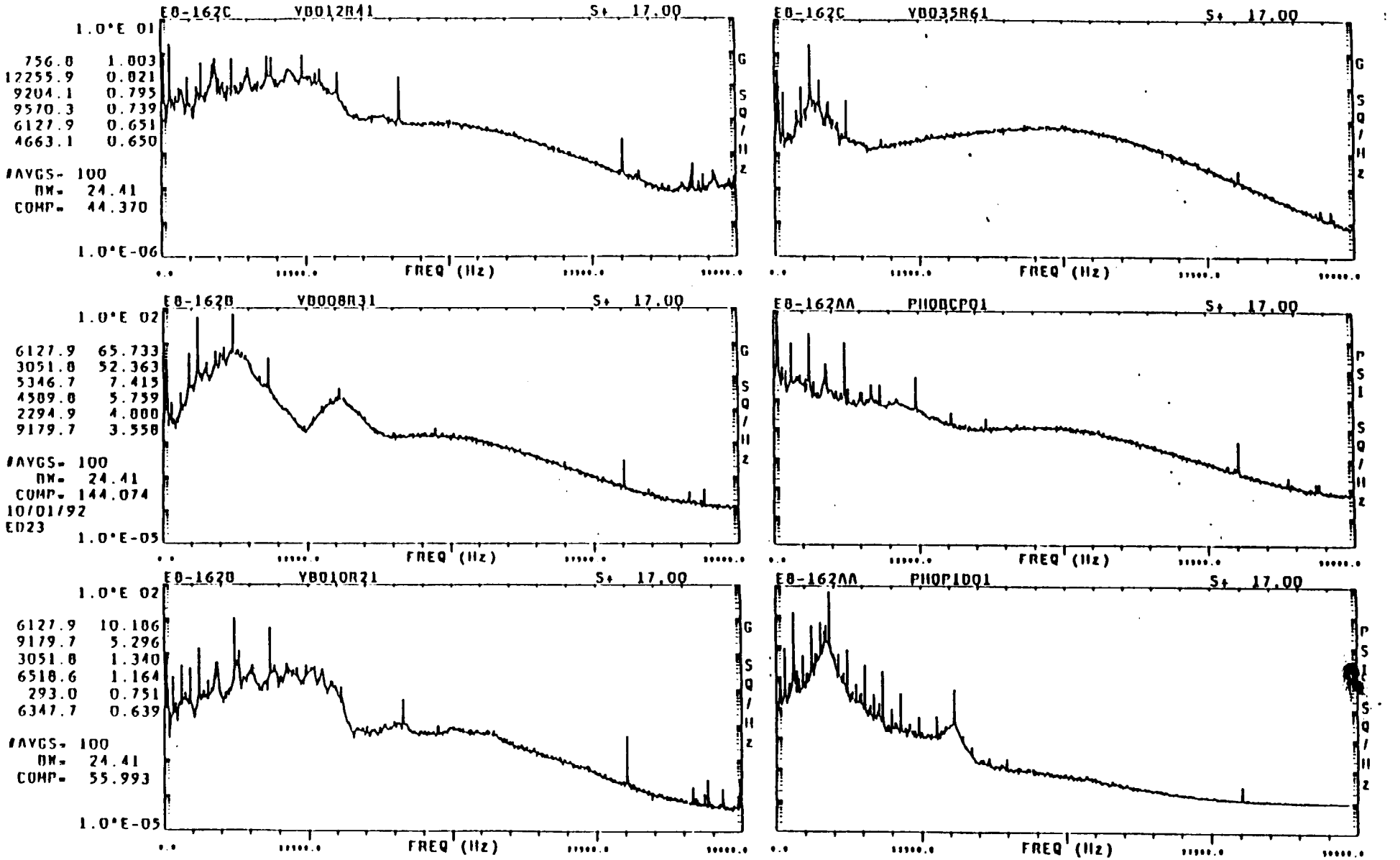

5 KHZ WBD PSD

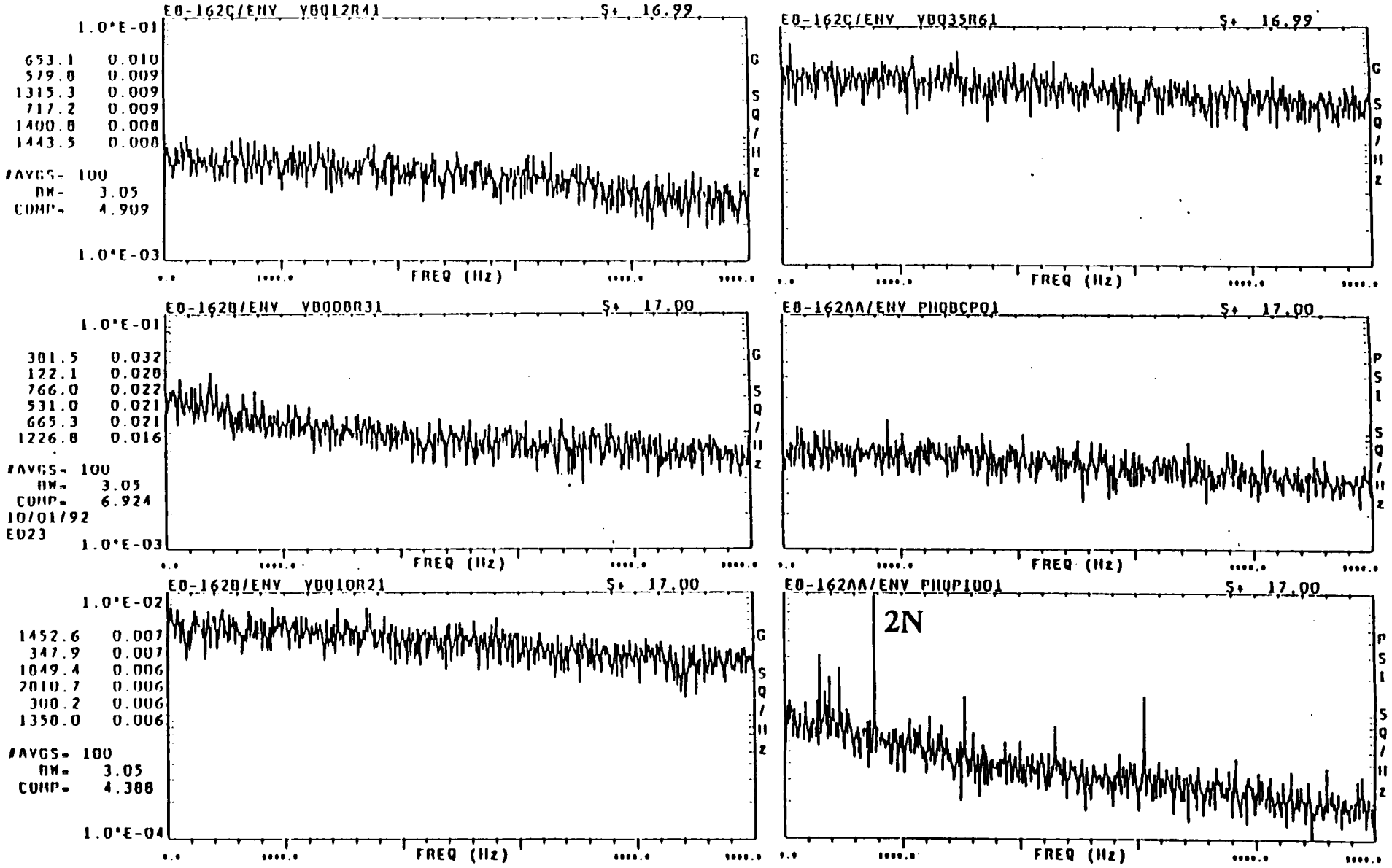
E0-162C/ENV YD012R41
S+ 16.99
1.0*E-01
653.1 0.010
579.0 0.009
1315.3 0.009
717.2 0.009
1400.8 0.008
1443.5 0.008
#AVGS= 100
BW= 3.05
COMP= 4.909
1.0*E-03
FREQ (Hz)
G SQ/Hz
E0-162C/ENV YD035R61
S+ 16.99
FREQ (Hz)
G SQ/Hz
E0-162D/ENV YD000R31
S+ 17.00
1.0*E-01
301.5 0.032
122.1 0.028
766.0 0.022
531.0 0.021
665.3 0.021
1226.8 0.016
#AVGS= 100
BW= 3.05
COMP= 6.924
10/01/92
E023
1.0*E-03
FREQ (Hz)
G SQ/Hz
E0-162AA/ENV PHQDCP01
S+ 17.00
FREQ (Hz)
PSI SQ/Hz
E0-162D/ENV YD010R21
S+ 17.00
1.0*E-02
1452.6 0.007
347.9 0.007
1049.4 0.006
2010.7 0.006
300.2 0.006
1350.0 0.006
#AVGS= 100
BW= 3.05
COMP= 4.388
1.0*E-04
FREQ (Hz)
G SQ/Hz
E0-162AA/ENV PHQP1D01
S+ 17.00
2N
FREQ (Hz)
PSI SQ/Hz

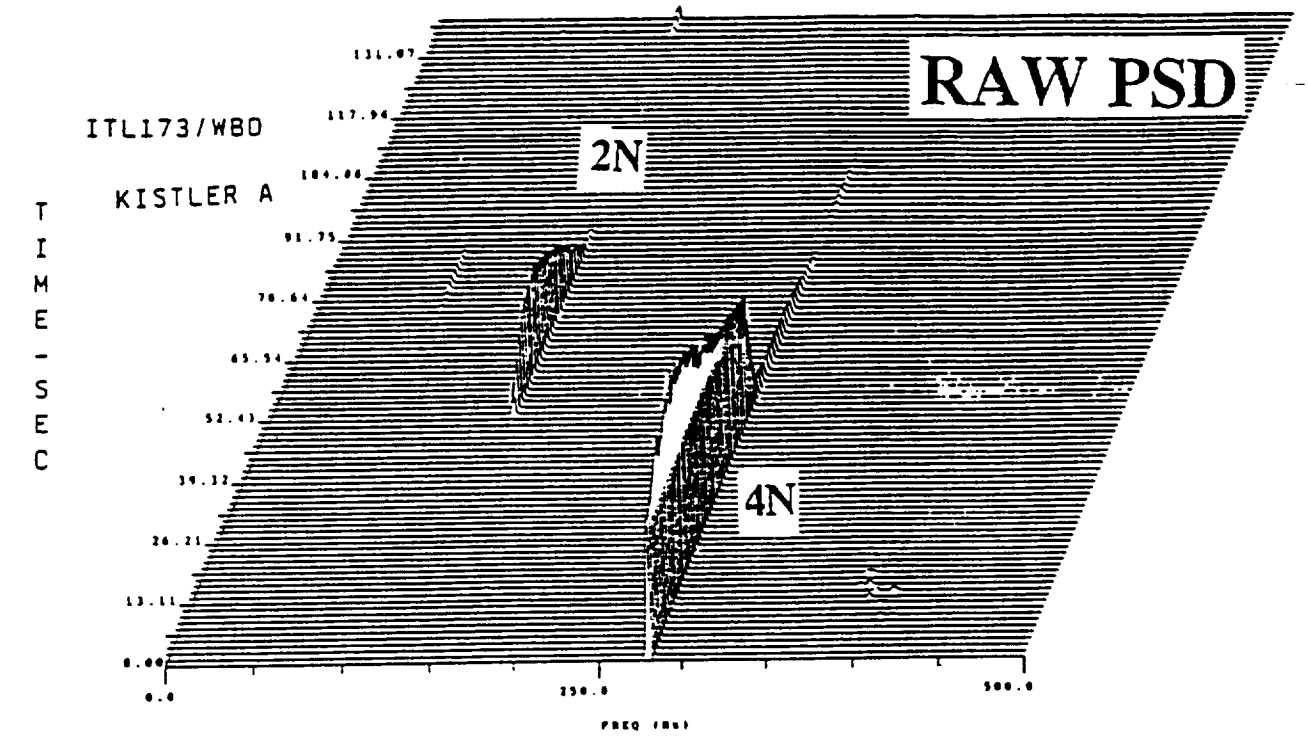
RAW PSD
ITL173/WBD
KISTLER A
2N
4N
TIME-SEC
131.07
117.96
104.86
91.75
78.64
65.54
52.43
39.32
26.21
13.11
0.00
0.0
250.0
500.0
FREQ (Hz)

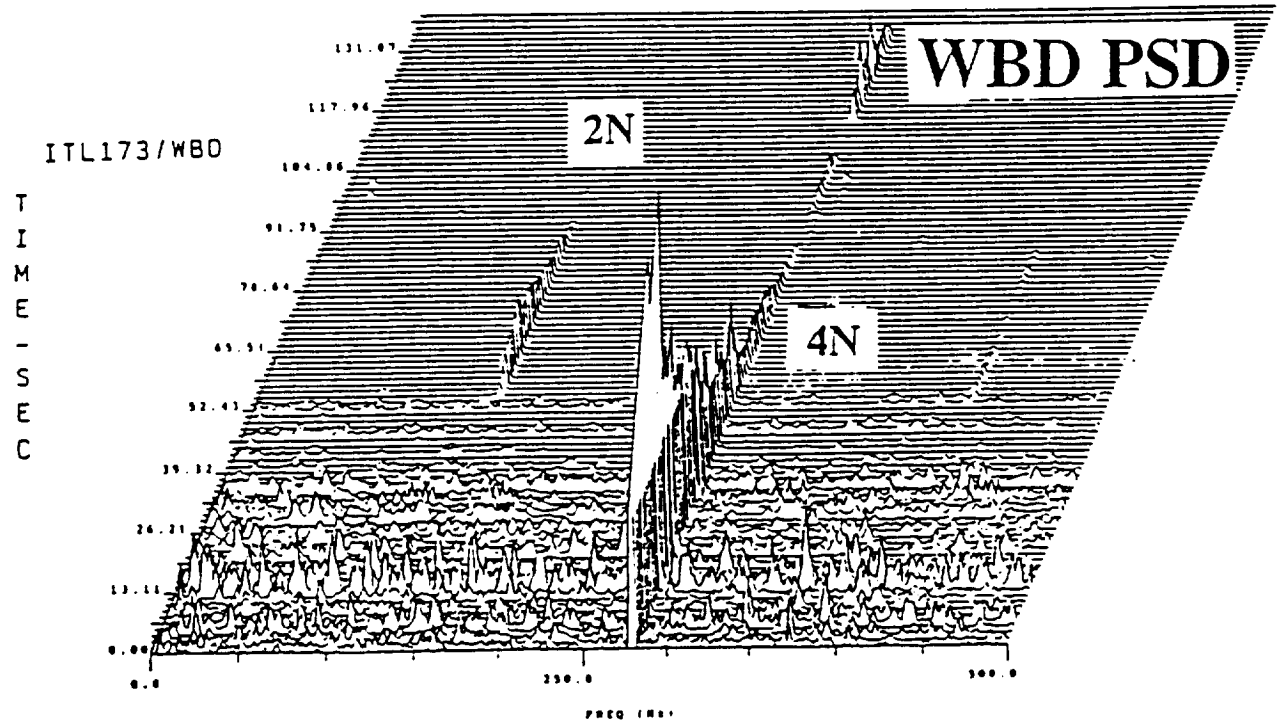
WBD PSD
ITL173/WBD
2N
4N
TIME-SEC
131.07
117.96
104.86
91.75
78.64
65.51
52.43
39.32
26.21
13.11
0.00
0.0
250.0
500.0
FREQ (Hz)

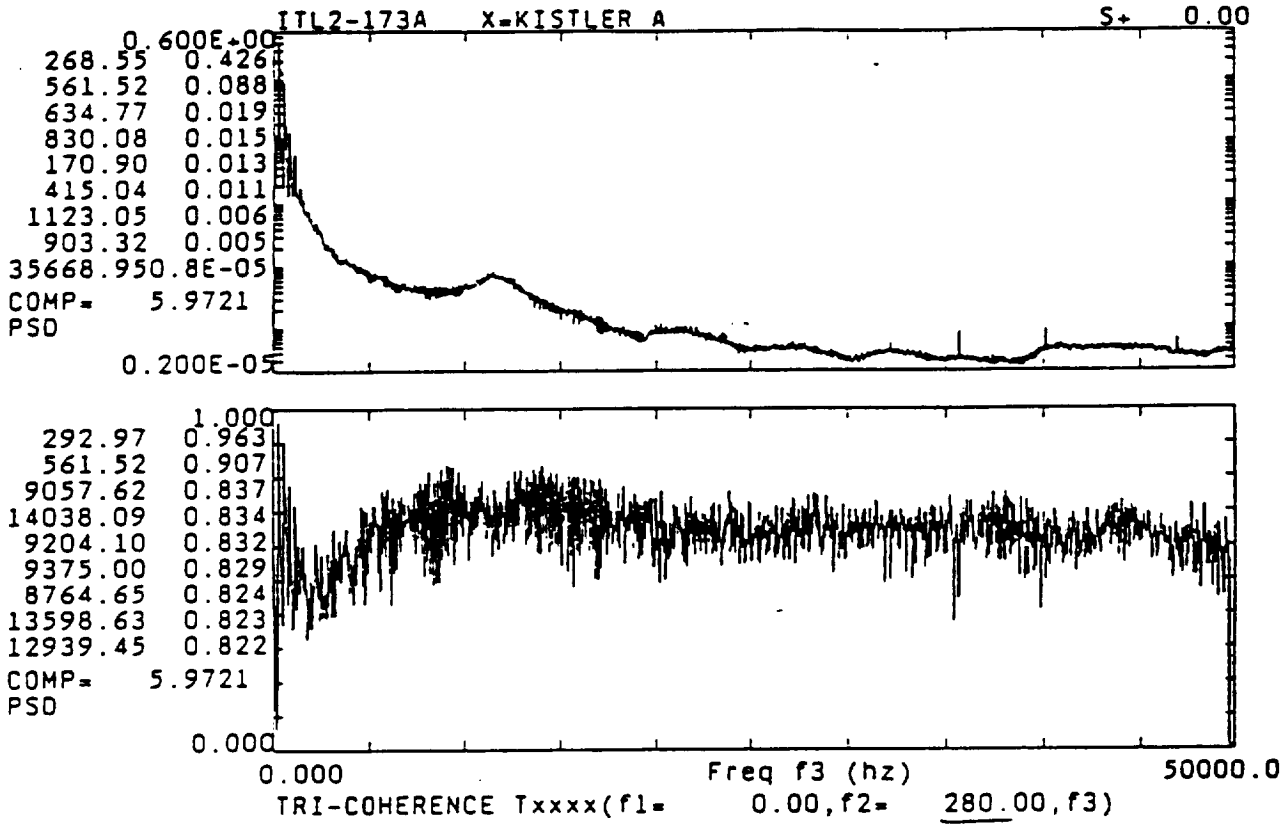
ITL2-173A X=KISTLER A
S+ 0.00
0.600E+00
268.55 0.426
561.52 0.088
634.77 0.019
830.08 0.015
170.90 0.013
415.04 0.011
1123.05 0.006
903.32 0.005
35668.95 0.8E-05
COMP= 5.9721
PSD
0.200E-05
1.000
292.97 0.963
561.52 0.907
9057.62 0.837
14038.09 0.834
9204.10 0.832
9375.00 0.829
8764.65 0.824
13598.63 0.823
12939.45 0.822
COMP= 5.9721
PSD
0.000
0.000
Freq f3 (hz)
50000.0
TRI-COHERENCE Txxxx(f1= 0.00,f2= 280.00,f3)

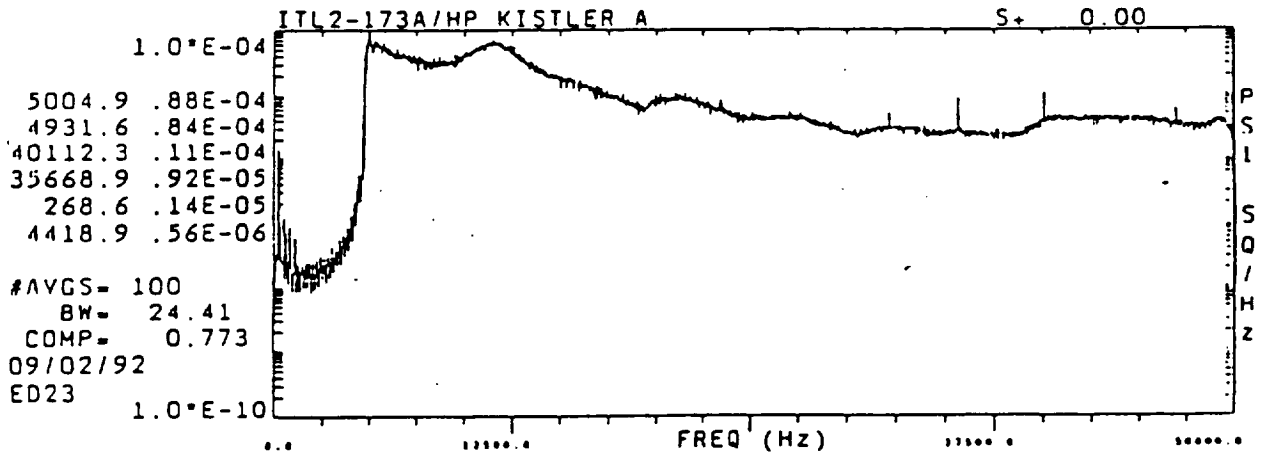
ITL2-173A/HP KISTLER A
S+ 0.00
1.0*E-04
5004.9 .88E-04
4931.6 .84E-04
40112.3 .11E-04
35668.9 .92E-05
268.6 .14E-05
4418.9 .56E-06
#AVGS= 100
BW= 24.41
COMP= 0.773
09/02/92
ED23
1.0*E-10
FREQ (Hz)
PSI/SQ/Hz

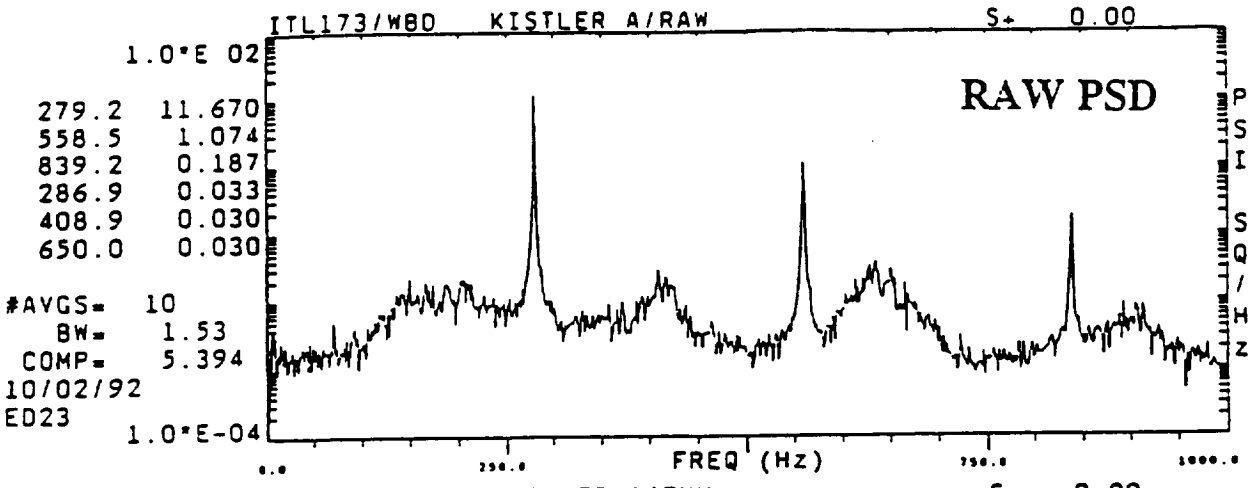
ITL173/WBD KISTLER A/RAW S+ 0.00
1.0*E 02
279.2 11.670
558.5 1.074
839.2 0.187
286.9 0.033
408.9 0.030
650.0 0.030
#AVGS= 10
BW= 1.53
COMP= 5.394
10/02/92
ED23
1.0*E-04
RAW PSD
PSI SQ/HZ
FREQ (Hz)

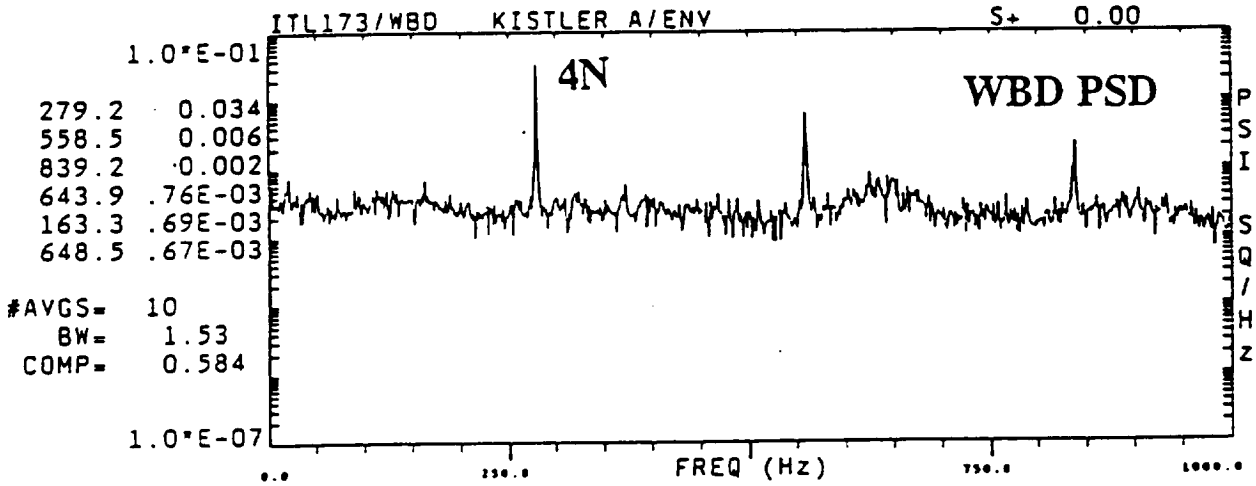
ITL173/WBD KISTLER A/ENV S+ 0.00
1.0*E-01
279.2 0.034
558.5 0.006
839.2 0.002
643.9 .76E-03
163.3 .69E-03
648.5 .67E-03
#AVGS= 10
BW= 1.53
COMP= 0.584
1.0*E-07
4N
WBD PSD
PSI SQ/HZ
FREQ (Hz)

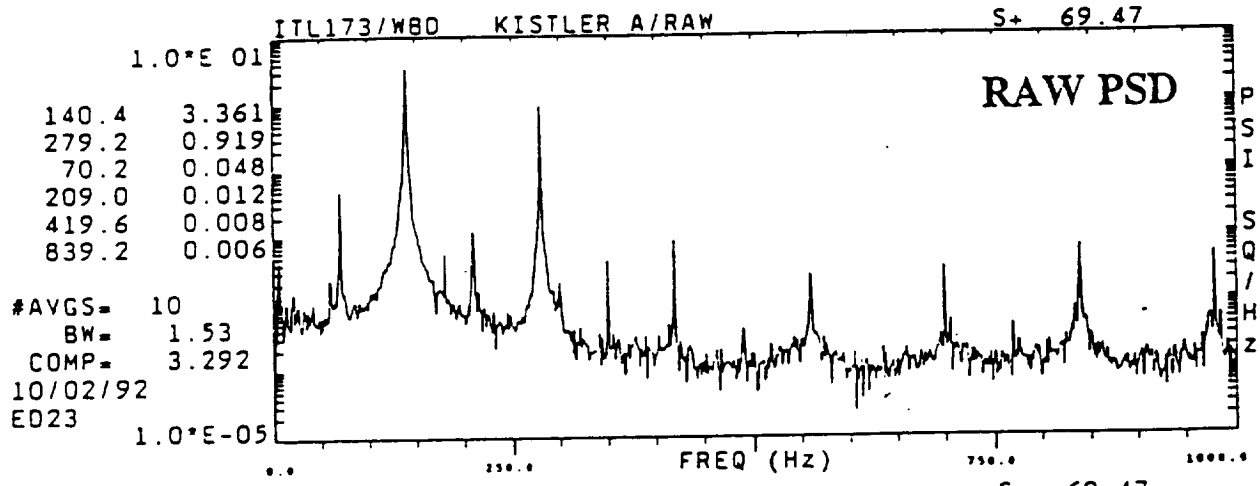
ITL173/WBD KISTLER A/RAW S+ 69.47
1.0*E 01
140.4 3.361
279.2 0.919
70.2 0.048
209.0 0.012
419.6 0.008
839.2 0.006
#AVGS= 10
BW= 1.53
COMP= 3.292
10/02/92
ED23
1.0*E-05
RAW PSD
PSI SQ/HZ
FREQ (Hz)

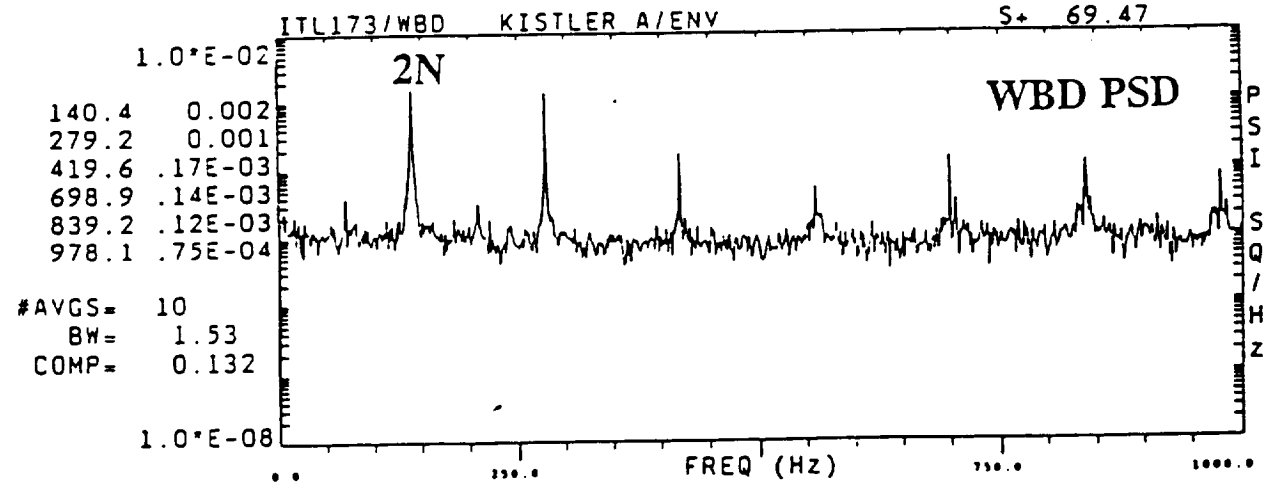
ITL173/WBD KISTLER A/ENV S+ 69.47
1.0*E-02
140.4 0.002
279.2 0.001
419.6 .17E-03
698.9 .14E-03
839.2 .12E-03
978.1 .75E-04
#AVGS= 10
BW= 1.53
COMP= 0.132
1.0*E-08
2N
WBD PSD
PSI SQ/HZ
FREQ (Hz)

RAW PSD

E8-161

PHOPI001

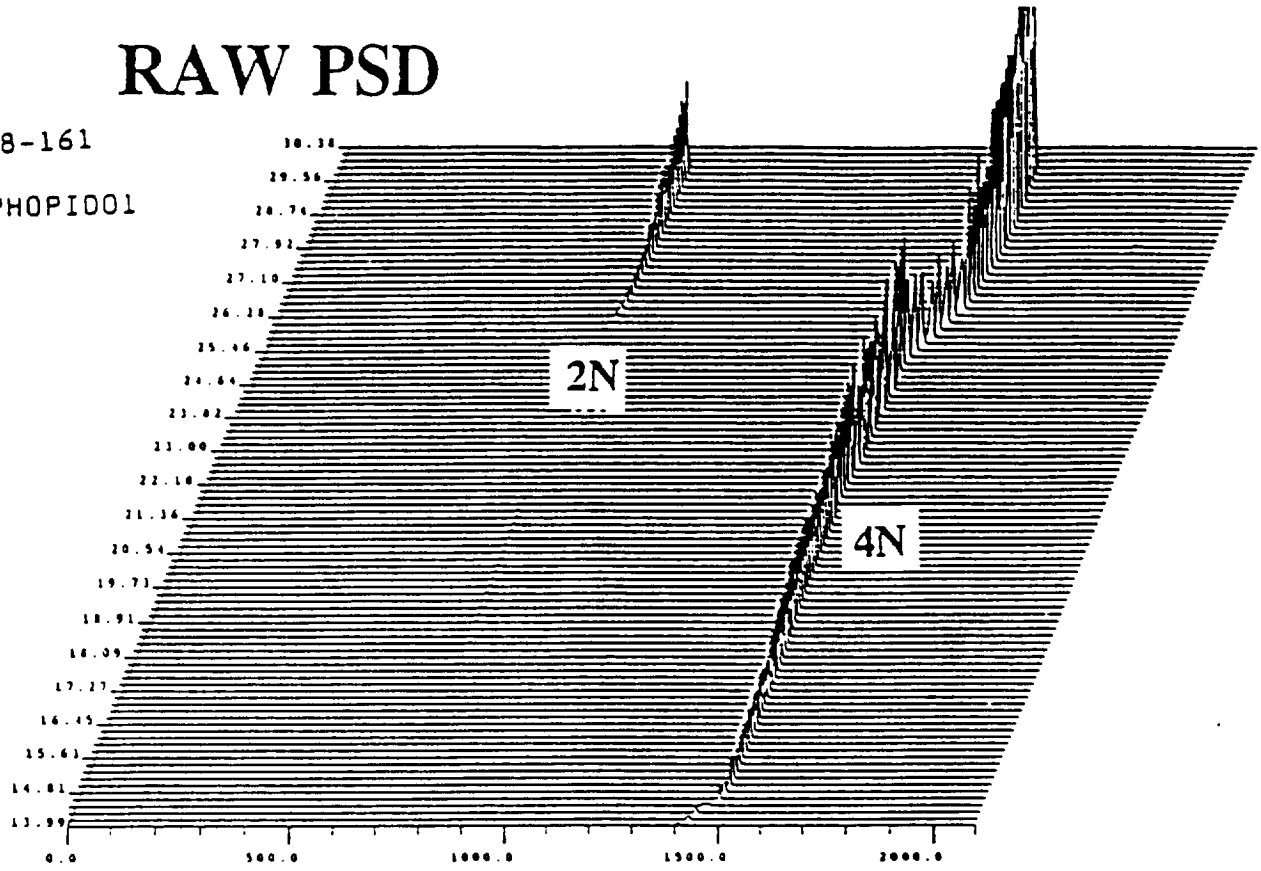

WBD PSD

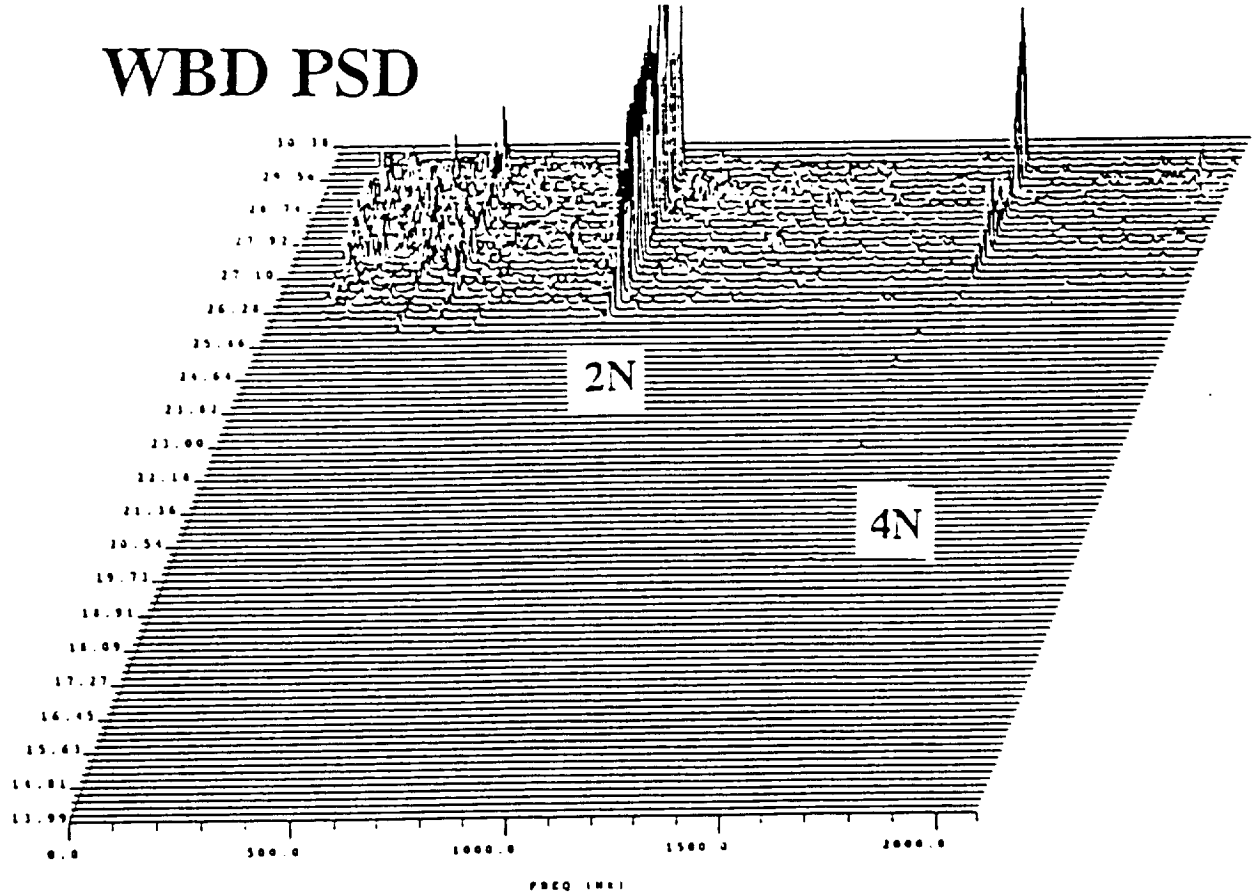

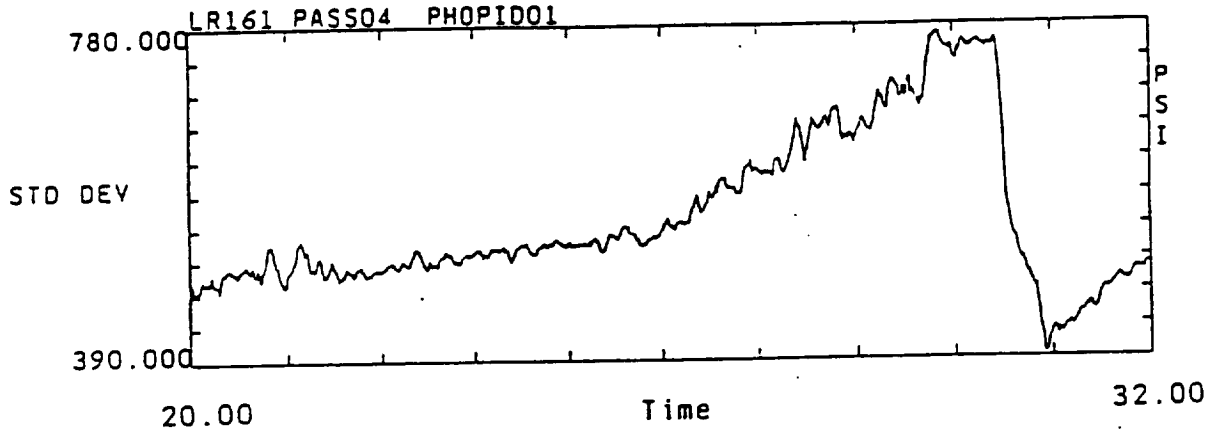
LR161 PASS04 PHOPID01
780.000
390.000
STD DEV
P
S
I
20.00
Time
32.00

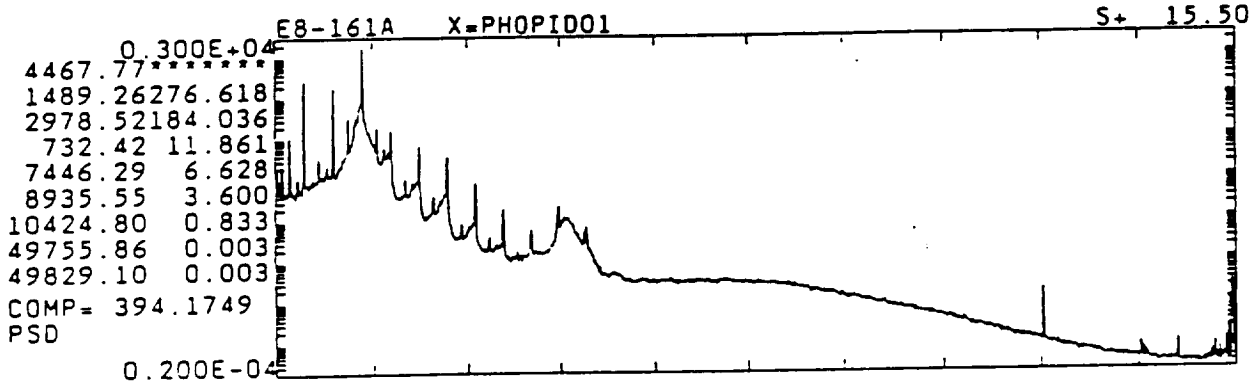
E8-161A X=PHOPID01
S+ 15.50
0.300E+04
4467.77*******
1489.26276.618
2978.52184.036
732.42 11.861
7446.29 6.628
8935.55 3.600
10424.80 0.833
49755.86 0.003
49829.10 0.003
COMP= 394.1749
PSD
0.200E-04

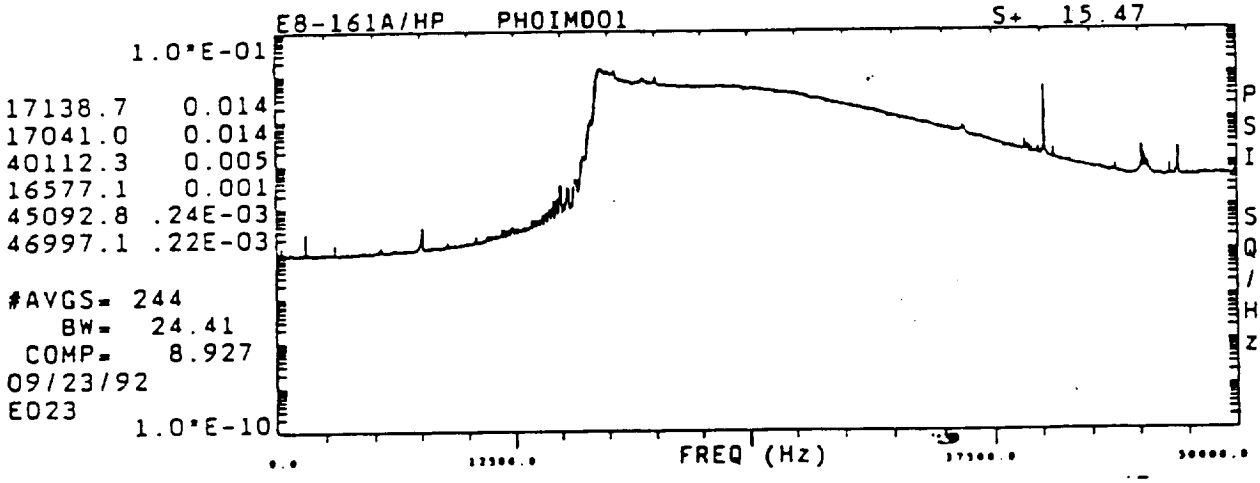
E8-161A/HP PHOIMD01
S+ 15.47
1.0*E-01
17138.7 0.014
17041.0 0.014
40112.3 0.005
16577.1 0.001
45092.8 .24E-03
46997.1 .22E-03
#AVGS= 244
BW= 24.41
COMP= 8.927
09/23/92
E023
1.0*E-10
P
S
I
S
Q
/
H
z
FREQ (Hz)

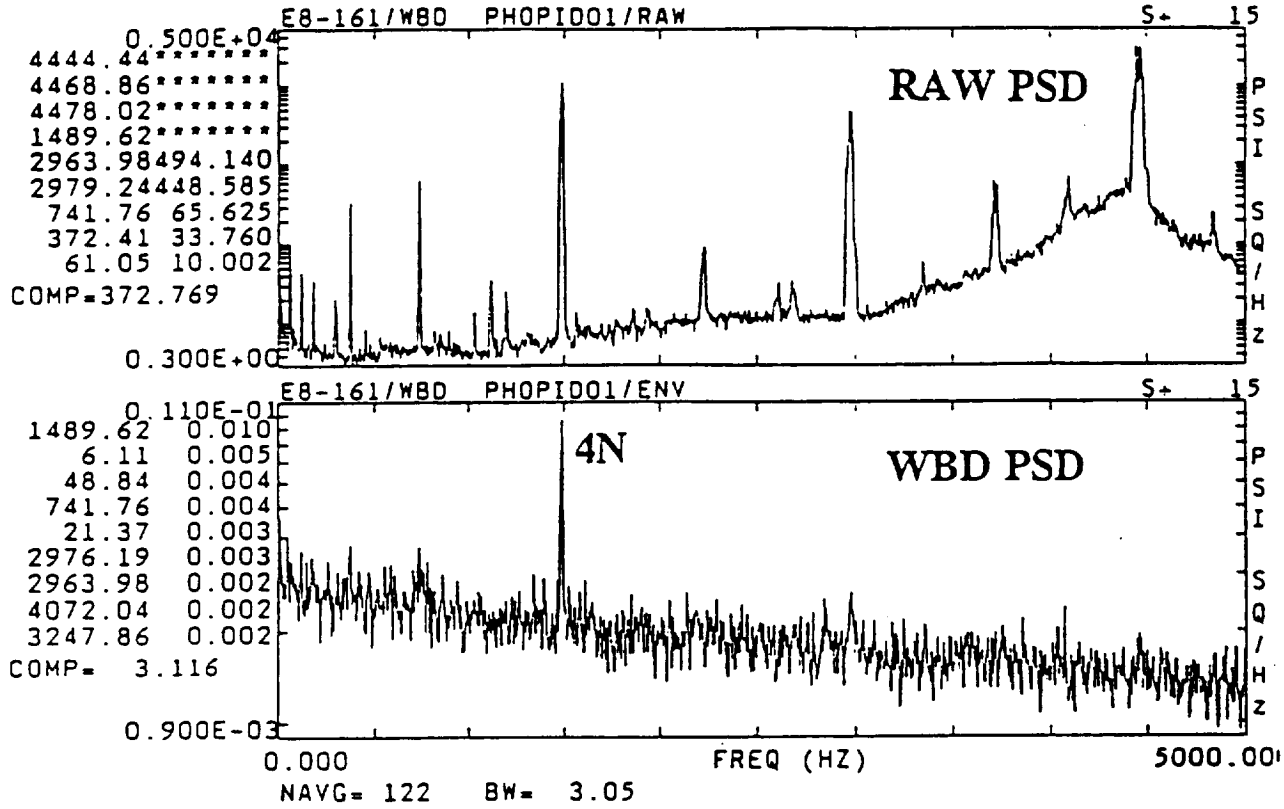
E8-161/WBD PHOPID01/RAW
S+ 15
0.500E+04
4444.44*******
4468.86*******
4478.02*******
1489.62*******
2963.98494.140
2979.24448.585
741.76 65.625
372.41 33.760
61.05 10.002
COMP=372.769
0.300E+00
RAW PSD
PSI SQ/Hz
E8-161/WBD PHOPID01/ENV
S+ 15
0.110E-01
1489.62 0.010
6.11 0.005
48.84 0.004
741.76 0.004
21.37 0.003
2976.19 0.003
2963.98 0.002
4072.04 0.002
3247.86 0.002
COMP= 3.116
0.900E-03
4N
WBD PSD
PSI SQ/Hz
0.000
FREQ (HZ)
5000.00
NAVG= 122 BW= 3.05

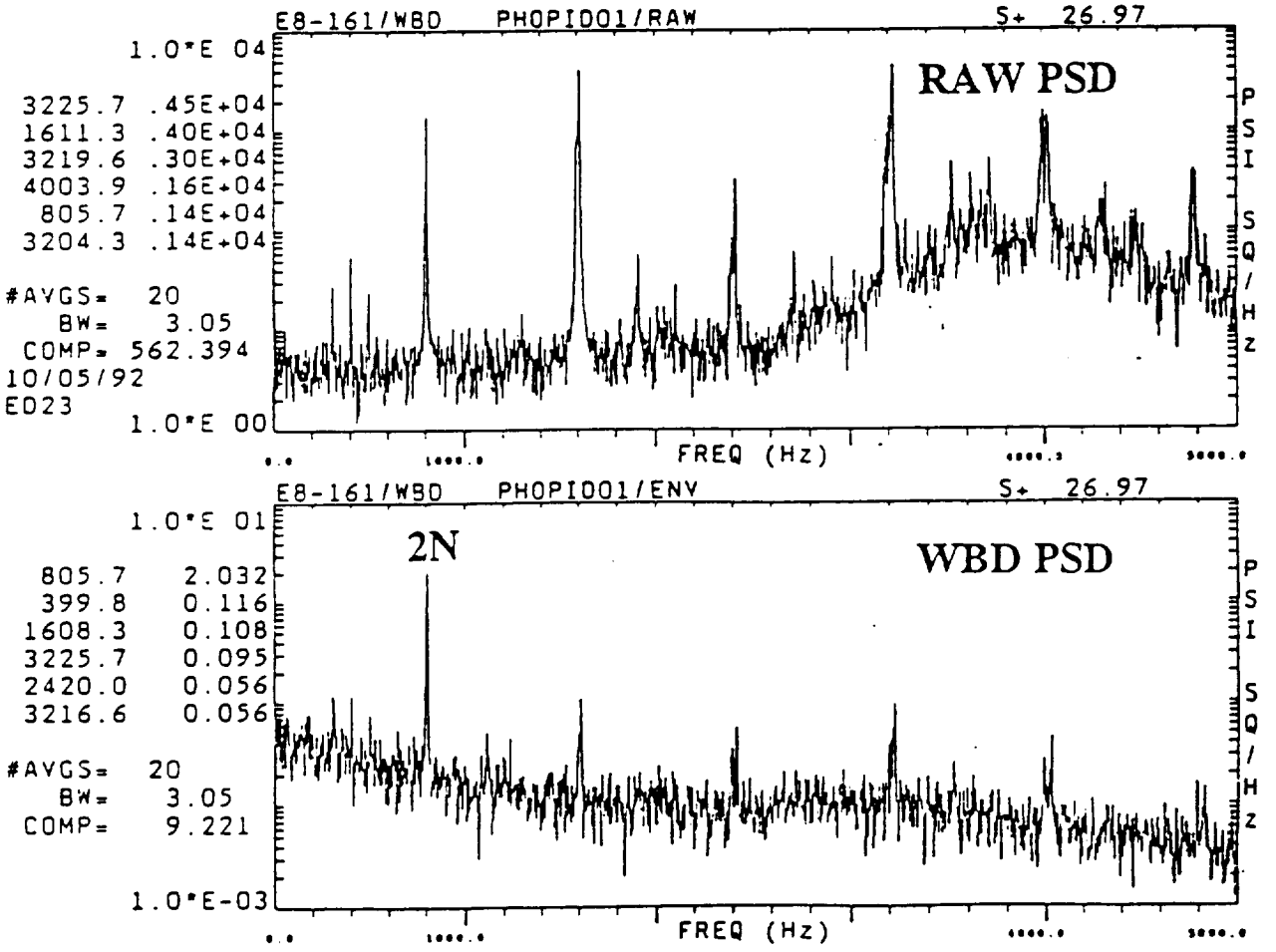
E8-161/WBD PHOPID01/RAW
S+ 26.97
1.0*E 04
3225.7 .45E+04
1611.3 .40E+04
3219.6 .30E+04
4003.9 .16E+04
805.7 .14E+04
3204.3 .14E+04
#AVGS= 20
BW= 3.05
COMP= 562.394
10/05/92
ED23
1.0*E 00
RAW PSD
PSI SQ/Hz
FREQ (Hz)
E8-161/WBD PHOPID01/ENV
S+ 26.97
1.0*E 01
805.7 2.032
399.8 0.116
1608.3 0.108
3225.7 0.095
2420.0 0.056
3216.6 0.056
#AVGS= 20
BW= 3.05
COMP= 9.221
1.0*E-03
2N
WBD PSD
PSI SQ/Hz
FREQ (Hz)

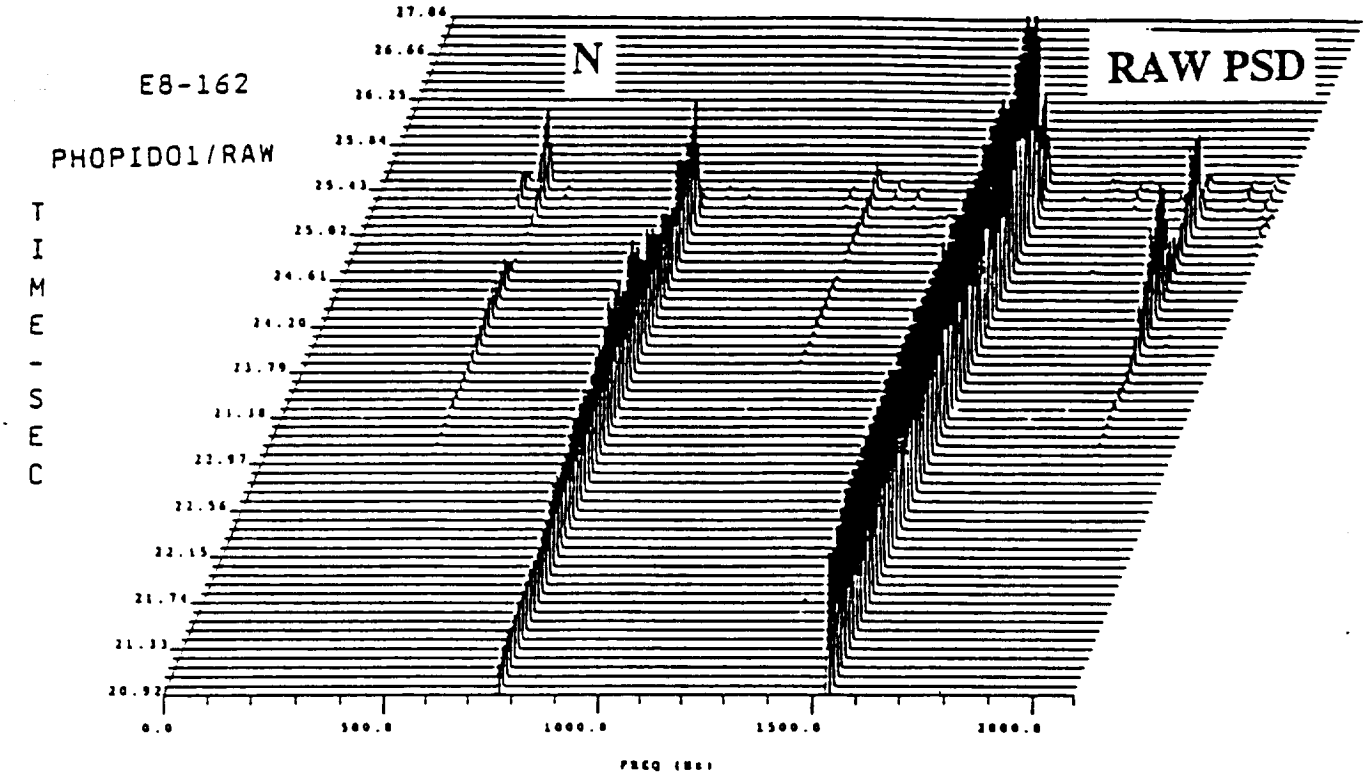
E8-162
PHOPIDO1/RAW
N
RAW PSD
TIME-SEC
27.06
26.66
26.25
25.84
25.43
25.02
24.61
24.20
23.79
23.38
22.97
22.56
22.15
21.74
21.33
20.92
0.0
500.0
1000.0
1500.0
2000.0
FREQ (Hz)

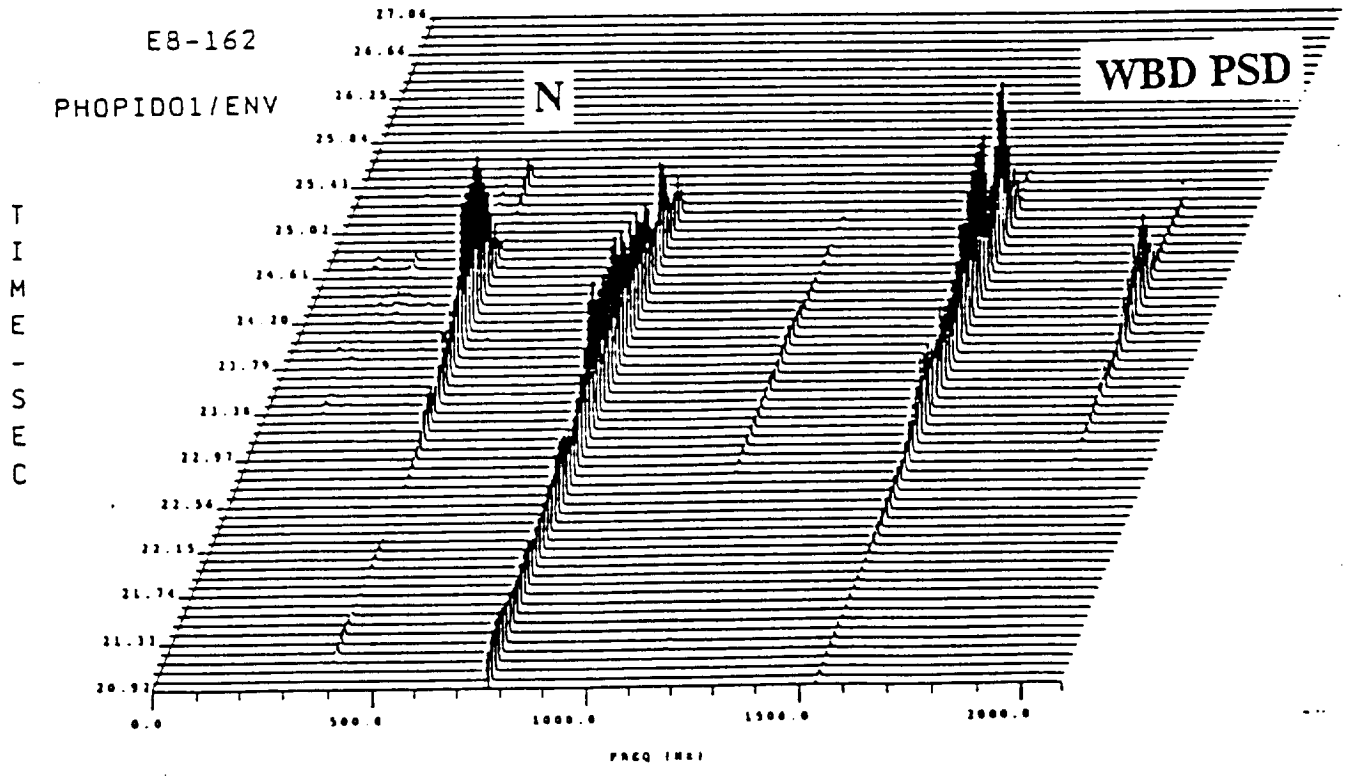
E8-162
PHOPIDO1/ENV
N
WBD PSD
TIME-SEC
27.06
26.64
26.25
25.84
25.43
25.02
24.61
24.20
23.79
23.38
22.97
22.54
22.15
21.74
21.33
20.92
0.0
500.0
1000.0
1500.0
2000.0
FREQ (Hz)

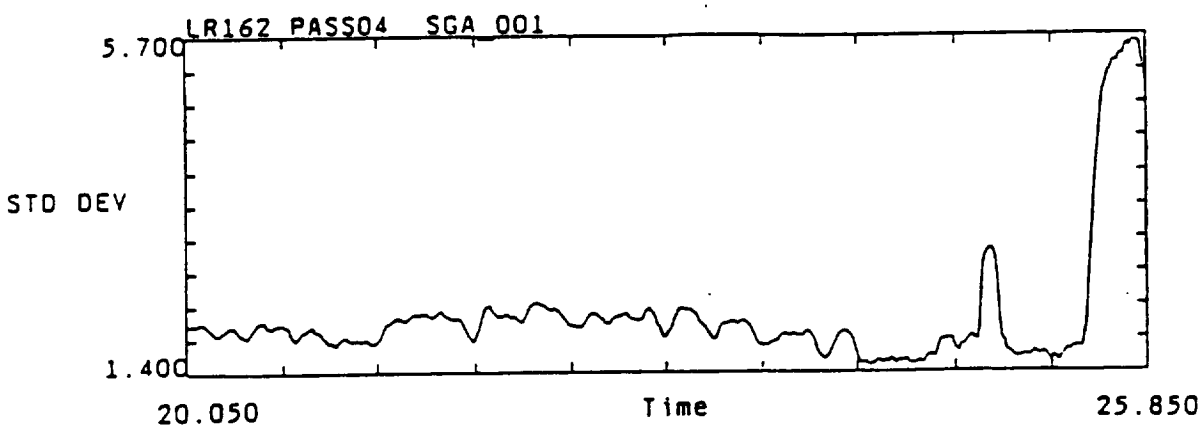
LR162 PASS04 SGA 001
5.700
STD DEV
1.400
20.050
Time
25.850

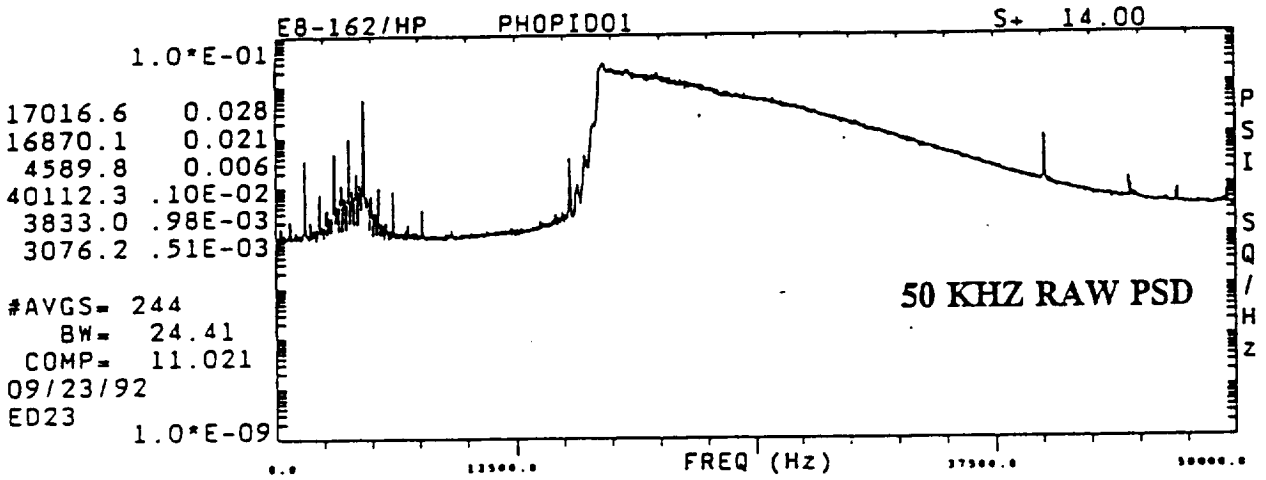
E8-162/HP PHOPID01
S+ 14.00
1.0*E-01
17016.6 0.028
16870.1 0.021
4589.8 0.006
40112.3 .10E-02
3833.0 .98E-03
3076.2 .51E-03
#AVGS= 244
BW= 24.41
COMP= 11.021
09/23/92
ED23
1.0*E-09
50 KHZ RAW PSD
PSI SQ/Hz
FREQ (Hz)

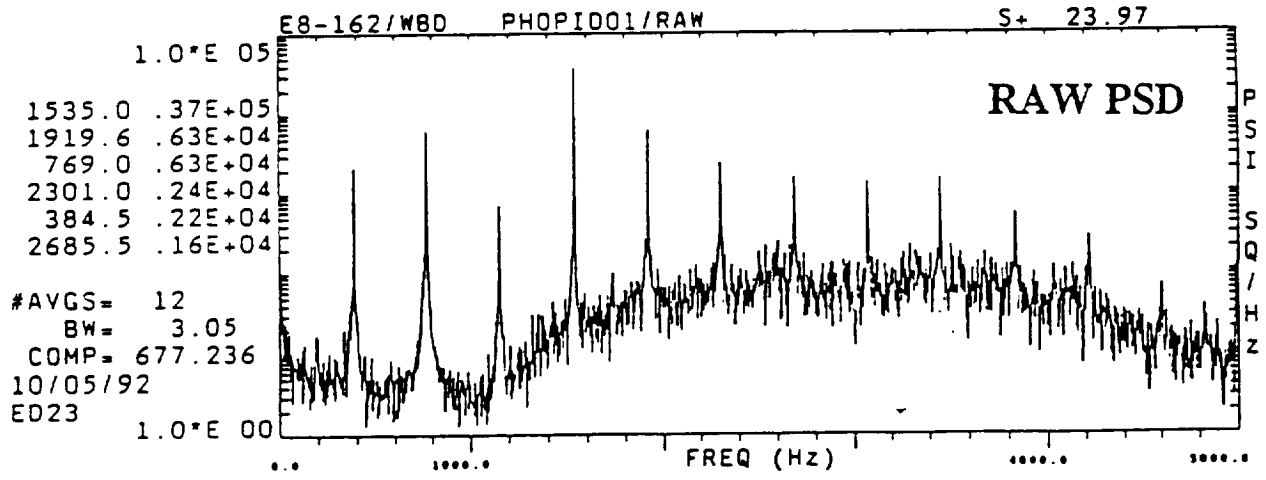
E8-162/WBD PHOPID01/RAW
S+ 23.97
1.0*E 05
1535.0 .37E+05
1919.6 .63E+04
769.0 .63E+04
2301.0 .24E+04
384.5 .22E+04
2685.5 .16E+04
#AVGS= 12
BW= 3.05
COMP= 677.236
10/05/92
ED23
1.0*E 00
RAW PSD
PSI SQ/Hz
FREQ (Hz)

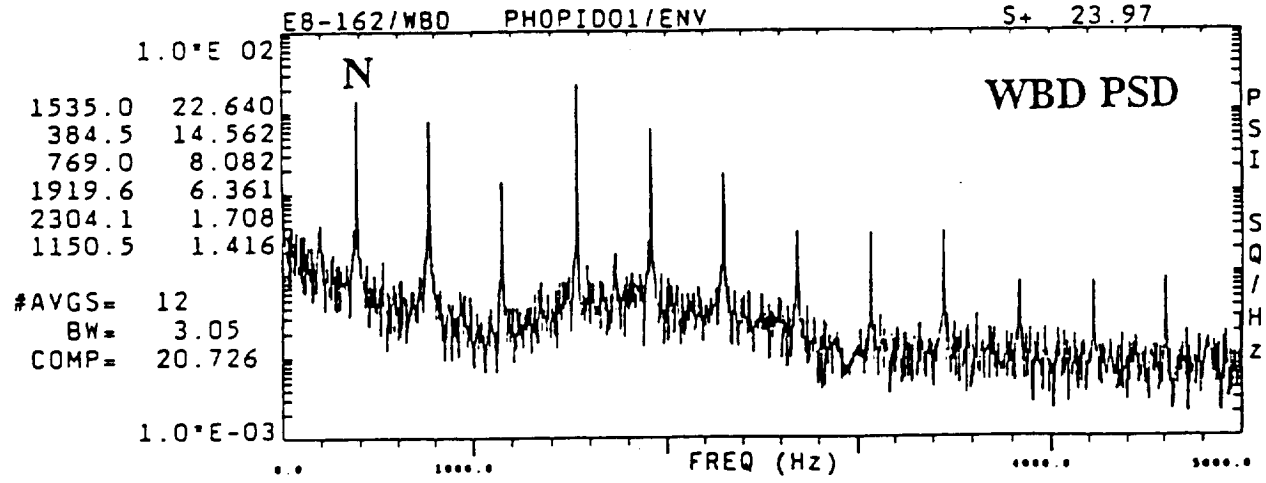
E8-162/WBD PHOPID01/ENV
S+ 23.97
1.0*E 02
N
1535.0 22.640
384.5 14.562
769.0 8.082
1919.6 6.361
2304.1 1.708
1150.5 1.416
#AVGS= 12
BW= 3.05
COMP= 20.726
1.0*E-03
WBD PSD
PSI SQ/Hz
FREQ (Hz)

Anomaly Identification for Space Shuttle Main Engine Diagnostics

Jen Jong
Jess Jones, Preston Jones, Thomas Zolladz
Thomas Coffin

Turbomachinery fault detection and diagnosis represents a significant technical challenge in the aeronautics, transportation, and power industry. A reliable health monitoring system can prevent catastrophic failures and costly down time due to false alarms. As computer information processing technology continues to advance, the major challenge associated with machinery monitoring and diagnosis is shifting from how to obtain machinery vibration data to methods of information extraction and interpretation. Therefore, the incorporation of intelligent information processing capability has become invaluable to the machinery diagnostic process. Such an element can provide valuable dynamic information regarding the machine operational condition and greatly improve system reliability.

During the development of the Space Shuttle Main Engine (SSME), significant progress has been made in both the NASA and aerospace communities toward performance of the fault diagnostic function in instrumentation, modeling, and signal analysis techniques, in order to enhance the safety and reliability of Space Shuttle operations. A hierarchy of Anomaly Identification (AI) techniques for mechanical signature analysis has been developed to process and identify intelligent information hidden in a measurement signal which is often unidentifiable using conventional signal analysis methods. The AI methods can better identify well-hidden defect symptoms as well as false-alarm signatures. Within the SSME as well as other propulsion environments, dynamic measurements suffer from severe noise contamination associated with fluid flow, combustion processes, structural resonance, couplings, modulations, and other unknown mechanisms. Whenever an anomaly is detected, the AI function must determine if such anomaly is associated with a false-alarm or true defect signature. It will perform a detailed analysis and verification through the AI techniques. The ultimate effectiveness of this AI technology will depend upon its ability to optimally extract available machinery operational state information from a monitoring signal. A number of techniques have been developed and applied to SSME hot-firing test and flight data, and they appear to be highly promising for failure analysis and detection in other complex machinery applications.

Bi-spectral analysis is illustrated to identify the existence of amplitude modulation (quadratic correlation) among spectral components. The characteristics of such

quadratic interactions are usually reflected in its coherent phase relationship. It has been applied to identify the quadratic phenomenon of a synchronous frequency component modulated by the cage frequency components in a ball bearing system.

Tri-spectrum analysis identifies cubic correlation among four different spectral components. A special case of its application is to identify whether an apparent side-band structure is really due to modulation or not. Such a sideband structure is another commonly observed nonlinear defect signature. A typical example is a bearing cage frequency component periodically excites a structure mode at its natural frequency.

The hyper-coherence function was developed to detect the correlation between synchronous frequency characteristics and any harmonic component. A major benefit is to determine whether an apparent harmonic in a complex vibration signal is correlated with the fundamental or caused by extraneous noise. This analysis has been extended to a time-domain algorithm (hyper-coherence filtering) for the extraction of period signals in noisy data.

The generalized hyper-coherence, more recently applied, permits estimation of the nonlinear correlation between a selected frequency (e.g., shaft speed) and an arbitrary frequency component. The spectral components to be identified by higher order spectra are required to satisfy certain frequency combinations (e.g., the sum of arguments is zero). However, in many situations, we wish to identify the correlation between two arbitrary frequency components that do not satisfy any such requirements. The generalized hyper-coherence (GHC) was developed to deal with this situation.

A Modified Wigner Distribution has proven useful in resolving time-frequency characteristics of highly nonstationary data typical of engine startup, cutoff, and throttling. The technique effectively suppresses the spurious spectral peaks inherent with the standard Wigner spectrum for a signal with multiple frequency components.

This paper reviews some recent AI methodologies for mechanical fault detection and identification. We briefly summarize the analytical basis for the above algorithms. Practical application of the methods is then demonstrated through the evaluation of vibration measurements from SSME hot firing tests exhibiting anomalous behavior.

WYLE LABORATORIES
Engineering Division

Technical Note TN 60900-90-611

STATISTICAL ANALYSIS OF SSME TURBOPUMP VIBRATION LEVELS

Part I, High Pressure Oxidizer Turbopump

by

Wayne L. Swanson

June 1990

FOREWORD

Wyle Laboratories' Engineering Division prepared this report for the National Aeronautics and Space Administration, George C. Marshall Space Flight Center. The work was performed under contract NAS8-38156, entitled "Data Analysis and Diagnostic Evaluation of Space Shuttle Main Engine (SSME) Dynamic Measurements."

Technical direction, assistance, and modification to the Diagnostic Data Base computer program was provided by J. McBride and S. Gallik of MSFC/ED 23, with members of BCSS providing the computer output support. This is part I in a series presently in various stages of preparation. The topics treated include

Part I: Statistical Analysis of Vibration Levels on the SSME High Pressure Oxidizer Turbopumps

Part II: Statistical Analysis of Vibration Levels on the SSME High Pressure Fuel Turbopumps

Part III: Statistical Analysis of Vibration Levels on the SSME Low Pressure Oxidizer Turbopumps

Part IV: Statistical Analysis of Vibration Levels on the SSME Low Pressure Fuel Turbopumps

TABLE OF CONTENTS

FOREWORD		ii
1.0	TECHNICAL DISCUSSION	1
2.0	SYNCHRONOUS STATISTICAL DATA PLOTS	15
3.0	COMPOSITE STATISTICAL DATA PLOTS	29
4.0	FASCOS SYNCHRONOUS AND COMPOSITE STATISTICAL DATA PLOTS	43
5.0	SSME DIAGNOSTIC DATA BASE DIRECTORY	53
6.0	SYNCHRONOUS FREQUENCY VS POWER LEVEL	77
7.0	DEC PROFESSIONAL 380 COMPUTER PROGRAM "GAMGREENA"	81

1.0 TECHNICAL DISCUSSION

This document is an updated version of a previously published report[1] on the vibration level statistics of the Phase II High Pressure Oxidizer Turbopumps (HPOTP) at different power levels. The purpose of this document was to evaluate if a significant change has occurred in the vibration statistics since the last report was published in November 1987.

Both the mean or average value and standard deviation do not indicate a significant change other than what would be expected from random chance for both the synchronous and composite vibration levels of the HPOTP. The updated version now includes 1217 measurements at the 100-percent power level, while the previous data base contained 429, or an increase of 788 in sample size. The average pump end vibration level changed from 1.33 Grms to 1.45 Grms, or 0.12, which is not considered significant. The standard deviation increased from 0.67 to 0.85, which also is not significant. On the turbine end measurements, the change was slightly less—from 1.23 to 1.28 Grms—with a change of the standard deviation from 0.56 to 0.68, which is also not significant. The composite levels, however, did indicate a slight decrease, which could be attributed to a decrease in the noise floor of the measurements. Additional analysis will be required to verify this hypothesis. A comparison of the calculated statistics in reference 1 is shown in Figures 1 through 4, with the updated statistics shown in Figures 5 through 8.

Again, for this study (for comparison with the reference 1 data base) only valid data from Phase II turbopumps that operated under normal conditions was included. Therefore, questionable data points (excessive noise, etc.), early cutoff, high running main impellors (0307 series of pumps), and pump S/N 2412 were deleted from this data base. However, including these pumps with the large data base presently available would still not significantly change the calculated statistics (mean and standard deviation). For studies that require information other than normal operational conditions (i.e., extreme values, higher moments, etc.), the complete data base should be utilized.

---

[1]Swanson, W. L. "Statistical Analysis of Vibration Levels on the SSME Turbopumps; Volume I, Calculation of RMS Overlay Vibration Levels for the SSME Phase II High Pressure Oxidizer Turbopumps." Wyle Laboratories TM 68101-20, November 1987.

Section 2 contains plots of the cumulative distribution, probability density or histogram, and a table of the mean and standard deviation for each test stand. Power levels analyzed for this report include 65 percent, 100 percent, 104 percent, and 109 percent. Sufficient data was not available to perform a statistical analysis at 111 percent or the other power levels (i.e., 80 percent, 90 percent, etc.) although some data is available in the Diagnostic Data Base at these power levels. Section 3 contains plots of the FASCOS vibration levels (PBP 45–2, PBP 135–1, and PBP 135–3) utilized for flight vibration monitoring. The synchronous vibration levels are comparable to the RASCOS measurements, although FASCOS composite vibration levels are slightly lower since the cut-off filter is set at 800 Hz for these measurements, as opposed to 1000 Hz. A comparison of the RASCOS and FASCOS measurements are shown in Figures 9 and 10. The small differences noted from this study do not warrant any change in the overlay plots and/or green-run specifications for the SSME HPOTP at this time. Studies will continue on more sophisticated methods to evaluate the significance and/or comparison of data groups using recently received PC software (i.e., SYSTAT, IGOR, ETATALYZER).

WYLE LABORATORIES
Engineering Division

Technical Note TN 60900-90-611

STATISTICAL ANALYSIS OF SSME TURBOPUMP VIBRATION LEVELS

Part II, High Pressure Fuel Turbopump

by

Wayne L. Swanson

June 1990

FOREWORD

Wyle Laboratories' Engineering Division prepared this report for the National Aeronautics and Space Administration, George C. Marshall Space Flight Center. The work was performed under contract NAS8-38156, entitled "Data Analysis and Diagnostic Evaluation of Space Shuttle Main Engine (SSME) Dynamic Measurements."

Technical direction, assistance, and modification to the Diagnostic Data Base computer program was provided by J. McBride and S. Gallik of MSFC/ED 23, with members of BCSS providing the computer output support. This is part II in a series of reports presently in various stages of preparation. The tentative topics of these reports are

Part I: Statistical Analysis of Vibration Levels on the SSME High Pressure Oxidizer Turbopumps

Part II: Statistical Analysis of Vibration Levels on the SSME High Pressure Fuel Turbopumps

Part III: Statistical Analysis of Vibration Levels on the SSME Low Pressure Oxidizer Turbopumps

Part IV: Statistical Analysis of Vibration Levels on the SSME Low Pressure Fuel Turbopumps

TABLE OF CONTENTS

FOREWORD		ii
1.0	TECHNICAL DISCUSSION	1
2.0	RASCOS SYNCHRONOUS SSME HPFP STATISTICAL PLOTS	1
3.0	FASCOS SYNCHRONOUS SSME HPFP STATISTICAL PLOTS	19
4.0	RASCOS COMPOSITE SSME HPFP STATISTICAL PLOTS	37
5.0	FASCOS COMPOSITE SSME HPFP STATISTICAL PLOTS	61
6.0	COMPLETE DATA BASE SYNCHRONOUS AND COMPOSITE SSME HPFP STATISTICAL PLOTS	71
7.0	SSME DIAGNOSTIC DATA BASE DIRECTORY	89
8.0	HPFP SYNCHRONOUS FREQUENCY VS POWER LEVEL	103
9.0	COMPUTER PROGRAM	107

WYLE LABORATORIES
Engineering Division

Technical Note TN 60900-90-611

STATISTICAL ANALYSIS OF SSME TURBOPUMP VIBRATION LEVELS

Part III, Low Pressure Oxidizer Turbopump

by

Wayne L. Swanson

June 1990

FOREWORD

Wyle Laboratories' Engineering Division prepared this report for the National Aeronautics and Space Administration, George C. Marshall Space Flight Center. The work was performed under contract NAS8-38156, entitled "Data Analysis and Diagnostic Evaluation of Space Shuttle Main Engine (SSME) Measurements."

Technical direction, assistance, and modification to the Diagnostic Data Base computer program was provided by J. McBride and S. Gallik of MSFC/ED 23, with members of BCSS providing the computer output support. This is part III in a series presently in various stages of preparation. The tentative topics of these reports are

Part I: Statistical Analysis of Vibration Levels on the SSME High Pressure Oxidizer Turbopumps

Part II: Statistical Analysis of Vibration Levels on the SSME High Pressure Fuel Turbopumps

Part III: Statistical Analysis of Vibration Levels on the SSME Low Pressure Oxidizer Turbopumps

Part IV: Statistical Analysis of Vibration Levels on the SSME Low Pressure Fuel Turbopumps

TABLE OF CONTENTS

FOREWORD		ii
1.0	TECHNICAL DISCUSSION	1
2.0	SYNCHRONOUS AND COMPOSITE STATISTICAL DATA PLOTS, DEC. '78 - JUNE '90	9
3.0	SYNCHRONOUS AND COMPOSITE STATISTICAL DATA PLOTS, TOTAL DATABASE	23
4.0	SSME DIAGNOSTIC DATA BASE DIRECTORY	37
5.0	LPOP SYNCHRONOUS FREQUENCY VS POWER LEVEL	61
6.0	COMPUTER PROGRAM	65

WYLE LABORATORIES
Engineering Division

Technical Note TN 60900-90-611

STATISTICAL ANALYSIS OF SSME TURBOPUMP VIBRATION LEVELS

Part IV, Low Pressure Fuel Turbopump

by

Wayne L. Swanson

June 1990

FOREWORD

Wyle Laboratories' Engineering Division prepared this report for the National Aeronautics and Space Administration, George C. Marshall Space Flight Center. The work was performed under contract NAS8-38156, entitled "Data Analysis and Diagnostic Evaluation of Space Shuttle Main Engine (SSME) Dynamic Measurements."

Technical direction, assistance, and modification to the Diagnostic Data Base computer program was provided by J. McBride and S. Gallik of MSFC/ED 23, with members of BCSS providing the computer output support. This is part II in a series presently in various stages of preparation. The tentative topics include

Part I: Statistical Analysis of Vibration Levels on the SSME High Pressure Oxidizer Turbopumps

Part II: Statistical Analysis of Vibration Levels on the SSME High Pressure Fuel Turbopumps

Part III: Statistical Analysis of Vibration Levels on the SSME Low Pressure Oxidizer Turbopumps

Part IV: Statistical Analysis of Vibration Levels on the SSME Low Pressure Fuel Turbopumps

1.0 TECHNICAL DISCUSSION

This document is an updated version of a previous study of the vibration level statistics for the Low Pressure Fuel Turbopumps (LPFTP) at different power levels. The previous unpublished work was to evaluate the green-run specifications and establish an overlay plot for data evaluation comparison, including all LPFP and LPFT vibration data in the Diagnostic Data Base up to December 1987.

Figures 1 through 4 compare the previous vibration data with the data rolled into the data base from December 1987 to June 1990. No significant change is noted for the synchronous data groups. However, the composite levels, especially at 104% power level, may contain some outliers that will require further checking to ensure that a valid data base was utilized for the previous (December 1987) study. Figures 5 through 8 are the statistical data for the total data group, which is more applicable for comparison with future individual measurements and/or data groups.

Sections 2 and 3 contain plots of the synchronous and composite (50 to 1000 Hz) cumulative distribution, probability density or histogram, and a table of the mean, standard deviation for each individual measurement location for each test stand and data group. Section 4 is a listing of the present SSME Diagnostic Data Directory, and Section 5 contains plots and tabulations of the synchronous frequency versus power level calculated using the engine balance data.

WYLE LABORATORIES
Engineering Division

Technical Note TN 60900-92-01

STATISTICAL SUMMARY OF SSME TURBOPUMP VIBRATION LEVELS

Part I
High Pressure Oxidizer Turbopump

by

Wayne L. Swanson

June 1992

FOREWORD

Wyle Laboratories' Engineering Division prepared this report for the National Aeronautics and Space Administration, George C. Marshall Space Flight Center. The work was performed under contract NAS8-38156, entitled "Data Analysis and Diagnostic Evaluation of Space Shuttle Main Engine Dynamic Measurements."

Technical direction, assistance, and maintenance of the Diagnostic Data Base computer program was provided by J. McBride and S. Gallik of MSFC/ED 23, with members of BCSS providing the computer output support. This is part I in a series of reports published and/or in preparation.

Statistical Summary of SSME Turbopump Vibration Levels

- **Part I, High Pressure Oxidizer Turbopump**
- Part II, High Pressure Fuel Turbopump
- Part III, Low Pressure Oxidizer Turbopump
- Part IV, Low Pressure Fuel Turbopump

TABLE OF CONTENTS

		Page
FOREWORD		(iii)
1.0	TECHNICAL DISCUSSION	1
2.0	COMPOSITE STATISTICAL DATA PLOTS	17
3.0	SYNCHRONOUS STATISTICAL DATA PLOTS	43
4.0	2 * SYNCH STATISTICAL DATA PLOTS	69
5.0	3 * SYNCH STATISTICAL DATA PLOTS	95
6.0	4 * SYNCH STATISTICAL DATA PLOTS	121
7.0	FASCOS COMPOSITE STATISTICAL DATA PLOTS	147
8.0	FASCOS SYNCHRONOUS STATISTICAL DATA PLOTS	161
9.0	SSME DIAGNOSTIC DATA BASE DIRECTORY	175
10.0	GAMMA DISTRIBUTION	203
11.0	SYNCHRONOUS FREQUENCY (HZ) VS POWER LEVEL	205

1.0 TECHNICAL DISCUSSION

This document is an updated version of previously published reports[1,2] on the vibration statistics of the Phase II High Pressure Oxidizer Turbopumps (HPOTP) at different power levels. The purpose of this document is to evaluate and document any significant change that has occurred in the vibration statistics since the last reports were published in November 1987 and June 1990. This report will also update and provide additional values (2N, 3N, 4N, etc) for overlay plots in the data analysis routines.

The first two moments—the mean (average value) and the standard deviation (variance)—do not indicate a significant change other than what would be expected from random chance for both the synchronous and composite (50-1000 Hz) vibration levels of the HPOTP. The updated version now includes 1796 measurements at the 100% power level, an increase of 579 from the June 1990 document. A comparison of the calculated statistics in references 1 and 2 are shown in Figures 1 through 6, with the updated statistics shown in Figures 7 through 11. The statistics for power levels at 63 percent and 64 percent and harmonics of synchronous (2N, 3N, and 4N) are also included in this document.

For the previous studies only valid data from Phase II turbopumps that operated under **normal** conditions were included in the data base analysis. Therefore, questionable data points (excessive noise, etc), early cutoff, high running main impellors and extreme outliers were not utilized. However, including these pumps or tests with the large data base presently available would still not significantly change the calculated statistics (mean and standard deviation). For studies that require information other than normal operational conditions (i.e., extreme values, higher moments, etc), the complete data base should be utilized. For this analysis, turbopumps with damping seals were defined as Phase II turbopumps since, during the development phase testing of the Phase II turbopumps, not all pumps contained the final design components during some of the tests.

Sections 2 through 8 contain plots of the cumulative distribution and probability density or histogram and a table of the mean and standard deviation for each test stand. The classical gamma function provides a convenient smoothing operation and computational method for evaluating the cumulative distribution of the data and is shown as an overlay on the plots. With the exception of one set of 4N plots and mean vibration levels below 0.5 Grms, the gamma distribution shows excellent fit to the measured data. At the low vibration levels, a smaller bin size should be used to analyze the data. Power levels analyzed for this report include 63 percent, 64 percent, 65 percent, 100 percent, 104 percent, and 109 percent. Sufficient data was not considered available to perform a statistical analysis at 111 percent or the other levels(i.e., 80 percent, 90 percent, etc.) although data is available in the Diagnostic Data Base at these power levels. Sections 7 and 8 contain plots of the FASCOS vibration levels (PBP RAD 45-2, PBP RAD 135-1, and PBP RAD 135-3) utilized for flight vibration monitoring. A slight increase from the previous study (approximately 0.25 Grms) was noted in the statistics for the composite FASCOS vibration levels (Figure 5). However, this is not considered significant since a much smaller increase (approximately 0.15 Grms) was noted for the synchronous levels (Figure 6). Studies will continue on

---

[1] Swanson, W. L. "Statistical Analysis of Vibration Levels on the SSME Turbopumps: Volume 1, Calculation of RMS Overlay Vibration Levels for SSME Phase II High Pressure Oxidizer Turbopumps." Wyle Laboratories technical memorandum TM 68101-20, November 1987.

[2] Swanson, W. L. "Statistical Analysis of SSME Turbopump Vibration Levels: Part I, High Pressure Oxidizer Turbopump." Wyle Laboratories technical note TN 60900-90-611, June 1990.

more sophisticated methods to evaluate the significance and/or compare different size data groups using recently received PC software (e.g., SYSTAT, IGOR statistical packages). Confidence intervals could be calculated based upon the Student t and Chi Square methods but are not included in this report. Additional study will be required to determine what degree of freedom applies to the data sample (number of pumps, with or without revisions, number of tests, total data sample, etc). Depending on the selection of the degree of freedom, a very wide variation can be obtained for the confidence interval, which places very little confidence in the confidence interval calculations.

Sections 9, 10, and 11 are included for reference. Section 9 is a listing of the tests, date of test, test duration, turbopump serial number, and the power levels where data is available from the Diagnostic Data Base program. Section 10 provides the synchronous frequency of the SSME turbopumps versus power levels, and Section 11 is a listing of the program written for calculation of the Gamma Cumulative Distribution Function. A bin size of 0.01 was used to calculate the 50%, 90% and 99% gamma values listed in Figures 7 through 11.

PHASE II
HIGH PRESSURE OXYGEN TURBOPUMP

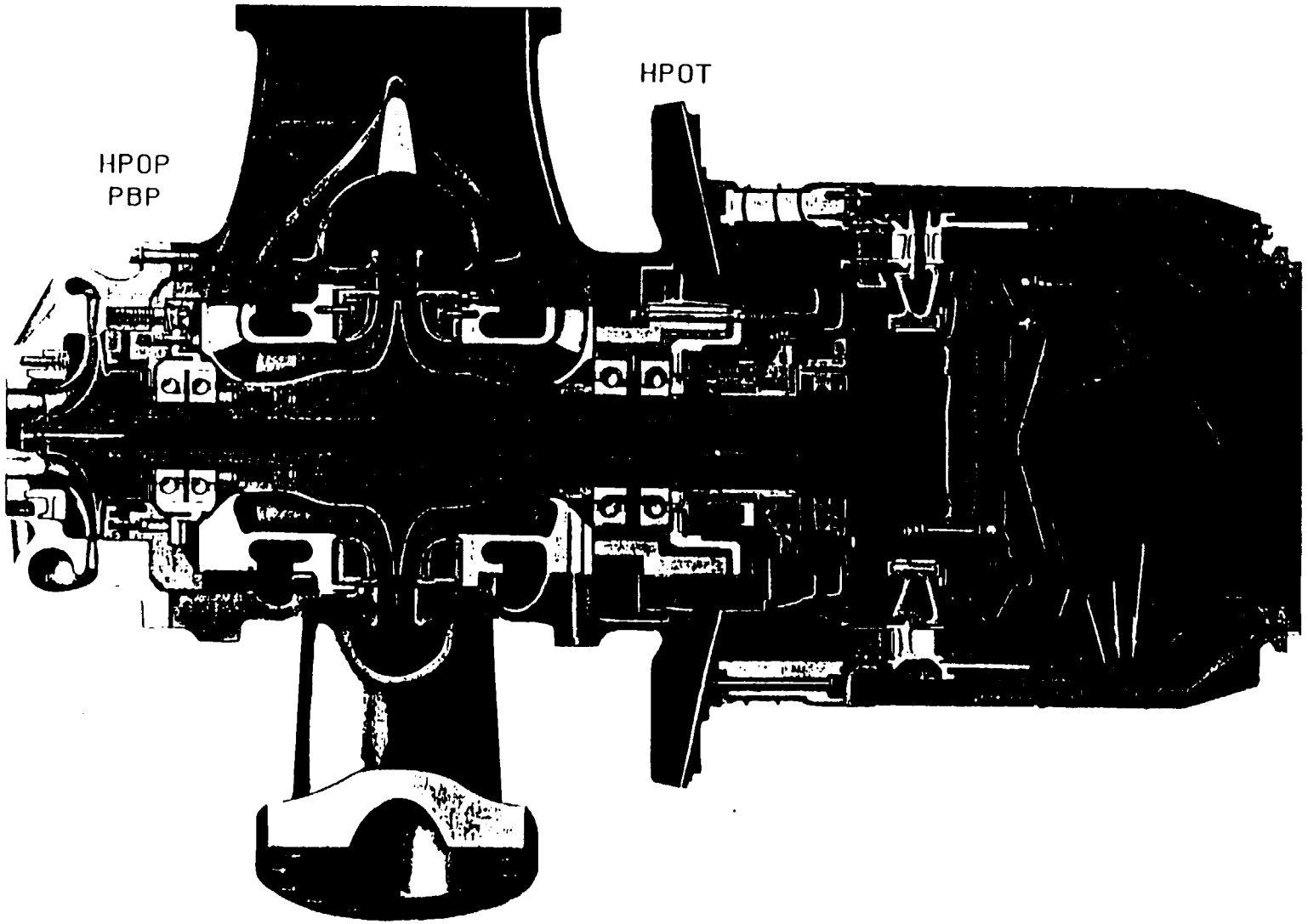

HISTORICAL STATISTICAL DATA COMPARISON
LOX PBP (PHASE II)
COMPOSITE Grms LEVELS

65% PWL	AVERAGE	STD DEV	NBR DATA SAMPLE
NOV. 1987	1.45	0.36	110
JUN. 1990	1.33	0.34	493
JUN. 1992	1.39	0.54	635

100% PWL	AVERAGE	STD DEV	NBR DATA SAMPLE
NOV. 1987	3.15	0.91	429
JUN. 1990	2.92	0.88	1217
JUN. 1992	2.91	0.86	1796

104% PWL	AVERAGE	STD DEV	NBR DATA SAMPLE
NOV. 1987	3.77	1.12	290
JUN. 1990	3.43	1.09	944
JUN. 1992	3.29	1.03	1426

109% PWL	AVERAGE	STD DEV	NBR DATA SAMPLE
NOV. 1987	4.63	1.71	171
JUN. 1990	3.73	1.35	599
JUN. 1992	3.52	1.22	961

Figure 1. Historical Statistical Data Comparison of RASCOS HPOTP PBP RAD (PHASE II) Composite Vibration Levels

HISTORICAL STATISTICAL DATA COMPARISON
LOX PBP (PHASE II)
SYNCHRONOUS Grms LEVELS

65% PWL	AVERAGE	STD DEV	NBR DATA SAMPLE
NOV. 1987	0.36	0.16	110
JUN. 1990	0.36	0.17	493
JUN. 1992	0.36	0.15	635

100% PWL	AVERAGE	STD DEV	NBR DATA SAMPLE
NOV. 1987	1.33	0.67	429
JUN. 1990	1.45	0.85	1217
JUN. 1992	1.51	0.85	1796

104% PWL	AVERAGE	STD DEV	NBR DATA SAMPLE
NOV. 1987	1.67	0.69	290
JUN. 1990	1.77	0.89	944
JUN. 1992	1.76	0.92	1426

109% PWL	AVERAGE	STD DEV	NBR DATA SAMPLE
NOV. 1987	1.59	0.88	171
JUN. 1990	1.64	0.87	599
JUN. 1992	1.63	0.90	961

Figure 2. Historical Statistical Data Comparison of RASCOS HPOTP PBP RAD (PHASE II) Synchronous Vibration Data

HISTORICAL STATISTICAL DATA COMPARISON
LOX TURB (PHASE II)
COMPOSITE Grms LEVELS

65% PWL	AVERAGE	STD DEV	NBR DATA SAMPLE
NOV. 1987	1.91	0.72	74
JUN. 1990	1.56	0.52	330
JUN. 1992	1.61	0.65	445

100% PWL	AVERAGE	STD DEV	NBR DATA SAMPLE
NOV. 1987	2.85	0.63	284
JUN. 1990	2.70	0.73	795
JUN. 1992	2.71	0.75	1204

104% PWL	AVERAGE	STD DEV	NBR DATA SAMPLE
NOV. 1987	3.13	0.57	192
JUN. 1990	2.95	0.73	620
JUN. 1992	2.89	0.76	976

109% PWL	AVERAGE	STD DEV	NBR DATA SAMPLE
NOV. 1987	3.56	0.90	114
JUN. 1990	3.11	0.79	402
JUN. 1992	3.04	0.73	670

Figure 3. Historical Statistical Data Comparison of RASCOS HPOTP TURB RAD (PHASE II) Composite Vibration Data

HISTORICAL STATISTICAL DATA COMPARISON
LOX TURB (PHASE II)
SYNCHRONOUS Grms LEVELS

65% PWL	AVERAGE	STD DEV	NBR DATA SAMPLE
NOV. 1987	0.26	0.13	74
JUN. 1990	0.24	0.11	330
JUN. 1992	0.25	0.12	445

100% PWL	AVERAGE	STD DEV	NBR DATA SAMPLE
NOV. 1987	1.23	0.56	284
JUN. 1990	1.28	0.68	795
JUN. 1992	1.25	0.65	1204

104% PWL	AVERAGE	STD DEV	NBR DATA SAMPLE
NOV. 1987	1.42	0.54	192
JUN. 1990	1.44	0.73	620
JUN. 1992	1.41	0.75	976

109% PWL	AVERAGE	STD DEV	NBR DATA SAMPLE
NOV. 1987	1.41	0.69	114
JUN. 1990	1.31	0.66	402
JUN. 1992	1.32	0.68	670

Figure 4. Historical Statistical Data Comparison of RASCOS HPOTP TURB RAD (PHASE II) Synchronous Vibration Data

HISTORICAL STATISTICAL DATA COMPARISON
FASCOS LOX PBP (PHASE II)
COMPOSITE Grms LEVELS

65% PWL	AVERAGE	STD DEV	NBR DATA SAMPLE
JUN. 1990	0.85	0.30	283
JUN. 1992	0.96	0.56	412
DIFFERENCE	0.11	0.26	129

100% PWL	AVERAGE	STD DEV	NBR DATA SAMPLE
JUN. 1990	1.92	0.67	559
JUN. 1992	2.19	0.77	897
DIFFERENCE	0.27	0.1	338

104% PWL	AVERAGE	STD DEV	NBR DATA SAMPLE
JUN. 1990	2.20	0.70	481
JUN. 1992	2.42	0.81	703
DIFFERENCE	0.22	0.11	222

109% PWL	AVERAGE	STD DEV	NBR DATA SAMPLE
JUN. 1990	2.26	0.63	311
JUN. 1992	2.51	0.80	448
DIFFERENCE	0.25	0.17	137

Figure 5. Historical Statistical Data Comparison of FASCOS HPOTP PBP (PHASE II) Composite Vibration Data

HISTORICAL STATISTICAL DATA COMPARISON
FASCOS LOX PBP (PHASE II)
SYNCHRONOUS Grms LEVELS

65% PWL	AVERAGE	STD DEV	NBR DATA SAMPLE
JUN. 1990	0.34	0.19	283
JUN. 1992	0.35	0.16	412
DIFFERENCE	0.01	-0.03	129

100% PWL	AVERAGE	STD DEV	NBR DATA SAMPLE
JUN. 1990	1.24	0.77	559
JUN. 1992	1.36	0.78	897
DIFFERENCE	0.12	0.01	338

104% PWL	AVERAGE	STD DEV	NBR DATA SAMPLE
JUN. 1990	1.50	0.78	481
JUN. 1992	1.61	0.85	703
DIFFERENCE	0.11	0.07	222

109% PWL	AVERAGE	STD DEV	NBR DATA SAMPLE
JUN. 1990	1.39	0.76	311
JUN. 1992	1.55	0.82	448
DIFFERENCE	0.16	0.06	137

Figure 6. Historical Statistical Data Comparison of FASCOS HPOTP PBP (PHASE II) Synchronous Vibration Data

HIGH PRESSURE OXIDIZER TURBOPUMP (HPOTP)						
RASCOS PBP 45-1, 45-3, 135-2, 225						
COMPOSITE	63%	64%	65%	100%	104%	109%
Mean	1.27	1.31	1.39	2.91	3.29	3.52
Std Dev	0.30	0.38	0.54	0.86	1.03	1.22
Data Sample	233	230	635	1796	1426	961
1-Sigma	1.57	1.69	1.93	3.77	4.32	4.74
2-Sigma	1.87	2.07	2.47	4.63	5.35	5.96
3-Sigma	2.17	2.45	3.01	5.49	6.38	7.18
50% Gamma	1.25	1.27	1.32	2.83	3.18	3.38
90% Gamma	1.67	1.81	2.11	4.05	4.66	5.15
99% Gamma	2.07	2.35	2.94	5.27	6.15	6.96

HIGH PRESSURE OXIDIZER TURBOPUMP (HPOTP)						
RASCOS PBP 45-1,45-3, 135-2, 225						
SYNCH	63%	64%	65%	100%	104%	109%
Mean	0.29	0.30	0.36	1.51	1.76	1.63
Std Dev	0.11	0.12	0.15	0.85	0.92	0.90
Data Sample	233	230	635	1796	1426	961
1-Sigma	0.40	0.42	0.51	2.36	2.68	2.53
2-Sigma	0.51	0.54	0.66	3.21	3.60	3.43
3-Sigma	0.62	0.66	0.81	4.06	4.52	4.33
50% Gamma	0.28	0.28	0.34	1.35	1.60	1.47
90% Gamma	0.44	0.46	0.56	2.65	2.99	2.84
99% Gamma	0.60	0.65	0.80	4.15	4.57	4.41

Figure 7. Statistical Vibration Data HPOTP PBP RAD
Composite and Synchronous

HIGH PRESSURE OXIDIZER TURBOPUMP (HPOTP)						
RASCOS PBP 45-1,45-3, 135-2, 225						
2*SYNCH	63%	64%	65%	100%	104%	109%
Mean	0.19	0.19	0.23	0.77	1.13	1.01
Std Dev	0.08	0.08	0.12	0.46	0.70	0.61
Data Sample	233	230	635	1796	1426	961
1-Sigma	0.27	0.27	0.35	1.23	1.83	1.62
2-Sigma	0.35	0.35	0.47	1.69	2.53	2.23
3-Sigma	0.43	0.43	0.59	2.15	3.23	2.84
50% Gamma	0.18	0.18	0.21	0.68	0.99	0.89
90% Gamma	0.30	0.30	0.39	1.39	2.07	1.83
99% Gamma	0.42	0.42	0.60	2.22	3.35	2.93

HIGH PRESSURE OXIDIZER TURBOPUMP (HPOTP)						
RASCOS PBP 45-1,45-3, 135-2, 225						
3*SYNCH	63%	64%	65%	100%	104%	109%
Mean	0.16	0.16	0.21	0.82	1.06	0.87
Std Dev	0.05	0.05	0.15	0.29	0.48	0.46
Data Sample	233	230	635	1796	1426	961
1-Sigma	0.21	0.21	0.36	1.11	1.54	1.33
2-Sigma	0.26	0.26	0.51	1.40	2.02	1.79
3-Sigma	0.31	0.31	0.66	1.69	2.50	2.25
50% Gamma	0.15	0.15	0.18	0.79	0.99	0.79
90% Gamma	0.23	0.23	0.41	1.21	1.70	1.49
99% Gamma	0.30	0.30	0.71	1.64	2.48	2.28

HIGH PRESSURE OXIDIZER TURBOPUMP (HPOTP)						
RASCOS PBP 45-1,45-3, 135-2, 225						
4*SYNCH	63%	64%	65%	100%	104%	109%
Mean	0.94	0.98	1.11	6.56	6.39	5.23
Std Dev	0.55	0.61	0.59	2.74	2.77	2.71
Data Sample	233	230	635	1834	14.24	940
1-Sigma	1.49	1.59	1.70	9.30	9.16	7.94
2-Sigma	2.04	2.20	2.29	12.04	11.93	10.65
3-Sigma	2.59	2.81	2.88	14.78	14.70	13.36
50% Gamma	0.84	0.86	1.01	6.18	5.99	4.77
90% Gamma	1.68	1.80	1.90	10.22	10.10	8.86
99% Gamma	2.66	2.92	2.92	14.55	14.52	13.49

Figure 8. Statistical Vibration Data HPOTP RASCOS PBP RAD
2*Synch, 3*Synch and 4*Synch

HIGH PRESSURE OXIDIZER TURBOPUMP (HPOTP)						
RASCOS HPOT RAD 45, 90, 135						
COMPOSITE	63%	64%	65%	100%	104%	109%
Mean	1.40	1.43	1.61	2.71	2.89	3.04
Std Dev	0.44	0.45	0.65	0.75	0.76	0.73
Data Sample	169	167	445	1204	976	670
1-Sigma	1.84	1.88	2.26	3.46	3.65	3.77
2-Sigma	2.28	2.33	2.91	4.21	4.41	4.50
3-Sigma	2.72	2.78	3.56	4.96	5.17	5.23
50% Gamma	1.35	1.38	1.52	2.64	2.82	2.98
90% Gamma	1.99	2.03	2.48	3.70	3.90	4.00
99% Gamma	2.62	2.68	3.49	4.75	4.94	4.99

HIGH PRESSURE OXIDIZER TURBOPUMP (HPOTP)						
RASCOS HPOT RAD 45, 90, 135						
SYNCH	63%	64%	65%	100%	104%	109%
Mean	0.16	0.16	0.25	1.25	1.41	1.32
Std Dev	0.08	0.09	0.12	0.65	0.75	0.68
Data Sample	169	167	445	1204	976	670
1-Sigma	0.24	0.25	0.37	1.90	2.16	2.00
2-Sigma	0.32	0.34	0.49	2.55	2.91	2.68
3-Sigma	0.40	0.43	0.61	3.20	3.66	3.36
50% Gamma	0.15	0.14	0.23	1.14	1.28	1.21
90% Gamma	0.27	0.28	0.41	2.12	2.42	2.23
99% Gamma	0.40	0.44	0.61	3.23	3.71	3.39

Figure 9. Statistical Vibration Data HPOTP RASCOS TURB RAD
Composite and Synchronous

HIGH PRESSURE OXIDIZER TURBOPUMP (HPOTP)						
RASCOS HPOT RAD 45, 90, 135						
2*SYNCH	63%	64%	65%	100%	104%	109%
Mean	0.16	0.17	0.22	0.99	1.25	1.22
Std Dev	0.06	0.06	0.09	0.61	0.63	0.58
Data Sample	169	167	445	1204	976	670
1-Sigma	0.22	0.23	0.31	1.60	1.88	1.80
2-Sigma	0.28	0.29	0.40	2.21	2.51	2.38
3-Sigma	0.34	0.35	0.49	2.82	3.14	2.96
50% Gamma	0.15	0.16	0.21	0.87	1.15	1.13
90% Gamma	0.24	0.25	0.34	1.81	2.09	2.00
99% Gamma	0.33	0.34	0.48	2.92	3.16	2.96

HIGH PRESSURE OXIDIZER TURBOPUMP (HPOTP)						
RASCOS HPOT RAD 45, 90, 135						
3*SYNCH	63%	64%	65%	100%	104%	109%
Mean	0.18	0.19	0.27	0.48	0.58	0.53
Std Dev	0.05	0.06	0.18	0.15	0.18	0.17
Data Sample	169	167	445	1204	976	670
1-Sigma	0.23	0.25	0.45	0.63	0.76	0.70
2-Sigma	0.28	0.31	0.63	0.78	0.94	0.87
3-Sigma	0.33	0.37	0.81	0.93	1.12	1.04
50% Gamma	0.18	0.18	0.23	0.46	0.56	0.51
90% Gamma	0.25	0.27	0.51	0.68	0.82	0.76
99% Gamma	0.32	0.36	0.85	0.90	1.08	1.00

HIGH PRESSURE OXIDIZER TURBOPUMP (HPOTP)						
RASCOS HPOT RAD 45, 90, 135						
4*SYNCH	63%	64%	65%	100%	104%	109%
Mean	0.42	0.43	0.51	1.63	2.63	3.94
Std Dev	0.20	0.21	0.23	0.86	1.5	2.03
Data Sample	169	167	445	1248	973	655
1-Sigma	0.62	0.64	0.74	2.49	4.13	5.97
2-Sigma	0.82	0.85	0.97	3.35	5.63	8.00
3-Sigma	1.02	1.06	1.20	4.21	7.13	10.03
50% Gamma	0.39	0.40	0.48	1.48	2.35	3.60
90% Gamma	0.69	0.71	0.82	2.78	4.64	6.66
99% Gamma	1.02	1.06	1.19	4.26	7.30	10.12

Figure 10. Statistical Vibration Data HPOTP RASCOS TURB RAD
2*Synch, 3*Synch, and 4*Synch

HIGH PRESSURE OXIDIZER TURBOPUMP (HPOTP)						
FASCOS PBP 45-2, 135-1, 135-2						
COMPOSITE	63%	64%	65%	100%	104%	109%
Mean	0.72	0.74	0.96	2.19	2.42	2.51
Std Dev	0.20	0.21	0.56	0.77	0.81	0.80
Data Sample	172	172	412	897	703	448
1-Sigma	0.92	0.95	1.52	2.96	3.23	3.31
2-Sigma	1.12	1.16	2.08	3.73	4.04	4.11
3-Sigma	1.32	1.37	2.64	4.50	4.85	4.73
50% Gamma	0.70	0.72	0.85	2.10	2.33	2.43
90% Gamma	0.99	1.02	1.71	3.22	3.50	3.57
99% Gamma	1.26	1.31	2.71	4.37	4.69	4.73
HIGH PRESSURE OXIDIZER TURBOPUMP (HPOTP)						
FASCOS PBP 45-2, 135-1, 135-2						
SYNCHRONOUS	63%	64%	65%	100%	104%	109%
Mean	0.24	0.25	0.35	1.36	1.61	1.55
Std Dev	0.11	0.12	0.16	0.78	0.85	0.82
Data Sample	172	172	412	897	703	448
1-Sigma	0.35	0.37	0.51	2.14	2.46	2.37
2-Sigma	0.46	0.49	0.67	2.92	3.31	3.19
3-Sigma	0.57	0.61	0.83	3.70	4.16	4.01
50% Gamma	0.22	0.23	0.33	1.21	1.46	1.41
90% Gamma	0.39	0.41	0.56	2.41	2.75	2.65
99% Gamma	0.57	0.61	0.82	3.79	4.21	4.06

Figure 11. Statistical Vibration Data HPOTP FASCOS PBP RAD
Composite and Synchronous

WYLE LABORATORIES
Engineering Division

Technical Note TN 60900-92-01

STATISTICAL SUMMARY OF SSME TURBOPUMP VIBRATION LEVELS

Part II
High Pressure Fuel Turbopump

by

Wayne L. Swanson

June 1992

FOREWORD

Wyle Laboratories' Engineering Division prepared this report for the National Aeronautics and Space Administration, George C. Marshall Space Flight Center. The work was performed under contract NAS8-38156, entitled "Data Analysis and Diagnostic Evaluation of Space Shuttle Main Engine Dynamic Measurements."

Technical direction, assistance, and maintenance of the Diagnostic Data Base computer program was provided by J. McBride and S. Gallik of MSFC/ED 23, with members of BCSS providing the computer output support. This is part II in a series of reports published and/or in preparation.

Statistical Summary of SSME Turbopump Vibration Levels

- Part I, High Pressure Oxidizer Turbopump
- **Part II, High Pressure Fuel Turbopump**
- Part III, Low Pressure Oxidizer Turbopump
- Part IV, Low Pressure Fuel Turbopump

TABLE OF CONTENTS

		Page
FOREWORD		(iii)
1.0	TECHNICAL DISCUSSION	1
2.0	COMPOSITE STATISTICAL DATA PLOTS	23
3.0	SYNCHRONOUS STATISTICAL DATA PLOTS	49
4.0	2 * SYNCH STATISTICAL DATA PLOTS	75
5.0	3 * SYNCH STATISTICAL DATA PLOTS	101
6.0	4 * SYNCH STATISTICAL DATA PLOTS	127
7.0	FASCOS COMPOSITE STATISTICAL DATA PLOTS	153
8.0	FASCOS SYNCHRONOUS STATISTICAL DATA PLOTS	167
9.0	SSME DIAGNOSTIC DATA BASE DIRECTORY	181
10.0	GAMMA DISTRIBUTION	209
11.0	SYNCHRONOUS FREQUENCY (HZ) VS POWER LEVEL	211

Appendix: Historical Vibration Data Trend Analysis Test List and Cumulative Distribution Plots

1.0 TECHNICAL DISCUSSION

This document is an updated version of previously published reports[1] on the vibration statistics of the Phase II High Pressure Fuel Turbopumps (HPFTP) at different power levels. The purpose of this document is to evaluate and document any significant change that has occurred in the vibration statistics since the last report was published in June 1990. This report will also update and provide additional values (2N, 3N, 4N, and PWLs) for overlay plots in the data analysis routines.

A comparison of the FASCOS vibration levels (HPFP RAD 0, HPFP RAD 174, and HPFP RAD 186) utilized for flight vibration monitoring are shown in Figures 1 and 2. When compared to the previously published data[2] for the first two moments—the mean (average) and standard deviation (variance)—no significant change was noted except for what would be expected from random chance. Figure 1 shows the composite (50 to 1000 Hz) and Figure 2 shows the synchronous vibration levels.

An additional historical vibration data trend analysis was also performed for each year from 1987 to the first half of 1992. All available test data in the SSME diagnostic data base was grouped by pump and turbine end for each power level. Power levels at 100 percent, 104 percent, and 109 percent for the composite (50 to 1000 Hz) and synchronous were included in the analysis. The results of this study are shown in Figures 3 through 8. The most significant feature over the past one and a half decades is the steady decrease of the pump end vibration for both the composite and synchronous data. For the turbine end measurements, however, the change is much less and could be considered insignificant when factored by the number of data samples available in the early part of the program. Figure 9 more clearly illustrates the difference between the pump end and turbine end data trend at the 100% power level. Since all data was included in this analysis, the results should not be directly compared to the data from turbopumps under normal operation. The extreme outliers (obviously invalid data) was not included, however, but included was data from early cut-off tests, abnormal operation, etc. For future reference, the SSME diagnostic data plot output and test input list for each year are included as an appendix.

Figures 10 and 11 illustrate the type of analysis that can be easily performed using the data in the SSME diagnostic data base program. Note the very slight upward trend of the 1992 data when compared to 1991 and 1990. The distribution of the data plotted for each of the three years is shown in Figure 10, and a different type of plot format is shown in Figure 11. When compared to the previous years, the upward trend is insignificant since the data shift is only one bin (0.5 Grms) and approximately one half less data samples were available for 1992. Also, it can be noted that the mean value was not influenced by a series of higher than usual vibration levels for a series of tests and/or turbopumps.

The next analyses were performed to evaluate and update the values for overlay plots in the data analysis routines at additional power levels of 63 percent and 64 percent and the harmonics of synchronous (2N, 3N, and 4N). Selected as the start of the data set, was the point where the measurement scheme was changed to separate the RASCOS and FASCOS measurements, which will provide a consistent data set for the analysis. Also, the data set

---

[1]Swanson, W. L. "Statistical Analysis of SSME Turbopump Vibration Levels: Part II, High Pressure Fuel Turbopump," Wyle Laboratories technical note TN 60900-90-611, June 1990.
[2]Ibid.

corresponds to the time period (1987) where the pump end measurements had stabilized to a reasonably constant level. Justification and/or validation for not using the total data set versus the data after 1987 is illustrated in Figure 12. The difference for composite vibration levels at 100% PWL is less than 0.6 Grms for the mean value and 0.8 for the standard deviation. Figures 13 through 17 include the 50%, 90%, and 99% values for the gamma distribution for the noted measurements. A bin size of 0.01 Grms was used to permit smooth plots and two-place tabulated values.

For the previous study,[3] only valid data from high pressure fuel turbopumps that operated under **normal** conditions was included in the the data base. The came criteria were applied for this analysis. Therefore, questionable data points (e.g., excessive noise), early cutoff, pseudo 3N (if identifiable), and extreme outliers were not utilized. Including these pumps or tests with the large data base presently available, however, would still not significantly change the calculated statistics (mean and standard deviation). For studies that require information other than normal operational conditions (i.e., extreme values, higher moments, etc), the complete data base should be utilized.

Sections 2 through 8 contain plots of the cumulative distribution, probability density or histogram, and a table of the mean and standard deviation for each test stand. The classical gamma function—shown as an overlay on the plots—provides a convenient smoothing operation and computational method for evaluating the cumulative distribution of the data. With the exception of isolated plots and mean vibration levels below 0.5 Grms, the gamma distribution shows excellent fit to the measured data. At the low vibration levels, a smaller bin size should be used to analyze the data. Power levels analyzed for this report include 63 percent, 64 percent, 65 percent, 100 percent, 104 percent, and 109 percent. Sufficient data was not considered available to perform a statistical analysis at 111 percent or the other levels (i.e., 80 percent, 90 percent, etc) although data is available in the diagnostic data base for these power levels. Sections 7 and 8 contain plots of the FASCOS vibration levels (HPFP RAD0, HPFP RAD 174, and HPFP RAD 186) utilized for flight vibration monitoring. From the previous study, a slight increase (approximately 0.25 Grms) was noted in the statistics for the composite FASCOS vibration levels (Figure 5). However, this is not considered significant since a much smaller increase (approximately 0.15 Grms) was noted for the synchronous levels (Figure 6). Studies will continue on more sophisticated methods of evaluating the significance and/or comparison of different size data groups using recently received PC software (i.e., SYSTAT, IGOR, and other statistical packages). Confidence intervals could be calculated based upon the Student t and Chi Square methods, but they are not included in this report. Additional study will be required to determine what degree of freedom applies to the data sample (number of pumps, with or without revisions; number of tests; total data sample; etc). Depending on the selection of the degree of freedom, a very wide variation can be obtained for the confidence interval, which places very little confidence in the calculations.

Sections 9, 10, and 11 are included for reference. Section 9 contains a list of the tests, date of tests, test duration, turbopump serial number, and the power levels, where data is available, from the diagnostic data base program. Section 10 contains a list of the program written for calculation of the gamma cumulative distribution function, and Section 11 provides the synchronous frequency of the SSME turbopumps versus power levels.

---

[3]Ibid.

HIGH PRESSURE FUEL TURBOPUMP

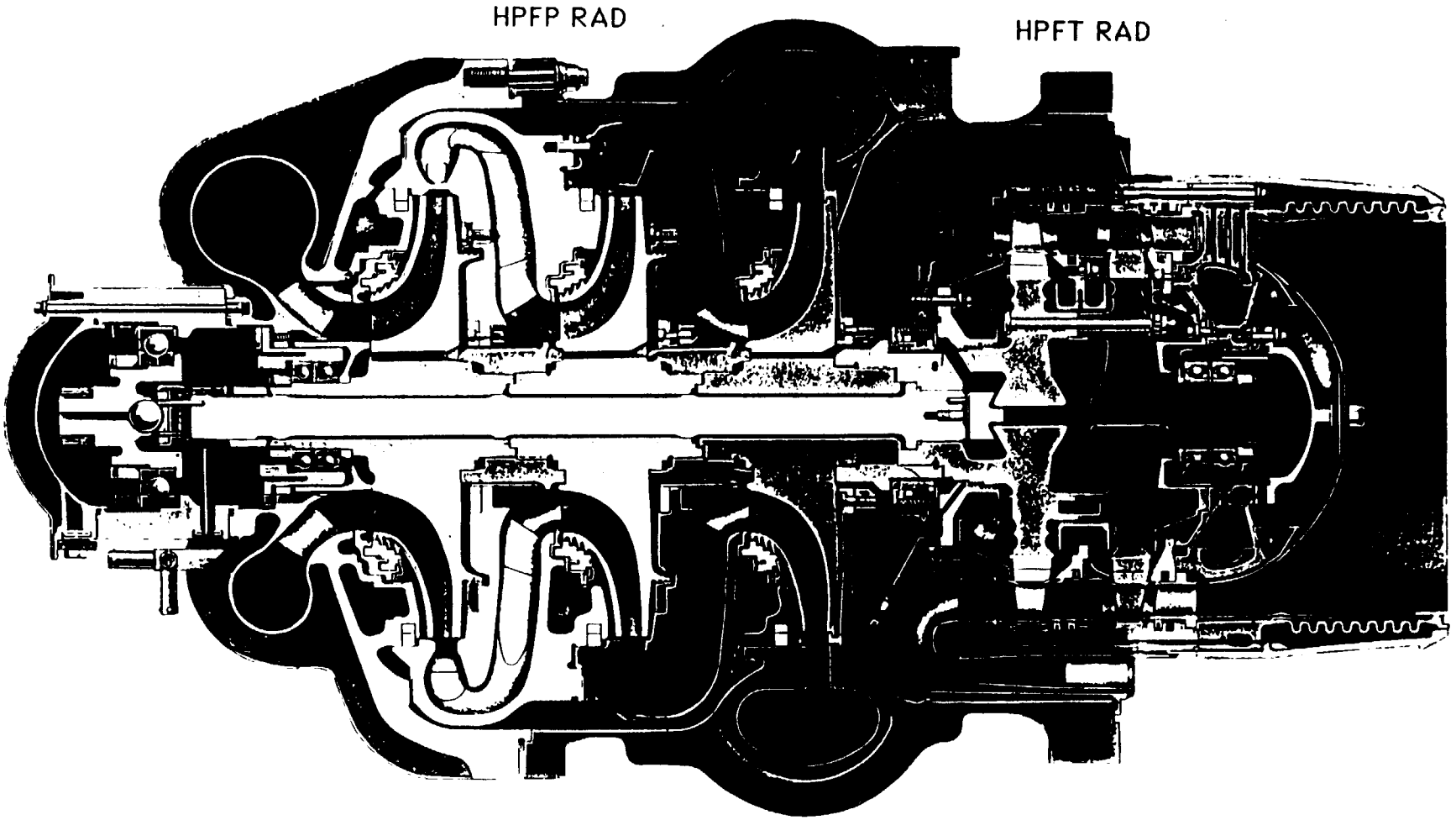

HISTORICAL STATISTICAL DATA COMPARISON
FASCOS HPFP RAD 0, 174, and 186
COMPOSITE Grms LEVELS

65% PWL	AVERAGE	STD DEV	NBR DATA SAMPLE
JUN. 1990	1.11	0.58	286
JUN. 1992	1.22	0.70	458
DIFFERENCE	0.11	0.12	172

100% PWL	AVERAGE	STD DEV	NBR DATA SAMPLE
JUN. 1990	2.77	1.14	566
JUN. 1992	2.86	1.14	884
DIFFERENCE	0.09	0.00	318

104% PWL	AVERAGE	STD DEV	NBR DATA SAMPLE
JUN. 1990	3.57	1.44	485
JUN. 1992	3.48	1.34	707
DIFFERENCE	-0.09	-0.10	222

109% PWL	AVERAGE	STD DEV	NBR DATA SAMPLE
JUN. 1990	4.09	1.60	317
JUN. 1992	3.99	1.49	480
DIFFERENCE	-0.10	-0.11	163

Figure 1. Historical Statistical Data Comparison of FASCOS HPFP Composite Vibration Data

HISTORICAL STATISTICAL DATA COMPARISON
FASCOS HPFP RAD 0, 174, and 186
SYNCHRONOUS Grms LEVELS

65% PWL	AVERAGE	STD DEV	NBR DATA SAMPLE
JUN. 1990	0.71	0.44	286
JUN. 1992	0.79	0.45	458
DIFFERENCE	0.08	0.01	172

100% PWL	AVERAGE	STD DEV	NBR DATA SAMPLE
JUN. 1990	1.99	1.06	566
JUN. 1992	1.93	1.04	884
DIFFERENCE	-0.06	-0.02	318

104% PWL	AVERAGE	STD DEV	NBR DATA SAMPLE
JUN. 1990	2.67	1.36	485
JUN. 1992	2.44	1.29	707
DIFFERENCE	-0.23	-0.07	222

109% PWL	AVERAGE	STD DEV	NBR DATA SAMPLE
JUN. 1990	2.96	1.46	317
JUN. 1992	2.65	1.42	480
DIFFERENCE	-0.31	-0.04	163

Figure 2. Historical Statistical Data Comparison of FASCOS HPFP Synchronous Vibration Data

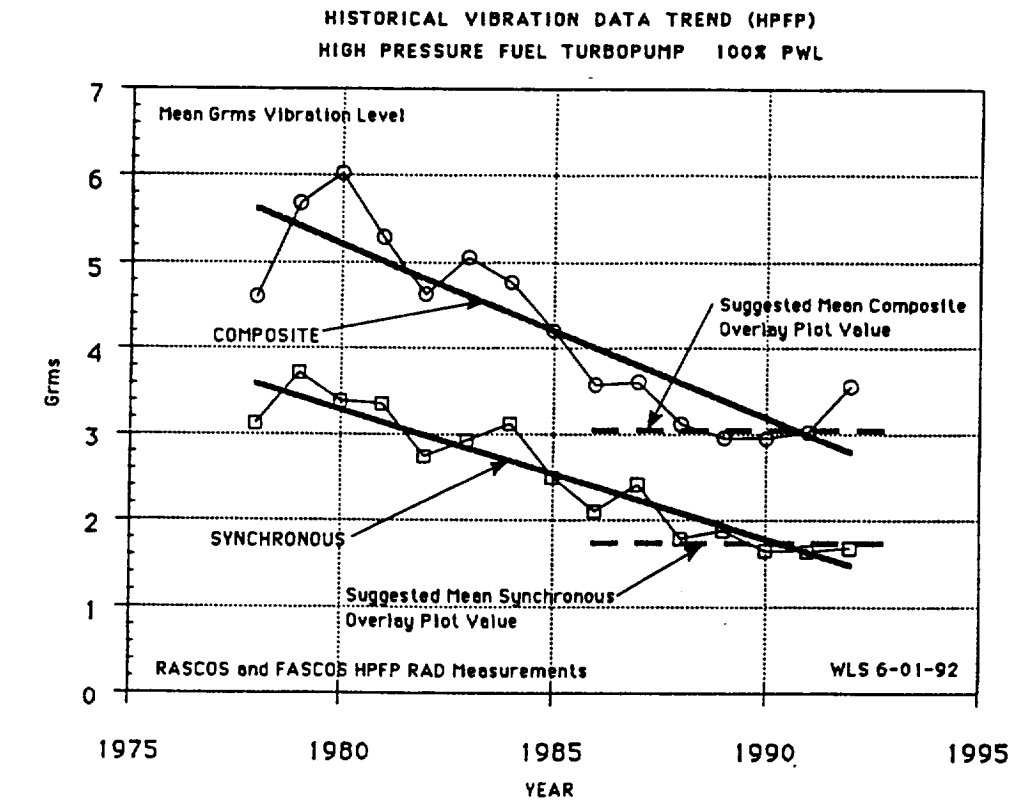

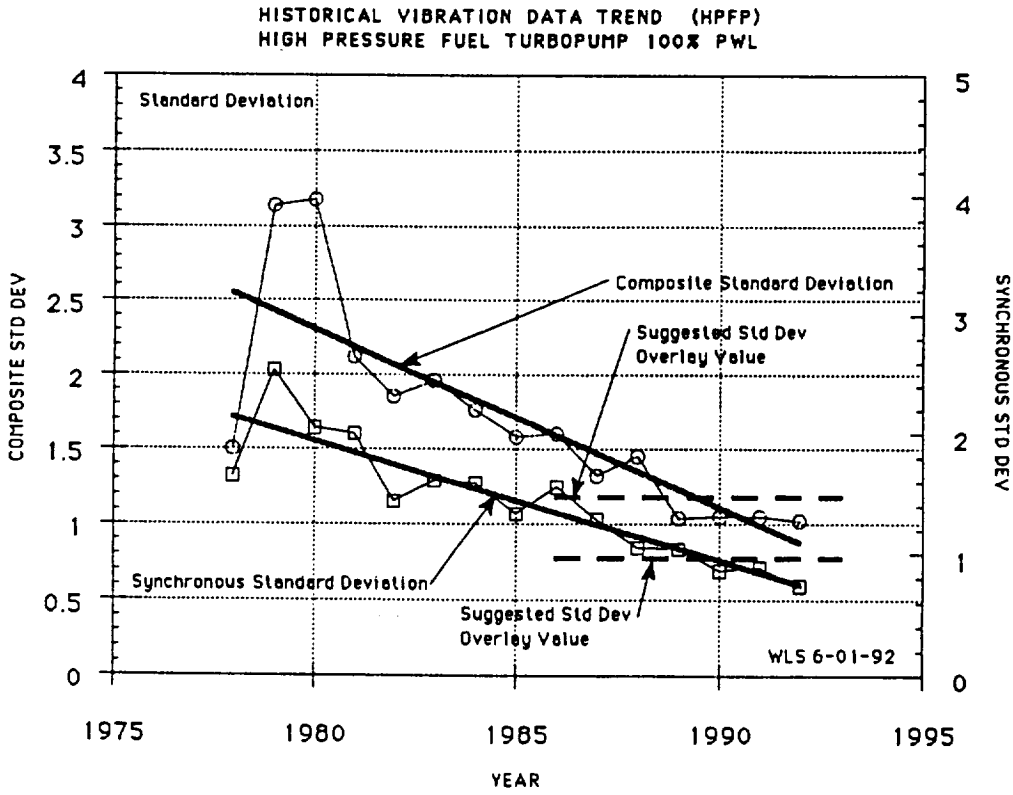

Figure 3. HPFP Historical Vibration Data Trend, 100% PWL

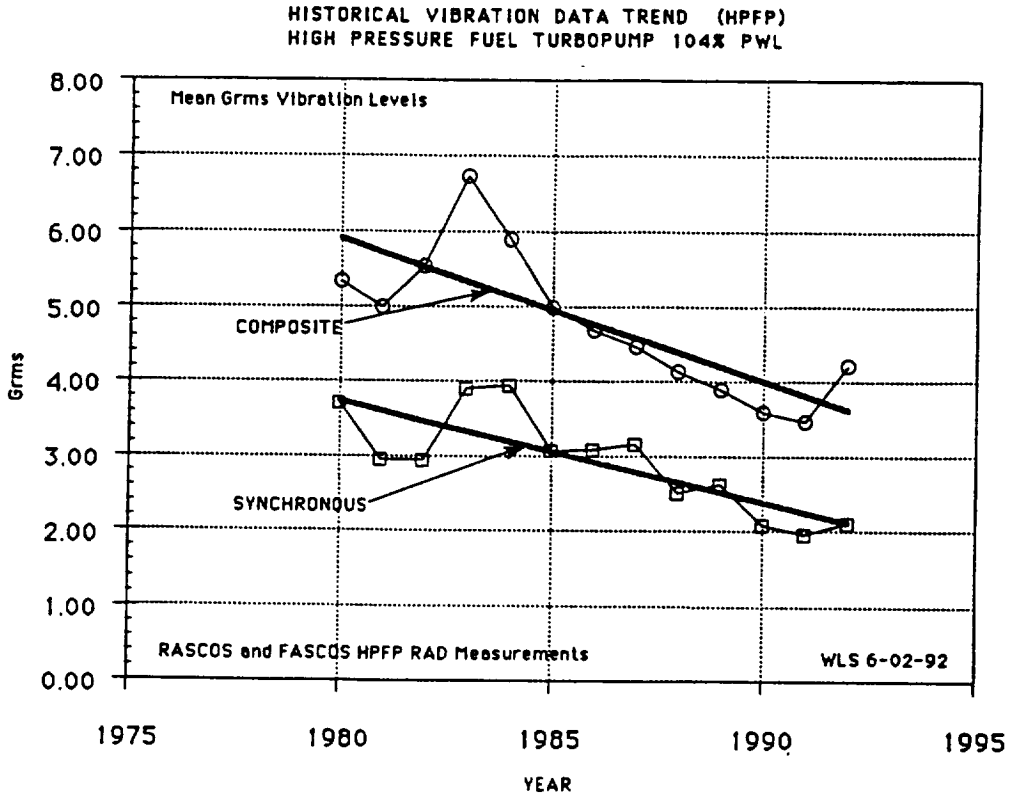

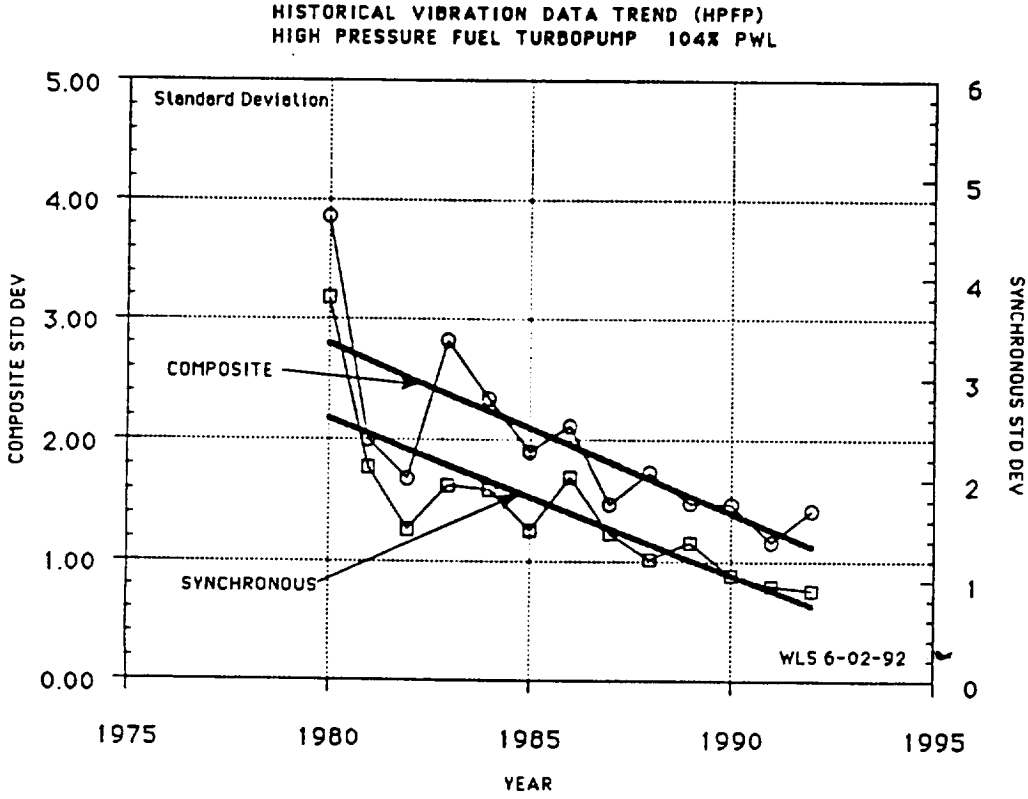

Figure 4. HPFP Historical Vibration Data Trend, 104% PWL

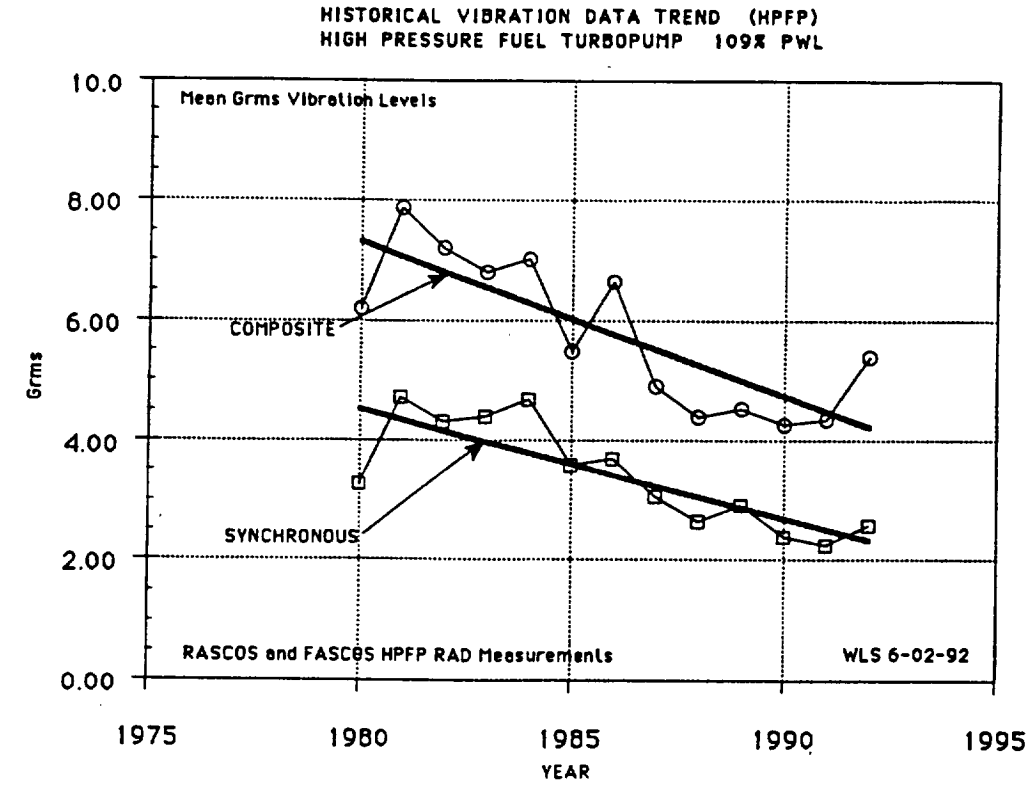

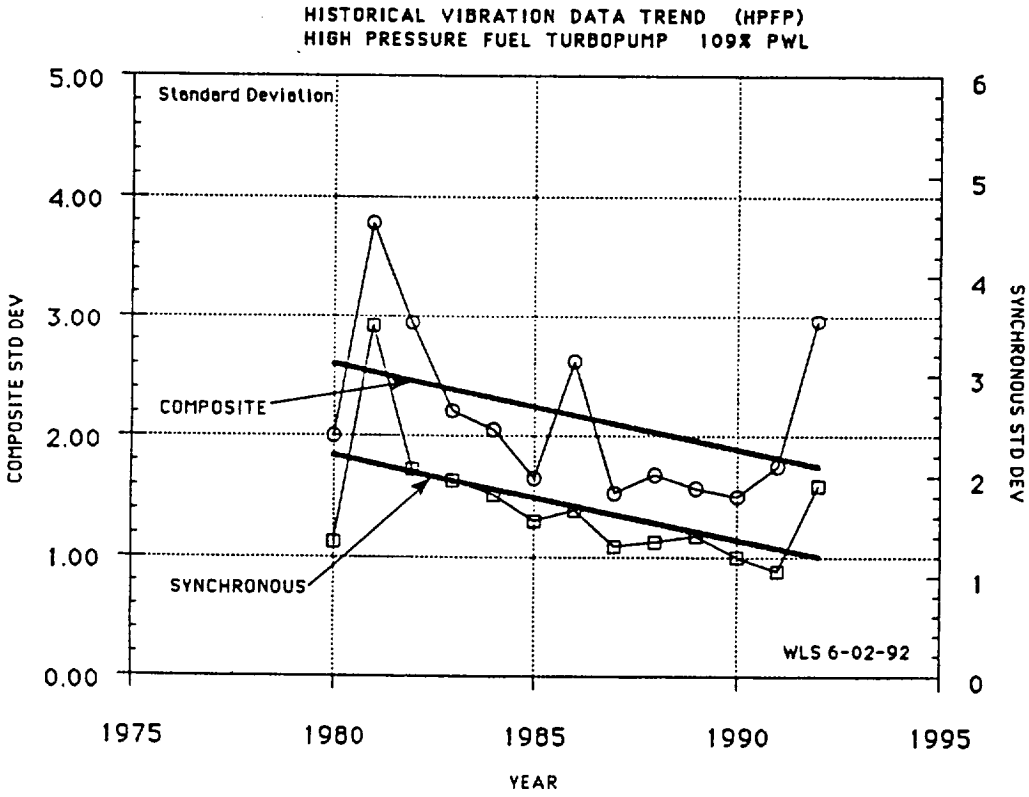

Figure 5. HPFP Historical Vibration Data Trend, 109% PWL

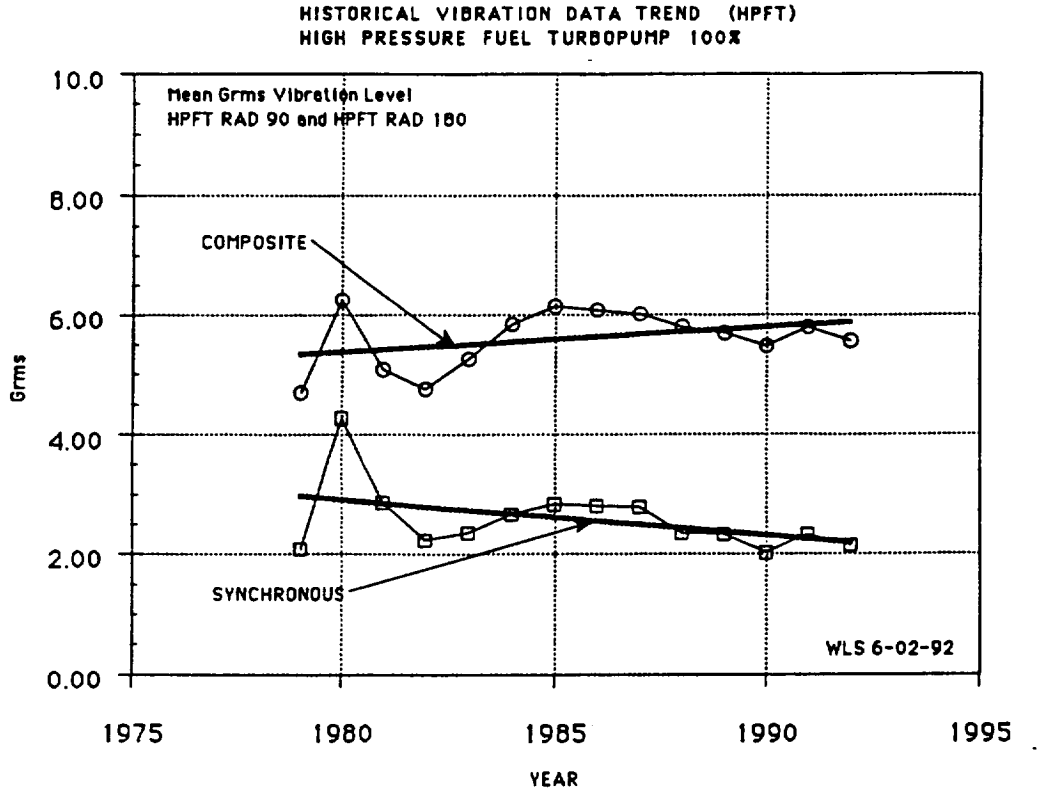

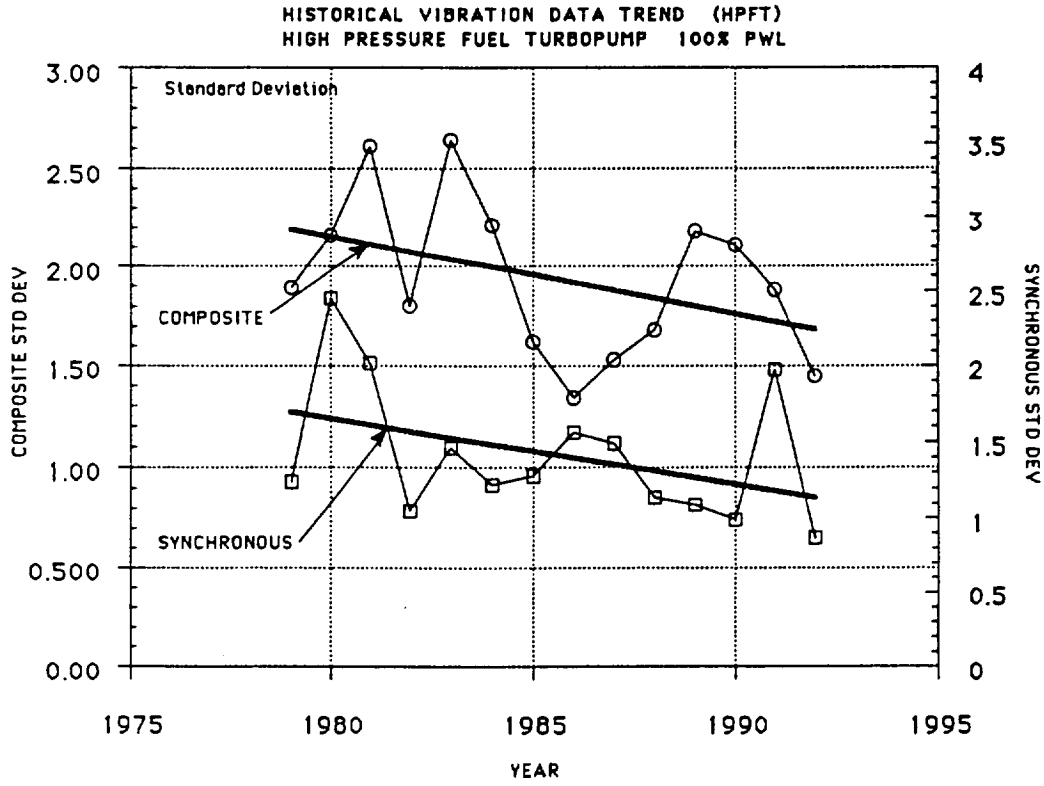

Figure 6. HPFT Historical Vibration Data Trend, 100% PWL

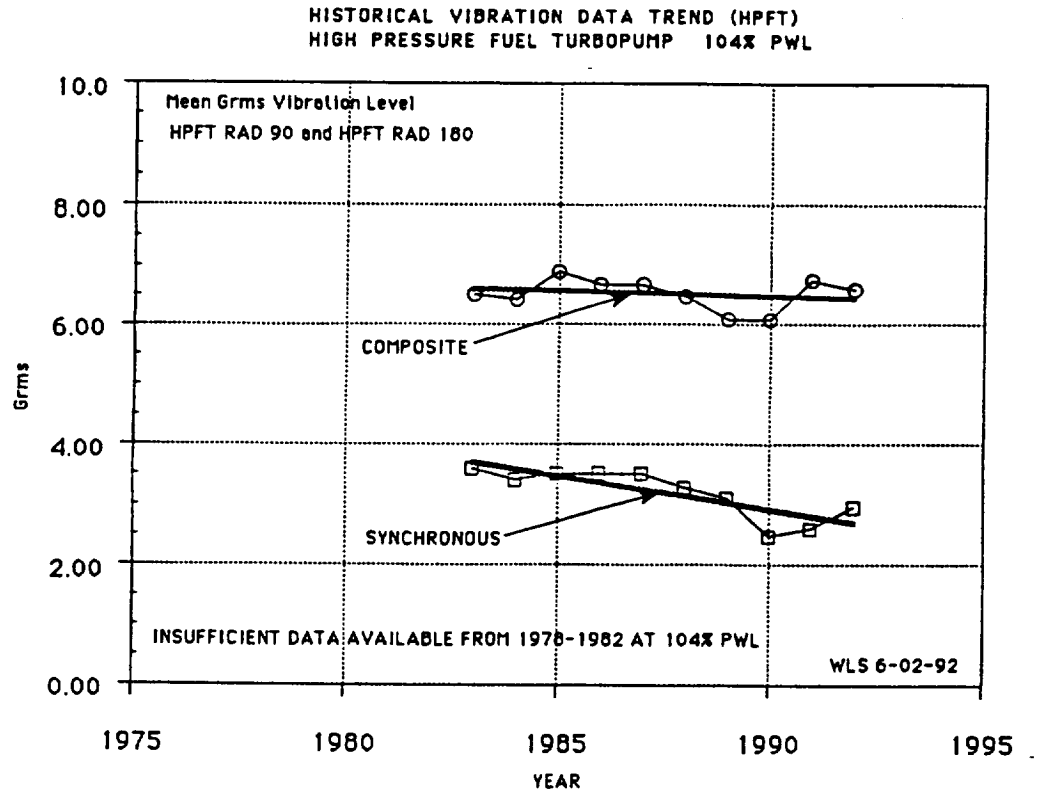

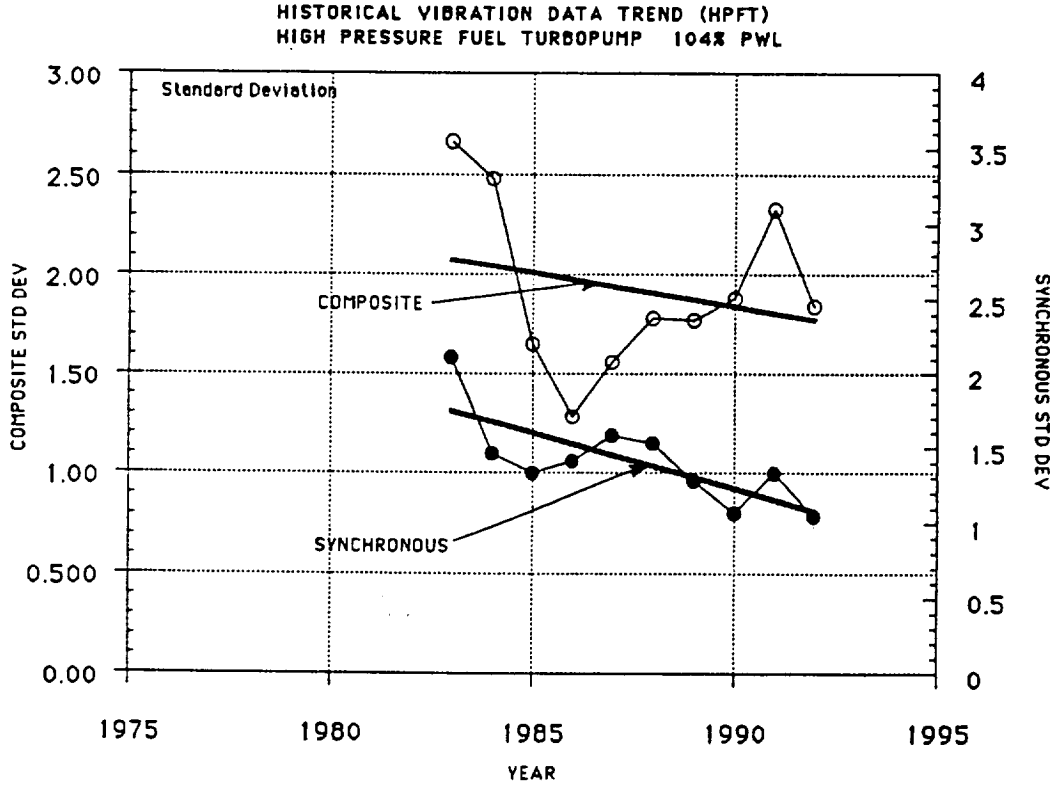

Figure 7. HPFT Historical Vibration Data Trend, 104% PWL

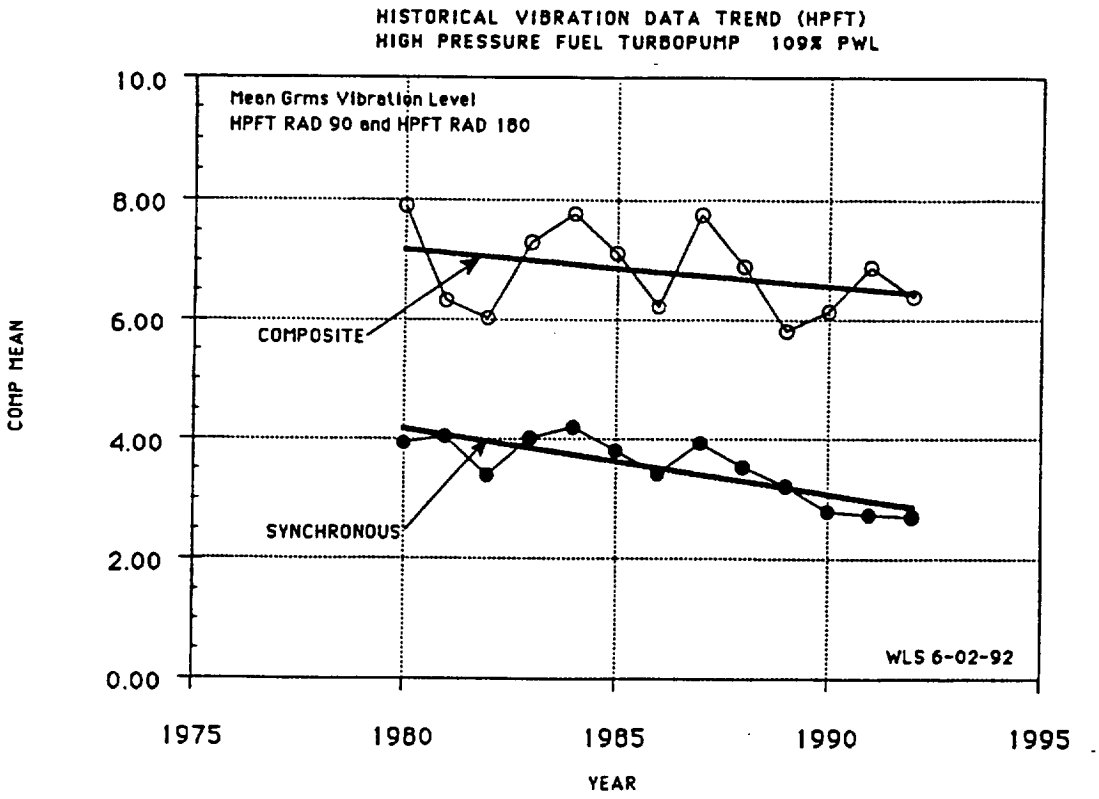

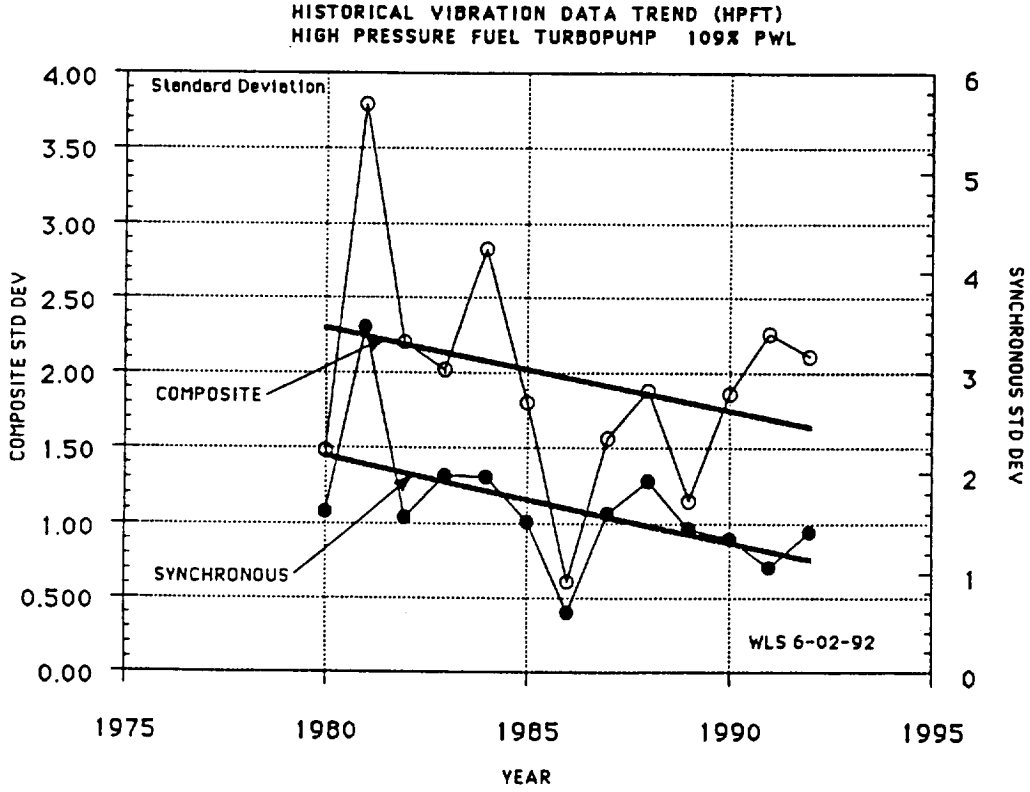

Figure 8. HPFT Historical Vibration Data Trend, 109% PWL

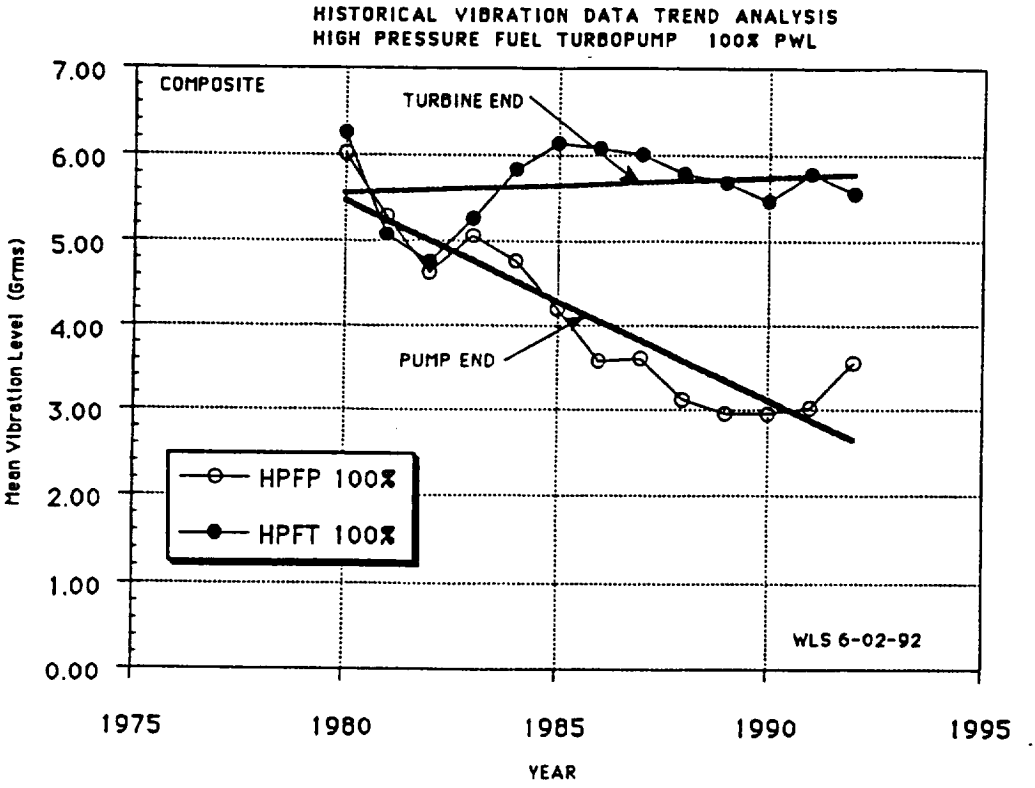

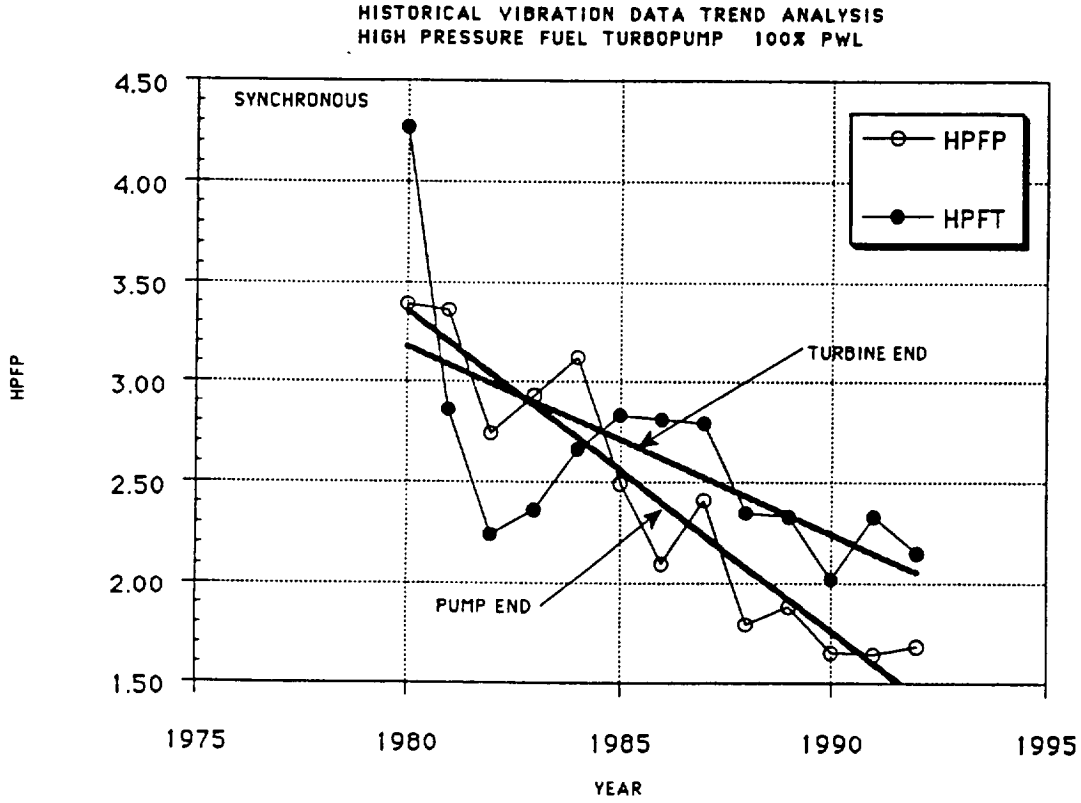

Figure 9. Comparison of HPFP and HPFT Historical Vibration Data Trend, 100% PWL

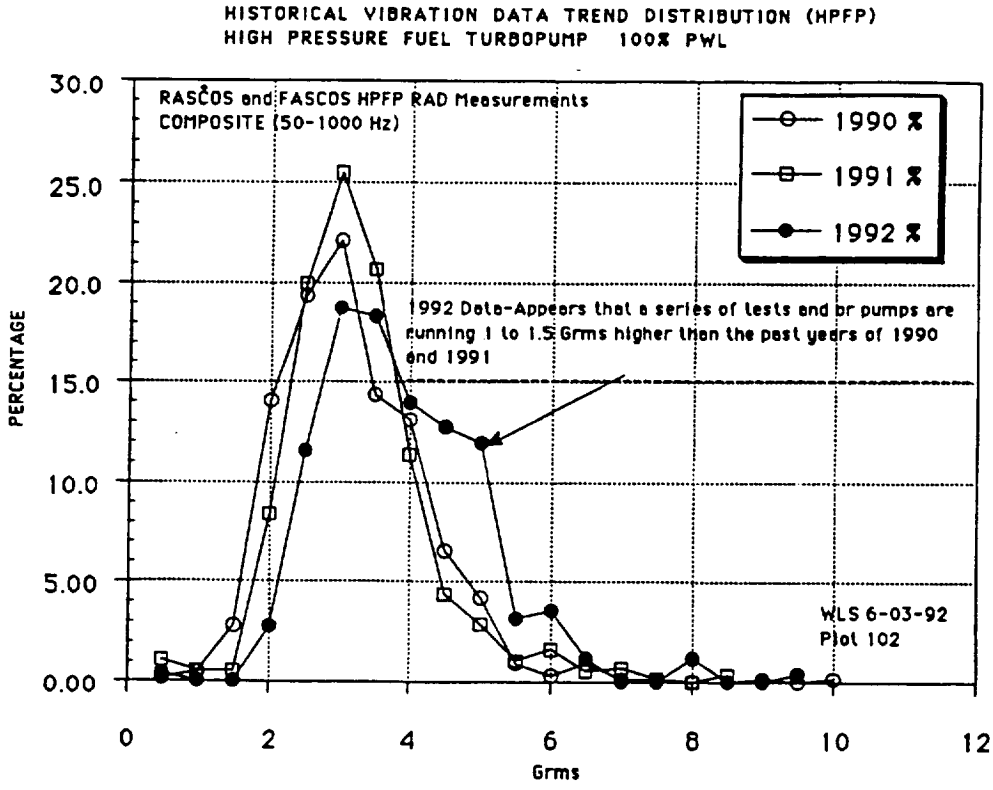

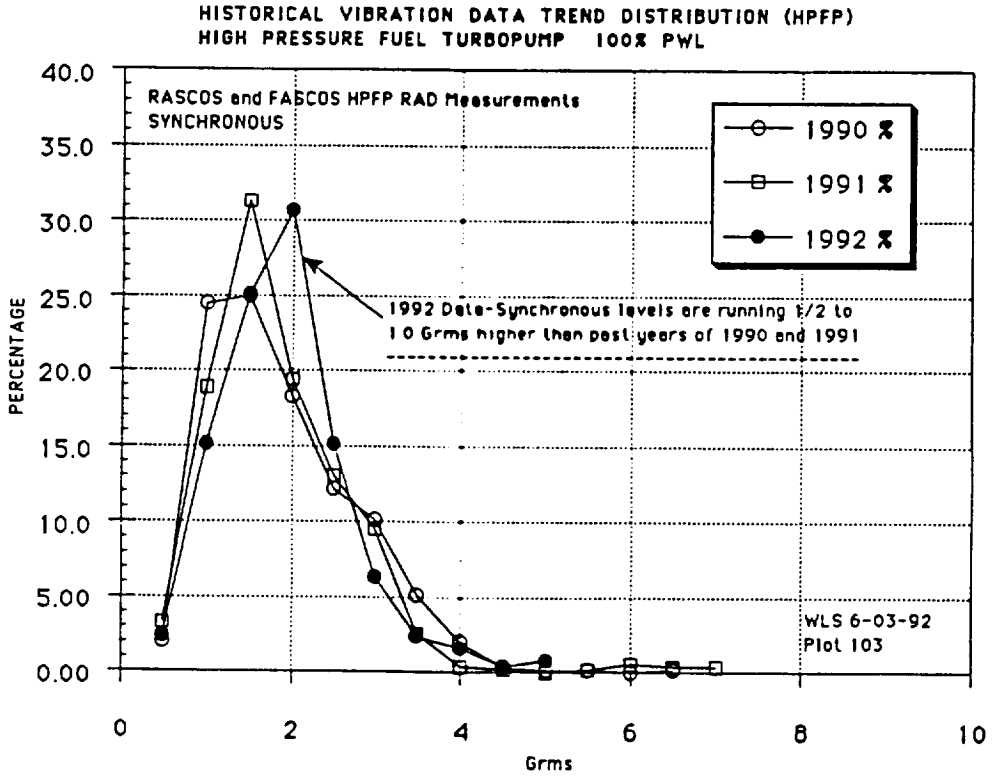

Figure 10. HPFP Historical Vibration Data Distribution, 100% PWL

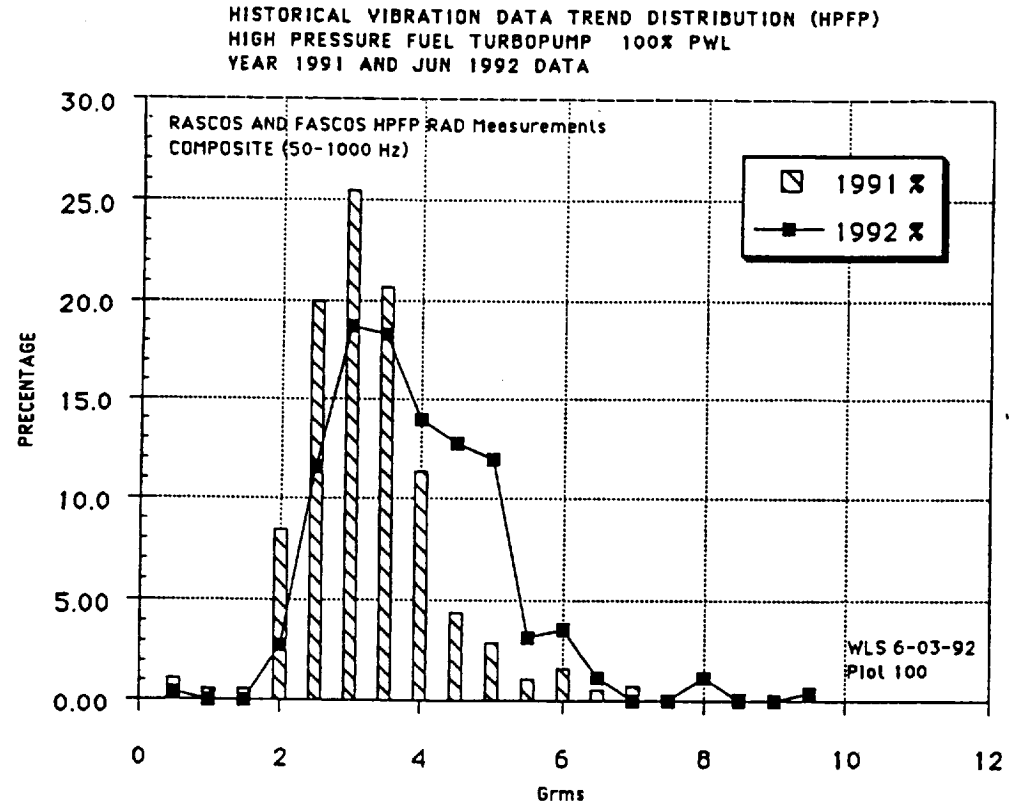

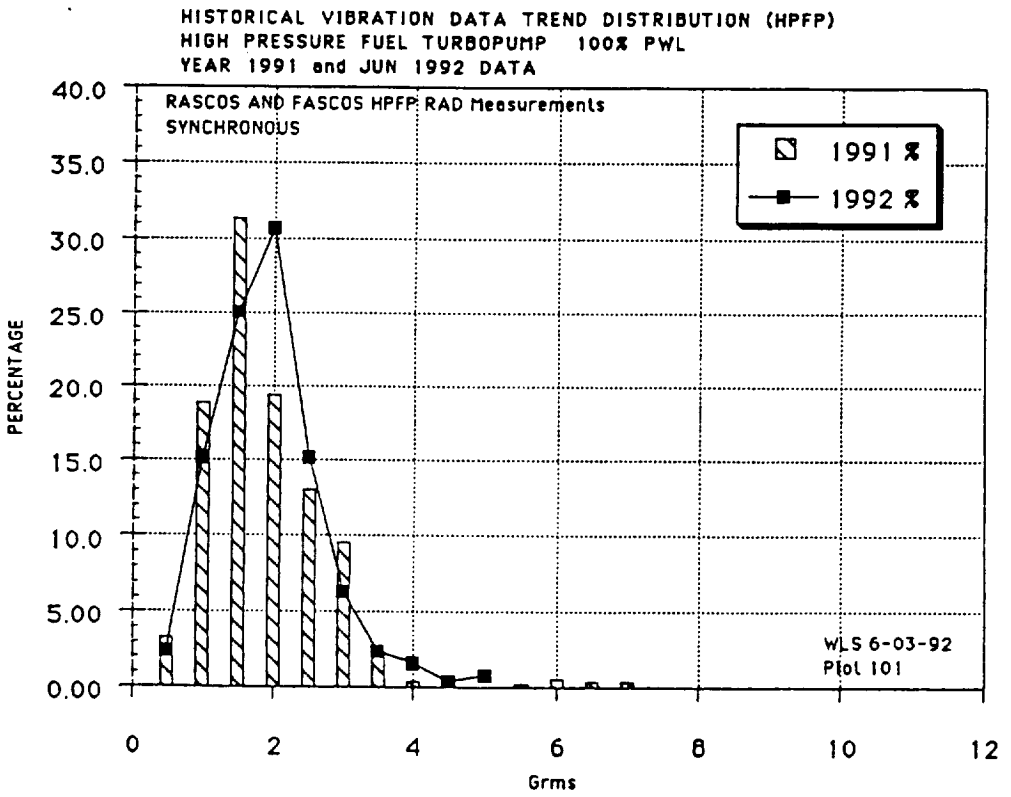

Figure 11. HPFP Historical Vibration Data Barchart, 100% PWL

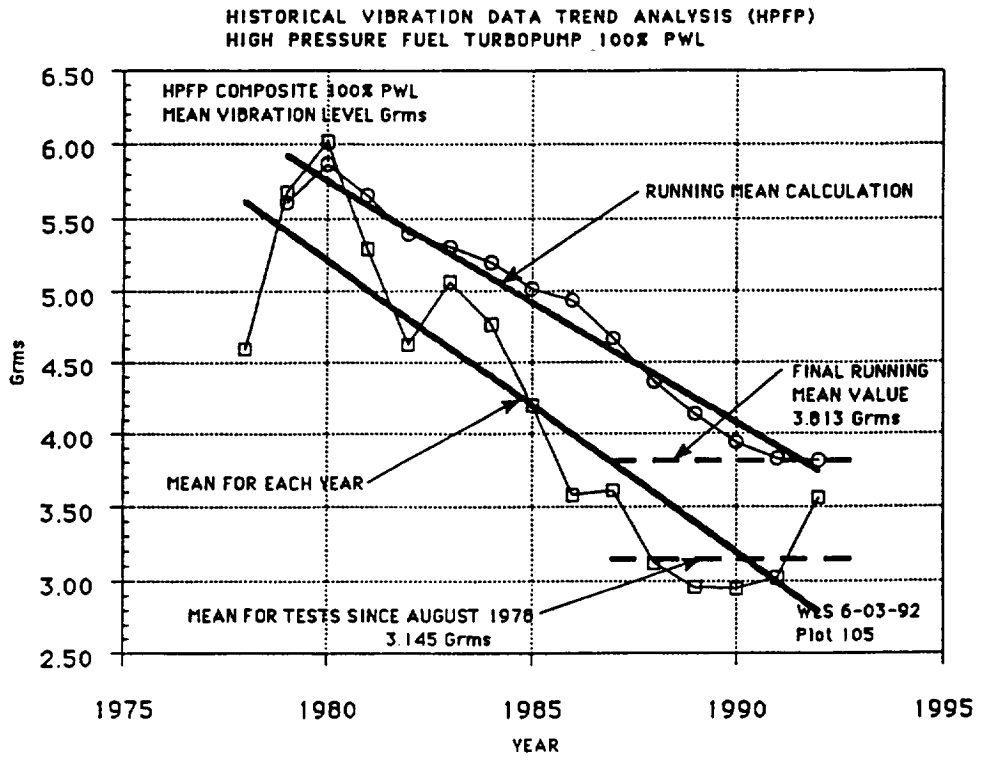

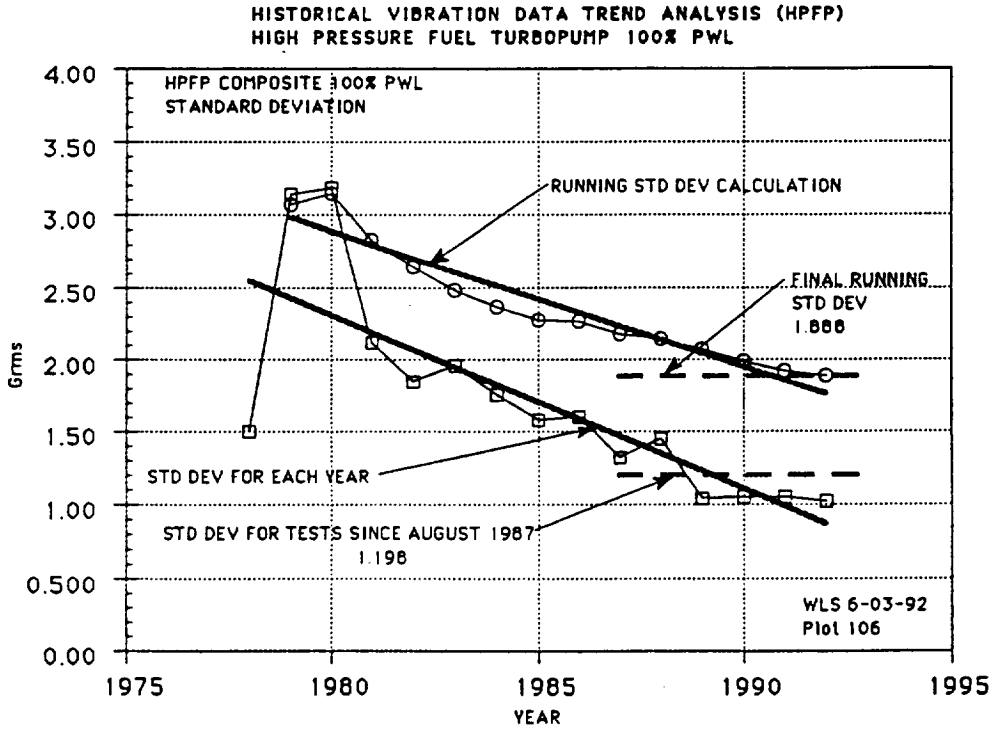

Figure 12. HPFP Comparison Total and 1987 Data Base, 100% PWL

HIGH PRESSURE FUEL TURBOPUMP						
RASCOS HPFP RAD 84, 96, 180, and 90						
COMPOSITE	63%	64%	65%	100%	104%	109%
Mean	1.43	1.45	1.46	3.19	4.03	4.68
Std Dev	0.57	0.56	0.51	1.19	1.56	1.69
Data Sample	308	312	639	1211	970	664
1-Sigma	2.00	2.01	1.97	4.38	5.59	6.37
2-Sigma	2.57	2.57	2.48	5.57	7.15	8.06
3-Sigma	3.14	3.13	2.99	6.76	8.71	9.75
50% Gamma	1.36	1.38	1.40	3.04	3.83	4.48
90% Gamma	2.19	2.20	2.14	4.78	6.11	6.93
99% Gamma	3.08	3.06	2.90	6.59	8.51	9.48
HIGH PRESSURE FUEL TURBOPUMP						
RASCOS HPFP RAD 84, 96, 180, and 90						
SYNCH	63%	64%	65%	100%	104%	109%
Mean	0.54	0.56	0.65	1.61	2.20	2.43
Std Dev	0.32	0.32	0.35	0.88	1.14	1.22
Data Sample	308	312	639	1211	970	664
1-Sigma	0.86	0.88	1.00	2.49	3.34	3.65
2-Sigma	1.18	1.20	1.35	3.37	4.48	4.87
3-Sigma	1.50	1.52	1.70	4.25	5.62	6.09
50% Gamma	0.48	0.50	0.59	1.45	2.01	2.23
90% Gamma	0.97	0.99	1.12	2.79	3.73	4.07
99% Gamma	1.54	1.56	1.73	4.32	5.67	6.12

Figure 13. Statistical Vibration Data RASCOS HPFP RAD 84, 96, 180, and 90 Composite and Synchronous

HIGH PRESSURE FUEL TURBOPUMP						
RASCOS HPFP RAD 84, 96, 180, and 90						
2*SYNCH	63%	64%	65%	100%	104%	109%
Mean	0.22	0.23	0.27	0.75	1.09	1.16
Std Dev	0.08	0.08	0.11	0.42	0.70	0.57
Data Sample	308	312	639	1211	970	664
1-Sigma	0.30	0.31	0.38	1.17	1.79	1.73
2-Sigma	0.38	0.39	0.49	1.59	2.49	2.30
3-Sigma	0.46	0.47	0.60	2.01	3.19	2.87
50% Gamma	0.21	0.22	0.26	0.67	0.94	1.07
90% Gamma	0.33	0.34	0.42	1.31	2.03	1.92
99% Gamma	0.45	0.46	0.59	2.05	3.33	2.88
HIGH PRESSURE FUEL TURBOPUMP						
RASCOS HPFP RAD 84, 96, 180, and 90						
3*SYNCH	63%	64%	65%	100%	104%	109%
Mean	0.22	0.22	0.27	2.69	3.78	3.49
Std Dev	0.08	0.10	0.15	1.76	2.20	2.07
Data Sample	308	312	639	1211	966	660
1-Sigma	0.30	0.32	0.42	4.45	5.98	5.56
2-Sigma	0.38	0.42	0.57	6.21	8.18	7.63
3-Sigma	0.46	0.52	0.72	7.97	10.38	9.70
50% Gamma	0.21	0.21	0.24	2.32	3.36	3.09
90% Gamma	0.33	0.35	0.47	5.05	6.73	6.27
99% Gamma	0.45	0.52	0.73	8.35	10.66	9.99
HIGH PRESSURE FUEL TURBOPUMP						
RASCOS HPFP RAD 84, 96, 180, and 90						
4*SYNCH	63%	64%	65%	100%	104%	109%
Mean	0.99	0.92	0.84	2.07	3.05	3.36
Std Dev	0.28	0.28	0.27	0.92	1.28	1.28
Data Sample	308	312	639	1211	970	664
1-Sigma	1.27	1.20	1.11	2.99	4.33	4.64
2-Sigma	1.55	1.48	1.38	3.91	5.61	5.92
3-Sigma	1.83	1.76	1.65	4.83	6.89	7.20
50% Gamma	0.96	0.89	0.81	1.94	2.87	3.20
90% Gamma	1.36	1.29	1.20	3.30	4.76	5.07
99% Gamma	1.75	1.69	1.59	4.78	6.78	7.03
Figure 14. Statistical Vibration Data RASCOS HPFP RAD 84, 96, 180, and 90						
2*Synch, 3*Synch and 4*Synch						

HIGH PRESSURE FUEL TURBOPUMP						
RASCOS HPFT RAD 90 and 180						
COMPOSITE	63%	64%	65%	100%	104%	109%
Mean	2.07	2.09	2.22	5.65	6.34	6.32
Std Dev	0.70	0.53	0.59	1.79	1.89	1.77
Data Sample	141	143	286	581	473	3.17
1-Sigma	2.77	2.62	2.81	7.44	8.23	8.09
2-Sigma	3.47	3.15	3.40	9.23	10.12	9.86
3-Sigma	4.17	3.68	3.99	11.02	12.01	11.63
50% Gamma	1.99	2.05	2.17	5.46	6.15	6.16
90% Gamma	3.00	2.79	3.00	8.03	8.85	8.67
99% Gamma	4.04	3.52	3.82	10.62	11.54	11.15
HIGH PRESSURE FUEL TURBOPUMP						
RASCOS HPFT RAD 90 and 180						
SYNCH	63%	64%	65%	100%	104%	109%
Mean	0.87	0.87	0.95	2.17	2.90	2.99
Std Dev	0.58	0.43	0.47	1.04	1.32	1.49
Data Sample	141	143	286	581	473	317
1-Sigma	1.45	1.30	1.42	3.21	4.22	4.48
2-Sigma	2.03	1.73	1.89	4.25	5.54	5.97
3-Sigma	2.61	2.16	2.36	5.29	6.86	7.46
50% Gamma	0.75	0.80	0.87	2.01	2.70	2.75
90% Gamma	1.65	1.45	1.58	3.56	4.67	4.99
99% Gamma	2.74	2.17	2.37	5.29	6.81	7.49

Figure 15. Statistical Vibration Data RASCOS HPFT RAD 90 and 180 Composite and Synchronous

HIGH PRESSURE FUEL TURBOPUMP						
RASCOS HPFT RAD 90 and 180						
2*SYNCH	63%	64%	65%	100%	104%	109%
Mean	0.38	0.38	0.44	2.31	3.23	4.04
Std Dev	0.21	0.18	0.19	1.01	1.30	1.40
Data Sample	141	143	286	581	473	317
1-Sigma	0.59	0.56	0.63	3.32	4.53	5.44
2-Sigma	0.80	0.74	0.82	4.33	5.83	6.84
3-Sigma	1.01	0.92	1.01	5.34	7.13	8.24
50% Gamma	0.34	0.35	0.41	2.16	3.06	3.88
90% Gamma	0.66	0.62	0.69	3.66	4.97	5.91
99% Gamma	1.03	0.92	1.00	5.28	6.99	7.99
HIGH PRESSURE FUEL TURBOPUMP						
RASCOS HPFT RAD 90 and 180						
3*SYNCH	63%	64%	65%	100%	104%	109%
Mean	0.82	0.82	0.96	3.57	4.37	3.91
Std Dev	0.42	0.33	0.36	1.85	2.21	1.72
Data Sample	141	143	286	581	471	315
1-Sigma	1.24	1.15	1.32	5.42	6.58	5.63
2-Sigma	1.66	1.48	1.68	7.27	8.79	7.35
3-Sigma	2.08	1.81	2.04	9.12	11.00	9.07
50% Gamma	0.75	0.78	0.92	3.26	4.00	3.66
90% Gamma	1.38	1.26	1.44	6.05	7.33	6.21
99% Gamma	2.10	1.78	1.99	9.21	11.07	8.97
HIGH PRESSURE FUEL TURBOPUMP						
RASCOS HPFT RAD 90 and 180						
4*SYNCH	63%	64%	65%	100%	104%	109%
Mean	1.06	1.07	1.22	2.96	3.84	4.06
Std Dev	0.64	0.36	0 45	1.66	2.10	2.04
Data Sample	141	143	286	581	473	317
1-Sigma	1.70	1 43	1 67	4.62	5.94	6.10
2-Sigma	2.34	1.79	2.12	6.28	8.04	8.14
3-Sigma	2.98	2.15	2.57	7.94	10.14	10.18
50% Gamma	0.93	1.03	1.17	2.66	3.46	3.72
90% Gamma	1.92	1.55	1.82	5.19	6.66	6.79
99% Gamma	3.08	2.08	2.50	8.11	10.31	10.23
Figure 16. Statistical Vibration Data RASCOS HPFT RAD 90 and 180						
2*Synch, 3*Synch and 4*Synch						

HIGH PRESSURE FUEL TURBOPUMP						
FASCOS HPFP RAD 0, 174, and 186						
COMPOSITE	63%	64%	65%	100%	104%	109%
Mean	1.03	1.03	1.22	2.86	3.48	3.99
Std Dev	0.54	0.55	0.70	1.14	1.34	1.49
Data Sample	228	231	458	884	707	480
1-Sigma	1.57	1.58	1.92	4.00	4.82	5.48
2-Sigma	2.11	2.13	2.62	5.14	6.16	6.97
3-Sigma	2.65	2.68	3.32	6.28	7.50	8.46
50% Gamma	0.94	0.93	1.09	2.71	3.31	3.81
90% Gamma	1.75	1.77	2.16	4.38	5.27	5.98
99% Gamma	2.68	2.72	3.40	6.15	7.33	8.25

HIGH PRESSURE FUEL TURBOPUMP						
FASCOS HPFT RAD 0, 174 and 186						
SYNCH	63%	64%	65%	100%	104%	109%
Mean	0.66	0.66	0.79	1.93	2.44	2.65
Std Dev	0.35	0.35	0.45	1.04	1.29	1.42
Data Sample	228	231	458	884	707	480
1-Sigma	1.01	1.01	1.24	2.97	3.73	4.07
2-Sigma	1.36	1.36	1.69	4.01	5.02	5.49
3-Sigma	1.71	1.71	2.14	5.05	6.31	6.91
50% Gamma	0.60	0.60	0.71	1.75	2.22	2.40
90% Gamma	1.13	1.13	1.39	3.32	4.17	4.55
99% Gamma	1.73	1.73	2.19	5.13	6.39	7.01

Figure 17. Statistical Vibration Data FASCOS HPFP RAD 0, 174, and 186
Composite and Synchronous

WYLE LABORATORIES
Engineering Division

Technical Note TN 60900-92-01

STATISTICAL SUMMARY OF SSME TURBOPUMP VIBRATION LEVELS

Part III
Low Pressure Oxidizer Turbopump

by

Wayne L. Swanson

June 1992

FOREWORD

Wyle Laboratories' Engineering Division prepared this report for the National Aeronautics and Space Administration, George C. Marshall Space Flight Center. The work was performed under contract NAS8-38156, entitled "Data Analysis and Diagnostic Evaluation of Space Shuttle Main Engine Dynamic Measurements."

Technical direction, assistance, and maintenance of the Diagnostic Data Base computer program was provided by J. McBride and S. Gallik of MSFC/ED 23, with members of BCSS providing the computer output support. This is part III in a series of reports published and/or in preparation.

Statistical Summary of SSME Turbopump Vibration Levels

- Part I, High Pressure Oxidizer Turbopump
- Part II, High Pressure Fuel Turbopump
- **Part III, Low Pressure Oxidizer Turbopump**
- Part IV, Low Pressure Fuel Turbopump

TABLE OF CONTENTS

		Page
FOREWORD		(iii)
1.0	TECHNICAL DISCUSSION	1
2.0	COMPOSITE STATISTICAL DATA PLOTS	11
3.0	SYNCHRONOUS STATISTICAL DATA PLOTS	21
4.0	2 * SYNCH STATISTICAL DATA PLOTS	31
5.0	3 * SYNCH STATISTICAL DATA PLOTS	41
6.0	4 * SYNCH STATISTICAL DATA PLOTS	51
7.0	SSME DIAGNOSTIC DATA BASE DIRECTORY	61
8.0	COMPUTER PROGRAM	85
9.0	SYNCHRONOUS FREQUENCY (HZ) VS POWER LEVEL	87

1.0 TECHNICAL DISCUSSION

This document is an updated version of a previously published report[1] on the vibration statistics of the Low Pressure Oxidizer TurboPumps (LPOTP) at different power levels. The purpose of this document is to evaluate and document any significant change that has occurred in the vibration statistics since the last report was published in June 1990. This report will also update and provide additional values (2N, 3N, 4N, and PWLs) for overlay plots in the data analysis routines.

Figures 1 through 3 compares the first two moments—the mean (average value) and the standard deviation (variance)—with the previous statistics for the LPOTP. No significant change is indicated other than what would be expected from random chance. Additional investigation will be required to explain the slightly lower mean value at 109-percent power level when compared to the 104-percent power level. The updated statistics are shown in Figures 4 and 5 for power levels at 63 percent, 64 percent, 65 percent, 100 percent, 104 percent, and 109 percent. The mean, standard deviation; one sigma; three sigma; and 50%, 90%, and 99% gamma are included. An interpretation of the gamma function at 50 percent is half the data should fall above and half below the listed value. For 90 percent, 10 percent of the data are expected to be above and 90 percent below the listed value. Other percentage point can be easily calculated using the program listed in section 8. This type of interpretation for the sigma values is much less accurate since the discrete gamma cumulative distribution function provides a much better fit to the measured data than a normal or Gaussian distribution.

For the previous study,[2] only valid data from low pressure oxidizer turbopumps that operated under **normal** conditions was included in the the data base analysis. Therefore, questionable data points (e.g., excessive noise), early cutoff, and extreme outliers were not utilized. Including these pumps or tests with the large data base presently available, however, would not significantly change the calculated statistics (mean and standard deviation). For studies that require information other than normal operational conditions (i.e., extreme values, higher moments, etc), the complete data base should be utilized.

Sections 2 through 6 contain plots of the cumulative distribution, probability density or histogram, and a table of the mean and standard deviation for each test stand. The classical gamma function—shown as an overlay on the plots— provides a convenient smoothing operation and computational method for evaluating the cumulative distribution of the data. For this study, the bin size was changed to 0.20 Grms from the normally used bin size of 0.50 Grms. In most cases, the gamma function provides an excellent fit to the data. Power levels analyzed for this report include 63, 64, 65, 100, 104, and 109 percent. Sufficient data was not available to perform a statistical analysis at 111 percent or the other levels (i.e., 80 percent, 90 percent, etc) although data is available in the diagnostic data base at these power levels.

Sections 7, 8, and 9 are included for reference. Section 7 contains a list of the tests, date of tests, test duration, turbopump serial number, and the power levels, where data is available, from the diagnostic data base program. Section 8 contains a list of the program

---

[1]Swanson, W. L. "Statistical Analysis of SSME Turbopump Vibration Levels: Part III, Low Pressure Oxidizer Turbopump," Wyle Laboratories technical note TN 60900-90-611, June 1990.
[2]Ibid.

written for calculation of the gamma cumulative distribution function. A bin size of 0.01 Grms was used to calculate the 50%, 90%, and 99% gamma values listed in Figures 4 and 5. Section 9 provides the synchronous frequency of the SSME turbopumps versus power levels.

LOW PRESSURE OXYGEN TURBOPUMP

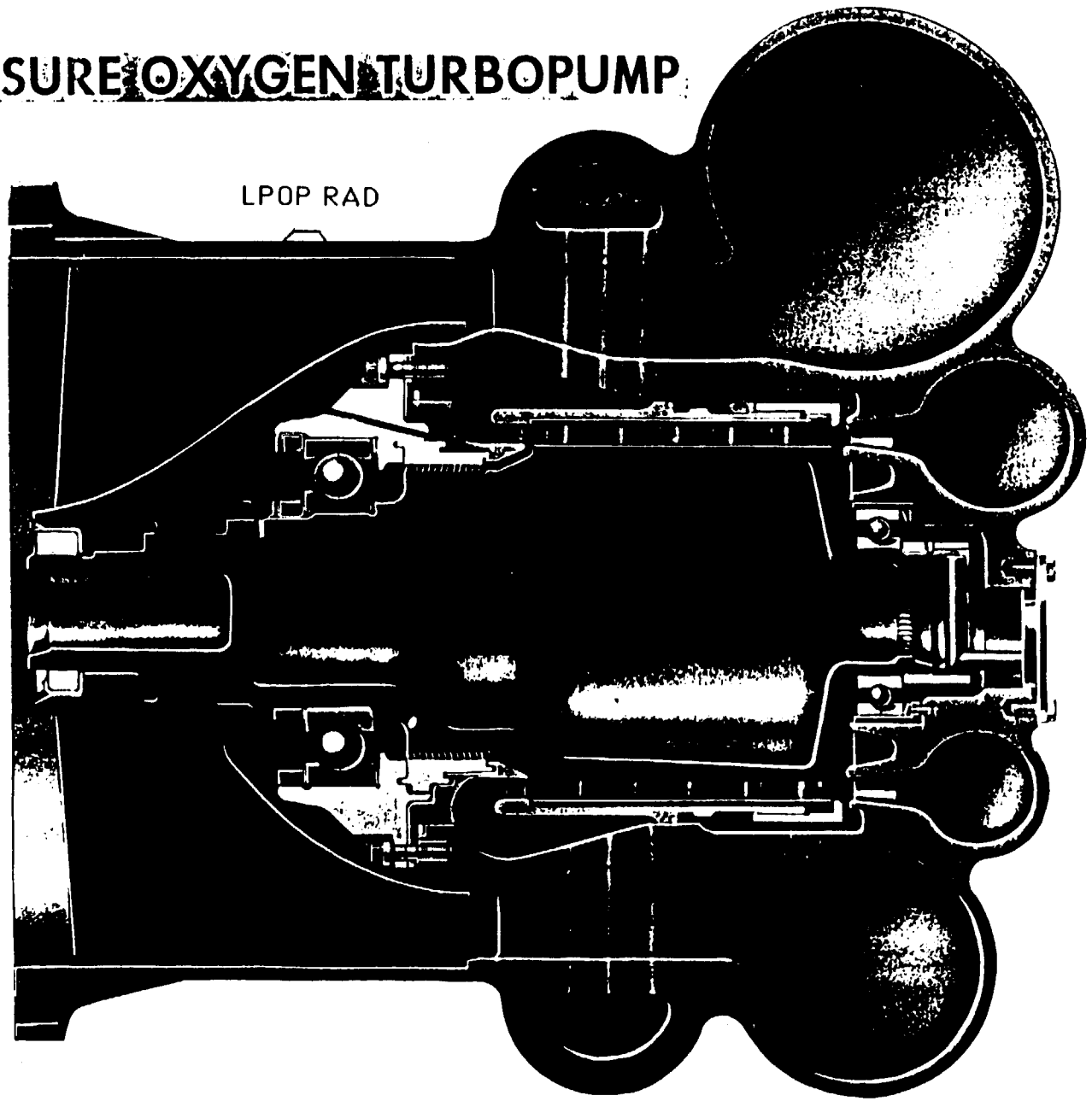

HISTORICAL STATISTICAL DATA COMPARISON
LOW PRESSURE OXIDIZER TURBOPUMP (LPOP)
COMPOSITE Grms LEVELS

100% PWL	AVERAGE	STD DEV	NBR DATA SAMPLE
DEC. 1987	1.57	0.37	630
JUN. 1990	1.48	0.65	313
JUN. 1992	1.51	0.29	464
TOT. DATA BASE	1.51	0.37	1709

104% PWL	AVERAGE	STD DEV	NBR DATA SAMPLE
DEC. 1987	2.15	0.92	276
JUN. 1990	2.09	0.75	516
JUN. 1992	1.94	0.45	359
TOT. DATA BASE	2.04	0.56	1336

109% PWL	AVERAGE	STD DEV	NBR DATA SAMPLE
DEC. 1987	1.88	0.67	112
JUN. 1990	1.75	0.67	339
JUN. 1992	1.65	0.39	252
TOT. DATA BASE	1.73	0.48	825

file HISTORY LPOP COMP #2

Figure 1. Historical Statistical Data Comparison of LPOP RAD Composite Vibration Levels

HISTORICAL STATISTICAL DATA COMPARISON
LOW PRESSURE OXIDIZER TURBOPUMP (LPOP)
SYNCHRONOUS Grms LEVELS

100% PWL	AVERAGE	STD DEV	NBR DATA SAMPLE
DEC. 1987	0.17	0.15	313
JUN. 1990	0.22	0.18	630
JUN. 1992	0.21	0.14	464
TOT. DATA BASE	0.20	0.14	1709

104% PWL	AVERAGE	STD DEV	NBR DATA SAMPLE
DEC. 1987	0.26	0.18	276
JUN. 1990	0.30	0.31	516
JUN. 1992	0.24	0.13	359
TOT. DATA BASE	0.26	0.19	1336

109% PWL	AVERAGE	STD DEV	NBR DATA SAMPLE
DEC. 1987	0.21	0.11	112
JUN. 1990	0.26	0.24	339
JUN. 1992	0.22	0.13	252
TOT. DATA BASE	0.23	0.12	825

file HISTORY LPOP SYNCH #2

Figure 2. Historical Statistical Data Comparison of LPOP RAD Synchronous Vibration Levels

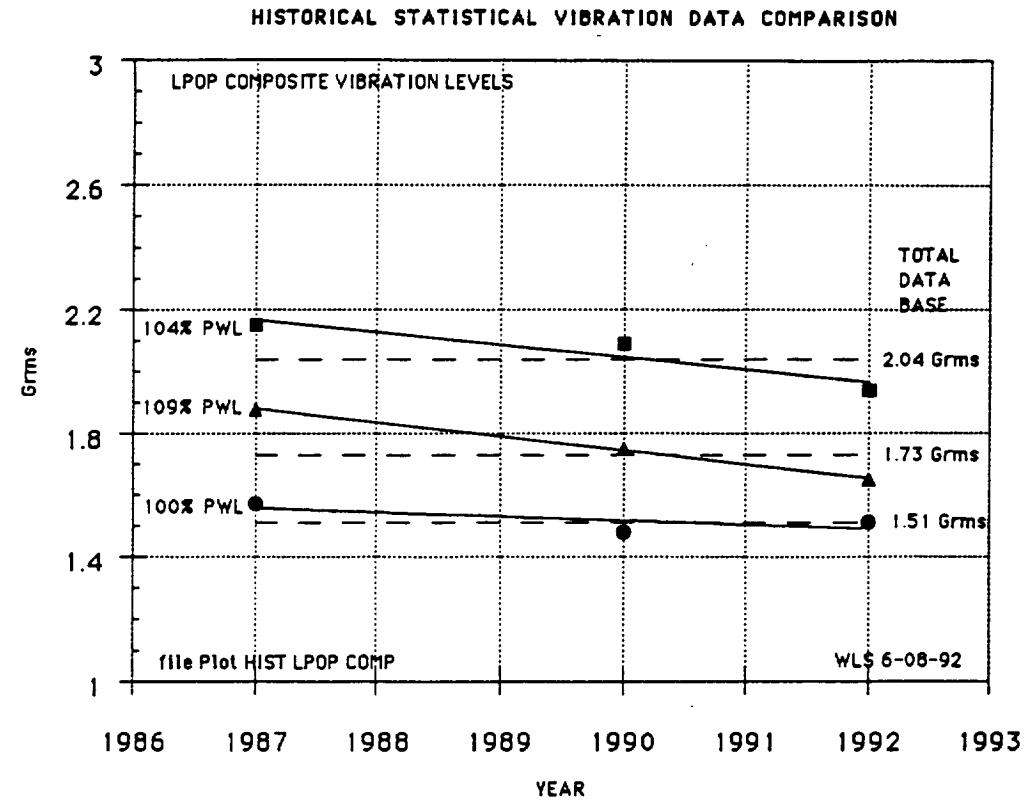

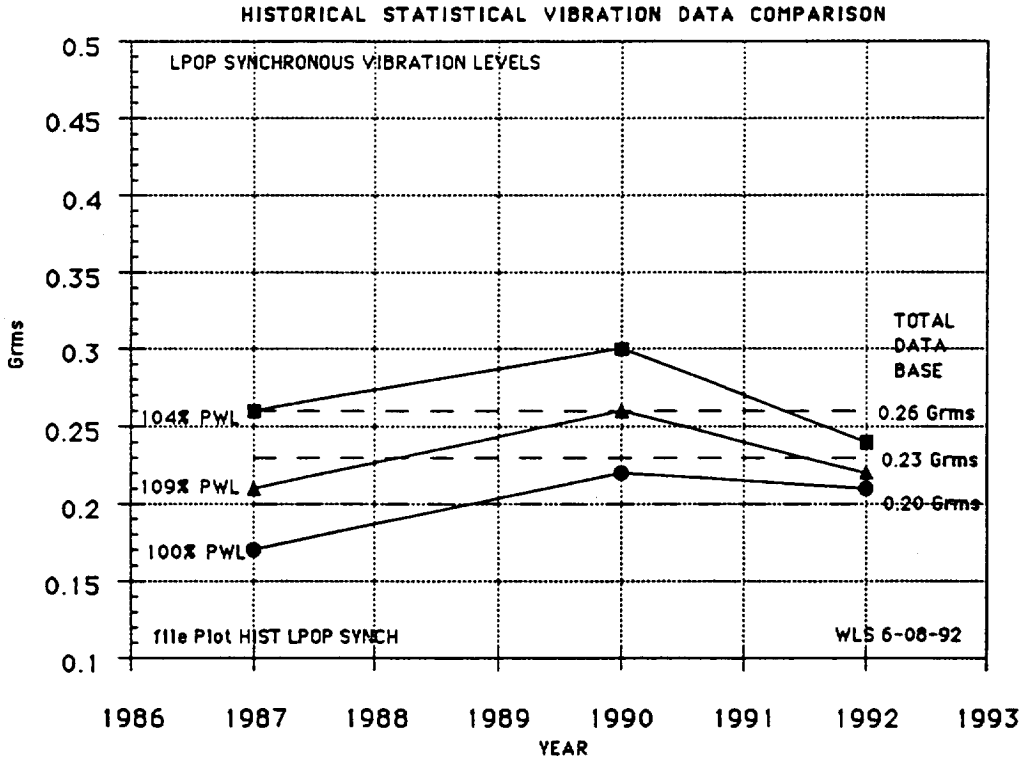

Figure 3. Historical Statistical Vibration Data Comparison, Composite and Synchronous

LOW PRESSURE OXIDIZER TURBOPUMP						
LPOP RAD 90, LPOP RAD 180, and LPOP RAD 270						
COMPOSITE	63%	64%	65%	100%	104%	109%
Mean	0.88	0.88	0.96	1.51	2.04	1.73
Std Dev	0.26	0.31	0.27	0.37	0.56	0.48
Data Sample	352	352	759	1709	1336	825
1-Sigma	1.14	1.19	1.23	1.88	2.60	2.21
2-Sigma	1.40	1.50	1.50	2.25	3.16	2.69
3-Sigma	1.66	1.81	1.77	2.62	3.72	3.17
50% Gamma	0.85	0.84	0.93	1.48	1.99	1.69
90% Gamma	1.23	1.29	1.32	2.00	2.78	2.37
99% Gamma	1.59	1.76	1.70	2.50	3.56	3.04
LOW PRESSURE OXIDIZER TURBOPUMP						
LPOP RAD 90, LPOP RAD 180, and LPOP RAD 270						
SYNCH	63%	64%	65%	100%	104%	109%
Mean	0.23	0.23	0.31	0.20	0.26	0.23
Std Dev	0.17	0.17	0.21	0.14	0.19	0.12
Data Sample	352	352	759	1709	1336	825
1-Sigma	0.40	0.40	0.52	0.34	0.45	0.35
2-Sigma	0.57	0.57	0.73	0.48	0.64	0.47
3-Sigma	0.74	0.74	0.94	0.62	0.83	0.59
50% Gamma	0.19	0.19	0.26	0.17	0.22	0.21
90% Gamma	0.46	0.46	0.59	0.39	0.51	0.39
99% Gamma	0.81	0.81	0.99	0.67	0.90	0.60

Figure 4. Statistical Vibration Data LPOP RAD 90, LPOP RAD 180, and LPOP RAD 270 Composite and Synchronous

LOW PRESSURE OXIDIZER TURBOPUMP						
LPOP RAD 90, LPOP RAD 180, and LPOP RAD 270						
2*SYNCH	63%	64%	65%	100%	104%	109%
Mean	0.15	0.14	0.15	0.16	0.21	0.21
Std Dev	0.05	0.04	0.05	0.11	0.09	0.10
Data Sample	352	352	759	1709	1336	825
1-Sigma	0.20	0.18	0.20	0.27	0.30	0.31
2-Sigma	0.25	0.22	0.25	0.38	0.39	0.41
3-Sigma	0.30	0.26	0.30	0.49	0.48	0.51
50% Gamma	0.14	0.14	0.14	0.14	0.20	0.19
90% Gamma	0.22	0.19	0.22	0.31	0.33	0.34
99% Gamma	0.29	0.25	0.29	0.53	0.47	0.51
LOW PRESSURE OXIDIZER TURBOPUMP						
LPOP RAD 90, LPOP RAD 180, and LPOP RAD 270						
3*SYNCH	63%	64%	65%	100%	104%	109%
Mean	0.26	0.24	0.22	0.13	0.18	0.17
Std Dev	0.12	0.11	0.13	0.08	0.09	0.13
Data Sample	352	352	759	1709	1336	825
1-Sigma	0.38	0.35	0.35	0.21	0.27	0.30
2-Sigma	0.50	0.46	0.48	0.29	0.36	0.43
3-Sigma	0.62	0.57	0.61	0.37	0.45	0.56
50% Gamma	0.24	0.22	0.19	0.11	0.17	0.14
90% Gamma	0.42	0.39	0.39	0.24	0.30	0.35
99% Gamma	0.62	0.57	0.63	0.38	0.45	0.65
LOW PRESSURE OXIDIZER TURBOPUMP						
LPOP RAD 90, LPOP RAD 180, and LPOP RAD 270						
4*SYNCH	63%	64%	65%	100%	104%	109%
Mean	0.10	0.11	0.13	0.17	0.20	0.16
Std Dev	0.04	0.04	0 05	0.11	0.12	0.11
Data Sample	352	352	759	1709	1336	825
1-Sigma	0.14	0.15	0.18	0.28	0.32	0.27
2-Sigma	0.18	0.19	0.23	0.39	0.44	0.38
3-Sigma	0.22	0.23	0.28	0.50	0.56	0.49
50% Gamma	0.09	0.11	0.12	0.15	0.18	0.14
90% Gamma	0.15	0.16	0.20	0.32	0.36	0.31
99% Gamma	0.22	0.22	0.27	0.53	0.58	0.53

Figure 5. Statistical Vibration Data LPOP RAD 90, LPOP RAD 180, and LPOP RAD 270 2*Synch, 3*Synch and 4*Synch

WYLE LABORATORIES
Engineering Division

Technical Note TN 60900-92-01

STATISTICAL SUMMARY OF SSME TURBOPUMP VIBRATION LEVELS

Part IV
Low Pressure Fuel Turbopump

by

Wayne L. Swanson

June 1992

WYLE LABORATORIES

FOREWORD

Wyle Laboratories' Engineering Division prepared this report for the National Aeronautics and Space Administration, George C. Marshall Space Flight Center. The work was performed under contract NAS8-38156, entitled "Data Analysis and Diagnostic Evaluation of Space Shuttle Main Engine Dynamic Measurements."

Technical direction, assistance, and maintenance of the Diagnostic Data Base computer program was provided by J. McBride and S. Gallik of MSFC/ED 23, with members of BCSS providing the computer output support. This is part II in a series of reports published and/or in preparation.

Statistical Summary of SSME Turbopump Vibration Levels

- Part I, High Pressure Oxidizer Turbopump
- Part II, High Pressure Fuel Turbopump
- Part III, Low Pressure Oxidizer Turbopump
- **Part IV, Low Pressure Fuel Turbopump**

TABLE OF CONTENTS

		Page
FOREWORD		(iii)
1.0	TECHNICAL DISCUSSION	1
2.0	COMPOSITE STATISTICAL DATA PLOTS	15
3.0	SYNCHRONOUS STATISTICAL DATA PLOTS	35
4.0	2 * SYNCH STATISTICAL DATA PLOTS	51
5.0	3 * SYNCH STATISTICAL DATA PLOTS	69
6.0	4 * SYNCH STATISTICAL DATA PLOTS	87
7.0	SSME DIAGNOSTIC DATA BASE DIRECTORY	105
8.0	COMPUTER PROGRAM	129
9.0	SYNCHRONOUS FREQUENCY (HZ) VS POWER LEVEL	131

1.0 TECHNICAL DISCUSSION

This document is an updated version of a previously published report[1] on the vibration statistics of the Low Pressure Fuel TurboPumps (LPFTP) at different power levels. The purpose of this document is to evaluate and document any significant change that has occurred in the vibration statistics since the last report was published in June 1990. This report will also update and provide additional values (2N, 3N, 4N, and PWLs) for overlay plots in the data analysis routines.

Figures 1 through 4 compare the first two moments—the mean (average value) and the standard deviation (variance)—with the previous statistics for the LPFTP. No significant change is indicated as shown in Figure 5, other than what would be expected from random chance. The updated statistics are shown in Figures 6 through 9 for power levels at 63, 64, 65, 100, 104, and 109 percent. The mean, standard deviation; one sigma; three sigma; and 50%, 90%, and 99% gamma are included. An interpretation of the gamma function at 50 percent is half the data would be expected to fall above and half below the listed value. For 90 percent, 10 percent of the data should be above and 90 percent below the listed value. Other percentage point can be easily calculated using the program listed in section 8. This type of interpretation for the sigma values is difficult since the distributions are skewed. The discrete gamma cumulative distribution function provides a much better fit to the measured data than a normal or Gaussian distribution.

For the previous study,[2] only valid data from low pressure fuel turbopumps that operated under **normal** conditions was included in the the data base analysis.The same criteria were applied for this analysis. Therefore, questionable data points (e.g.,excessive noise), early cutoff, and extreme outliers were not utilized. Included were the 2218, 4001, 9105 and 82106 series of turbopumps, which have a history of above normal vibration levels at some measurement locations. Including or not including these pumps or tests with the large data base presently available does not significantly change the calculated statistics (mean and standard deviation).

Sections 2 through 6 contain plots of the cumulative distribution, probability density or histogram, and a table of the mean and standard deviation for each test stand. The classical gamma function—shown as an overlay on the plots—provides a convenient smoothing operation and computational method for evaluating the cumulative distribution of the data. In most cases, the gamma function provides an excellent fit to the data. Power levels analyzed for this report include 63 percent, 64 percent, 65 percent, 100 percent, 104 percent, and 109 percent. Sufficient data was not available to perform a statistical analysis at 111 percent or the other levels (i.e., 80 percent, 90 percent, etc) although data is available in the diagnostic data base at these power levels.

Sections 7, 8, and 9 are included for reference. Section 7 contains a list of the tests, date of tests, test duration, turbopump serial number, and the power levels, where data is available, from the diagnostic data base program. Section 8 contains a list of the program written for calculation of the gamma cumulative distribution function. A bin size of 0.01 was used to calculate the 50%, 90%, and 99% gamma values listed in Figures 6 through 9

---

[1]Swanson, W. L. "Statistical Analysis of SSME Turbopump Vibration Levels: Part IV, Low Pressure Fuel Turbopump," Wyle Laboratories technical note TN 60900-90-611, June 1990.
[2]Ibid.

for smooth data plotting and two-place print of the calculated value. Section 9 provides a plot of the synchronous frequency of the SSME Low Pressure Fuel Turbopump vs power level. A table is included listing the synchronous frequency vs power level for the other three turbopumps.

ORIGINAL PAGE IS
OF POOR QUALITY

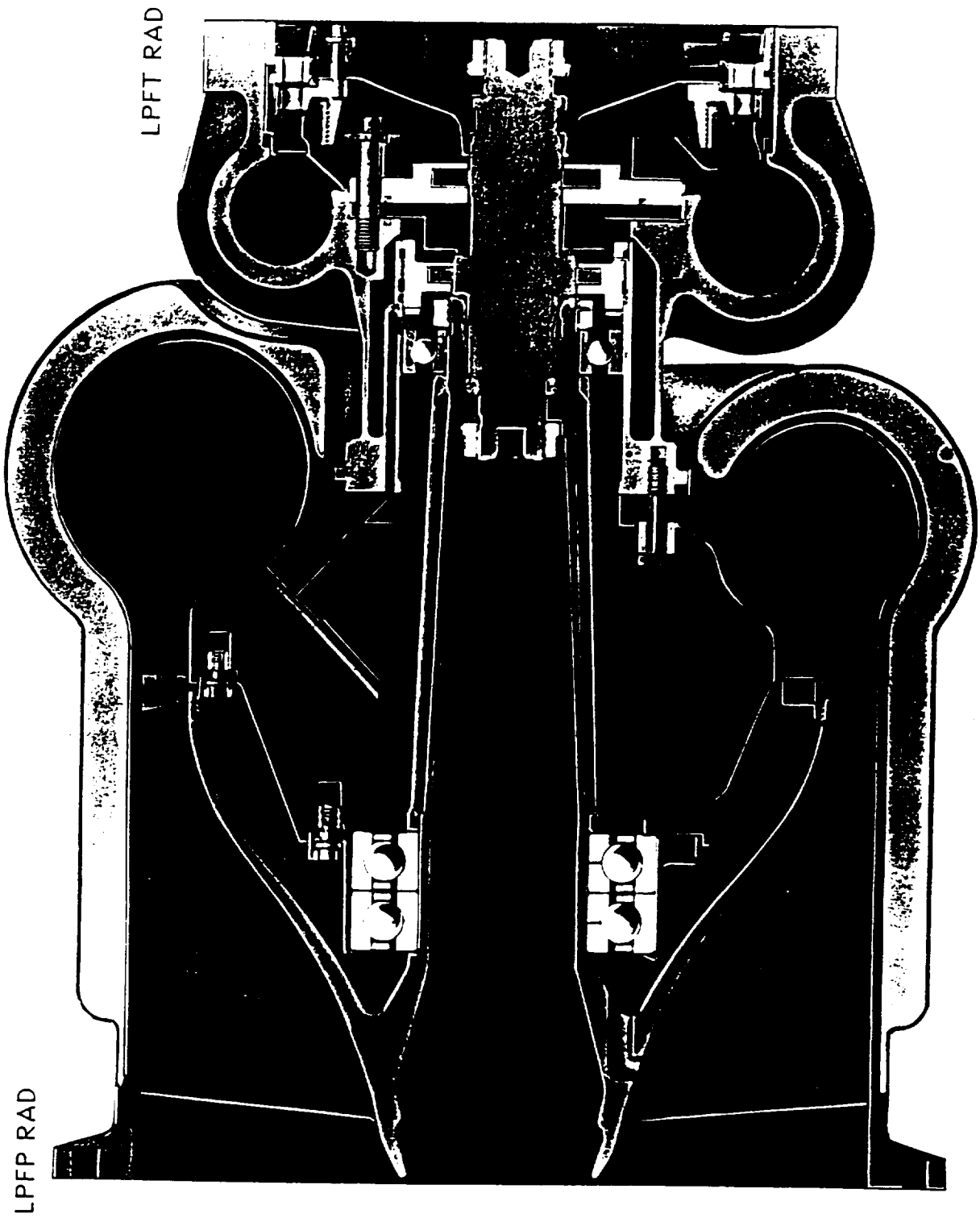

ORIGINAL PAGE IS
OF POOR QUALITY

HISTORICAL STATISTICAL DATA COMPARISON
LOW PRESSURE FUEL TURBOPUMP (LPFTP)
LPFP RAD 150, LPFP RAD 240, and LPFP RAD 330
COMPOSITE Grms LEVELS

100% PWL	AVERAGE	STD DEV	NBR DATA SAMPLE
DEC. 1987	4.55	1.94	303
JUN. 1990	4.25	1.33	631
JUN. 1992	4.31	1.42	1680

104% PWL	AVERAGE	STD DEV	NBR DATA SAMPLE
DEC. 1987	6.09	2.95	254
JUN. 1990	4.85	1.70	516
JUN. 1992	5.22	2.03	1299

109% PWL	AVERAGE	STD DEV	NBR DATA SAMPLE
DEC. 1987	5.59	2.70	98
JUN. 1990	5.25	1.69	341
JUN. 1992	5.17	1.83	773

file HISTORY LPFP COMP

Figure 1.Historical Statistical Data Comparison of LPFP RAD Composite Vibration Levels

HISTORICAL STATISTICAL DATA COMPARISON
LOW PRESSURE FUEL TURBOPUMP (LPFTP)
LPFP RAD 150, LPFP RAD 240, and LPFP RAD 330
SYNCHRONOUS Grms LEVELS

100% PWL	AVERAGE	STD DEV	NBR DATA SAMPLE
DEC. 1987	0.75	0.45	303
JUN. 1990	0.79	0.39	631
JUN. 1992	0.75	0.41	1680

104% PWL	AVERAGE	STD DEV	NBR DATA SAMPLE
DEC. 1987	1.03	0.62	254
JUN. 1990	1.05	0.69	516
JUN. 1992	0.97	0.59	1299

109% PWL	AVERAGE	STD DEV	NBR DATA SAMPLE
DEC. 1987	1.03	0.73	98
JUN. 1990	1.17	0.77	341
JUN. 1992	1.06	0.68	773

file HISTORY LPFP SYNCH

Figure 2.Historical Statistical Data Comparison of LPFP RAD Synchronous Vibration Levels

HISTORICAL STATISTICAL DATA COMPARISON
LOW PRESSURE FUEL TURBOPUMP (LPFTP)
LPFT RAD 180 and LPFT RAD 270
COMPOSITE Grms LEVELS

100% PWL	AVERAGE	STD DEV	NBR DATA SAMPLE
DEC. 1987	3.98	1.37	193
JUN. 1990	3.77	1.04	406
JUN. 1992	3.82	1.14	1107

104% PWL	AVERAGE	STD DEV	NBR DATA SAMPLE
DEC. 1987	N/A	N/A	171
JUN. 1990	4.30	1.40	331
JUN. 1992	4.44	1.55	864

109% PWL	AVERAGE	STD DEV	NBR DATA SAMPLE
DEC. 1987	5.03	1.89	62
JUN. 1990	4.81	1.60	214
JUN. 1992	4.88	1.53	514

file HISTORY LPFT COMP

Figure 3.Historical Statistical Data Comparison of LPFT RAD Composite Vibration Levels

HISTORICAL STATISTICAL DATA COMPARISON
LOW PRESSURE FUEL TURBOPUMP (LPFTP)
LPFT RAD 180 and LPFT RAD 270
SYNCHRONOUS Grms LEVELS

100% PWL	AVERAGE	STD DEV	NBR DATA SAMPLE
DEC. 1987	0.97	0.66	193
JUN. 1990	1.12	0.75	406
JUN. 1992	1.07	0.81	1107

104% PWL	AVERAGE	STD DEV	NBR DATA SAMPLE
DEC. 1987	1.50	1.26	171
JUN. 1990	1.73	1.48	331
JUN. 1992	1.57	1.34	864

109% PWL	AVERAGE	STD DEV	NBR DATA SAMPLE
DEC. 1987	1.61	1.36	62
JUN. 1990	2.22	1.76	214
JUN. 1992	1.97	1.53	514

file HISTORY LPFT SYNCH

Figure 4.Historical Statistical Data Comparison of LPFT RAD Synchronous Vibration Levels

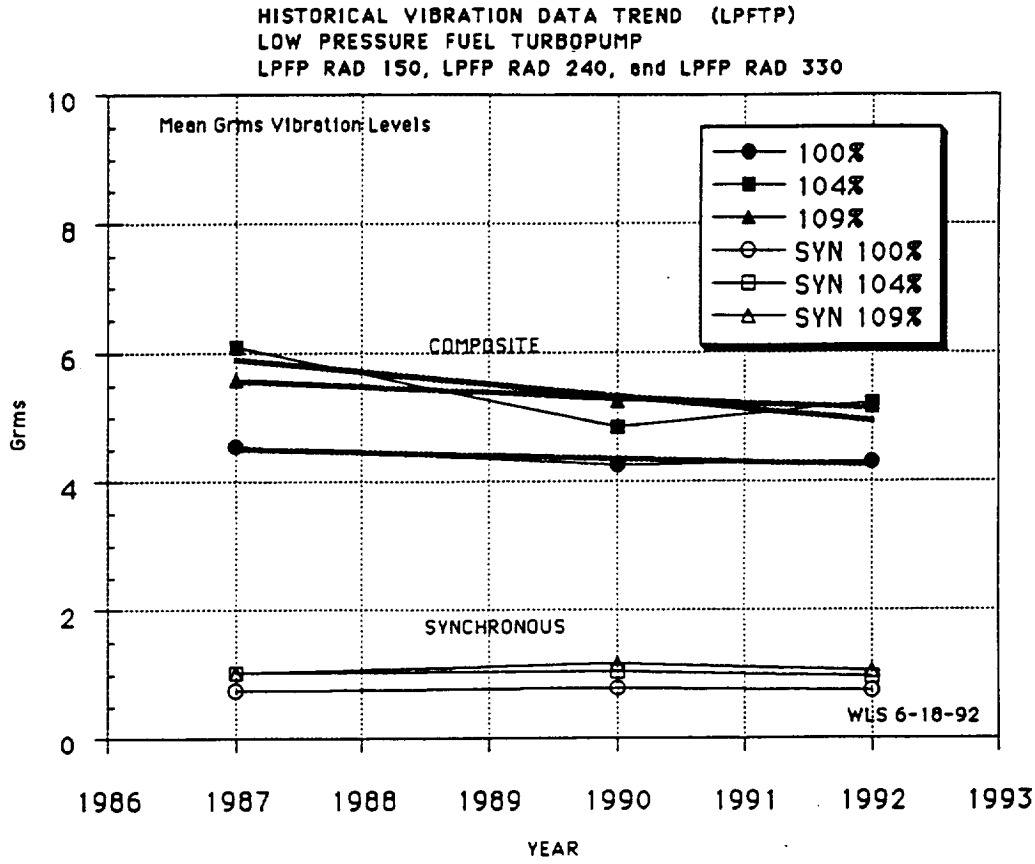

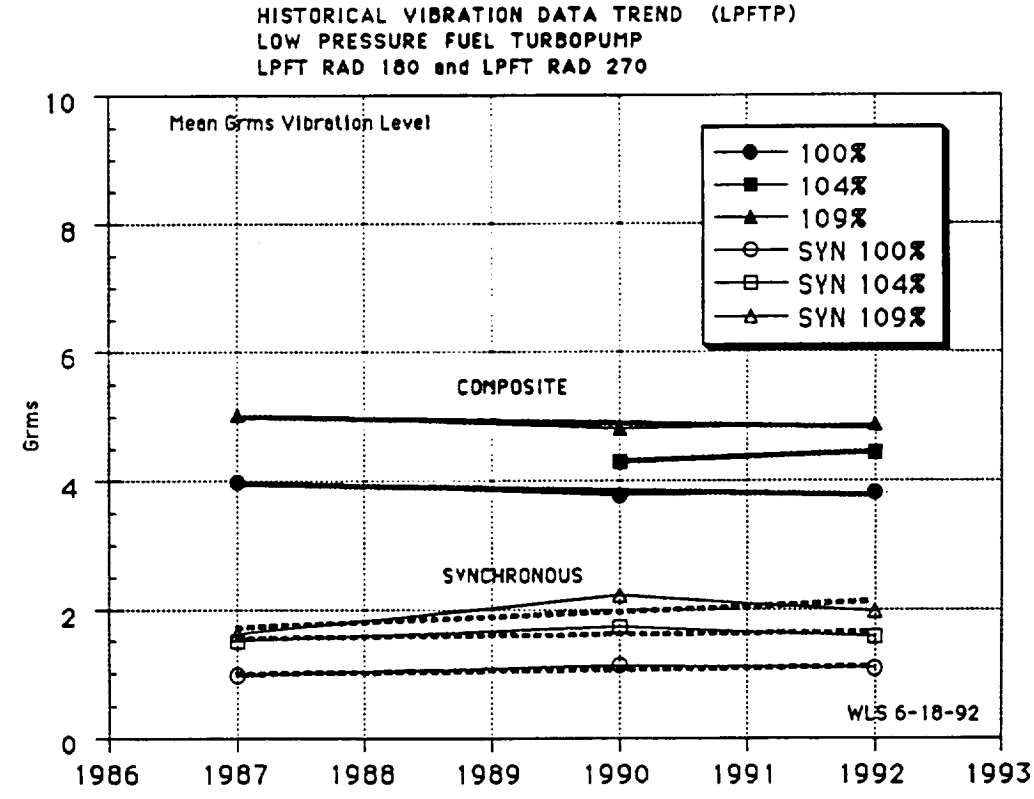

Figure 5. LPFTP Historical Vibration Trend

LOW PRESSURE FUEL TURBOPUMP						
LPFP RAD 150, LPFP RAD 240, and LPFP RAD 330						
COMPOSITE	63%	64%	65%	100%	104%	109%
Mean	2.76	2.63	3.08	4.31	5.22	5.17
Std Dev	0.58	0.52	0.86	1.42	2.03	1.83
Data Sample	351	354	751	1680	1299	773
1-Sigma	3.34	3.15	3.94	5.73	7.25	7.00
2-Sigma	3.92	3.67	4.80	7.15	9.28	8.83
3-Sigma	4.50	4.19	5.66	8.57	11.31	10.66
50% Gamma	2.72	2.60	3.00	4.16	4.96	4.96
90% Gamma	3.52	3.31	4.22	6.20	7.93	7.61
99% Gamma	4.29	3.99	5.42	8.28	11.06	10.35
LOW PRESSURE FUEL TURBOPUMP						
LPFP RAD 150, LPFP RAD 240, and LPFP RAD 330						
SYNCH	63%	64%	65%	100%	104%	109%
Mean	0.34	0.35	0.39	0.75	0.97	1.06
Std Dev	0.18	0.18	0.19	0.41	0.59	0.68
Data Sample	351	354	751	1680	1299	773
1-Sigma	0.52	0.53	0.58	1.16	1.56	1.74
2-Sigma	0.70	0.71	0.77	1.57	2.15	2.42
3-Sigma	0.88	0.89	0.96	1.98	2.74	3.10
50% Gamma	0.31	0.32	0.36	0.68	0.85	0.92
90% Gamma	0.58	0.59	0.64	1.30	1.76	1.97
99% Gamma	0.89	0.90	0.96	2.01	2.83	3.24

Figure 6. Statistical Vibration Data LPFP RAD 150, LPOP RAD 240, and LPFP RAD 330 Composite and Synchronous

LOW PRESSURE FUEL TURBOPUMP						
LPFP RAD 150, LPFP RAD 240, and LPFP RAD 330						
2*SYNCH	63%	64%	65%	100%	104%	109%
Mean	0.29	0.26	0.29	0.42	0.71	0.77
Std Dev	0.12	0.12	0.15	0.35	0.50	0.60
Data Sample	351	354	751	1680	1299	773
1-Sigma	0.41	0.38	0.44	0.77	1.21	1.37
2-Sigma	0.53	0.50	0.59	1.12	1.71	1.97
3-Sigma	0.65	0.62	0.74	1.47	2.21	2.57
50% Gamma	0.27	0.24	0.26	0.33	0.60	0.62
90% Gamma	0.45	0.42	0.49	0.89	1.38	1.57
99% Gamma	0.64	0.62	0.75	1.69	2.35	2.81
LOW PRESSURE FUEL TURBOPUMP						
LPFP RAD 150, LPFP RAD 240, and LPFP RAD 330						
3*SYNCH	63%	64%	65%	100%	104%	109%
Mean	0.40	0.37	0.50	0.69	1.02	0.89
Std Dev	0.14	0.12	0.23	0.42	0.60	0.53
Data Sample	351	354	751	1680	1299	773
1-Sigma	0.54	0.49	0.73	1.11	1.62	1.42
2-Sigma	0.68	0.61	0.96	1.53	2.22	1.95
3-Sigma	0.82	0.73	1.19	1.95	2.82	2.48
50% Gamma	0.38	0.36	0.47	0.61	0.91	0.79
90% Gamma	0.59	0.53	0.81	1.25	1.82	1.60
99% Gamma	0.80	0.70	1.18	2.02	2.90	2.56
LOW PRESSURE FUEL TURBOPUMP						
LPFP RAD 150, LPFP RAD 240, and LPFP RAD 330						
4*SYNCH	63%	64%	65%	100%	104%	109%
Mean	0.71	0.69	0.83	2.17	2.90	3.58
Std Dev	0.23	0.24	0.28	1.01	1.34	1.81
Data Sample	351	354	751	1680	1299	773
1-Sigma	0.94	0.93	1.11	3.18	4.24	5.39
2-Sigma	1.17	1.17	1.39	4.19	5.58	7.20
3-Sigma	1.40	1.41	1.67	5.20	6.92	9.01
50% Gamma	0.69	0.66	0.80	2.02	2.70	3.28
90% Gamma	1.02	1.01	1.20	3.52	4.69	6.01
99% Gamma	1.35	1.37	1.62	5.18	6.88	9.06

Figure 7. Statistical Vibration Data LPFP RAD 150, LPFP RAD 240, and LPFP RAD 330 2*Synch, 3*Synch and 4*Synch

LOW PRESSURE FUEL TURBOPUMP						
LPFT RAD 180 and LPFT RAD 270						
COMPOSITE	63%	64%	65%	100%	104%	109%
Mean	2.87	2.68	3.20	3.82	4.44	4.88
Std Dev	0.60	0.52	0.69	1.14	1.55	1.53
Data Sample	231	233	497	1107	864	514
1-Sigma	3.47	3.20	3.89	4.96	5.99	6.41
2-Sigma	4.07	3.72	4.58	6.10	7.54	7.94
3-Sigma	4.67	4.24	5.27	7.24	9.09	9.47
50% Gamma	2.83	2.65	3.15	3.71	4.26	4.72
90% Gamma	3.66	3.36	4.11	5.33	6.51	6.91
99% Gamma	4.45	4.04	5.02	6.96	8.82	9.12
LOW PRESSURE FUEL TURBOPUMP						
LPFT RAD 180 and LPFT RAD 270						
SYNCH	63%	64%	65%	100%	104%	109%
Mean	0.42	0.42	0.47	1.07	1.57	1.97
Std Dev	0.26	0.26	0.24	0.81	1.34	1.53
Data Sample	231	233	497	1107	864	514
1-Sigma	0.68	0.68	0.71	1.88	2.91	3.50
2-Sigma	0.94	0.94	0.95	2.69	4.25	5.03
3-Sigma	1.20	1.20	1.19	3.50	5.59	6.56
50% Gamma	0.37	0.37	0.43	0.87	1.21	1.59
90% Gamma	0.77	0.77	0.79	2.15	3.35	4.01
99% Gamma	1.25	1.25	1.20	3.78	6.24	7.12

Figure 8. Statistical Vibration Data LPFT RAD 180 and LPFT RAD 270
Composite and Synchronous

LOW PRESSURE FUEL TURBOPUMP						
LPFT RAD 180 and LPFT RAD 270						
2*SYNCH	63%	64%	65%	100%	104%	109%
Mean	0.50	0.48	0.53	0.67	0.87	0.94
Std Dev	0.20	0.20	0.23	0.72	0.69	0.69
Data Sample	231	233	497	1107	864	514
1-Sigma	0.70	0.68	0.76	1.39	1.56	1.63
2-Sigma	0.90	0.88	0.99	2.11	2.25	2.32
3-Sigma	1.10	1.08	1.22	2.83	2.94	3.01
50% Gamma	0.47	0.45	0.50	.45 **	0.70	0.78
90% Gamma	0.77	0.75	0.84	1.49 **	1.79	1.86
99% Gamma	1.08	1.06	1.21	2.71 **	3.22	3.23
**Invalid gamma calculation -standard deviation exceeds the mean-assume std dev= 0.67						
LOW PRESSURE FUEL TURBOPUMP						
LPFT RAD 180 and LPFT RAD 270						
3*SYNCH	63%	64%	65%	100%	104%	109%
Mean	0.45	0.42	0.51	0.75	1.01	0.83
Std Dev	0.15	0.13	0.20	0.46	0.69	0.49
Data Sample	231	233	497	1107	864	514
1-Sigma	0.60	0.55	0.71	1.21	1.70	1.32
2-Sigma	0.75	0.68	0.91	1.67	2.39	1.81
3-Sigma	0.90	0.81	1.11	2.13	3.08	2.30
50% Gamma	0.43	0.41	0.48	0.66	0.86	0.74
90% Gamma	0.65	0.59	0.78	1.37	1.93	1.49
99% Gamma	0.87	0.78	1.09	2.21	3.25	2.37
LOW PRESSURE FUEL TURBOPUMP						
LPFT RAD 180 and LPFT RAD 270						
4*SYNCH	63%	64%	65%	100%	104%	109%
Mean	0.46	0.45	0.51	0.82	1.07	1.46
Std Dev	0.21	0.21	0.24	0.51	0.58	0.94
Data Sample	231	233	497	1107	864	514
1-Sigma	0.67	0.66	0.75	1.33	1.65	2.40
2-Sigma	0.88	0.87	0.99	1.84	2.23	3.34
3-Sigma	1.09	1.08	1.23	2.35	2.81	4.28
50% Gamma	0.43	0.42	0.47	0.72	0.97	1.26
90% Gamma	0.74	0.73	0.83	1.50	1.85	2.72
99% Gamma	1.08	1.08	1.23	2.44	2.85	4.47

Figure 9. Statistical Vibration Data LPFT RAD 180 and LPFT RAD 270
2*Synch, 3*Synch and 4*Synch

WYLE LABORATORIES
Engineering Division

Technical Memorandum TM 62200-93-11

SYNCHRONOUS FREQUENCIES OF THE ATD HIGH PRESSURE OXIDIZER TURBOPUMP

by

Wayne L. Swanson

JUNE 11, 1993

WYLE
LABORATORIES

1.0 INTRODUCTION

The purpose of this study was to determine an equation for the calculation of the synchronous frequency of the ATD High Pressure Oxidizer Turbopump (HPOTP) vs. power level. This equation will be utilized in the Dynamic Analysis Programs which allows the computer to seek the synchronous frequency in a predetermined band of frequencies. The data for this study was obtained from the MSFC Dynamic Data Base Computer program. All calculations and plotting were performed on a Macintosh IIfx using KaleidaGraph software. The static firing test numbers, turbopump serial numbers, power level profile and output data sheets are included as enclosures for future reference.

2.0 DISCUSSION

Sixty-three static firing tests were available in the Diagnostic Data Base for analysis at power levels of 65%, 90%, 100%, 104%, and 109%. A quick review of the plotted data in Enclosure 1 indicates we do not have a consistent data set. The first five plots are the synchronous frequency at the different power levels as listed in the data base. At all power levels except the 65% an increase in the frequency is noted. The next five plots are histograms which clearly show a multiple modal distribution which indicates there is a marked difference in the turbopump builds or operational rotational speed. After discussion with ED-23 personnel, five turbopump builds were chosen which appear to represent the final ATD HPOTP configuration and operational synchronous frequencies. The serial numbers of the turbopumps are:

8003R6, 7, 8
8107R1, 2, 3, 4
8202R1, 2, 3
8106R4
8105R5

This provided a total of 28 static firing tests for the analysis. However, not all power levels were run on each test, therefore less than 28 data samples were available at each of the different power levels.

3.0 RESULTS

Figure 1 shows that a linear curve-fit equation will provide the necessary accuracy for synchronous frequency vs. power level (in percent) for the ATD HPOTP. The equation is:

$$\text{Syn Freq} = 98.691 + 2.788*\text{Pwl} \quad (1)$$

The calculated mean synchronous frequencies with the 3 Sigma values are shown in Table I and plotted in Figures 2 and 3 for each power level.

TABLE I

PWL %	Synch (Mean)	-3 Sigma	+3 Sigma
65	280	277	283
90	350	337	362
100	377	365	390
104	389	380	397
109	403	394	411

Figures 4 to 8 are the histograms and a comparison to the normal or Gaussian distribution at each power level. Considering the small sample size available for analysis, it appears a normal distribution can be assumed as a best fit to the data. The mean, standard deviation, minimum, maximum and number of data samples at each power level are listed on the plots. When more test data becomes available, additional analysis should be performed to verify the adequacy of equation 1 to determine the synchronous frequency vs. power level.

Enclosures:
1 - ATD Synchronous Frequencies vs. Power Level (All turbopump builds)
2 - ATD Lifetime Analysis Data Sheets
3 - ATD Data Summary Sheets
4 - ATD Listing of Synchronous Frequencies for Each Test

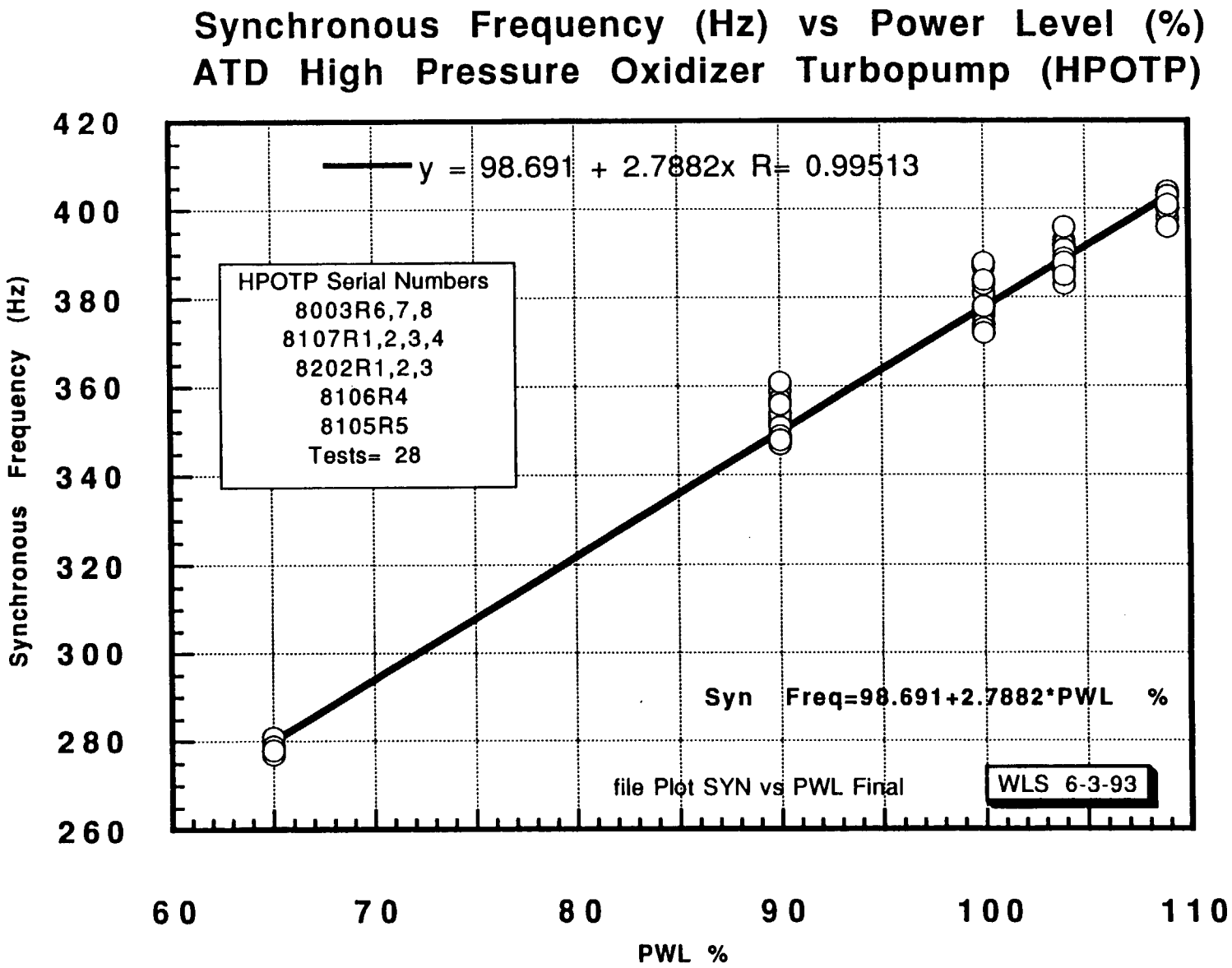

Figure 1. ATD Synchronous Frequency (Hz) vs. Power Level (%)

Figure 2. Synchronous Frequency (Hz) vs Power Level (%) ATD High Pressure Oxidizer Turbopump (HPOTP)

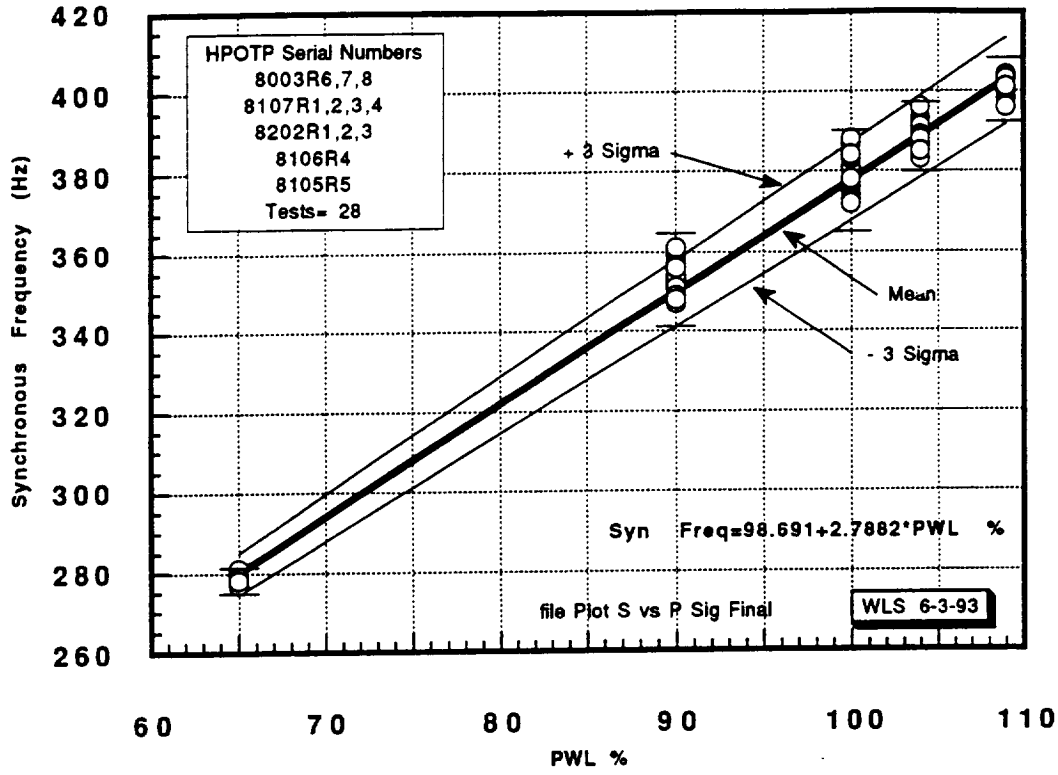

Figure 3. Synchronous Frequency (Hz) vs Power Level (%) ATD High Pressure Oxidizer Turbopump (HPOTP)

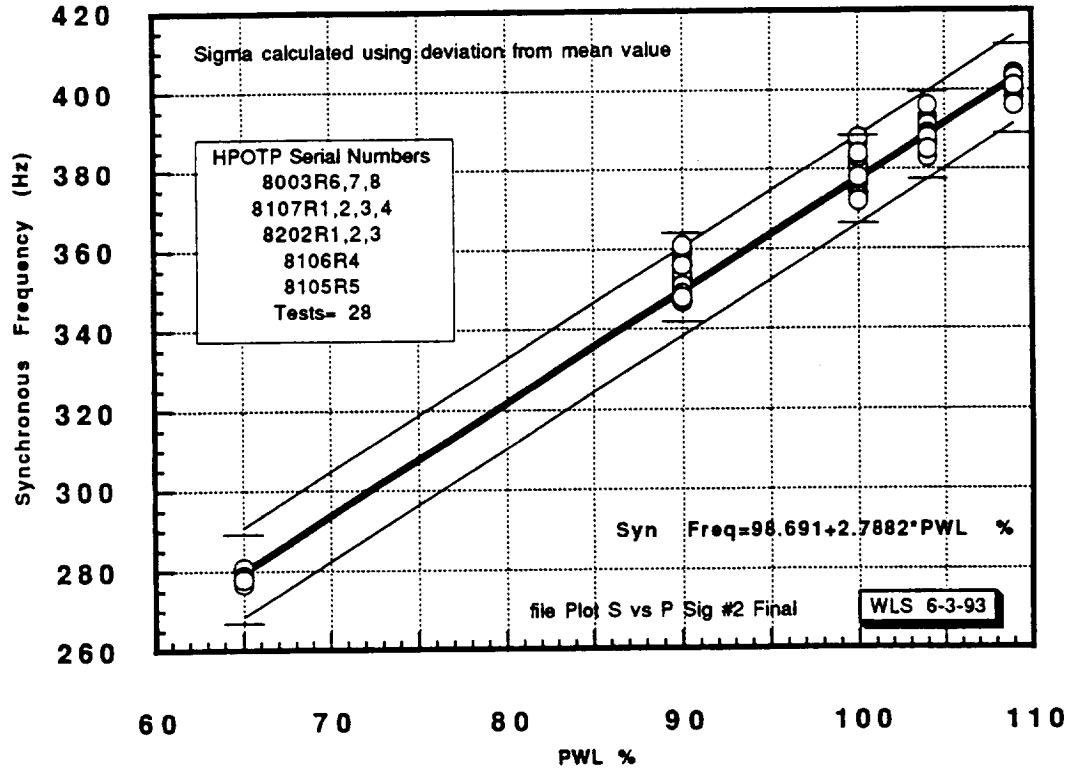

Figure 4. Histogram Synchronous Frequency (Hz) @ 65% PWL ATD High Pressure Oxidizer Turbopump (HPOTP)

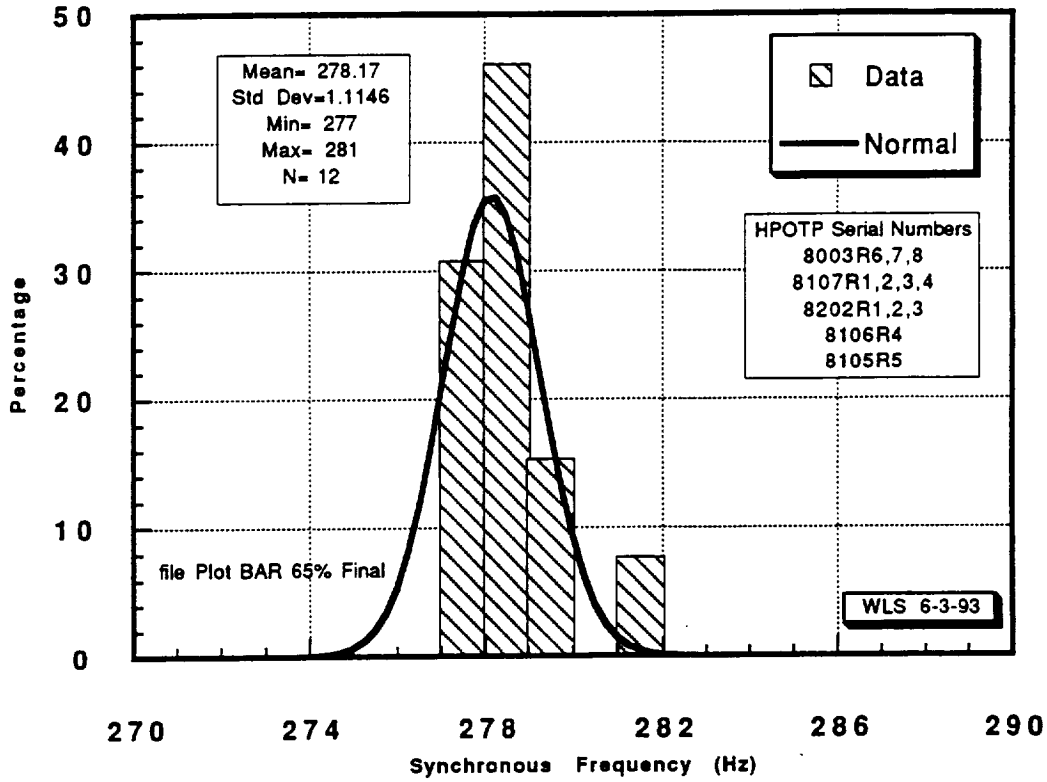

Figure 5. Histogram Synchronous Frequency (Hz) @ 90% PWL ATD High Pressure Oxidizer Turbopump (HPOTP)

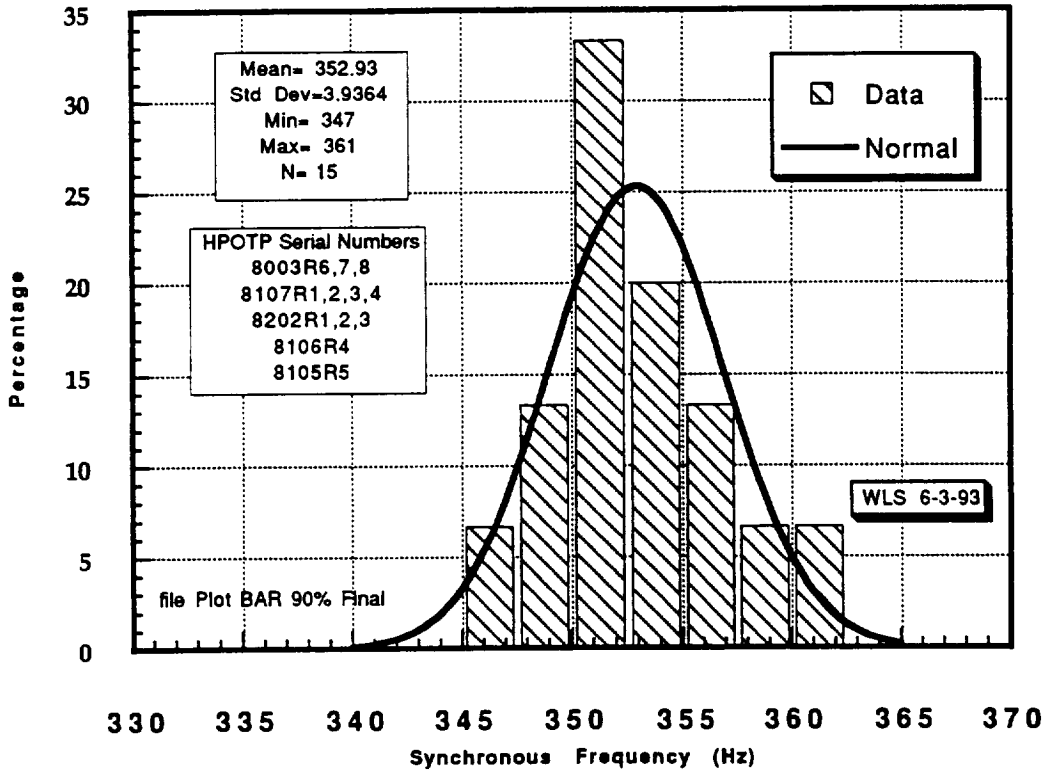

Figure 6. Histogram Synchronous Frequency @ 100% PWL ATD High Pressure Oxidizer Turbopump (HPOTP)

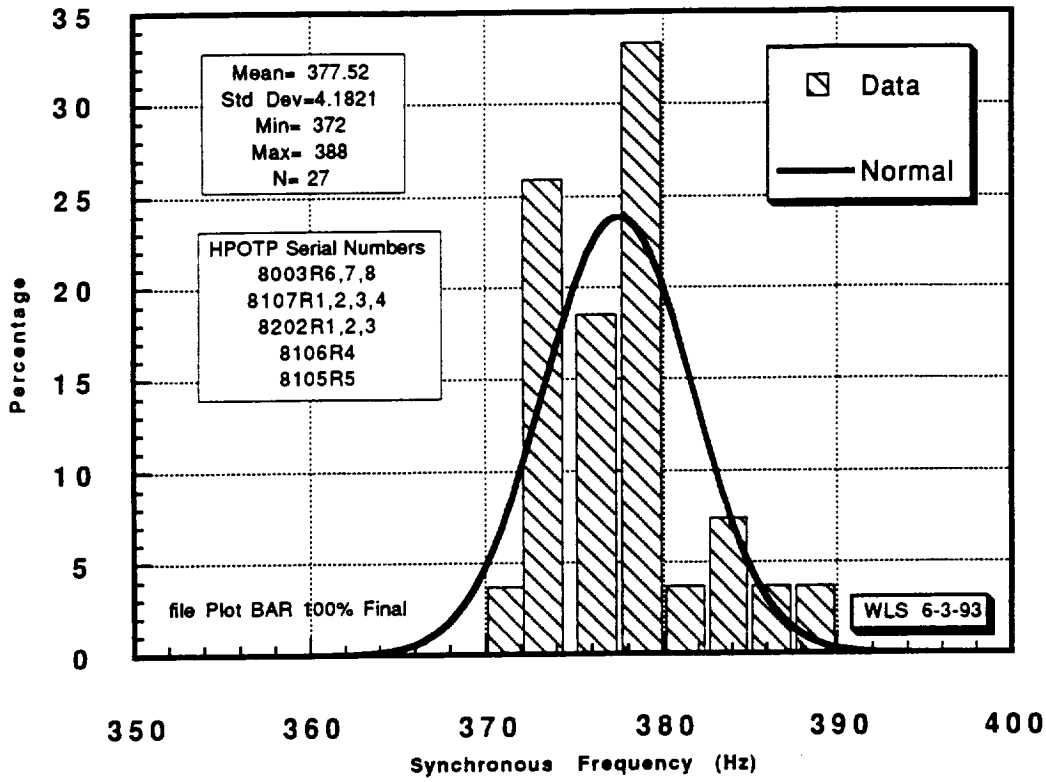

Figure 7. Histogram Synchronous Frequency @ 104% PWL ATD High Pressure Oxidizer Turbopump (HPOTP)

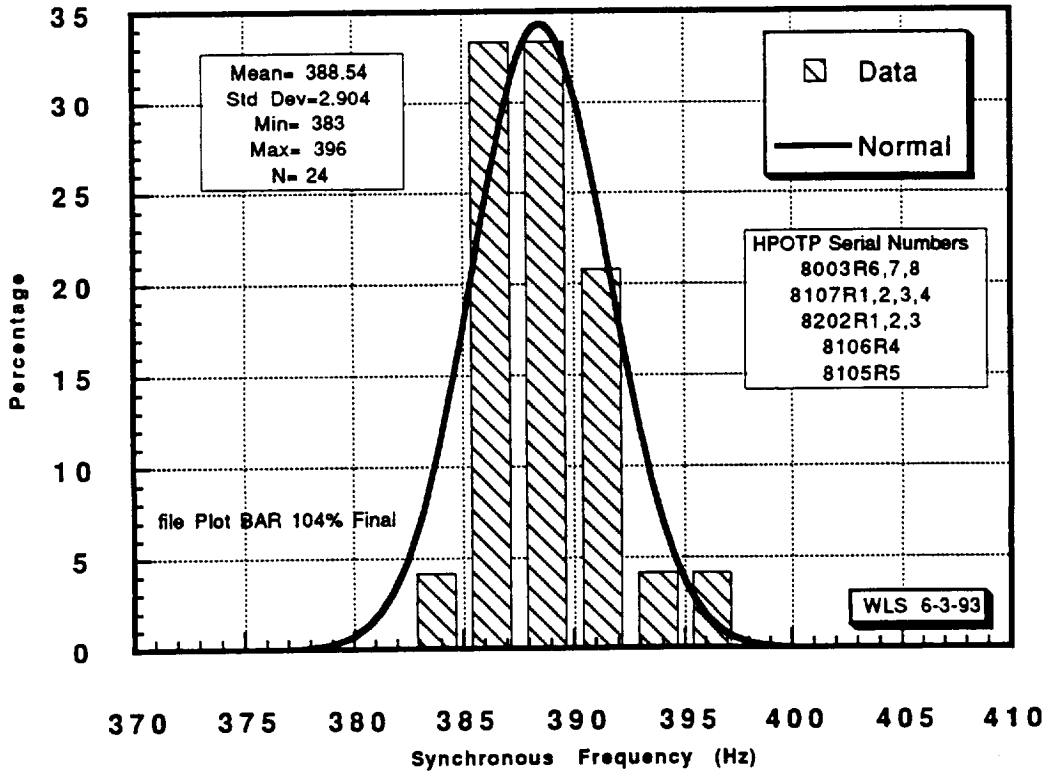

Figure 8. Histogram Synchronous Frequency (Hz) @ 109% PWL ATD High Pressure Oxidizer Turbopump (HPOTP)

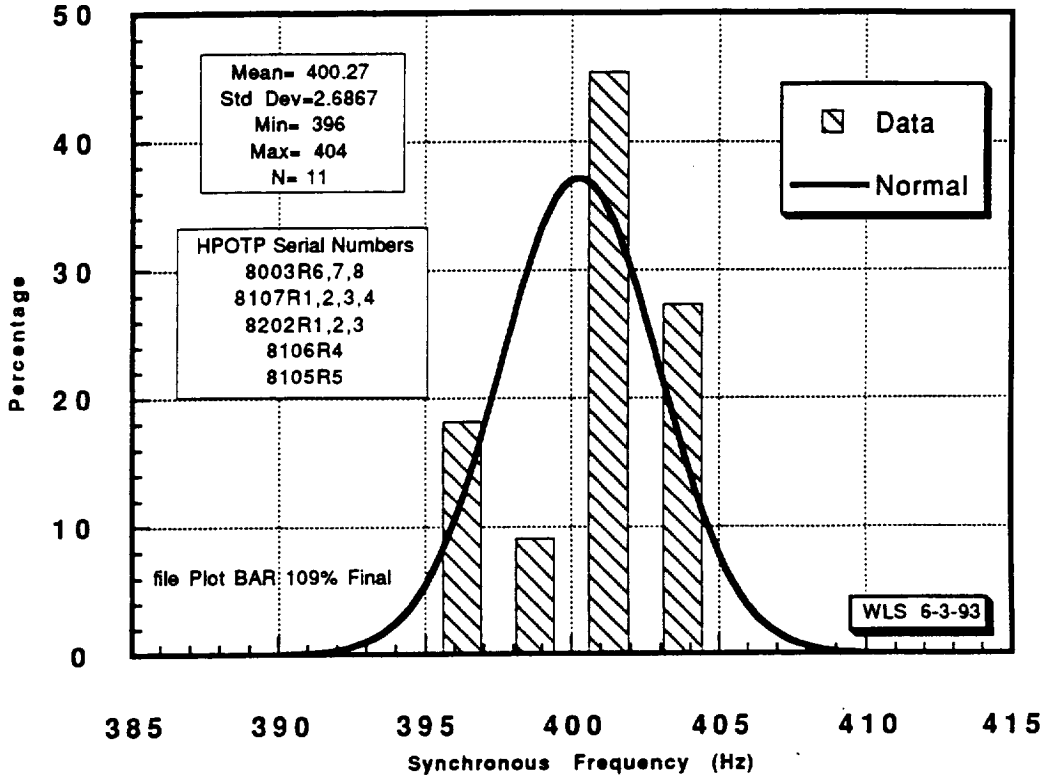

WYLE LABORATORIES
Engineering Division

Technical Memorandum TM 62200-93-12

COMPARISON OF GAMMA, WEIBULL AND NORMAL DISTRIBUTIONS WITH ATD HIGH PRESSURE OXIDIZER TURBOPUMP VIBRATION DATA

by

Wayne L. Swanson

JUNE 25, 1993

WYLE
LABORATORIES

1.0 INTRODUCTION AND SUMMARY

The purpose of this study was to evaluate if the classical gamma distribution function previously utilized for the Rocketdyne Space Shuttle Main Engines (SSME) Turbopumps is applicable to the P&W ATD High Pressure Oxidizer Turbopump (HPOTP) measured vibration data. Classical distribution functions provide a convenient smoothing operation and computational method for evaluating the cumulative and density distribution and measured data. The application is desirable for data characterization since this permits continuous statistical definition and manipulation from discrete measurement observations. Density plots are useful for an assessment of the historical data scatter or dispersion around the mid-point or mean value. The three classical functions in this study include the gamma, Weibull, and normal (gaussian) distributions. To check the functions for goodness-of-fit, the total mean-square error was calculated for each function for the ATD PBP RAD vibration measurements. The data from the Diagnostic Data Base for this study was the composite (50-1000 Hz) and synchronous Grms levels at 100% power level.

Other classical and more robust methods are available to evaluate the fit of distribution functions to measured data but were not utilized for this study since a visual analysis in many cases is adequate. A visual review of the plots (Figures 1 to 4) shows the discrete gamma function provides the best fit to the measured ATD HPOTP and Rocketdyne turbopump vibration data. (Ref. 1 to 4) The gamma distribution function also has the least mean-square error for both the composite and synchronous vibration levels. It is therefore recommended the gamma distribution be utilized for smoothing and evaluation of the P&W ATD HPOTP vibration data.

2.0 GAMMA DISTRIBUTION

The gamma distribution contains two parameters related to the mean and standard deviation and is defined as follows (ref. 6):

$$f(x) = \frac{\lambda}{\Gamma(r)} (\lambda x)^{(r-1)} e^{-\lambda x} \qquad x \geq 0 \qquad (1)$$

where $\Gamma(r)$ is the gamma, or generalized factorial, function and r; $\lambda > 0$.

The parameters λ and r, in terms of the mean $\bar{x}$ and variance (σ^2) are

$$\bar{x} = \frac{r}{\lambda}, \qquad \sigma^2 = \frac{r}{\lambda^2} \tag{2}$$

Solving each equation for r,

$$r = \bar{x}\lambda, \qquad r = \sigma^2\lambda^2 \tag{3}$$

or $$\lambda^2\sigma^2 = \lambda\bar{x} \tag{4}$$

$$\lambda = \bar{x}/\sigma^2 \tag{5}$$

From the first equation of 2 and equation 4

$$\bar{x} = \frac{r\,\sigma^2}{\bar{x}} \tag{6}$$

so $$r = \frac{\bar{x}^2}{\sigma^2} \tag{7}$$

Using equations 1, 5, and 7,

$$f(x) = \frac{\bar{x}}{\sigma^2\Gamma(\frac{\bar{x}^2}{\sigma^2})}\left[\frac{\bar{x}\ x}{\sigma^2}\right]^{(\bar{x}^2/\sigma^2 - 1)} e^{-\bar{x}x/\sigma^2} \tag{8}$$

Some important relationships of the gamma function are

$$\Gamma(n+1) = \int_0^\infty x^n e^{-x}\,dx \tag{9}$$

which leads to

$$\Gamma(n) = (n-1)\,\Gamma(n-1) \tag{10}$$

$$\Gamma(n) = (n-1)! \tag{11}$$

$$\Gamma(n+1) = n! \tag{12}$$

thus, the definition as a generalized factorial function.

For digital computation of the gamma term, the following polynomial approximation was used from reference 7.

$$\ln\Gamma(z) \sim \left(z-\frac{1}{2}\right) \ln z - z + \frac{1}{2} \ln 2\pi + \frac{1}{12\,z} - \frac{1}{360\,z^3} + \frac{1}{1260\,z^5} - \frac{1}{1680\,z^7} \qquad (13)$$

Therefore, in terms of the mean Grms and standard deviation, the gamma probability distribution function is

$$f(x) = \frac{m}{s^2\Gamma(m^2/s^2)} * \left[\frac{mx}{s^2}\right]^{(m^2/s^2-1)} * e^{-[mx/s^2]} * \Delta x \qquad (14)$$

m = mean Grms level
s = standard deviation
Δx = step size

Although the gamma distribution appears to provide a reasonable fit to the data, some additional improvements could be investigated. These include a change in the class interval width, unequal class intervals, and some type of truncated gamma to account for the low synchronous values approaching the noise floor of the measurement instrumentation system. It may be noted, F(x) and f(x) are not the continuous form of the cumulative probability function and probability density function but represent percentiles within discrete class intervals. This formulation permits direct comparison between classical function approximations and discrete frequency distributions representing empirical measurement characteristics.

3.0 WEIBULL DISTRIBUTION

The Weibull distribution is frequently used as a time-to-failure model. Its probability density function, from reference 6, is

$$f(x) = \left(\frac{\alpha}{\beta}\right)\left(\frac{x}{\beta}\right)^{\alpha-1} \exp\left[-\left(\frac{x}{\beta}\right)^{\alpha}\right], \quad x \geq 0, \alpha > 0, \beta > 0 \qquad (15)$$

where β is the scale parameter and α is the shape parameter. The cumulative Weibull distribution is

$$F(x) = \int_0^x \left(\frac{\alpha}{\beta}\right)\left(\frac{x}{\beta}\right)^{\alpha-1} \exp\left[-\left(\frac{x}{\beta}\right)^{\alpha}\right] dx \tag{16}$$

$$= 1 - \exp\left[-\left(\frac{x}{\beta}\right)^{\alpha}\right], \quad x \geq 0 \tag{17}$$

The two parameters α and β in terms of the mean and variance are

$$m = \beta\,\Gamma\left(\frac{1}{\alpha} + 1\right) \tag{18}$$

$$s^2 = \beta^2 \left\{\Gamma\left(\frac{2}{\alpha} + 1\right) - \Gamma^2\left(\frac{1}{\alpha} + 1\right)\right\} \tag{19}$$

where m = mean and s = standard deviation.

A closed form solution is not available for the nonlinear equations and the system must be solved by iteration. Define $g(\alpha)$ and $h(\alpha)$ in terms of the mean and standard deviation, then from equations 18 and 19,

$$\frac{m}{s} = \frac{\Gamma\left(\frac{1}{\alpha} + 1\right)}{\left[\Gamma\left(\frac{2}{\alpha} + 1\right) - \Gamma^2\left(\frac{1}{\alpha} + 1\right)\right]^{1/2}} = g(\alpha) \tag{20}$$

and, from equation 18,

$$\frac{m}{\beta} = \Gamma\left(\frac{1}{\alpha} + 1\right) = h(\alpha) \tag{21}$$

Iteration of equation 20 on α will provide the value of α when $g(\alpha)=m/s$ and β follows immediately from the numerator and equation 21.

$$\beta = \frac{m}{h(\alpha)} \tag{22}$$

The probability density and cumulative functions are then calculated from equations 15 and 17 using the α and β values of equations 20 and 22.

The fit of the Weibull distribution to the composite levels could be greatly improved by taking into account an arbitrary origin. Introducing the location parameter μ of 0.5 or 1.0 to account for the noise floor below which the values cannot fall and using the three-parameter Weibull probability density function defined as follows

$$f(x) = \frac{\alpha}{\beta}\left(\frac{x-\mu}{\beta}\right)^{\alpha-1} \exp\left[-\left(\frac{x-\mu}{\beta}\right)^{\alpha}\right] \tag{23}$$

which should shift the function to the right and provide a better fit to the data.

4.0 NORMAL (OR GAUSSIAN) DISTRIBUTION

The normal distribution is a frequently used statistical model. Its probability distribution function is

$$f(x_i) = \frac{1}{\sigma\sqrt{2\pi}} \exp\left[-\frac{(x_i-\mu)^2}{2\sigma^2}\right] \Delta x \tag{24}$$

where m and s are location and scale parameters, respectively, of the distribution. It should be noted that all normal distributions are symmetric and have the same shape—that is, the distribution has no shape factor. The cumulative normal distribution is

$$F(x_i) = \int_{-\infty}^{x_i} \frac{1}{\sigma\sqrt{2\pi}} \exp\left[-\frac{(x_i-\mu)^2}{2\sigma^2}\right] dx \tag{25}$$

The two parameters of the normal distribution are the mean and standard deviation. Using the previous notation, the probability distribution function is

$$f(x) = \frac{1}{s\sqrt{2\pi}} \exp\left[-\frac{(x-m)^2}{2s^2}\right] \Delta x \tag{26}$$

with the cumulative distribution calculated using $F(x) = \sum_{}^{N} f(x)$. (27)

5.0 MEAN-SQUARE ERROR

The mean-square error was defined as

$$MSEG = \sum_{i}^{B} (G_i - Grms_i)^2 \tag{28}$$

$$MSEW = \sum_{i}^{B} (W_i - Grms_i)^2 \tag{29}$$

$$MSEN = \sum_{i}^{B} (N_i - Grms_i)^2 \tag{30}$$

B = Number of bins

G_i = Gamma function

W_i = Weibull function

N_i = Normal function

$Grms_i$ = Measured data (percent) with bin width of 0.5

6.0 TECHNICAL DISCUSSION

A study to evaluate the vibration statistics of the ATD HPOTP for overlay plots in the test data analysis routines will utilize a classical distribution for calculation of the values. The overlay values will represent the ATD flight configuration when operating under normal conditions. Therefore, questionable data points (excessive noise, etc.) and extreme outliers will not be utilized for the overlay plot study. The same methodology was applied before the final comparison of the classical distributions to the measured ATD HPOTP vibration data. An illustration of the requirement to purge the data base of outliers is shown in Enclosure 1 for the composite and synchronous vibration levels at the 100% power level (PWL). The data values indicated as invalid were not included in the final analysis. It should be noted that even with the relatively small data sample, the invalid data points do not significantly effect the mean, but show a significant change in the higher moments (standard deviation, skewness, and kurtosis).

The computer program written in QuickBasic language is listed in Enclosure 2 and was utilized for all the classical distribution calculations. For future reference and cross checking, the composite vibration levels are included in Enclosure 3 with the synchronous vibration levels for this study extracted from Enclosure 3 of Reference 5.

Figures 5 to 8 are included for comparison of the vibration statistics and calculated gamma distribution of the Rocketdyne HPOTP. These plots were extracted from Reference 3 and illustrate the close fit the gamma distribution function provides for a larger data sample. A first-cut comparison between the P&W ATD and Rocketdyne HPOTP synchronous and composite vibration levels are shown in Figures 9 to 12. Additional analysis and data is required to evaluate if any significant difference is noted. Modifications to the computer program listed in Enclosure 2 are still required to vary the bin size and make the program more user friendly.

ENCLOSURES

1. ATD HPOTP Composite and Synchronous Vibration Levels
2. Macintosh IIfx - QuickBASIC Computer Program Listing
3. ATD Data Summary Sheets Composite Grms Vibration Levels

REFERENCES

1. Swanson, W.L. "Gamma, Weibull and Normal Distributions Applied to the SSME High Pressure Turbopump Vibration Data" Wyle Laboratories' Engineering Division, Technical Note TN-60900-92-02, August 1992.

2. Swanson, W.L. "Statistical Summary of SSME Turbopump Vibration Levels: Part I, High Pressure Oxidizer Turbopump," Wyle Laboratories' Engineering Division, technical note TN-60900-92-01, June 1992.

3. Swanson, W.L. "Statistical Analysis of Vibration Levels on the SSME Turbopumps: Volume 1, Calculation of RMS Overlay Vibration Levels for SSME Phase II High Pressure Oxidizer Turbopumps." Wyle Laboratories technical memorandum TM 68101-20, November 1987.

4. Swanson, W.L. "Statistical Analysis of SSME Turbopump Vibration Levels: Part I, High Pressure Oxidizer Turbopump." Wyle Laboratories technical note TN 60900-90-611, June 1990.

5. Swanson, W. L. "Synchronous Frequencies of the ATD High Pressure Oxidizer Turbopump," Wyle Laboratories' Engineering Division, Technical Memorandum TM 62200-93-11, page E3-1 to E3-35, June 11, 1993.

6. Hahn, G. J., and S. S. Shapiro. *Statistical Models in Engineering,* John Wiley & Sons, Inc., New York, 1967.

7. Abramowitz, M., and I. A. Stegum. *Handbook of Mathematical Functions with Formulas, Graphs, and Mathematical Tables,* Nat'l Bureau of Stds, Washington, D.C., p. 257, eq. 6.1.41, June 1964.

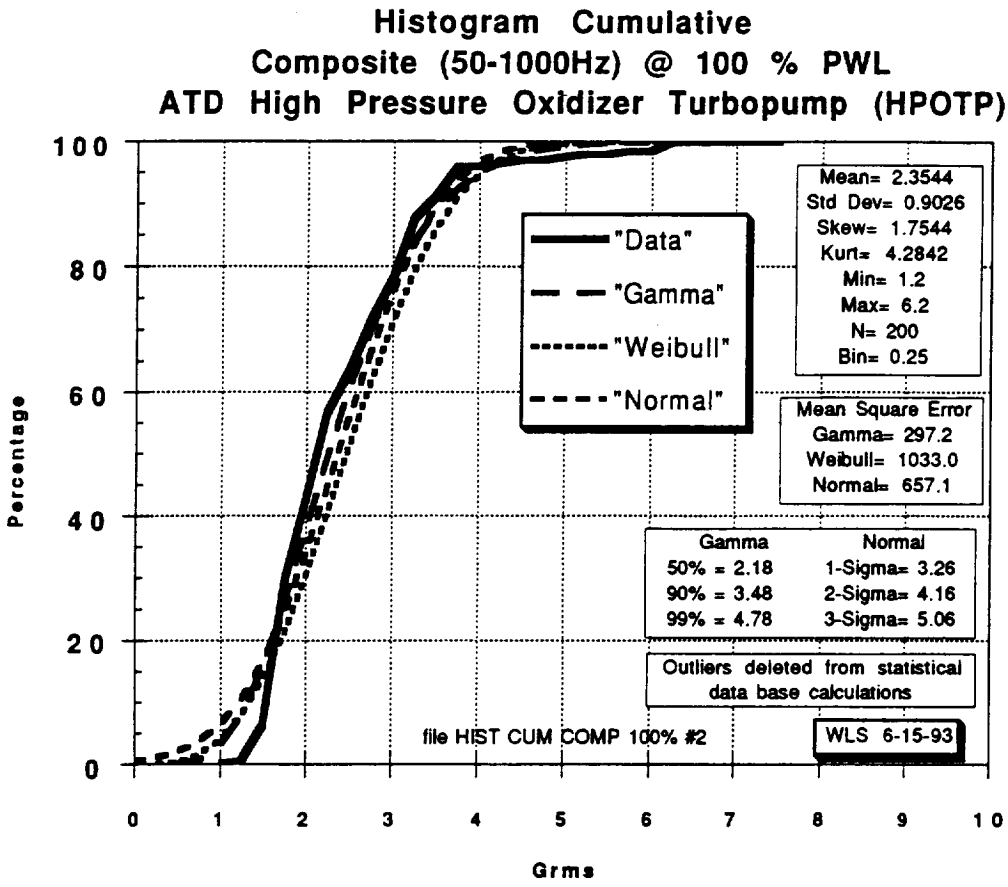

Figure 1. ATD Cumulative Histogram Composite @ 100 PWL

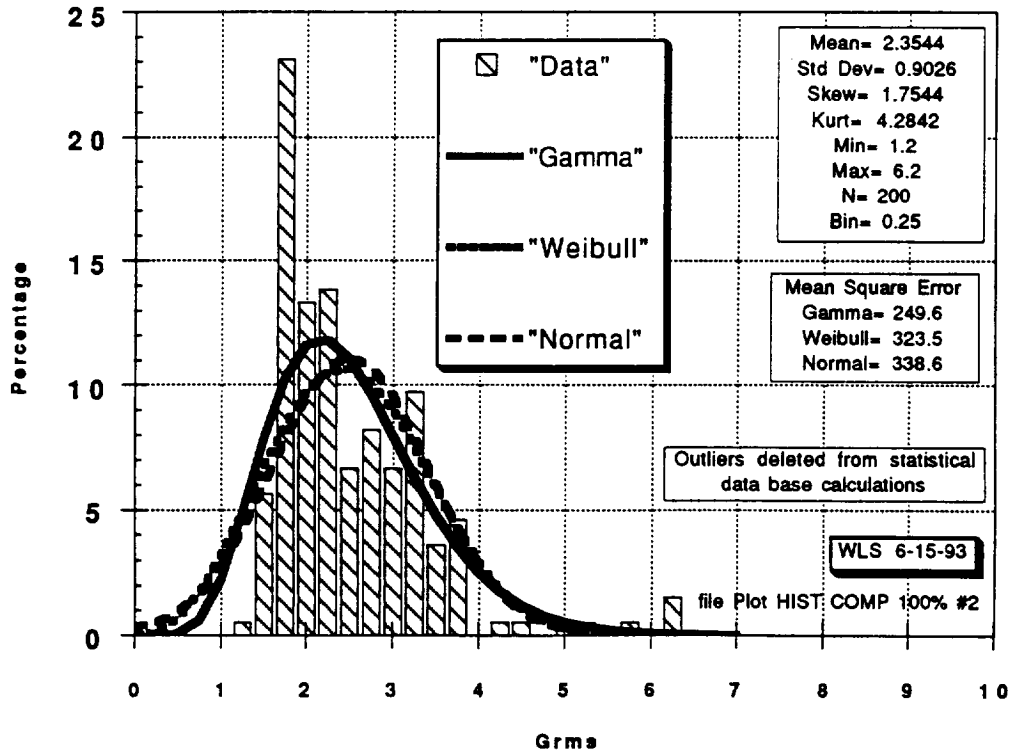

Figure 2. ATD Density Histogram Composite @ 100% PWL

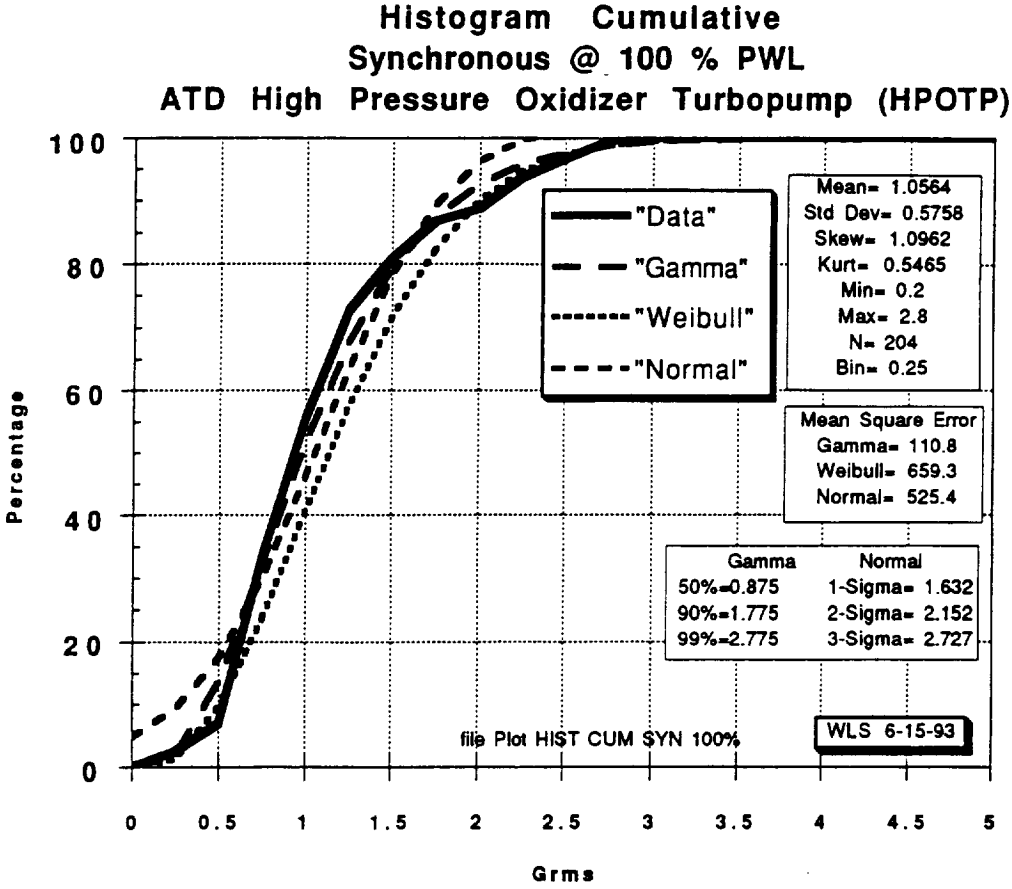

Figure 3. ATD Cumulative Histogram Synchronous @ 100% PWL

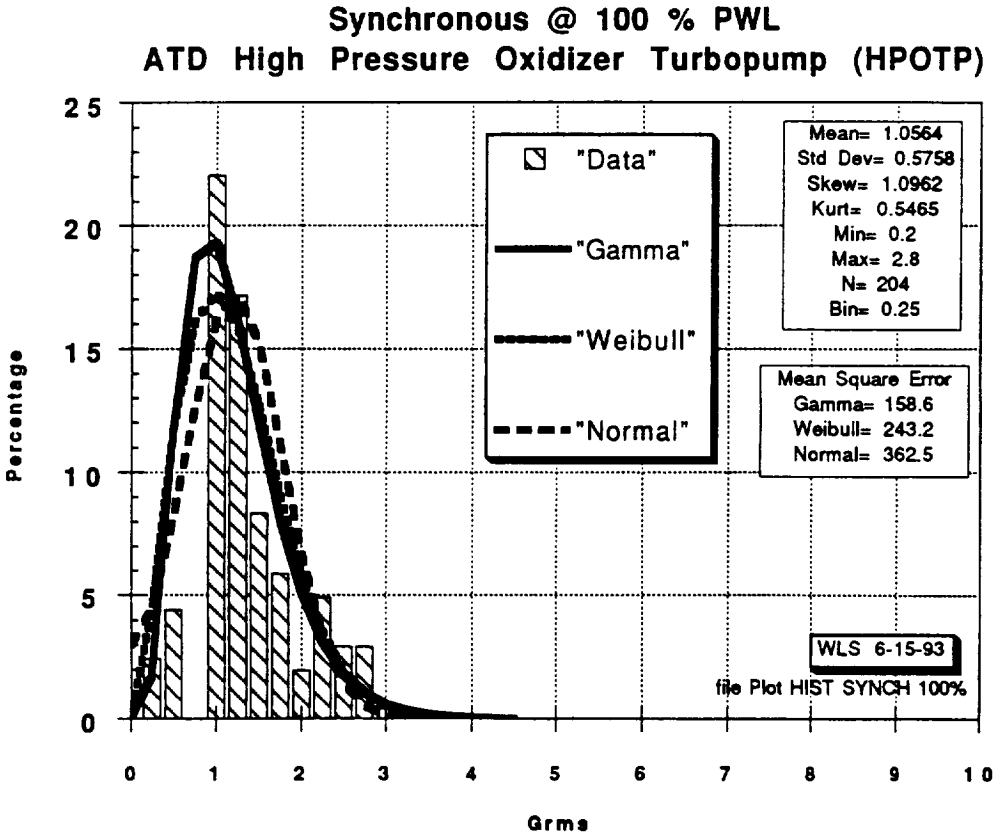

Figure 4. ATD Density Histogram Synchronous @ 100% PWL

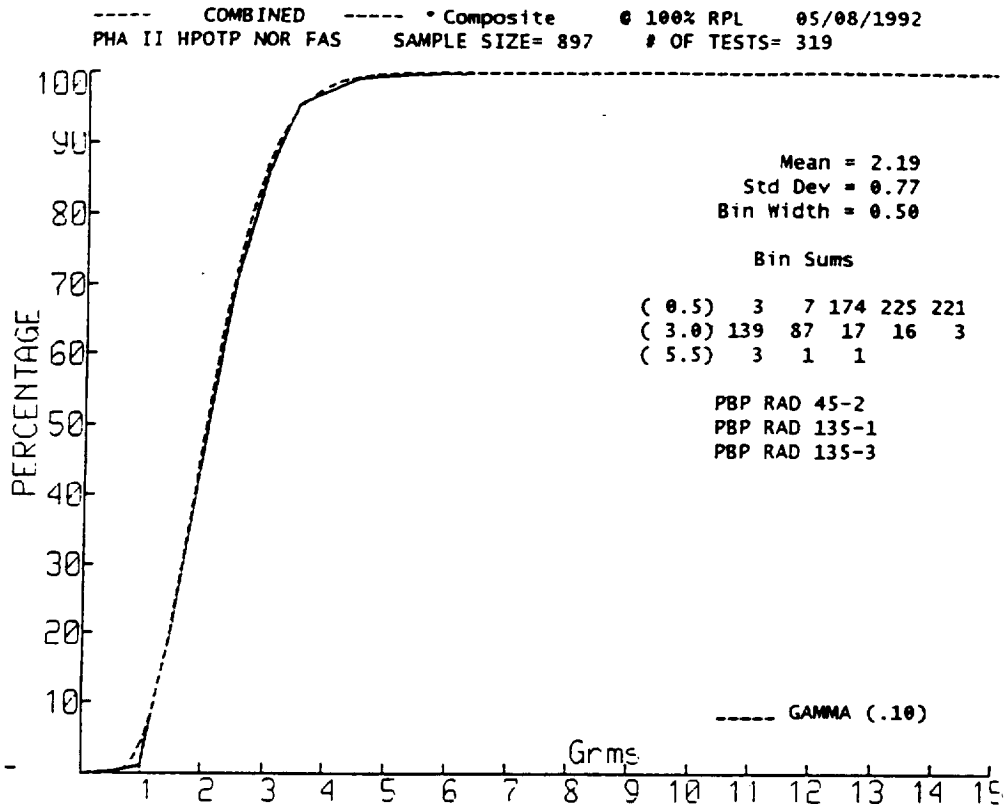

Figure 5. RD HPOTP Cumulative Histogram Composite @ 100% PWL

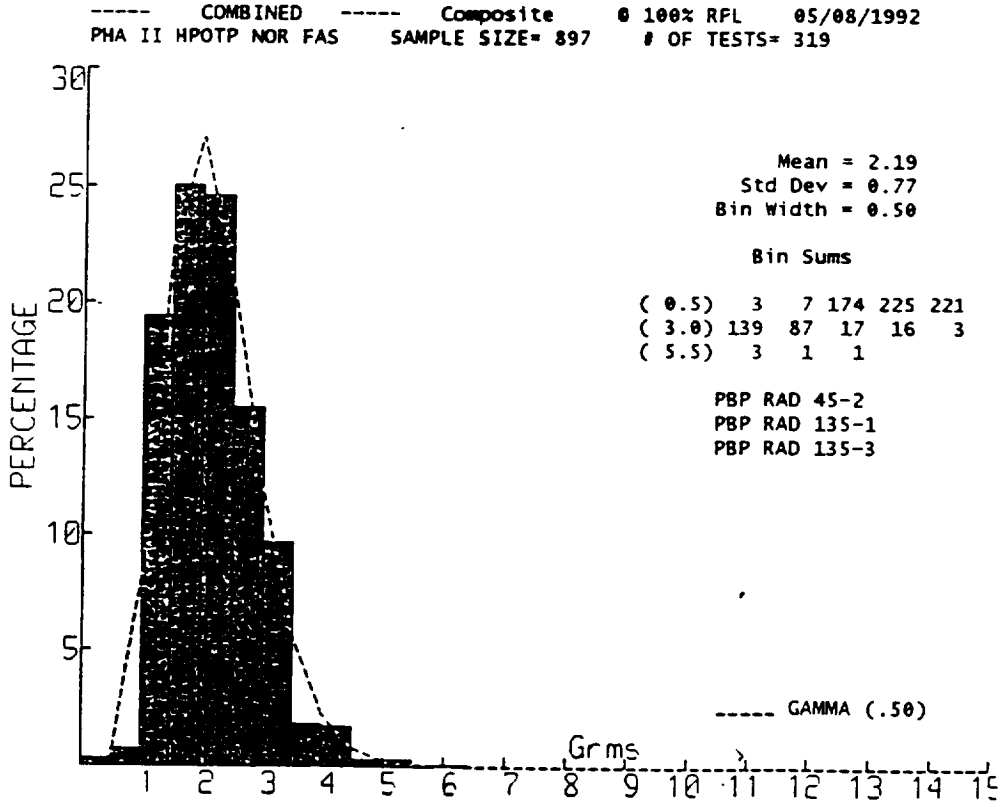

Figure 6. RD HPOTP Density Histogram Composite @ 100% PWL

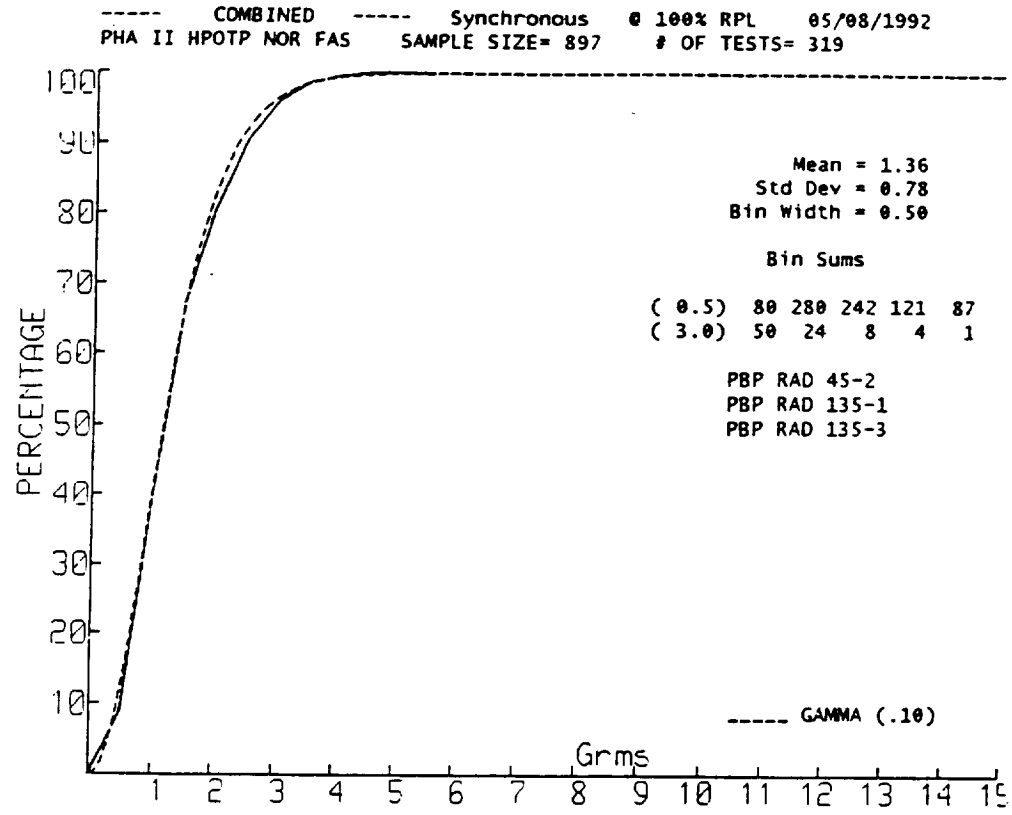

Figure 7. RD HPOTP Cumulative Histogram Synchronous @ 100% PWL

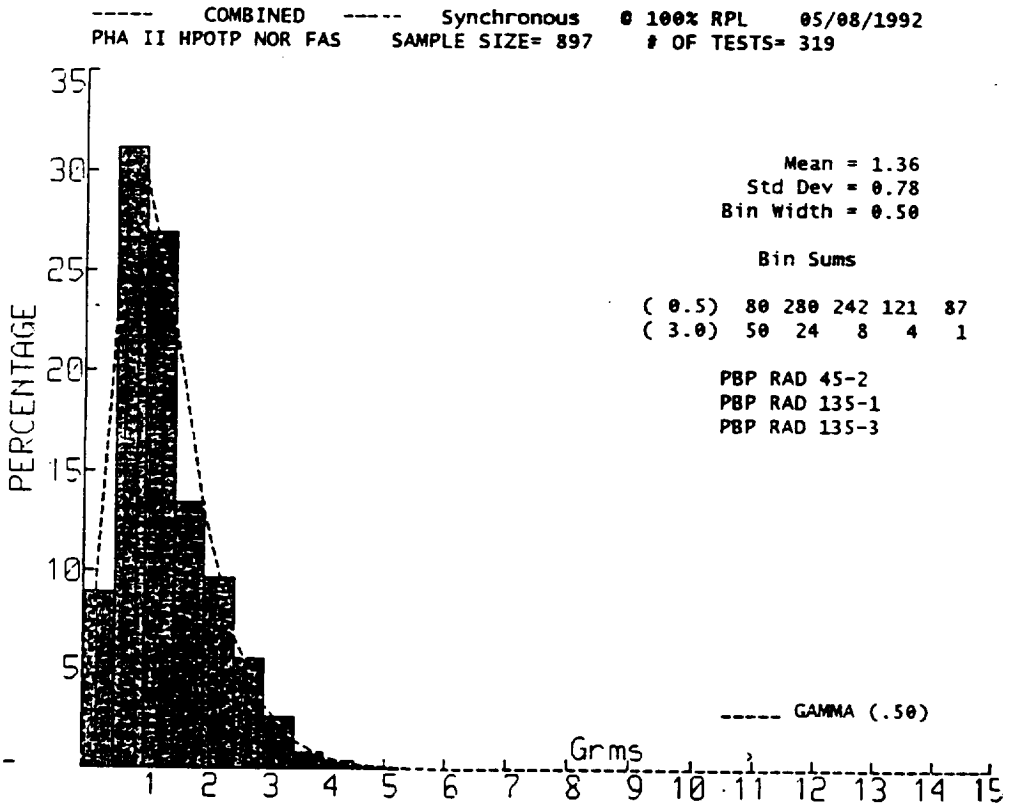

Figure 8. RD HPOTP Density Histogram Synchronous @ 100% PWL

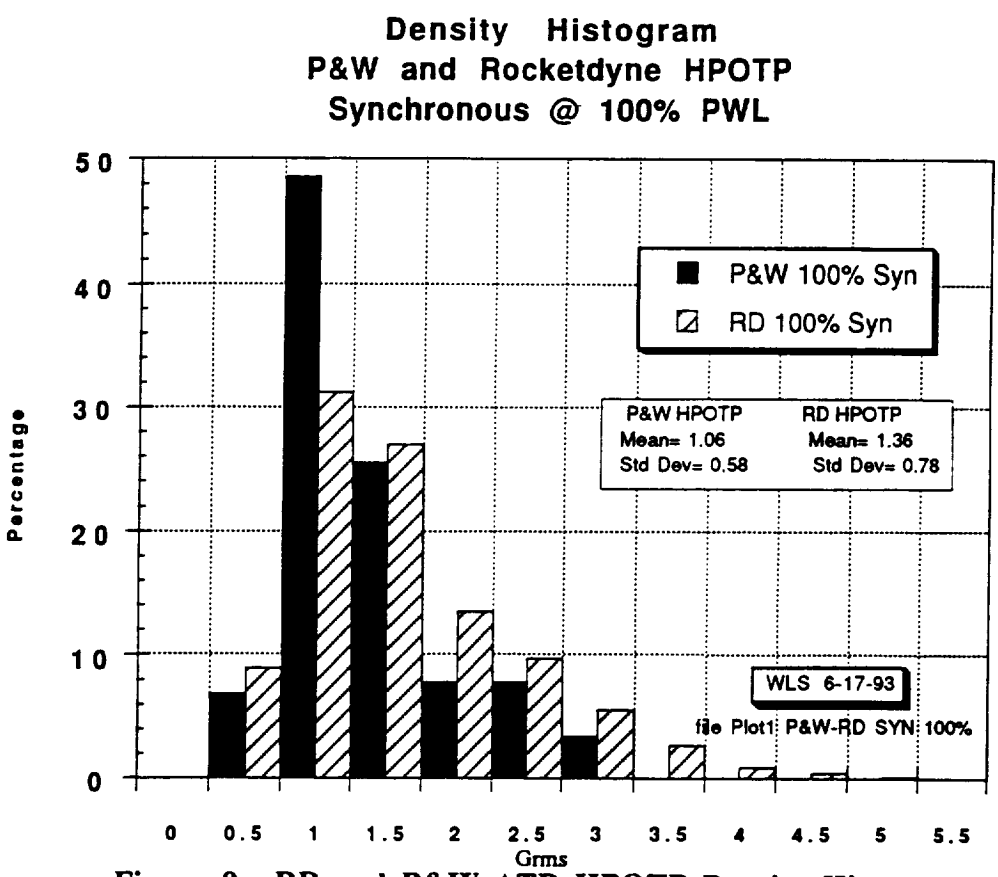

Figure 9. RD and P&W ATD HPOTP Density Histogram Synchronous @ 100% PWL

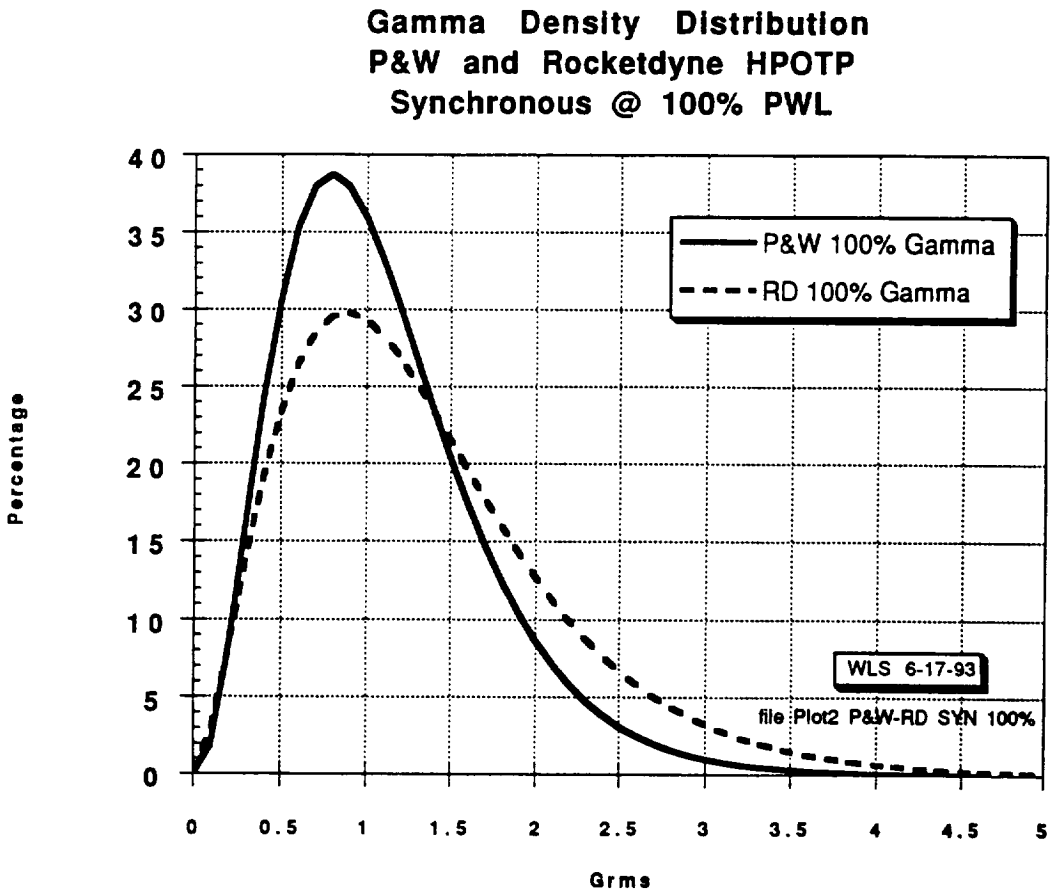

Figure 10. Calculated Synchronous Gamma Distribution for RD and P&W ATD HPOTP @ 100% PWL

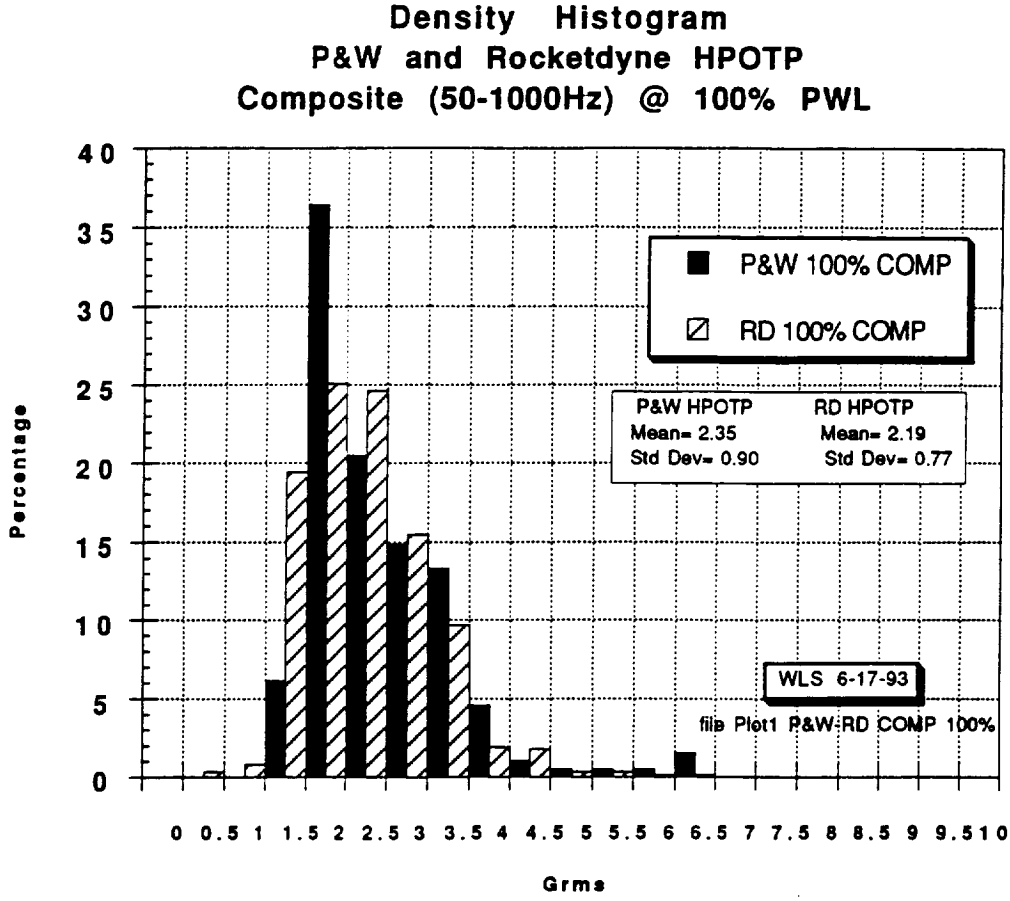

Figure 11. RD and P&W Density Histogram Composite @ 100% PWL

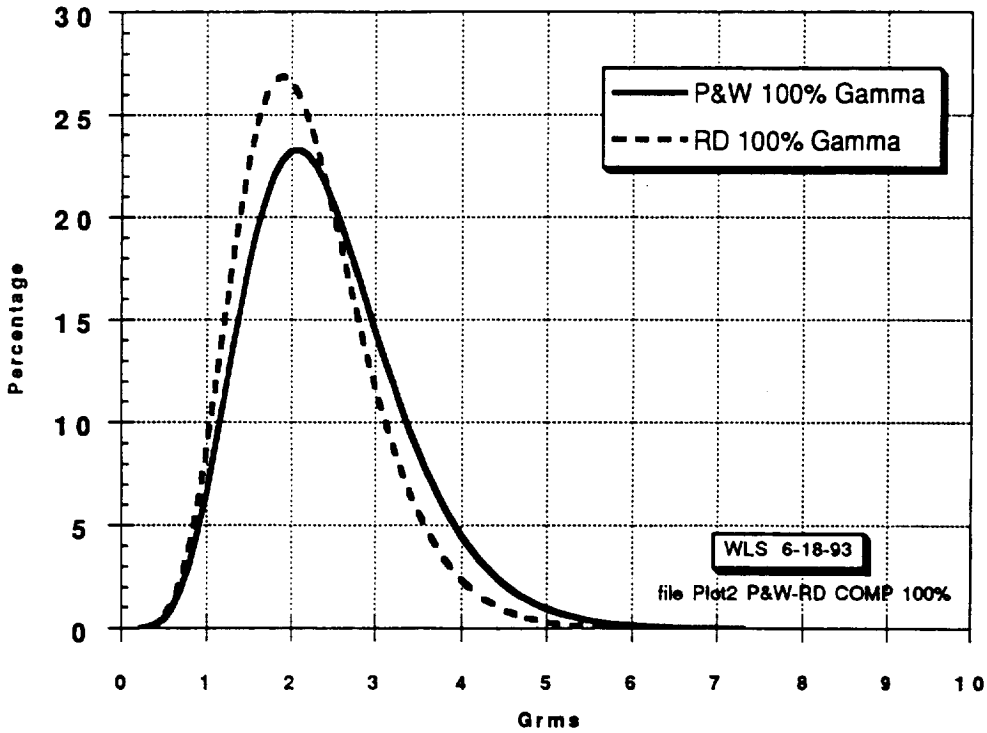

Figure 12. Calculated Composite Gamma Distribution for RD and P&W ATD HPOTP @ 100% PWL

APPENDIX B

SEMINAR NOTES

ON

SIGNAL PROCESSING TECHNIQUES FOR SPACE SHUTTLE MAIN ENGINE DIAGNOSTIC EVALUATION

by

Jen-Yi Jong

WYLE LABORATORIES

for

Structures and Dynamics Laboratory
Marshall Space Flight Center

Work Performed Under
Contract NAS8-38156

THEORY AND APPLICATION OF BI-SPECTRUM ANALYSIS

by

Jen-Yi Jong

September 1990

for

Structures And Dynamics Laboratory
Marshall Space Flight Center

Contract NAS8-38156

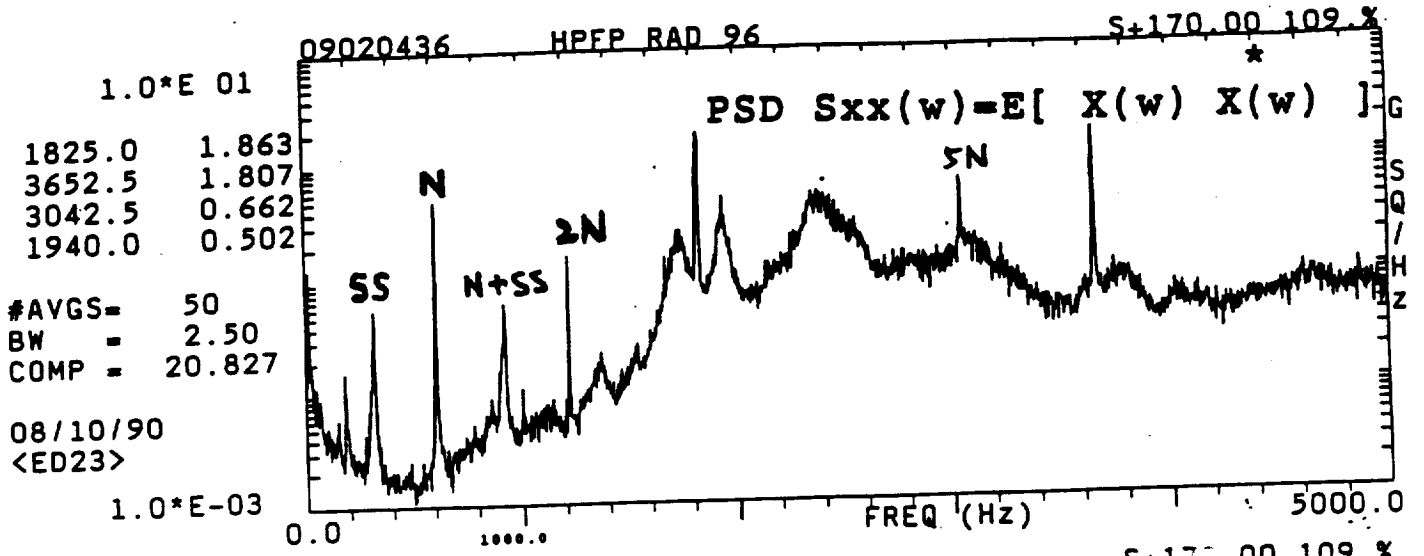

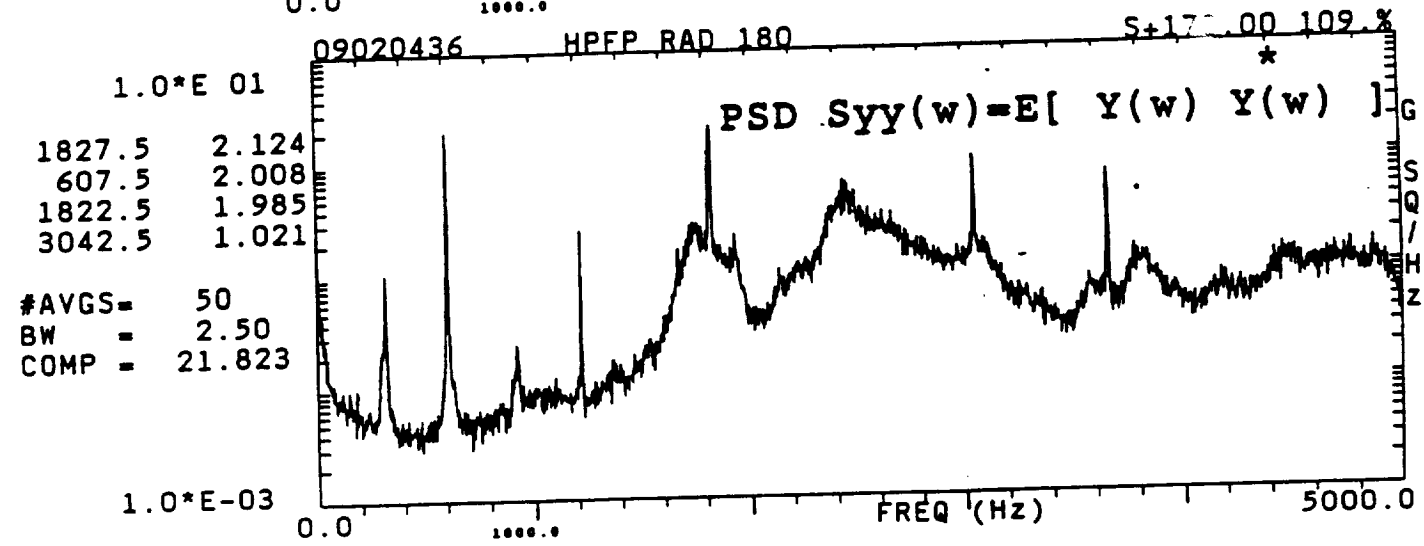

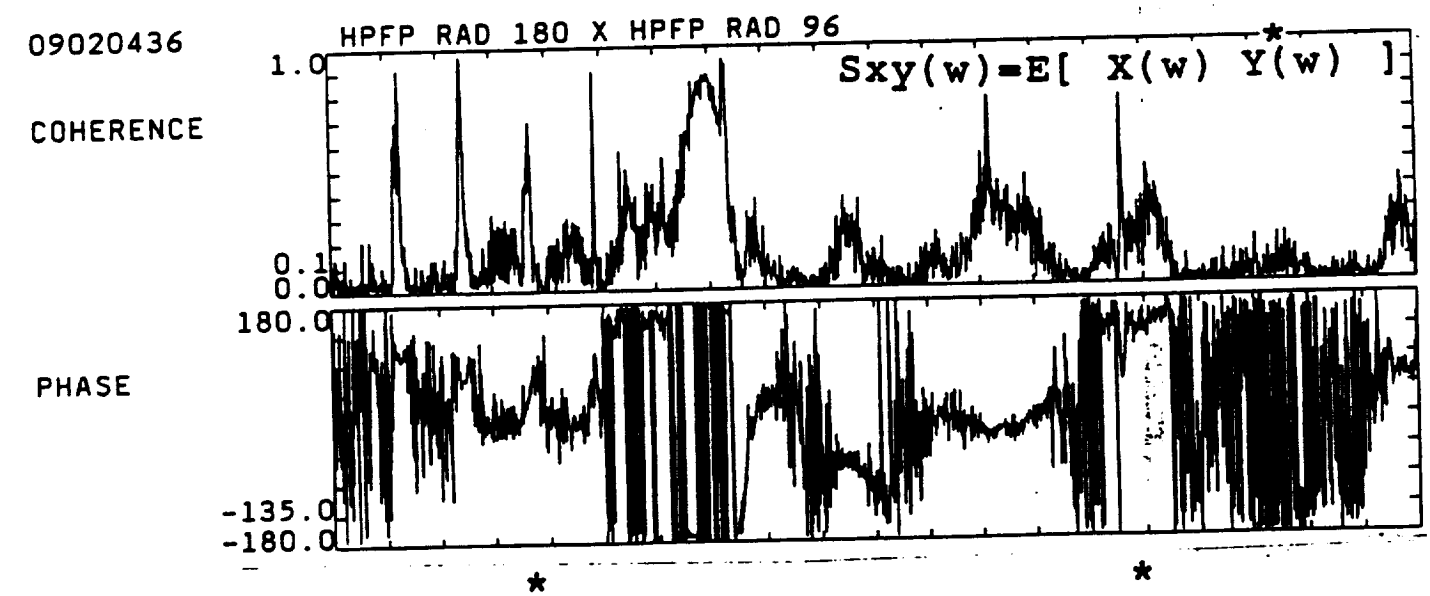

E[X(w1) X(w2)] or E[X(w1) Y(w2)] ???

HIGH ORDER SPECTRAL ANALYSIS

- RANDOM VARIABLES X1,X2,...Xn :
  - Joint Moment and Central Moment
  - Joint Cumulant
  - ---> Identify Correlation Among R.V.

- RANDOM TIME SERIES x(t) :
  - Cumulant Function:
  - Cumulant Spectrum:
  - ---> Identify Correlation Among Waves at Different Frequencies

- SECOND ORDER CUMULANT SPECTRUM:
  - Linear Spectrum
  - ---> Identify Correlation Between Waves at the Same Frequency

- THIRD ORDER CUMULANT SPECTRUM:
  - Bi-Spectrum
  - ---> Identify Correlation AMONG Three Waves at Frequencies (W1, W2, W1+W2)

- SIMULATIONS AND EXAMPLES FOR SSME DIAGNOSTICS

(1) MOMENT, CENTRAL MOMENT AND CUMULANT

1-1 MOMENT AND CHARACTERISTIC FUNCTION

For a single random variable (RV) x :

p(x) = pdf (probability density function)

Q(v) = Characteristic Functionis = FT[p(x)]

$$= \int p(x)\, \exp(jxv)\, dx = E\,[\, \exp(jxv)\,]$$

$$M1 = E[x] = \int x\, p(x)\, dx = (-j)\frac{\partial Q(v)}{\partial v}\Big|_{v=0} = \text{Mean}$$

$$M2 = E[x^2] = \int x^2\, p(x)\, dx = (-j)^2\frac{\partial^2 Q(v)}{\partial v^2}\Big|_{v=0} = \text{Mean Square}$$

$M3 = E[x^3]$ ==> Skewness ==> Indication of Symmetric/nonsymmetric distribution

$M4 = E[x^4]$ ==> Kurtosis ==> Indication of Impulsive data

.
.
.
.
.
.
.

$$Mn = E[x^n] = \int x^n\, p(x)\, dx = (-j)^n\frac{\partial^n Q(v)}{\partial v^n}\Big|_{v=0}$$

E[•] : expect value operator

1-2 JOINT MOMENT and CENTRAL MOMENT

for a set of random variable x1,x2,....xn:

p(x1,x2,..xn) = Joint probability Density Function

Q(v1,v2,..vn) = Characteristic Function

$$= \text{N-Dimensional FT}\{\ p(x1,x2,..xn)\ \}$$

$$= \iint\cdots\int p(x1,x2,..xn)\ \exp\left(j \sum_i x_i v_i\right)\ dx1\ dx2..\ dxn$$

$$= E\left[\ \exp\left(j \sum_i x_i v_i\right)\ \right]$$

--JOINT MOMENT:

$$M12...n = E[x1x2...xn] = (-j)^n \left.\frac{\partial^n Q(v1,v2,..vn)}{\partial v1\ \partial v2\ ...\partial vn}\right|_{v1,v2,..vn=0}$$

$$= \iint\cdots\int (x1x2...xn)\ p(x1,x2,..,xn)\ \ dx1\ dx2\ ...\ dxn$$

--CENTRAL MOMENT:

. for 2 RV x1 & x2:

C12 = Central Joint Moment (Covariance)

$$= E[\ (x1-M1)(x2-M2)\ ] = M12-M1M2$$

==>if x1 & x2 are independent of each other, then C12 will be zero

<pf> $$C12 = \iint (x1-M1)(x2-M2)\ p(x1,x2)\ dx1\ dx2$$

$$= \int (x1-M1)p(x1)\ dx1 \int (x2-M2)\ p(x2)\ dx2 = 0$$

. for 3 RV x1,x2 & x3:

C123 = E[(x1-M1)(x2-M2) (x3-M3)] = M123-M12M3-M13M2-M23M1+2M1M2M3

==>if (x1,x2,x3) can be devided into two or three groups that are statistically independent of each other, then C123 will be zero. C123 will be non-zero only if (x1,x2,x3) are correlated with one another

. For 4 RV x1,x2,x3 & x4:

C1234 = E[(x1-M1)(x2-M2)(x3-M3)(x4-M4)]

= M1234+ (M34M1M2+M14M2M3 +M24M1M3 +M13M2M4+M23M1M4+M12M3M4)

-(M134M2+M234M1+M124M3 +M123M4) -3M1M2M3M4

==>C1234=0, ONLY if (x1,x2,x3,x4) can be devided into SOME CERTAIN subset that are statistically independent of each other.

C1234 still be nonzero if (x1,x2,x3,x4) are correlated with one another. BUT C1234 will also be nonzero even though some subsets of RV are independent of other subsets.

FOR EXAMPLE, for 4 zero-mean RV (x1,x2,x3,x4), if (x1 cor x2) and (x3 cor x4), but (x1,x2) independent of (x3,x4)

===> M1=M2=M3=M4=0 M12≠0 M34≠0 M1234=M12M34≠0

C1234 = M1234 = M12 M34 ≠0

. When C1234 is non-zero, it is possible that some subsets of the RV are still independent of other subsets of RV. (Not Desired)

. Need a statistics: ====> CUMULANT

{ zero: As long as the RV's can be divided into two or more groups that are statistically independent of one another.

{ nonzero: All the RV's are correlated with one another.

1-3 CUMULANT

for a set of RV's x1,x2,....xn, with joint probability density function p(x1,x2,..xn) and characteristic function Q(v1,v2,...vn):

The joint cumulant K12...n:

$$K12...n = K[x1x2...xn] = (-j)^n \frac{\partial^n \ln [Q(v1,v2,..vn)]}{\partial v1\, \partial v2 \ldots \partial vn} \Bigg|_{v1,v2,..vn=0}$$

Relationship between Moment and Cumulant :

Note: $Q(v1,v2,\ldots vn)\big|_{v1,v2,\ldots,vn=0} = 1$

n=1

$$K1=(-j)\frac{\partial \ln [Q(v1)]}{\partial v1}\Big|_{v1=0} = (-j)\frac{\partial Q(v1)/\partial v1}{Q(v1)}\Big|_{v1=0} = (-j)\frac{\partial Q(v1)}{\partial v1}\Big|_{v1=0} = M1$$

n=2

$$K12=(-j)^2\frac{\partial^2 \ln [Q(v1,v2)]}{\partial v1\ \partial v2}\Big|_{v1,v2=0} = (-j)^2\frac{\partial}{\partial v2}\left\{\frac{\partial Q(v1,v2)/\partial v1}{Q(v1,v2)}\right\}\Big|_{v1,v2=0}$$

$$=(-j)^2\frac{[\partial^2 Q(v1,v2)/\partial v1\partial v2]\ Q(v1,v2) - \partial Q(v1,v2)/\partial v1\ \partial Q(v1,v2)/\partial v2}{Q(v1,v2)}\Big|_{v1,v2=0}$$

$$= M12 - M1\ M2 = C12$$

n=3:

$$K123 = M123 - M12M3 - M13M2 - M23M1 + 2M1M2M3 = C123$$

n=4:

$$K1234 = M1234 - (M12M34 + M13M24 + M14M23 + M123M4 + M124M3 + M134M2 + M234M1) + 2(M12M3M4 + M13M2M4 + M14M2M3 + M23M1M4 + M24M1M3 + M34M1M2) - 6M1M2M3M4$$

$$= 2*C1234 - M1234 + (M123M4 + M124M3 + M134M2 + M234M1) - (M12M34 + M13M24 + M14M23)$$

PROPERTY OF CUMULANT:

[1] if RV x1,x2,...xn can be divided into two or more groups that are statistically independent of each other, then its K12..n will be zero. (Note: the central moment C12...n would not necessarily be zero)

<proof> if(x1,x2,..xm, xm+1,....xn) can be divided into two independent groups: (x1,x2,...xm) & (xm+1,....xn)

then $p(x1,x2,...xn) = p1(x1,x2,...,xm)\ p2(xm+1,xm+2,...,xn)$

$$Q(v1,v2...vn) = \iint_{(n)}\cdots\int p(x1,x2,..xn)\ \exp(j\sum_{i=1}^{n} x_i v_i)\ dx1...dxn$$

$$= \iint_{(m)}\cdots\int p1(x1,..xm)\ \exp(j\sum_{i=1}^{m} x_i v_i)\ dx1\ dx2\ \ldots\ dxm$$

$$\iint_{(n-m)}\cdots\int p2(xm+1,..xn)\ \exp(j\sum_{i=m+1}^{n} x_i v_i)\ dxm+1\ \ldots\ dxn$$

$$= Q1(v1,..vm)\ Q2(vm+1,..vn)$$

$$K12..n = (-j)^n \frac{\partial^n \ln[Q(v1,..vn)]}{\partial v1\ \partial v2\ \ldots \partial vn}\Bigg|_{v1,..vn=0}$$

$$= (-j)^n \frac{\partial^n \ln[\ Q1(v1,..vm)\ Q2(vm+1,..vn)\ ]}{\partial v1\ \partial v2\ \ldots \partial vn}\Bigg|_{v1,..vn=0}$$

$$= (-j)^n \frac{\partial^n \{\ \ln[\ Q1(v1,..vm)] + \ln[\ Q2(vm+1,..vn)\ ]\ \}}{\partial v1\ \partial v2\ \ldots \partial vn}\Bigg|_{v1,..vn=0}$$

$$= 0$$

$\begin{cases} K12...n \neq 0 & \Longrightarrow \text{all of RV's (x1,x2,...xn) are correlated} \\ K12...n = 0 & \Longrightarrow \text{some sub-sets of RV's are independent of other subsets} \end{cases}$

[2] if $\underline{x}$ = (x1,x2,..xn) is joint Gaussian, then K12...n=0 for n>2

<proof>

Gaussian Probability Density Function:

$$p(x1,x2..xn) = \frac{\exp(-(\underline{X} - \underline{m}_x)^T \Lambda_x^{-1} (\underline{X} - \underline{m}_x)/2)}{(2\pi)^{N/2} |\Lambda_x|^{1/2}}$$

Gaussian Characterictic Function:

$$Q(v1,v2..vn) = \exp\left(j \underline{v}^T \underline{m}_{-x} - 0.5 \underline{v}^T \Lambda_{x-} \underline{v} \right)$$

==> ln [Q(v1,v2..vn)] = Quadratic function of (v1,v2,..,vn)

$$K12...n = K[x1x2...xn] = (-j)^n \frac{\partial^n \ln [Q(v1,v2,..vn)]}{\partial v1\, \partial v2 \ldots \partial vn}\Bigg|_{v1,v2,..vn=0} = 0 \text{ for } n > 2$$

Note: This can also be proof by using the property of Gaussian RV:
----

if (x1,x2,..xn) be a set of Gaussian RV with Cij being the covariance between xi & xj , then

$$\begin{cases} C12...n = 0 & \text{if n is odd} \\ C12...n = \sum C_{j1j2} C_{j3j4} \ldots C_{jn-1jn} & \text{if n is even} \end{cases}$$

The summation is over all distinct pairs of subscripts (j1,j2,...jn) that are permutation of (1,2,...,n)

Example: for n=4, C1234 = C12 C34 + C13 C24 + C14 C23
----

[3] IN GENERAL, treat K[] operator just as a symbol, which represents certain combination of E[], rather than being an operator that can skip over an operator on the RV.

EXAMPLE: RV's (x,y,z) transform into new RV's (r,s) as:

r=a x ; s= b yz (a,b= constant)

RIGHT: $K[rs] = E[rs] - E[r]\,E[s] = ab\,E[xyz] - ab\,E[x]E[y\,z]$

WRONG: $K[rs] = K[(ax)\,(byz)] = ab\,K[xyz]$

$= ab\{\,E[xyz] - E[xy]E[z] - E[xz]E[y] - E[yz]E[x] + 2E[x]E[y]E[z]\}$

. If L() represent a linear transformation operator which satisfy:

$L1(x1)\,L2(x2) = L1L2(x1x2)$, then $K[\,L()\,] = L(\,K[]\,)$

e.g. $L(x) =$ Fourier Transform $= \int x(t)\exp(j\,wt)\,dt$

$L1(x1)L2(x2) = \int x1(t1)\exp(j\,w1t1)\,dt1 \int x2(t2)\exp(j\,w2t2)\,dt2$

$= \iint x1(t1)\,x2(t2)\,\exp(j\,w1t1)\,(j\,w2t2)\,dt1\,dt2 = L1L2(x1x2)$

Example:

. $K[L1(x1)\,L2(x2)] = E[L1(x1)\,L2(x2)] - E[\,L1(x1)\,]\,E[\,L2(x2]\,)$

$= E[\,L1L2(x1x2)\,] - L1(E[x1]\,)\,L2(E[x2])$

$= L1L2(\,E[x1x2])\,] - L1L2(\,E[x1]\,E[x2]\,)$

. $K[L1(x1)\,L2(x2)] = K[L1L2(x1x2)] = L1L2(K[x1x2])$

$= L1L2(\,E[x1x2])\,] - L1L2(\,E[x1]\,E[x2]\,)$

(2) HIGH ORDER SPECTRUM

2-1 CUMULANT FUNCTION (TIME DOMAIN)

For a random time series x(t), the n-th order cumulant function:

$$Kn(t1,t2,...,tn) = K[\, x(t1)\, x(t2)....x(tn)\,]$$

if x(t) is stationary, it only depends on the n-1 time lag variables:

time lag variables: Ti=ti-tn

$$Kn(t1,t2,..,tn) = K[x(tn)\, x(tn+T1)\, x(tn+T2)...x(tn+Tn-1)]$$
$$= Kn(T1,T2,...Tn-1)$$

SPECIAL CASE WHEN n=2:

$K2(T) = K[\, x(t)\, x(t+T)\,] = Rxx(T)$ = auto-correlation function (a.c.f)

2-2 CUMULANT SPECTRUM (FREQUENCY DOMAIN):

Fn(w1,w2..,wn-1) =N-th ORDER CUMULANT SPECTRUM = $\underset{(n-1\ D)}{FT\{\, Kn(\, T1,T2...Tn-1)\, \}}$

$$Fn(w1,w2...wn-1) = \underbrace{\int\cdots\int}_{n-1} Kn(T1,T2...Tn-1)\exp\Big(j \sum_{i=1}^{n-1} wi\ Ti\Big)\ dT1\ dT2...dTn-1$$

==> This involves the estimation of cumulant function Kn(T1,T2,...Tn-1), as well as multi-dimensional Fourier Transform

==> Wish to find a direct relationship between cumulant spectrum and the FT of x(t).

Relationship Between Fn(w1,w2,..Wn-1) and X(w):

. If x(t) be real and stationary, $X(w) = FT[x(t)] = \int x(t)\exp(j\,wt)\,dt$

then X(w) will be zero-mean at non-zero frequency, i.e.

$$E[X(w)] = E[x(t)]\,\delta(w) \quad (\ E[X(0)] = E[x(t)]\ )$$

<proof> $E[X(w)] = E\left[\int x(t)\exp(j\,wt)\,dt\right] = \int E[x(t)]\exp(j\,wt)\,dt$

$= E[x(t)]\int \exp(j\,wt)\,dt = E[x(t)]\,\delta(w)$ #

- $K[\,X(w1)\,X(w2)\,\ldots\,X(wn)\,]$

$$= K\left[\int x(t1)\exp(j\,w1t1)\,dt1 \int x(t2)\exp(j\,w2t2)\,dt2 \ldots \int x(tn)\exp(j\,wntn)\,dtn\right]$$

$$= K\left[\underset{(n)}{\int\int\cdots\int} x(t1)x(t2)\ldots x(tn)\,\exp\left(j\sum_{i=1}^{n} wi\,ti\right)\,dt1\,dt2\ldots dtn\right]$$

$$= \underset{(n)}{\int\int\cdots\int} K[\,x(t1)\,x(t2)\ldots x(tn)]\exp\left(j\sum_{i=1}^{n} wi\,ti\right)\,dt1\,dt2\ldots dtn$$

$$= \underset{(n)}{\int\int\cdots\int} Kn(\,t1,t2\ldots,tn)\exp\left(j\sum_{i=1}^{n} wi\,ti\right)\,dt1\,dt2\ldots dtn$$

change of variable: Ti=ti-tn for i=1,2,...,n-1

ti ===> Ti+tn
dti ===> dTi
Kn(t1,t2 ...,tn)===> Kn(T1,T2,...,tn-1) (for stationary)

$$= \underset{(n)}{\int\int\cdots\int} Kn(\,T1,T2\ldots Tn-1)\exp\left[j\sum_{i=1}^{n} wi\,(Ti+tn)\right]\,dT1\,dT2\ldots dTn-1\,dtn$$

$$= \underset{(n-1)}{\int\int\cdots\int} Kn(T1,T2\ldots Tn-1)\exp\left(j\sum_{i=1}^{n-1} wiTi\right)\,dT1\,dT2\ldots dTn-1\int \exp\left(j\,tn\sum_{i=1}^{n} wi\right)\,dtn$$

$$= \{\ n-1\ \text{dimensional FT of}\ Kn(T1,T2,\ldots,Tn-1)\ \}\,\delta\left(\sum_{i=1}^{n} wi\right)$$

$$= \{\ Fn(w1,w2,\ldots,wn-1)\ \}\,\delta(\ w1+w2+\ldots+wn\ )$$

$$\boxed{K[X(w1)\,X(w2)\ldots X(wn)] = \{Fn(w1,w2,\ldots,wn-1)\}\,\delta(\ w1+w2+\ldots+wn\ )} \quad (*)$$

where, delta function: $\delta(u) = \int \exp(j\,tu)\,dt \begin{cases} = 1 & \text{for } u = 0 \\ = 0 & \text{for } u = 0 \end{cases}$

Two Important Statistical Concept From Equation (*):

[1] K[X(w1) X(w2)....X(wn)] will be non-zero, only w1+w2+...+wn=0

Because only in this case, the delta funtion becomes non-zero.

K[X(w1) X(w2)...X(wn)]=0 for any other arbitrary freq combination

EXAMPLE:

(1) observe { 50Hz signal in channel-x
50Hz signal in channel-y

can identify whether the 50Hz signal in channel x & y are correlated by examing the linear cross-spectrum (2nd order cumulant spectrum):

K[X(50Hz) Y(-50Hz)] = F2(50Hz) = Sxy(50Hz) ==> freq sum= zero

(2) observe { 50Hz signal in channel-x
80Hz signal in channel-y

can not simply exame the 2-nd order cumulant spectrum at these two frequencies as:

K[X(50 Hz) Y(+- 80Hz)] is always zero (sum freq is not zero)

[2] Sum frequency (w1+w2+...+wn)=0 ===> wn = -(w1+w2+...+wn-1)

===> Fn(w1,w2,...,wn-1)= K[X(w1) X(w2)....X(wn-1) X(-w1-w2-...-wn-1)]

$$Fn(w1,w2,\ldots,wn-1)= K[\, X(w1)\, X(w2)\ldots X(wn-1)\, X^{*}(w1+w2\ldots+wn-1)\,] \quad (**)$$

. This equation allows us to evaluate cumulant spectrum directly from the FT of x(t) without having to evalute cumulant function and performing multi-dimensional FT.

. Recall the property of cumulant average:
If RV x1,x2...xn can be divided into two or more groups which are statistically independent of each other, then K[x1 x2..xn] = 0

Equation (**) imply that:

If the waves at frequencies w1,w2...wn can be divided into two or more groups which are independent of each other, then Fn(w1,...wn-1) = 0

If the waves at these different frequencie are nonlinearly correlated with each other, then Fn(w1,w2,...wn-1) = 0

2-3 LINEAR SPECTRUM (SPECIAL CASES FOR n=2)

- Auto-correlation and auto-spectrum of x(t):

$$\begin{cases} K2xx(T) = K[\, x(t)\, x(t+T)\,] = Rxx(T) = \text{a.c.f.} \\ F2xx(w) = \int K2xx(T) \exp(j\, wT)\, dT = \int Rxx(T) \exp(i\, wT)\, dT = Sxx(w) = PSD \\ F2xx(w) = K[\, X(w)\, X^{*}(w)\,] = E[\, X(w)\, X^{*}(w)\,] = E[\, |X(W)|^{2}\,] = Sxx(w) = PSD \end{cases}$$

- Cross-Correlation, Cross-Spectrum, Cross-Coherence between x(t) & y(t)

$$\begin{cases} K2xy(T) = K[\, x(t)\, y(t+T)\,] = Rxy(T) = \text{c.c.f.} \\ F2xy(w) = \int K2xy(T) \exp(j\, wT)\, dT = \int Rxy(T) \exp(i\, wT)\, dT = Sxy(w) = CSD \\ F2xy(w) = K[\, X(w)\, Y^{*}(w)\,] = E[X(w)\, Y^{*}(w)\,] = Sxy(w) = CSD \end{cases}$$

$$r^{2}_{xy}(w) = \frac{|\, Sxy(w)\,|^{2}}{[\, Sxx(w)\, Syy(w)\,]} = \text{linear cross-coherence function}$$

Discrete form:

$$\hat{r}^{2}_{xy}(w) = \frac{|\, Xi(w) Yi(w))\,|^{2}}{[\, |\, Xi(w)|^{2}\,]\,[\, |\, Yi(w)|^{2}\,]} = \text{linear cross-coherence function}$$

- Coherence is bounded by one

  < proof> by using Cauchy's Inequality:

  (i) for any random variables x,y, real or complex

$$|\, E[xy]\,|^{2} \le E[\, |x|^{2}\,]\, E[\, |y|^{2}\,]$$

  (ii) for any sequences xi,yi, real or complex

$$\left|\, \sum_i x_i y_i \,\right|^{2} \le \sum |x_i|^{2} \sum |y_i|^{2}$$

- System Identification for Linear Time Invariant (LTI) system:

$$x(t) \longrightarrow \boxed{\; h(t),\ H(w) \;} \longrightarrow y(t)$$

$$y(t) = x(t) * h(t) = \int x(t-a)\, h(a)\, da \Longrightarrow Y(w) = X(w)\ H(w)$$

$$Sxy(w) = E[\, X(w)\, Y(-w)\,] = E[\, X(w)\, X(-w)\, H(-w)\,] = Sxx(w)\, H(w)$$

$$\Longrightarrow \quad H(w) = \frac{Sxy(w)}{Sxx(w)}$$

2-4 BISPECTRUM (WHEN n=3)

Auto-Bispectrum

. Auto-bicorrelation, auto-bispectrum & auto-bicoherence of x(t):

$$\begin{cases} K3xxx(T1,T2) = K\,[\, x(t)\; x(t+T1)\; x(t+T2)\,] = Rxxx(T1,T2) = a.b.c.f \\ F3xxx(w1,w2) = K3xxx(T1,T2)\; \exp[j\,(w1T1+w2T2)]\; dT1\; dT2 = Bxxx(w1,w2) \\ F3xxx(w1,w2) = K\,[\, X(w1)\; X(w2)\; X^{*}(w1+w2)\,] = Bxxx(w1,w2) = ABS \end{cases}$$

$$b^{2}_{xxx}(w1,w2) = \frac{\dfrac{1}{2}\; Bxxx(w1,w2)\; \dfrac{1}{2}}{E[\; \dfrac{1}{2}\; X(w1)X(w2)\; \dfrac{1}{2}\;]\; Sxx(w1+w2)} = \text{Auto-Bi-coherence (ABC)}$$

Discrete form:

$$\hat{b}^{2}_{xxx}(w1,w2) = \frac{|\; Xi(w)\; Xi(w2)\; Xi^{*}(w1+w2)\;|^{2}}{[\;|\; Xi(w1)\; Xi(w2)|\;]\;[\;|\; Xi(w1+w2)|\;]}$$

Region of ABS:

Maximum frequency = Nyquist Frequency Wq = Sampling Frequency/2

Auto-Bispectrum will only be defined over a hexagon:

$$-Wq < w1,w2 < Wq \quad \text{and} \quad -Wq < w1+w2 < Wq$$

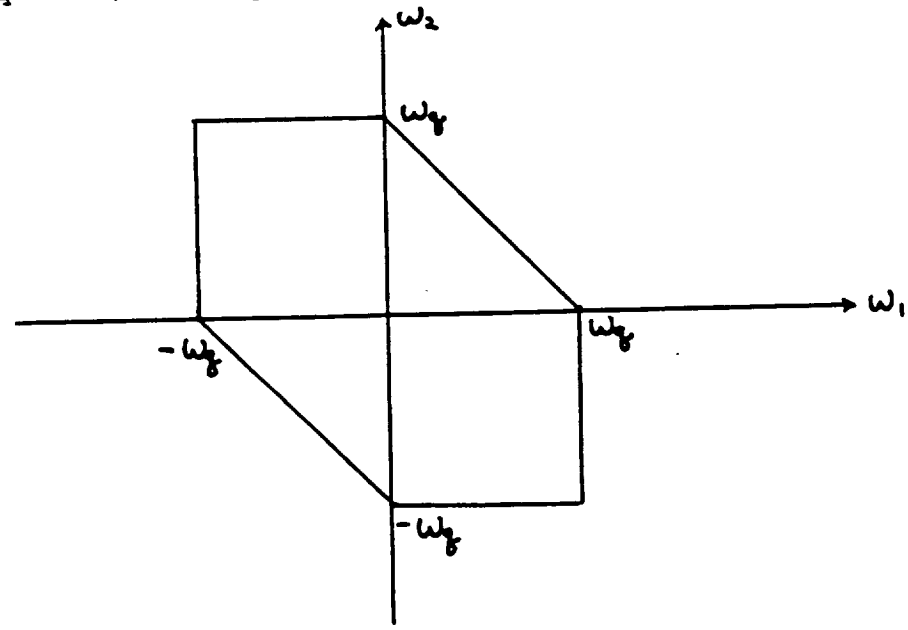

SYMMETRIC PROPERTY:

$B(w1,w2)=K[\ X(w1)\ X(w2)\ X(-w1-w2)\ ]$ ===> 6 different permutation:

$(w1,w2;\ -w1-w2)\ (w2,-w1-w2;\ w1)\ (-w1-w2,w1;\ w2)$

$(w2,w1;\ -w1-w2)\ (w1,-w1-w2;\ w2)\ (-w1-w2,w2;\ w1)$

$\overset{*}{B}(w1,w2)=K[\overset{*}{X}(w1)\overset{*}{X}(w2)\overset{*}{X}(-w1-w2)]=K[X(-w1)X(-w2)X(w1+w2)]$

==> 6 more permutation:

$(-w1,-w2;\ w1+w2)\ (-w2,w1+w2;\ -w1)\ (w1+w2,-w1;\ -w2)$

$(-w2,-w1;\ w1+w2)\ (-w1,w1+w2;\ -w2)\ (w1+w2,-w2;\ -w1)$

=====> $Bxxx(w1,w2) = Bxxx(w2,-w1-w2) = Bxxx(-w1-w2,w1)$

$= Bxxx(w2,w1) = Bxxx(w1,-w1-w2) = Bxxx(-w1-w2,w2)$

$= \overset{*}{Bxxx}(-w1,-w2) = \overset{*}{Bxxx}(-w2,w1+w2) = \overset{*}{Bxxx}(w1+w2,-w1)$

$= \overset{*}{Bxxx}(-w2,-w1) = \overset{*}{Bxxx}(-w1,w1+w2) = \overset{*}{Bxxx}(w1+w2,-w2)$

$Bxxx(w1,w2)=Bxxx(w2,w1)$ / MP=(w1+w2/2,w2+w1/2)==> SYM wrt 45° line

$Bxxx(w1,w2)=\overset{*}{Bxxx}(-w2,-w1)$/ MP=(w1-w2/2,w2-w1/2)==> Conj SYM WRT -45° line

$Bxxx(w1,w2)=Bxxx(w1,-w1-w2)$/ MP=(w1,-w1/2) ==> Sym vertically WRT Middle Line: w1=-2w2

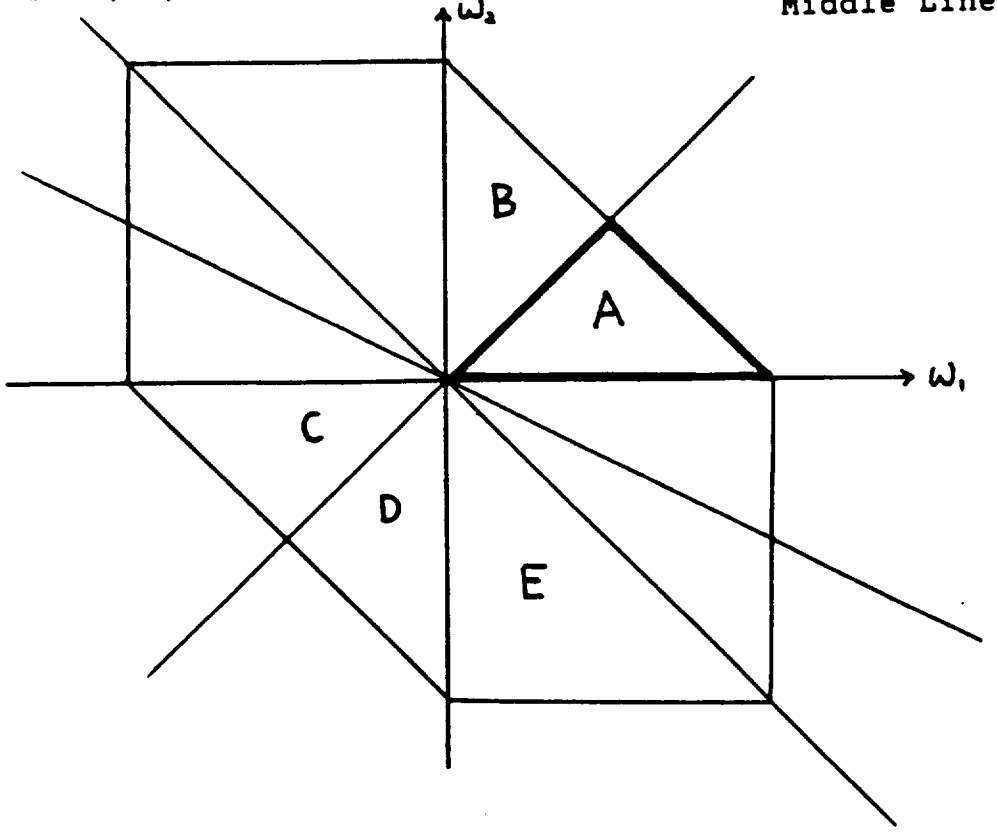

Cross-Bispectrum

. Cross-Bicorrelation, Cross-Bispectrum, Cross-Bicoherence between x & y

$$\begin{cases} K3xxy(T1,T2) = K\,[\, x(t)\, x(t+T1)\, y(t+T2)\,] = Rxxy(T1,T2) = c.b.c.f \\ F3xxy(w1,w2) = \int\int K3xxy(T1,T2)\, \exp[j(w1T1+w2T2)]\, dT1\, dT2 = Bxxy(w1,w2) \\ F3xxy(w1,w2) = K\,[\, X(w1)\, X(w2)\, Y^*(w1+w2)\,] = Bxxy(w1,w2) = CBS \end{cases}$$

$$b^2_{xxy}(w1,w2) = \frac{|\, Bxxy(w1,w2)\,|^2}{E[\,|\, X(w1)\, X(w2)\,|^2\,]\, Syy(w1+w2)} = \text{Cross-Bi-coherence (CBC)}$$

Discrete form:

$$\hat{b}^2_{xxy}(w1,w2) = \frac{|\, Xi(w)\, Xi(w2)\, Yi^*(w1+w2))\,|^2}{[\,|\, Xi(w1)\, Xi(w2)|^2\,]\,[\,|\, Yi(w1+w2)|^2\,]}$$

Region of CBS: Same Hexagon = $-Wq < w1,w2 < Wq$ & $-Wq < w1+w2 < Wq$

Symmetric Property:

$$Bxxy(w1,w2) = K[X(w1)X(w2)Y^*(-w1-w2)] = K[X(w2)X(w1)Y^*(-w1-w2)] = Bxxy(w2,w1)$$

$$Bxxy^*(-w1,-w2) = K[X^*(-w1)X^*(-w2)Y(w1+w2)] = K[X(-w2)X(-w1)Y(w1+w2)] = Bxxy(-w2,-w$$

$$\Longrightarrow Bxxy(w1,w2) = Bxxy(w2,w1) = Bxxy^*(-w1,-w2) = Bxxy^*(-w2,-w1)$$

$Bxxy(w1,w2) = Bxxy(w2,w1)$ / MP=(w1+w2/2, w2+w1/2) ==> SYM WRT 45 line

$Bxxy(w1,w2) = Bxxy^*(-w2,-w1)$ / MP=(w1-w2/2, w2-w1/2) ==> Conj SYM WRT -45 line

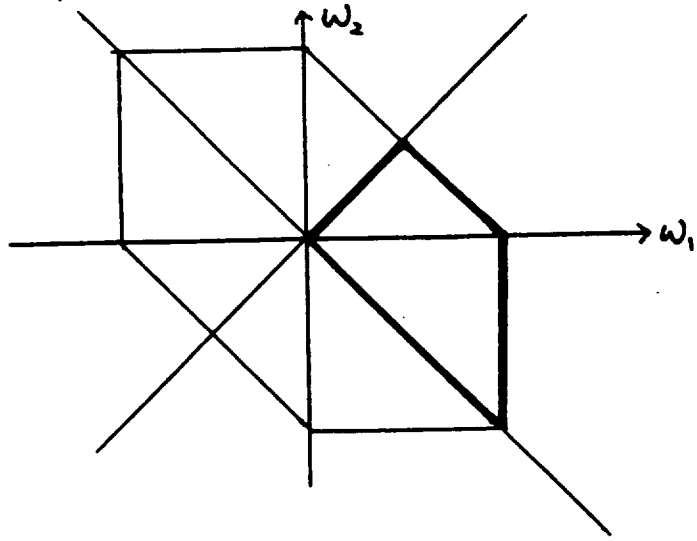

2-5 System Identification for Quadratic Time Invariant (QTI) system:

INPUT/OUTPUT RELATIONSHIP:

Let x(t) be zero-mean, and y(t) be the output of a quadratic system:

$$x(t) \longrightarrow \boxed{\; g(t1,t2),\ G(w1,w2) \;} \longrightarrow y(t)$$

$G(w1,w2)$ = Quadratic Transfer Function (QTF) = $FT\{\, g(t1,t2) \,\}$

$$G(w1,w2) = \int\int g(t1,t2)\, \exp[j\,(w1t1+w2t2)]\, dt1\, dt2$$

Note: . $G(w1,w2) = G^{*}(w2,w1)$

. $G(w1,w2) = G(-w1,-w2)$

. $Y(0) = \int G(a,-a)\, X(a)\, X(-a)\, da$

$$\Longrightarrow E[y(t)] = E[Y(0)] = \int G(a,-a)\, E[X(a)X(-a)]\, da$$

$$= \int G(a,-a)\, Sxx(a)\, da$$

$$y(t) = x(t) ** g(t1,t2) = \iint x(t-a)x(t-b)\, g(a,b)\, da\, db$$

$$= \int\int g(a,b) \int X(w1)\exp[-j(t-a)w1]dw1 \int X(w2)\exp[-j(t-b)w2]dw2\, da\, db$$

$$= \int\int \{\iint g(a,b)\, \exp[j(aw1+bw2)]\, da\, db\}\, X(w1)X(w2)\exp[-j(w1+w2)t]\, dw1\, dw2$$

$$= \int\int G(w1,w2)\, X(w1)X(w2)\exp[-j(w1+w2)t]\, dw1\, dw2$$

$$Y(w) = \int\int G(w1,w2)\, X(w1)X(w2)\, FT\{\, \exp[-j(w1+w2)t] \,\}\, dw1\, dw2$$

$$= \int\int G(w1,w2)\, X(w1)X(w2)\, \delta(w-w1-w2)\, dw1\, dw2$$

$$= \int G(w1,w-w1)\, X(w1)X(w-w1)\, dw1$$

$$\Longrightarrow \boxed{\; Y(w) = \int G(a,w-a)\, X(a)X(w-a)\, da \;}$$

QTF IDENTIFICATION:

$$B_{xxy}(w_1,w_2) = E[\,X(w_1)\,X(w_2)\,Y(-w_1-w_2)\,]$$

$$= E[\,X(w_1)\,X(w_2)\,Y(-w_1-w_2)\,] - E[\,X(w_1)\,X(w_2)\,]\,E[\,Y(-w_1-w_2)\,]$$
$$- E[X(w_1)Y(-w_1-w_2)]\,E[X(w_2)] - E[X(w_2)Y(-w_1-w_2)]\,E[X(w_1)]$$

$$= E\left[X(w_1)X(w_2)\int G(a,-w_1-w_2-a)X(a)X(-w_1-w_2-a)\,da\right]$$
$$- E[X(w_1)X(w_2)]\,E[Y(-w_1-w_2)]$$

$$= \int G(a,-w_1-w_2-a)\,E[X(w_1)X(w_2)X(a)X(-w_1-w_2-a)]\,da$$
$$- E[X(w_1)X(w_2)]\,E[Y(-w_1-w_2)]$$

$$= \int G(a,-w_1-w_2-a)\{\,E[\,X(w_1)\,X(a)\,]\,E[\,X(w_2)\,X(-w_1-w_2-a)]$$
$$+ E[\,X(a)\,X(w_2)\,]\,E[\,X(w_1)\,X(-w_1-w_2-a)]$$
$$+ E[\,X(w_1)\,X(w_2)]\,E[\,X(a)\,X(-w_1-w_2-a)\,]\,\}\,da$$
$$- E[\,X(w_1)X(w_2)]\,E[Y(-w_1-w_2)]$$

$$= \int G(a,-w_1-w_2-a)\{\,E[\,X(w_1)\,X(a)\,]\,E[\,X(w_2)\,X(-w_1-w_2-a)]\,\delta(w_1+a)$$
$$+ E[\,X(a)\,X(w_2)\,]\,E[\,X(w_1)\,X(-w_1-w_2-a)]\,\delta(w_2+a)$$
$$+ E[\,X(w_1)\,X(w_2)]\,E[\,X(a)\,X(-w_1-w_2-a)\,]\,\delta(w_1+w_2)\}\,da$$
$$- E[\,X(w_1)X(w_2)]\,E[Y(-w_1-w_2)]\qquad\delta(w_1+w_2)$$

$$= G(-w_1,-w_2)\,S_{xx}(w_1)\,S_{xx}(w_2) + G(-w_2,-w_1)\,S_{xx}(w_2)\,S_{xx}(w_1)$$
$$+ S_{xx}(w_1)\int G(a,-a)\,S_{xx}(a)\,da - S_{xx}(w_1)\quad E[y(t)]$$

$$= 2\,S_{xx}(w_1)\,S_{xx}(w_2)\,G(w_1,w_2) + S_{xx}(w_1)\{\int G(a,-a)\,S_{xx}(a)\,da - E[y(t)\,\}$$

$$= 2\,S_{xx}(w_1)\,S_{xx}(w_2)\,G(w_1,w_2)$$

$$\Longrightarrow\quad \boxed{G^{\star}(w_1,w_2) = \frac{B_{xxy}(w_1,w_2)}{2\,S_{xx}(w_1)\,S_{xx}(w_2)}}$$

EXAMPLE:

If x(t) is zero-mean Gaussian White Noise (GWN), and Sxx(w) = 1

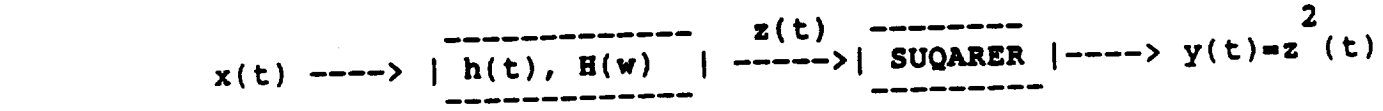

I/O relationship ==> $Y(w) = \int G(a,w-a)\, X(a)X(w-a)\, da$

$y(t) = z(t)\, z(t)$ ==> $Y(w) = \int Z(a)Z(w-a)\, da = \int H(a)H(w-a)\, X(a)X(w-a)\, da$

===> $G(w1,w2) = H(w1)\, H(w2) = \overset{*}{B}xxy(w1,w2)/2$

w1=w2=w ===> $H^2(w) = \overset{*}{B}xxy(w,w)/2$ ===> $H(w) = \{\, 0.5\, \overset{*}{B}xxy(w,w) \,\}^{0.5}$

SIMULATION EXAMPLE FOR AUTO-BICOHERENCE

$$\begin{cases} X_1(t) = \cos(W_1 t + \phi_1) + \cos(W_2 t + \phi_2) + \cos\left[(W_1 + W_2)t + (\phi_1 + \phi_2)\right] + N_1(t) \\ X_2(t) = \cos(W_1 t + \phi_1) + \cos(W_2 t + \phi_2) + \cos\left[(W_1 + W_2)t + \phi_3\right] + N_2(t) \\ X_3(t) = \cos(W_1 t + \phi_1) + \cos(W_2 t + \phi_2) + 0.5\cos\left[(W_1 + W_2)t + (\phi_1 + \phi_2)\right] + \\ \qquad 0.5\cos\left[(W_1 + W_2)t + \phi_3\right] + N_3(t) \end{cases}$$

Where: $\begin{cases} \phi_1, \phi_2, \phi_3 \text{ are random phase} \\ N_1, N_2, N_3 \text{ are independent GWN} \end{cases}$

$\begin{cases} X_1(t) = (W_1, W_2, W_3) \text{ are perfectly correlated} \\ X_2(t) = (W_1, W_2, W_3) \text{ are independent} \\ X_3(t) = 50\% \text{ Power at } W_3 \text{ are correlated with } W_1 \text{ and } W_2 \\ \qquad \text{the remaining } 50\% \text{ power at } W_3 \text{ are independent of } W_1 \text{ and } W_2 \end{cases}$

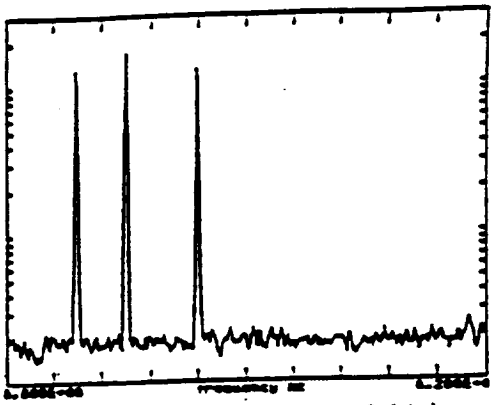

PSD S(W) of x1(t)

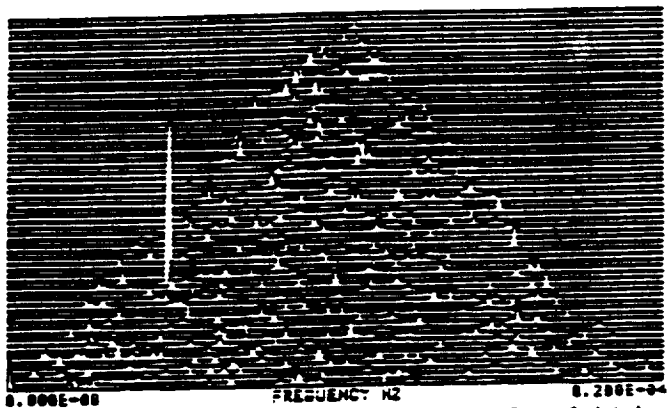

ABC B(W1,W2) of x1(t)

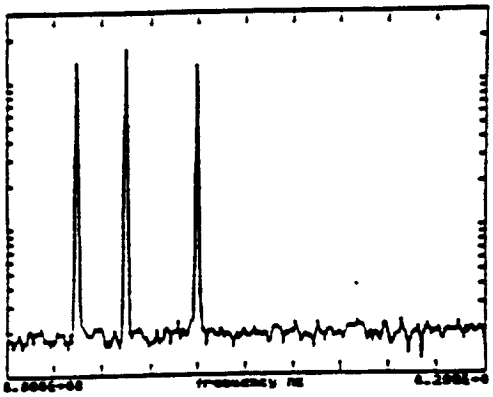

PSD S(W) of x2(t)

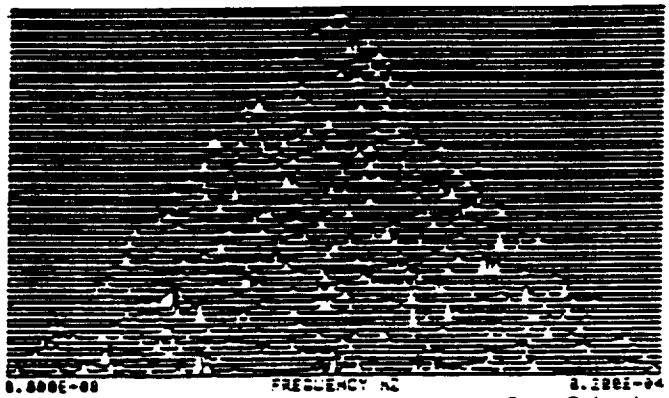

ABC B(W1,W2) of x2(t)

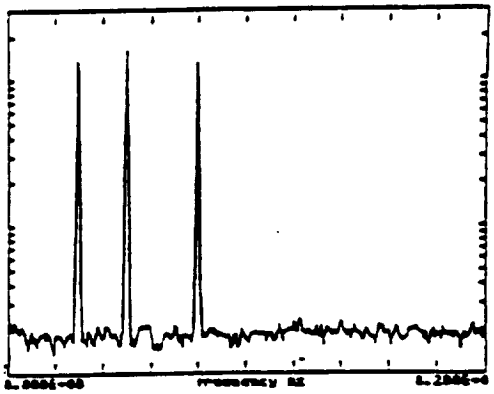

PSD S(W) of x3(t)

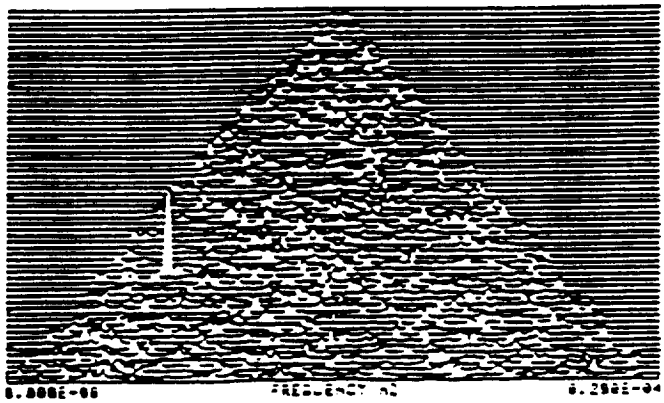

ABC B(W1,W2) of x3(t)

CROSS-BI-COHENERCE SIMULATION

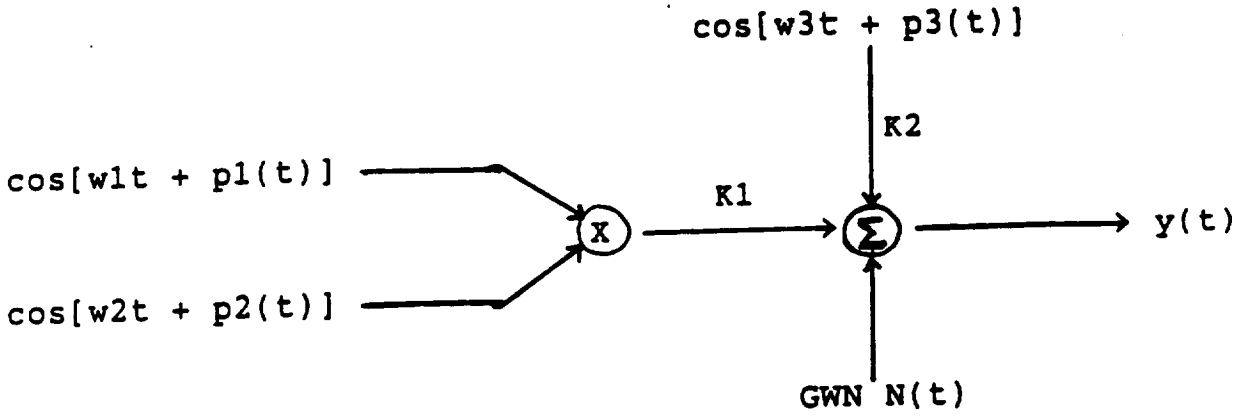

w3=w1+w2
p1(t), p2(t), p3(t) are independent slowly varying phase
N(t), N1(t), N2(t), N3(t) are independent Gaussian White Noise

INPUT: $x(t) = \cos[w1t + p1(t)] + \cos[w2t + p2(t)] + N(t)$

OUTPUT 1: $y1(t) = \cos[w1t + p1(t)] \times \cos[w2t + p2(t)] + N1(t)$
(K1=1 K2=0)

OUTPUT 2: $y2(t) = \cos[w3t + p3(t)] + N2(t)$
(K1=0 K2=1)

OUTPUT 3: $y3(t) = \cos[w1t + p1(t)] \times \cos[w2t + p2(t)] + 0.5 \cos[w3t + p3(t)] + N3(t)$
(K1=1 K2=0.5)

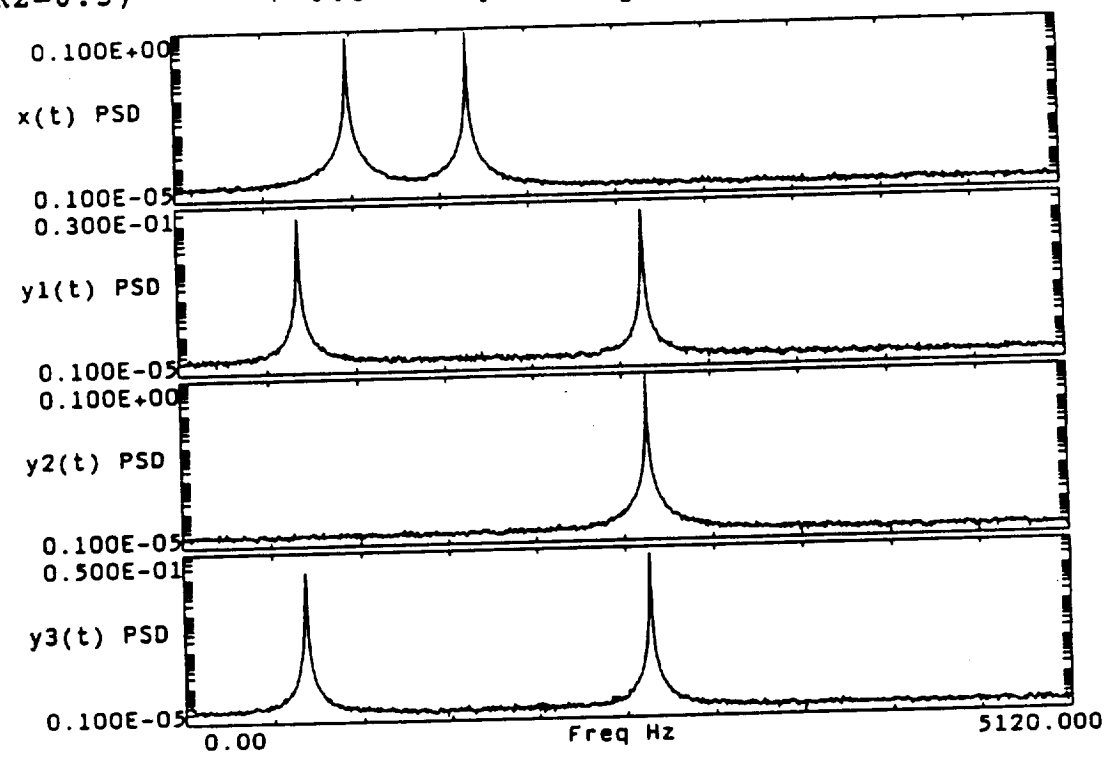

BW=5 Hz Navg=64

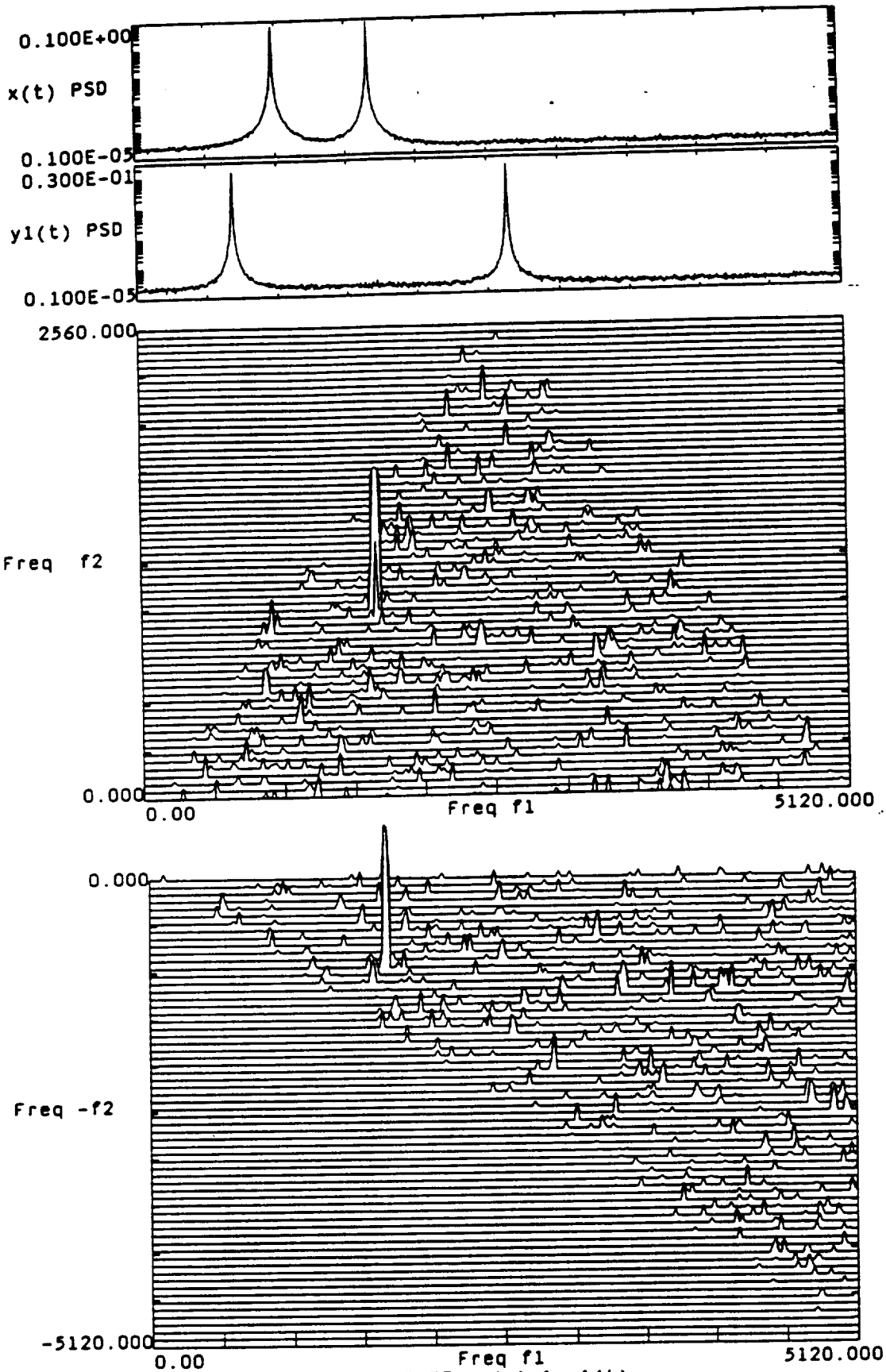

CROSS-BI-COHERENCE BETWEEN x(y) & y1(t)
Bxxy1(f1, -f2)

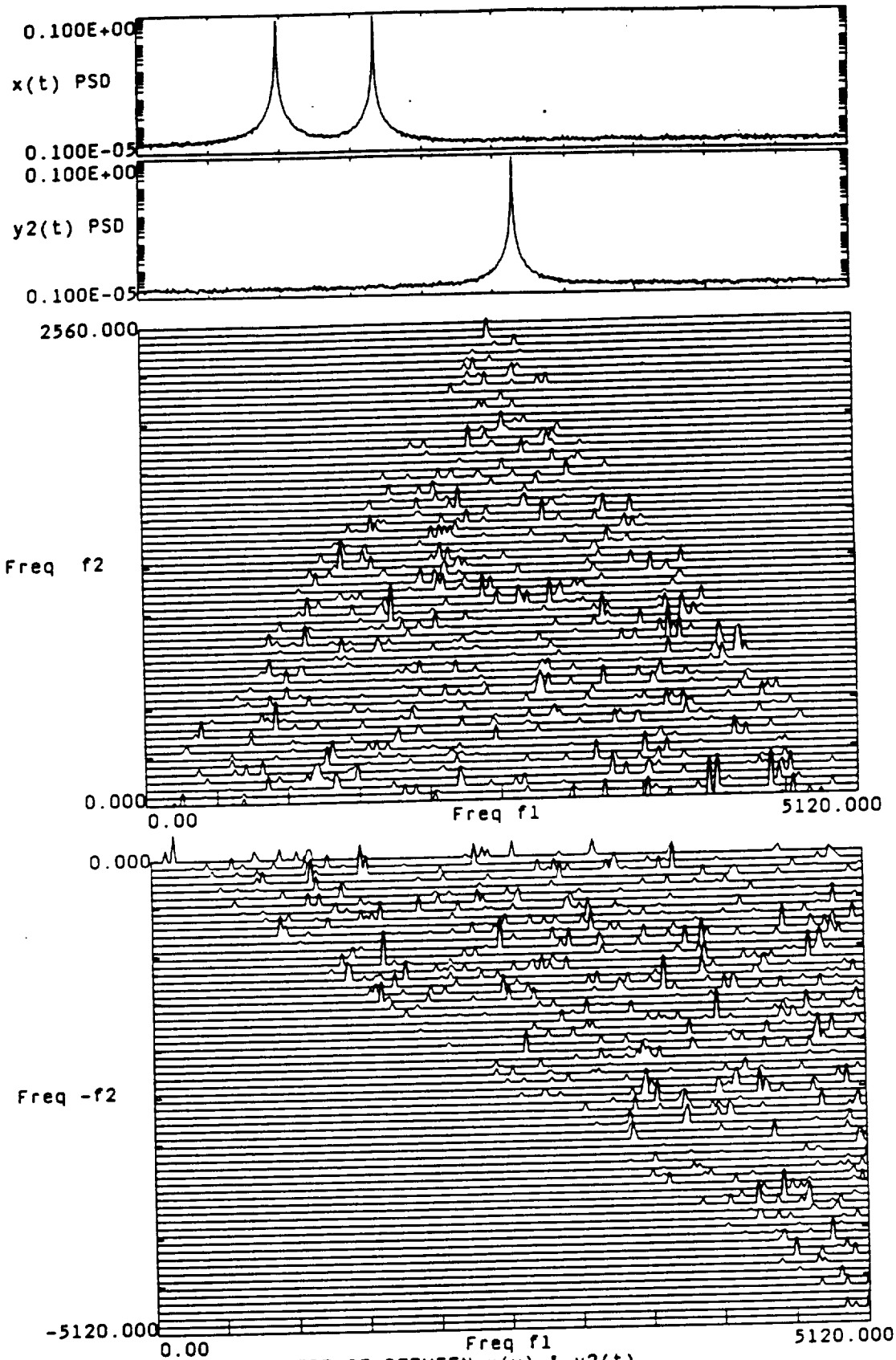

CROSS-BI-COHERENCE BETWEEN x(y) & y2(t)
Bxxy2(f1, -f2)

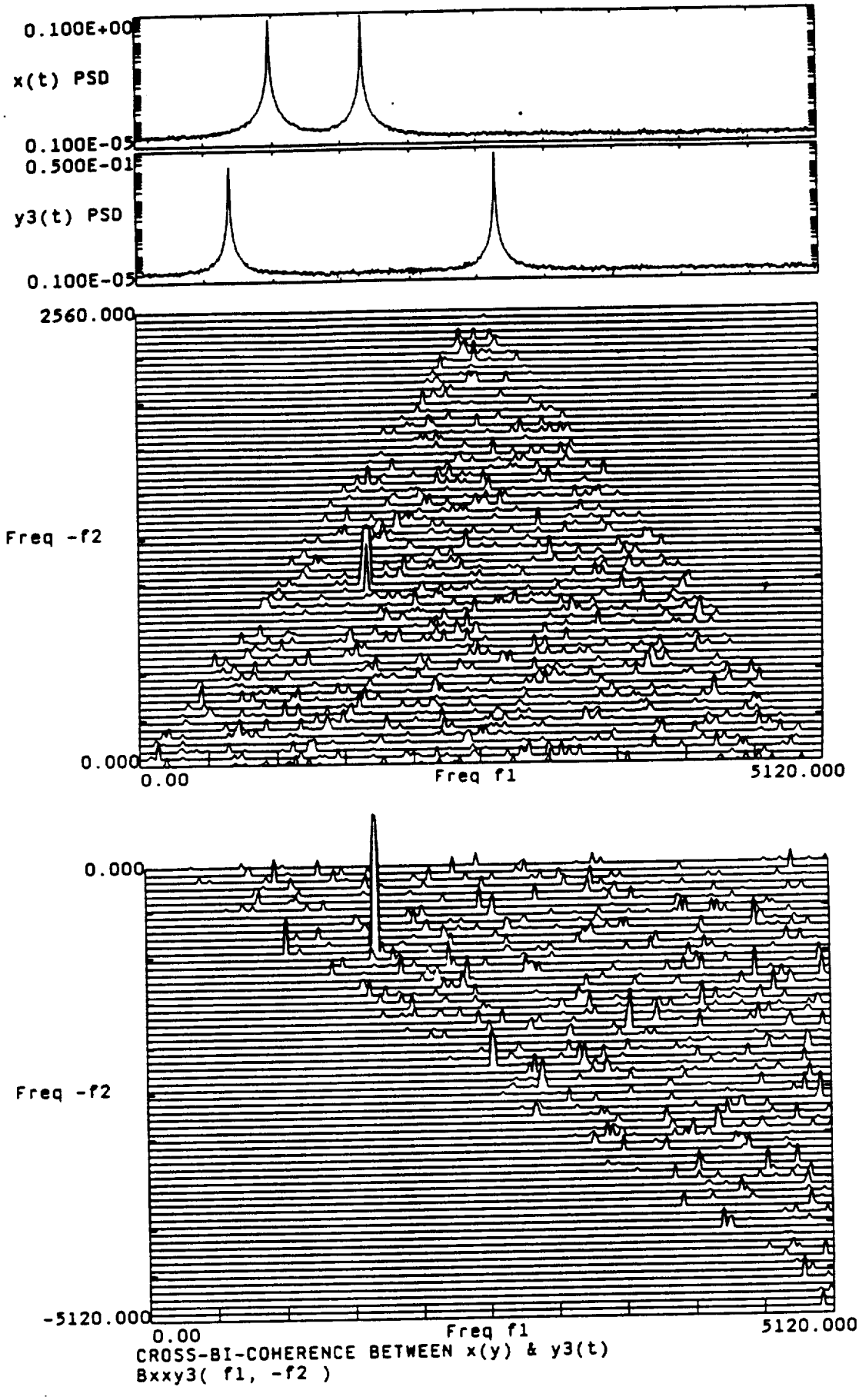
0.100E+00
x(t) PSD
0.100E-05
0.500E-01
y3(t) PSD
0.100E-05
2560.000
Freq -f2
0.000
0.00
Freq f1
5120.000
0.000
Freq -f2
-5120.000
0.00
Freq f1
5120.000
CROSS-BI-COHERENCE BETWEEN x(y) & y3(t)
Bxxy3(f1, -f2)

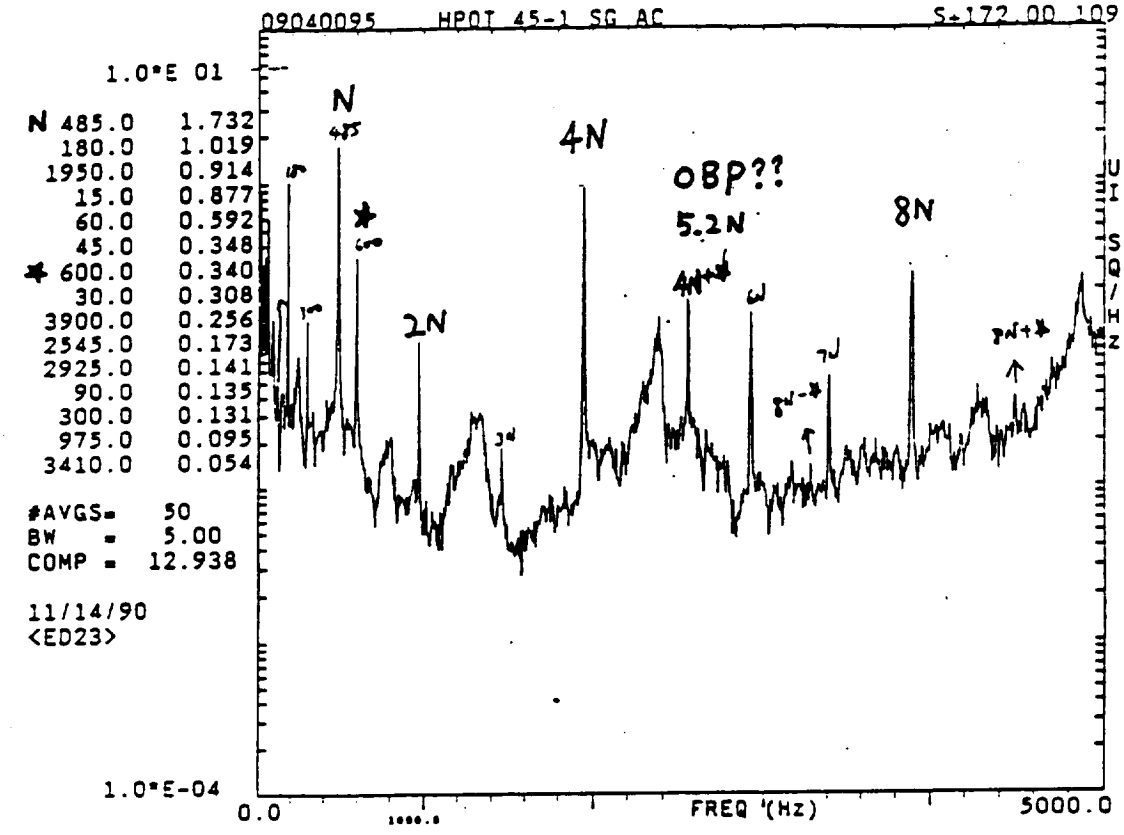
09040095 HPOT 45-1 SG AC
S+172.00 109.
1.0*E 01
N 485.0 1.732
180.0 1.019
1950.0 0.914
15.0 0.877
60.0 0.592
45.0 0.348
* 600.0 0.340
30.0 0.308
3900.0 0.256
2545.0 0.173
2925.0 0.141
90.0 0.135
300.0 0.131
975.0 0.095
3410.0 0.054
#AVGS= 50
BW = 5.00
COMP = 12.938
11/14/90
<ED23>
1.0*E-04
0.0
FREQ (Hz)
5000.0
N
4N
OBP??
5.2N
8N
2N
UH SQ/HZ

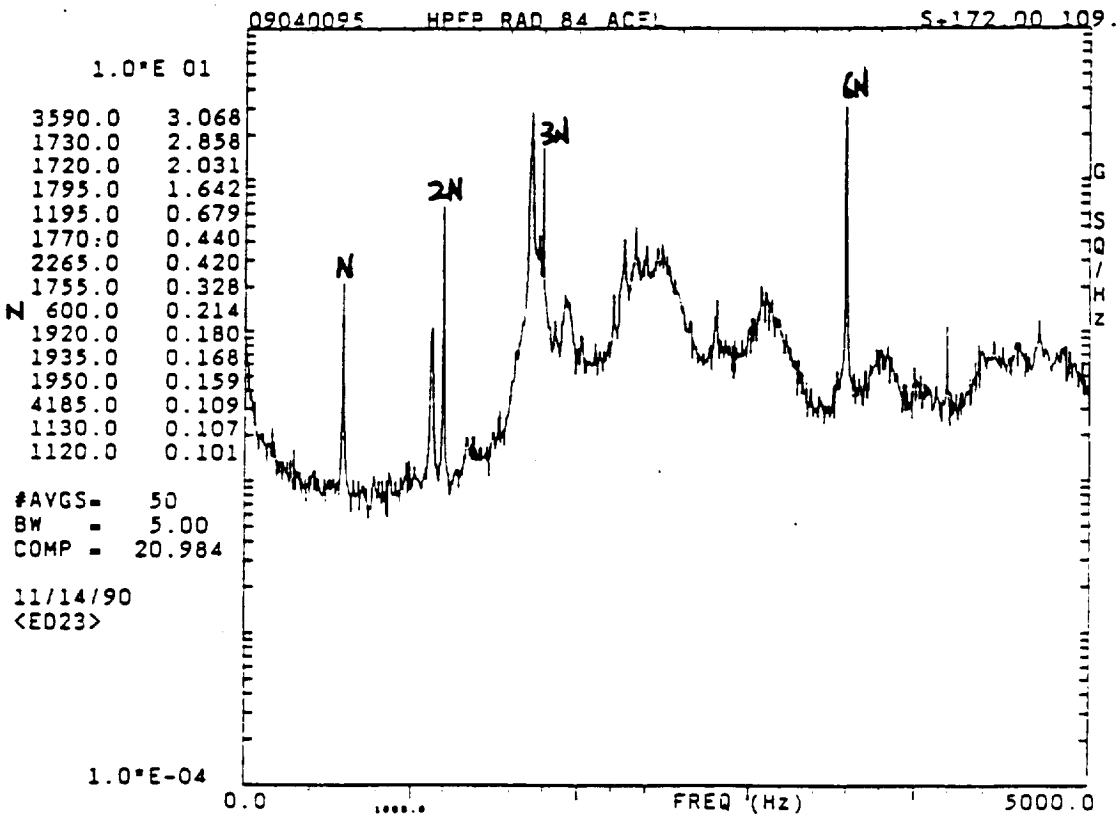
09040095 HPFP RAD 84 ACE
S+172.00 109.
1.0*E 01
3590.0 3.068
1730.0 2.858
1720.0 2.031
1795.0 1.642
1195.0 0.679
1770.0 0.440
2265.0 0.420
1755.0 0.328
N 600.0 0.214
1920.0 0.180
1935.0 0.168
1950.0 0.159
4185.0 0.109
1130.0 0.107
1120.0 0.101
#AVGS= 50
BW = 5.00
COMP = 20.984
11/14/90
<ED23>
1.0*E-04
0.0
FREQ (Hz)
5000.0
N
2N
3N
6N
G SQ/HZ

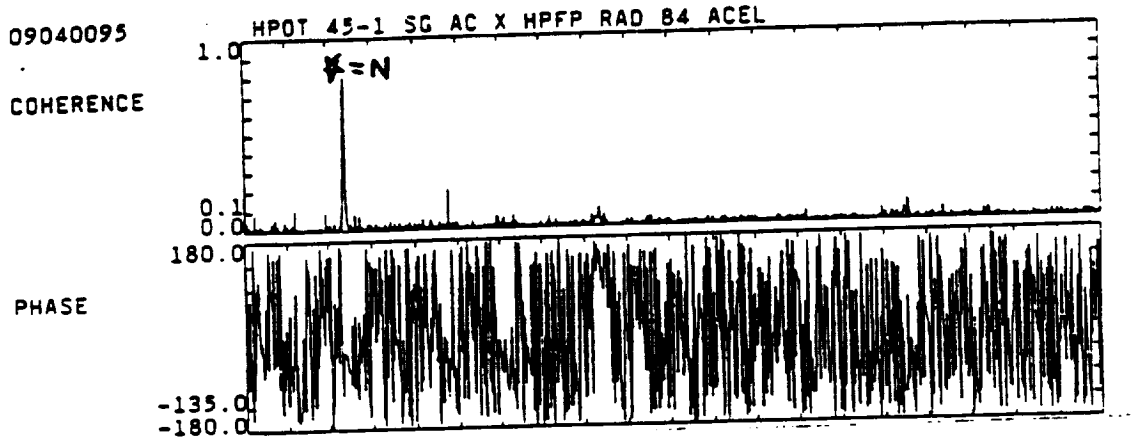
09040095
HPOT 45-1 SG AC X HPFP RAD 84 ACEL
COHERENCE
1.0
0.1
0.0
X=N
PHASE
180.0
-135.0
-180.0

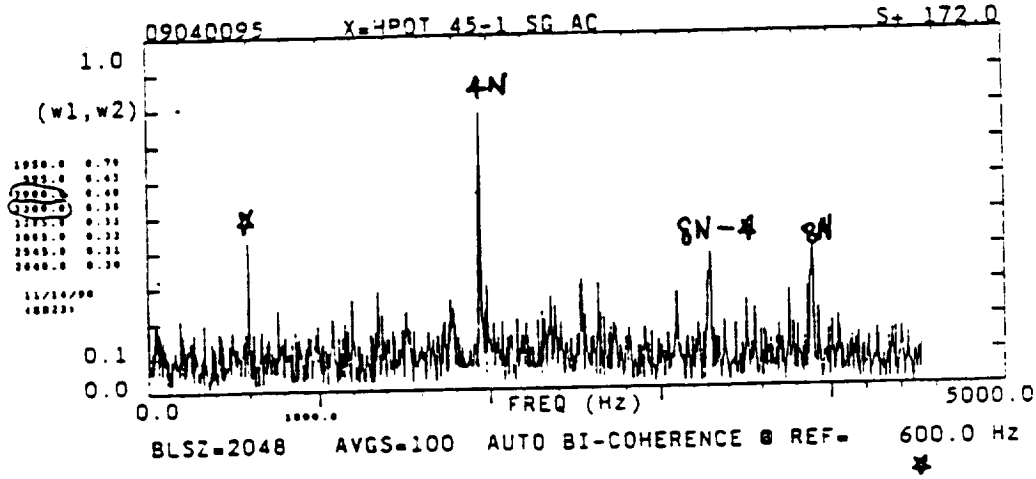
09040095
X=HPOT 45-1 SG AC
S+ 172.0
1.0
(w1,w2)
0.1
0.0
X
4N
8N-4
8N
0.0
FREQ (Hz)
5000.0
BLSZ=2048 AVGS=100 AUTO BI-COHERENCE @ REF= 600.0 Hz

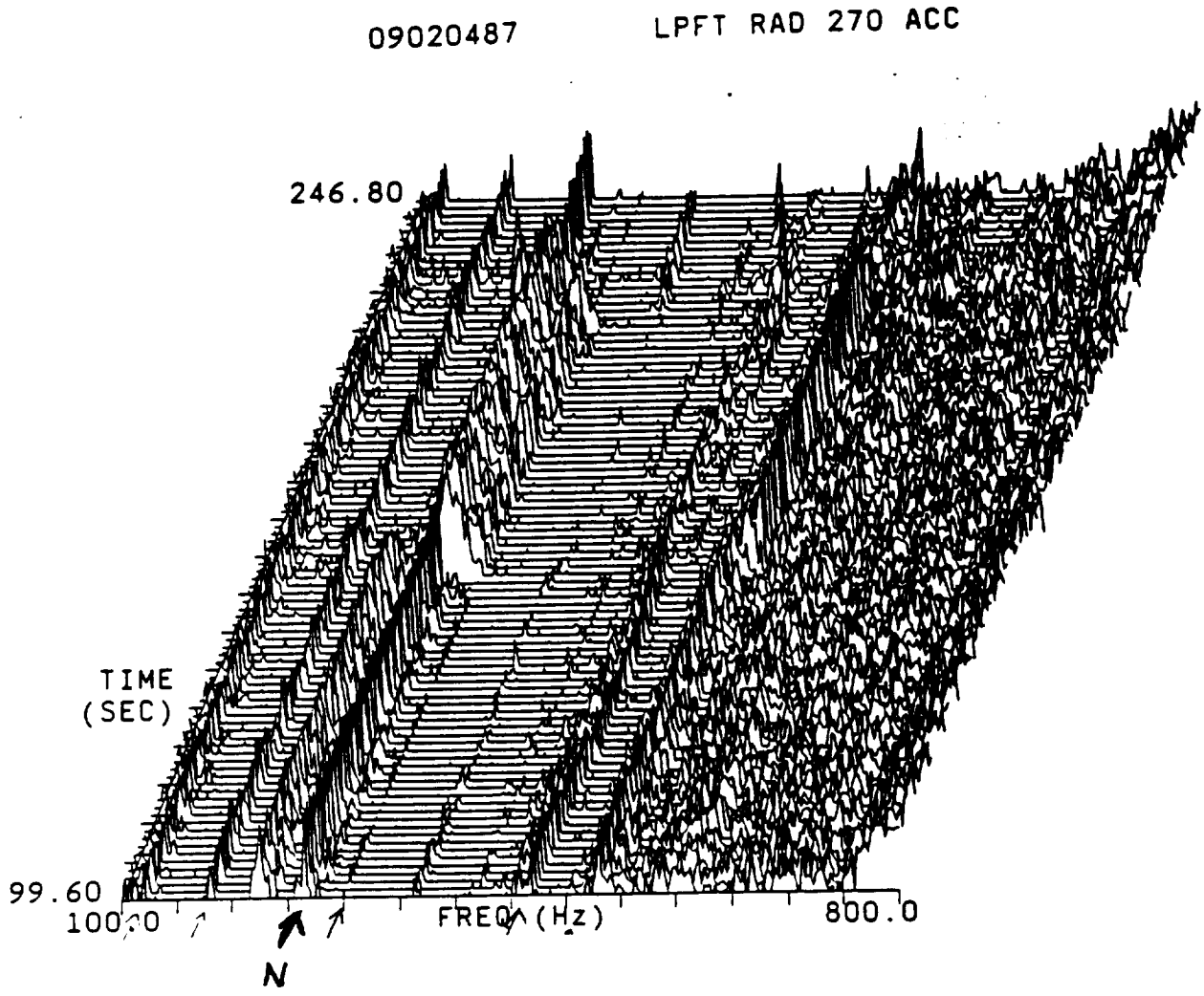
09020487
LPFT RAD 270 ACC
246.80
TIME
(SEC)
99.60
100.0
FREQ (Hz)
800.0
N

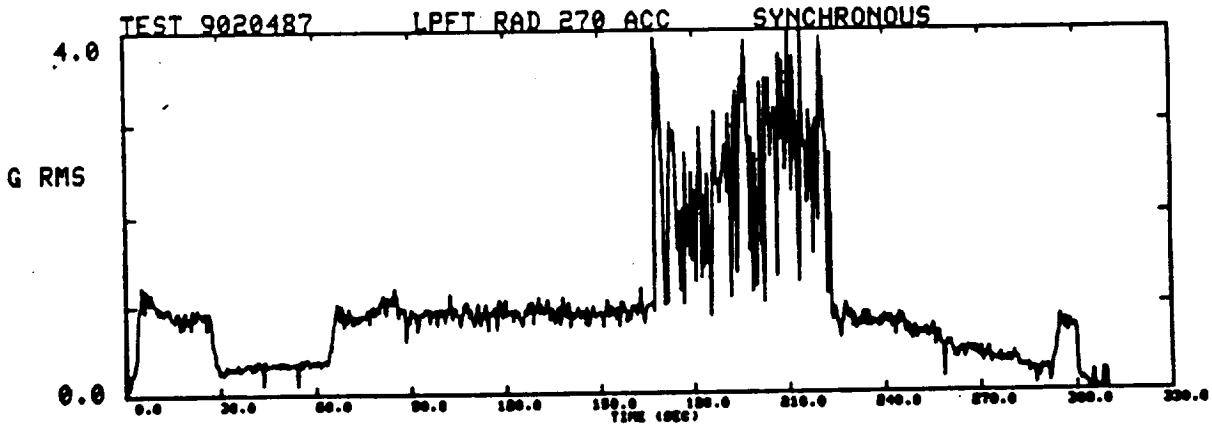
TEST 9020487
LPFT RAD 270 ACC
SYNCHRONOUS
4.0
G RMS
0.0
TIME (SEC)

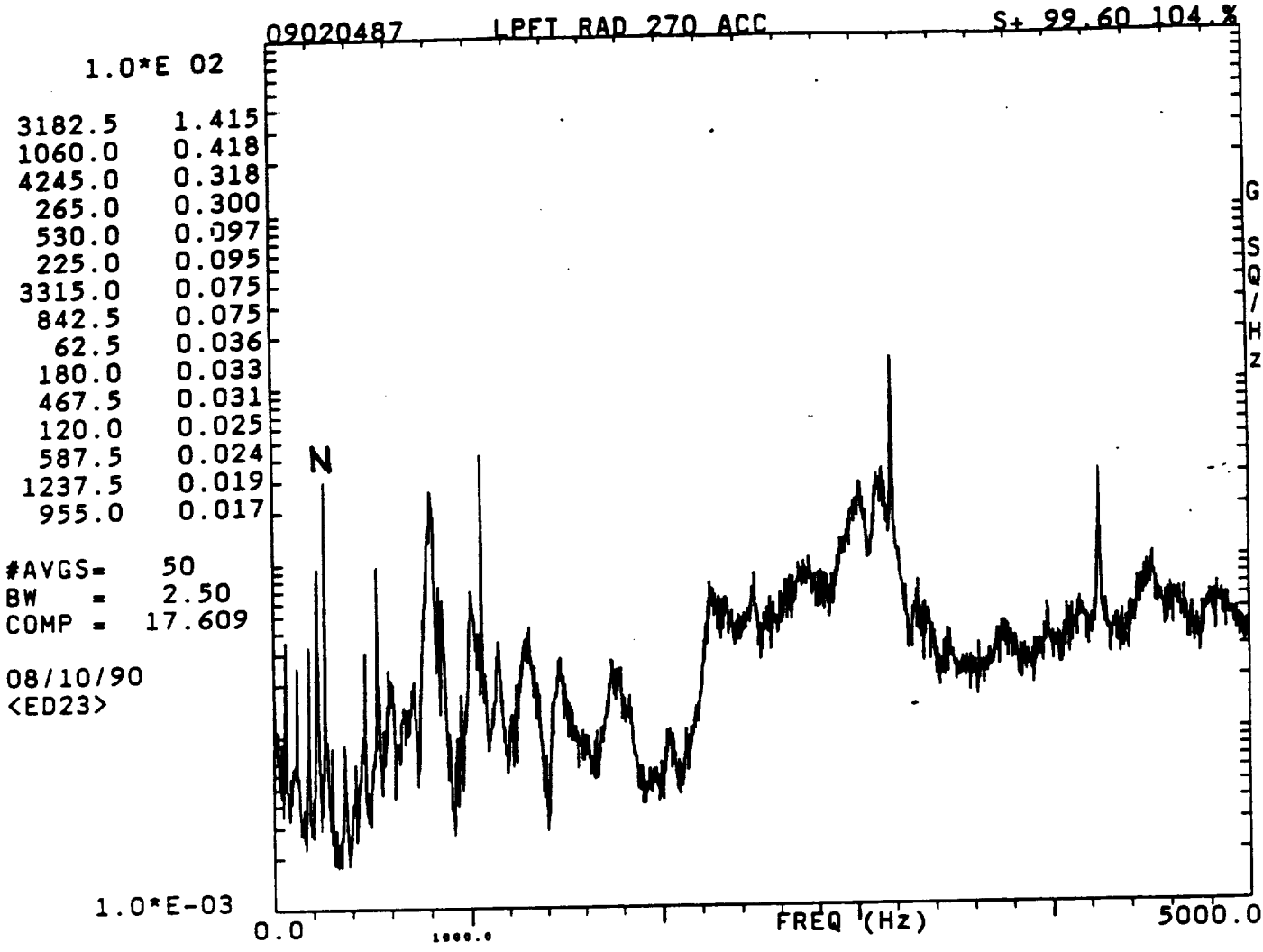
09020487 LPFT RAD 270 ACC S+ 99.60 104.%
1.0*E 02
3182.5 1.415
1060.0 0.418
4245.0 0.318
265.0 0.300
530.0 0.097
225.0 0.095
3315.0 0.075
842.5 0.075
62.5 0.036
180.0 0.033
467.5 0.031
120.0 0.025
587.5 0.024
1237.5 0.019
955.0 0.017
#AVGS= 50
BW = 2.50
COMP = 17.609
08/10/90
<ED23>
N
1.0*E-03
0.0
1000.0
FREQ (Hz)
5000.0
G
SQ/Hz

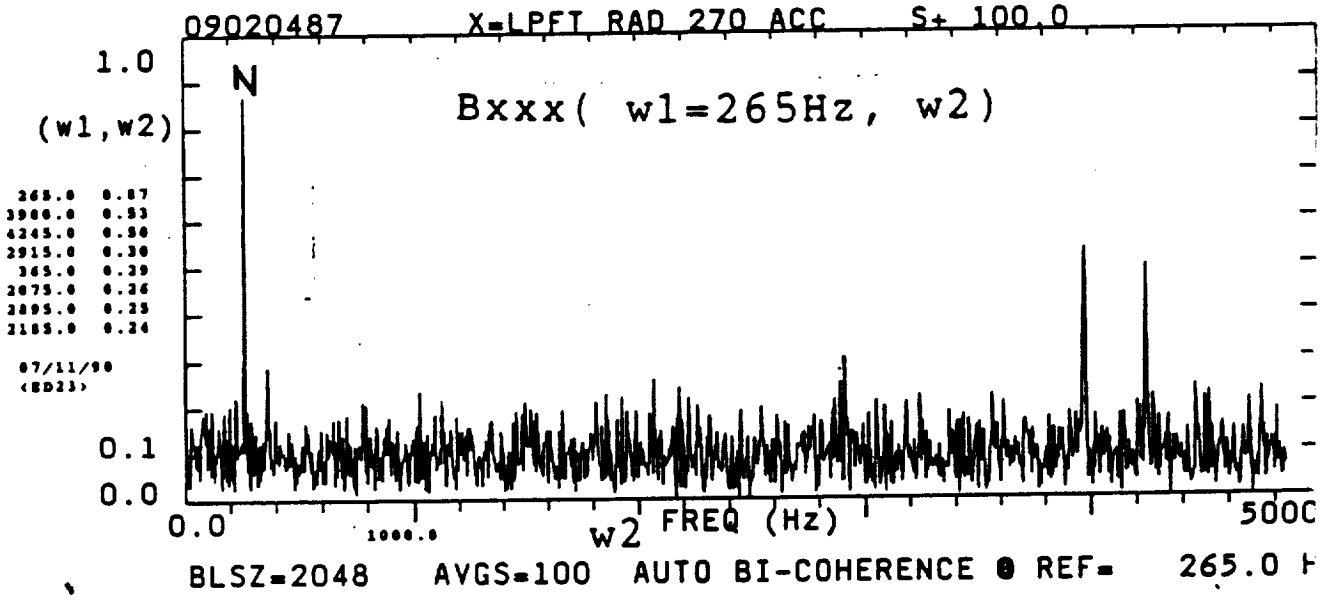
09020487 X=LPFT RAD 270 ACC S+ 100.0
1.0
(w1,w2)
N
Bxxx(w1=265Hz, w2)
265.0 0.87
3980.0 0.53
4245.0 0.50
2915.0 0.30
265.0 0.29
2075.0 0.26
2385.0 0.25
2185.0 0.24
07/11/90
<ED23>
0.1
0.0
0.0
1000.0
w2 FREQ (Hz)
5000
BLSZ=2048 AVGS=100 AUTO BI-COHERENCE @ REF= 265.0 H

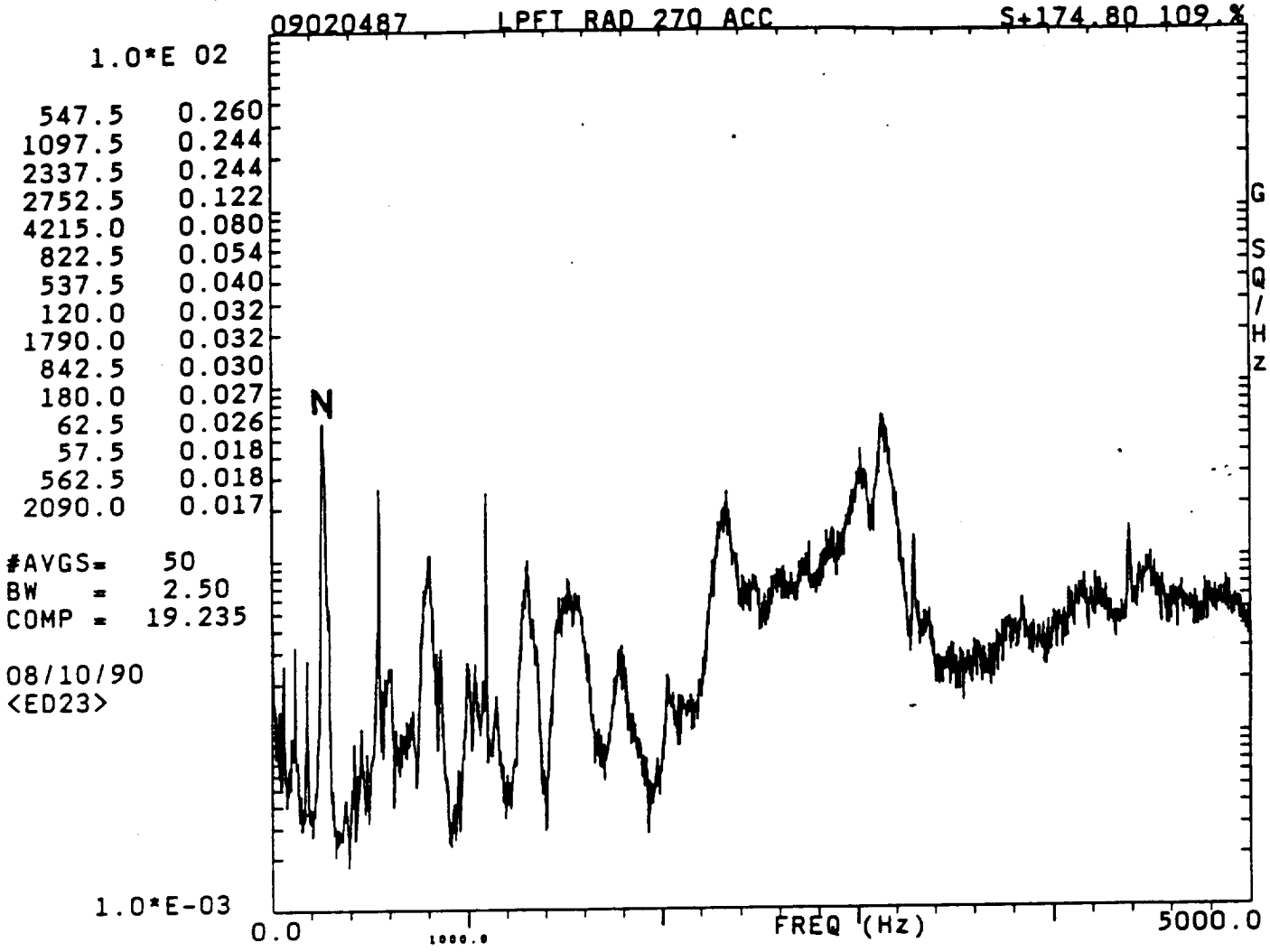
09020487 LPFT RAD 270 ACC S+174.80 109.%
1.0*E 02
547.5 0.260
1097.5 0.244
2337.5 0.244
2752.5 0.122
4215.0 0.080
822.5 0.054
537.5 0.040
120.0 0.032
1790.0 0.032
842.5 0.030
180.0 0.027
62.5 0.026
57.5 0.018
562.5 0.018
2090.0 0.017
#AVGS= 50
BW = 2.50
COMP = 19.235
08/10/90
<ED23>
N
G
S
Q
/
H
z
1.0*E-03
0.0
1000.0
FREQ (Hz)
5000.0

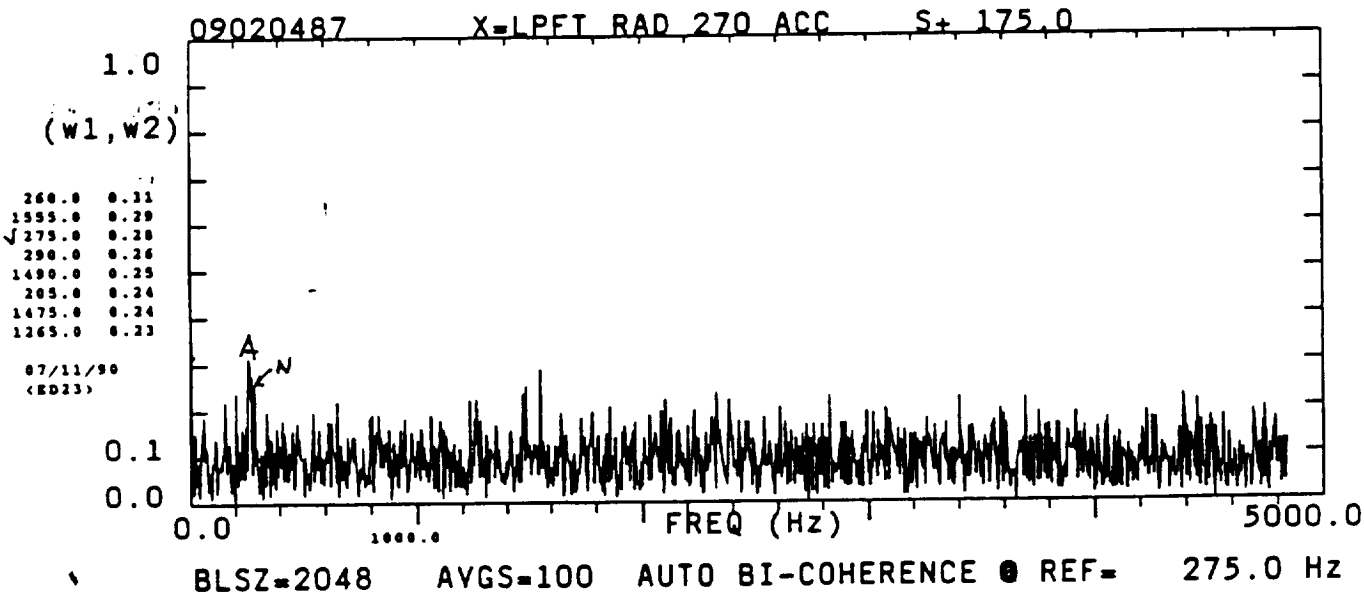
09020487 X=LPFT RAD 270 ACC S+ 175.0
1.0
(w1,w2)
260.0 0.31
1555.0 0.29
275.0 0.28
290.0 0.26
1490.0 0.25
285.0 0.24
1475.0 0.24
1265.0 0.23
07/11/90
<ED23>
A
N
0.1
0.0
0.0
1000.0
FREQ (Hz)
5000.0
BLSZ=2048 AVGS=100 AUTO BI-COHERENCE @ REF= 275.0 Hz

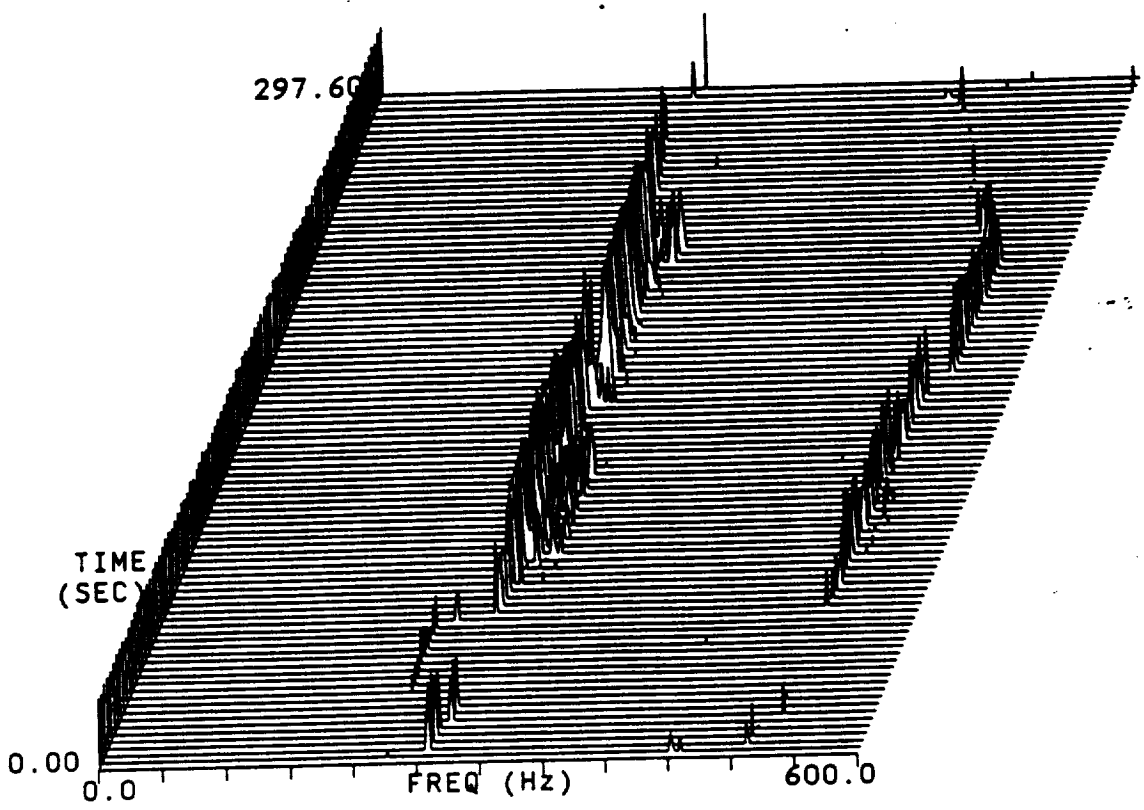
902-501 LPFP LPFT RAD 180
297.60
TIME (SEC)
0.00
0.0
FREQ (Hz)
600.0

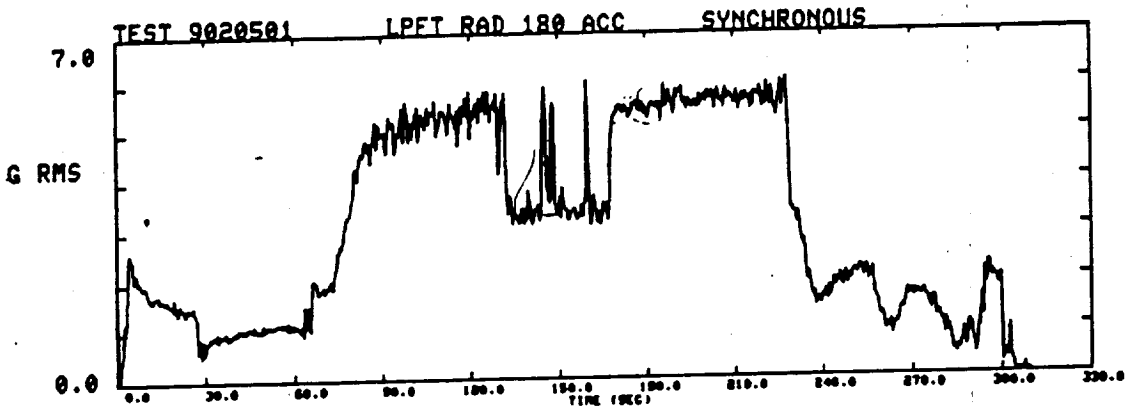
TEST 9020501 LPFT RAD 180 ACC SYNCHRONOUS
7.0
G RMS
0.0
TIME (SEC)

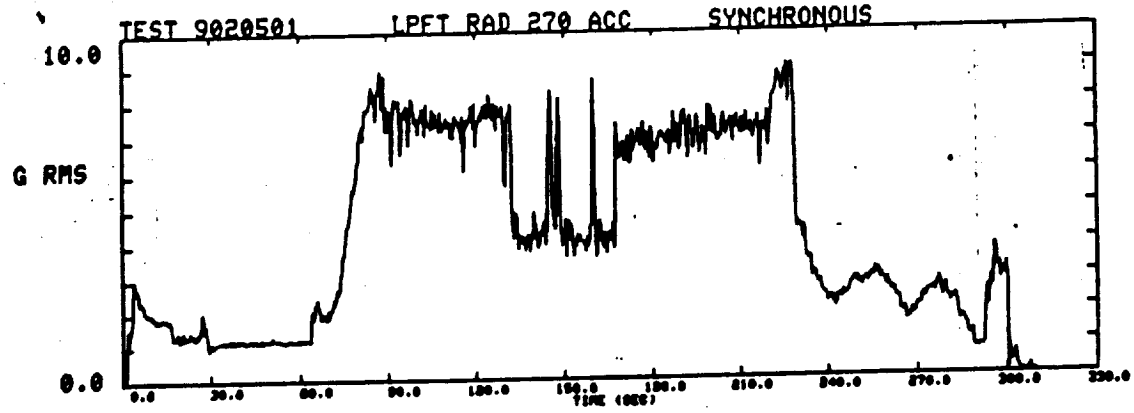
TEST 9020501 LPFT RAD 270 ACC SYNCHRONOUS
10.0
G RMS
0.0
TIME (SEC)

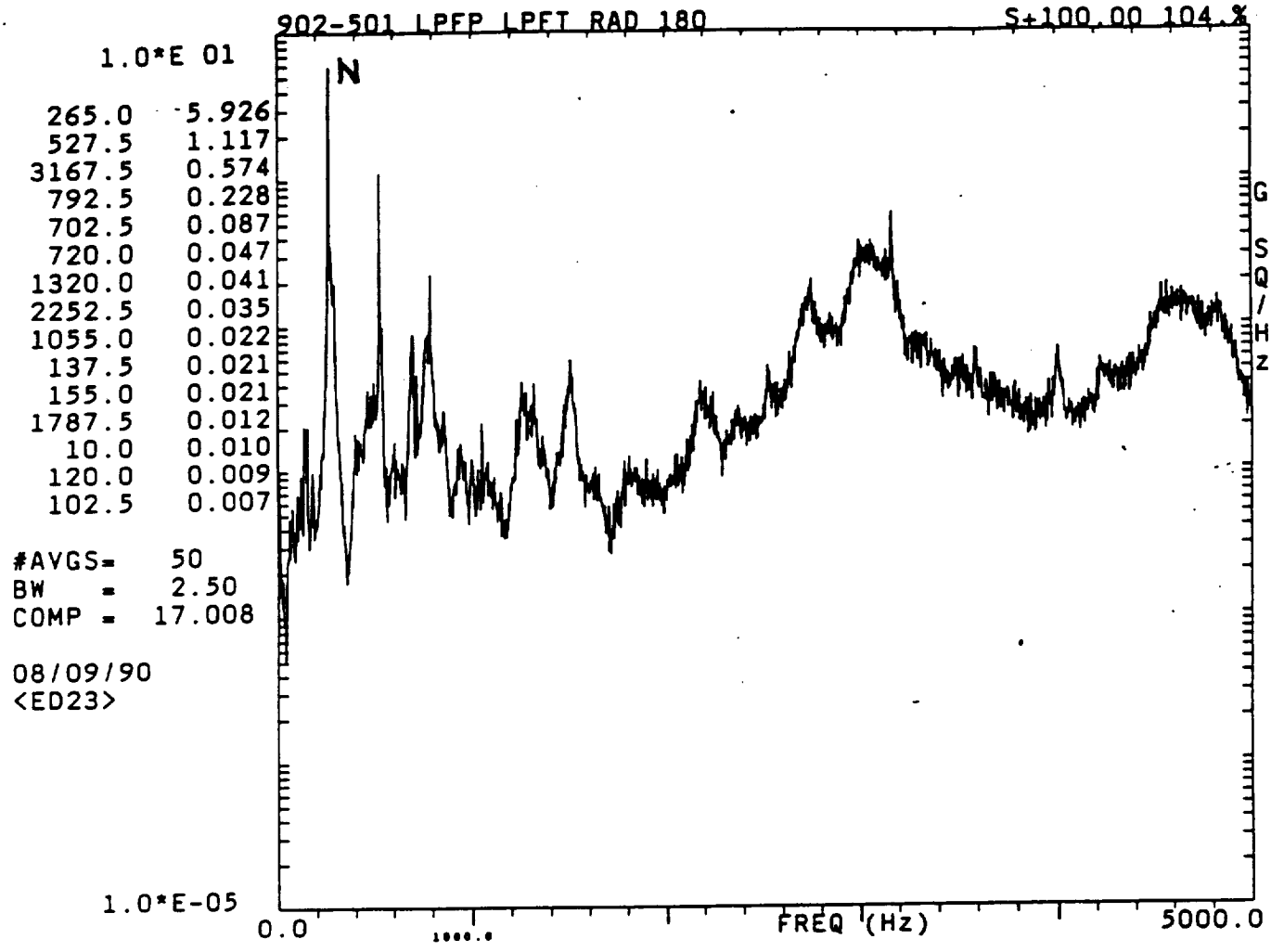
902-501 LPFP LPFT RAD 180
S+100.00 104.%
1.0*E 01
N
265.0 5.926
527.5 1.117
3167.5 0.574
792.5 0.228
702.5 0.087
720.0 0.047
1320.0 0.041
2252.5 0.035
1055.0 0.022
137.5 0.021
155.0 0.021
1787.5 0.012
10.0 0.010
120.0 0.009
102.5 0.007
#AVGS= 50
BW = 2.50
COMP = 17.008
08/09/90
<ED23>
G SQ/HZ
1.0*E-05
0.0
1000.0
FREQ (Hz)
5000.0

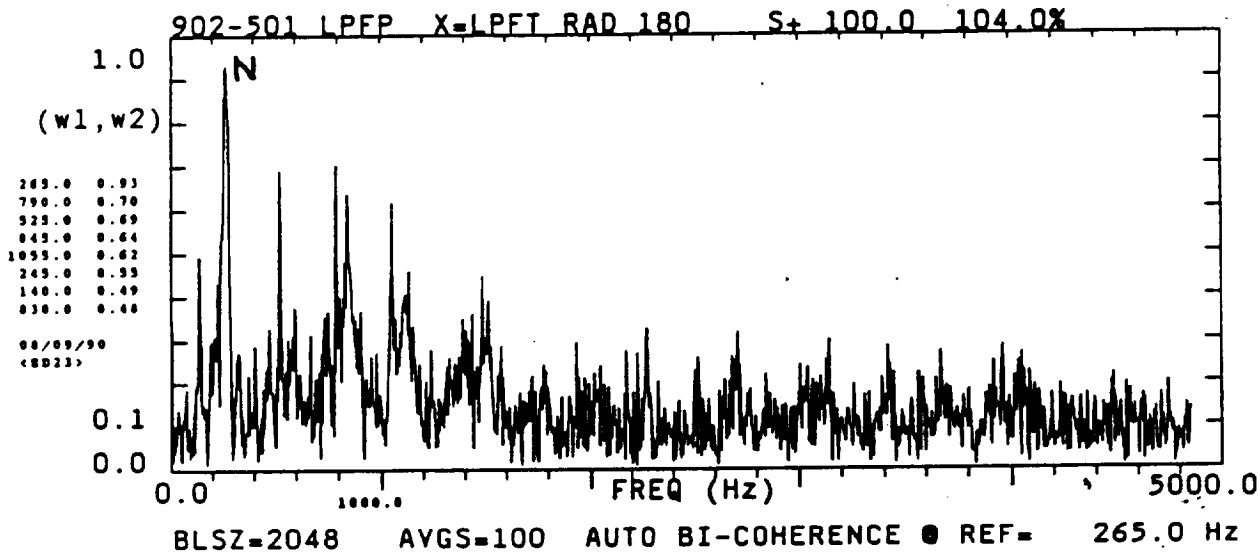
902-501 LPFP X=LPFT RAD 180
S+ 100.0 104.0%
1.0
(w1,w2)
N
0.1
0.0
0.0
1000.0
FREQ (Hz)
5000.0
BLSZ=2048 AVGS=100 AUTO BI-COHERENCE ● REF= 265.0 Hz

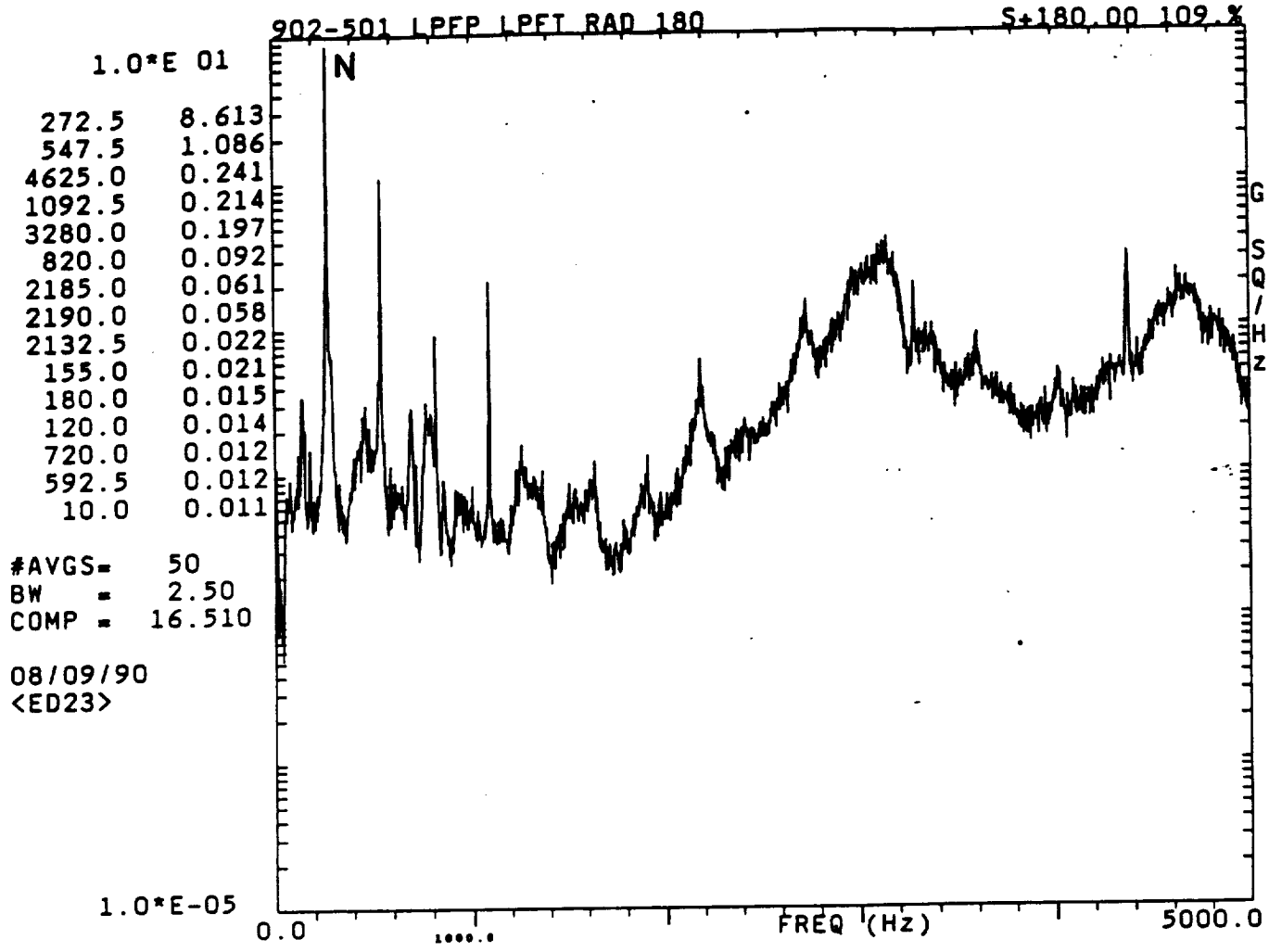
902-501 LPFP LPFT RAD 180
S+180.00 109.%
1.0*E 01
N
272.5 8.613
547.5 1.086
4625.0 0.241
1092.5 0.214
3280.0 0.197
820.0 0.092
2185.0 0.061
2190.0 0.058
2132.5 0.022
155.0 0.021
180.0 0.015
120.0 0.014
720.0 0.012
592.5 0.012
10.0 0.011
#AVGS= 50
BW = 2.50
COMP = 16.510
08/09/90
<ED23>
G
S
Q
/
H
z
1.0*E-05
0.0
1000.0
FREQ (Hz)
5000.0

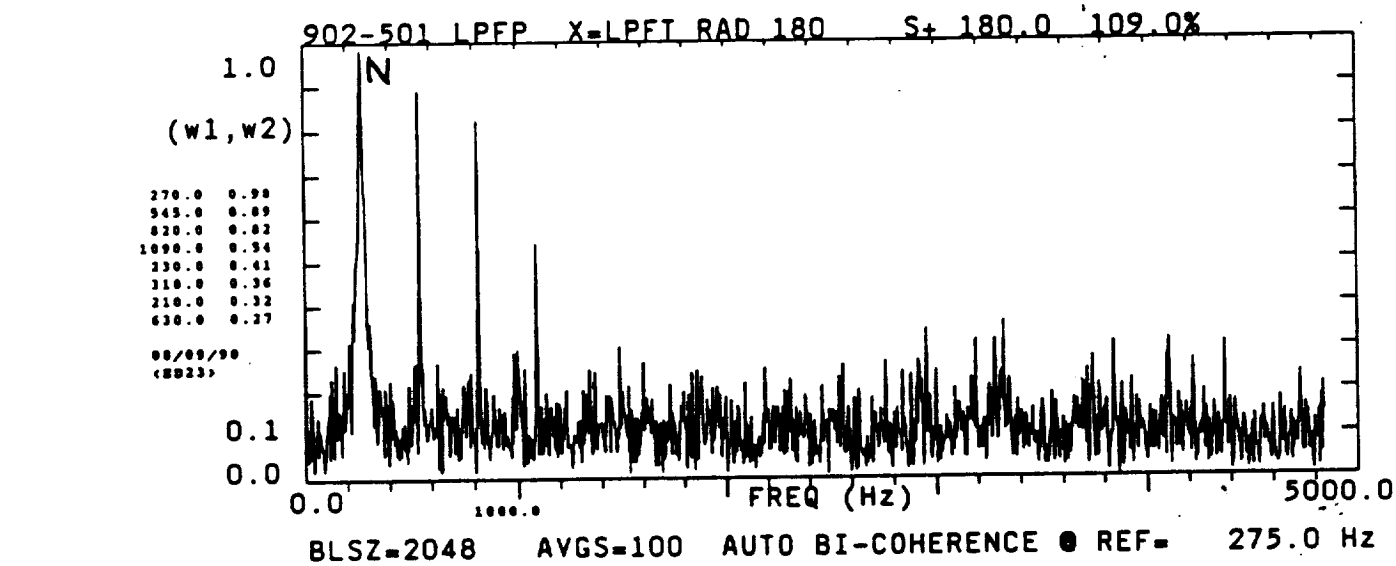
902-501 LPFP X=LPFT RAD 180
S+ 180.0 109.0%
1.0
N
(w1,w2)
0.1
0.0
0.0
1000.0
FREQ (Hz)
5000.0
BLSZ=2048 AVGS=100 AUTO BI-COHERENCE @ REF= 275.0 Hz

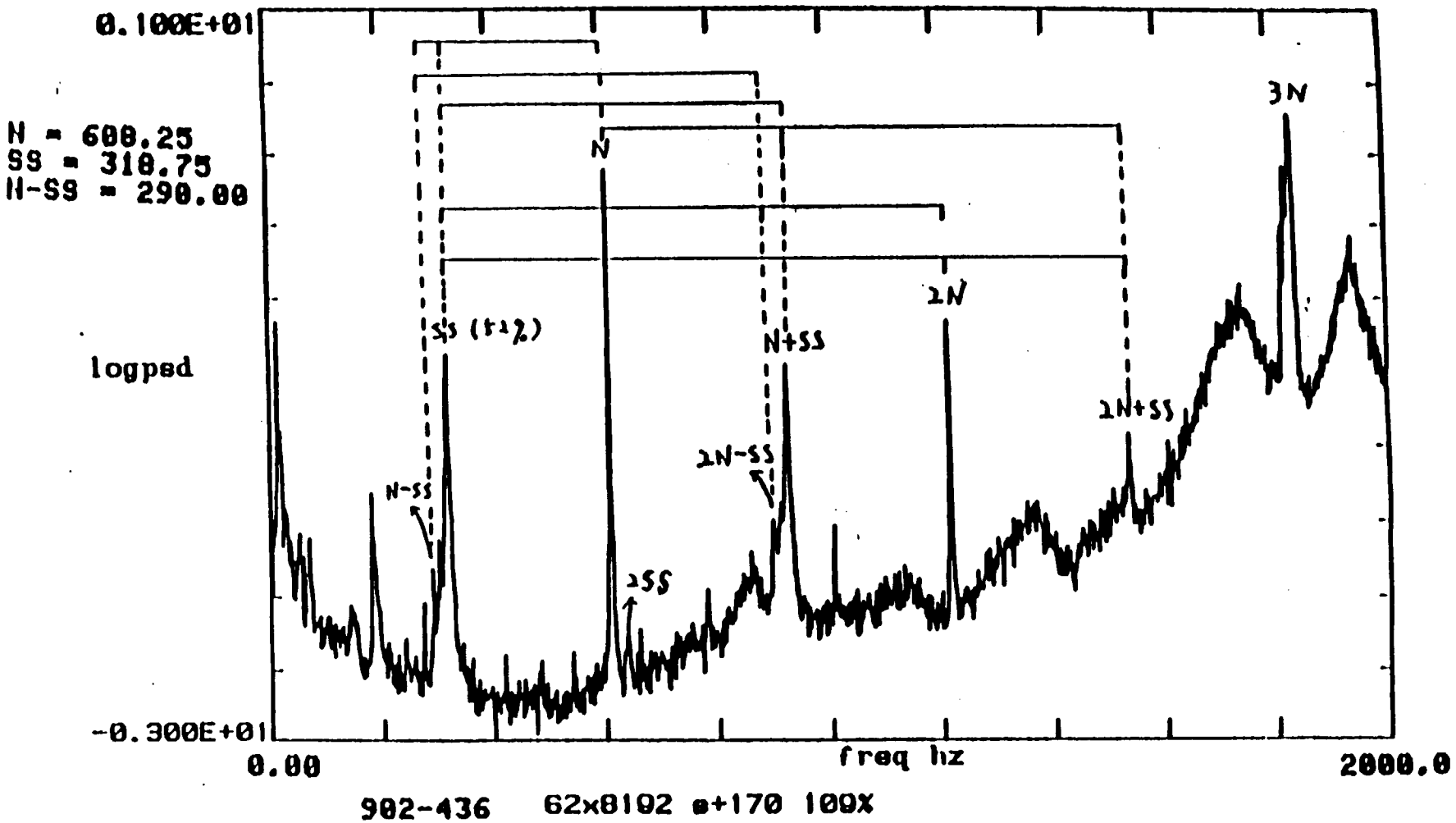
0.100E+01
N = 600.25
SS = 318.75
N-SS = 290.00
logpsd
-0.300E+01
0.00
freq hz
2000.0
N
3N
2N
SS (±2)
N+SS
2N+SS
2N-SS
N-SS
2SS
902-436 62x8192 e+170 100X

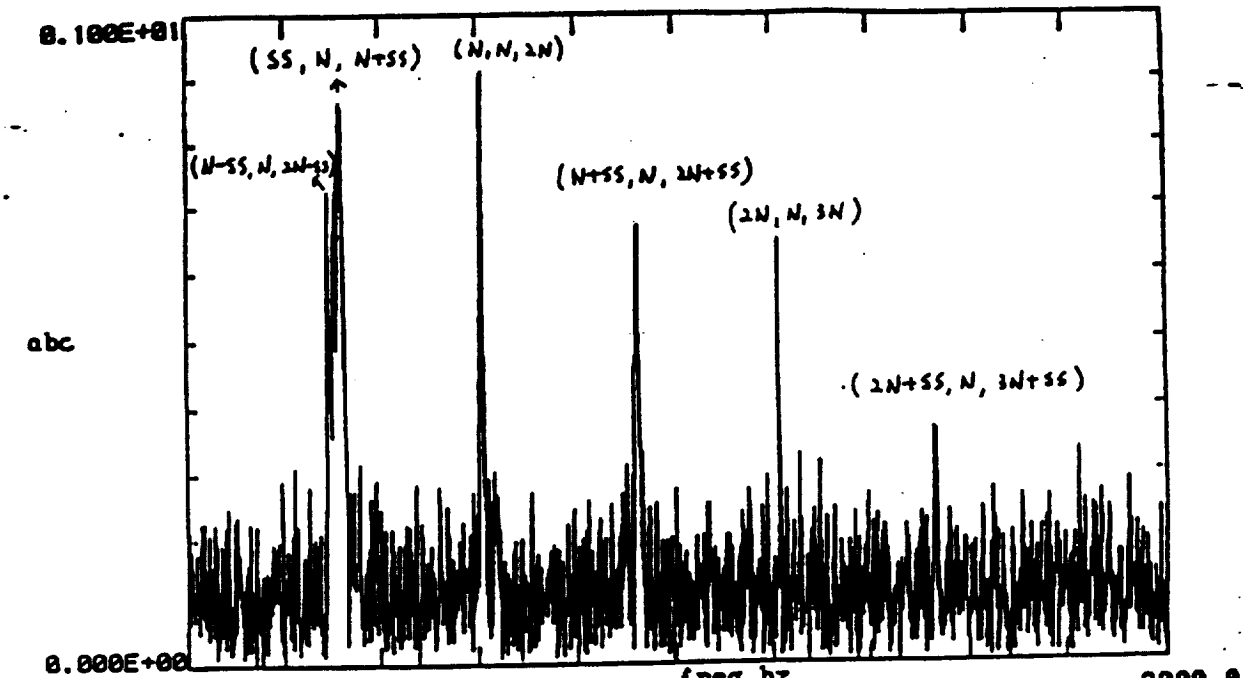

902-436 Bxxx(f , 608.75) 62x8192 e+170 100x

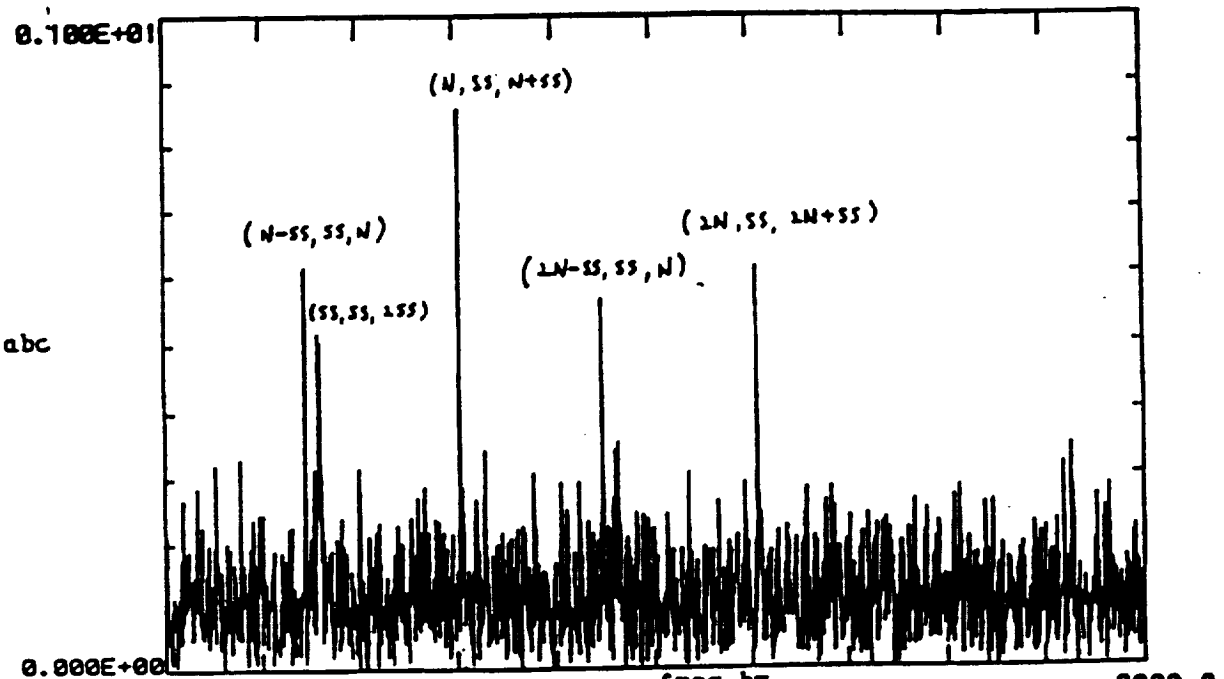

902-436 Bxxx(f , 318.75) 62x8192 e+170 100x

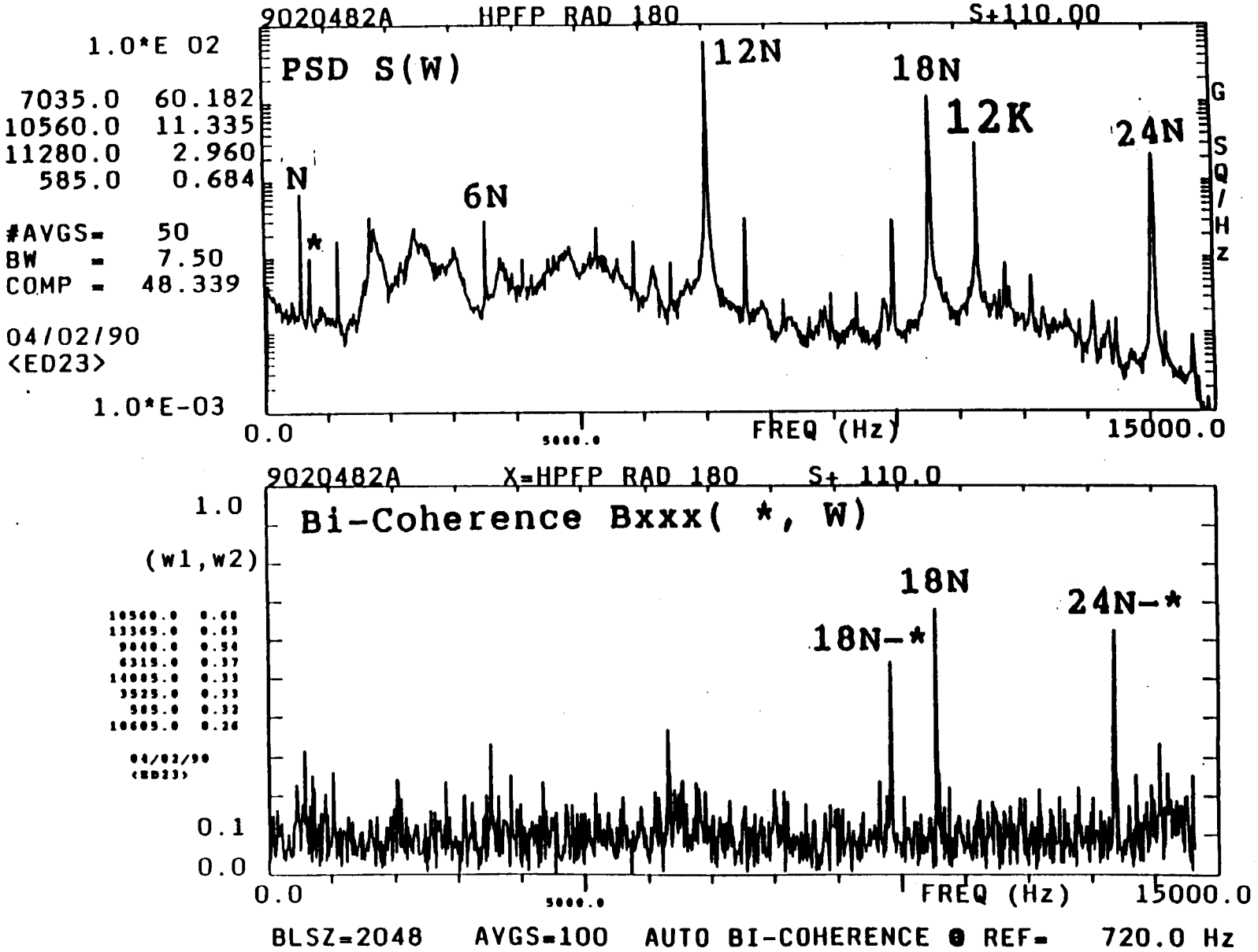
9020482A HPFP RAD 180 S+110.00
1.0*E 02
PSD S(W)
12N
18N
12K
24N
N
6N
*
7035.0 60.182
10560.0 11.335
11280.0 2.960
585.0 0.684
#AVGS= 50
BW = 7.50
COMP = 48.339
04/02/90
<ED23>
1.0*E-03
G
S
Q
/
H
z
0.0
FREQ (Hz)
15000.0
9020482A X=HPFP RAD 180 S+ 110.0
1.0
Bi-Coherence Bxxx(*, W)
(w1,w2)
18N
24N-*
18N-*
0.1
0.0
0.0
FREQ (Hz)
15000.0
BLSZ=2048 AVGS=100 AUTO BI-COHERENCE @ REF= 720.0 Hz

NONLINEAR SPECTRAL ANALYSIS METHODS FOR SSME DIAGNOSTICS

by

Jen-Yi Jong

October 1990

for

Structures and Dynamics Laboratory
Marshall Space Flight Center

Contract NAS8-38156

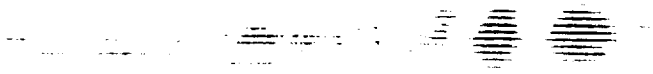

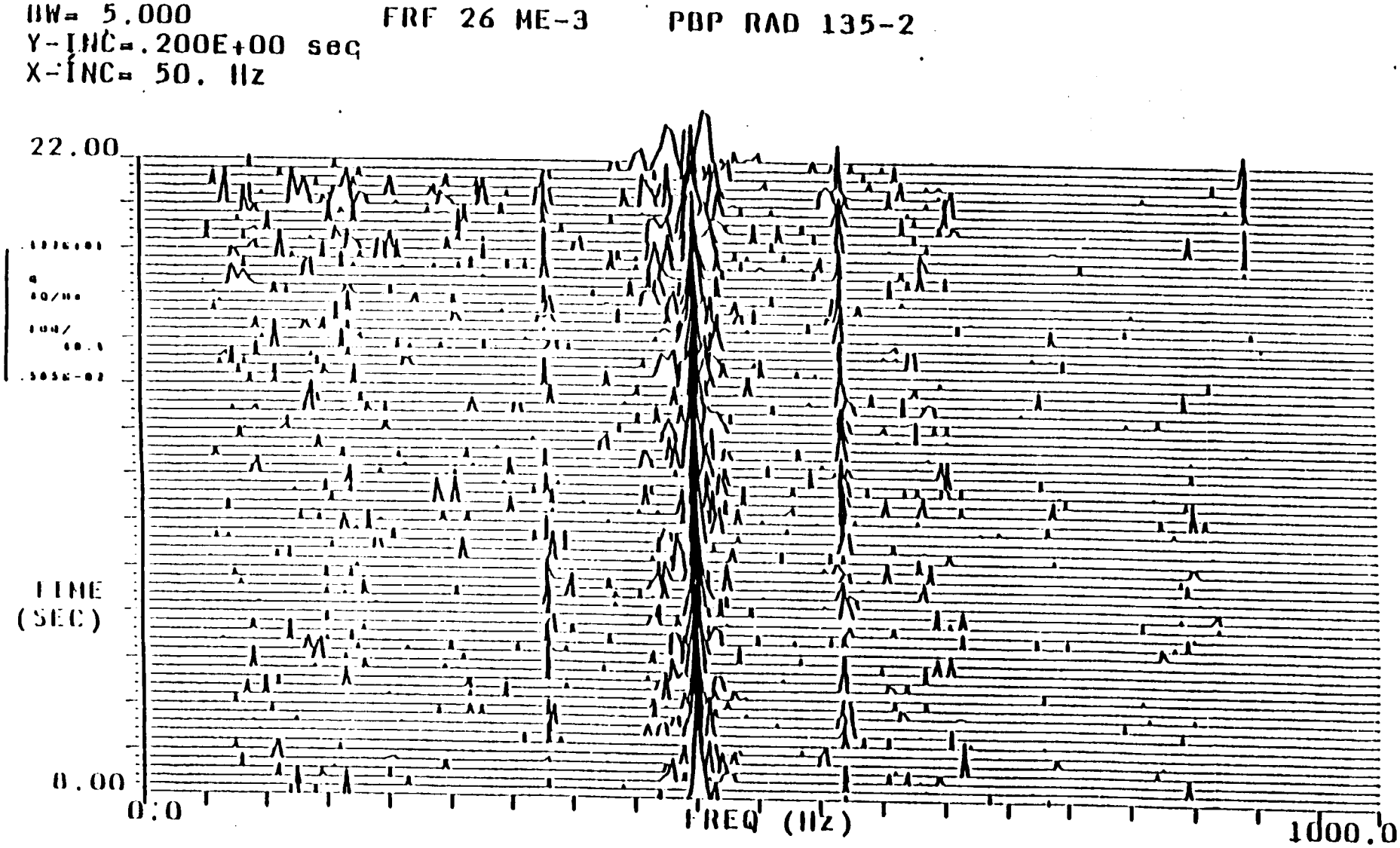

FIGURE 50. ISOPLOT OF PREBURNER PUMP RADIAL (135-2) ACCEL. FROM TEST FRF-26 ON ME-3

(1) SIDE-BAND PSD STRUCTURE DUE TO MODULATION:

Consider a vibration signal due to periodic impact on a structure with resonant freq Wc

e.g. cage frequency component periodically excite a structure mode at its natural frequency (or a sensor's natural frequecy)

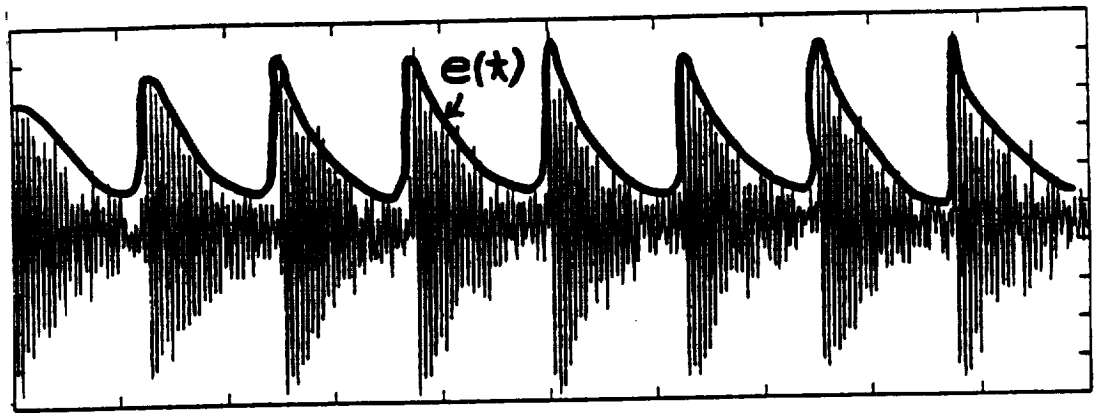

Time Domain model: $x(t) = e(t) \cos[\, Wct + p(t) \,]$

- e(t) = envelope = periodic impact signal with dominant frequency We
- cos[Wct+pt(t)] = carrier = structural response at natural frequency Wc

Frequency Domain: ===> Side-Band Structure (Wc-We, Wc, Wc+We)

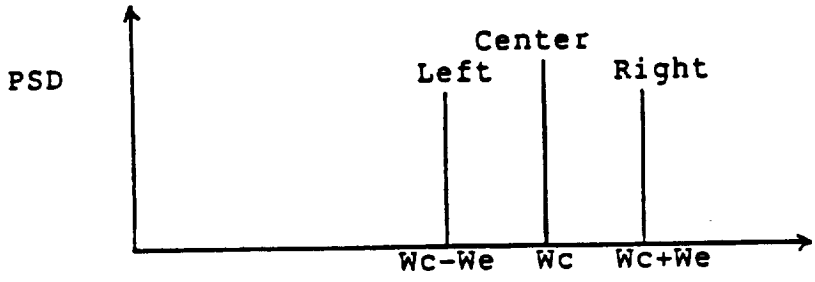

(2) Envelope Detection :

$$\begin{cases} \text{measured signal: } x(t) = e(t)\cos[Wct + p(t)] \\ \text{90 phase shift: } y(t) = e(t)\sin[Wct + p(t)] \end{cases} \Longrightarrow \text{envelope } e(t) = \sqrt{x^2(t) + y^2(t)}$$

. Hilbert Transform:

$$y(t) = HT[\,x(t)\,] = x(t) * h(t) \quad \Longleftrightarrow \quad Y(w) = X(w)\;H(w)$$

$$H(w) = \text{90 phase shiftor} = -j\,\text{sgn}(w) = \begin{cases} -j = \exp(-j\,pi/2) & \text{for } w > 0 \\ +j = \exp(+j\,pi/2) & \text{for } w < 0 \end{cases}$$

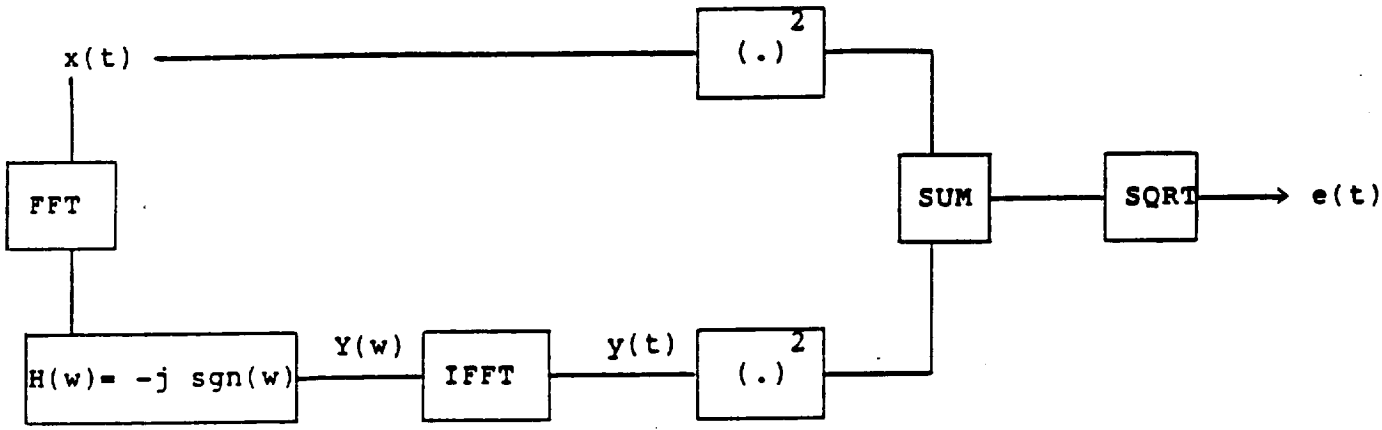

====> PSD at Output of Squarer for Both x(t) and y(t):

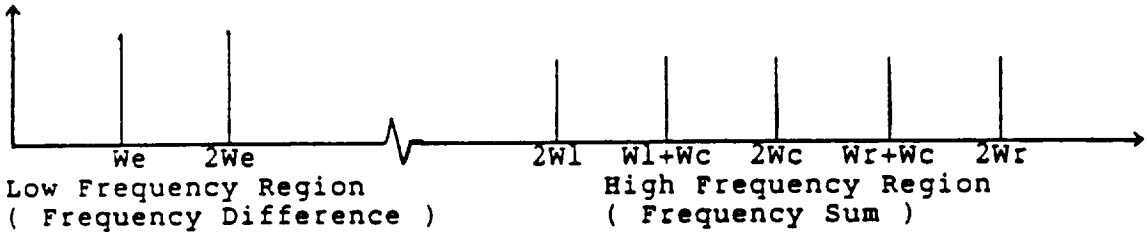

==> PSD of Envelope:

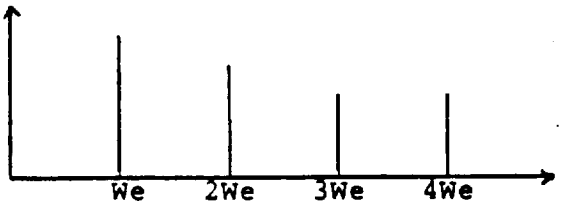

Note: Harmonics Might Show Up Due to The SQUARE and SQUARE ROOT Operation in The Envelope Detection, and Is Dependent On the MODULATION INDEX

TRISPECTRAL ANALYSIS

(3) AUTO/CROSS TRISPECTRUM & TRICOHERENCE

Auto-tricorrelation, auto-trispectrum & auto-tricoherence of x(t):

$$K4xxxx(T1,T2,T3) = K[x(t)x(t+T1)x(t+T2)x(t+T3)] = Rxxxx(T1,T2,T3) = a.t.c.$$

$$F4xxxx(w1,w2,w3) = \iiint K4xxxx(T1,T2,T3)\ \exp[j(w1T1+w2T2+w3T3)]\ dT1\ dT2\ dT3$$

$$= Txxxx(w1,w2,w3) = \text{Auto-Tri-Spectrum (ATS)}$$

$$F4xxxx(w1,w2,w3) = K[\ X(w1)X(w2)X(w3)X^{*}(w1+w2+w3)\ ] = Txxxx(w1,w2,w3) = ATS$$

$$= E[\ X(w1)X(w2)X(w3)X^{*}(w1+w2+w3)\ ] - E[\ X(w1)X(w2)\ ]\ E[\ X(w3)X^{*}(w1+w2+w3)\ ]$$

$$-E[X(w1)X(w3)]\ E[X(w2)X^{*}(w1+w2+w3)] - E[X(w2)X(w3)]\ E[X(w1)X^{*}(w1+w2+w3)]$$

$$t^{2}_{xxxx}(w1,w2,w3) = \frac{1\ \ Txxxx(w1,w2,w3)\ \ 1^{2}}{E[\ 1\ X(w1)X(w2)X(w3)\ 1\ ]\ E[\ 1\ X(w1+w2+w3)\ 1\ ]} = (ATC)$$

Discrete Form:

$$\hat{t}^{2}_{xxxx}(w1,w2,w3) = \frac{1\ \ \hat{T}xxxx(w1,w2,w3)\ \ 1^{2}}{[\ \Sigma 1\ Xi(w1)Xi(w2)Xi(w3)\ 1^{2}\ ]\ \ [\ \Sigma 1\ Xi(w1+w2+w3)\ 1^{2}\ ]}$$

Where:

$$\hat{T}xxxx(w1,w2,w3) = |\Sigma Xi(w1)\ Xi(w2)\ Xi(w3)\ Xi^{*}(w1+w2+w3)\ |$$

$$- |\Sigma Xi(w1)\ Xi(w2)|\ \ |\ \Sigma\ Xi(w3)\ Xi^{*}(w1+w2+w3)\ |$$

$$- |\Sigma Xi(w1)\ Xi(w3)|\ \ |\ \Sigma\ Xi(w2)\ Xi^{*}(w1+w2+w3)\ |$$

$$- |\Sigma Xi(w2)\ Xi(w3)|\ \ |\ \Sigma\ Xi(w1)\ Xi^{*}(w1+w2+w3)\ |$$

Xi(w) = Fourier Transform of x(t) at i-th ensemble Average Block

(4) Tri-Spectral Analysis for Side-Band Identification:

$$x(t) = [\, A + e(t) \,] \cos[\, Wc\, t + Pc(t)]$$

Where: $e(t)$ = envelope = $\cos[\, We\, t + Pe(t)]$

$$\Longrightarrow \begin{cases} \text{left side-band} & \cos[\, \{Wc-We\}\, t + \{\, Pc(t)-Pe(t)\,\}\,] \\ \text{center} & \cos[\, Wc\, t + Pc(t)\,] \\ \text{right side+band} & \cos[\, \{Wc+We\}\, t + \{\, Pc(t)+Pe(t)\,\}\,] \end{cases}$$

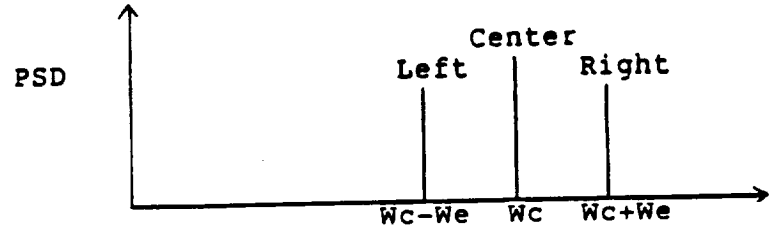

OBSERVATION: NOT ONLY the frequencies become sum and difference, BUT ALSO their phase drifting become sum and difference. This Phase correlation can be identified by using the Tri-Coherence:

Txxxx(W1= Wc-We, W2= -Wc, W3=W) NOTE: SUM FREQ = W-We
(W1 = LEFT; W2 = -CENTER)

$$\begin{cases} \text{MODULATION SIDE-BAND} \Longrightarrow Txxxx(\ LEFT,\ -CENTER,\ W3=\ RIGHT\ ) = 1 \\ \text{INDEPENDENT SIDE-BAND} \Longrightarrow Txxxx(\ LEFT,\ -CENTER,\ W3=\ RIGHT\ ) = 0 \end{cases}$$

Txxxx(LEFT, -CENTER, W3= RIGHT)

= Ensemble Average of { Phase(LEFT) + Phase(RIGHT) - 2 Phase(CENTER) }

$$= \begin{cases} \text{constant compound phase for modulation side-band} \\ \text{random compound phase for independent side-band} \end{cases} = \begin{cases} 1 \\ 0 \end{cases}$$

(5) **SIMULATION:**

[1] Modulation Side-Band :

$$x(t) = \underbrace{\{\ 5 + \cos[\ We\ t + p1(t)\ ]\ \}}_{\text{Envelope}}\ \underbrace{\cos[\ Wc\ t + p2(t)\ ]}_{\text{Carrier}} + N(t)$$

PSD:

$$\begin{cases}\text{Envelope at We= 200 Hz}\\ \text{Carrier at Wc= 3000 Hz}\end{cases} \longrightarrow \begin{cases}\text{Left Side-Band Wc-We = 2800 Hz}\\ \text{Center Frequency Wc = 3000 Hz}\\ \text{Right Side-Band Wc+We = 3200 Hz}\end{cases}$$

[2] Independent Side-Band :

$$y(t) = \cos[\ (Wc-We)t + p3(t)\ ] + 10\cos[\ Wc\ t + p4(t)\ ]$$
$$+ \cos[\ (Wc+We)t + p5(t)\ ] + N(t)$$

PSD:

$$\begin{cases}\text{Left Side-Band Wc-We = 2800 Hz}\\ \text{Center Frequency Wc = 3000 Hz}\\ \text{Right Side-Band Wc+We = 3200 Hz}\end{cases}$$

Where:

$$\begin{cases}p1(t),\ p2(t),\ p3(t),\ p4(t),\ p5(t) = \text{Independent Phase Drifting}\\ N(t) = \text{Gaussian White Noise}\end{cases}$$

ORIGINAL PAGE IS
OF POOR QUALITY

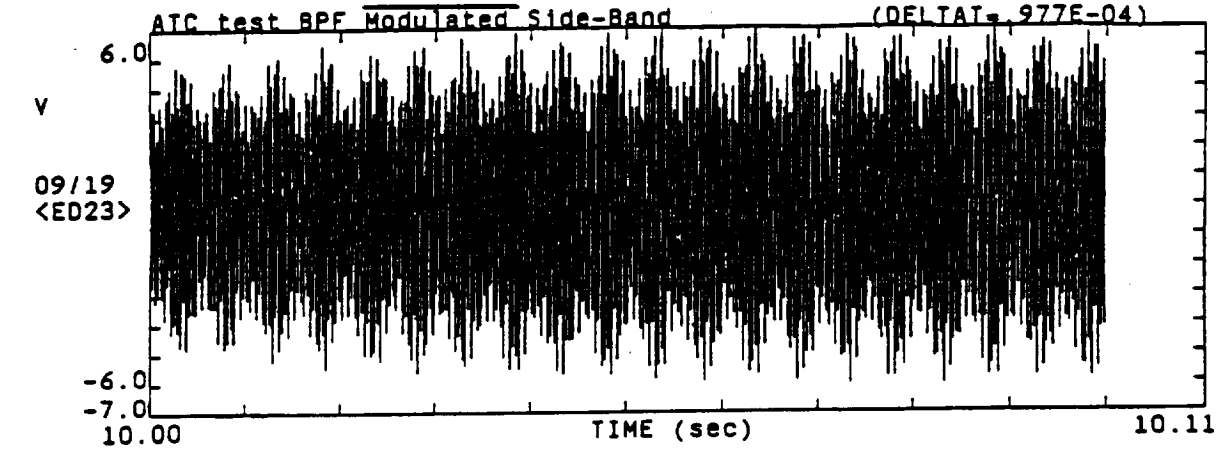
ATC test BPF Modulated Side-Band
(DELTAT= .977E-04)
6.0
V
09/19
<ED23>
-6.0
-7.0
10.00
TIME (sec)
10.11

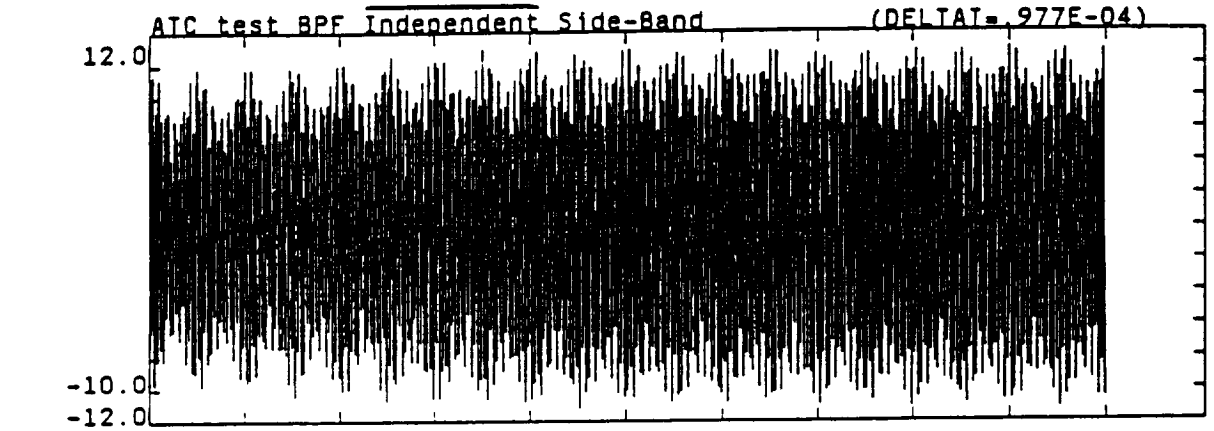
ATC test BPF Independent Side-Band
(DELTAT= .977E-04)
12.0
-10.0
-12.0

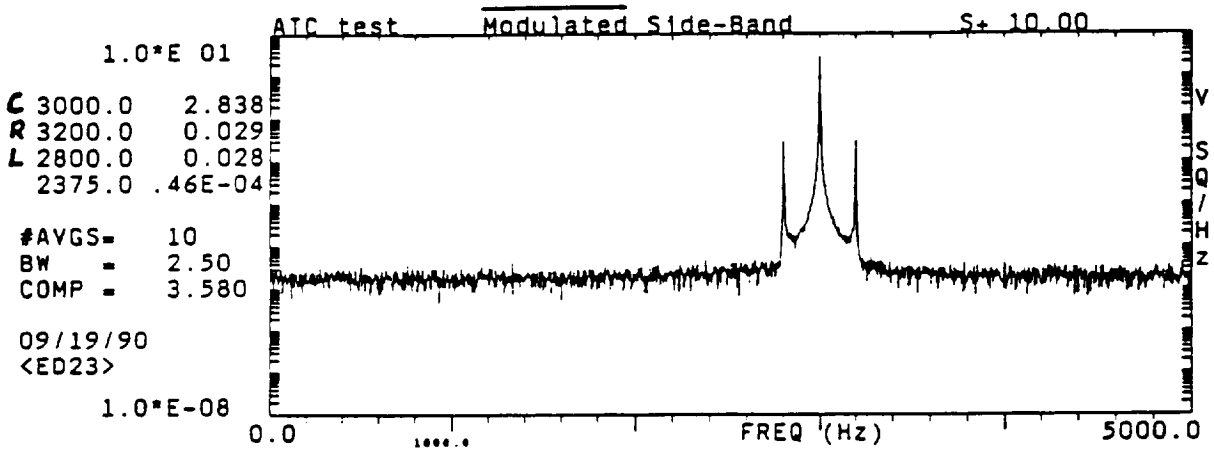
ATC test Modulated Side-Band
S+ 10.00
1.0*E 01
C 3000.0 2.838
R 3200.0 0.029
L 2800.0 0.028
2375.0 .46E-04
#AVGS= 10
BW = 2.50
COMP = 3.580
09/19/90
<ED23>
1.0*E-08
V SQ/Hz
0.0
FREQ (Hz)
5000.0

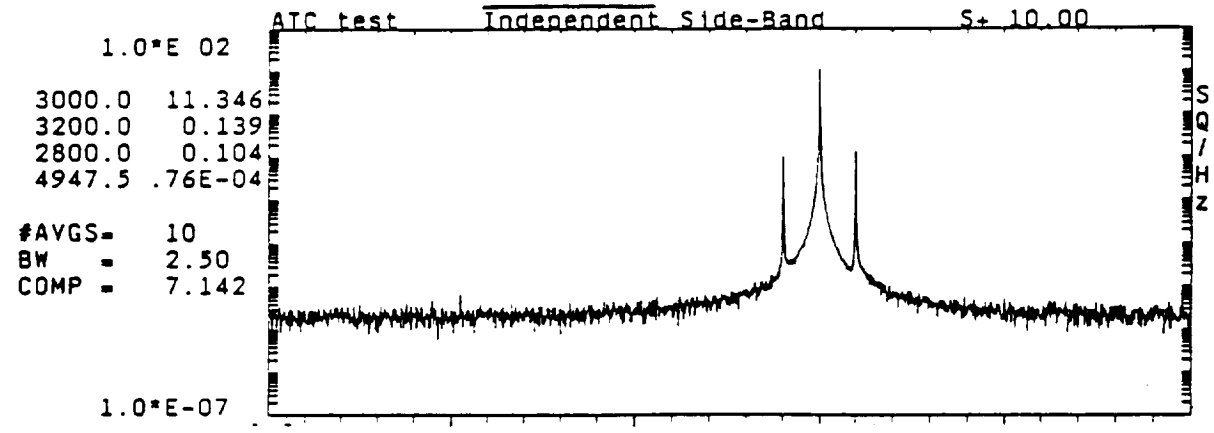
ATC test Independent Side-Band
S+ 10.00
1.0*E 02
3000.0 11.346
3200.0 0.139
2800.0 0.104
4947.5 .76E-04
#AVGS= 10
BW = 2.50
COMP = 7.142
1.0*E-07
SQ/Hz

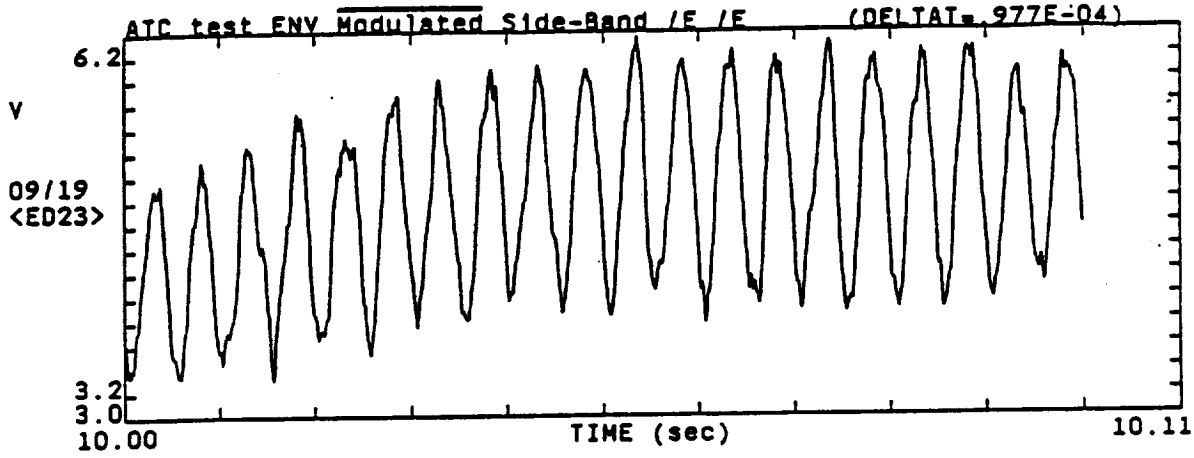
ATC test ENV Modulated Side-Band /E /E (DELTAT= .977E-04)
6.2
V
09/19
<ED23>
3.2
3.0
10.00
TIME (sec)
10.11

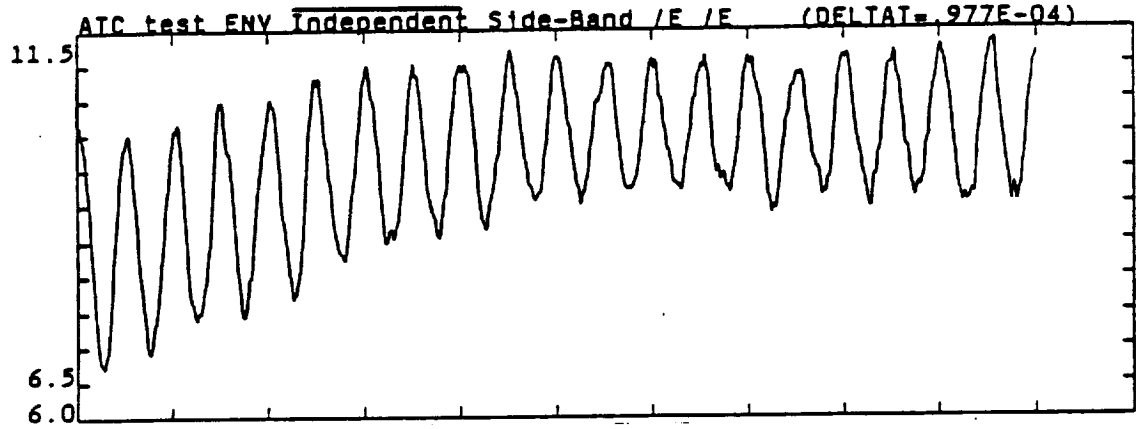
ATC test ENV Independent Side-Band /E /E (DELTAT= .977E-04)
11.5
6.5
6.0

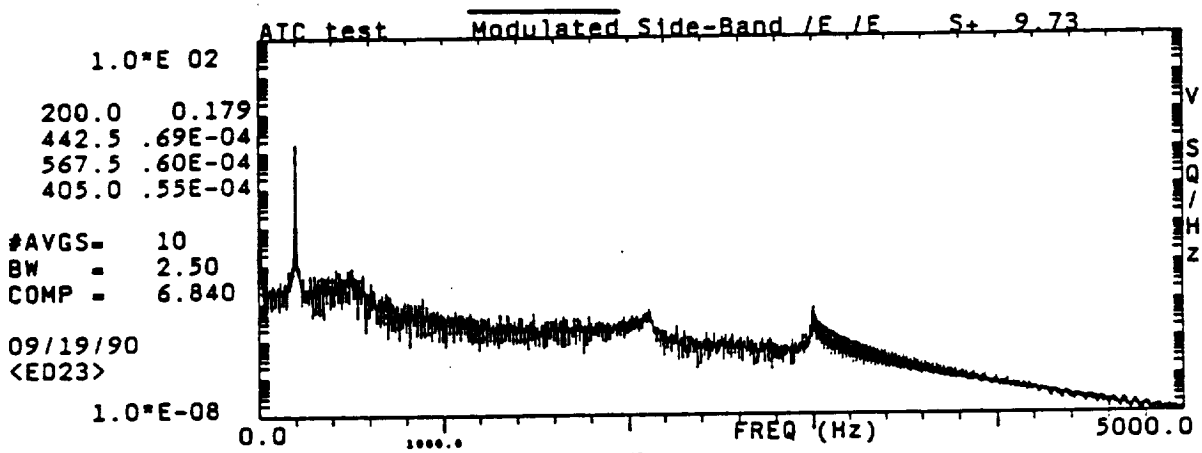
ATC test Modulated Side-Band /E /E S+ 9.73
1.0*E 02
200.0 0.179
442.5 .69E-04
567.5 .60E-04
405.0 .55E-04
#AVGS= 10
BW = 2.50
COMP = 6.840
09/19/90
<ED23>
1.0*E-08
0.0
FREQ (Hz)
5000.0
V SQ/Hz

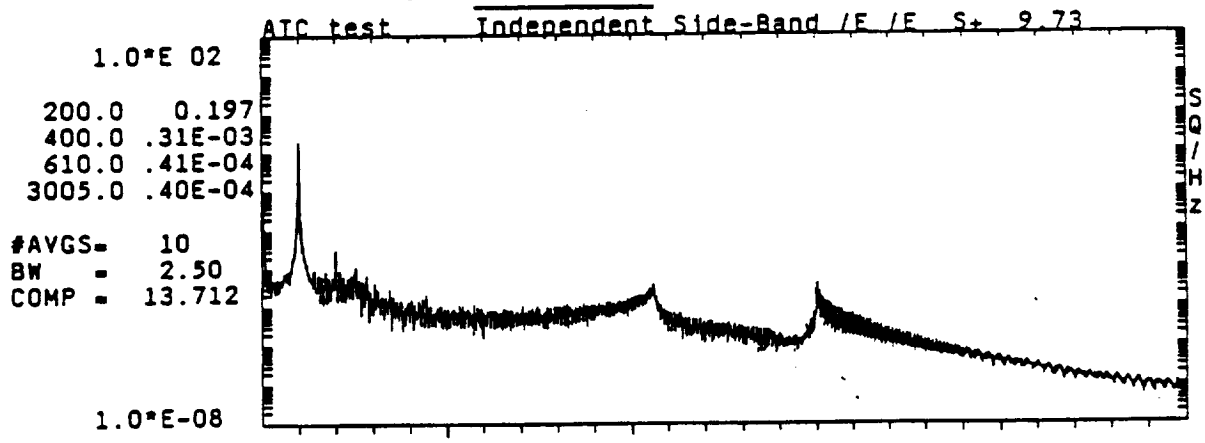
ATC test Independent Side-Band /E /E S+ 9.73
1.0*E 02
200.0 0.197
400.0 .31E-03
610.0 .41E-04
3005.0 .40E-04
#AVGS= 10
BW = 2.50
COMP = 13.712
1.0*E-08
SQ/Hz

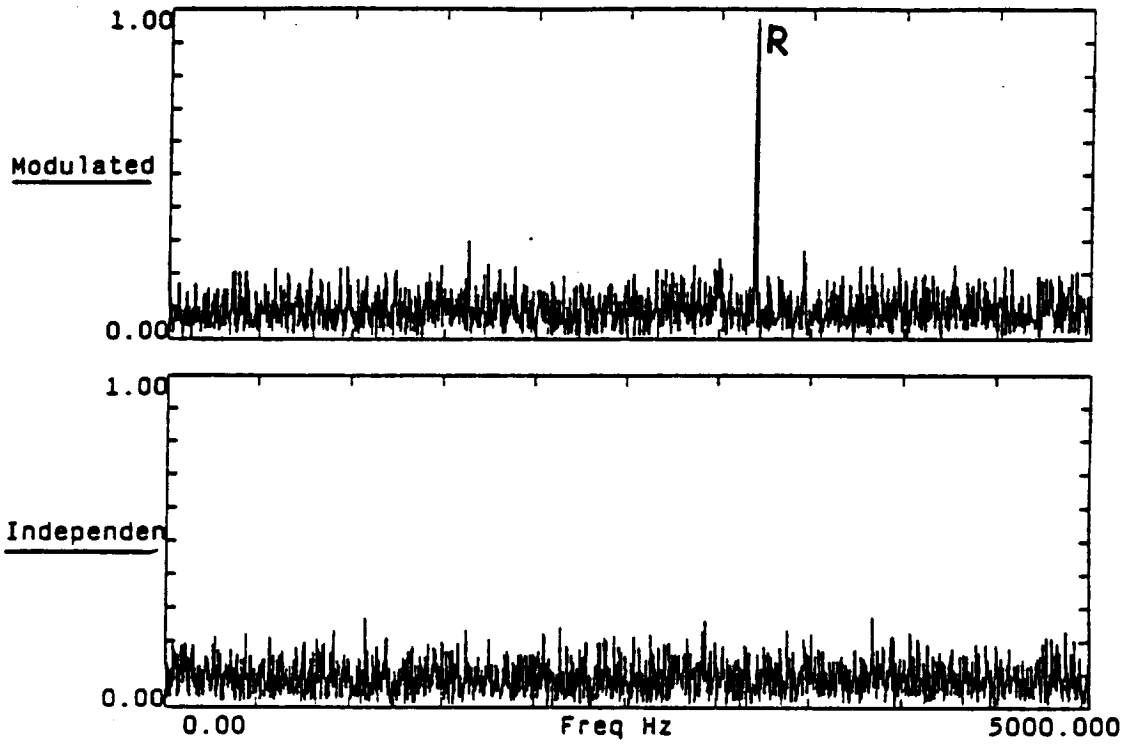

Auto Tri-Coherence T(2800, -3000, f)

↑ L ↑ -C

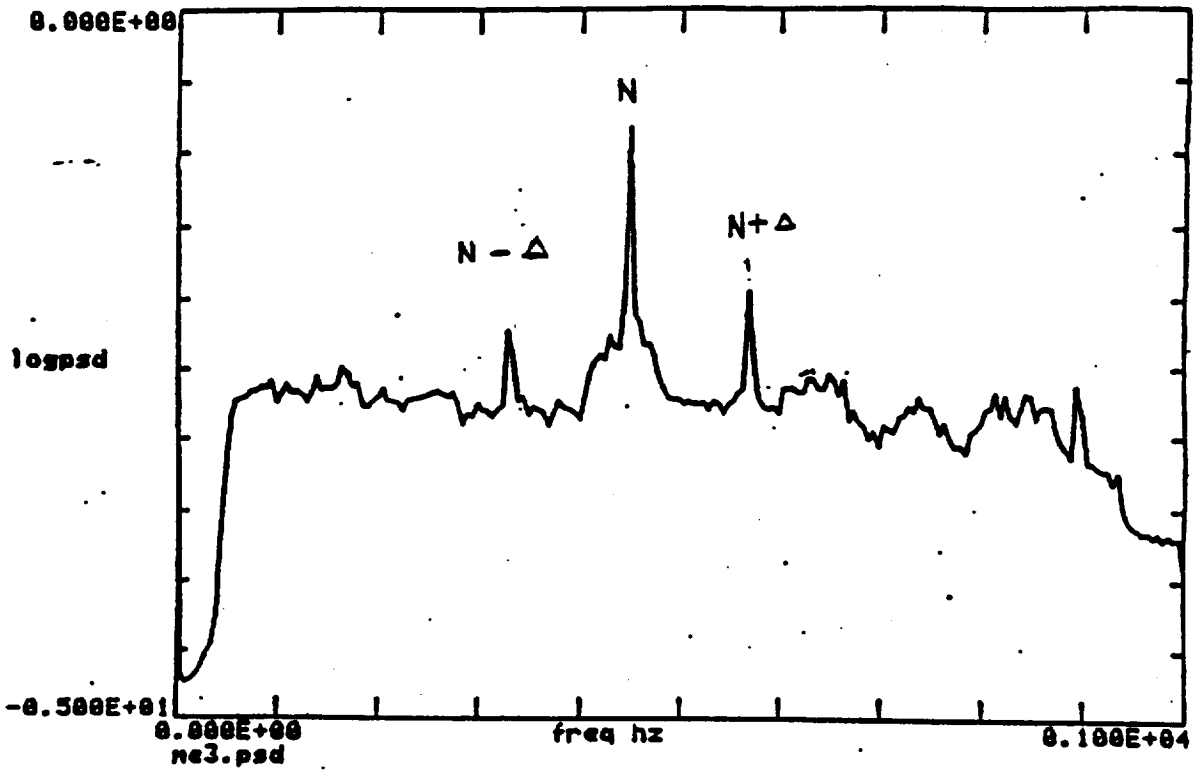

FIGURE 51. ENSEMBLE AVERAGE PSD
(PBP RAD 135-2) FROM FRF-26

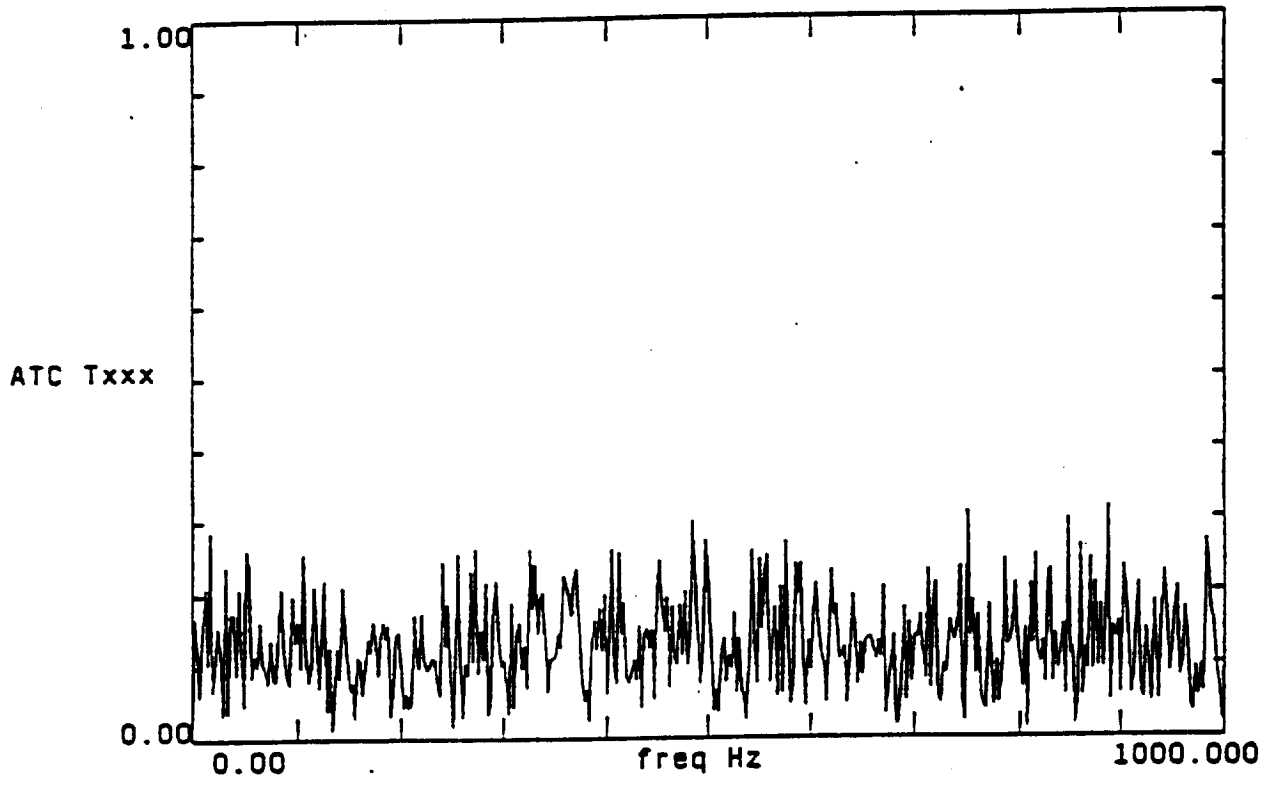

(b) FRF-26 Data

Auto-Tri-coherence Txxx(330, -450, f; f-120)

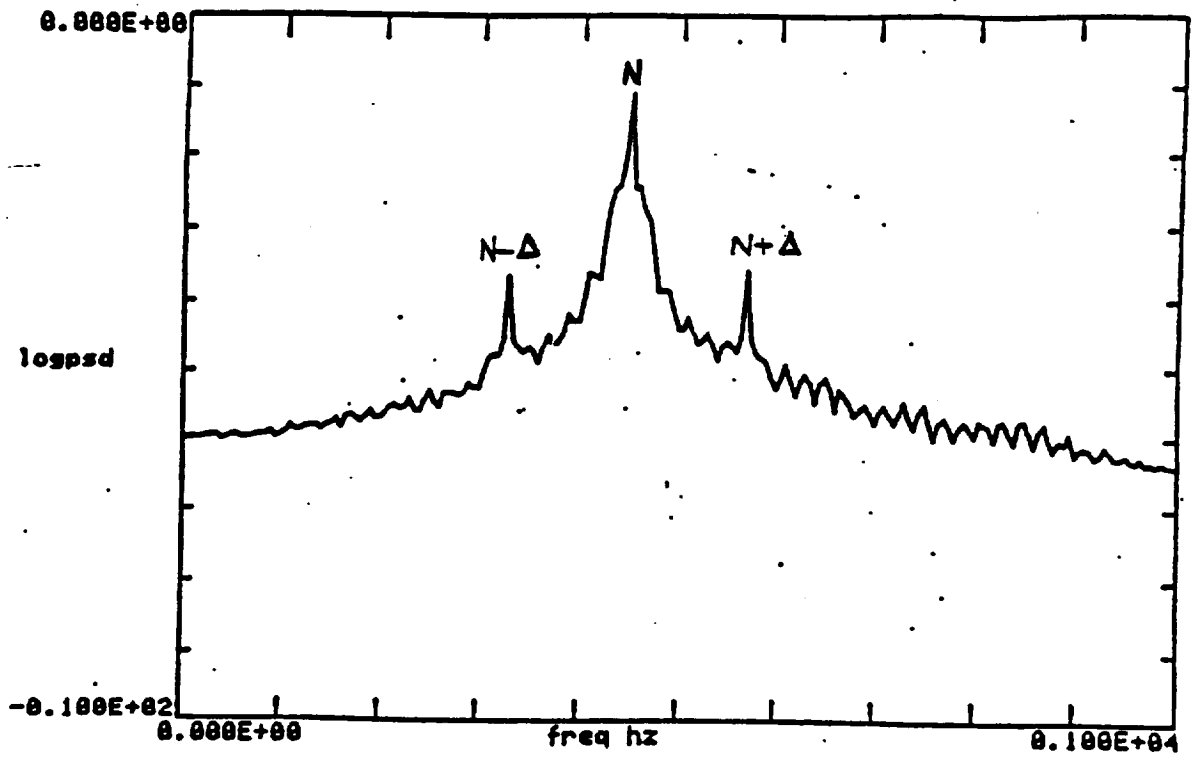

FIGURE 53. BAND-PASS FILTERED PSP 135-2
WITH PURE SINE WAVE MODULATION

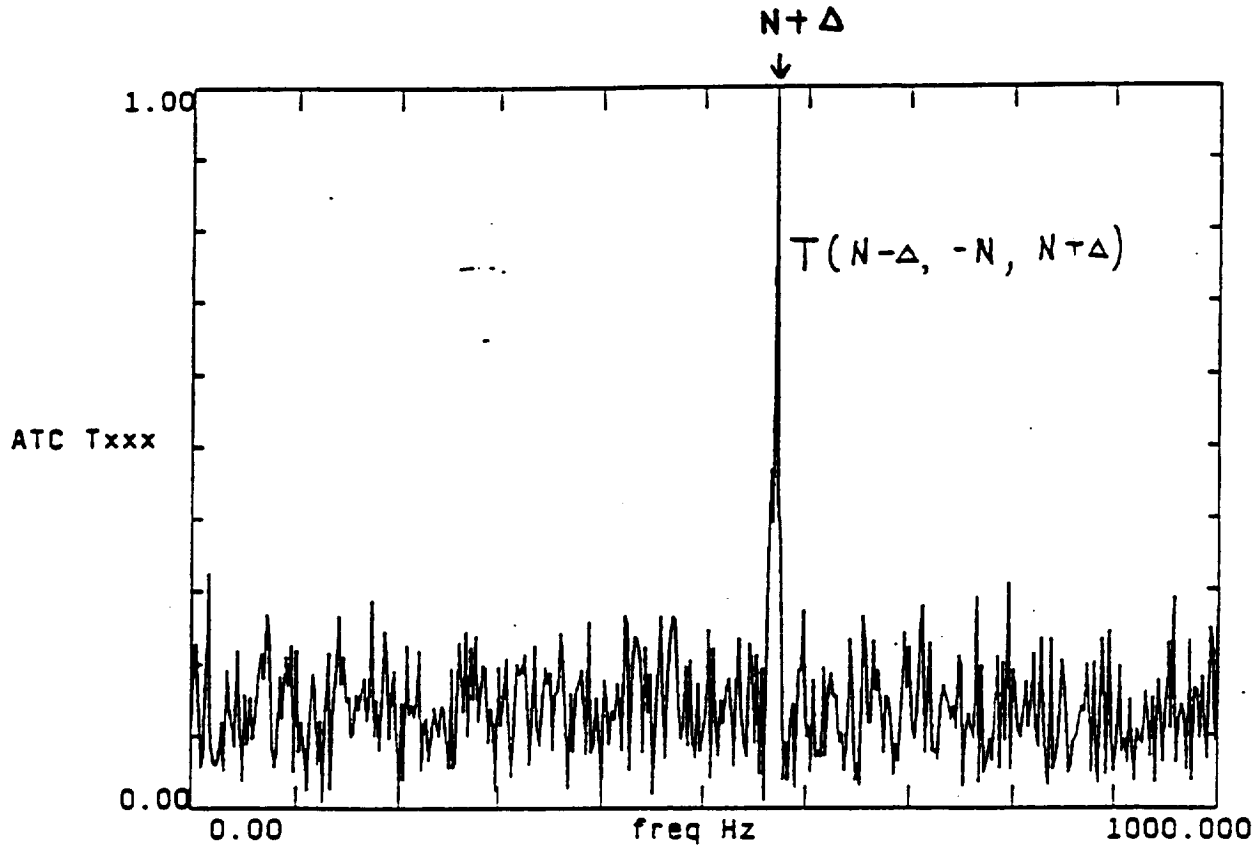

(a) Simulation data with true sideband due to modulation

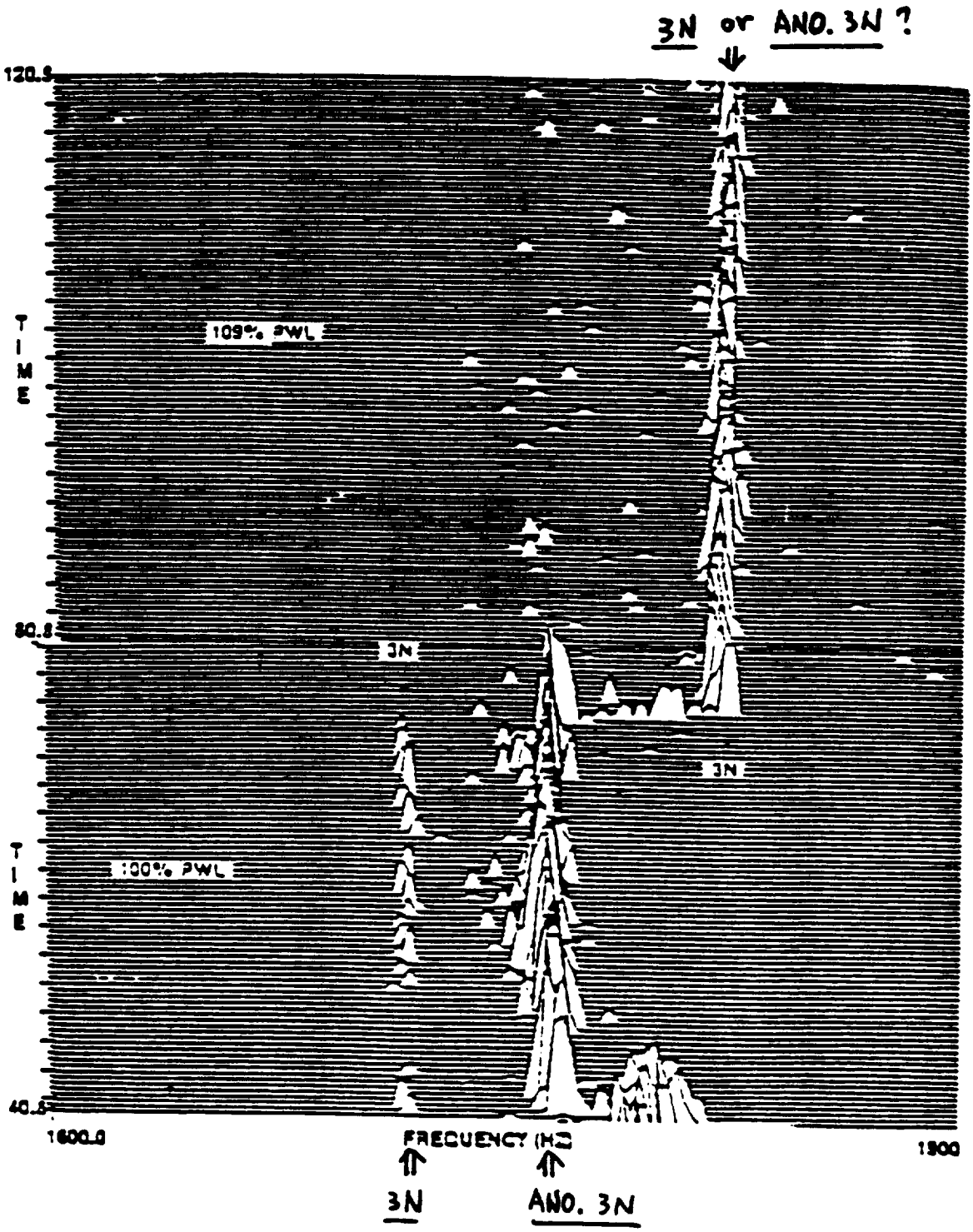

Figure 8. Isoplot of Measurement from Test 901-471

HYPER-COHERENCE AND HYPER-COHERENCE FILTERING

(1) PERIODIC SIGNAL

. Periodic Signal With $\begin{cases} T = \text{Period} \\ f1 = 1/T = \text{Fundamental Frequecy } (W1 = 2\pi f1) \end{cases}$

$$\begin{cases} \text{Time Domain:} & x(t) = x(t+T) \\ \text{Frequency Domain:} & X(W) = X(W)\exp(jWT) \end{cases}$$

If $X(W) \neq 0$, then $\exp(jWT) = 1 \Rightarrow WT = 2\pi f/f1 = k\,2\pi \Rightarrow f = k\,f1$

Therefore, for a periodic signal, its Fourier Transform X(W) can be non-zero only at the integer-multiple of the fundamental frequency:

(f1, 2*f1, 3*f1, ..., k*f1,...)

Any other non-zero X(W) at non-integer-multiple frequency will violate the periodicity assumption.

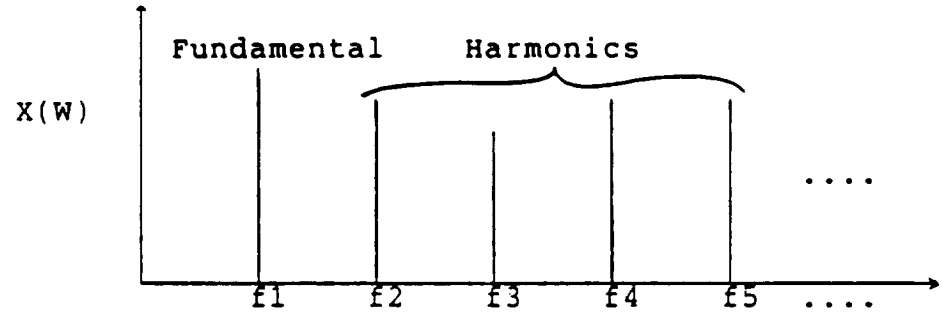

===> time domain model: $x(t) = \sum_{n=1} An \cos(n\,W1\,t + Pn)$

. In order to maintain a fixed pattern of waveform, the phase between the fundamental frequency component and all of its harmonics must maintain some constant phase relationship.

===> HOW to identify and establish such phase relationship between different frequency components ????

(2) HYPER-COHERENCE

$$\begin{cases} Bxxx(w1,w1) = K[\ X(w1)\ X(w1)\ X(2\ W1)] \\ Txxxx(w1,w1,w1) = K[\ X(w1)\ X(w1)\ X(w1)\ X(3\ W1)] \\ Qxxxxx(w1,w1,w1,w1) = K[\ X(w1)\ X(w1)\ X(w1)\ X(W1)\ X(4\ w1)] \\ \cdot \\ \cdot \\ \cdot \\ Fn(w1,w1,w1,...) = K[\ X(w1)\ X(w1)\ ....\ X(n\ w1)] \end{cases}$$

Hyper-Spectrum:

$$HS(Wn;\ W1) = K\ [\ X^{n}(W1)\ X^{*}(n\ W1)\ ] = E\ [\ X^{n}(W1)\ X^{*}(n\ W1)\ ]$$

Hyper-Coherence:

$$HC^{2}(Wn;\ W1) = \frac{|\ HS(\ Wn;\ W1)\ |^{2}}{E[\ |\ X(W1)\ |^{2}]\ \ E[\ |\ X(n\ W1)\ |^{2}]}$$

. PHASE OF HYPER-SPECTRUM:

$$HS(Wn;\ W1) = E\ [\ X^{n}(W1)\ X^{*}(n\ W1)\ ]$$

$$= E\ [\ |X(W1)\ X(nW1)\ |\ \ e^{\,j\ \{\ \overbrace{n\ P(W1) - P(Wn)}^{\text{Compound Phase } Q(Wn;W1)}\ \}}\ ]$$

Original model:

$$x(t) = \sum_{n=1} An\ \cos[\ Wn\ t + P(Wn)\ ] \qquad \text{where } Wn = n * W1$$

If we take measurement at any arbitrary time t0:

$$\begin{cases} y(t) = x(t-t0) = \sum An\ \cos[\ Wn\ (t-t0) + P(Wn)\ ] \\ \qquad\qquad = \sum An\ \cos[\ Wn\ t + P(Wn) - Wn\ t0\ ] \\ Y(W) \Longrightarrow \text{the observed Phase at } Wn = P'(Wn) = P(Wn) - Wn\ t0, \text{ which} \end{cases}$$

depends on the starting time of measurement t0, BUT the compound phase

$$Q'(Wn;W1) = n\ P'(W1) - P'(Wn) = n\ [\ P(W1) - W1\ t0\ ] - [\ P(Wn) - Wn\ t0\ ]$$

$$= n\ P(W1) - P(Wn) = \text{independent of } t0$$

[1] This compound phase Q(Wn;W1) = n P(W1) - P(Wn), provides an inherent phase relationship between the fundamental component and its n-th order harmonic. It will remain a constant phase for a fixed pattern of periodic waveform.

EX: We observe 100 Hz and 400 Hz spectral component in a signal.

If 400 Hz is 4th Harmonic of 100 Hz: Q(Wn;W1) = constant phase

==> Hyper-Coherence HC(4N, N) = 1

If 400 Hz is from other independent source: Q(Wn;W1) = random phase

==> Hyper-Coherence HC(4N, N) = 0

====> Hyper-Coherence can be used to identify whether an apparent harmonic of some reference component is truely a harmonic of it or not

[2] If the periodic signal is corrupted by noise, then this inherent phase relationship can provide a way to perform waveform enhancement through ensemble average of the compound phase.

===> Hyper-Coherence Filtering:

- Phase Information Recovery

At the n-th harmonic of the i-th ensemble average block:

Qi(Wn;W1)= n Pi(W1) -Pi(Wn) =n P(W1) -P(Wn) +Noise = Q(Wn;W1) +Noise

= will be fluctuating around the true Q(Wn;W1) due to noise

Ensemble average of Qi(Wn;W1) ====> Noise Effect will be reduced

===> P(Wn) = Phase at Wn can be better estimated

- Amplitude Information Recovery

$HC^2(Wn;W1)$ = Hypercoherence Square = Percentage of power at Wn which is correlated with the fundamental frequency component.

===> $Sxx(Wn)\ HC^2(Wn;W1)$ ===> Amplitude at Wn (An) can be estimated

$x(t) = \sum_{n=1} An \cos[\ Wn\ t + P(Wn)\ ]$ can be recovered and enhanced

POWER SPECTRA FOR TWO SIMULATED TIME SERIES

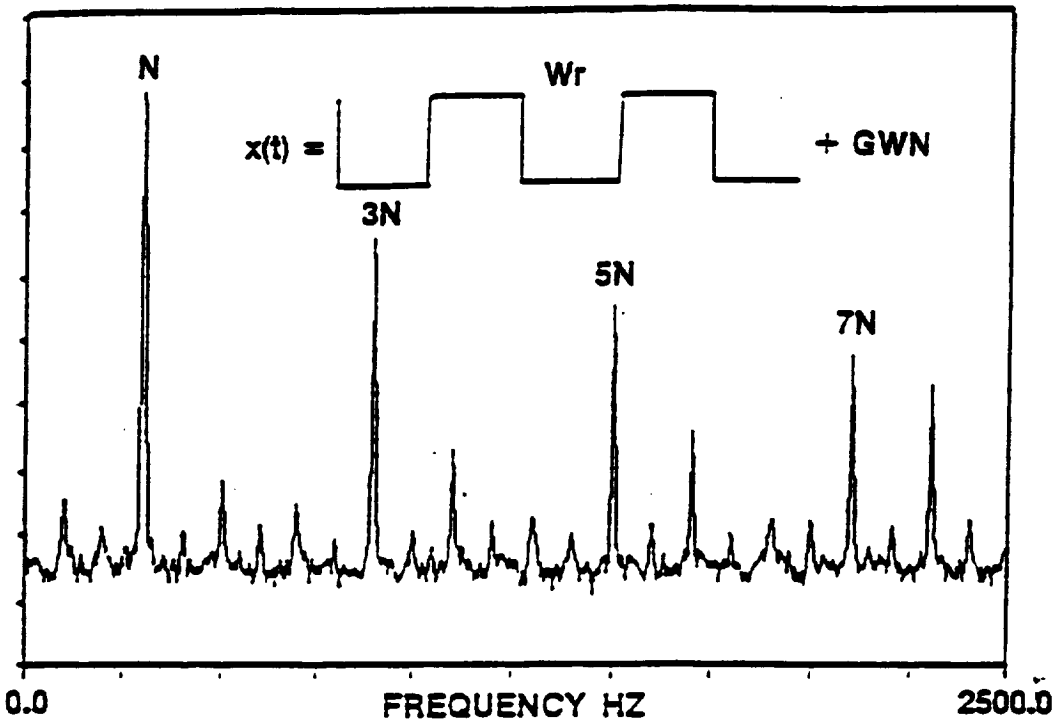

POWER SPECTRUM OF SQUARE WAVE + NOISE

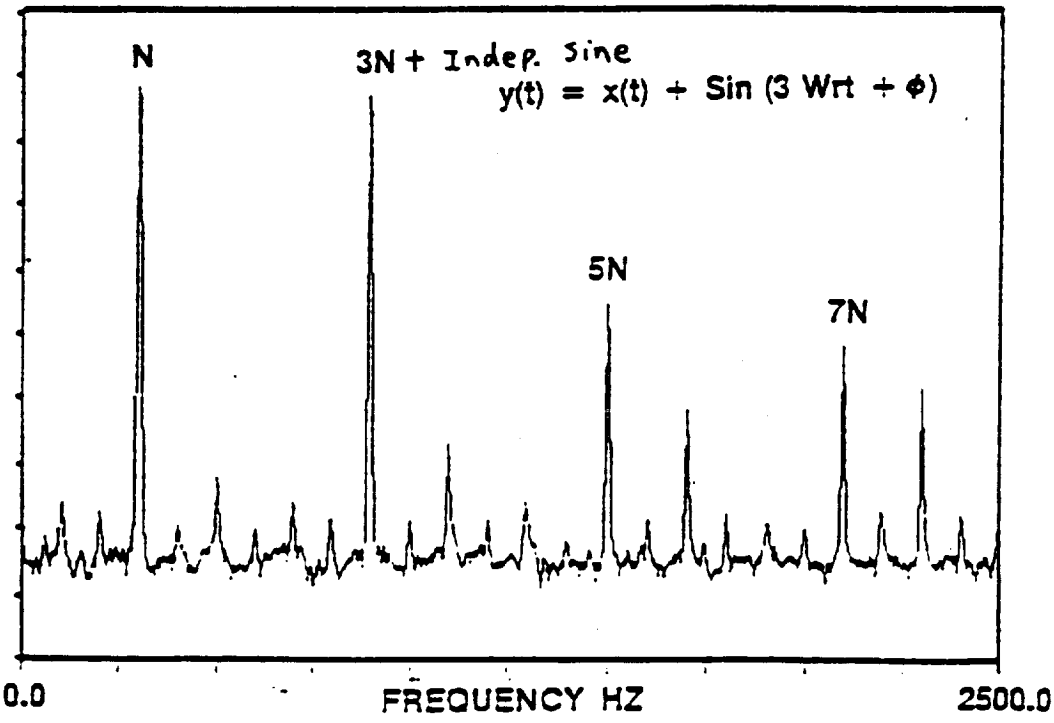

POWER SPECTRUM OF SQUARE WAVE + UNCORRELATED SINE WAVE + NOISE

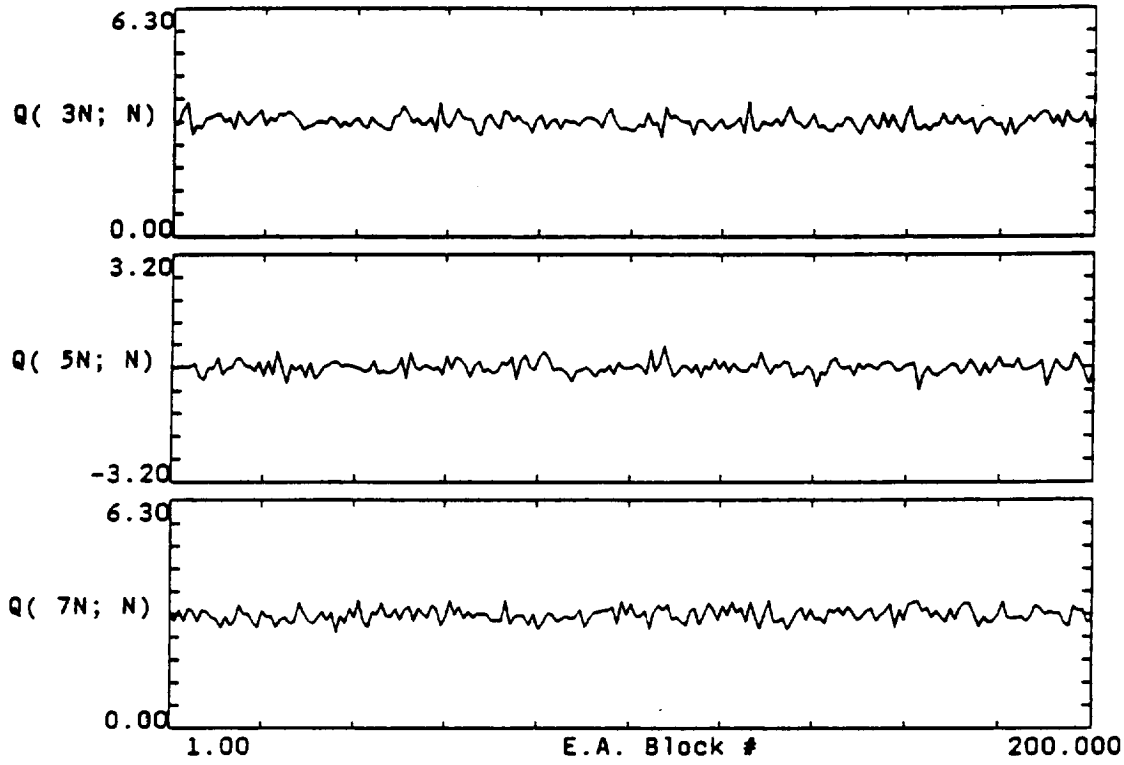

COMPOUND PHASE OF SQUARE WAVE + NOISE $X(t)$

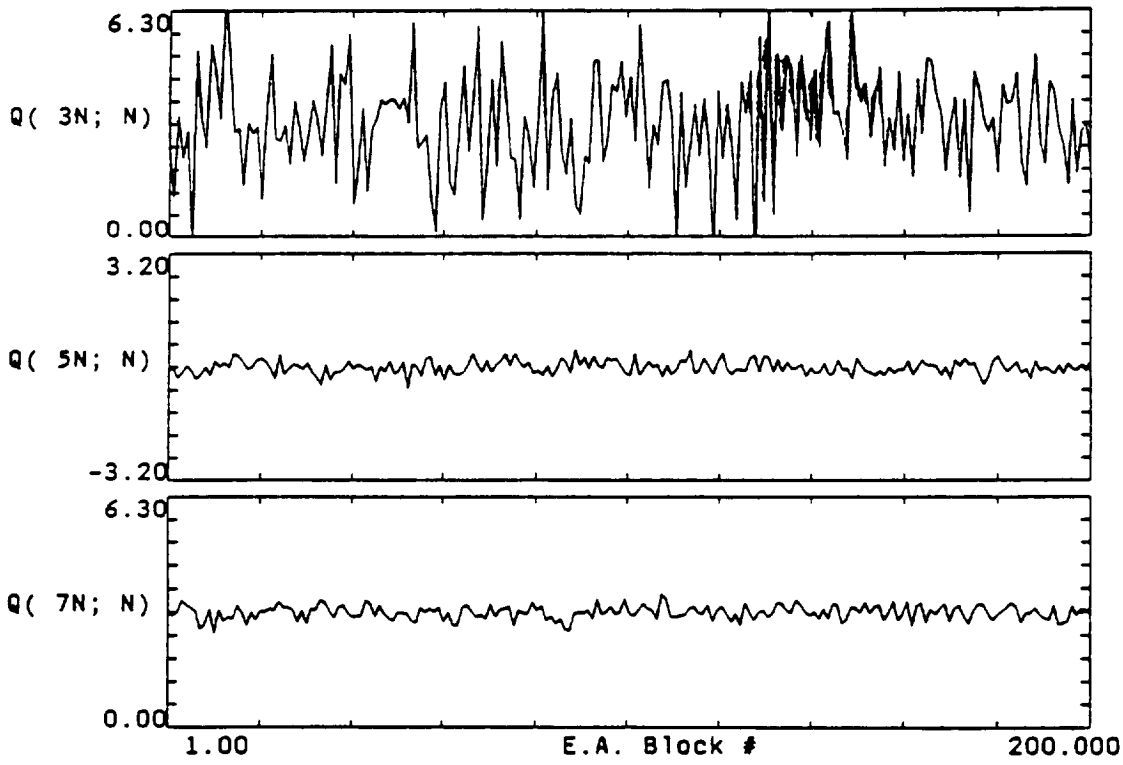

COMPOUND PHASE OF SQUARE WAVE + UNCORRELATED SINE + NOISE $y(t)$

HYPER-COHERENCE SPECTRUM OF TWO SIMULATED TIME SERIES

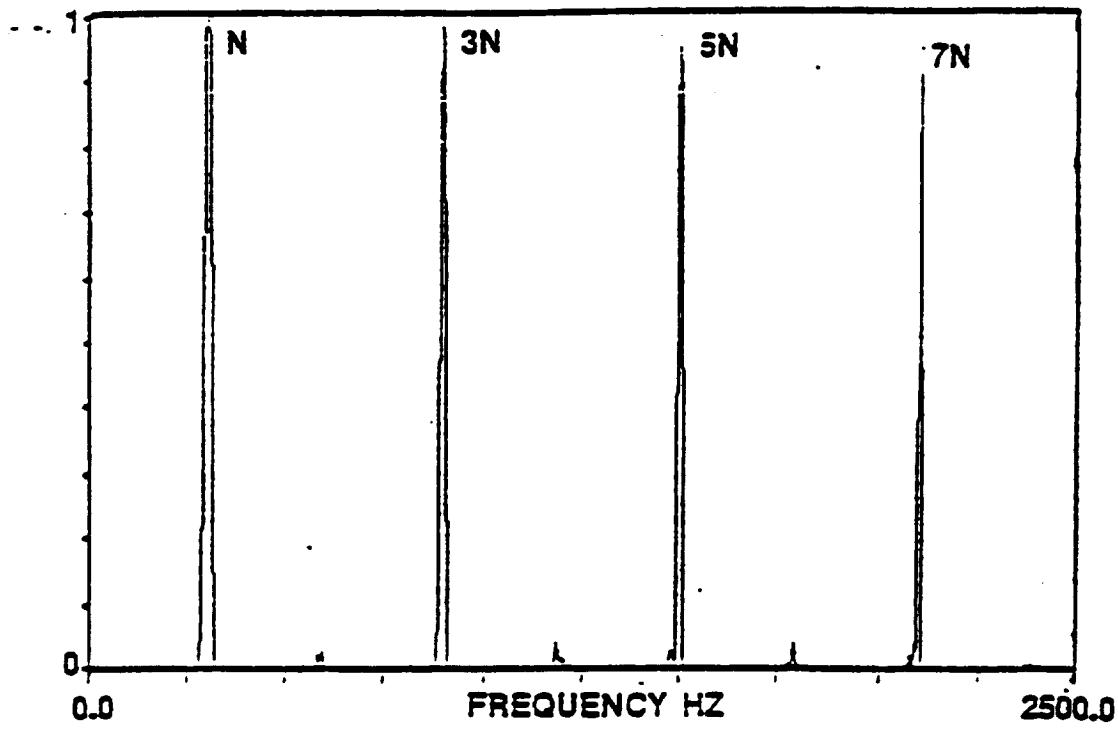

HYPER-COHERENCE SPECTRUM OF SQUARE WAVE + NOISE

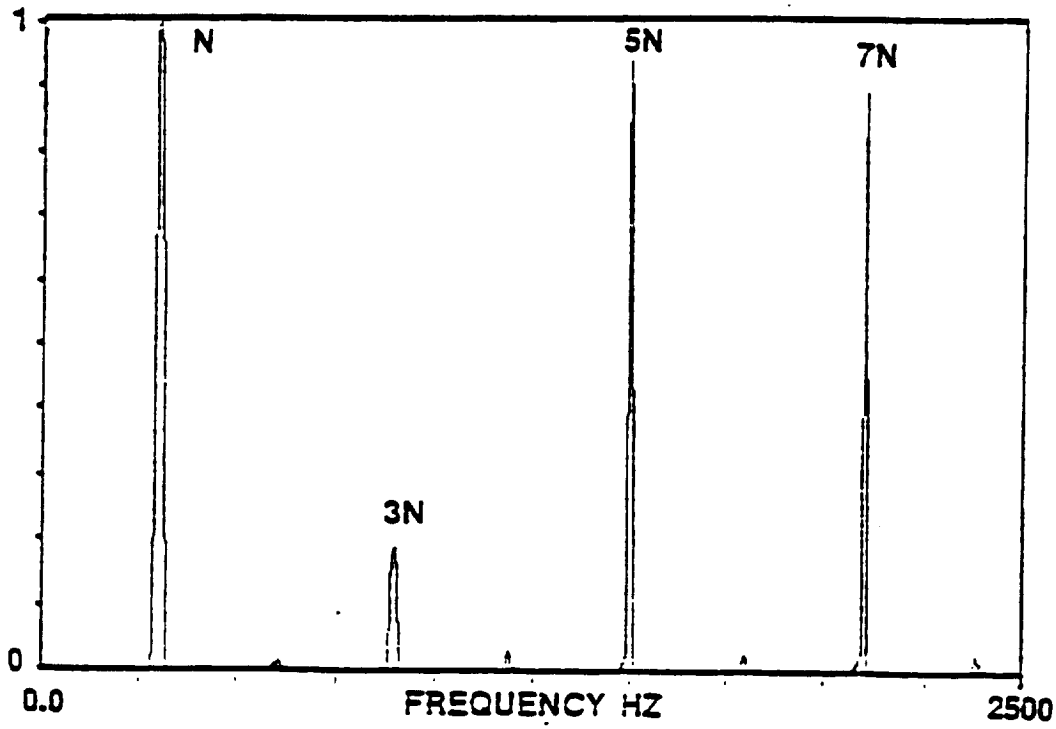

HYPER-COHERENCE SPECTRUM OF SQUARE WAVE
+ UNCORRELATED SINE WAVE + NOISE

P-11-85-21

POWER SPECTRA FROM ROCKET ENGINE TURBOPUMP

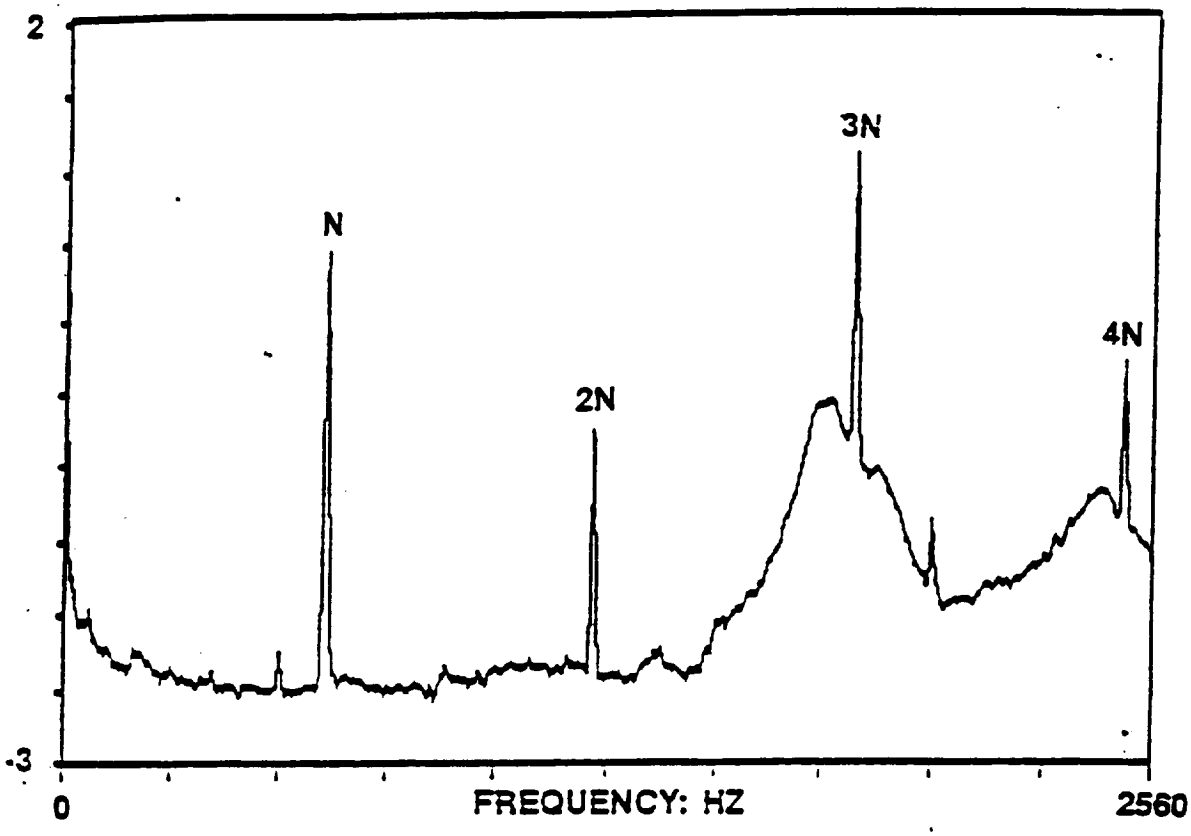

TEST 901-436

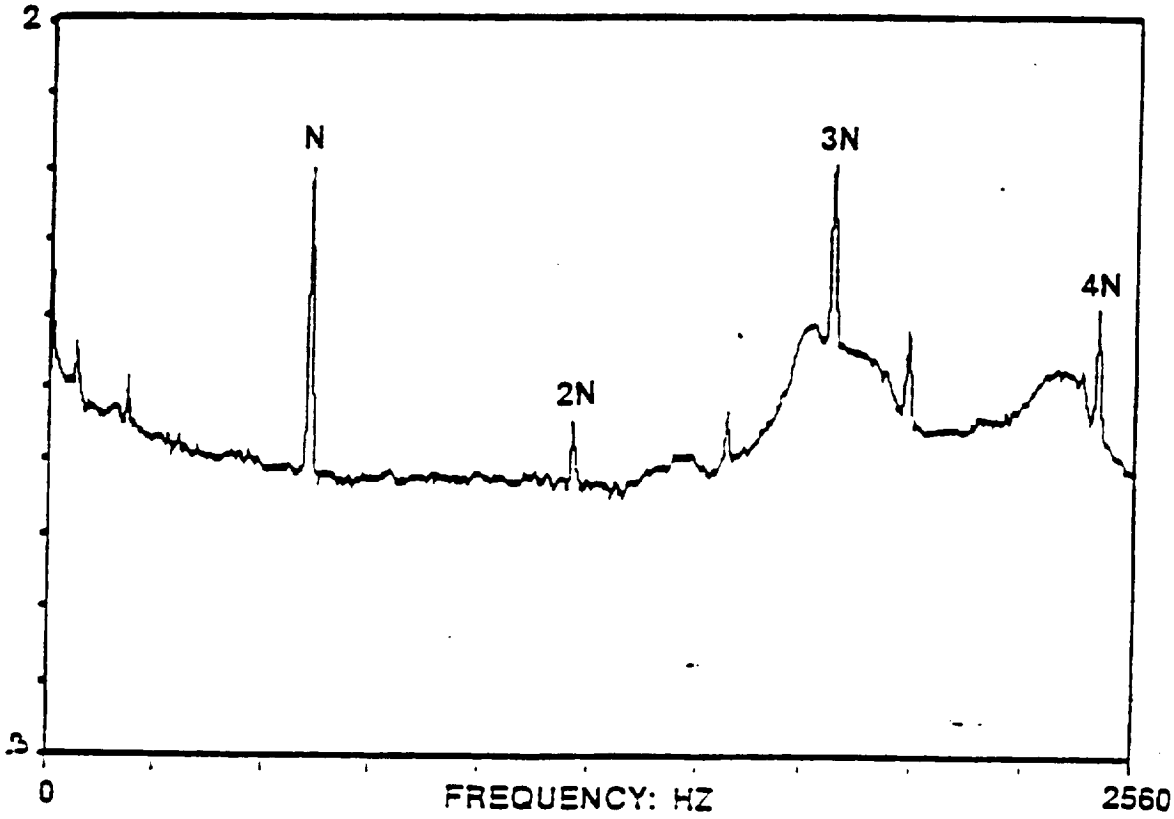

TEST 901-471

P-11-85-Z1

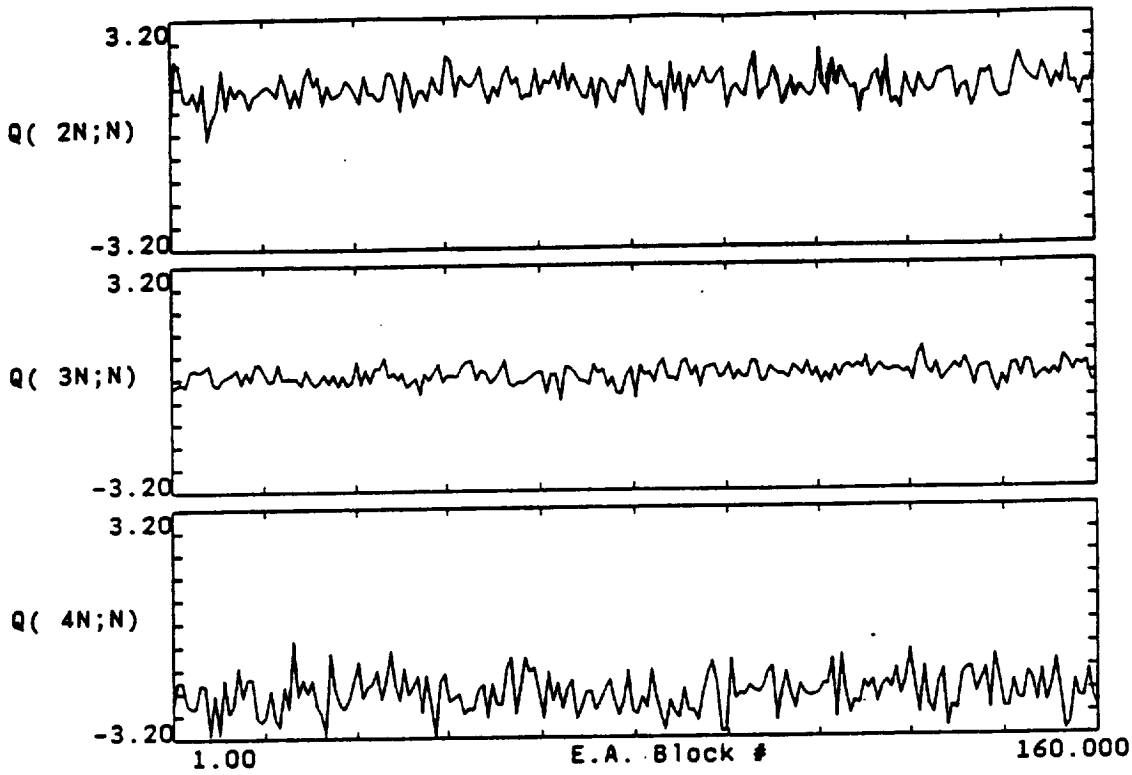

COMPOUND PHASE OF TEST 901-436 S+150

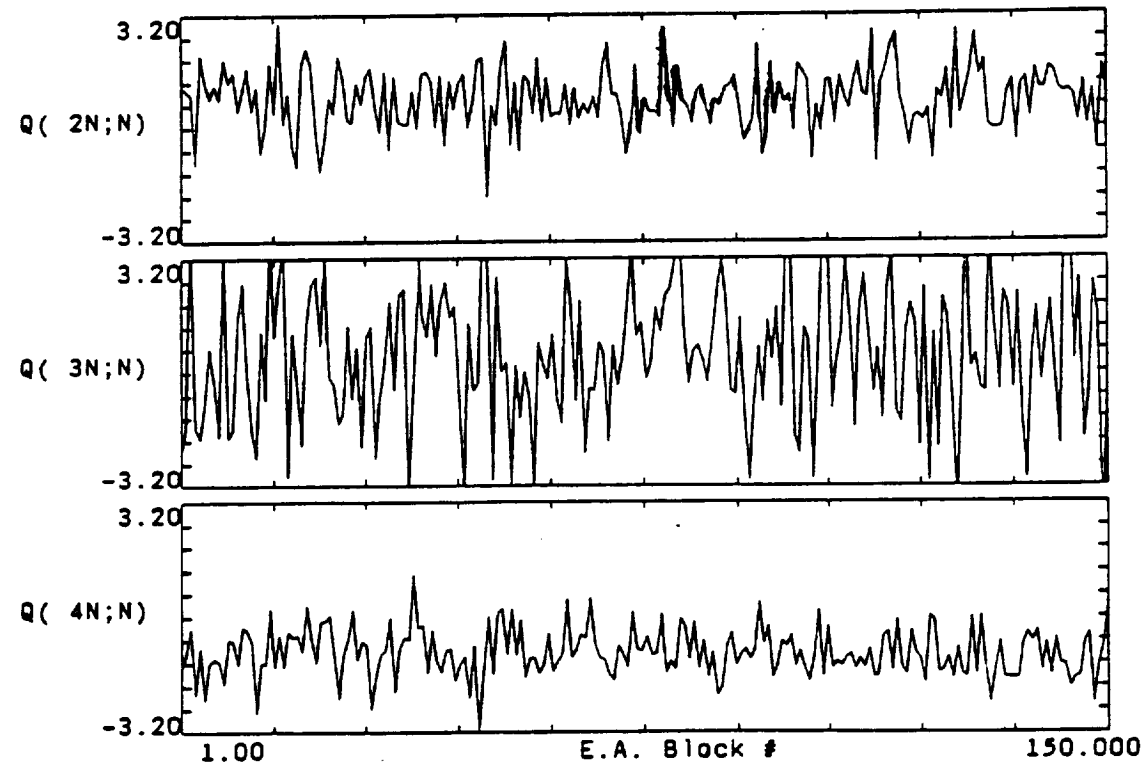

COMPOUND PHASE OF TEST 901-471 S+76

SIMULATION EXAMPLE FOR HYPER-COHERENCE FILTERING

- Noise free periodic signal:

$$\begin{cases} x(t)=\sin(W1t) + 0.7\sin(W2\,t+P2) + 0.5\sin(W3\,t+P3) + 0.3\sin(W4t+P4) \\ y(t)=\sin(W1t+P0) + 0.5\sin(W2\,t+P5) + 0.5\sin(W3\,t+P6) + 0.3\sin(W4t+P7) \end{cases}$$

Where: P2,P3,P4,P0,P5,P6,P7 are fixed initial phases which are not randomized for each ensemble average block.

===> continuous waveform

Orbit plot: x(t) v.s. y(t)

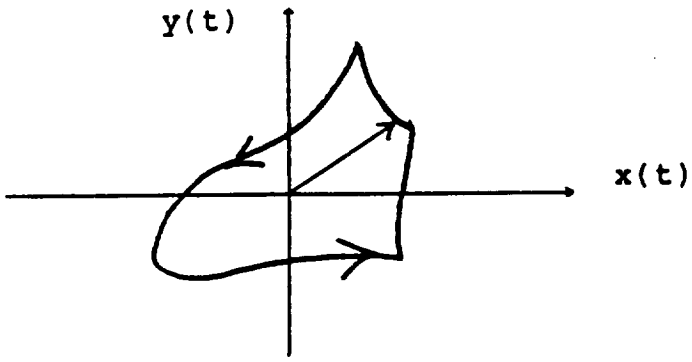

CASE-1: Corruption With Noise

$$\begin{cases} x1(t) = x(t) + GWN1 \text{ (GAUSSIAN WHITE NOISE)} \\ y1(t) = y(t) + GWN2 \end{cases}$$

Where: GWN1 & GWN2 are independent Gaussian White Noise.

CASE-2: Corruption With Noise and Independent Sine Wave at 2N in x2(t) and 3N in y2(t)

$$\begin{cases} x2(t) = x(t) + GWN1 + 0.5\sin(W2\,t + P8) \\ y2(t) = y(t) + GWN2 + 0.5\sin(W3\,t + P9) \end{cases}$$

Where: P8 & P9 are independent random phases, which are randomized for each ensemble average block.

HYPER-COHERENCE SPECTRUM OF TURBOPUMP MEASUREMENT

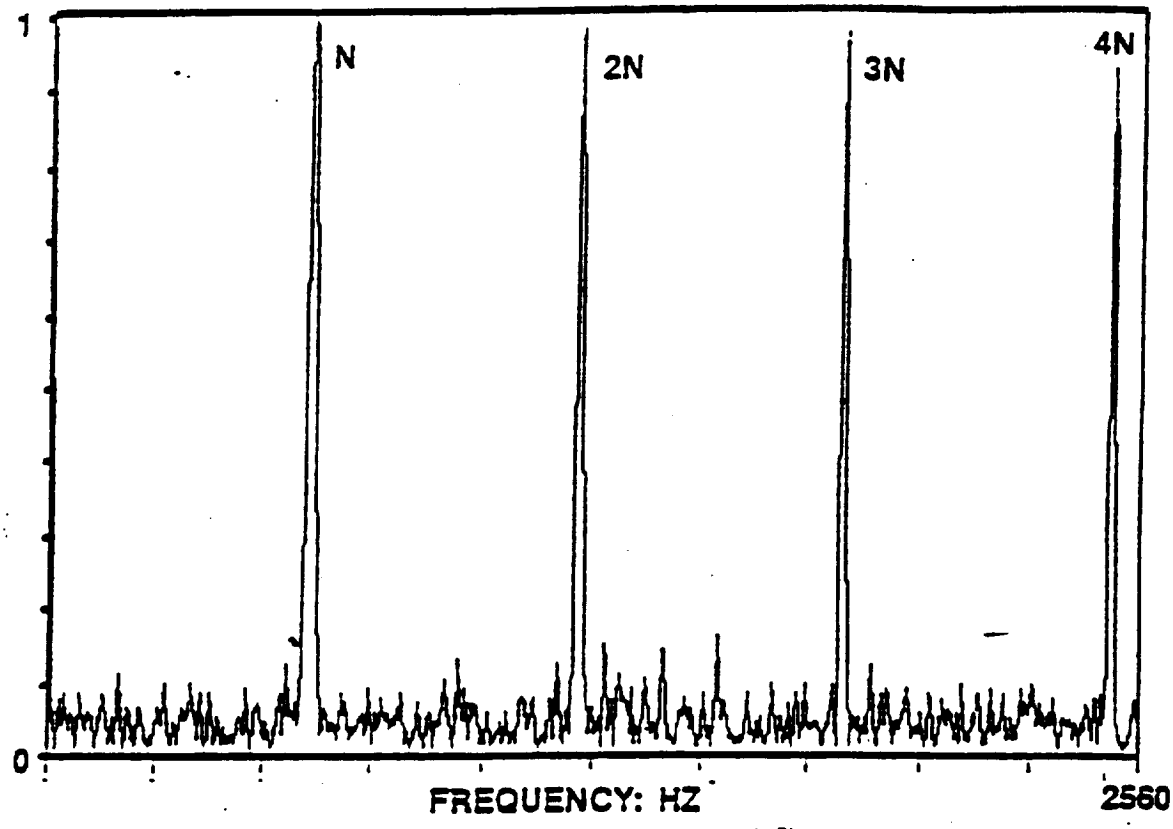

TEST 901-436

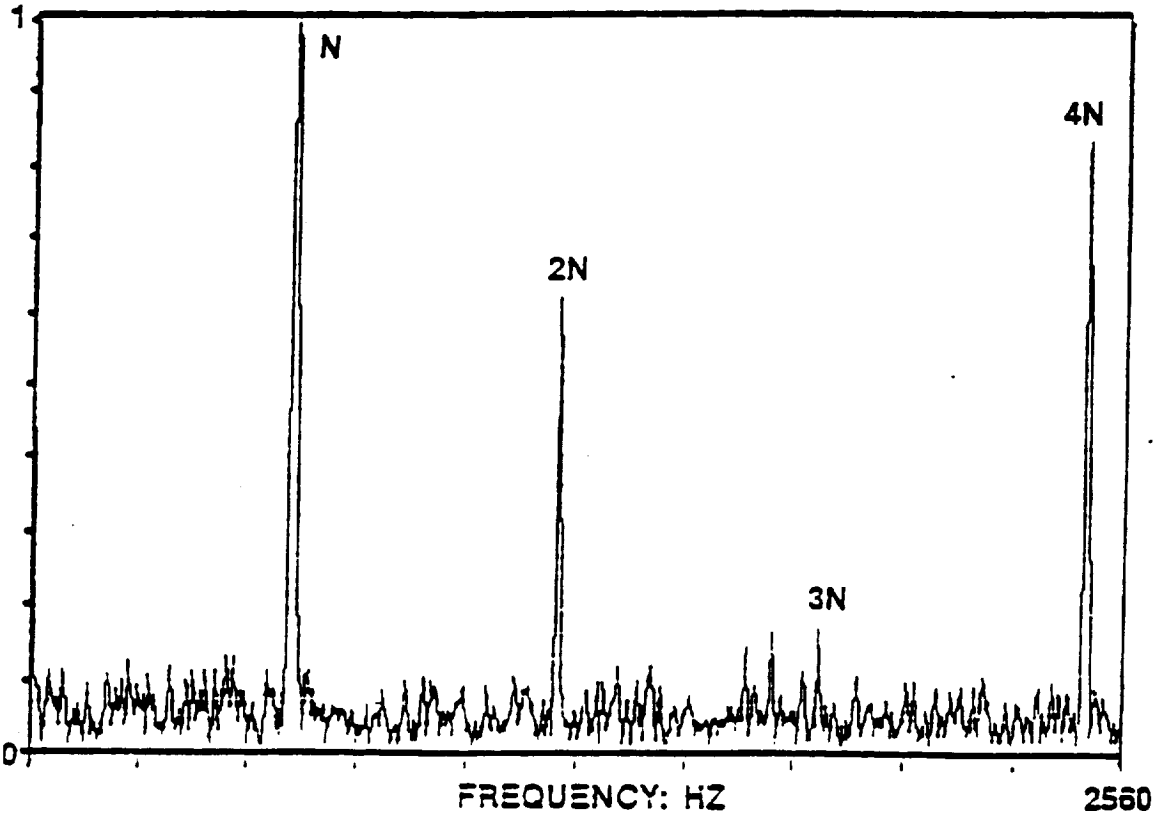

TEST 901-471

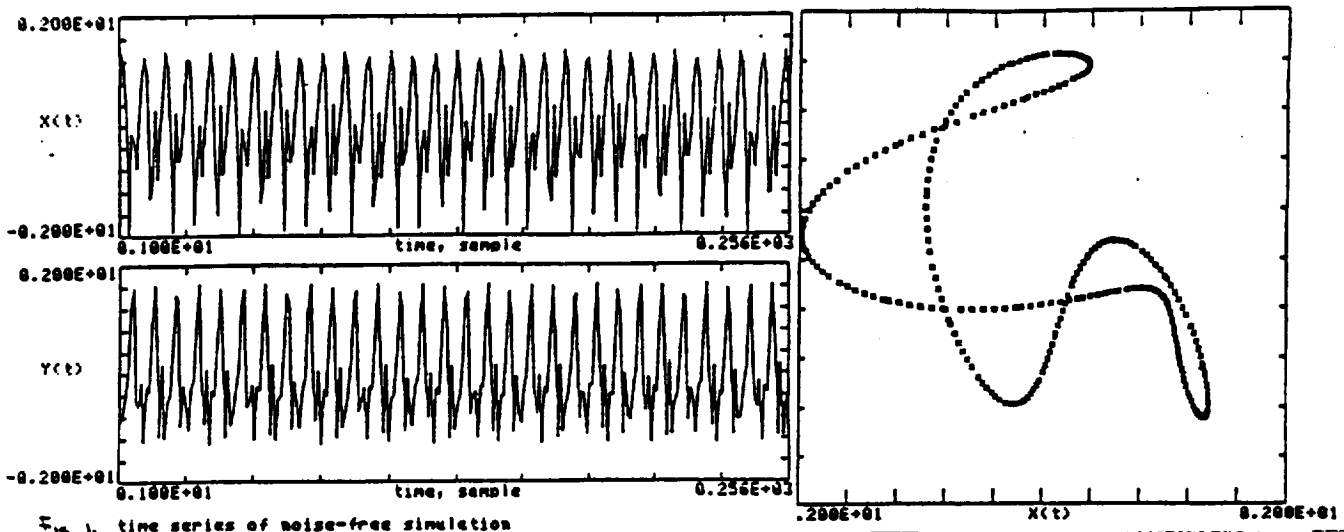

Fig 1. time series of noise-free simulation

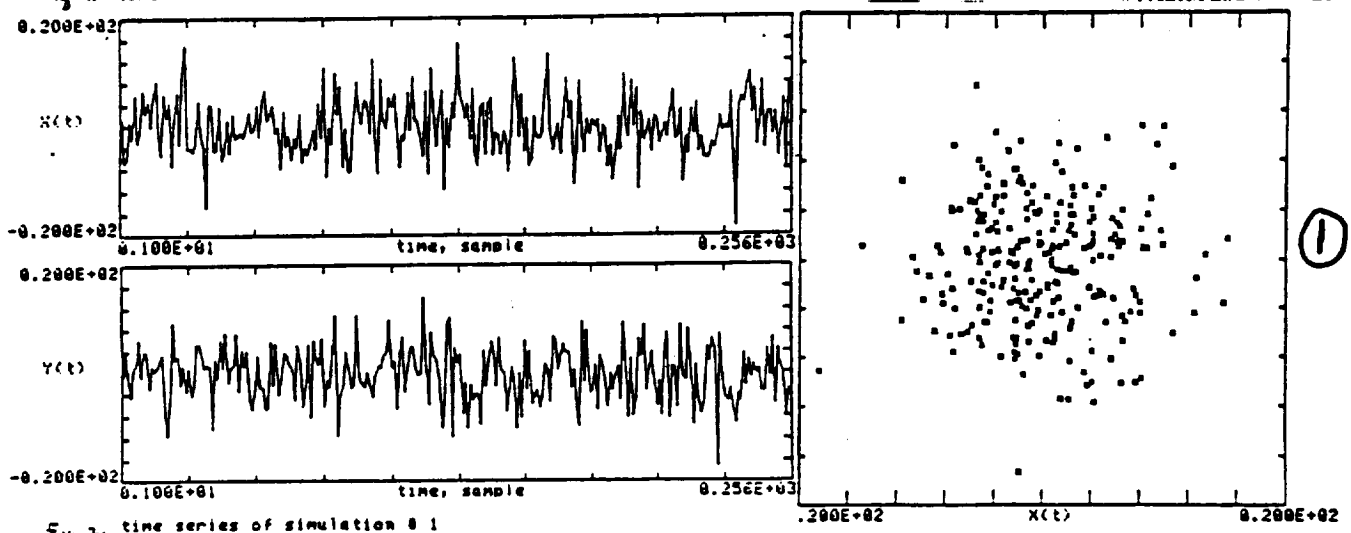

(1)

Fig 2. time series of simulation # 1 with additive gaussian white noise

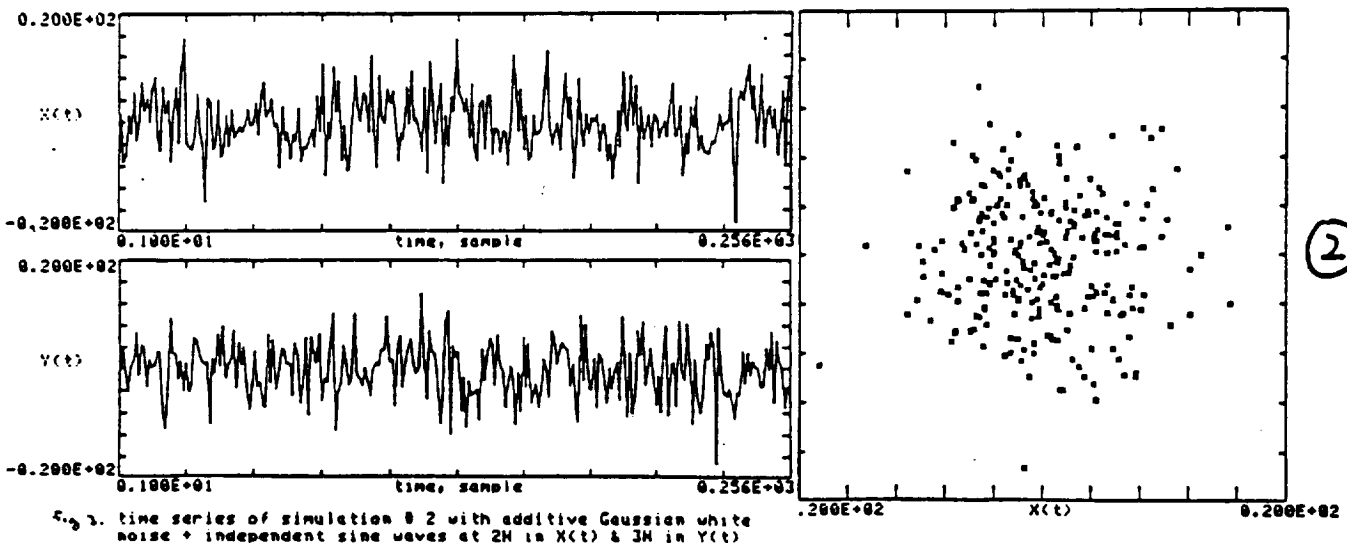

(2)

Fig 3. time series of simulation # 2 with additive Gaussian white noise + independent sine waves at 2H in X(t) & 3H in Y(t)

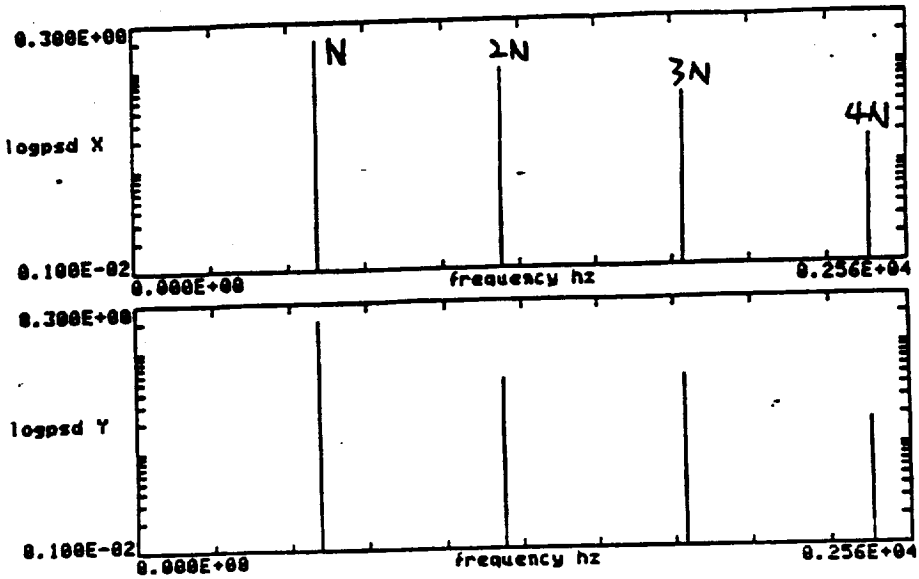

FIG 4: PSD OF NOISE-FREE SIMULATION

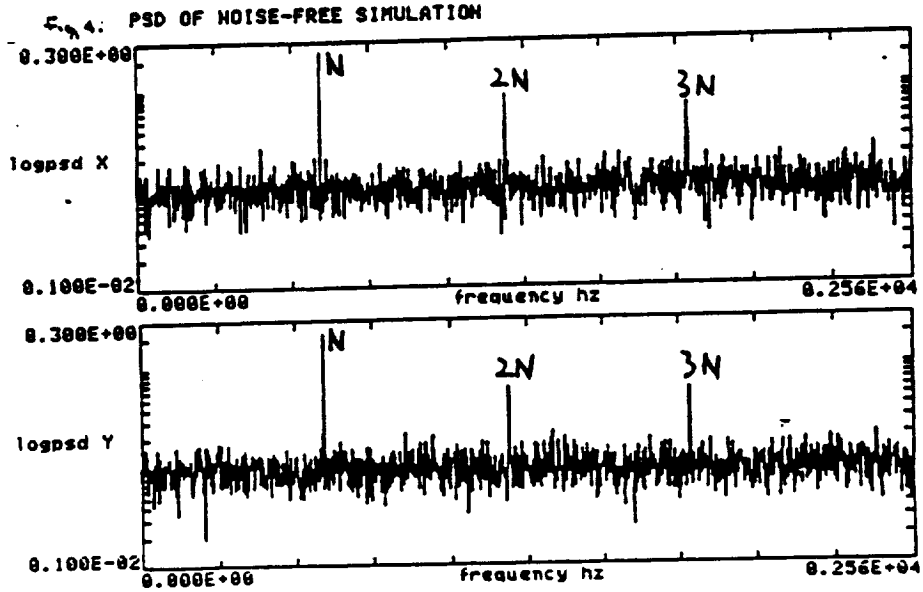

(1)

FIG 5. PSD OF SIMULATION # 1 WITH ADDITIVE GAUSSIAN WHITE NOISE

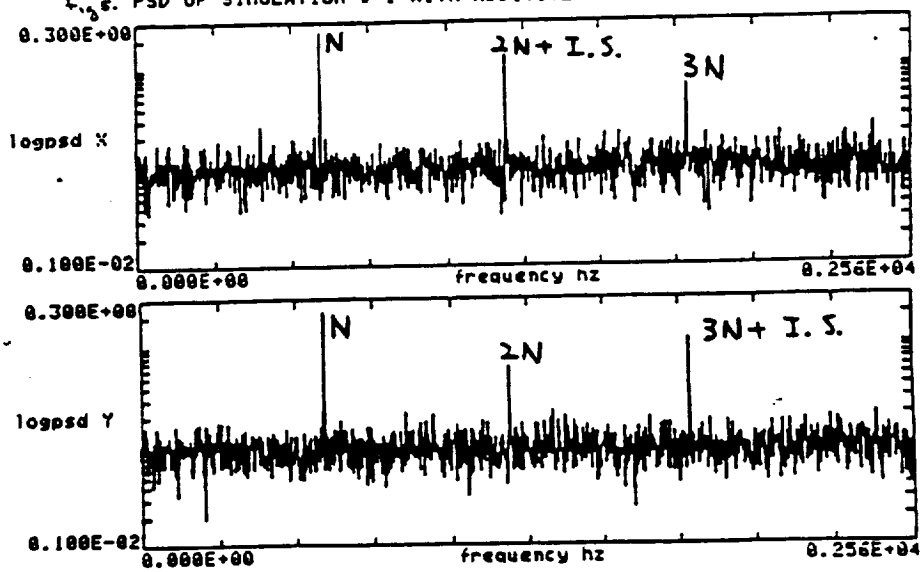

(2)

FIG 6. PSD OF SIMULATION # 2 WITH ADDITIVE GAUSSIAN WHITE NOISE + INDEPENDENT SINE WAVES AT 2N IN X(T) & 3N IN Y(T)

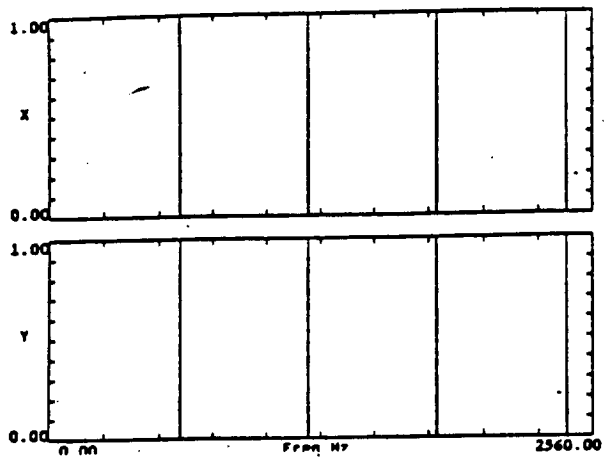

HYPER-COHERENCE FOR NOISE-FREE SIMULATION SIGNAL
REFERENCE FREQ = 610 Hz

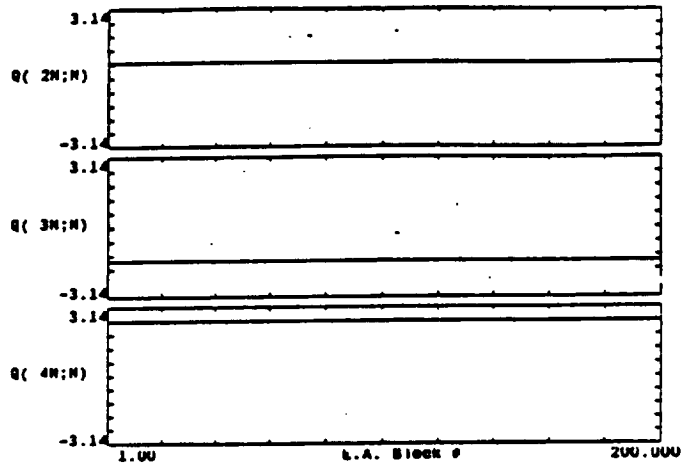

COMPOUND PHASE OF NOISE-FREE DATA x(t)

(1)

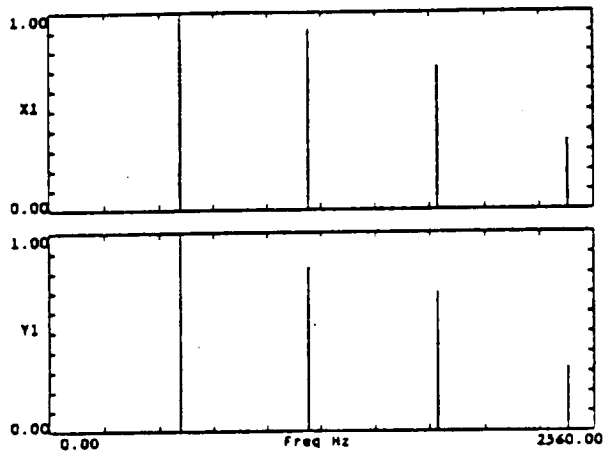

HYPER-COHERENCE FOR CASE-1 (SIN + GWN)
REFERENCE FREQ = 610 Hz

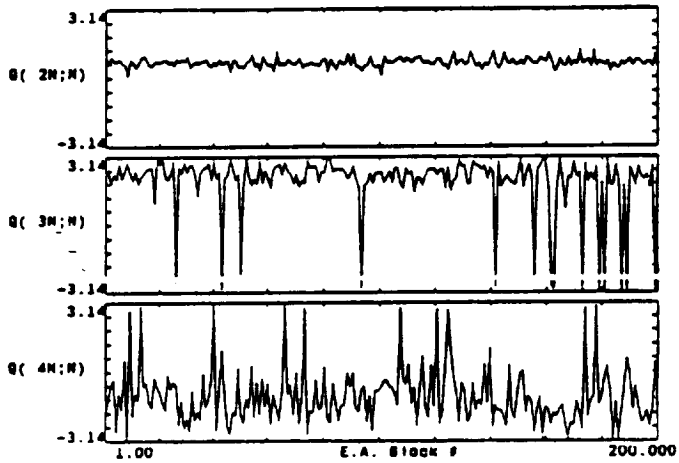

COMPOUND PHASE OF CASE-1 SIN+GWN x1(t)

(2)

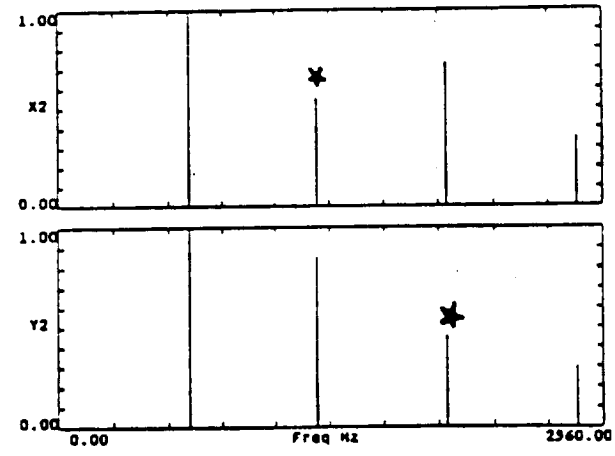

HYPER-COHERENCE FOR CASE-2 (SIN + GWN + INDEPENDENT SIN)
REFERENCE FREQ = 610 Hz

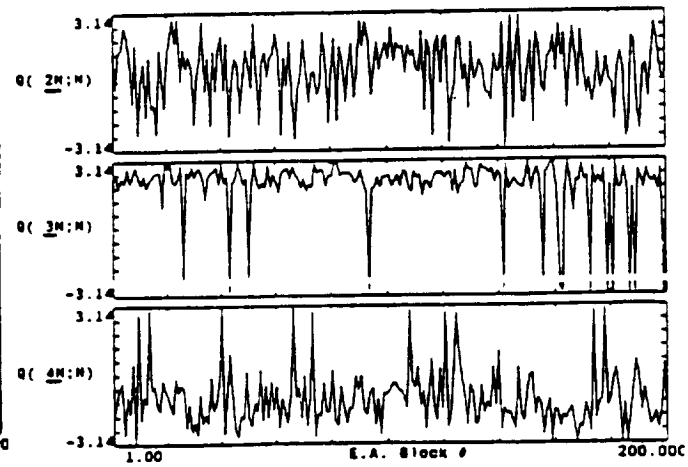

COMPOUND PHASE OF CASE-2 SIN+GWN+INDEPENDENT SIN x2(t)

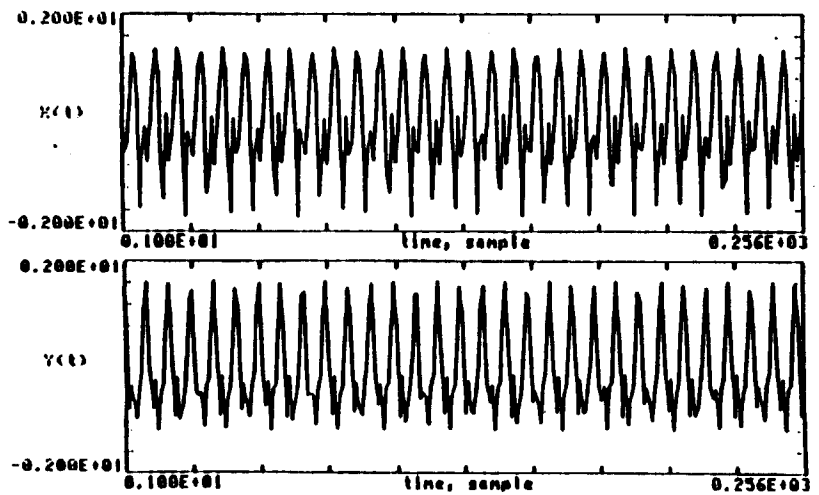

(1)

Fig 13. RECOVERED TIME SERIES OF SIMULATION 8 1
BY USING HYPER-COHERENCE FILTERING

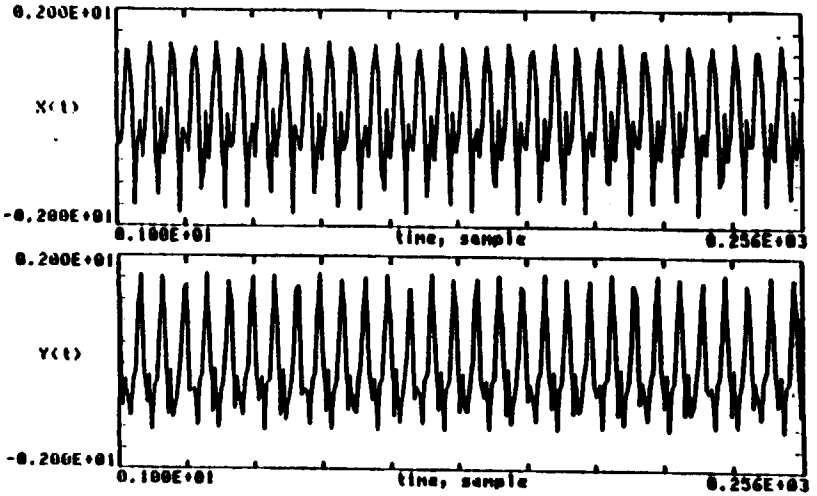

(2)

Fig 14. RECOVERED TIME SERIES OF SIMULATION 8 2
BY USING HYPER-COHERENCE FILTERING

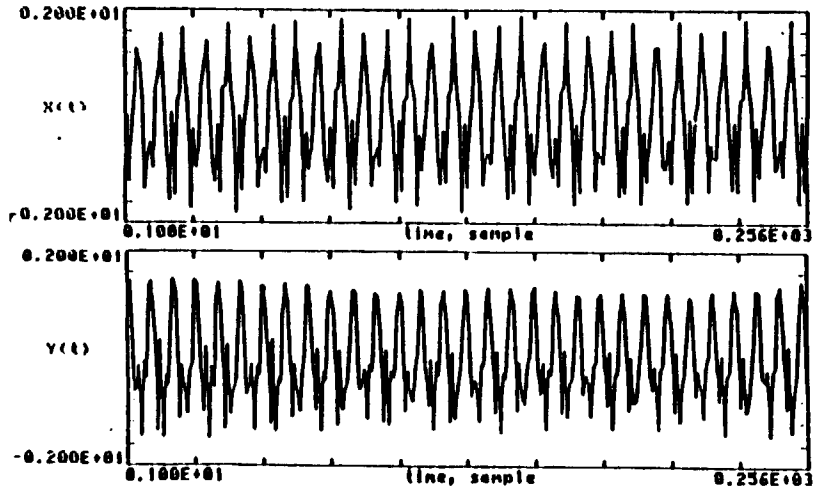

Fig 15. RECOVERED TIME SERIES OF SIMULATION 8 1
BY USING COMB FILTERING

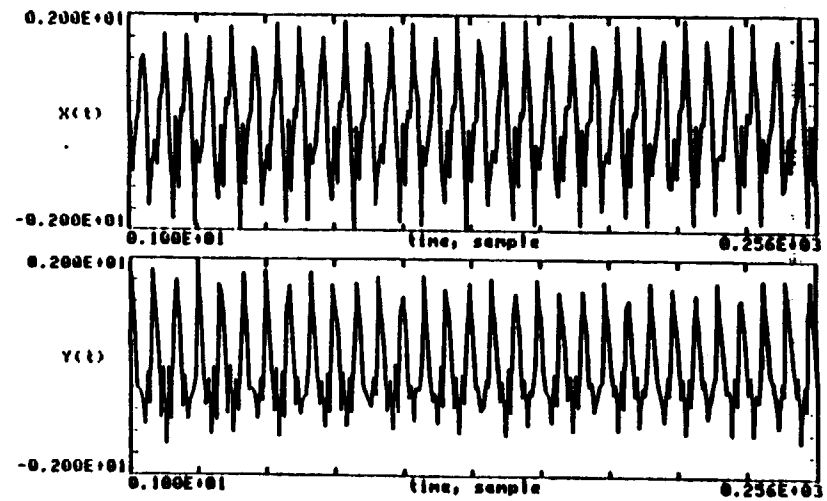

Fig 16. RECOVERED TIME SERIES OF SIMULATION 8 2
BY USING COMB FILTERING

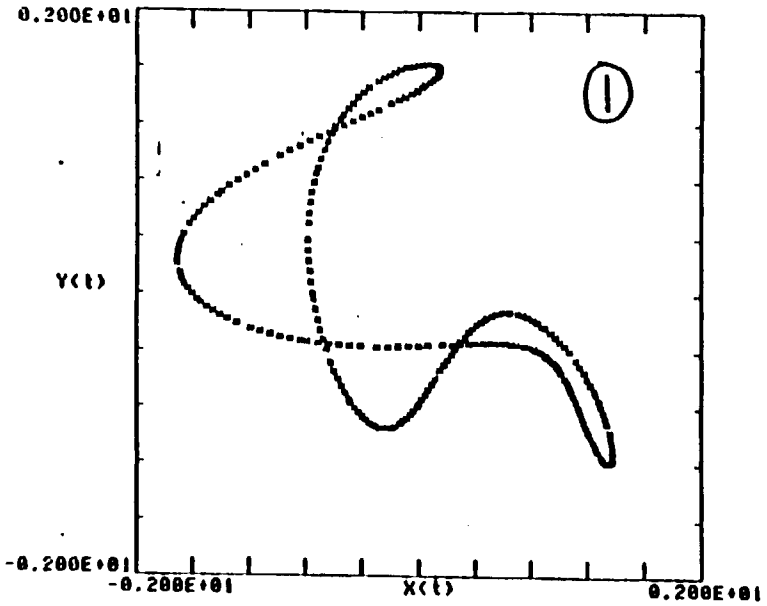

Fig 12. RECOVERED ORBITAL DIAGRAM OF SIMULATION # 1 BY USING HYPER-COHERENCE FILTERING

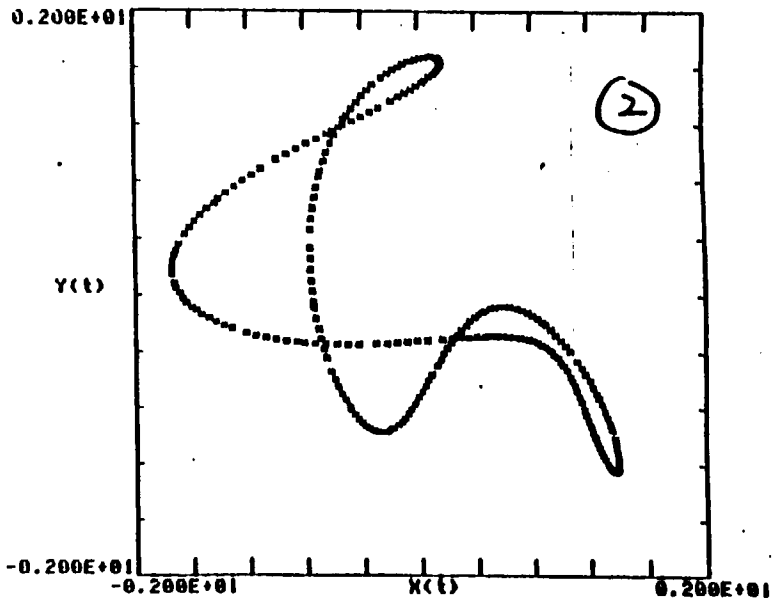

Fig 13. RECOVERED ORBITAL DIAGRAM OF SIMULATION # 2 BY USING HYPER-COHERENCE FILTERING

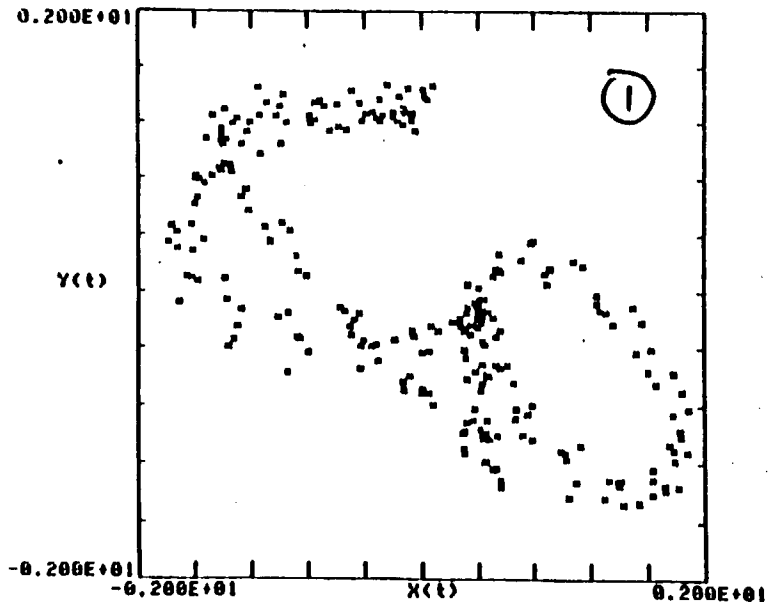

Fig 14. RECOVERED ORBITAL DIAGRAM OF SIMULATION # 1 BY USING COMB FILTERING

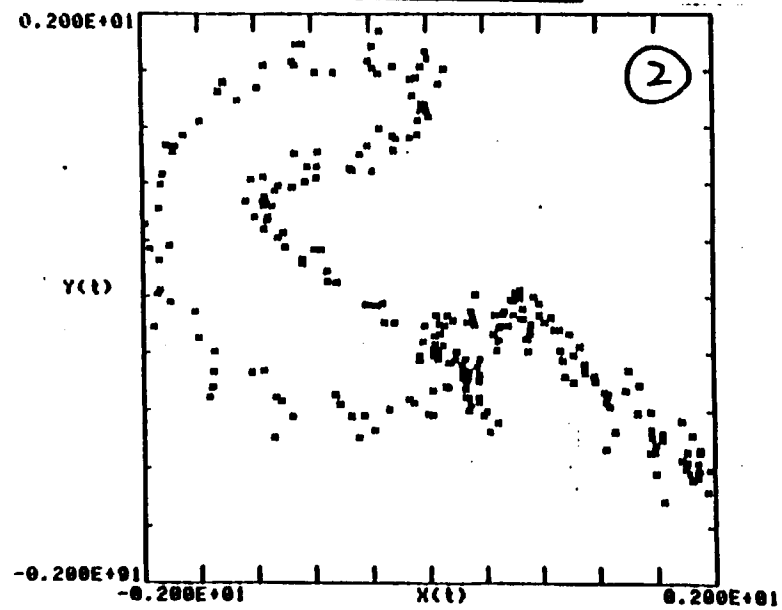

Fig 15. RECOVERED ORBITAL DIAGRAM OF SIMULATION # 2 BY USING COMB FILTERING

901-436

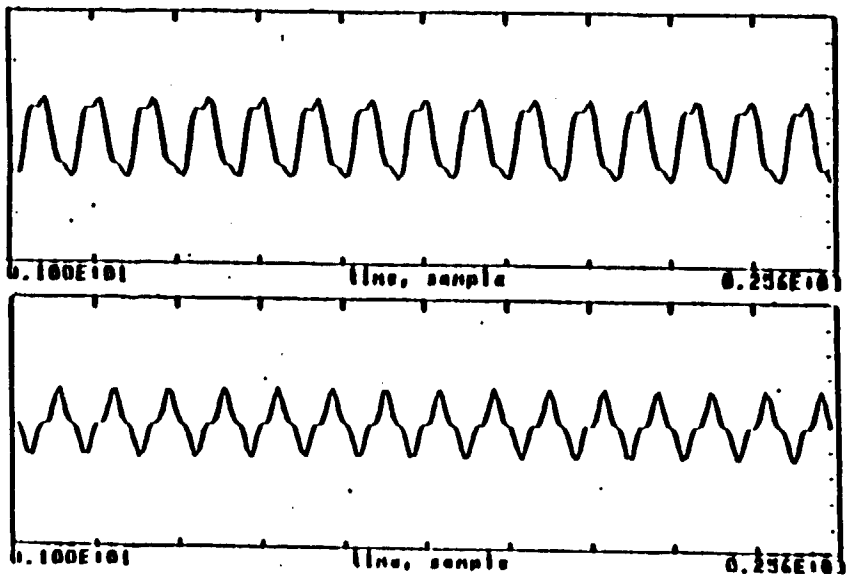

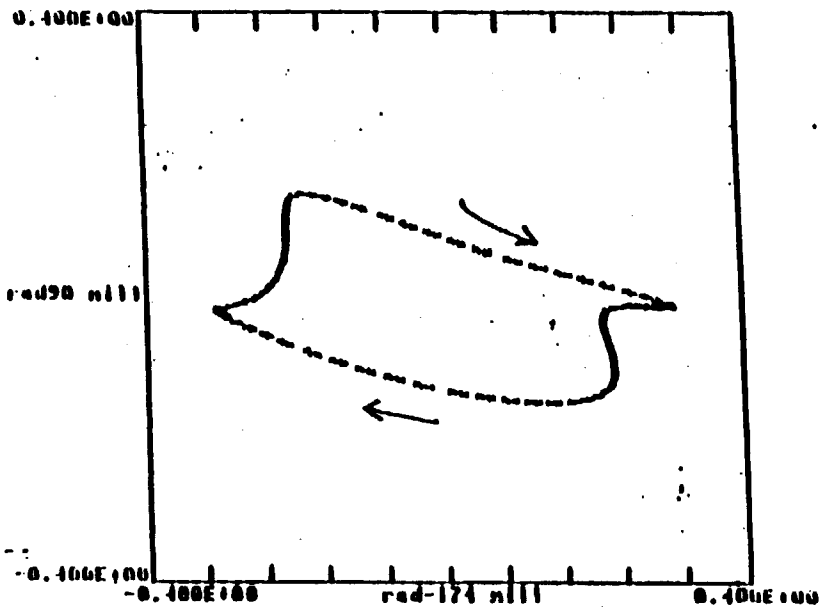

ORBITAL DIAGRAM OF 901-436 BY HUMAN CONTROL

901-471

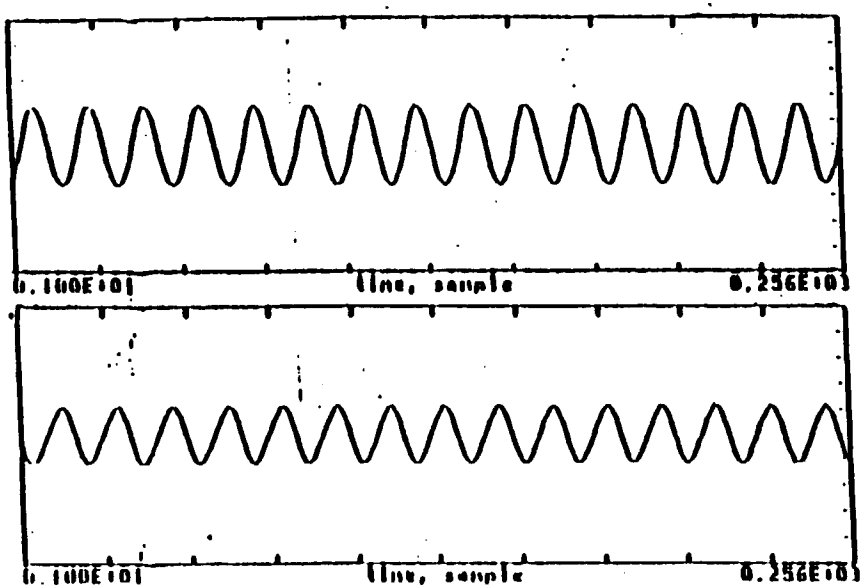

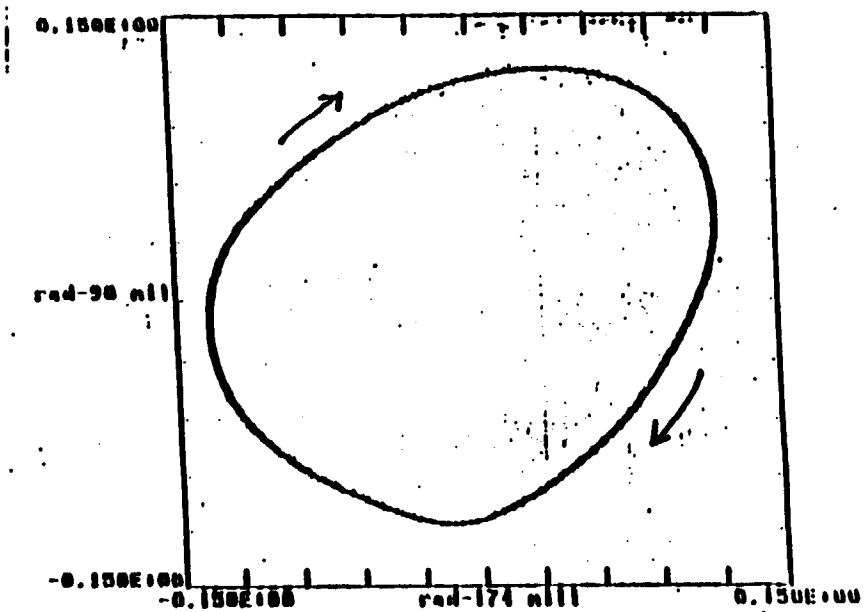

901-471 s176 100 x 2048 fr-693.75

PSD ISOPLOT FOR TEST 901-436

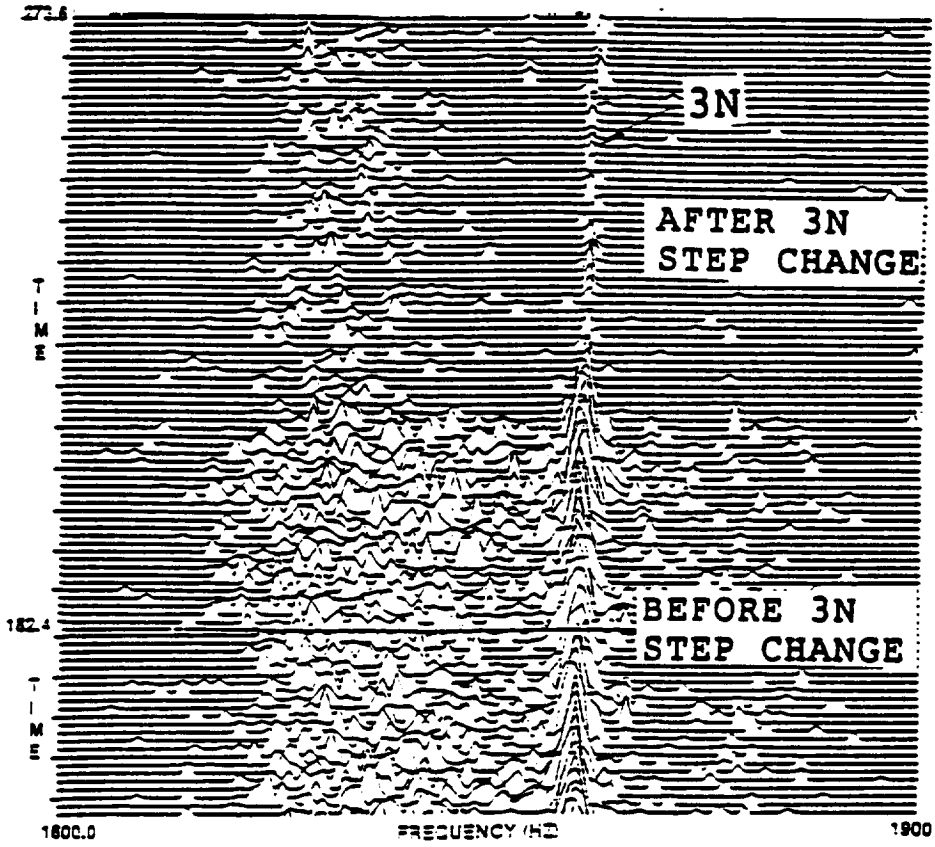

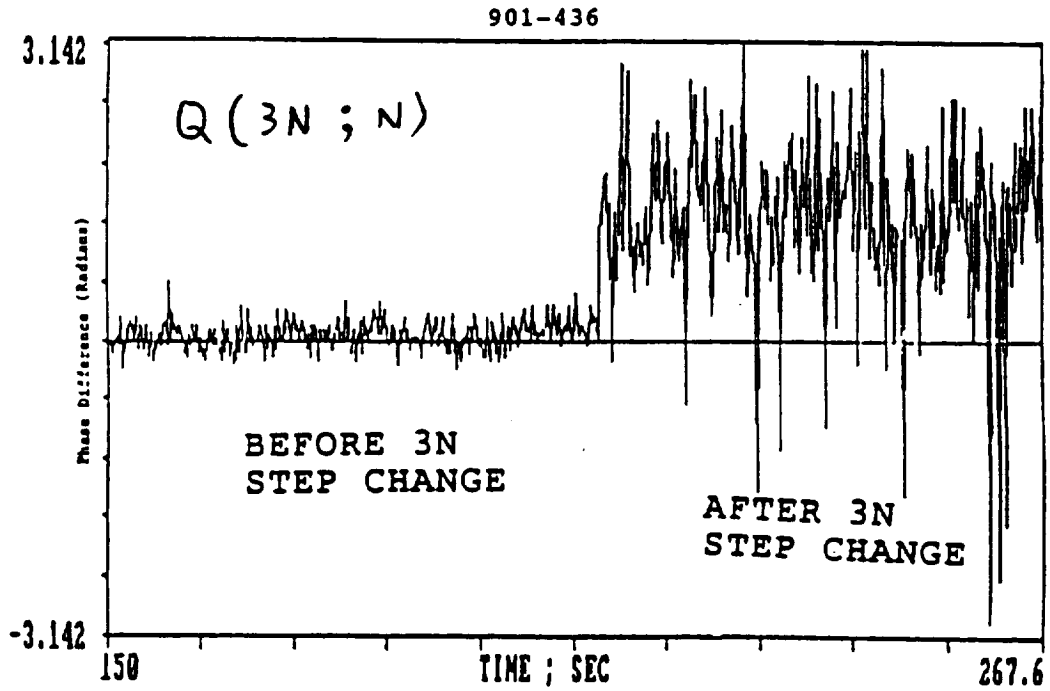

PHASE OF HYPER-COHERENCE AT 3N

901-436

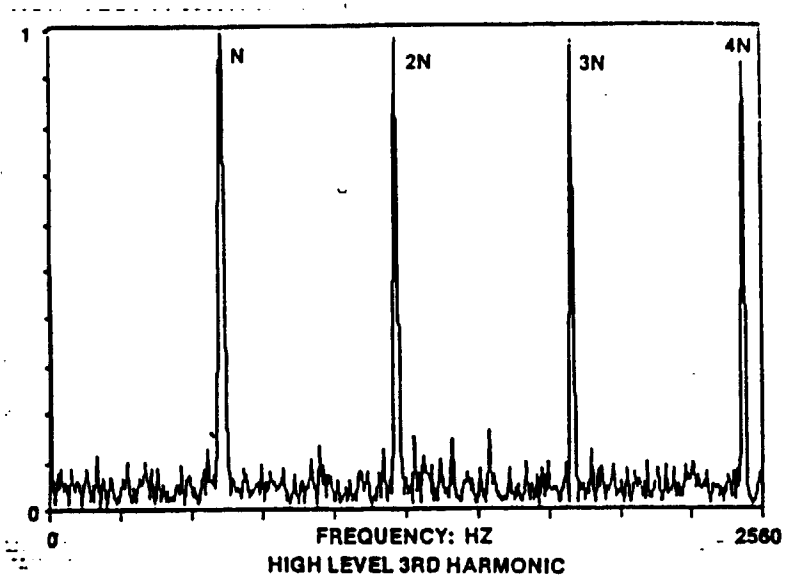

HIGH LEVEL 3RD HARMONIC

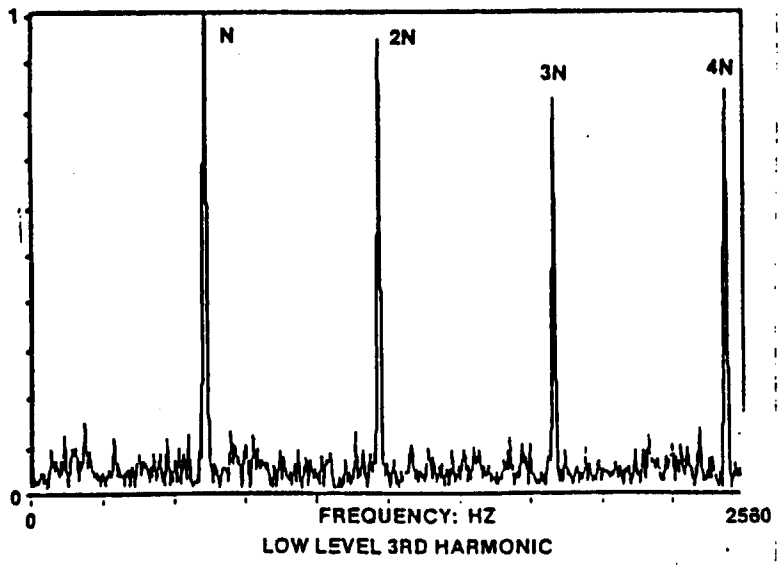

LOW LEVEL 3RD HARMONIC

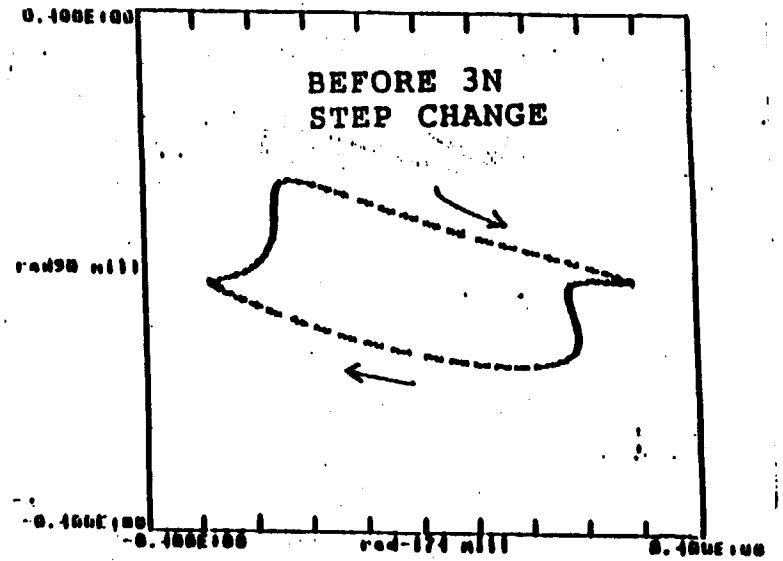

ORBITAL DIAGRAM OF 901-436 BY HYPER-COHERENCE FILTERING 8:168 BEFORE 3N DIMINISHED

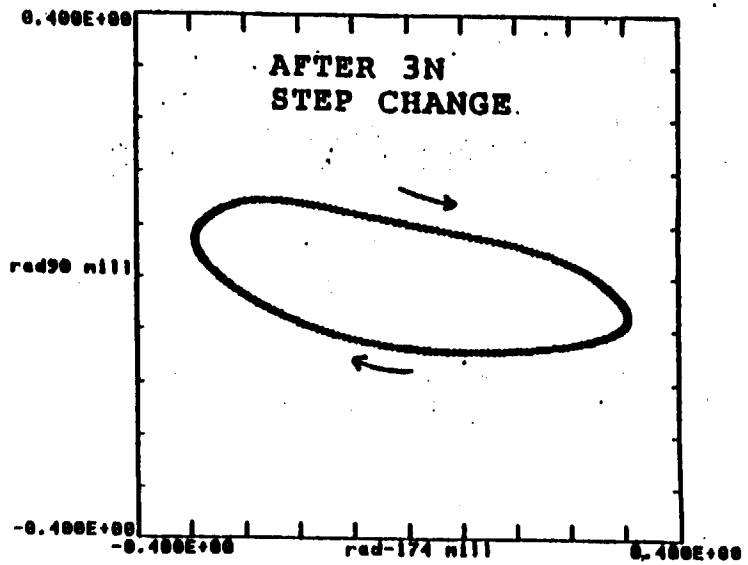

ORBITAL DIAGRAM OF 901-436 BY HYPER-COHERENCE FILTERING 8:215 AFTER 3N DIMINISHED

LIMITATION OF HYPER-COHERENCE

Q(Wn; W1)= n P(W1) - P(Wn)

- The noise presented in P(W1) will be enlarged by n times.
  When n is large, this noise component will be expanded over the $-\pi$ to π cycle, and folded back onto this $-\pi$ to π cycle.
  ===> smear the phase coherence.

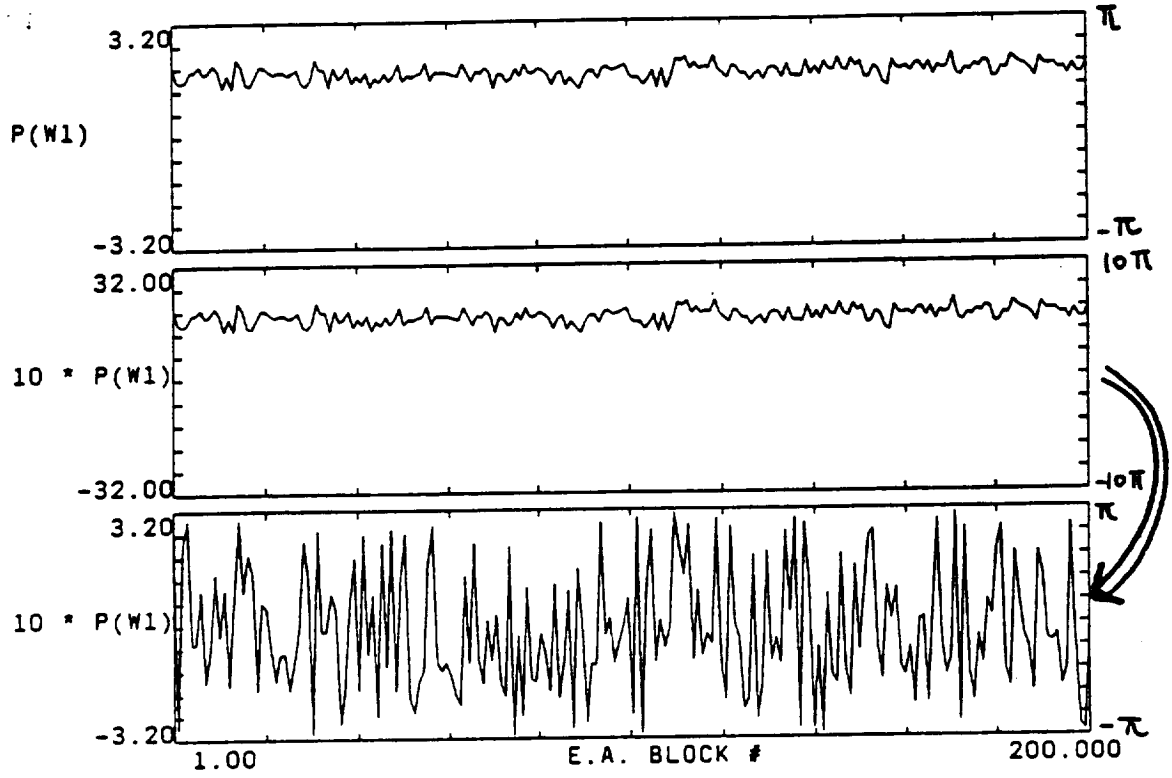

(1) n should not be too large. (LE 5 for typical SSME data)

(2) Choose fundamental component with good SNR

GENERALIZED HYPER-COHERENCE (GHC)

-- Frequency Combination Requirement:

- Bispectrum ==> (W1, W2, W1+W2 or W1-W2)
- Trispectrum ==> (W1, W2, W3, W1+W2+W3)
- Hyper-Coherence ==> (W1, N * W1) N = Integer
- ???????? ==> (W1, W2) Arbitrary Frequency Pair

-- 4KHz Example:

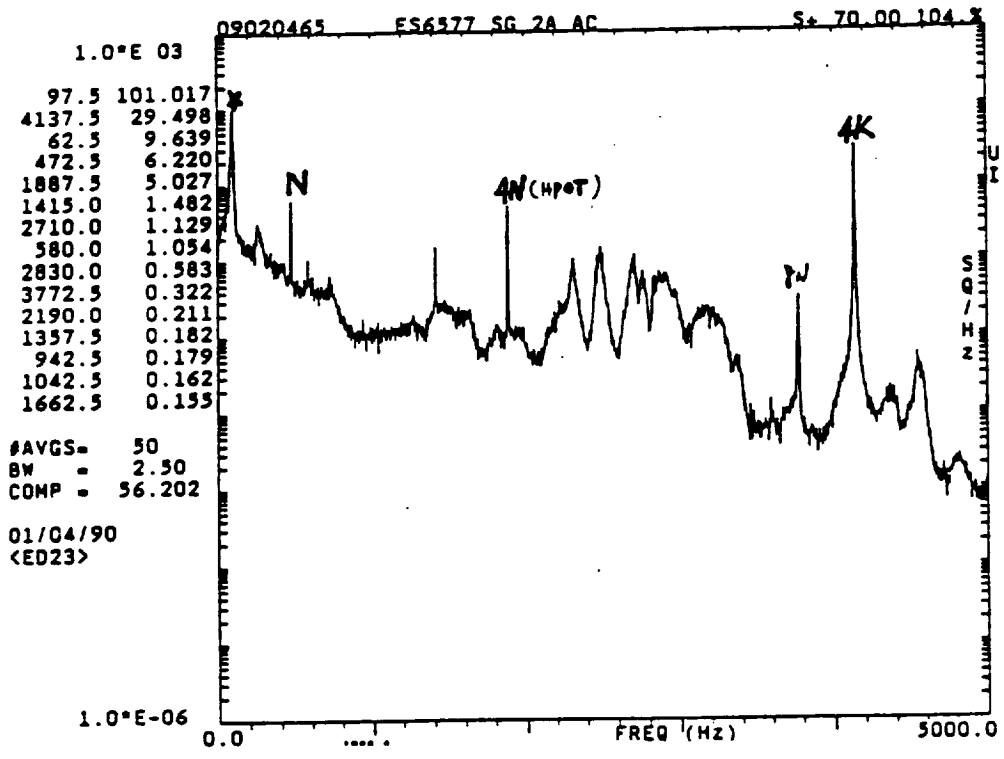

====> Components at (4KHz, *, N, 4N) do not satisfy any of the above frequency combination requirements.

GHC: Identify the correlation between two spectral components at arbitrary frequencies (W1, W2) in the sense of frequency lock-in (Frequency synchronous).

- Gear Box With Non-Integer Gear Ratio (R)

Gear#1 (N1-Tooth)

Gear#2 (N2-Tooth)

===> Gear Ratio R = N1/N2

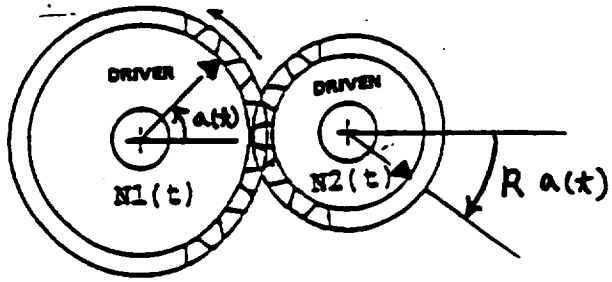

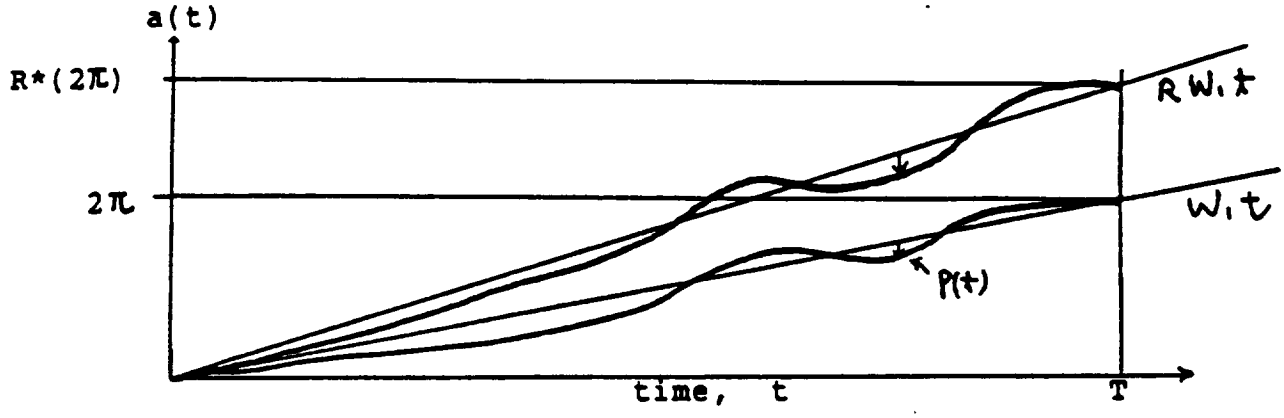

ASSUMPTION: Perfect Gear Mesh (No Broken Or Worn Gear-Tooth)

- If Key-Phasor A goes through one cycle of rotation with angular displacement a(t), then Key-Phasor B will finish R cycle of rotation with angular displacement R*a(t)
- The angular displacement a(t) can be modeled as:

$$a(t) = \begin{cases} W1\ t & \text{for pure harmonic motion (sine wave)} \\ \underline{W1\ t + p(t)} & \text{for motion with } \underline{\text{slowly phase drifting p(t)}} \end{cases}$$

$$\begin{cases} \text{Gear\#1} \Longrightarrow \cos[\ a(t)\ ] = \cos[\ W1\ t + p(t)\ ] \\ \text{Gear\#2} \Longrightarrow \cos[\ R*a(t)\ ] = \cos[\ R*W1\ t + R*p(t)\ ] \end{cases}$$

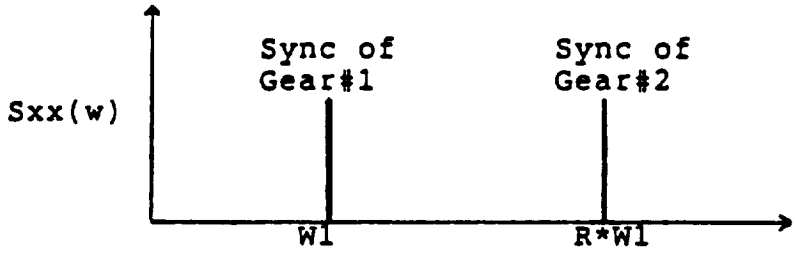

- If Gear Ratio R is an integer: (R=n)

Hyper-Coherence ==> Compound Phase Q(Wn,W1) = n P(W1) -P(Wn)

$$\text{FFT} \Longrightarrow \begin{cases} P(W1) = p(t) + k1(2\pi) \\ P(Wn) = n\,p(t) + k2(2\pi) \end{cases}$$

===> $Q(Wn,W1) = [n\,p(t) + n\,k1\,(2\pi)\,] - [\,n\,p(t) + k2(2\pi)\,]$

$= \underline{n\,k1(2\pi) - k2(2\pi)}$ = constant phase

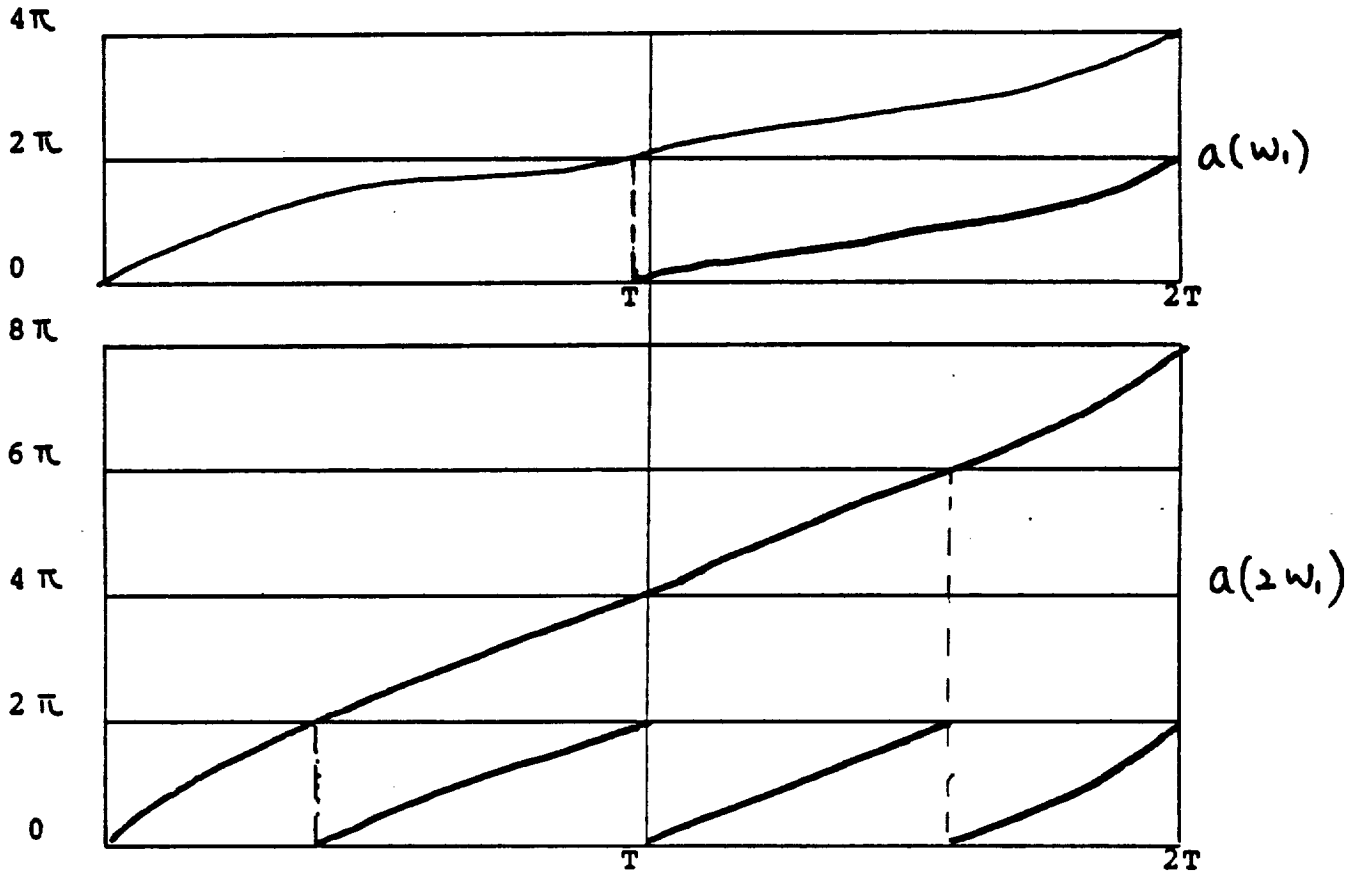

- If Gear Ratio R is not an integer: (R=R)

$$\text{FFT} \Longrightarrow \begin{cases} P(W1) = p(t) + k1(2\pi) \\ P(WR) = R\,p(t) + k2(2\pi) \end{cases}$$

===> $Q(WR,W1) = \underline{R\,k1(2\pi) - k2(2\pi)}$ = ambiguous phase (not unique)

- GHC
  - . use the RATE OF CHANGE OF PHASE (INSTANTANEOUS FREQUENCY)
  - . avoid the ambiguity of arbitrary integer multiple of 2π
  - . Frequency Synchronous: p(t) = R p(t)

NARROW-BAND RANDOM -- $x(t)=A(t)\ \mathrm{Cos}[\ Wc\ t + p(t)\ ]$

Instantaneous Amplitude = $A(t)$
Instantaneous Frequency = $Wc + d\ p(t)/dt = Wc + Wi(t)$

---> Intellegence $Wi(t)$ is Frequency Modulated in $x(t)$

FM Demodulator (FM-D) Algorithm:

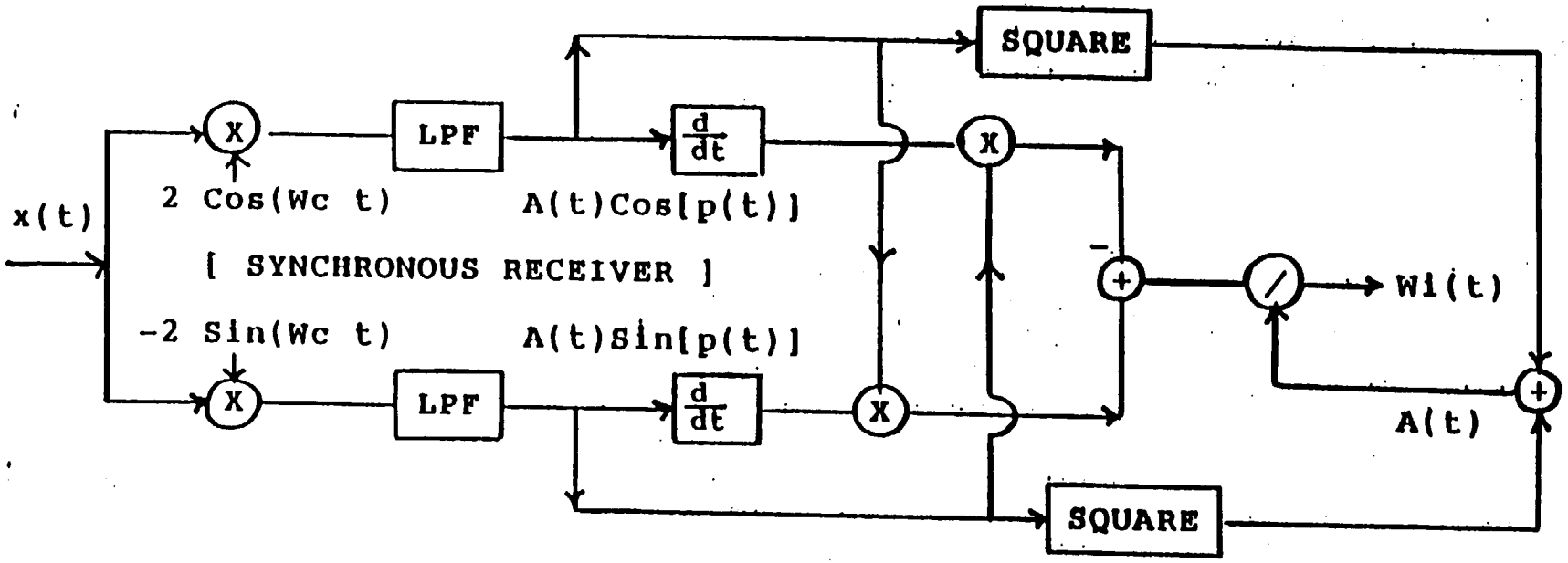

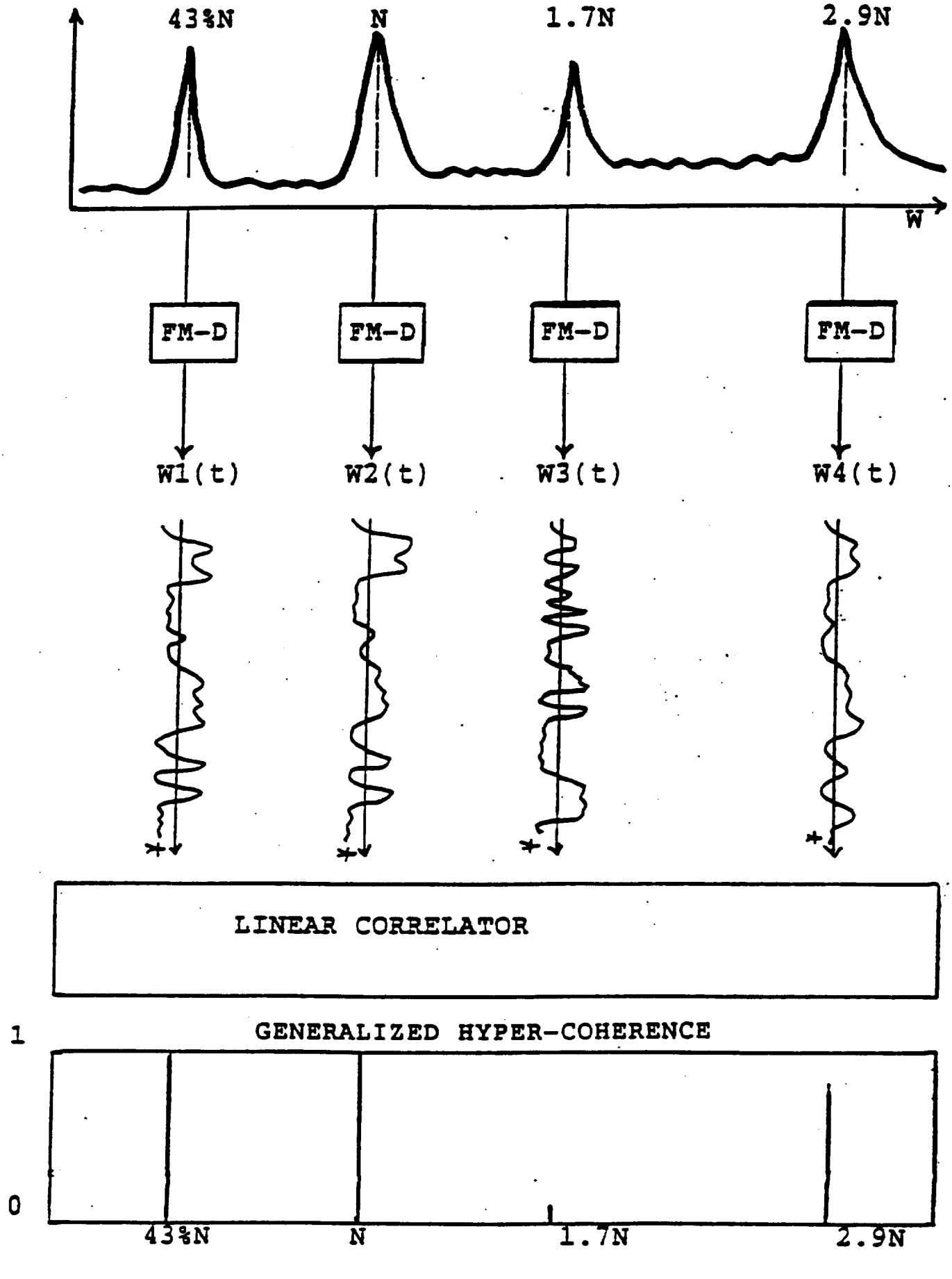
43%N
N
1.7N
2.9N
W
FM-D
FM-D
FM-D
FM-D
W1(t)
W2(t)
W3(t)
W4(t)
LINEAR CORRELATOR
1
GENERALIZED HYPER-COHERENCE
0
43%N
N
1.7N
2.9N

SIMULATION FOR GHC

- Gear Box With Non-Integer Gear Ratio (R)

  Gear#1 (16-Tooth)

  Gear#2 (9-Tooth)

  ===> R = 16/9 =1.78

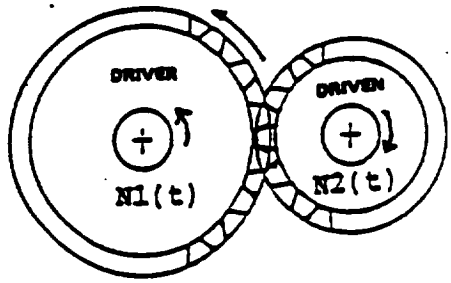

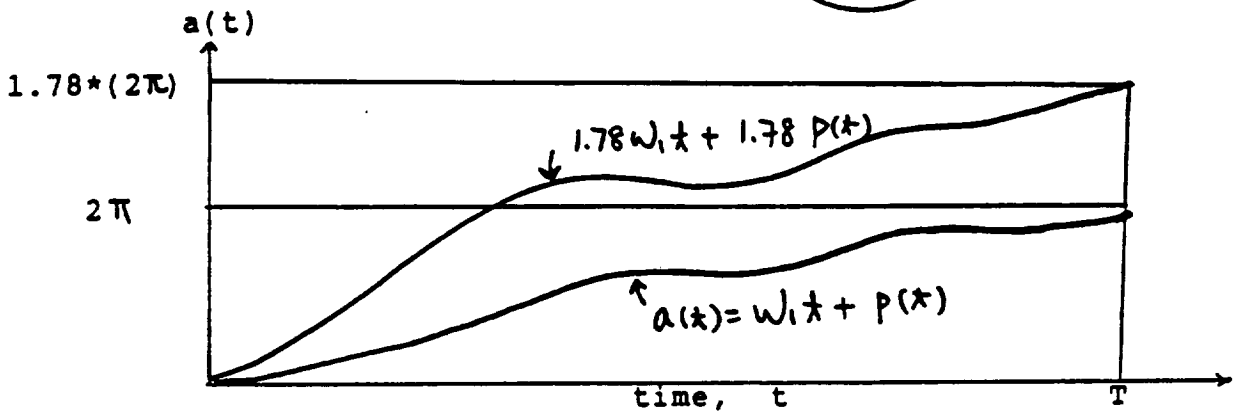

$$\begin{cases} x1(t) = \cos[\,a(t)\,] = \cos[\,W1t + p(t)\,] \\ x2(t) = \cos[1.78\,a(t)] = \cos[1.78*W1t + 1.78*p(t)\,] \\ x3(t) = \cos[\,1.36*W1t + q(t)] \end{cases}$$

Where: { Angular displacement a(t)= W1t + p(t)
{ p(t) and q(t) are independent phase drifting signal

===> simulation signal x(t) = x1(t) + x2(t) + x3(t) + GWN

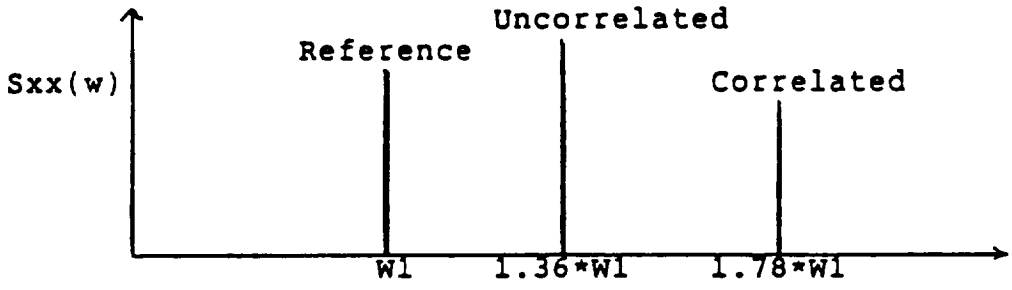

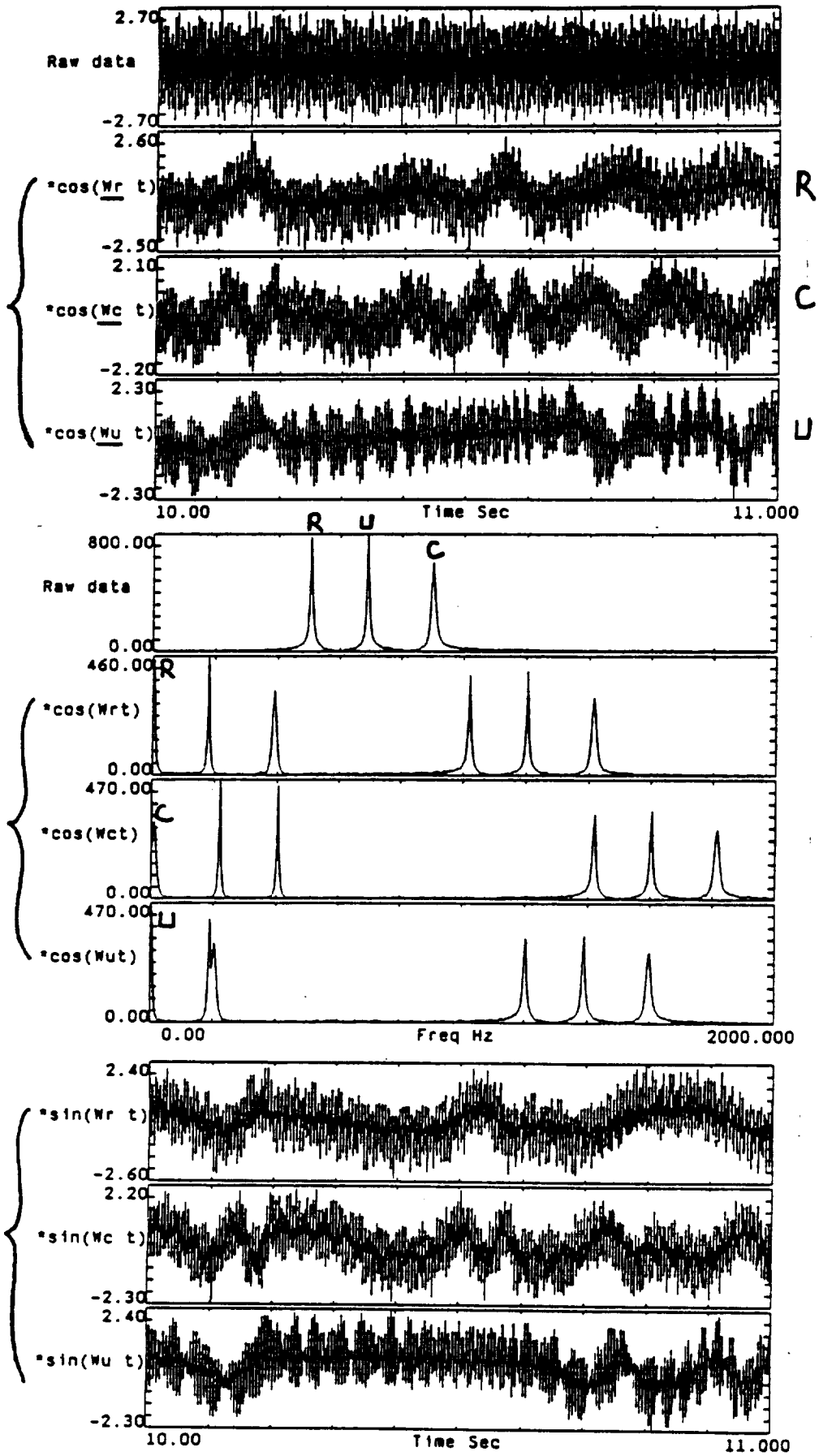
2.70
Raw data
-2.70
2.60
*cos(Wr t)
-2.50
R
2.10
*cos(Wc t)
-2.20
C
2.30
*cos(Wu t)
-2.30
U
10.00
Time Sec
11.000
R
U
C
800.00
Raw data
0.00
460.00
R
*cos(Wrt)
0.00
470.00
C
*cos(Wct)
0.00
470.00
U
*cos(Wut)
0.00
0.00
Freq Hz
2000.000
2.40
*sin(Wr t)
-2.60
2.20
*sin(Wc t)
-2.30
2.40
*sin(Wu t)
-2.30
10.00
Time Sec
11.000

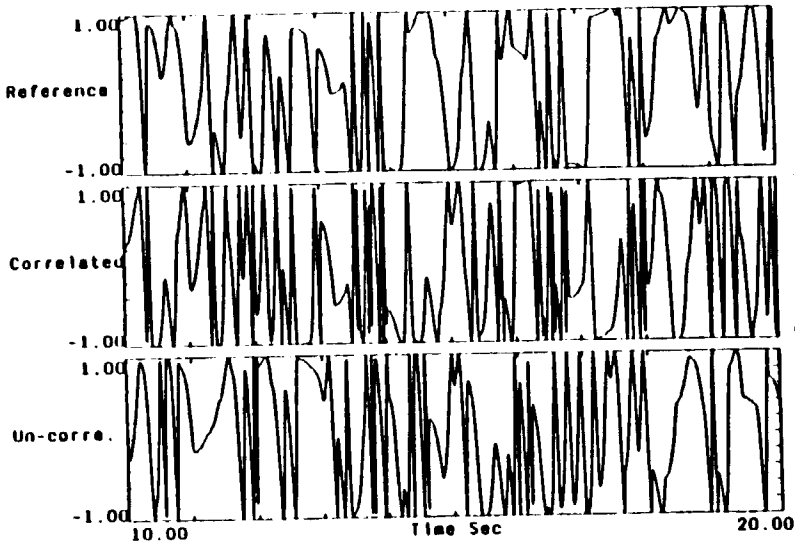

cos[wt+p(t)] + cos[1.78*[wt+p(t)]] + cos[1.36*[wt+q(t)]]
Low-Passed x(t)*cos(Wct)

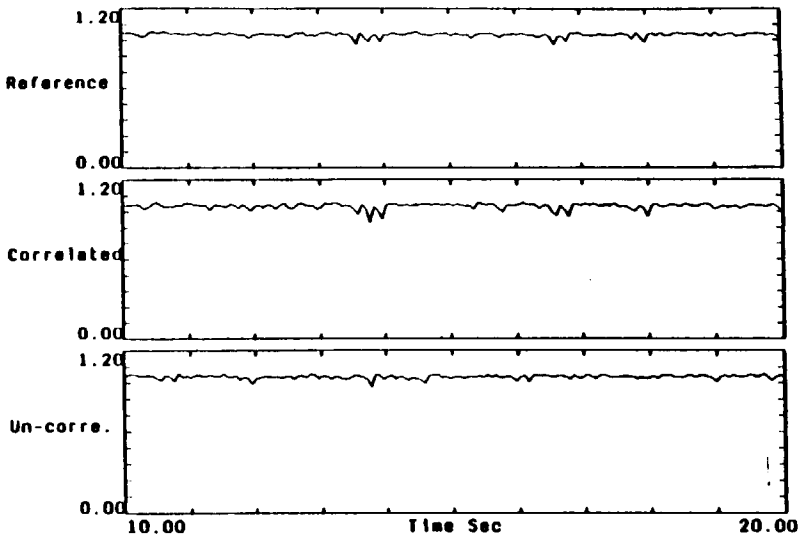

cos[wt+p(t)] + cos[1.78*[wt+p(t)]] + cos[1.36*[wt+q(t)]]
Instantaneous Envelope

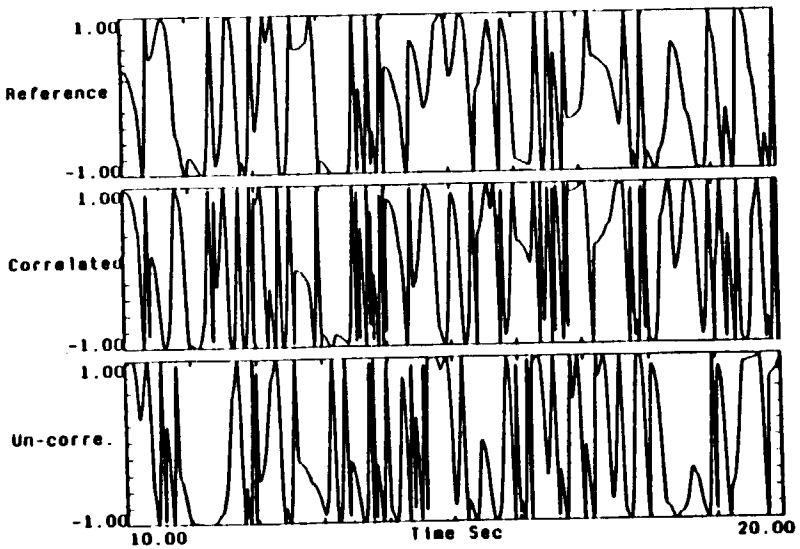

cos[wt+p(t)] + cos[1.78*[wt+p(t)]] + cos[1.36*[wt+q(t)]]
Low-Passed x(t)*sin(Wct)

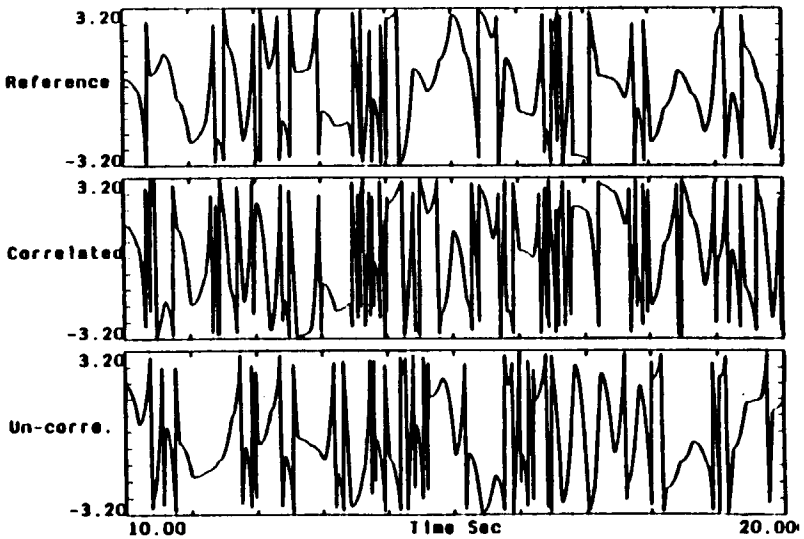

cos[wt+p(t)] + cos[1.78*[wt+p(t)]] + cos[1.36*[wt+q(t)]]
Instantaneous Phases

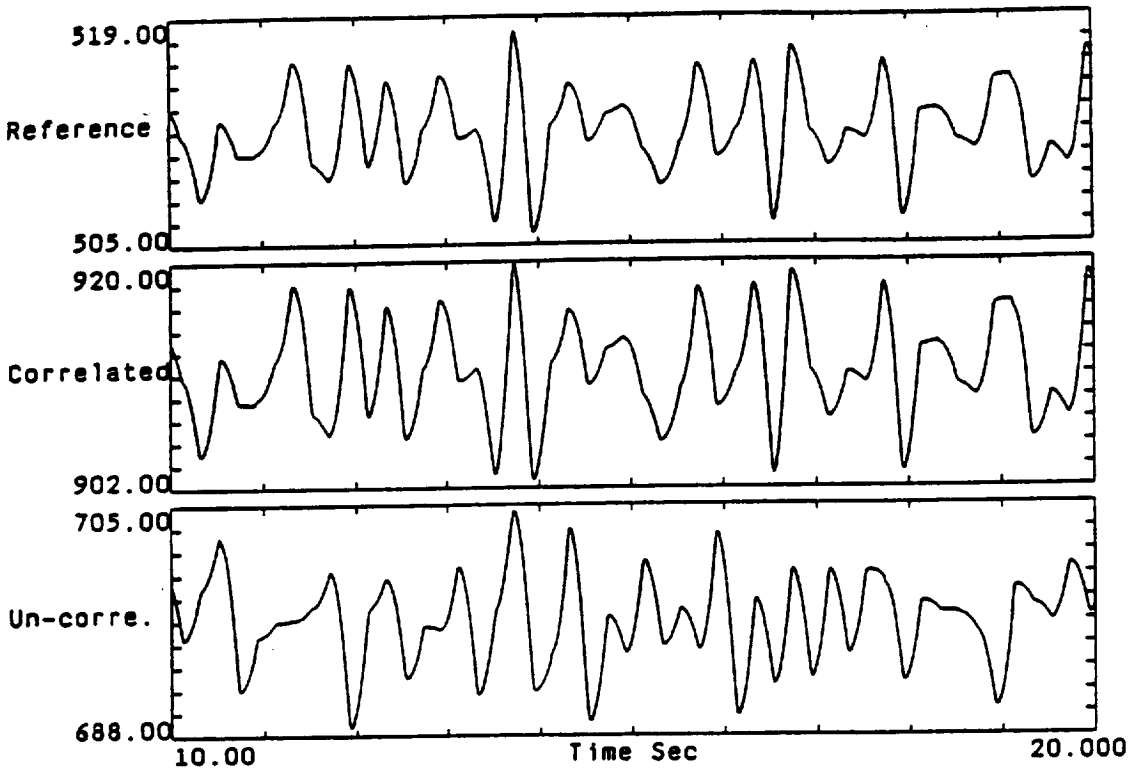

cos[wt+p(t)] + cos{1.78*[wt+p(t)]} + cos{1.36*[wt+q(t)]}
Instantaneous Frequency

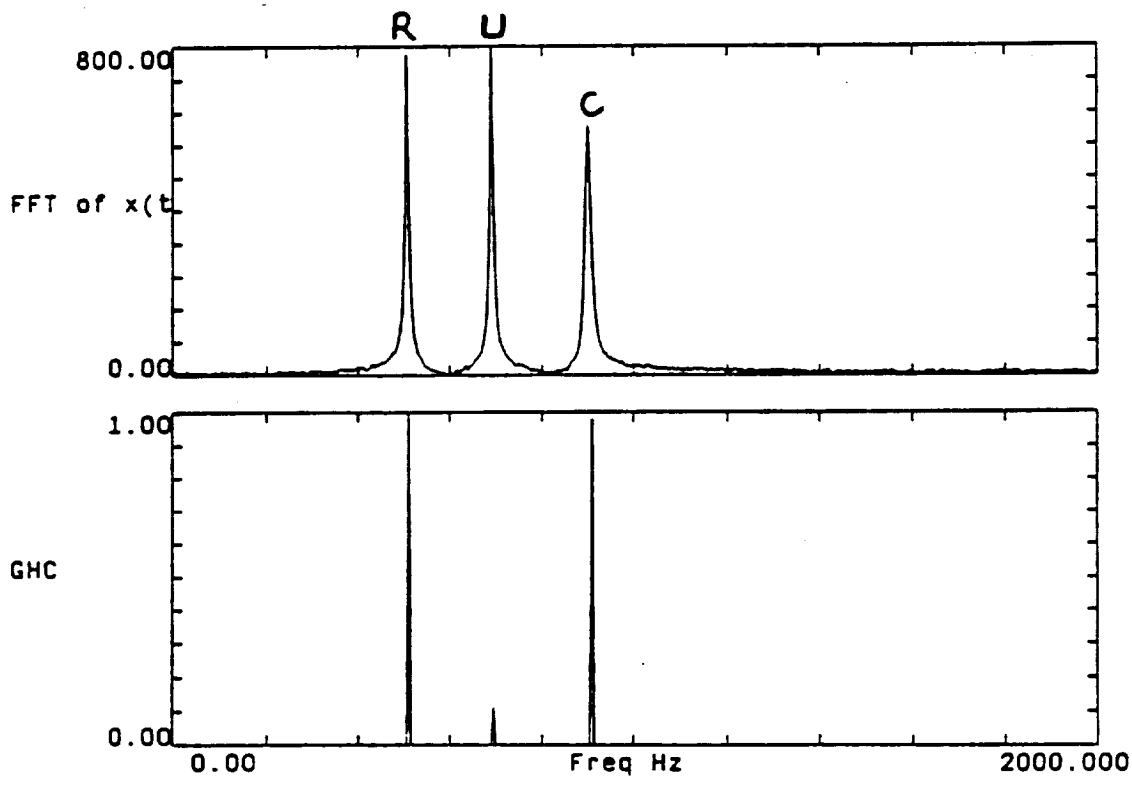

cos[wt+p(t)] + cos{1.78*[wt+p(t)]} + cos{1.36*[wt+q(t)]}
GHC with Reference component at Wr=512 Hz

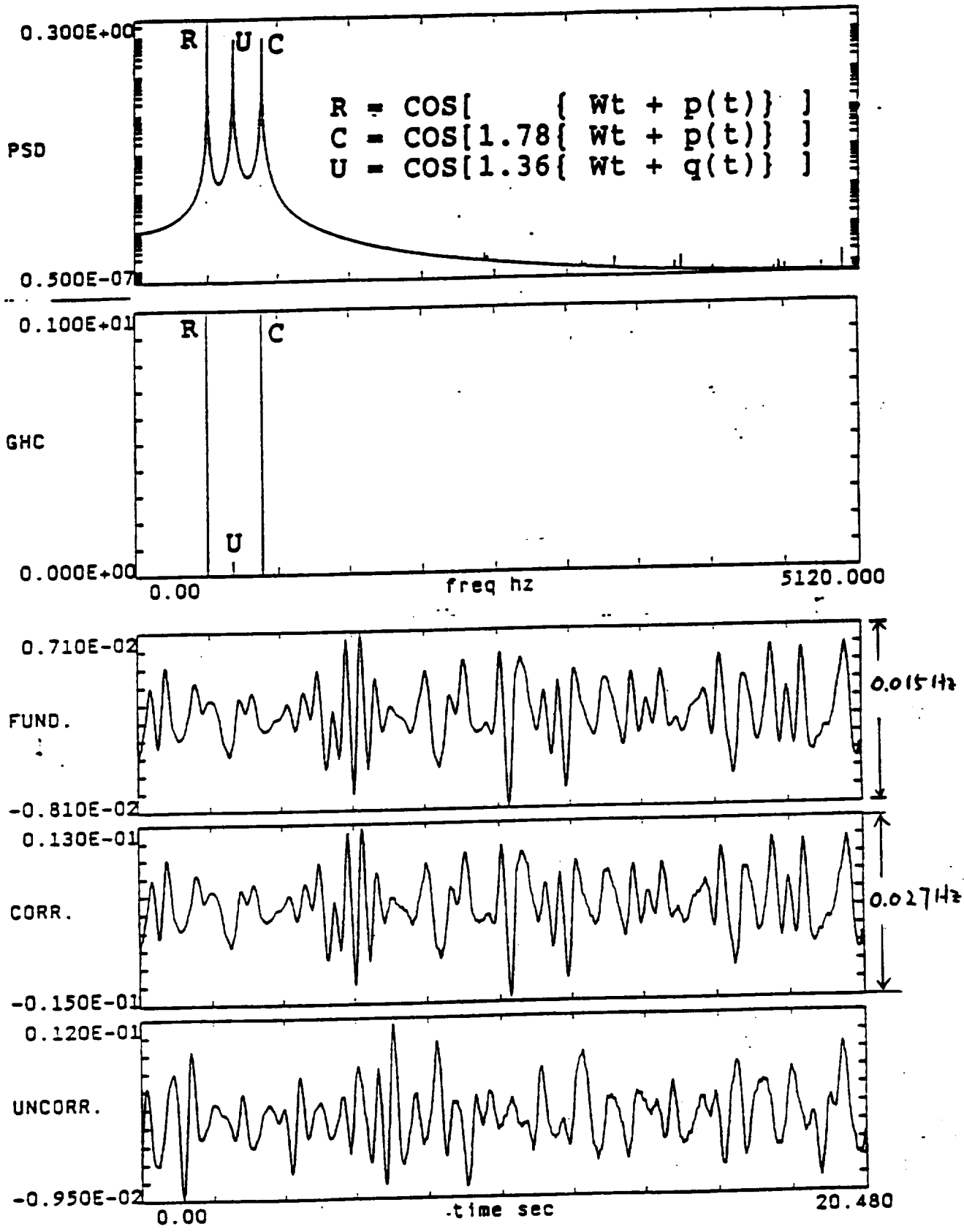

cos[wt+p(t)]+ cos[1.78*[wt+p(t)]]+ cos[1.36*[wt+q(t)]]
test0 dev(GWN)=0
instantaneous frequency variation

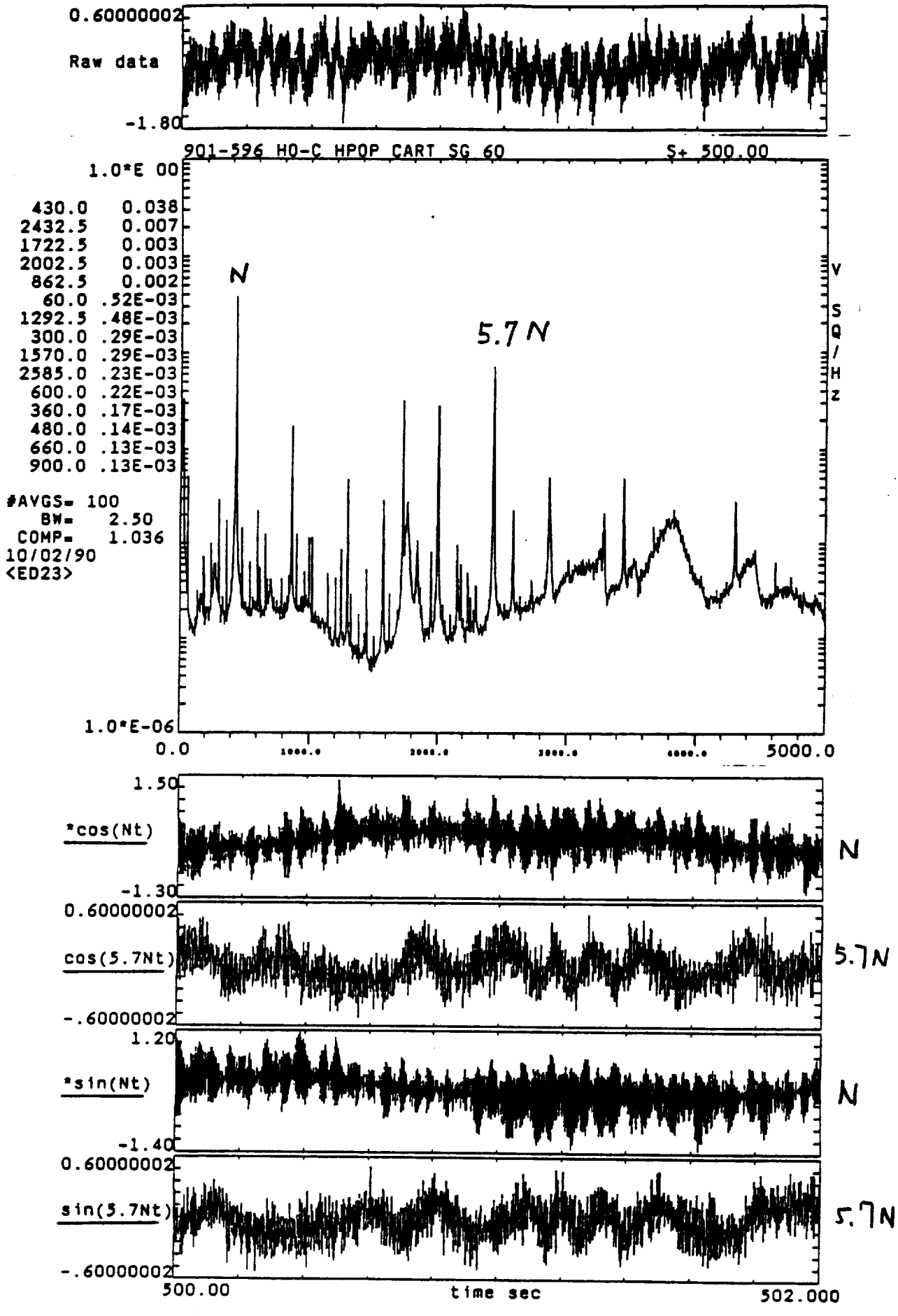
0.60000002
Raw data
-1.80
901-596 HO-C HPOP CART SG 60
S+ 500.00
1.0*E 00
430.0 0.038
2432.5 0.007
1722.5 0.003
2002.5 0.003
862.5 0.002
60.0 .52E-03
1292.5 .48E-03
300.0 .29E-03
1570.0 .29E-03
2585.0 .23E-03
600.0 .22E-03
360.0 .17E-03
480.0 .14E-03
660.0 .13E-03
900.0 .13E-03
#AVGS= 100
BW= 2.50
COMP= 1.036
10/02/90
<ED23>
N
5.7 N
V
S
Q
/
H
z
1.0*E-06
0.0
5000.0
1.50
*cos(Nt)
-1.30
N
0.60000002
cos(5.7Nt)
-.60000002
5.7N
1.20
*sin(Nt)
-1.40
N
0.60000002
sin(5.7Nt)
-.60000002
5.7N
500.00
time sec
502.000

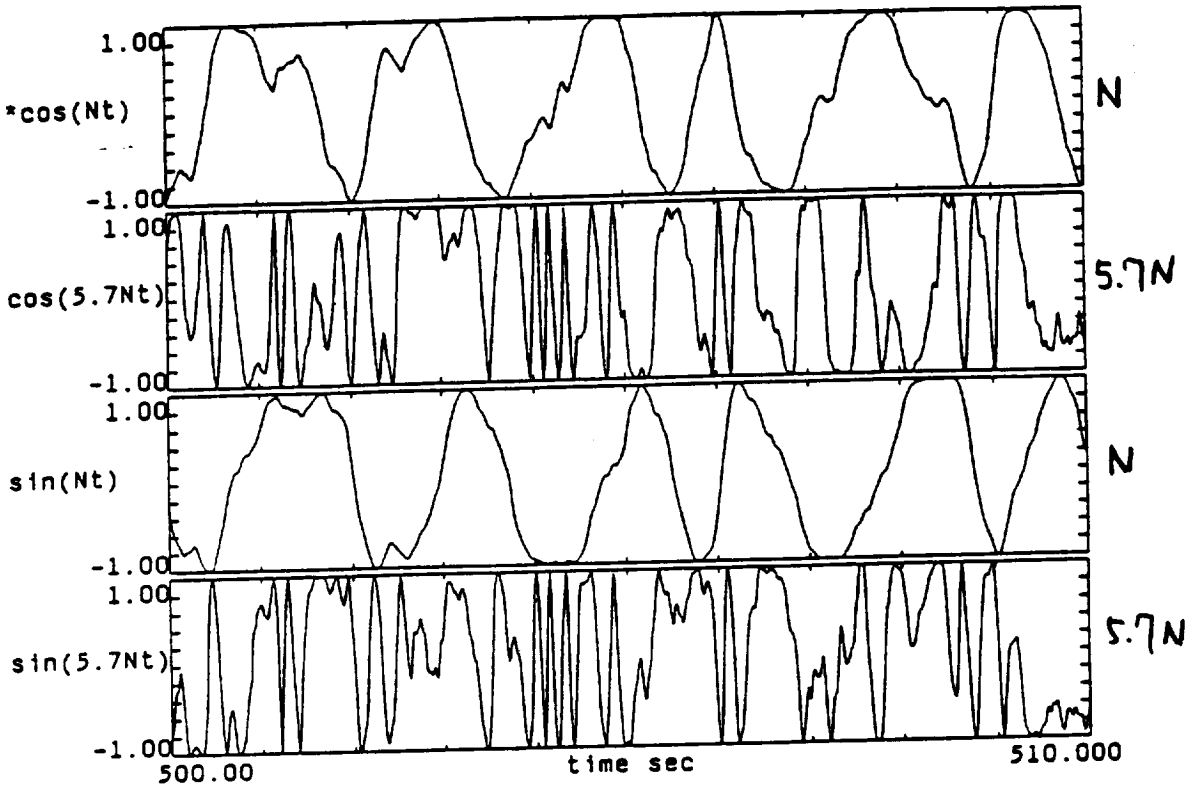

901-596 HPOP CART SG 60
Low-Passed x(t)*cos(Wct) and x(t)*sin(Wct)

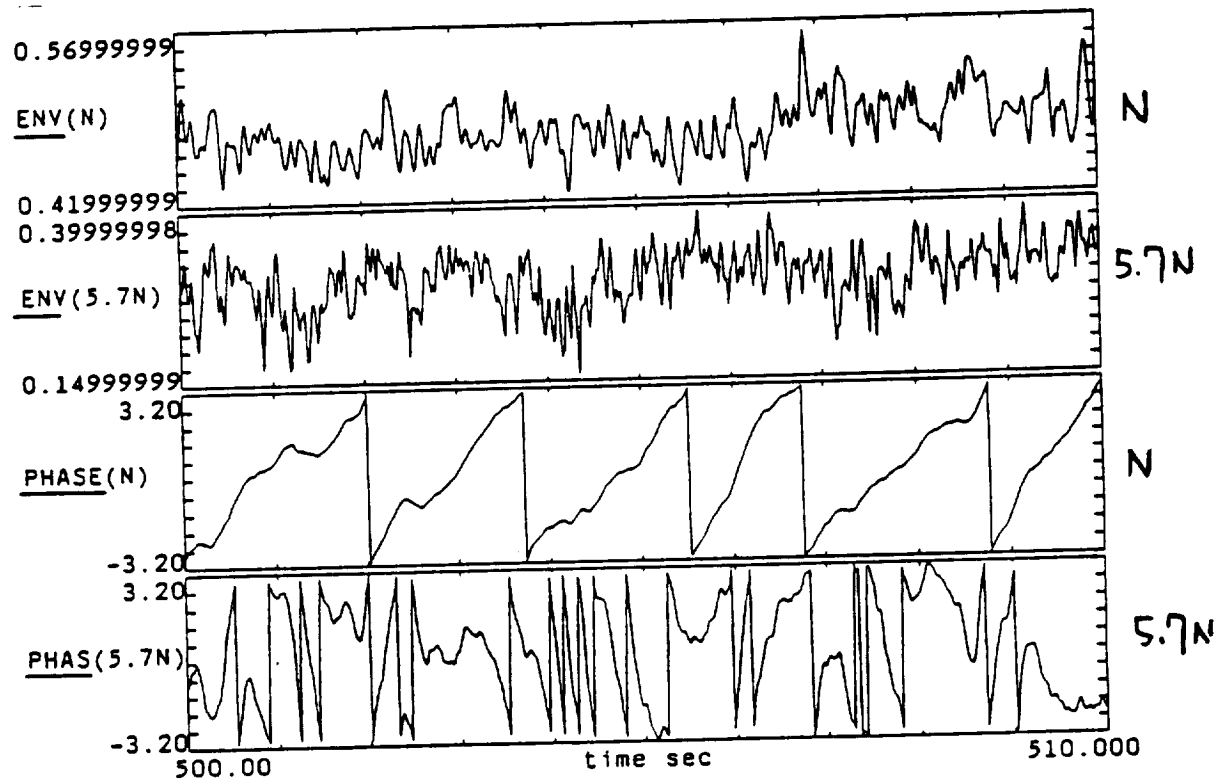

901-596 HPOP CART SG 60
Envelope and Phase

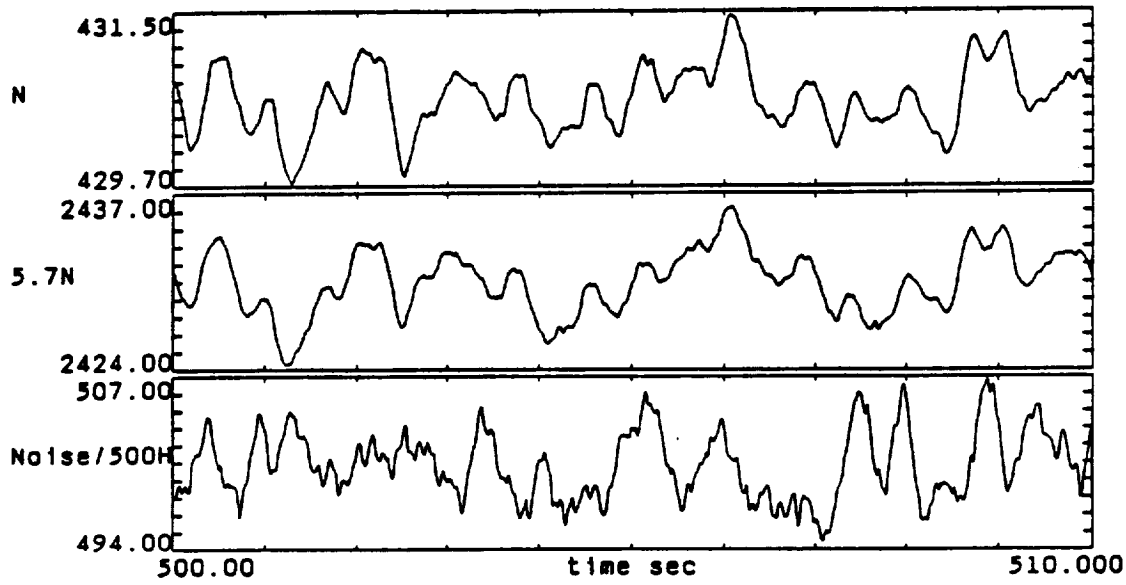

901-596 HPOP CART SG 60
Instantaneous Frequency

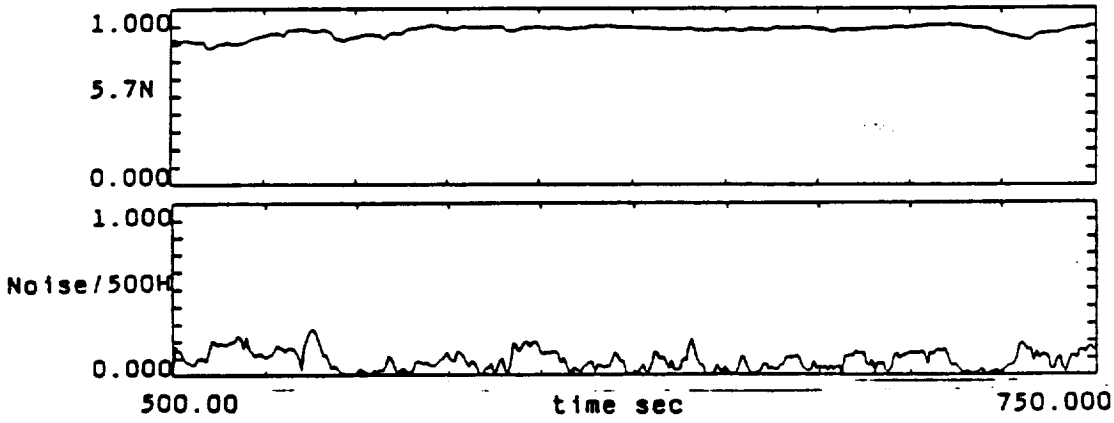

901-596 Moving-averaged G.H.C. Window=20 sec Advance=1 sec
reference component = SYNC of HPOP

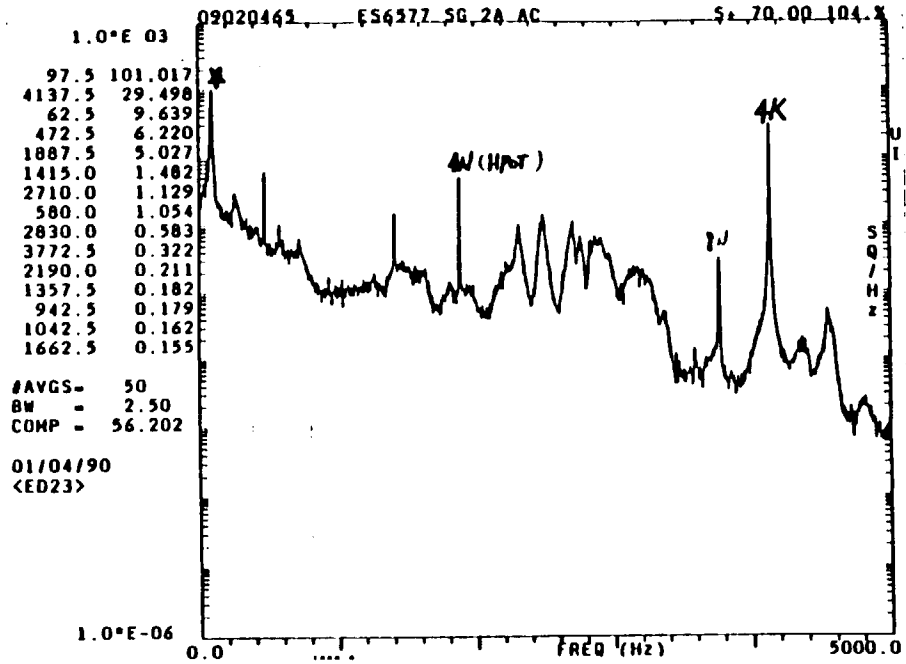
09020465 ES6577 SG 2A AC S= 70.00 104.%
1.0*E 03
97.5 101.017
4137.5 29.498
62.5 9.639
472.5 6.220
1887.5 5.027
1415.0 1.482
2710.0 1.129
580.0 1.054
2830.0 0.583
3772.5 0.322
2190.0 0.211
1357.5 0.182
942.5 0.179
1042.5 0.162
1662.5 0.155
#AVGS= 50
BW = 2.50
COMP = 56.202
01/04/90
<ED23>
1.0*E-06
4W (HPOT)
4K
FREQ (Hz)
0.0
5000.0

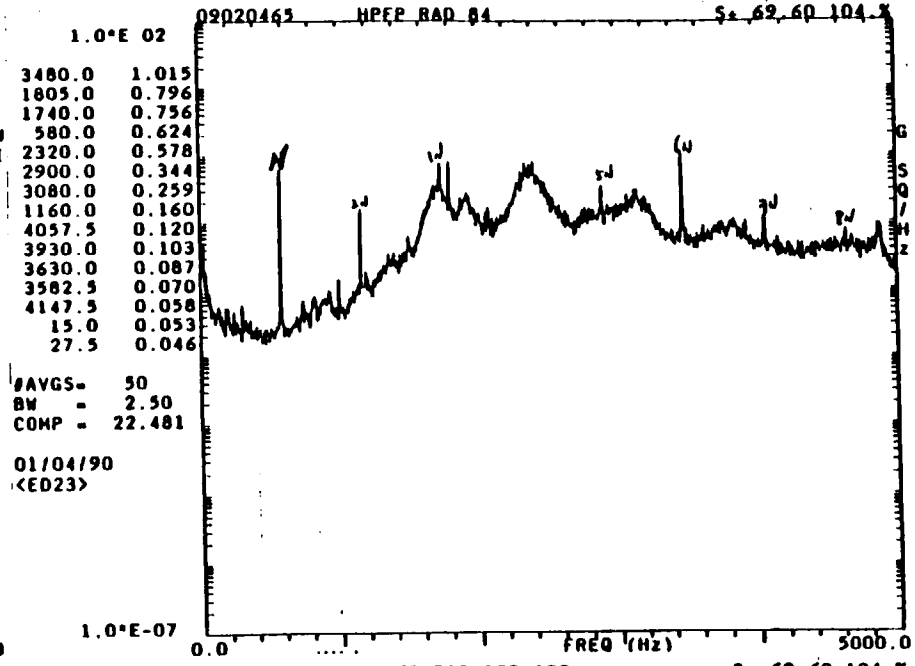
09020465 HPEP RAD 84 S= 69.60 104.%
1.0*E 02
3480.0 1.015
1805.0 0.796
1740.0 0.756
580.0 0.624
2320.0 0.578
2900.0 0.344
3080.0 0.259
1160.0 0.160
4057.5 0.120
3930.0 0.103
3630.0 0.087
3582.5 0.070
4147.5 0.058
15.0 0.053
27.5 0.046
#AVGS= 50
BW = 2.50
COMP = 22.481
01/04/90
<ED23>
1.0*E-07
FREQ (Hz)
0.0
5000.0

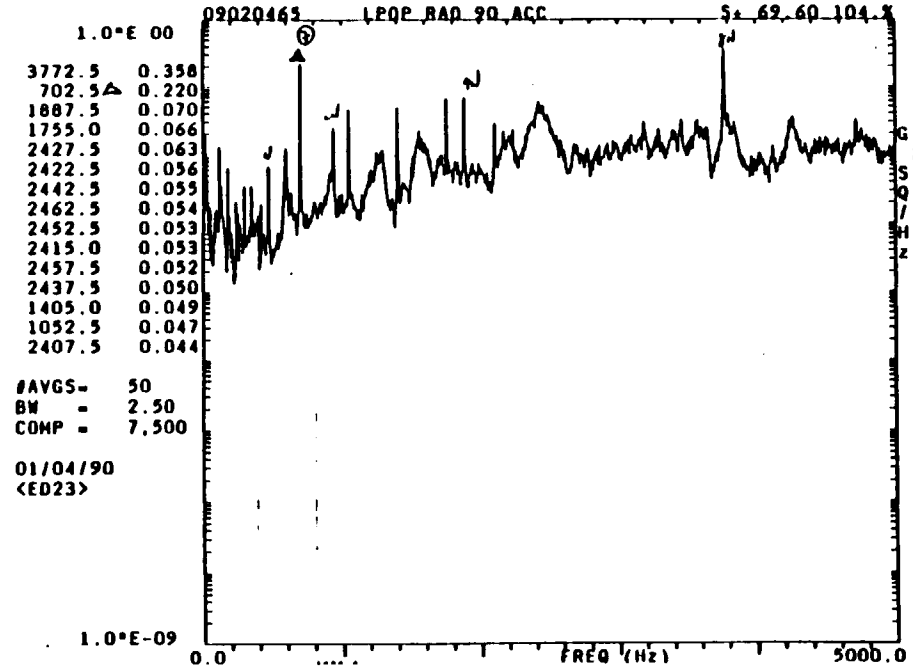
09020465 LPQP RAD 90 ACC S= 69.60 104.%
1.0*E 00
3772.5 0.358
702.5 0.220
1887.5 0.070
1755.0 0.066
2427.5 0.063
2422.5 0.056
2442.5 0.055
2462.5 0.054
2452.5 0.053
2415.0 0.053
2457.5 0.052
2437.5 0.050
1405.0 0.049
1052.5 0.047
2407.5 0.044
#AVGS= 50
BW = 2.50
COMP = 7.500
01/04/90
<ED23>
1.0*E-09
FREQ (Hz)
0.0
5000.0

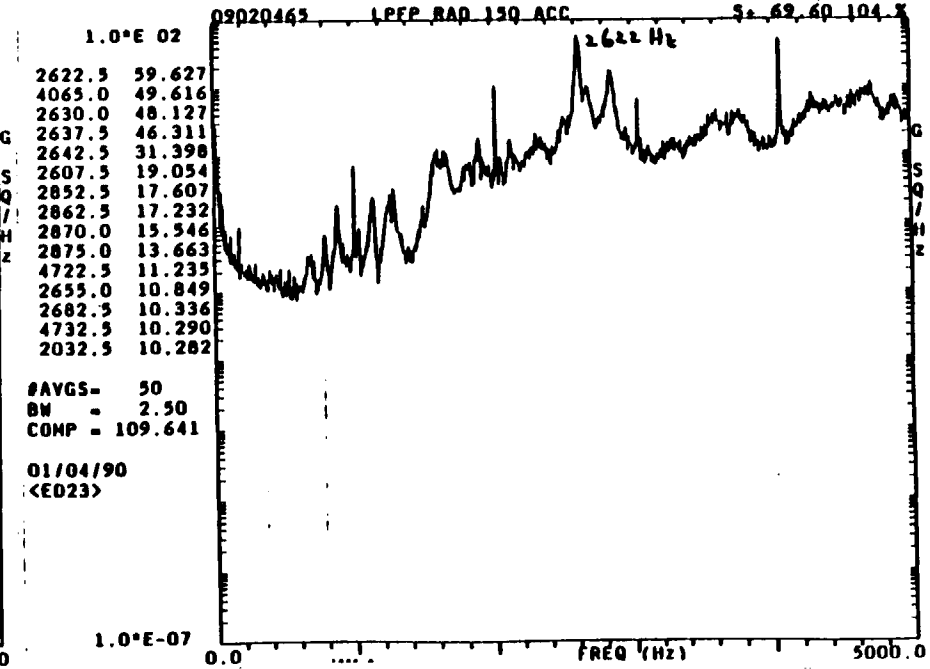
09020465 LPEP RAD 150 ACC S= 69.60 104.%
1.0*E 02
2622.5 59.627
4065.0 49.616
2630.0 48.127
2637.5 46.311
2642.5 31.398
2607.5 19.054
2852.5 17.607
2862.5 17.232
2870.0 15.546
2875.0 13.663
4722.5 11.235
2655.0 10.849
2682.5 10.336
4732.5 10.290
2032.5 10.282
#AVGS= 50
BW = 2.50
COMP = 109.641
01/04/90
<ED23>
1.0*E-07
2622 Hz
FREQ (Hz)
0.0
5000.0

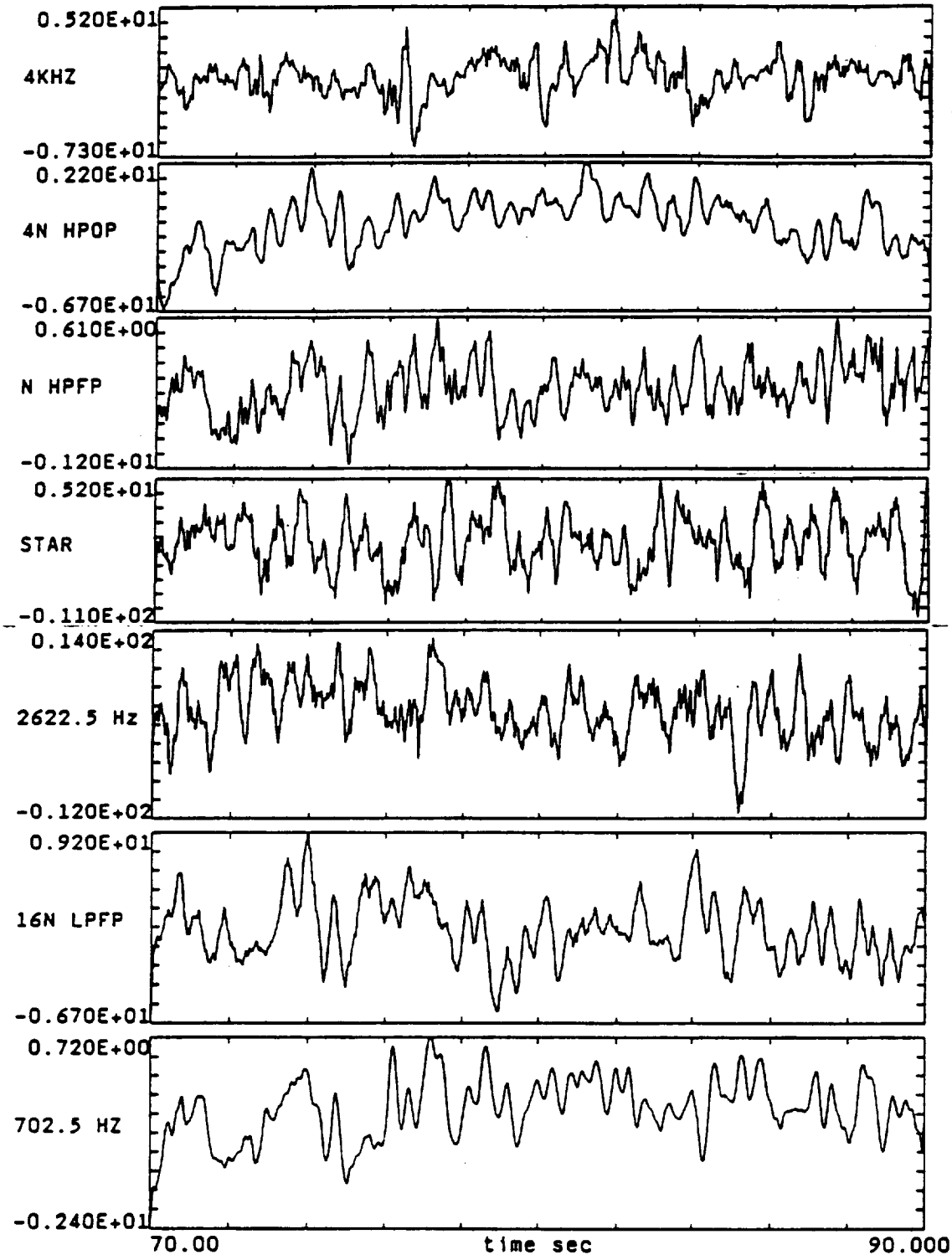

A2-465 ES6577 SG 2A AC

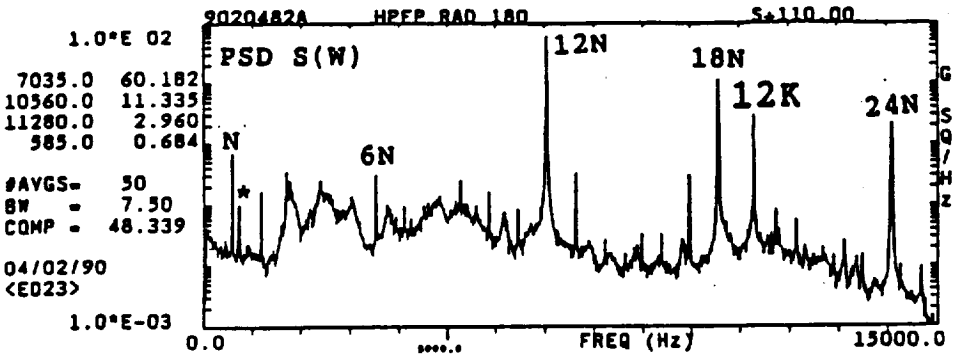

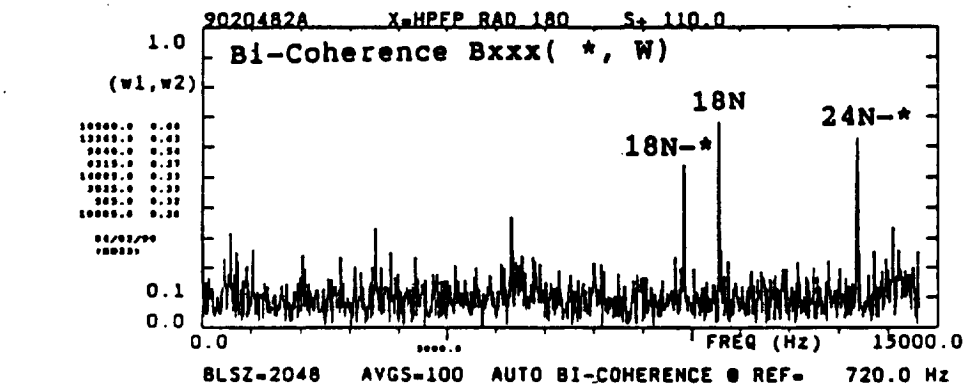

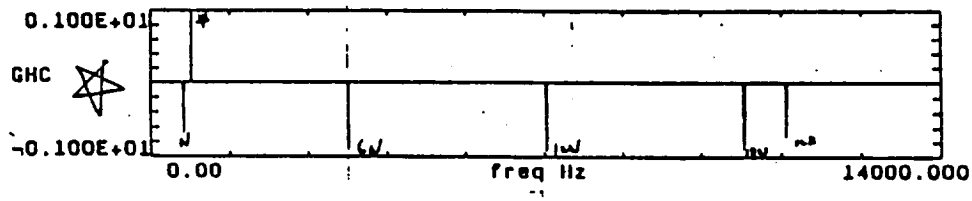

A2-482A HPFP RAD 90
NA1=2048/1024/512 NA2=128 NPASS=19

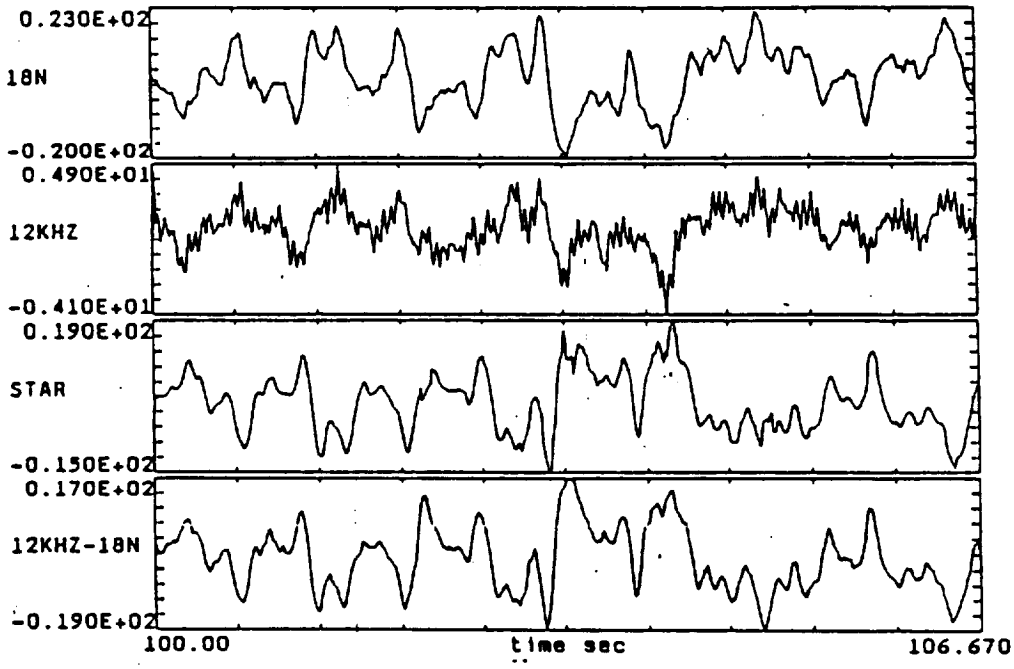

A2-482A HPFP RAD 90
NA1=2048/1024/512 NA2=128 NPASS=19

901-596

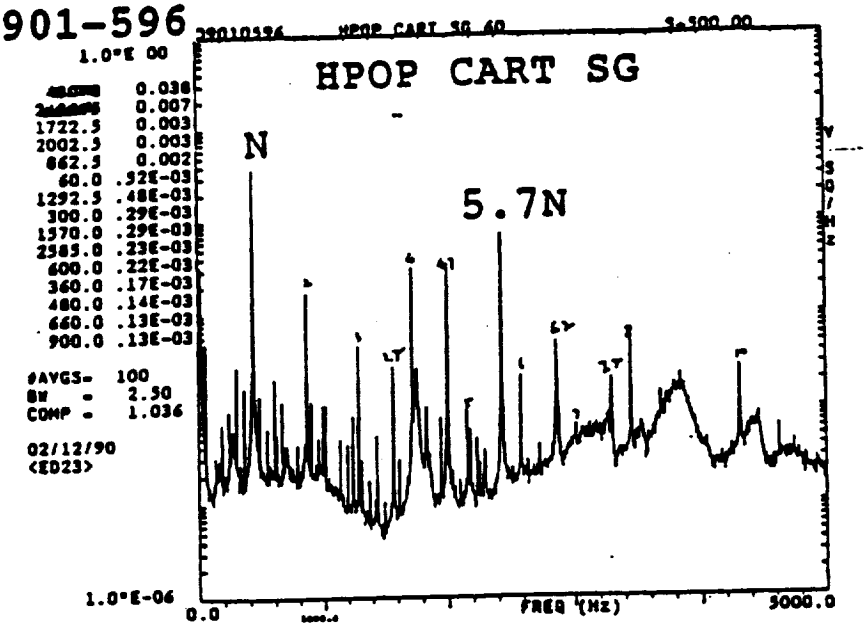
HPOP CART SG
N
5.7N
1.0*E 00
0.038
0.007
1722.5 0.003
2002.5 0.003
862.5 0.002
60.0 .92E-03
1292.5 .48E-03
300.0 .29E-03
1570.0 .29E-03
2585.0 .23E-03
600.0 .22E-03
360.0 .17E-03
480.0 .14E-03
660.0 .13E-03
900.0 .13E-03
#AVGS= 100
BW = 2.50
COMP = 1.036
02/12/90
<ED23>
1.0*E-06
0.0
FREQ (Hz)
5000.0

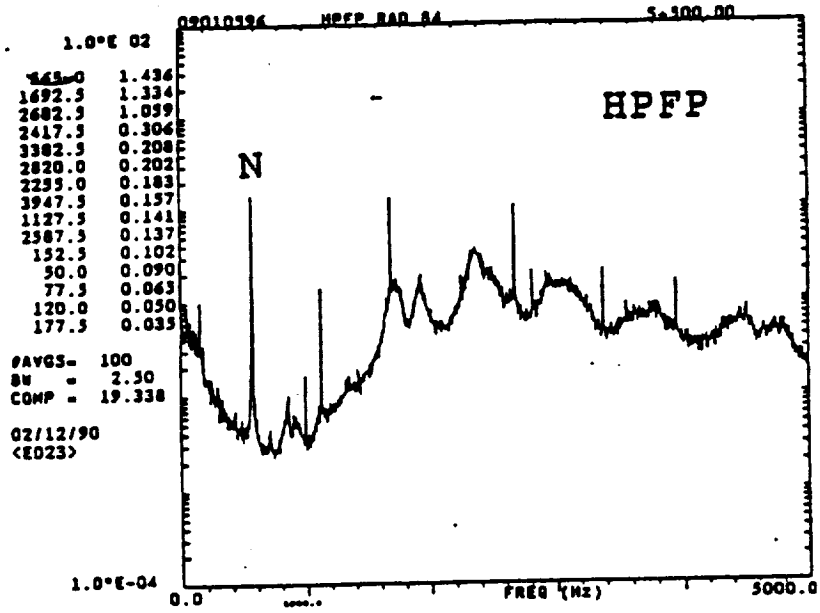
HPFP
N
1.0*E 02
1692.5 1.334
2682.5 1.039
2417.5 0.306
3382.5 0.208
2820.0 0.202
2295.0 0.183
3947.5 0.157
1127.5 0.141
2587.5 0.137
152.5 0.102
50.0 0.090
77.5 0.065
120.0 0.050
177.5 0.035
#AVGS= 100
BW = 2.50
COMP = 19.338
02/12/90
<ED23>
1.0*E-04
0.0
FREQ (Hz)
5000.0

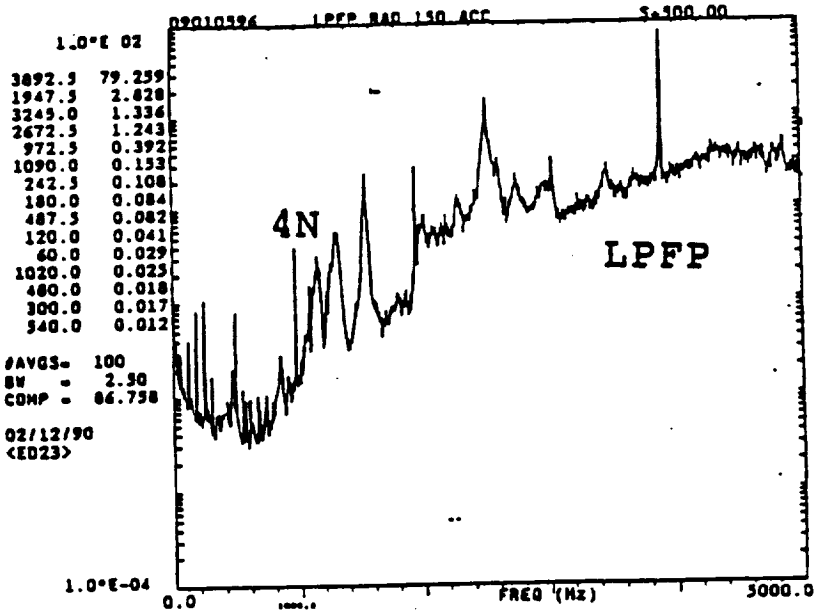
4N
LPFP
1.0*E 02
3892.5 79.259
1947.5 2.628
3245.0 1.336
2672.5 1.243
972.5 0.392
1090.0 0.153
242.5 0.108
180.0 0.084
487.5 0.082
120.0 0.041
60.0 0.029
1020.0 0.025
480.0 0.018
300.0 0.017
540.0 0.012
#AVGS= 100
BW = 2.50
COMP = 86.758
02/12/90
<ED23>
1.0*E-04
0.0
FREQ (Hz)
5000.0

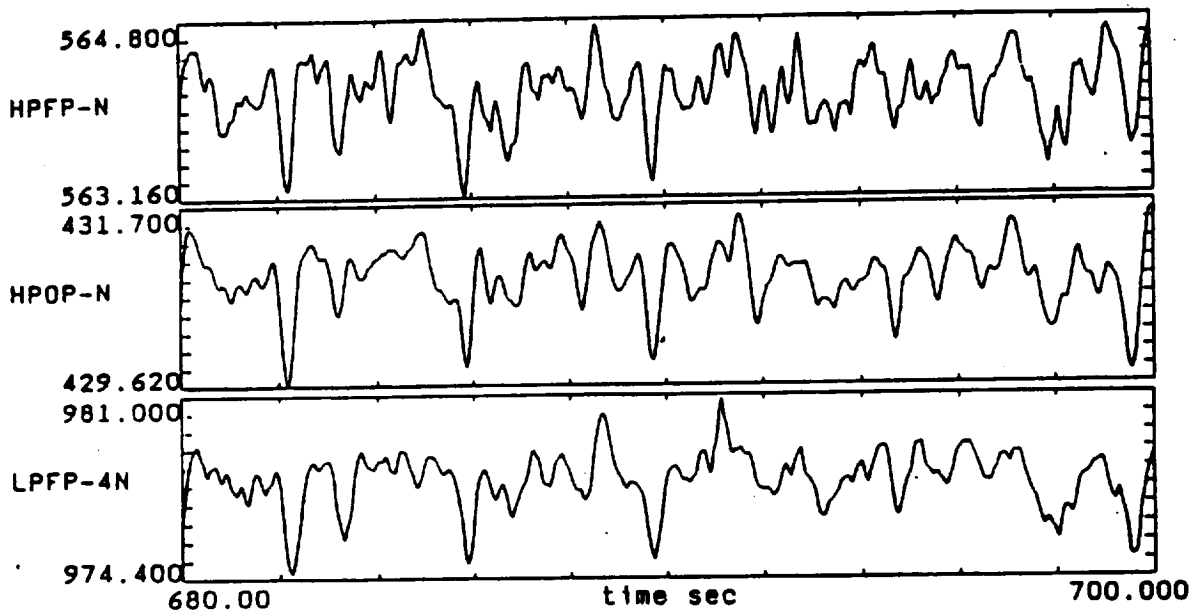

901-596 Instantaneous Frequency
HPOP-CART-SG 60

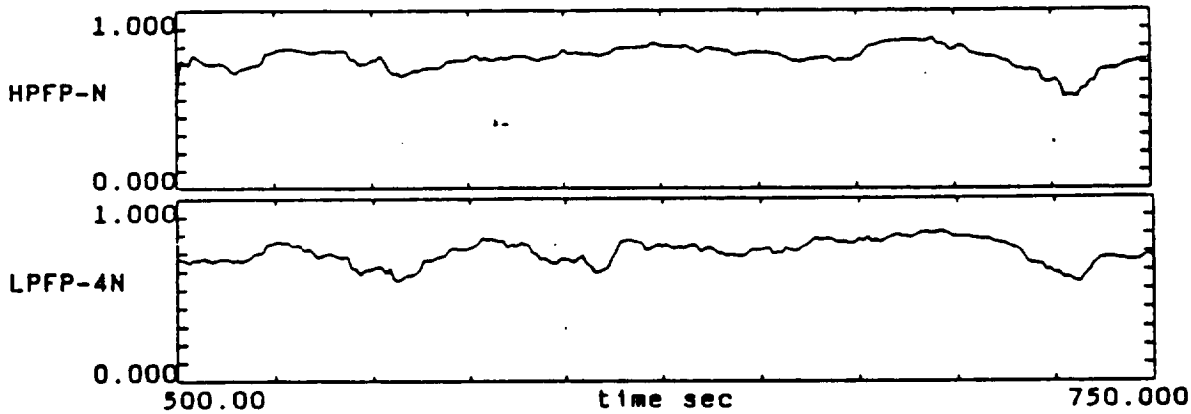

901-596 Moving-averaged G.H.C. Window=20 sec Advance=1 sec
reference component = SYNC of HPOP-ISO-SG
HPOP-ISOSG-41%N HPOP-CARTSG-5.7N

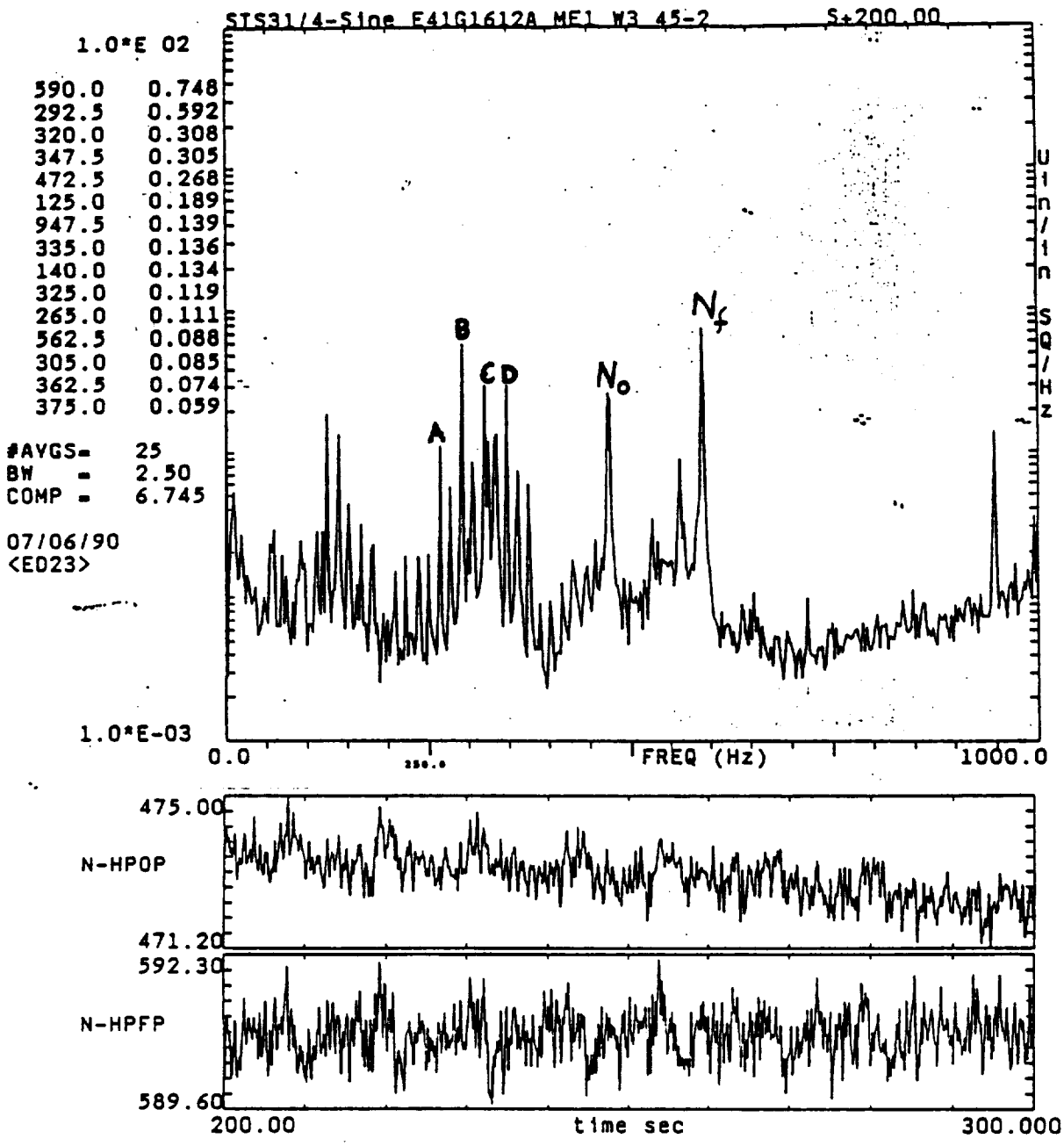

STS-31 SG E41G1612A ME1 W3 45-2
Inst. Freq

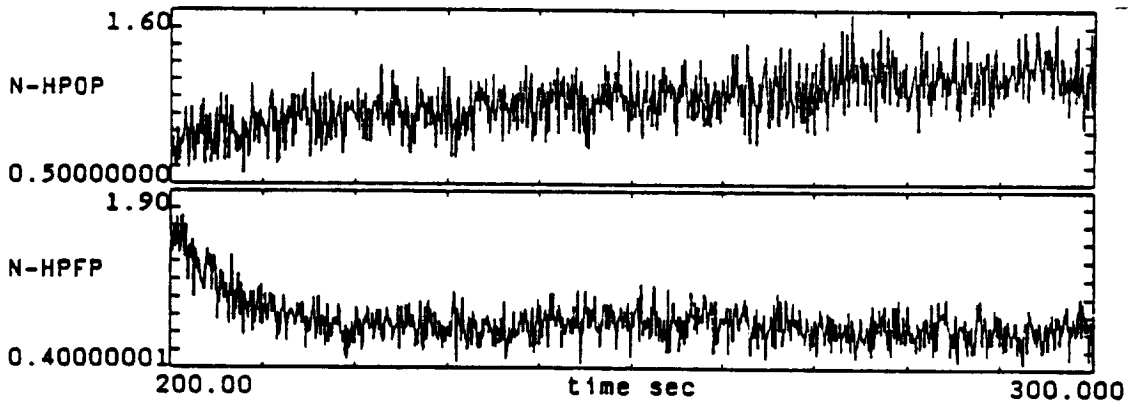

STS-31 SG E41G1612A ME1 W3 45-2
Inst. Amp

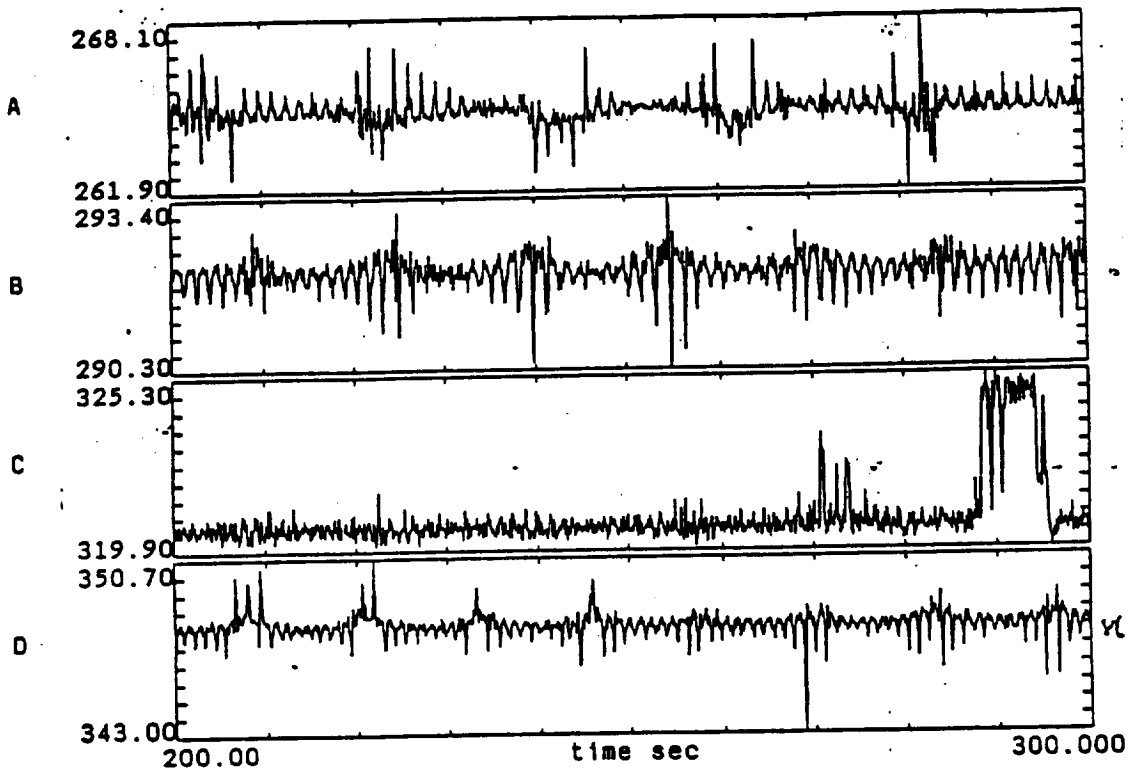

STS-31 SG E41G1612A ME1 W3 45-2
Instantaneous Frequency

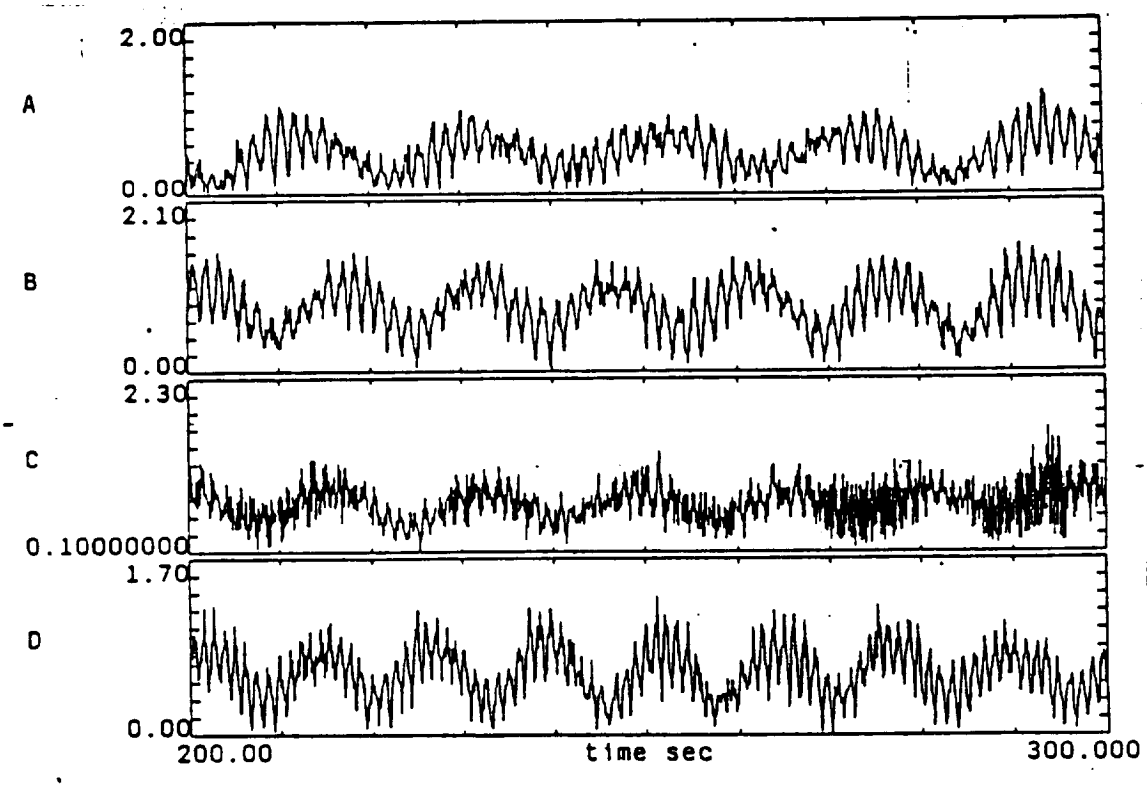

STS-31 SG E41G1612A ME1 W3 45-2
Inst. Amp

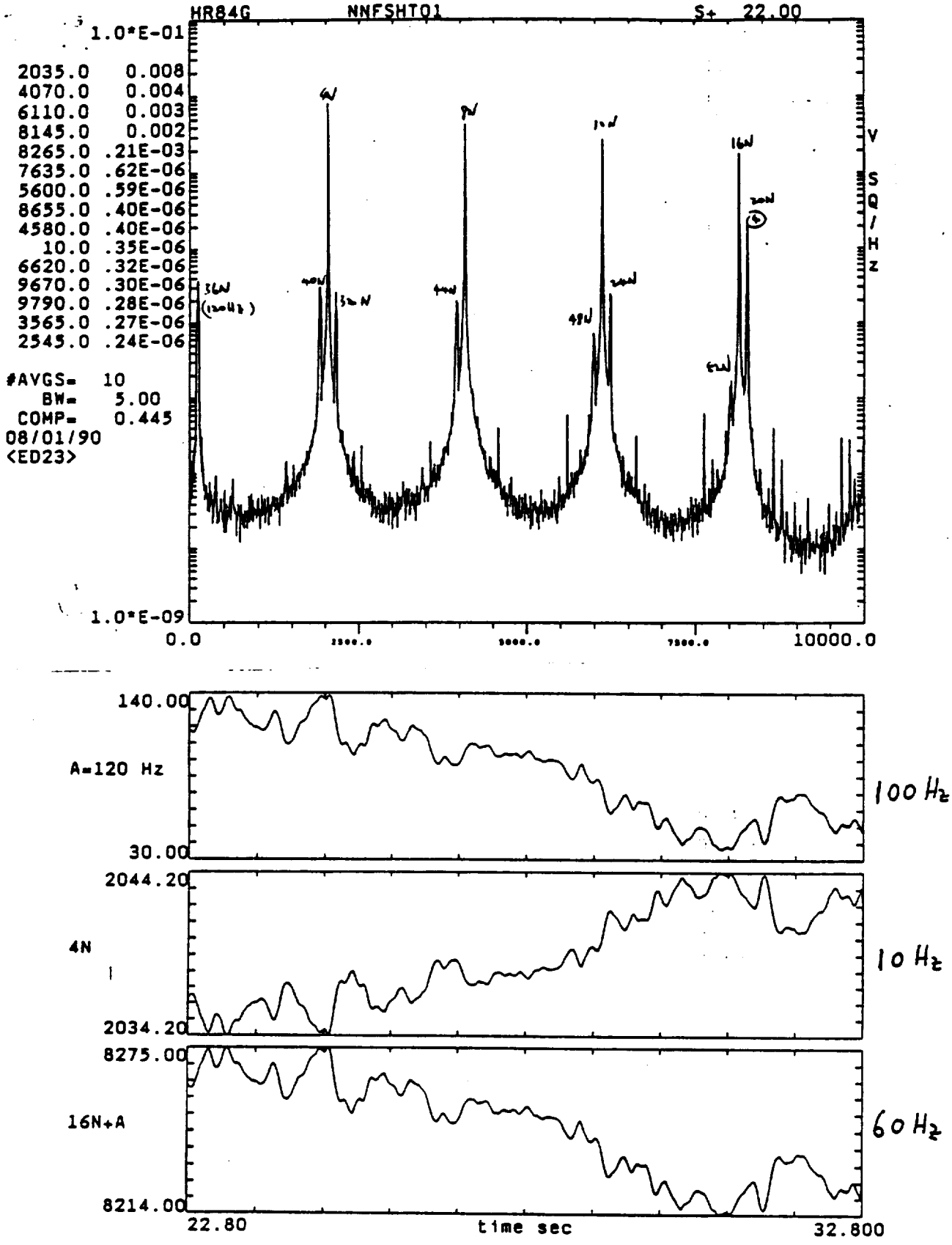

HR84 NNFSHTO1
GHC INSTANTANEOUS AMP

MEM SPECTRAL ANALYSIS AND ADAPTIVE FILTER

by

Jen-Yi Jong

January 1991

for

Structures and Dynamics Laboratory
Marshall Space Flight Center

Contract NAS8-38156

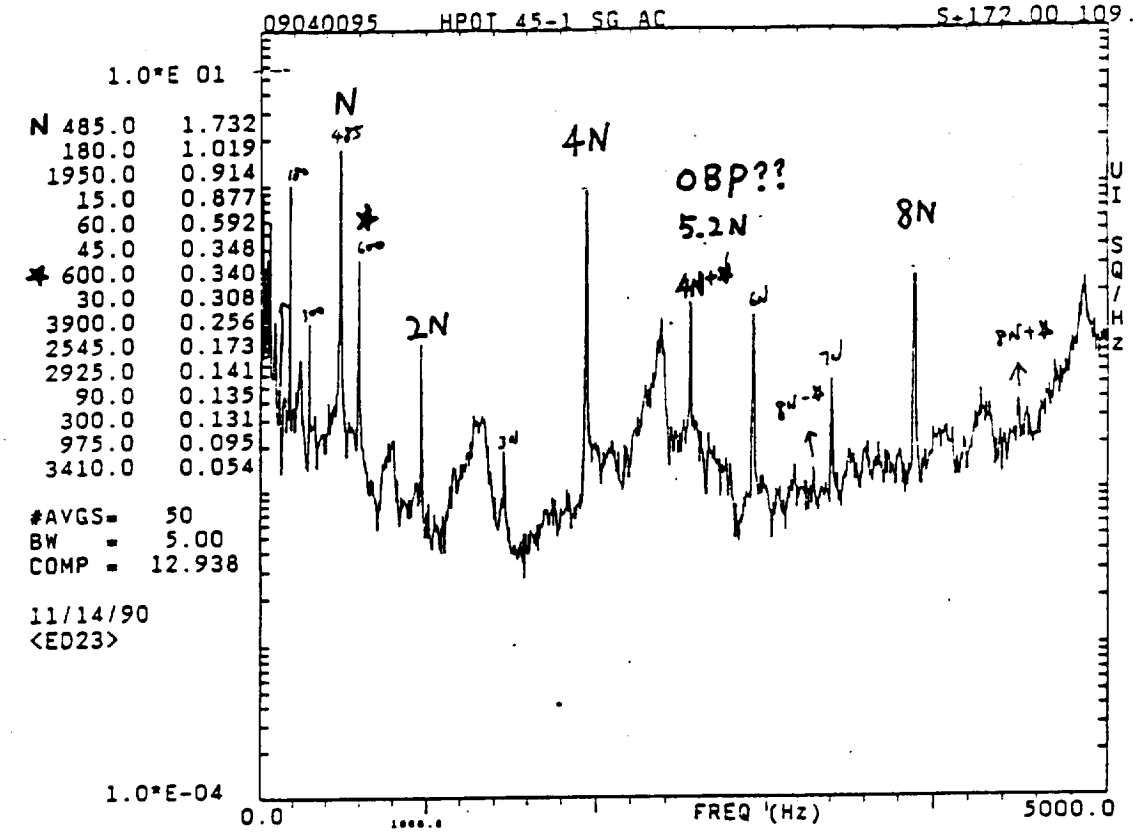
09040095 HPOT 45-1 SG AC
S-172 00 109
1.0*E 01
N 485.0 1.732
180.0 1.019
1950.0 0.914
15.0 0.877
60.0 0.592
45.0 0.348
* 600.0 0.340
30.0 0.308
3900.0 0.256
2545.0 0.173
2925.0 0.141
90.0 0.135
300.0 0.131
975.0 0.095
3410.0 0.054
#AVGS= 50
BW = 5.00
COMP = 12.938
11/14/90
<ED23>
1.0*E-04
N
4N
OBP??
5.2N
8N
2N
0.0
FREQ (Hz)
5000.0

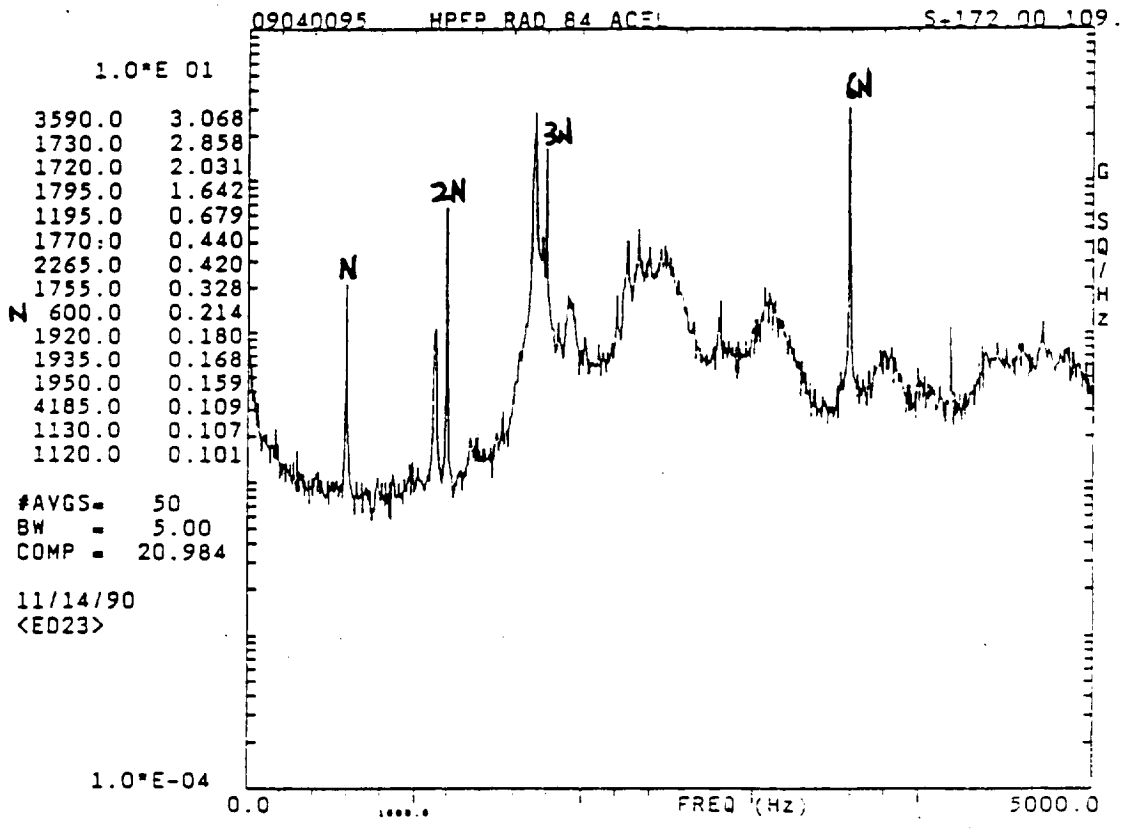
09040095 HPFP RAD 84 ACE
S-172 00 109
1.0*E 01
3590.0 3.068
1730.0 2.858
1720.0 2.031
1795.0 1.642
1195.0 0.679
1770.0 0.440
2265.0 0.420
1755.0 0.328
N 600.0 0.214
1920.0 0.180
1935.0 0.168
1950.0 0.159
4185.0 0.109
1130.0 0.107
1120.0 0.101
#AVGS= 50
BW = 5.00
COMP = 20.984
11/14/90
<ED23>
1.0*E-04
N
2N
3N
6N
0.0
FREQ (Hz)
5000.0

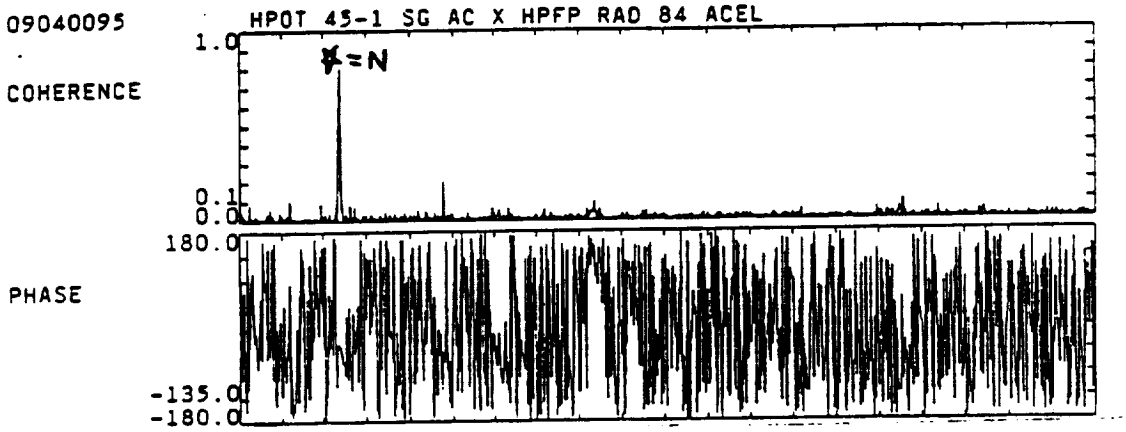
09040095
HPOT 45-1 SG AC X HPFP RAD 84 ACEL
COHERENCE
PHASE
1.0
0.1
0.0
180.0
-135.0
-180.0
1X=N

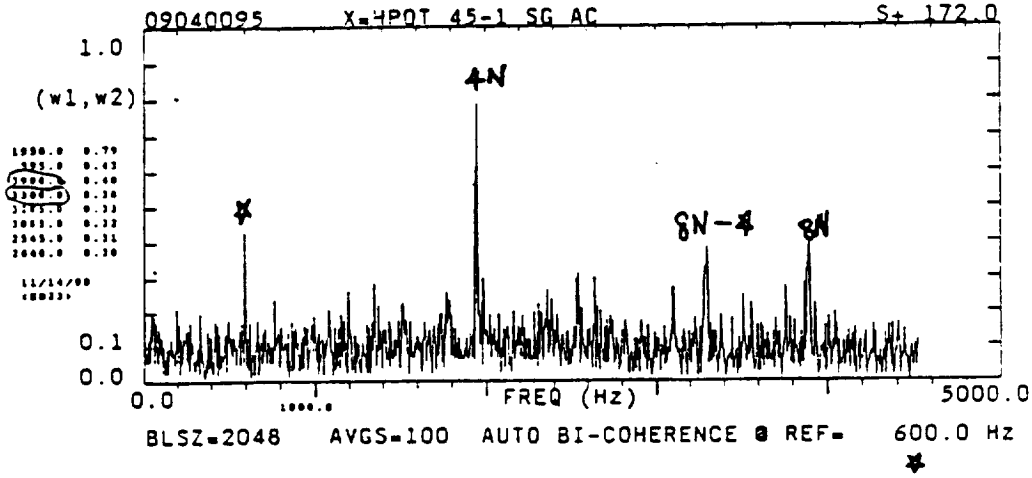
09040095
X=HPOT 45-1 SG AC
S+ 172.0
1.0
(w1,w2)
0.1
0.0
0.0
FREQ (Hz)
5000.0
1X
4N
8N-4
8N
BLSZ=2048 AVGS=100 AUTO BI-COHERENCE @ REF= 600.0 Hz

SPECTRUM ESTIMATION

(1) FFT (DIRECT) METHOD

$$Xw(f) = \int_{-T/2}^{T/2} w(t)\, x(t)\, e^{-j2\,ft}\, dt \;=\; X(f) * W(f)$$

$$\hat{S}(f) = |\, Xw(f)\,|^2 = |\, X(f) * W(f)\,|^2$$

. STATISTICS:

$$\begin{cases} \text{Mean}[\, \hat{S}(f|T)\,] = E[\, \hat{S}(f|T)\,] = \int S(v)\, W(f-v)\, W^*(f-v)\, dv \\ \text{Cov}[\, \hat{S}(f|T)\,] = E[\, \hat{S}(f1|T)\, \hat{S}(f2|T)\,] \end{cases}$$

$$= |\, \int S(v)\, W(f1-v)\, W^*(f2-v)\, dv\,|^2$$

(2) BLACKMAN-TURKEY (INDIRECT) METHOD

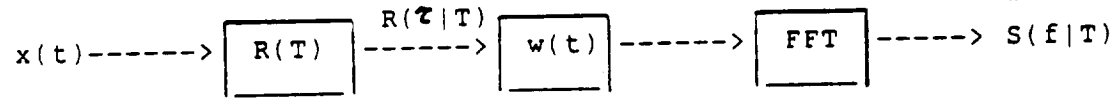

$$\hat{R}(\tau|T) = \frac{1}{T} \int_{-T/2+\tau}^{T/2} x(t)\, x(t-\tau)\, dt$$

$$\hat{S}(f/T) = \int_{-T/2}^{T/2} w(\tau)\, \hat{R}(\tau|T)\, e^{-j2\,f\tau}\, d\tau$$

. STATISTICS:

$$\begin{cases} \text{Mean}[\, \hat{S}(f|T)\,] = E[\, \hat{S}(f|T)\,] = \int S(v)\, W(f-v)\, dv \\ \text{Cov}[\, \hat{S}(f|T)\,] = E[\, \hat{S}(f1|T)\, \hat{S}(f2|T)\,] \end{cases}$$

$$= \frac{1}{T} \int S^2(v)\, [\, W(f1-v)\, W^*(f2-v) + W(f1-v)\, W(f2+v)\,]\, dv$$

Maximum Entropy Method (MEM) of Spectral Analysis (by J.P. Burg)

Entropy: a measure of average information content in a data set

(1) Discrete Random variable:

. A communication system transmits M different messages m1,m2,.. with probabilities of occurrence P1,P2... respectively. Suppose that, during a long period of time, a total sequence of messages L has been generated. Then we would expect to find L*P1 messages of m1, L*P2 messages of m2,...and so on.

. The occurrence of a rare event contains more valuable information.
  ==> The value (weight) of each message is inversely proportional to its probability of occurrence.
  ==> total information in such a sequence can be defined as:

$$I = L\,P1\,\log(1/P1) + L\,P2\,\log(1/P2) \ldots\ldots = L \sum_{k=1} Pk\,\log(1/Pk)$$

Entropy (H) = The average information per message

$$\boxed{H = I/L = \sum_{k=1} Pk\ \log(1/Pk)}$$

(2) Continuous Random variable:

$$\boxed{\text{Entropy } H = \int \underset{-}{p(x)}\ \log[\ 1/\underset{-}{p(x)}\ ]\ d\underset{-}{x}}$$

$\underset{-}{p(x)}$ = joint p.d.f. of time series { x1, x2, x3,....xn}

- if { x1, x2, x3,....xn } is Gaussian:

$$p(x) = \frac{1}{[(2\pi)^{n}\det(C_x)]^{\frac{1}{2}}} \exp\left[-\tfrac{1}{2}(x-\mu_x)^{H} C_x^{-1}(x-\mu_x)\right].$$

where Cx = covariance matrix; Cij = E[(xi-M1)(xj-M1)]

====> H = 0.5 log[det(Cx)]

- if { x1, x2, x3,....xn } is zero-mean Gaussian:

Cx = Rx = auto-correlation matrix; Rij = E[xi xj]

====> H = 0.5 log[det(Rx)]

- From the relationship between Rx(T) and Sx(f)

====> $\boxed{H=0.5\ \log(2B) + 1/(4B) \int \log[\ Sx(f)\ ]\ df}$

MEM SPECTRUM ESTIMATION

Problem:

given measured $R(m)$, $m=1,M$, wish to find $\hat{R}x(m)$ and $\hat{S}x(f)$

such that:

(1) Entropy is maximized: $d\,H/d\hat{R}(m) = 0$ for $|m| > M$

(2) Constrain: $\hat{R}(m) = R(m)$ for $|m| < M$

Where $\hat{R}x(m) \xleftrightarrow{FFT} \hat{S}x(f)$

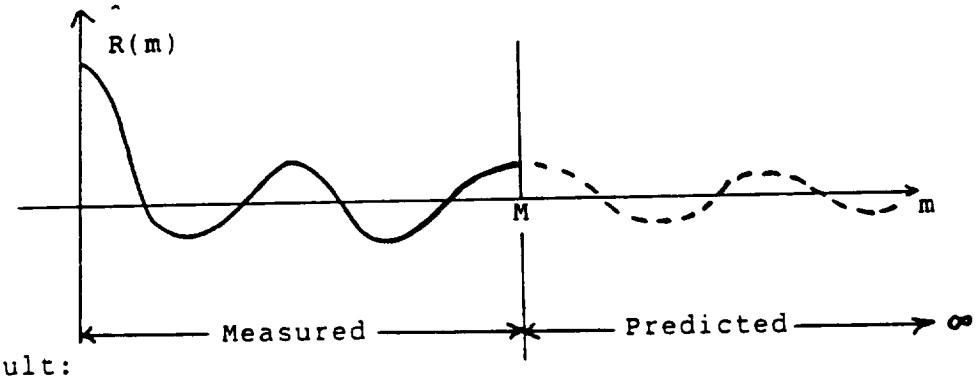

Result:

$$\hat{R}x(m) = \sum_{n=1}^{M} A(n)\,\hat{R}(m-n)$$

$$\hat{S}x(f) = \frac{2\,PE}{fs\,\left|\,1 - \sum_{m=1} A(n)\,\exp[\,-j2\pi m\,f/fs\,]\,\right|^2}$$

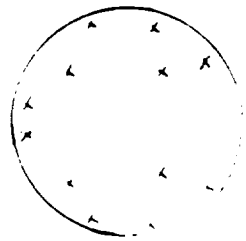

7

. Coefficients A(n) & PE can be obtained by solving Wiener-Levinson equation:

$$\begin{bmatrix} R(0) & R(1) & R(2)\ldots\ldots R(M) \\ R(1) & R(0) & R(1)\ldots\ldots R(M-1) \\ R(2) & R(1) & R(0)\ldots\ldots R(M-2) \\ \vdots & \vdots & \vdots \\ R(M) & R(M-1) & R(M-2)\ldots R(0) \end{bmatrix} \begin{Bmatrix} 1 \\ -A(1) \\ -A(2) \\ \vdots \\ -A(M) \end{Bmatrix} = \begin{Bmatrix} PE \\ 0 \\ 0 \\ \vdots \\ 0 \end{Bmatrix}$$

. Levinson-Durbin Recursive Algorithm for Toeplitz matrix

AUTO-REGRESSIVE (AR) MODEL (by Van den Bos)

- AR Model: $x(n) = \sum_{m=1}^{M} A(m)\, x(n-m) + e(n) \quad n=1,M$

=> current data x(n) can be predicted from past data x(n-m) m=1,M with prediction error e(n) representing white noise

white noise has no memory ==> un-predictable

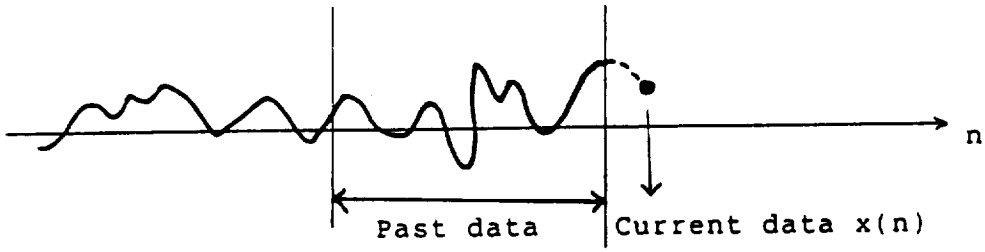

- Whitening Filter: $x(n) - \sum_{m=1}^{M} A(m)\, x(n-m) = e(n)$

==> $x(n) * h(n) = e(n)$; where: $h(0)=1,\ h(m)=-A(m)$

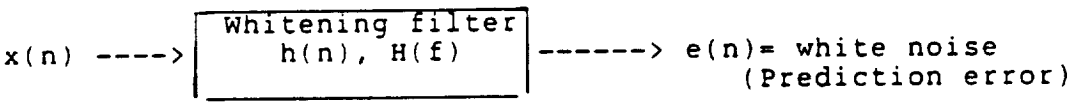

==> $Se(f) = Sx(f) \mid H(f) \mid^2$

==> $Sx(f) = Se(f) / \mid H(f) \mid^2$

Where : $\begin{cases} Se(f) = 2\ PE\ /\ fs \\ H(f) = 1 - \sum_{m=1} A(m)\ \exp[\ -j2\ \ m\ f/fs] \end{cases}$

====> $Sx(f) = \dfrac{2\ PE}{fs \mid 1 - \sum_{m=1} A(m)\ \exp[\ -j2\pi m\ f/fs] \mid^2}$

LEAST SQUARE ESTIMATION OF AR COEFFICIENTS A(m)

Problem:

given signal Model (AR): $x(n) = \sum_{m=1}^{M} A(m)\, x(n-m) + e(n) \quad n=1,M$

wish to find A(m) such that the expect value of $e^2(t)$ is minimized

$$PE = E\left[\, e^2(n) \,\right] = E\left[\, \left\{ x(n) - \sum_{m=1} A(m)\, x(n-m) \right\}^2 \,\right]$$

(1) $d\,PE \,/\, d\,A(k) = 0 \quad$ for $k=1,M$

$$d\,PE \,/\, d\,A(k) = -E\left[\, \left\{ x(n) - \sum_{m=1} A(m)\, x(n-m) \right\} x(n-k) \,\right]$$

$$= -R(k) + \sum_{m=1} A(m)\, R(m-k) = 0$$

$$\Longrightarrow \sum_{m=1} A(m)\, R(m-k) = R(k) \quad k=1,M \quad \text{(Yule-Walker equation)}$$

$$\begin{bmatrix} R(0) & R(1) & R(2) \ldots\ldots R(M-1) \\ R(1) & R(0) & R(1) \ldots\ldots R(M-2) \\ R(2) & R(1) & R(0) \ldots\ldots R(M-3) \\ \vdots & \vdots & \vdots \\ R(M-1) & R(M-2) & R(M-3) \ldots R(0) \end{bmatrix} \begin{Bmatrix} A(1) \\ A(2) \\ A(3) \\ \vdots \\ A(M) \end{Bmatrix} = \begin{Bmatrix} R(1) \\ R(2) \\ R(3) \\ \vdots \\ R(M) \end{Bmatrix}$$

(2) $PE,min = E\left[\left\{x(n) - \sum_{m=1} A(m)\, x(n-m)\right\}\left\{x(n) - \sum_{k=1} A(k)\, x(n-k)\right\}\right]$

$$= E\left[\left\{x(n) - \sum_{m=1} A(m)\, x(n-m)\right\} x(n)\right] = R(0) - \sum_{m=1} A(m)\, R(m)$$

(3) Combine (1) and (2) ===> Wiener-Levinson equation:

$$\begin{bmatrix} R(0) & R(1) & R(2) \ldots\ldots R(M) \\ R(1) & R(0) & R(1) \ldots\ldots R(M-1) \\ R(2) & R(1) & R(0) \ldots\ldots R(M-2) \\ \vdots & \vdots & \vdots \\ R(M) & R(M-1) & R(M-2) \ldots R(0) \end{bmatrix} \begin{Bmatrix} 1 \\ -A(1) \\ -A(2) \\ \vdots \\ -A(M) \end{Bmatrix} = \begin{Bmatrix} PE,min \\ 0 \\ 0 \\ \vdots \\ 0 \end{Bmatrix}$$

Conclusion:

====> MEM-PSD is identical to AR-PSD

. MEM: Extending R(t) such that its entropy is maximized

. AR : Assuming AR model, minimizing its prediction error

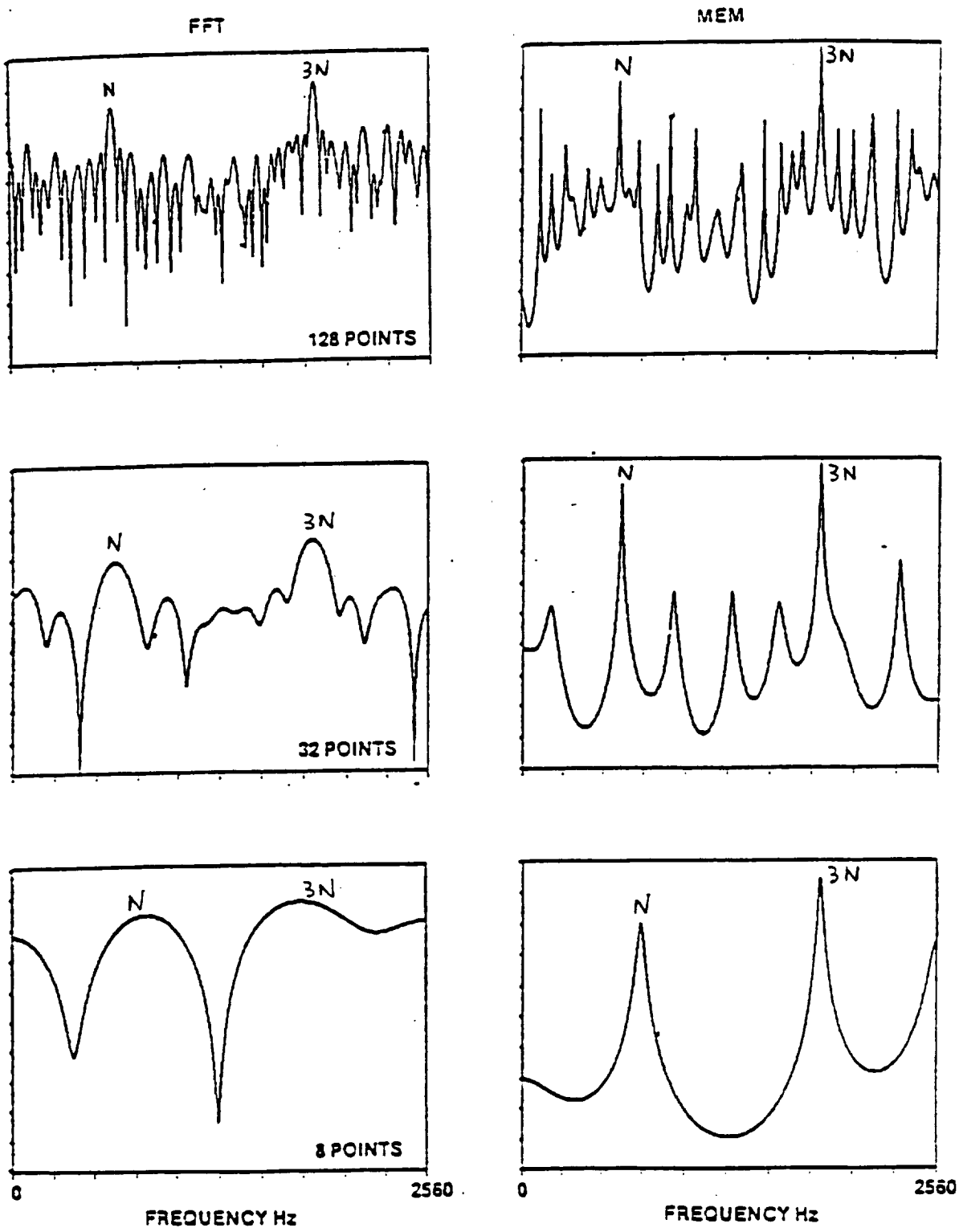

FIGURE 4-50. COMPARISON BETWEEN FFT AND MEM SPECTRUM FOR LIMITED SAMPLE SIZE

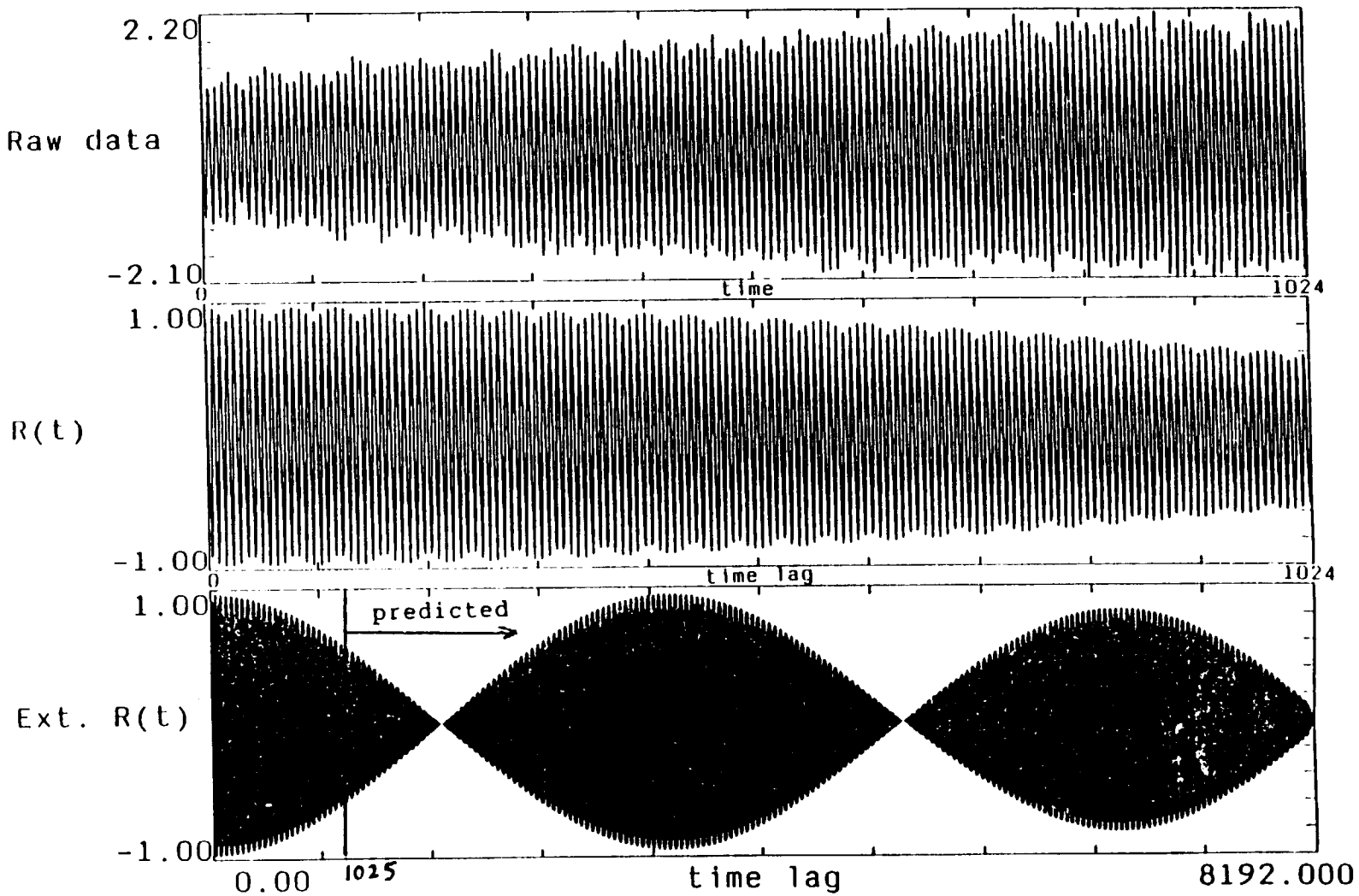

(a) Raw data (1024 samples)
(b) original a.c.f R(t) from 1024 data samples
(c) MEM extended R(t)

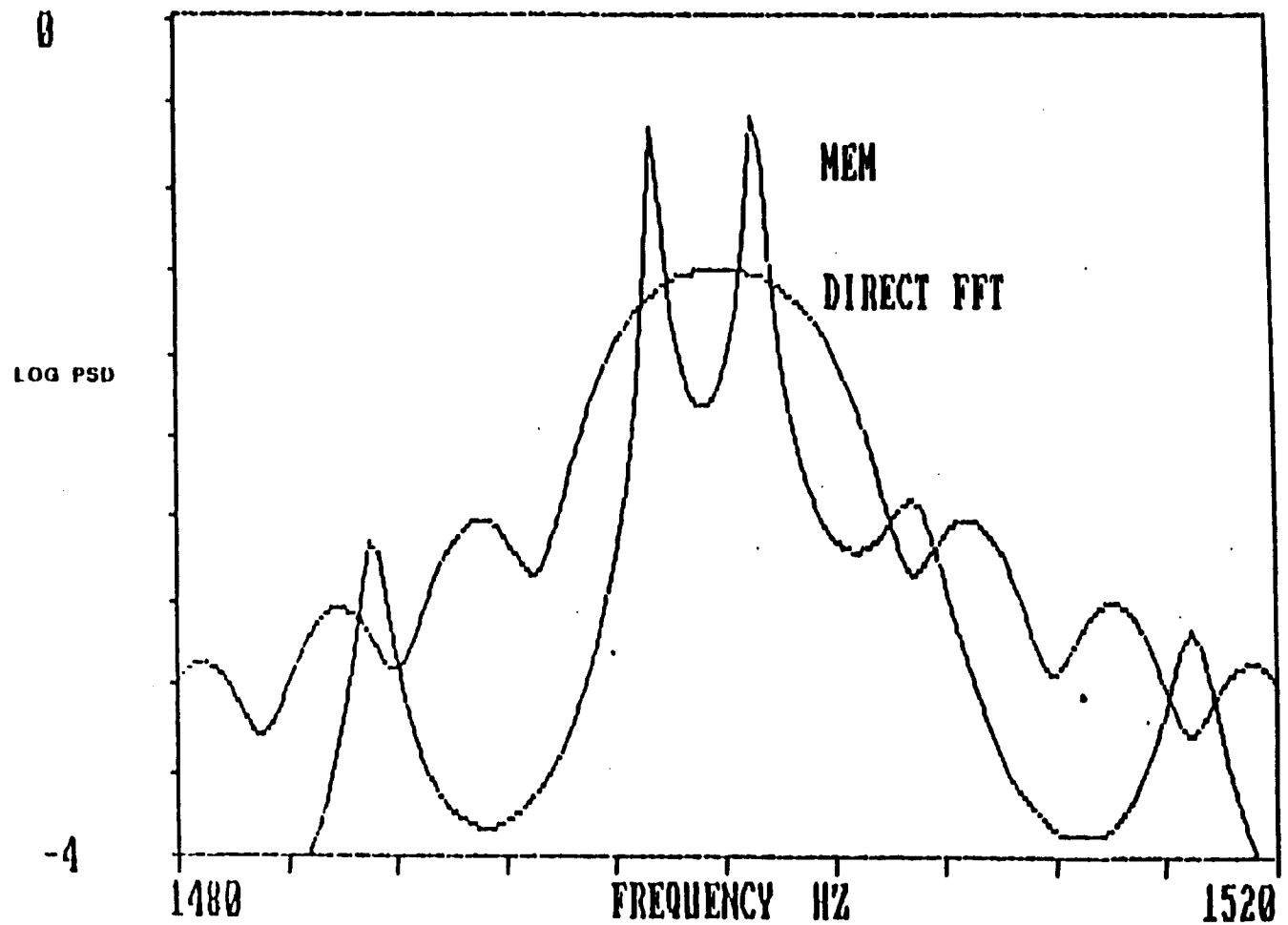
0
LOG PSD
-4
MEM
DIRECT FFT
1480
FREQUENCY HZ
1520

WIENER FILTER (by N. Wiener)

EXAMPLE:

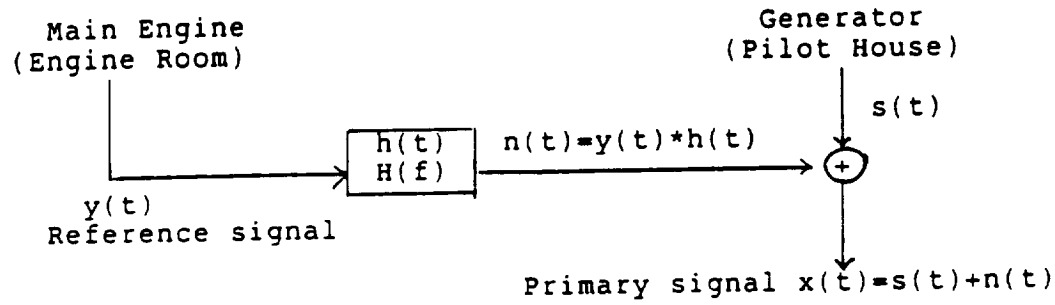

. wish to study the vibration response of the generator s(t).

. measurement x(t) at the generator will be corrupted by the background noise n(t) from the main engine

. n(t) is transmitted from the engine room to the pilot house through a unknown linear transfer function H(f)

. Noise Cancellation --
  . take additional measurement y(t) (reference signal)
  . estimate of h(t).
  . predict background noise n(t) (N(t) = y(t) * h(t)
  . noise in the primary signal can be canceled

WIENER FILTER:

- Assumption:

  1. s(t) and y(t) are independent
  2. y(t) and n(t) are linearly correlated; n(t)=y(t)*h(t)
  3. all signal are stationary
  4. H(f) is linear time invariant (LTI) system

- Wish to estimate I.R.F h(t):

Prediction $\hat{n}(t) = y(t) * \hat{h}(t)$ = estimation of n(t)

Prediction error $e(t) = x(t) - \hat{n}(t)$ = estimation of s(t)

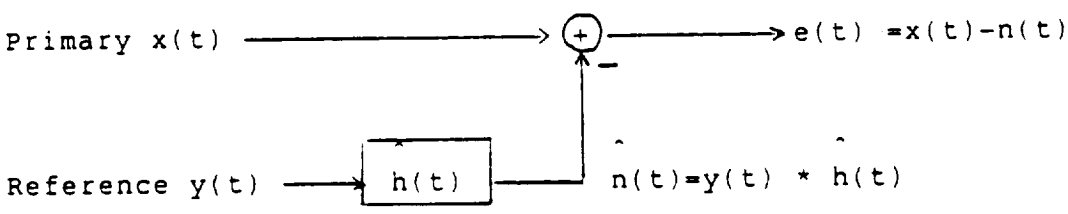

LEAST SQUARE ESTIMATION:

==> Find h(t) such that $PE = E[\,|e(t)|^2\,]$ is minimized

$$PE = E[\,|e(t)|^2\,] = E[\,\{\,x(t)-y(t)*h(t)\,\}^2\,]$$

Minimize PE with respect to h(t)

. discrete time, matrix form:

$$PE = Rxx(0) - 2\,h^T\,Rxy + h^T\,Ryy\,h$$

$$\frac{d\,PE}{d\,h} = 0 \quad ===> \quad R_{yy}\,h = R_{xy} \qquad \text{Wiener-Hopf Equation}$$

$$\begin{bmatrix} Ryy(0) & Ryy(1) & Ryy(2)\ldots\ldots Ryy(M-1) \\ Ryy(1) & Ryy(0) & Ryy(1)\ldots\ldots Ryy(M-2) \\ Ryy(2) & Ryy(1) & Ryy(0)\ldots\ldots Ryy(M-3) \\ \vdots & \vdots & \vdots \\ Ryy(M-1) & Ryy(M-2) & Ryy(M-3)\ldots Ryy(0) \end{bmatrix} \begin{Bmatrix} h(1) \\ h(2) \\ h(3) \\ \vdots \\ h(M) \end{Bmatrix} = \begin{Bmatrix} Rxy(0) \\ Rxy(1) \\ Rxy(2) \\ \\ \\ Rxy(M-1) \end{Bmatrix}$$

=====> optimal h(t)

predict background noise $\hat{n}(t)$

perform noise cancellation $s(t) = x(t) - \hat{n}(t)$

Disadvantage:

1. signal must be stationary
2. system must be time invariant
3. need block of data to calculate h(t)

   ==> difficult to perform on-line real-time processing

====> Adaptive Filter

FINITE IMPULSE RESPONSE (FIR) ADAPTIVE FILTER

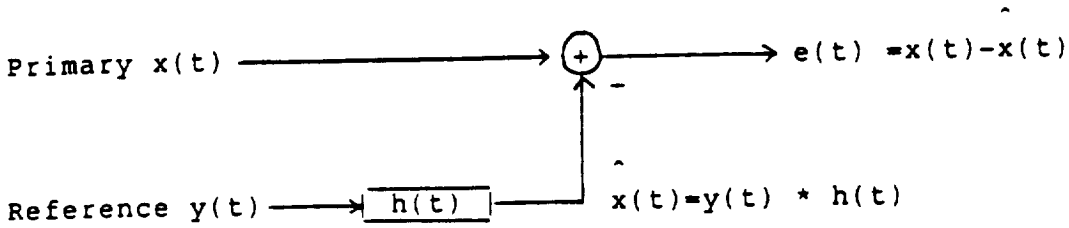

$$\text{Prediction Error } PE(t) = \sum_{s=0}^{t} q^{t-s} \, e^{2}(s)$$

q = forgetting factor

- update filter coeff. h(t) at every new data point:
  at next time step t+1: h(t+1) = h(t) + correction term
- estimate new filter coeff. h(t+1) by modifying the old filter coeff h(t) with a correction term such that the new prediction error PE(t+1) is minimized
- Memory can be introduced into the Prediction Error PE(t) by putting more weight on recent data and less weight on old data
- Adjustable weighting : { when q=1, infinite memory
  { when q<1, exponential weighting

  ===> non-stationary data and time-varying system

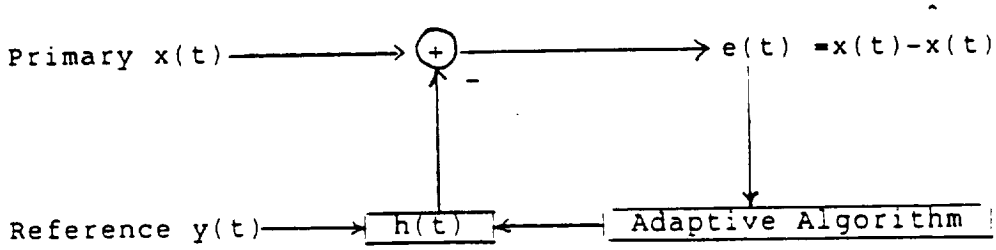

(A) LEAST SQUARE ESTIMATION

Define:

$$x(n) = [\, x(0)\ x(1)\ \ldots\ldots\ x(n-1)\ x(n) \,]^T$$

$$y(n) = [\, y(0)\ y(1)\ \ldots\ldots\ y(n-1)\ y(n) \,]^T$$

$$e(n) = [\, e(0)\ e(1)\ \ldots\ldots\ e(n-1)\ e(n) \,]^T$$

$$H(n) = [\, h1\ h2\ h3\ \ldots\ldots\ hN \,]^T$$

$$Q = \mathrm{Diag}[\, q^{**}n\ \ q^{**}(n-1)\ \ \ldots\ \ q^{**}2\ \ q\ \ 1 \,]$$

$$Y(n) = \begin{bmatrix} 0 & 0 & 0 & 0 & . & . \\ y(0) & 0 & 0 & 0 & . & \\ y(1) & y(0) & 0 & 0 & . & \\ . & & & & & \\ . & & & & & \\ . & & & & & \\ y(n-1) & \ldots\ldots\ldots\ldots\ldots\ldots & & & & y(n-N) \end{bmatrix}$$

$$\text{Prediction Error } PE(n) = \sum_{s=0}^{n} q^{n-s}\, e(s)^2$$

$$PE(n) = e(n)^T\ Q(n)\ e(n) \quad \text{where:} \quad e(n) = x(n) - Y(n)\ H(n)$$

$$PE(n) = x(n)^T\ Q\ x(n) - 2H(n)^T\ Y(n)^T\ Q(n)\ x(n) + H(n)^T\ Y(n)^T\ Q(n)\ Y(n)\ H(n)$$

$$\frac{d\ PE(n)}{d\ H(h)} = 0 \quad \Longrightarrow \quad H(n) = [\, Y(n)^T\ Q(n)\ Y(n) \,]^{-1}\ Y(n)^T\ Q(n)\ x(n)$$

- This equation estimates the filter coefficients at time step n from the entire past data. It provides the basis for the adaptive filtering problem:

  At next time step n+1, adaptive filter updates the filter coefficients through a recursive relationship between H(n) and H(n+1), which can be derived from this equation.

RECURSIVE LEAST SQUARE (RLS) ADAPTIVE ALGORITHM

Least Square Est.==> $H(n) = \underline{\underline{[\ Y^T(n)\ Q(n)\ Y(n)\ ]}}^{-1}\ Y^T(n)\ Q(n)\ x(n)$

Define $P(n) = [\ Y^T(n)\ Q(n)\ Y(n)\ ]^{-1}$

$$\begin{cases} \text{at time step n:} & H(n) = P(n)\ Y^T(n)\ Q(n)\ x(n) \\ & \Downarrow \\ \text{at time step n+1:} & H(n+1) = P(n+1)\ Y^T(n+1)\ Q(n+1)\ x(n+1) \end{cases}$$

From Matrix Partition, find recursive relationship between $P(n)$ and $P(n+1)$ as:

$$P(n+1) = \{P(n) - P(n)\ y(n+1)[\ q+y^T(n+1)P(n)y(n+1)]^{-1}\ y^T(n+1)\ P(n)\}/q$$

====> recursive relationship between between H(n) and H(n+1):

$$H(n+1) = H(n) + P(n+1)\ y(n+1)\ [\ x(n+1) - y^T(n+1)\ H(n)\ ] \quad .....(1)$$

Adaptive Procedure:

. at time step n, only coefficients H(n) and P(n) are stored

. at time step n+1 with new observations x(n+1) and y(n+1)

- Prediction: $\hat{x}(n+1) = y^T(n+1)\ H(n)$
- Prediction error: $e(n+1) = x(n+1) - \hat{x}(n+1)$
- update P(n+1) from P(n) and new observation x(n+1) & y(n+1)
- update H(n+1) from H(n), P(n+1), x(n+1) & y(n+1)

. H(n+1) updated from H(n) is identical to the least square estimation from the entire past data ===> exact adaptation

. P(n) is N x N matrix. N= filter order

===> large computation and storage requirement

Equation (1): $H(n+1) = H(n) + P(n+1)\, y(n+1)\, [\, x(n+1) - y(n+1)\, H(n)]$

Prediction: $\hat{x}(n+1) = y^{T}(n+1)\, H(n)$

Prediction error: $e(n+1) = x(n+1) - \hat{x}(n+1)$

Define Kalman gain vector $K(n+1) = P(n+1)\, y(n+1)$

Equation (1) becomes: $\boxed{H(n+1) = H(n) + e(n+1)\, K(n+1) \ldots\ldots(2)}$

correction vector = $e(n+1)\, K(n+1)$:

- Prediction error $e(n+1)$ ===> the correction step size is proportional to $e(n+1)$
- Kalman gain vector $K(n+1)$ ===> the correction step direction

. Fast Kalman Algorithm:

$H(n+1) = H(n) + e(n+1)\, K(n+1)$

recursive relationship to update $K(n+1)$ from $K(n)$ exactly

. Widrow's LMS Adaptive Algorithm:

- The Steepest Decent optimization method:

wish to search the minimal location of PE w.r.t. to H,

searching method: $H(n+1) = H(n) - s\ GRAD$

where: GRAD = Gradient Vector = $d\ PE / d\ H$

s = searching step size (scalar)

-

$$GRAD = \frac{d\ PE}{d\ H} = \frac{d\ E[\ e^{2}(n)\ ]}{d\ H}$$

$$\hat{GRAD} = \frac{d\ [\ e^{2}(n)\ ]}{d\ H(n)} = 2\, e(n)\, \frac{d\ e(n)}{d\ H(n)}$$

where $e(n) = x(n) - y(n)\, H(n)$ ===> $d\ e(t) / d\ H(n) = -y(n)$

====> $\hat{GRAD} = -2\, e(n)\, y(n)$

Widrow's algorithm: $\boxed{H(n+1) = H(n) + 2\, \mu\, e(n)\, y(n) \ldots\ldots(3)}$

μ = parameter controls stability and rate of convergence

SIMULATION EXAMPLES FOR ADAPTIVE FILTER

tksin(t) = Truncated Sine Wave (Amp=1, 80% truncation)

gwn(t) = Gaussian White Noise (variance =1)

fgwn(t) = Filtered Gaussian White Noise = gwn(t) * h(t)

where: $h(t) = [\ 1,\ 3,\ 5,\ 7,\ 9,\ 7,\ 5,\ 3,\ 1,\ 1\ ]^T$

ch1(t) = tksin(t) + 10 gwn(t)

ch2(t) = tksin(t) + fgwn(t)

ch3(t) = tksin(t) + 10 fgwn(t)

ch4(t) = gwn(t)

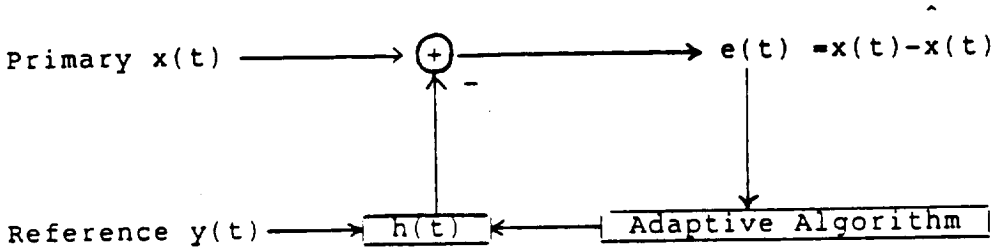

Case 1: {Primary Signal = ch1(t) = tksin(t) + 10 gwn(t)
{Reference Signal = ch4(t) = gwn(t)

====> $\hat{h}(t) = [\ 10,\ 0,\ 0,\ 0,\ 0,\ 0,\ 0,\ 0,\ 0,\ 0,\ ]$
PD = 10 gwn(t) PE=tksin(t)

Case 2: {Primary Signal = ch2(t) = tksin(t) + fgwn(t)
{Reference Signal = ch4(t) = gwn(t)

====> $\hat{h}(t) = [\ 1,\ 3,\ 5,\ 7,\ 9,\ 7,\ 5,\ 3,\ 1,\ 1\ ]$
PD = fgwn(t) PE=tksin(t)

Case 3: {Primary Signal = ch3(t) = tksin(t) + 10 fgwn(t)
{Reference Signal = ch4(t) = gwn(t)

====> $\hat{h}(t) = 10\ [\ 1,\ 3,\ 5,\ 7,\ 9,\ 7,\ 5,\ 3,\ 1,\ 1\ ]$
PD = 10 fgwn(t) PE=tksin(t)

Case 4: {Primary Signal = ch2(t) = tksin(t) + fgwn(t)
{Reference Signal = ch1(t) = tksin(t) + 10 gwn(t)

====> $\hat{h}(t) = ??$
PD = fgwn(t) ?? PE=tksin(t) ??

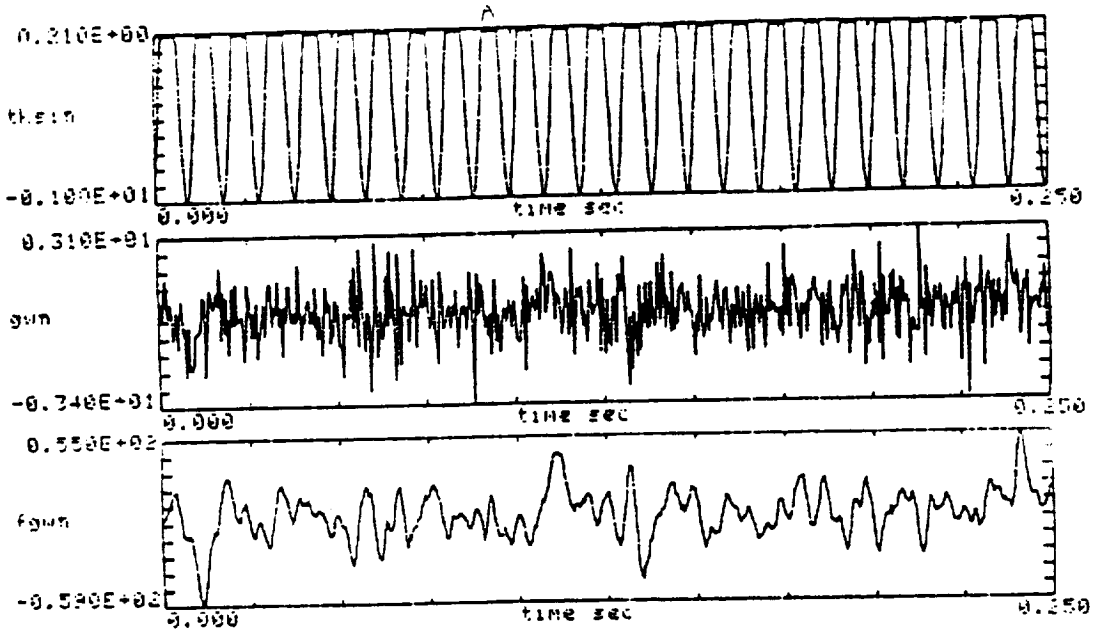

(1) truncated sine wave (90% truncation)
(2) GWN
(3) filter GWN

$fgwn = gwn \leftarrow R(f)$ $\quad R(f) = 1, 3, 5, 7, 9, 7, 5, 3, 1, 1$

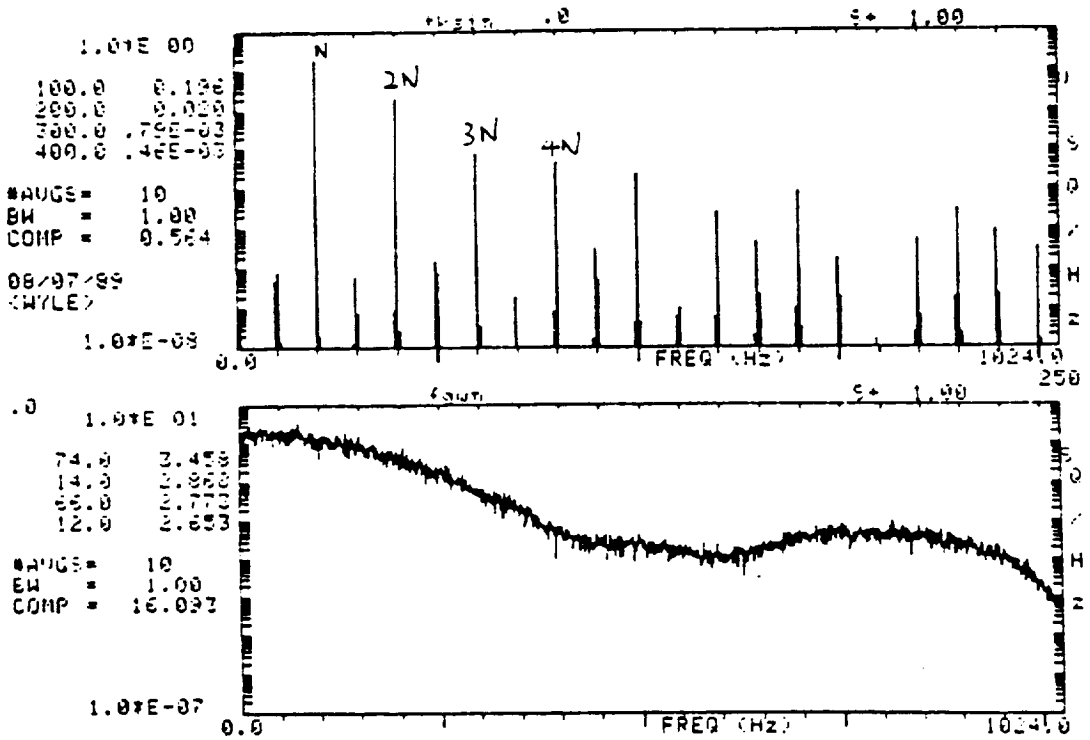

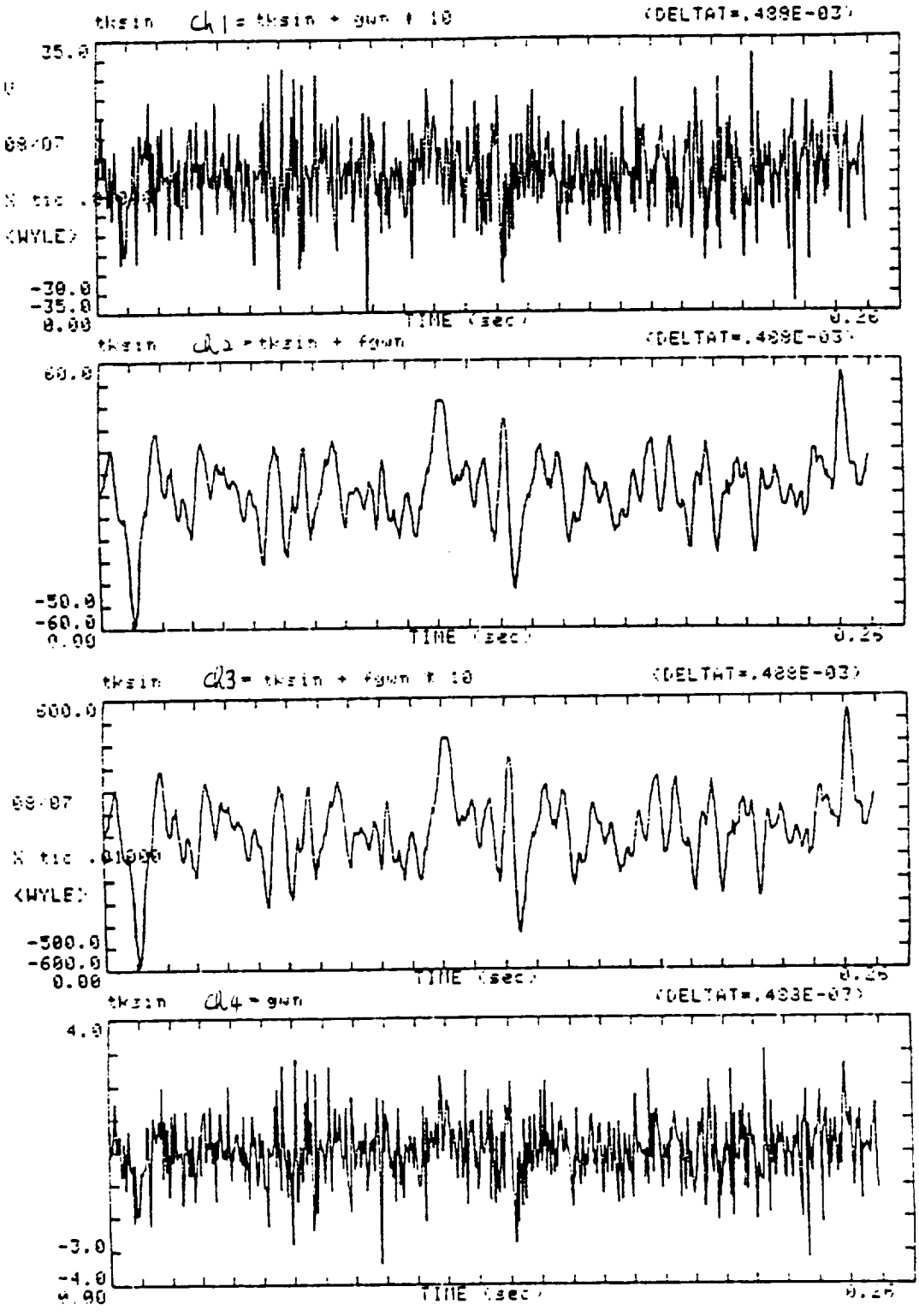
tksin ch1 = tksin + gwn * 10
(DELTAT=.488E-03)
35.0
-30.0
-35.0
0.00
TIME (sec)
0.25
tksin ch2 = tksin + fgwn
(DELTAT=.488E-03)
60.0
-50.0
-60.0
0.00
TIME (sec)
0.25
tksin ch3 = tksin + fgwn * 10
(DELTAT=.488E-03)
500.0
-500.0
-600.0
0.00
TIME (sec)
0.25
tksin ch4 = gwn
(DELTAT=.488E-03)
4.0
-3.0
-4.0
0.00
TIME (sec)
0.25

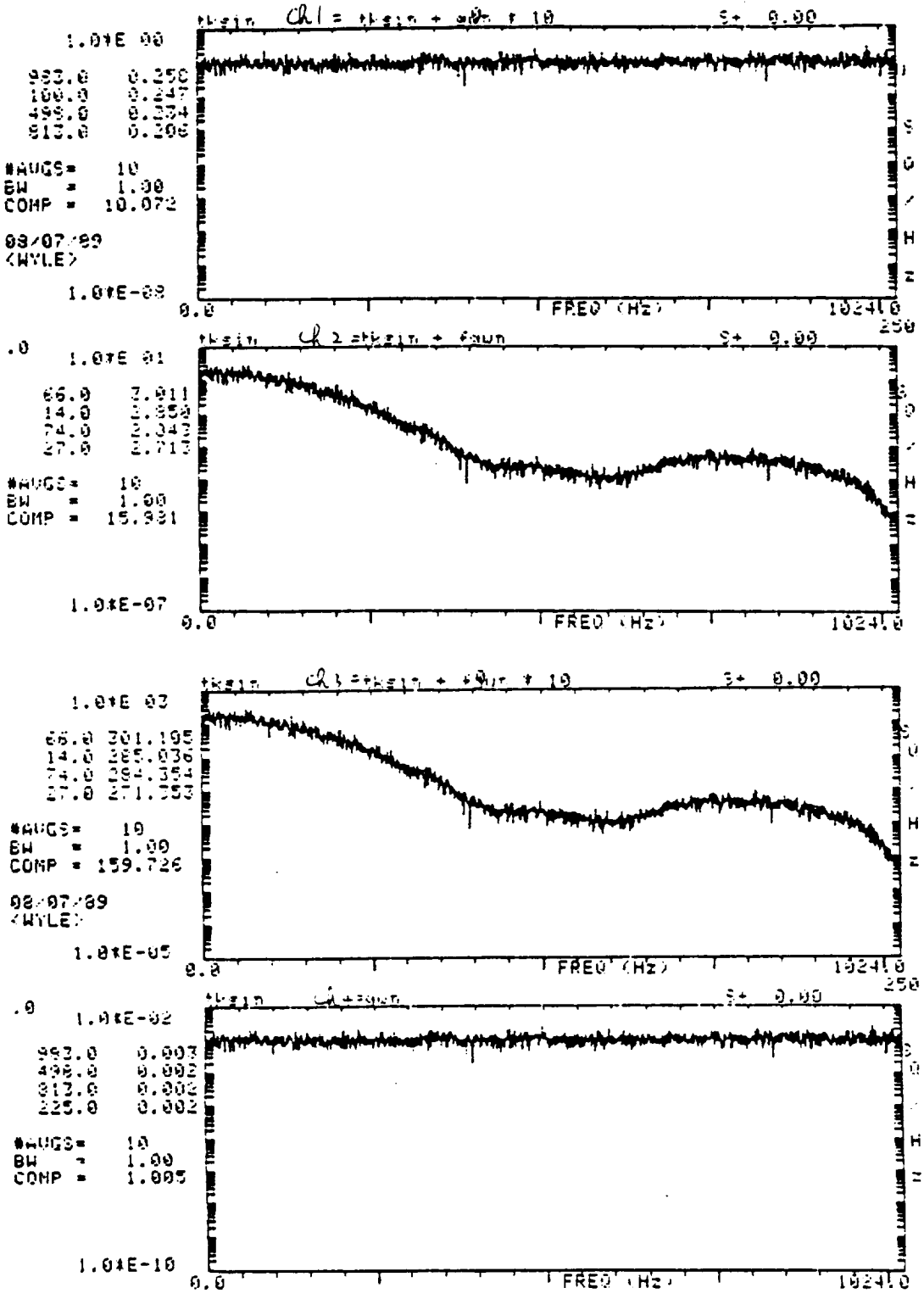
1.0*E 00
993.0 0.250
498.0 0.334
313.0 0.206
#AVGS= 10
BW = 1.00
COMP = 10.072
08/07/89
<WYLE>
1.0*E-08
0.0
FREQ (Hz)
1024.0
1.0*E 01
66.0 7.911
14.0 3.858
74.0 2.049
27.0 3.713
#AVGS= 10
BW = 1.00
COMP = 15.931
1.0*E-07
0.0
FREQ (Hz)
1024.0
1.0*E 03
66.0 301.195
14.0 385.036
74.0 284.354
27.0 271.353
#AVGS= 10
BW = 1.00
COMP = 159.726
08/07/89
<WYLE>
1.0*E-05
0.0
FREQ (Hz)
1024.0
1.0*E-02
993.0 0.003
498.0 0.002
313.0 0.002
225.0 0.002
#AVGS= 10
BW = 1.00
COMP = 1.005
1.0*E-10
0.0
FREQ (Hz)
1024.0

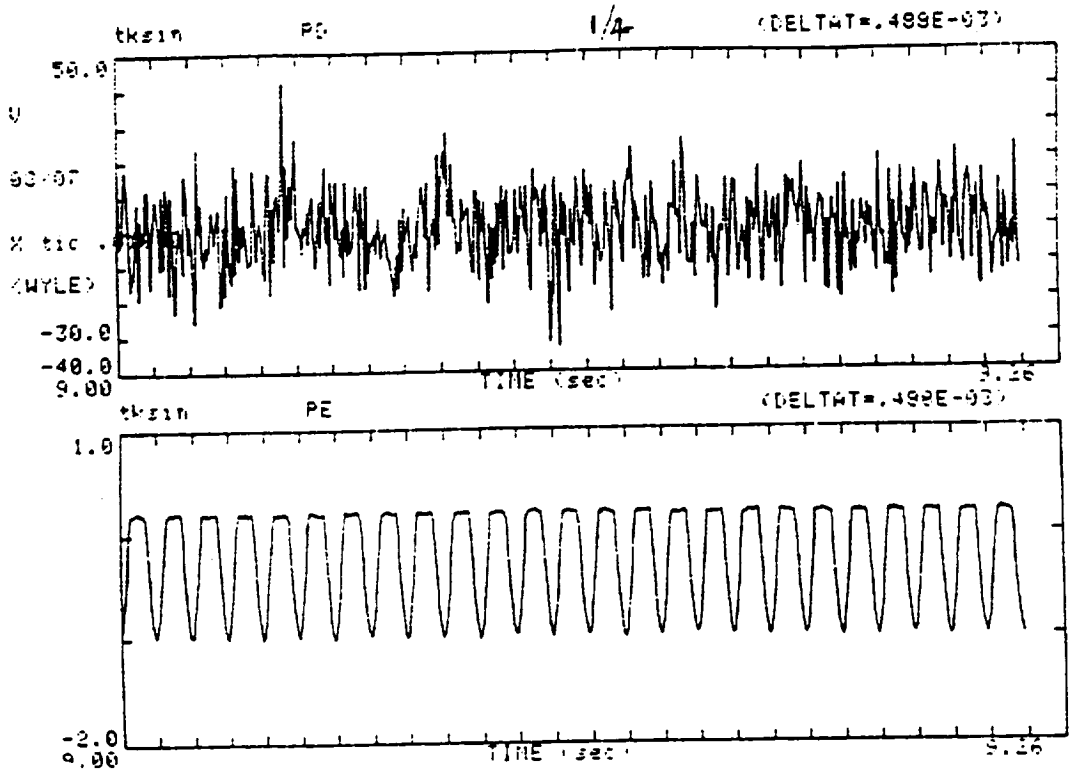
tksin
PD
1/4
(DELTAT=.489E-03)
50.0
V
03/07
X tic
(WYLE)
-30.0
-40.0
9.00
TIME (sec)
9.26
tksin
PE
(DELTAT=.498E-03)
1.0
-2.0
9.00
TIME (sec)
9.26

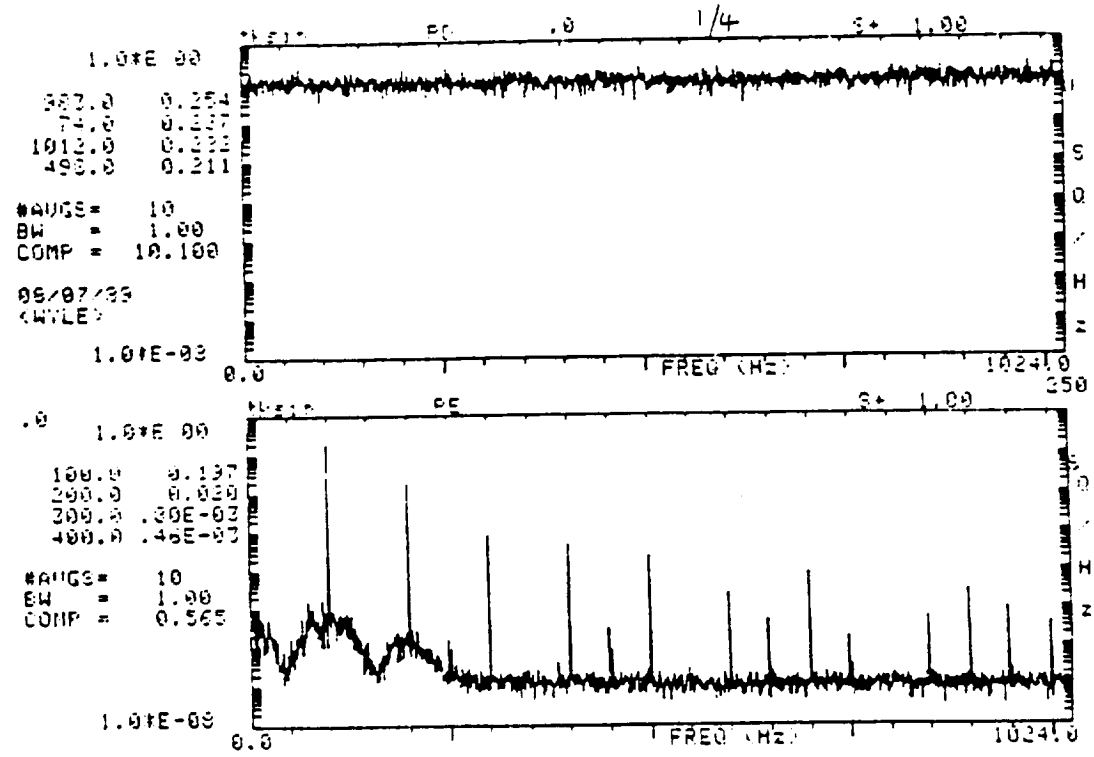
tksin
PD
.0
1/4
S+ 1.00
1.0*E 00
983.0 0.254
74.0 0.237
1012.0 0.232
498.0 0.211
#AVGS= 10
BW = 1.00
COMP = 10.100
06/07/89
(WYLE)
1.0*E-03
0.0
FREQ (Hz)
1024.0
250
S
Q
/
H
z
.0
1.0*E 00
100.0 0.197
200.0 0.020
300.0 .30E-03
400.0 .46E-03
#AVGS= 10
BW = 1.00
COMP = 0.565
1.0*E-08
0.0
FREQ (Hz)
1024.0

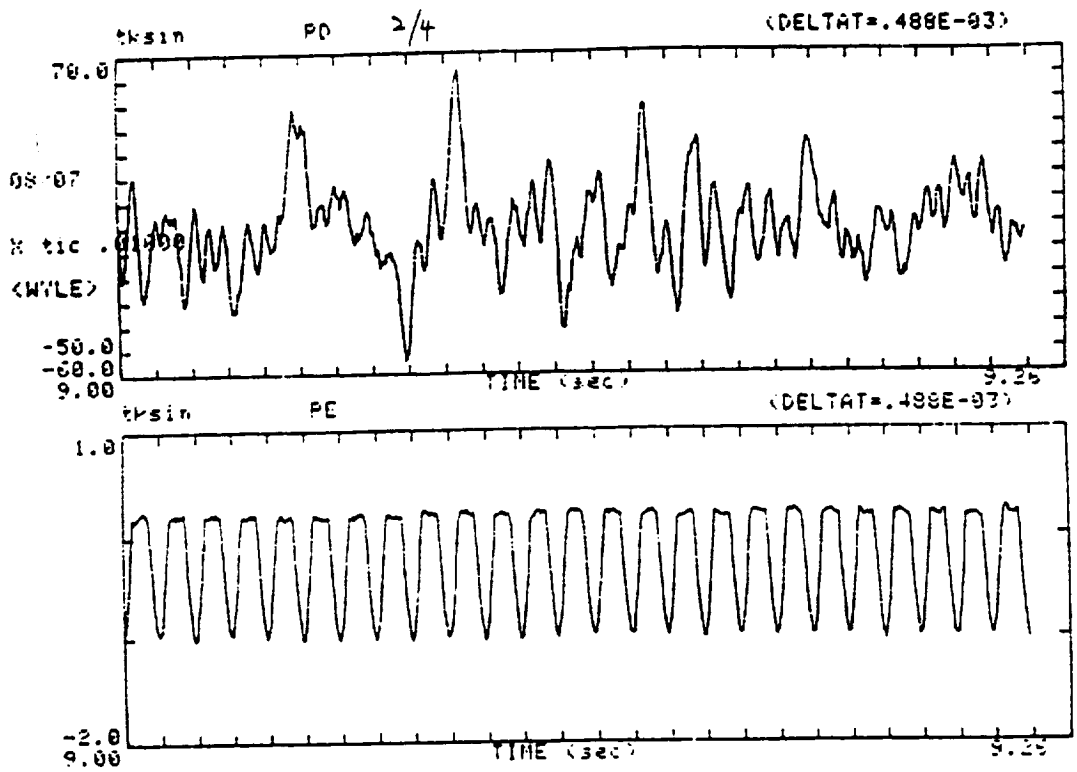
tksin
PD
2/4
(DELTAT=.488E-03)
70.0
08/07
X tic
(WYLE)
-50.0
-60.0
9.00
TIME (sec)
9.25
tksin
PE
(DELTAT=.488E-03)
1.0
-2.0
9.00
TIME (sec)
9.25

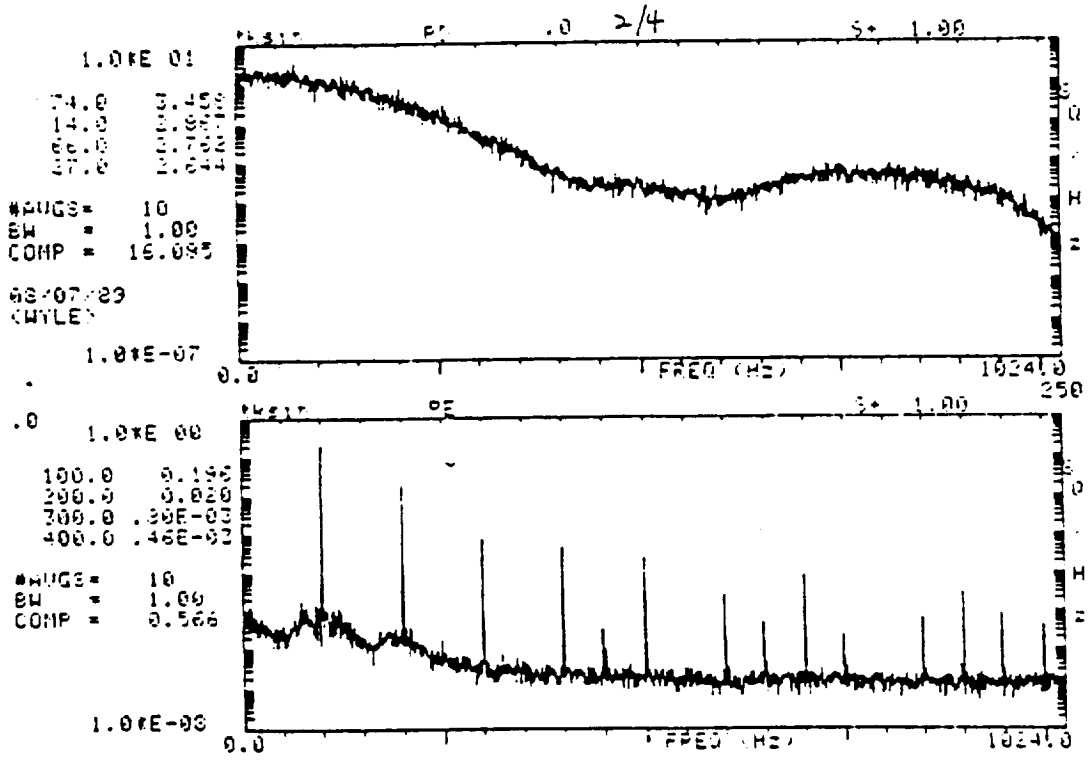
2/4
1.0*E 01
#AVGS= 10
BW = 1.00
COMP = 16.095
08/07/89
(WYLE)
1.0*E-07
0.0
FREQ (Hz)
1024.0
250
.0
1.0*E 00
100.0 0.196
200.0 0.020
300.0 .80E-03
400.0 .46E-03
#AVGS= 10
BW = 1.00
COMP = 0.566
1.0*E-08
0.0
FREQ (Hz)
1024.0

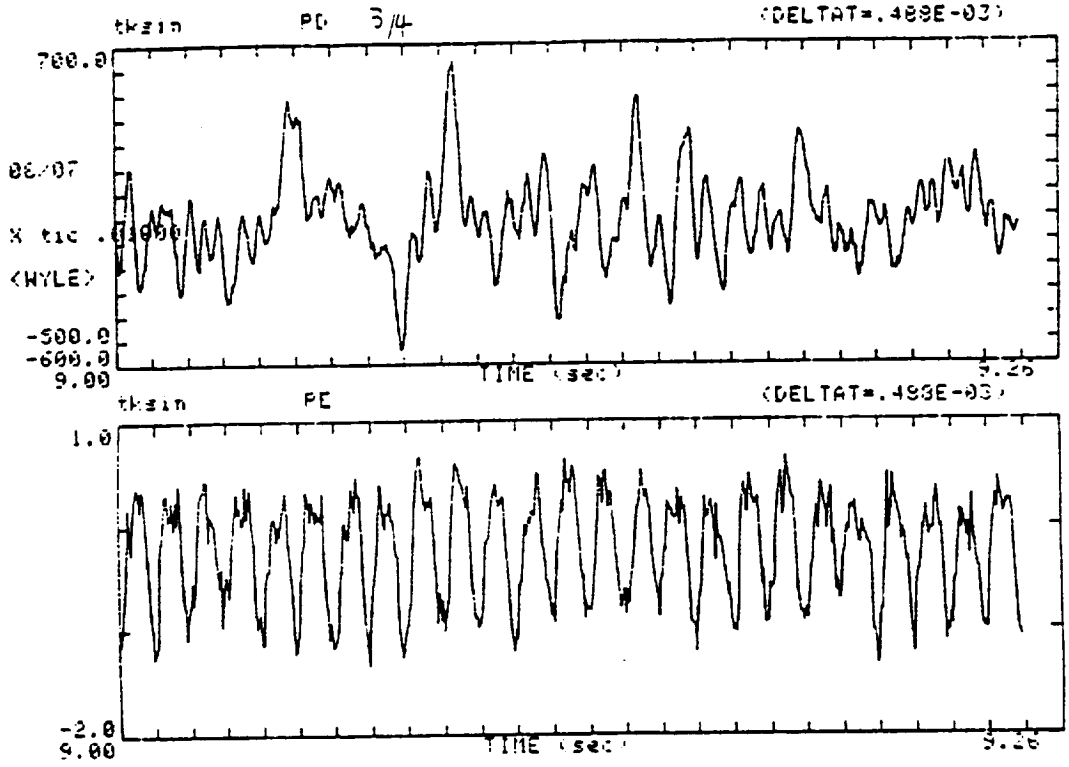
PD 3/4
<DELTAT=.488E-03>
700.0
08/07
X tic
<HYLE>
-500.0
-600.0
9.00
TIME (sec)
PE
<DELTAT=.488E-03>
1.0
-2.0
9.00
TIME (sec)

3/4

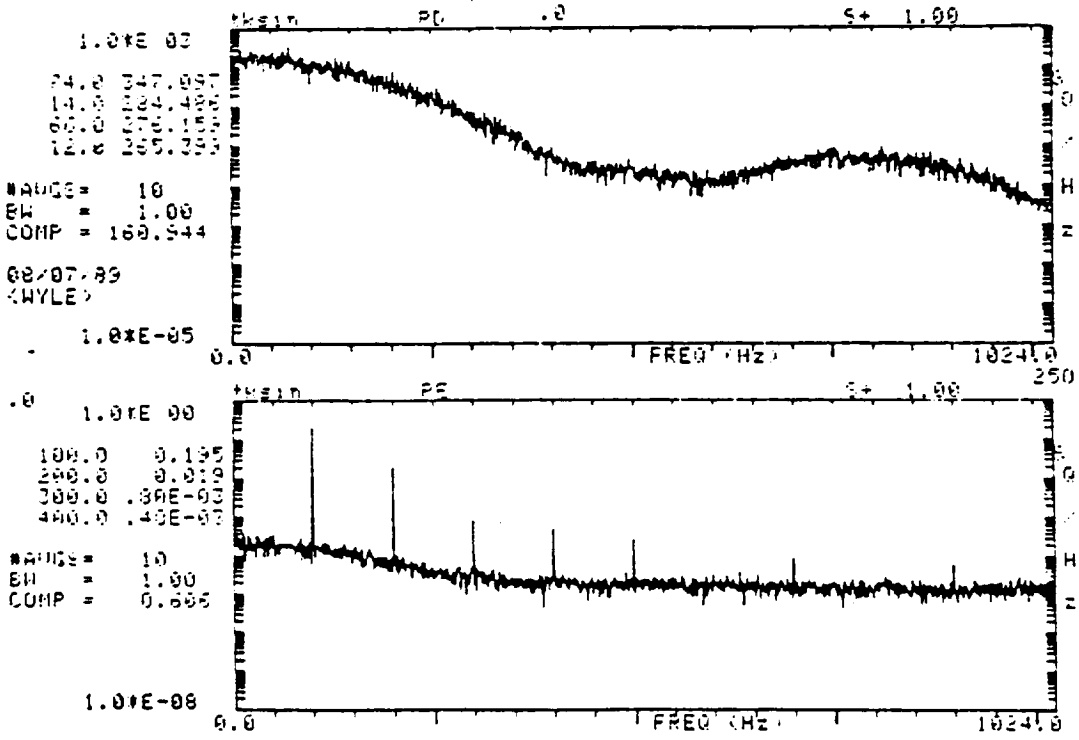
PD .2 S+ 1.00
1.0*E 03
BW = 1.00
COMP = 160.544
08/07/89
<HYLE>
1.0*E-05
0.0
FREQ (Hz)
1024.0
250
PE S+ 1.00
1.0*E 00
BW = 1.00
COMP = 0.666
1.0*E-08
0.0
FREQ (Hz)
1024.0

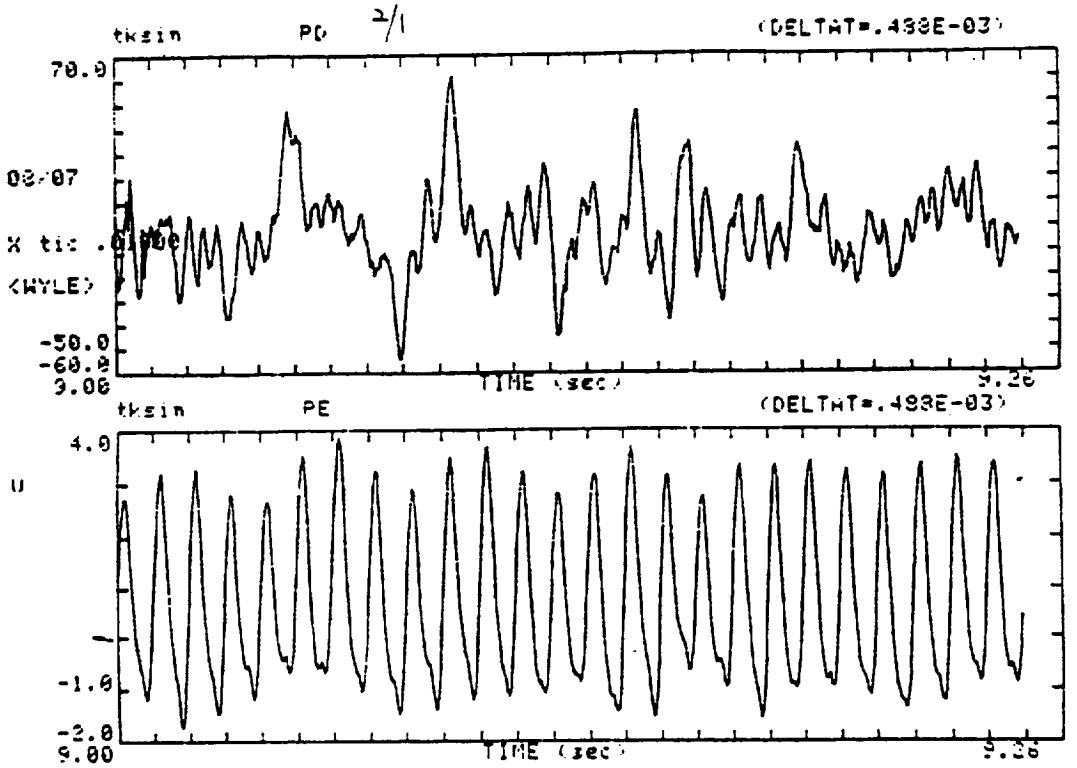
tksin
PD
2/1
(DELTHT=.488E-03)
70.0
08/07
X tic .0100
(WYLE)
-50.0
-60.0
9.00
TIME (sec)
9.20
tksin
PE
(DELTHT=.488E-03)
4.0
U
-1.0
-2.0
9.00
TIME (sec)
9.20

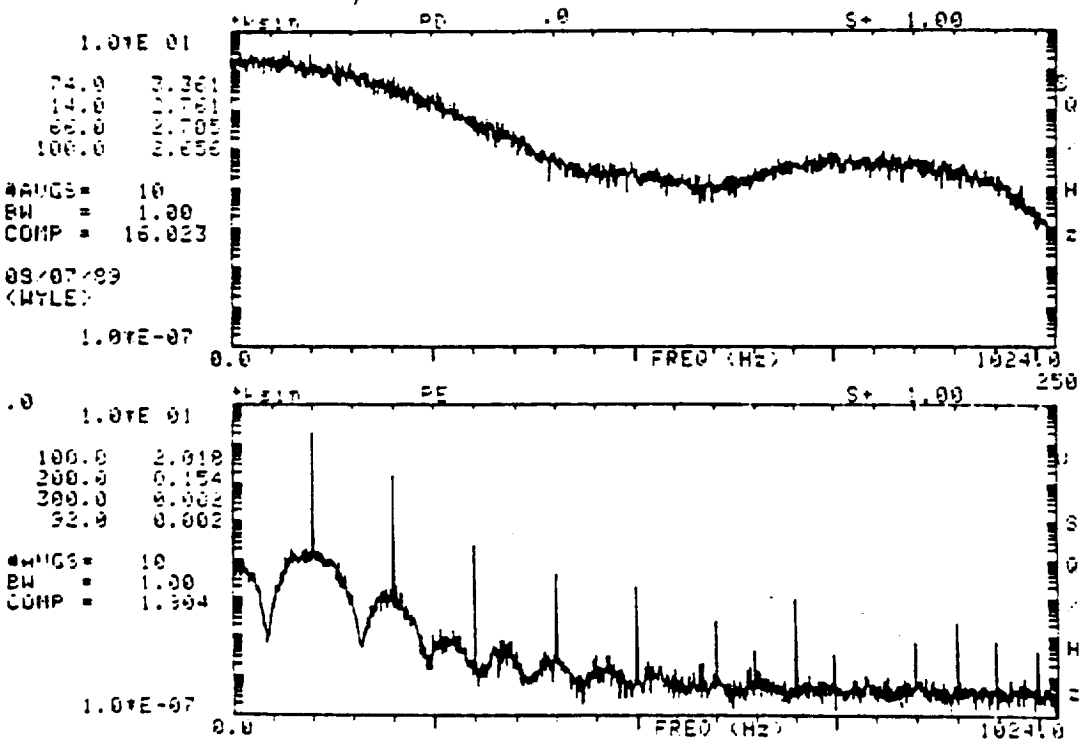
2/1
1.01E 01
#AVGS= 10
BW = 1.00
COMP = 16.023
08/07/89
(WYLE)
1.01E-07
tksin
PD
.0
S+ 1.00
0.0
FREQ (HZ)
1024.0
250
.0
1.01E 01
100.0 2.018
200.0 0.154
300.0 0.002
32.0 0.002
#AVGS= 10
BW = 1.00
COMP = 1.304
1.01E-07
tksin
PE
S+ 1.00
0.0
FREQ (HZ)
1024.0

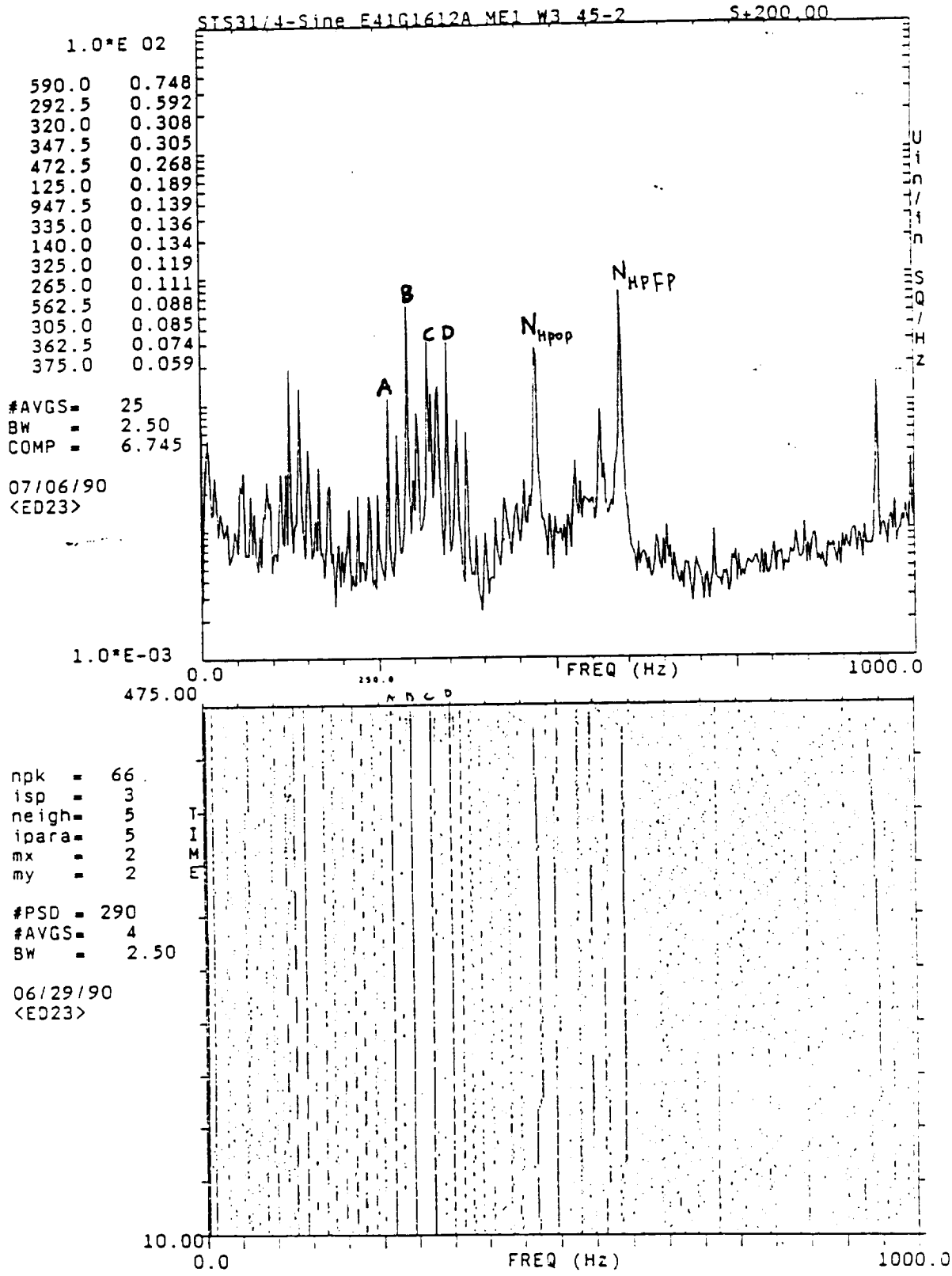
STS31/4-Sine E41G1612A ME1 W3 45-2
S+200.00
1.0*E 02
590.0 0.748
292.5 0.592
320.0 0.308
347.5 0.305
472.5 0.268
125.0 0.189
947.5 0.139
335.0 0.136
140.0 0.134
325.0 0.119
265.0 0.111
562.5 0.088
305.0 0.085
362.5 0.074
375.0 0.059
#AVGS= 25
BW = 2.50
COMP = 6.745
07/06/90
<ED23>
1.0*E-03
A
B
C D
N Hpop
N HPFP
Uin/in SQ/Hz
0.0
FREQ (Hz)
1000.0
475.00
A B C D
npk = 66
isp = 3
neigh= 5
ipara= 5
mx = 2
my = 2
#PSD = 290
#AVGS= 4
BW = 2.50
06/29/90
<ED23>
TIME
10.00
0.0
FREQ (Hz)
1000.0

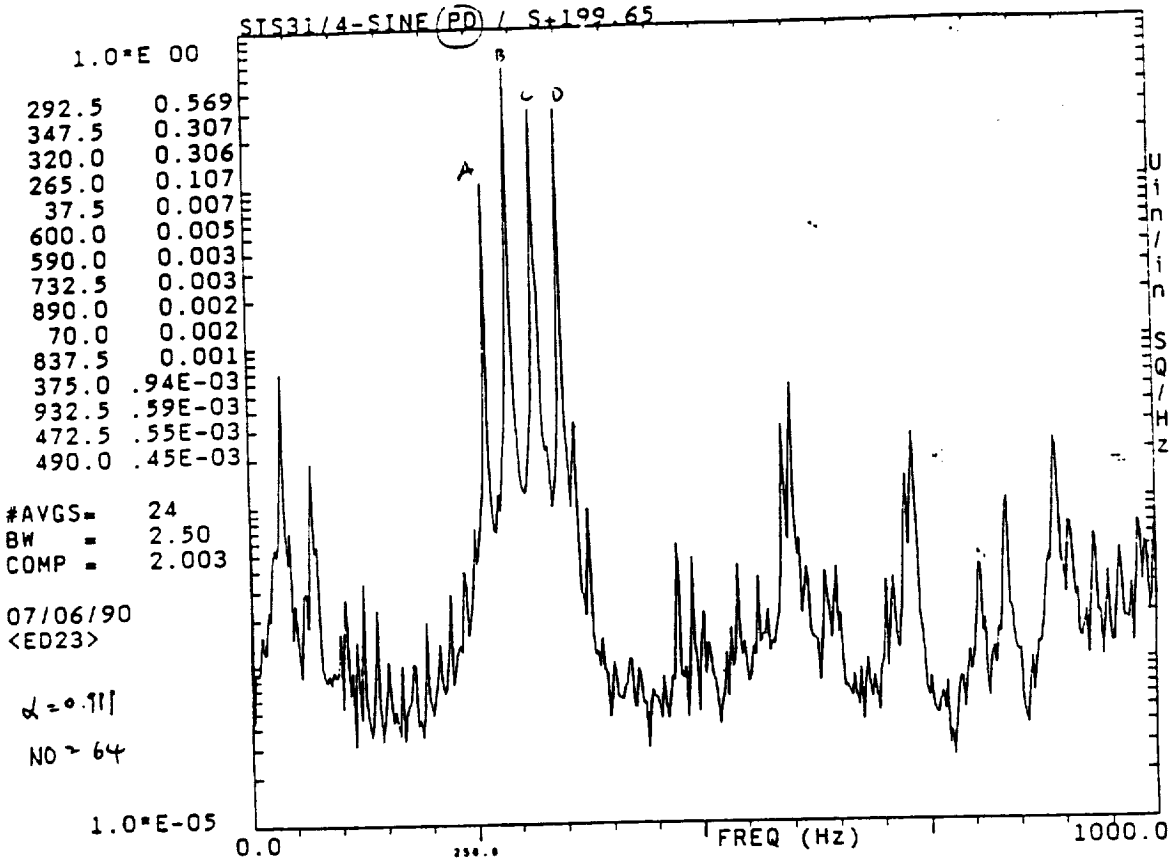
SIS31/4-SINE (PD) / S+199.65
1.0*E 00
292.5 0.569
347.5 0.307
320.0 0.306
265.0 0.107
37.5 0.007
600.0 0.005
590.0 0.003
732.5 0.003
890.0 0.002
70.0 0.002
837.5 0.001
375.0 .94E-03
932.5 .59E-03
472.5 .55E-03
490.0 .45E-03
#AVGS= 24
BW = 2.50
COMP = 2.003
07/06/90
<ED23>
α = 0.111
NO = 64
1.0*E-05
A
B
C
D
0.0
FREQ (Hz)
1000.0
V SQ/HZ

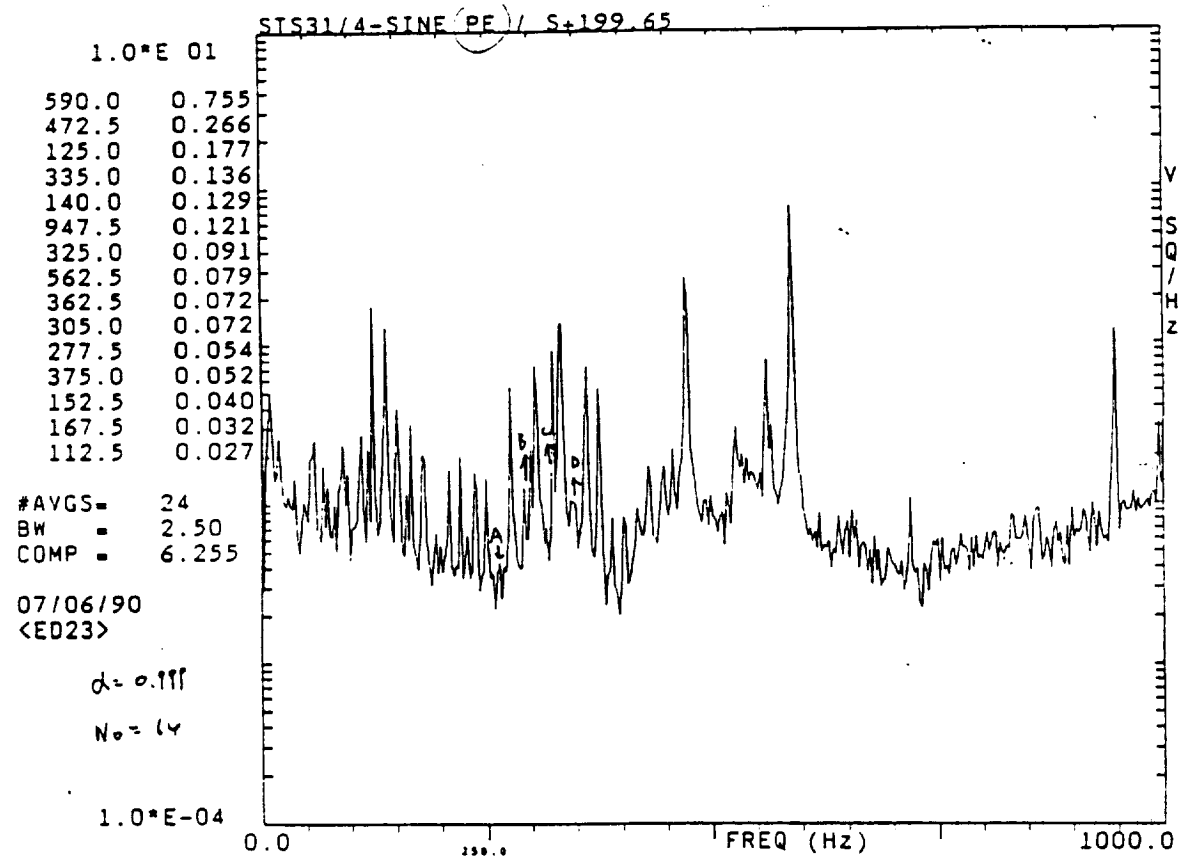
SIS31/4-SINE (PE) / S+199.65
1.0*E 01
590.0 0.755
472.5 0.266
125.0 0.177
335.0 0.136
140.0 0.129
947.5 0.121
325.0 0.091
562.5 0.079
362.5 0.072
305.0 0.072
277.5 0.054
375.0 0.052
152.5 0.040
167.5 0.032
112.5 0.027
#AVGS= 24
BW = 2.50
COMP = 6.255
07/06/90
<ED23>
α = 0.111
No = 64
1.0*E-04
0.0
FREQ (Hz)
1000.0
V SQ/HZ

C-5

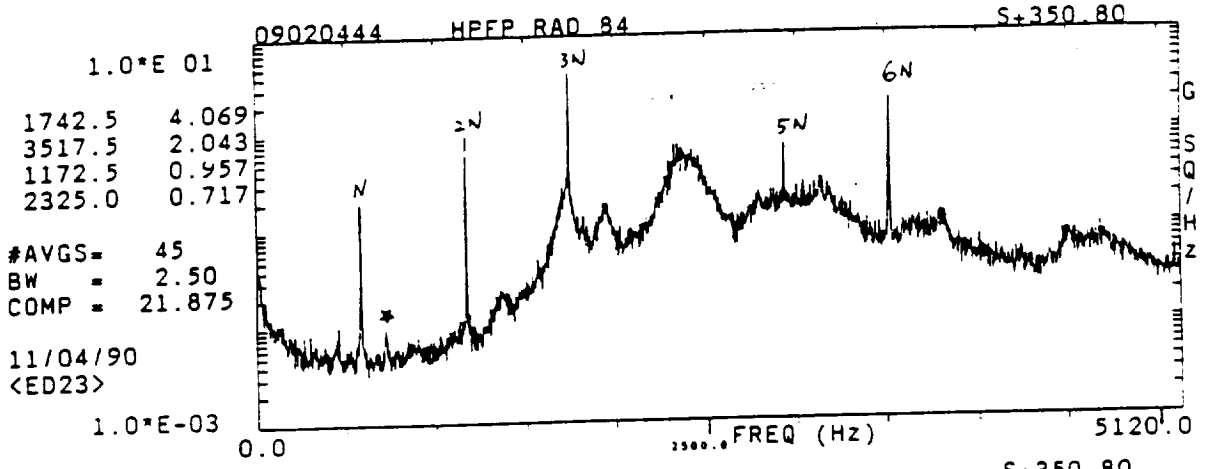
09020444 HPFP RAD 84
S+350.80
1.0*E 01
1742.5 4.069
3517.5 2.043
1172.5 0.957
2325.0 0.717
#AVGS= 45
BW = 2.50
COMP = 21.875
11/04/90
<ED23>
1.0*E-03
N
2N
3N
5N
6N
G S Q / H z
0.0
FREQ (Hz)
5120.0

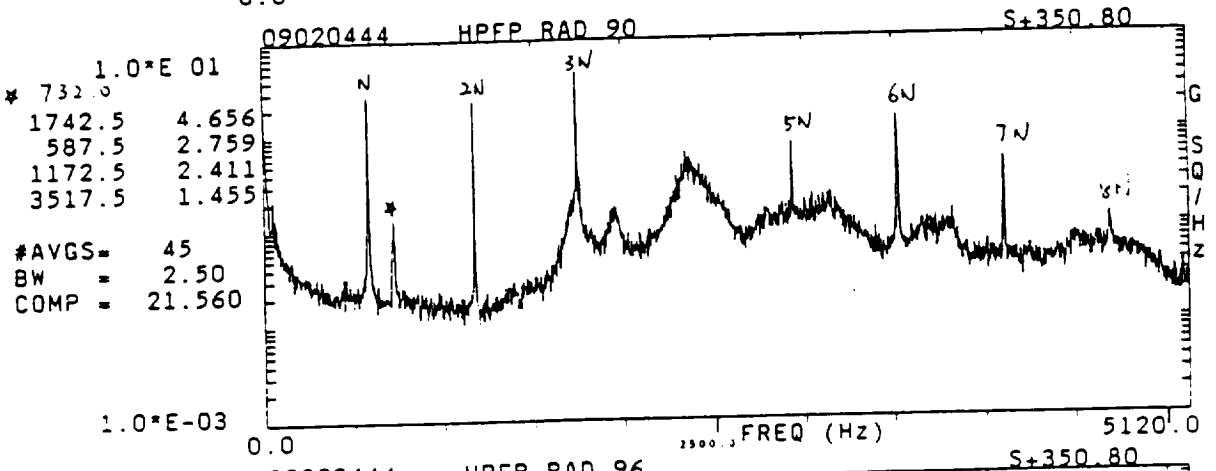
09020444 HPFP RAD 90
S+350.80
1.0*E 01
1742.5 4.656
587.5 2.759
1172.5 2.411
3517.5 1.455
#AVGS= 45
BW = 2.50
COMP = 21.560
1.0*E-03
N
2N
3N
5N
6N
7N
G S Q / H z
0.0
FREQ (Hz)
5120.0

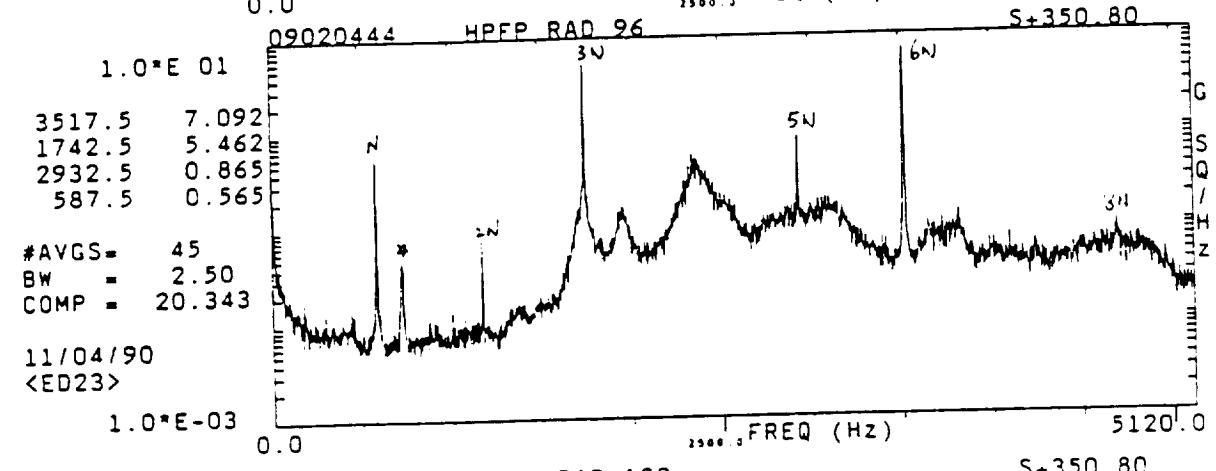
09020444 HPFP RAD 96
S+350.80
1.0*E 01
3517.5 7.092
1742.5 5.462
2932.5 0.865
587.5 0.565
#AVGS= 45
BW = 2.50
COMP = 20.343
11/04/90
<ED23>
1.0*E-03
N
2N
3N
5N
6N
G S Q / H z
0.0
FREQ (Hz)
5120.0

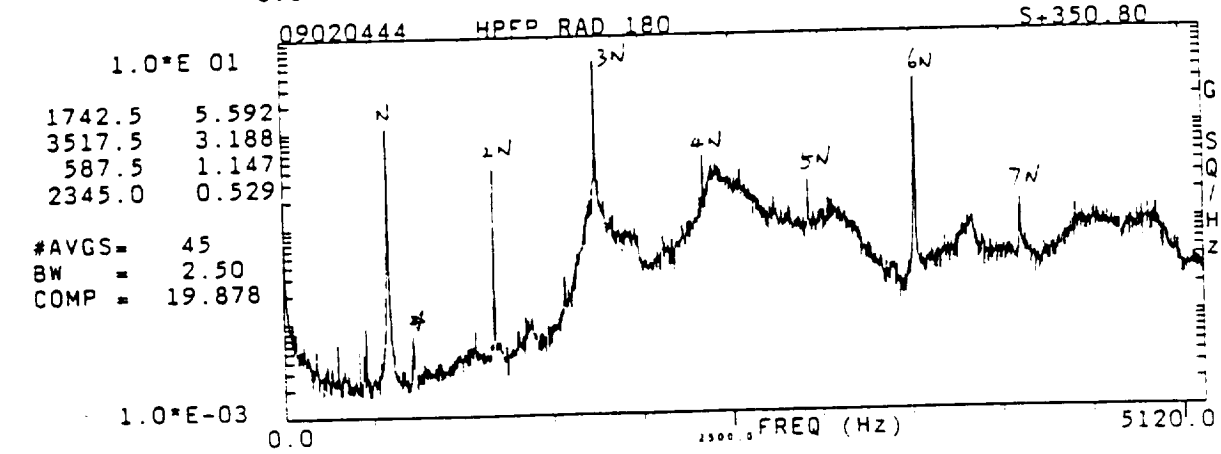
09020444 HPFP RAD 180
S+350.80
1.0*E 01
1742.5 5.592
3517.5 3.188
587.5 1.147
2345.0 0.529
#AVGS= 45
BW = 2.50
COMP = 19.878
1.0*E-03
N
2N
3N
4N
5N
6N
7N
G S Q / H z
0.0
FREQ (Hz)
5120.0

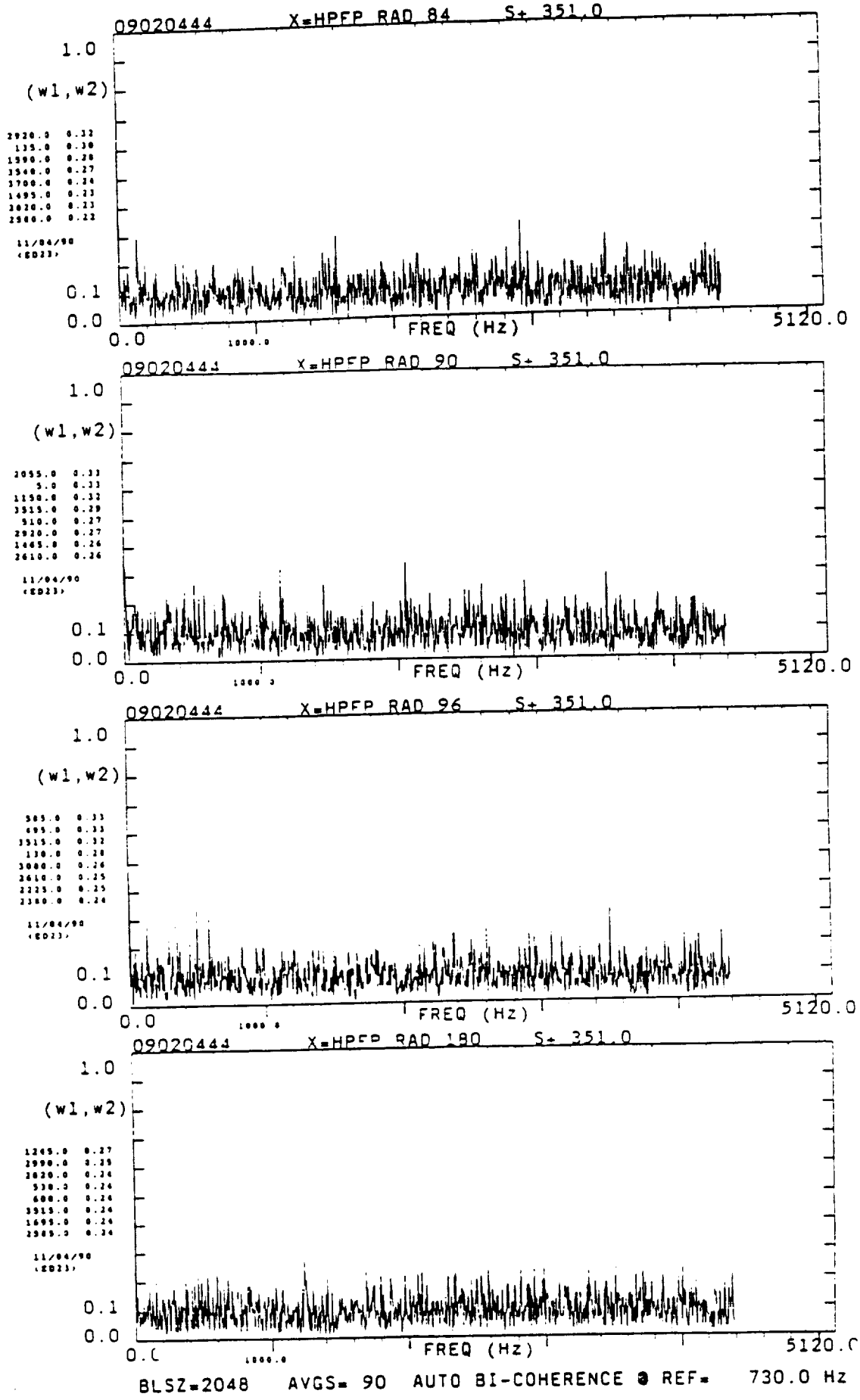
09020444 X=HPFP RAD 84 S+ 351.0
1.0
(w1,w2)
0.1
0.0
0.0
FREQ (Hz)
5120.0
09020444 X=HPFP RAD 90 S+ 351.0
1.0
(w1,w2)
0.1
0.0
0.0
FREQ (Hz)
5120.0
09020444 X=HPFP RAD 96 S+ 351.0
1.0
(w1,w2)
0.1
0.0
0.0
FREQ (Hz)
5120.0
09020444 X=HPFP RAD 180 S+ 351.0
1.0
(w1,w2)
0.1
0.0
FREQ (Hz)
5120.0
BLSZ=2048 AVGS= 90 AUTO BI-COHERENCE REF= 730.0 Hz

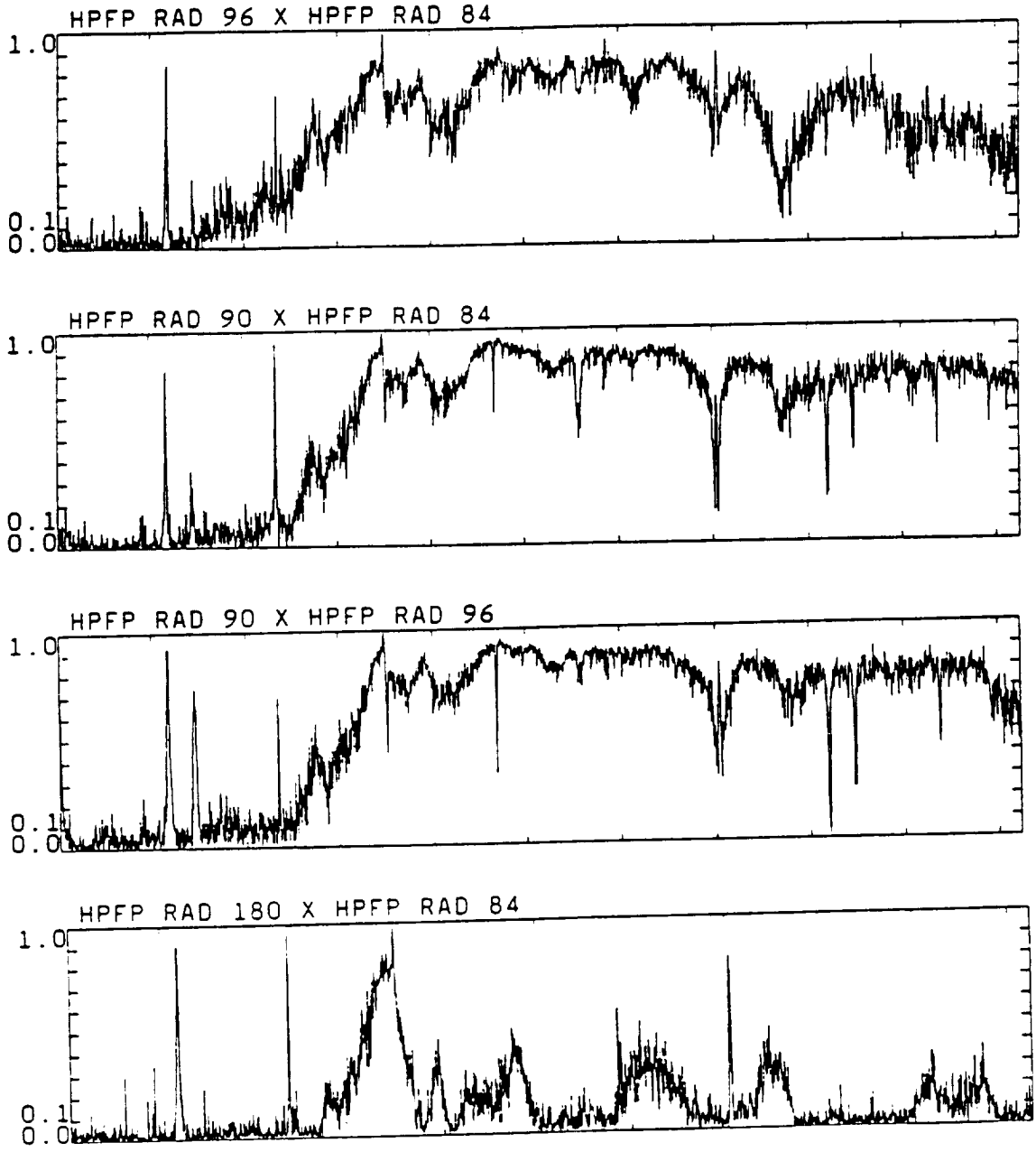

09020444 COHERENCE

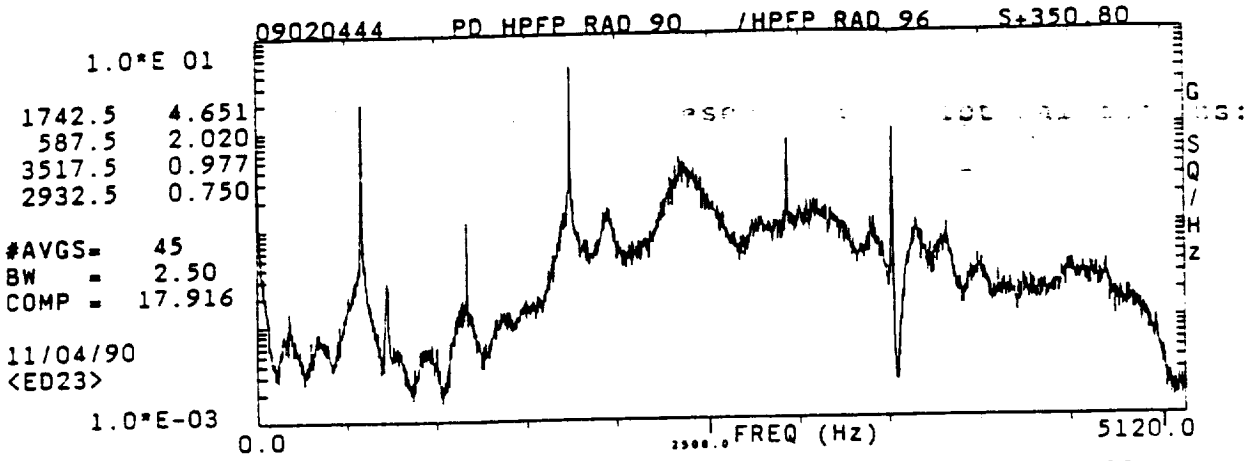
09020444 PD HPFP RAD 90 /HPFP RAD 96 S+350.80
1.0*E 01
1742.5 4.651
587.5 2.020
3517.5 0.977
2932.5 0.750
#AVGS= 45
BW = 2.50
COMP = 17.916
11/04/90
<ED23>
1.0*E-03
G SQ/Hz
0.0
2560.0 FREQ (Hz)
5120.0

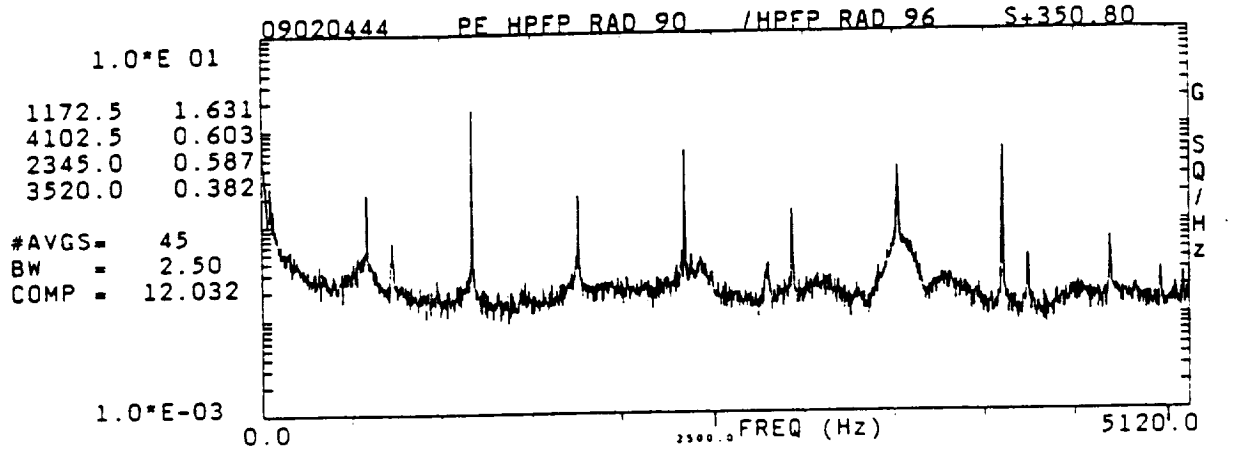
09020444 PF HPFP RAD 90 /HPFP RAD 96 S+350.80
1.0*E 01
1172.5 1.631
4102.5 0.603
2345.0 0.587
3520.0 0.382
#AVGS= 45
BW = 2.50
COMP = 12.032
1.0*E-03
G SQ/Hz
0.0
2560.0 FREQ (Hz)
5120.0

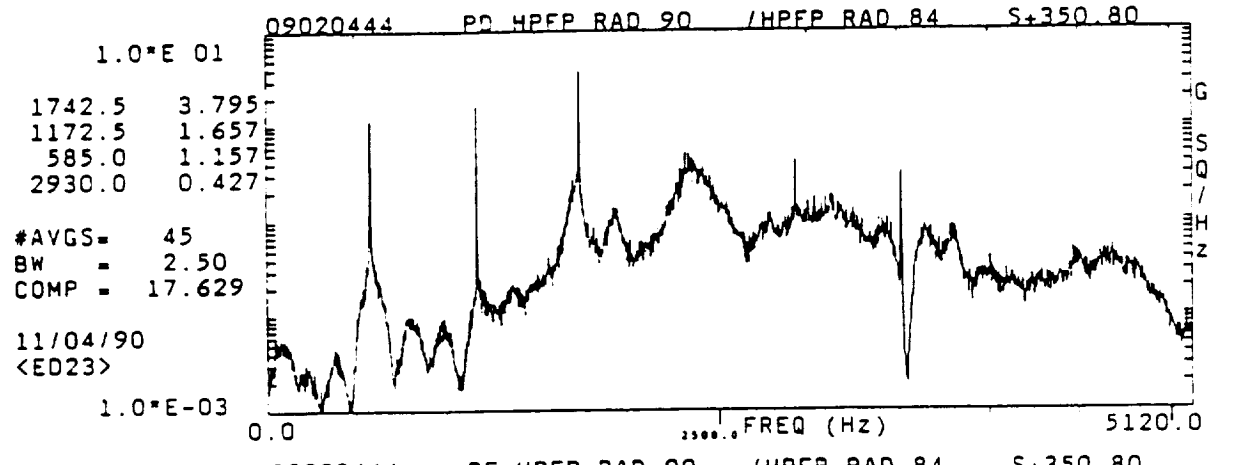
09020444 PD HPFP RAD 90 /HPFP RAD 84 S+350.80
1.0*E 01
1742.5 3.795
1172.5 1.657
585.0 1.157
2930.0 0.427
#AVGS= 45
BW = 2.50
COMP = 17.629
11/04/90
<ED23>
1.0*E-03
G SQ/Hz
0.0
2560.0 FREQ (Hz)
5120.0

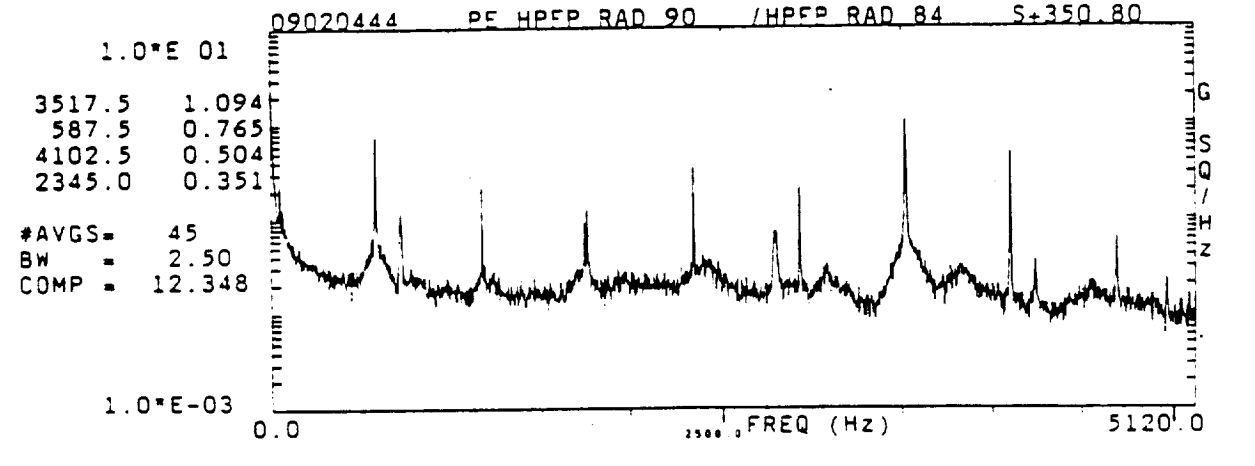
09020444 PF HPFP RAD 90 /HPFP RAD 84 S+350.80
1.0*E 01
3517.5 1.094
587.5 0.765
4102.5 0.504
2345.0 0.351
#AVGS= 45
BW = 2.50
COMP = 12.348
1.0*E-03
G SQ/Hz
0.0
2560.0 FREQ (Hz)
5120.0

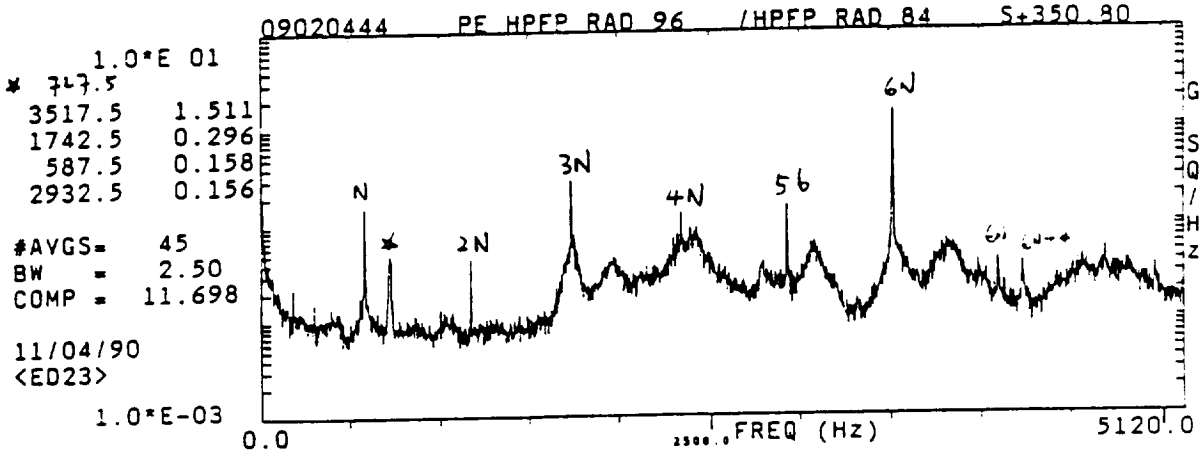
09020444 PE HPFP RAD 96 /HPFP RAD 84 S+350.80
1.0*E 01
* 747.5
3517.5 1.511
1742.5 0.296
587.5 0.158
2932.5 0.156
#AVGS= 45
BW = 2.50
COMP = 11.698
11/04/90
<ED23>
1.0*E-03
N
2N
3N
4N
5 6
6N
0.0
2500.0 FREQ (Hz)
5120.0
G
S
Q
/
H
z

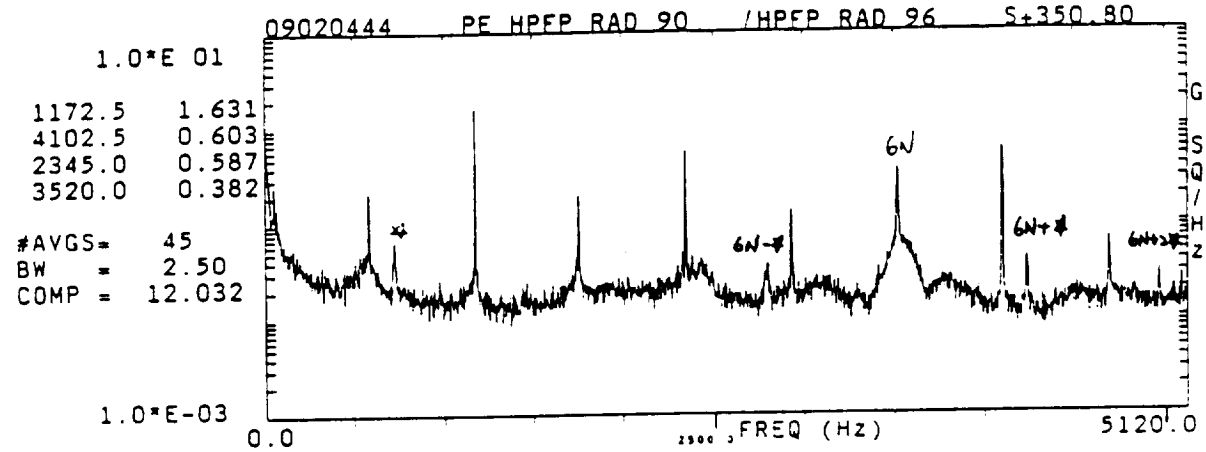
09020444 PE HPFP RAD 90 /HPFP RAD 96 S+350.80
1.0*E 01
1172.5 1.631
4102.5 0.603
2345.0 0.587
3520.0 0.382
#AVGS= 45
BW = 2.50
COMP = 12.032
1.0*E-03
6N
6N-*
6N+*
0.0
2500.0 FREQ (Hz)
5120.0
G
S
Q
/
H
z

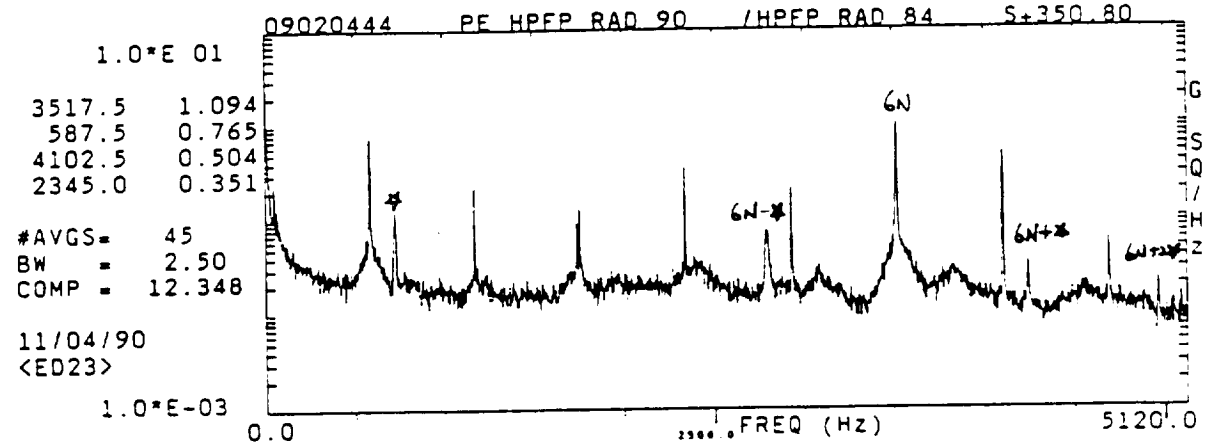
09020444 PE HPFP RAD 90 /HPFP RAD 84 S+350.80
1.0*E 01
3517.5 1.094
587.5 0.765
4102.5 0.504
2345.0 0.351
#AVGS= 45
BW = 2.50
COMP = 12.348
11/04/90
<ED23>
1.0*E-03
6N
6N-*
6N+*
0.0
2500.0 FREQ (Hz)
5120.0
G
S
Q
/
H
z

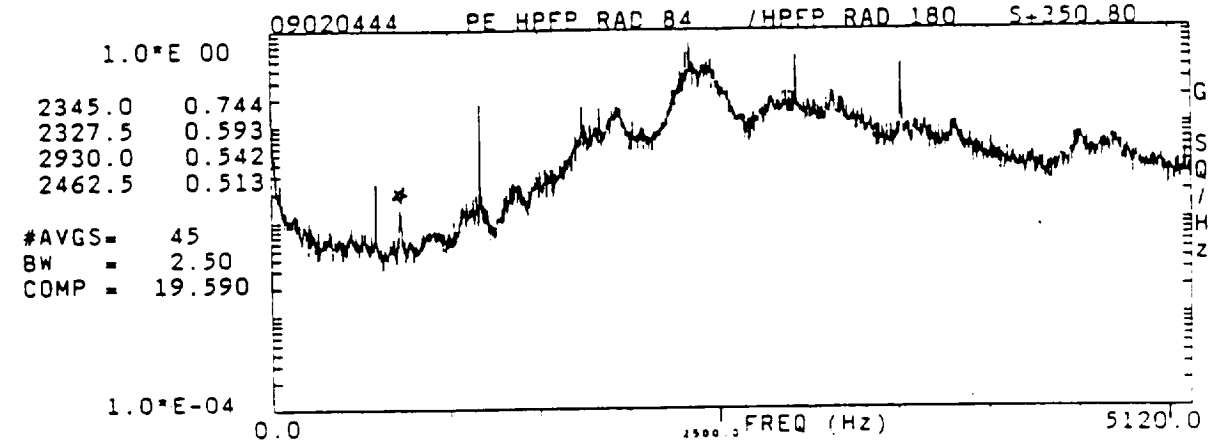
09020444 PE HPFP RAD 84 /HPFP RAD 180 S+350.80
1.0*E 00
2345.0 0.744
2327.5 0.593
2930.0 0.542
2462.5 0.513
#AVGS= 45
BW = 2.50
COMP = 19.590
1.0*E-04
0.0
2500.0 FREQ (Hz)
5120.0
G
S
Q
/
H
z

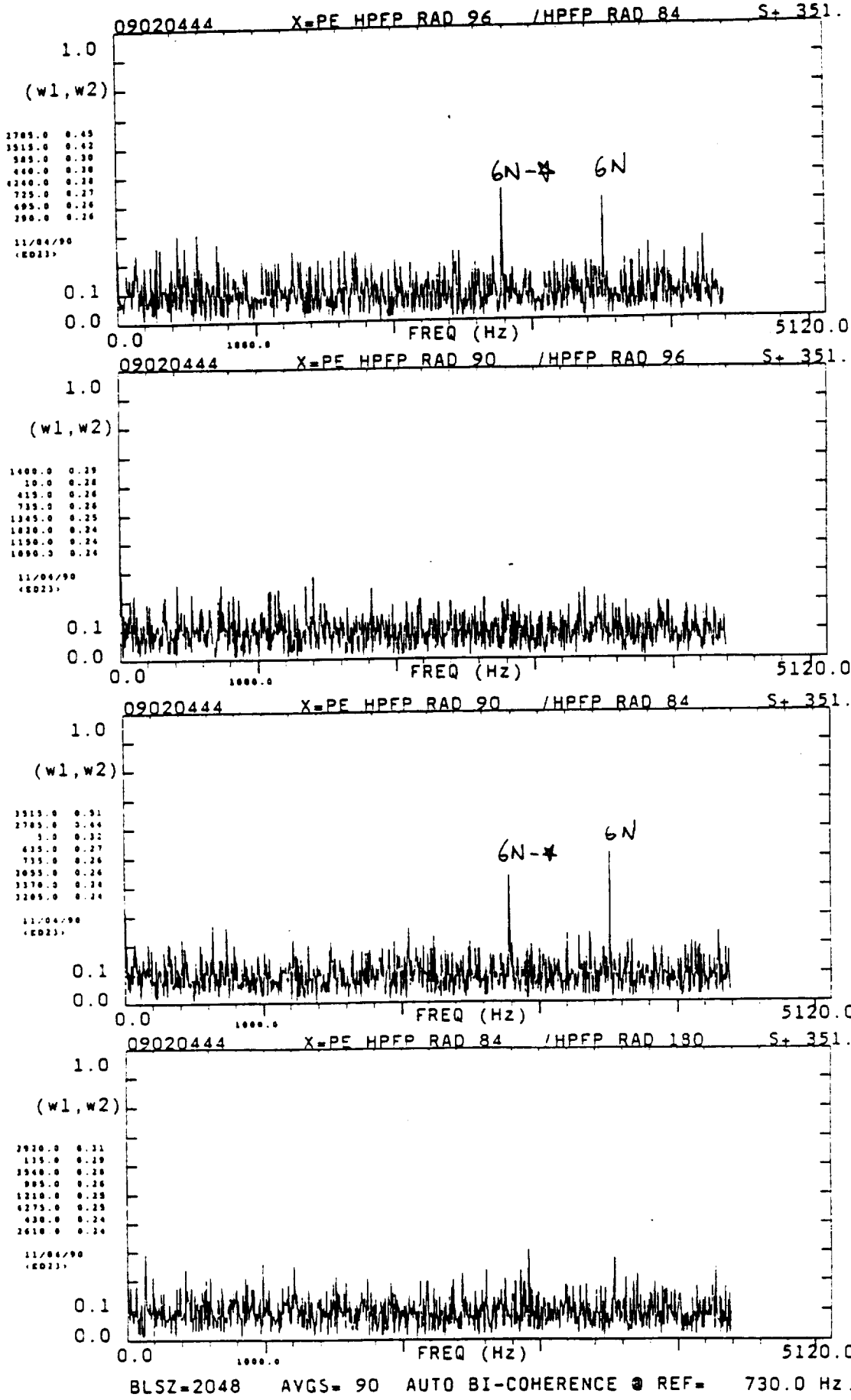
09020444 X=PF HPFP RAD 96 /HPFP RAD 84 S+ 351.
1.0
(w1,w2)
0.1
0.0
0.0
FREQ (Hz)
5120.0
6N-1
6N
09020444 X=PF HPFP RAD 90 /HPFP RAD 96 S+ 351.
1.0
(w1,w2)
0.1
0.0
0.0
FREQ (Hz)
5120.0
09020444 X=PF HPFP RAD 90 /HPFP RAD 84 S+ 351.
1.0
(w1,w2)
0.1
0.0
0.0
FREQ (Hz)
5120.0
6N-1
6N
09020444 X=PF HPFP RAD 84 /HPFP RAD 180 S+ 351.
1.0
(w1,w2)
0.1
0.0
0.0
FREQ (Hz)
5120.0
BLSZ=2048 AVGS= 90 AUTO BI-COHERENCE @ REF= 730.0 Hz

CEPSTRUM
ROTARY SPECTRUM
FREQUENCY-WAVENUMBER SPECTRUM
PHASE DOMAIN AVERAGE COHERENCE
COMPLEX TOPO DATABASE

by

Jen-Yi Jong

February 1991

for

Structures and Dynamics Laboratory
Marshall Space Flight Center

Contract NAS8-38156

COMPLEX CEPSTRUM ANALYSIS

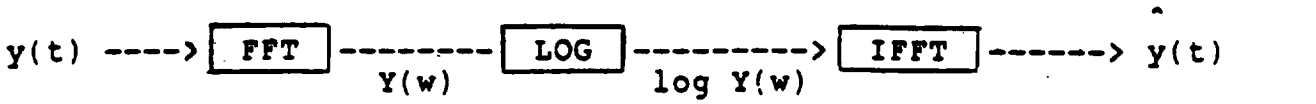

$x(t) * h(t) \Longrightarrow X(w)\,H(w) \Longrightarrow \log[X(w)] + \log[H(w)] \Longrightarrow \hat{x}(t) + \hat{h}(t)$

Convolution Multiplication Addition Addition

====> in quefrency domain: linear filtering

NOTE: X(w) is complex ===> phase unwrape of X(W) ===> log[X(w)]

. Deconvolution:

Given: $y(t) = x(t) * h(t)$

Wish to recover $x(t)$ and $h(t)$ from $y(t)$

- if X(w) is low frequency (smooth) ====> $\hat{x}(t)$ is low-time

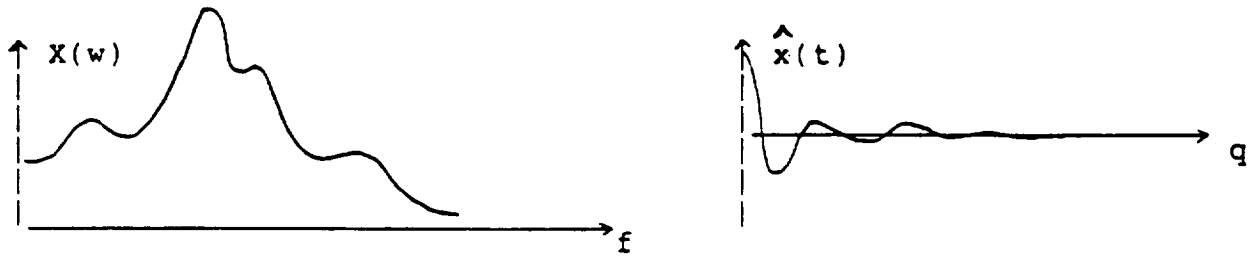

- if H(w) is high frequency (fluctuating) ====> $\hat{h}(t)$ is high-time

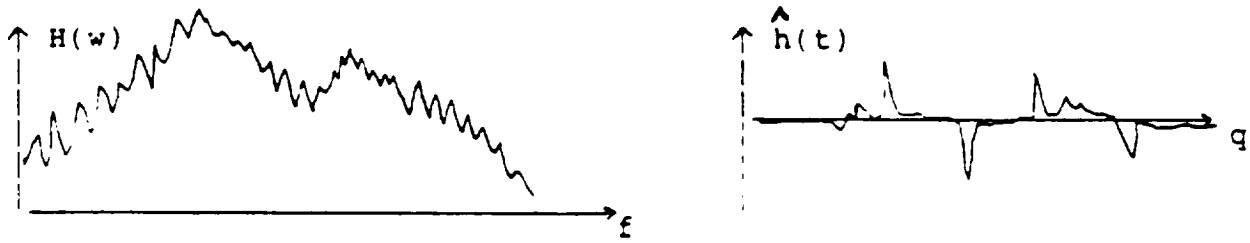

- since $\hat{y}(t) = \hat{x}(t) + \hat{h}(t)$

====> { low-time filter: $\hat{x}(t)$; high-time filter: $\hat{h}(t)$ } ===> [INVERSE CEPSTRUM TRANSFORM] ===> $x(t)$, $h(t)$

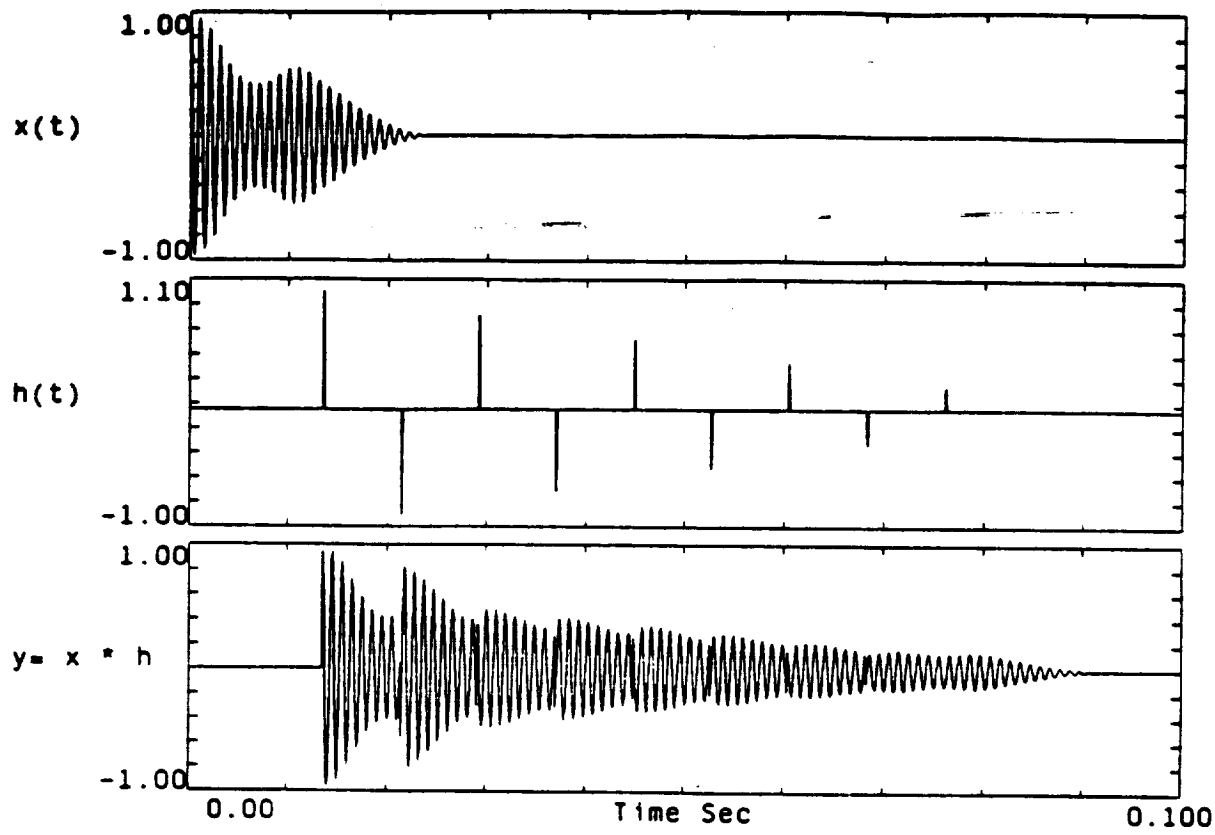

simulation for cepstrum analysis
x(t)=raw signal h(t)= I.R.F. y(t)= x(t)*h(t) with echo

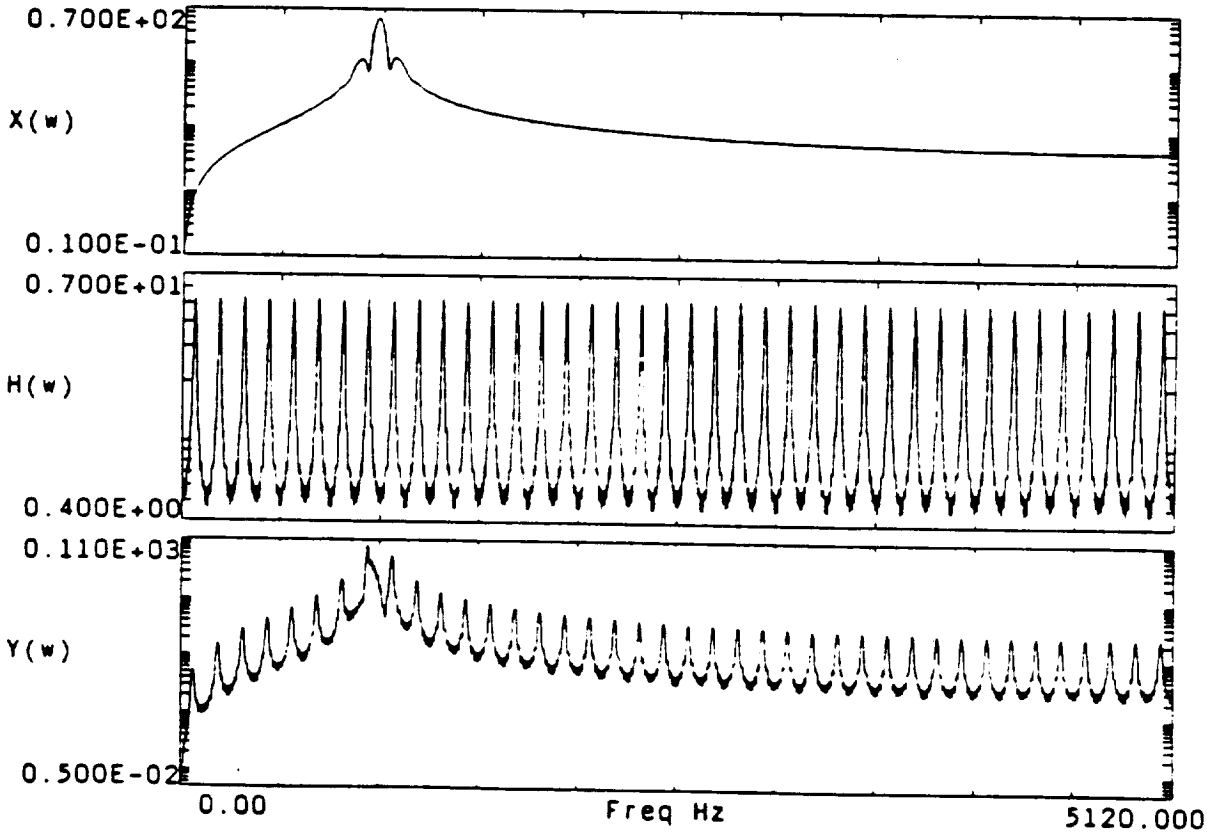

log FFT of x(t), h(t), y(t)
Y(W) = X(w) H(W)

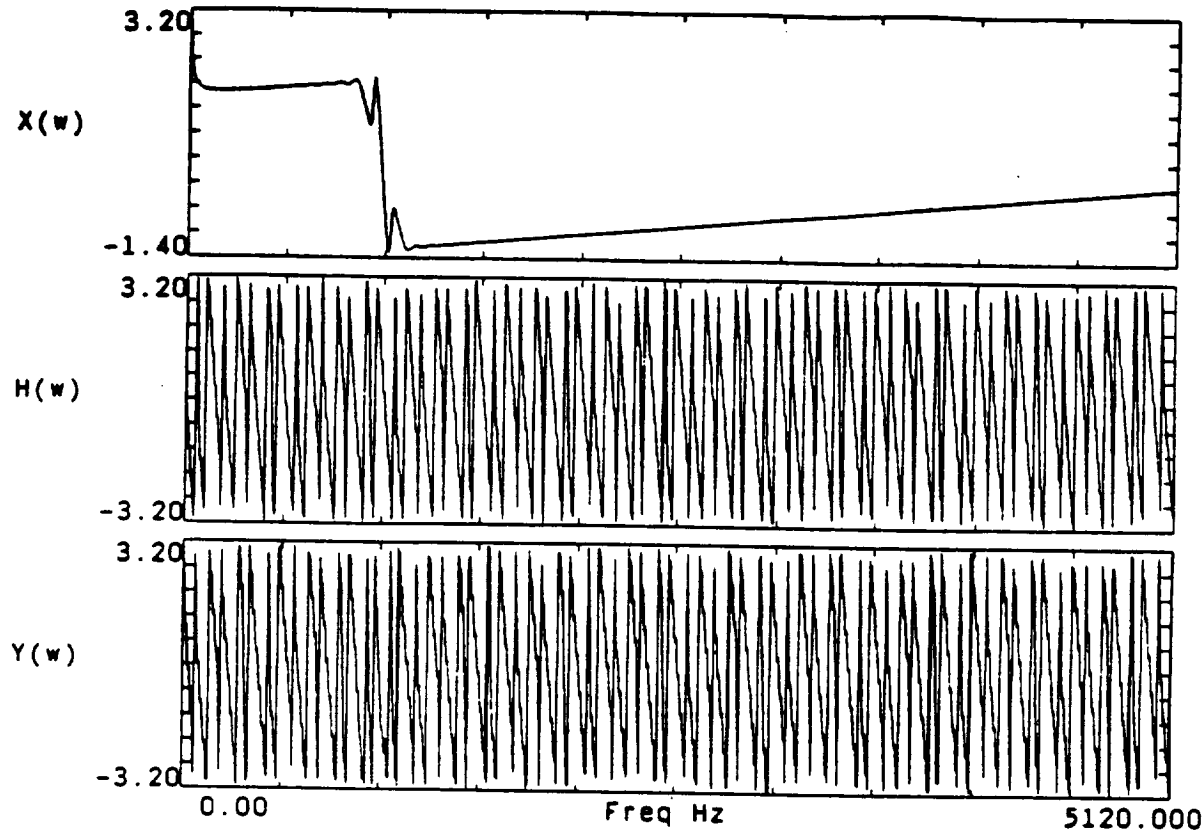

PRINCIPLE VALUE OF PHASE OF X(w) H(w), Y(w)

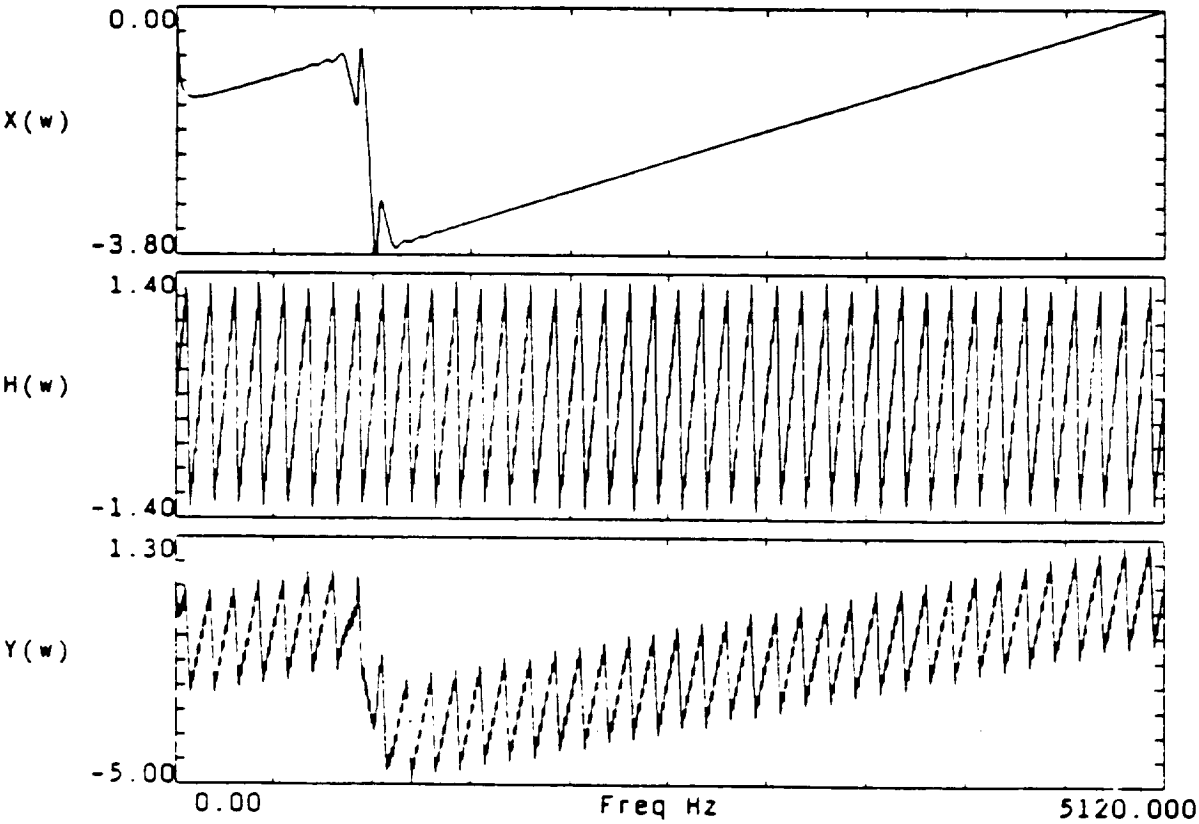

UNWRAPED PHASE OF X(W), H(W), Y(W)

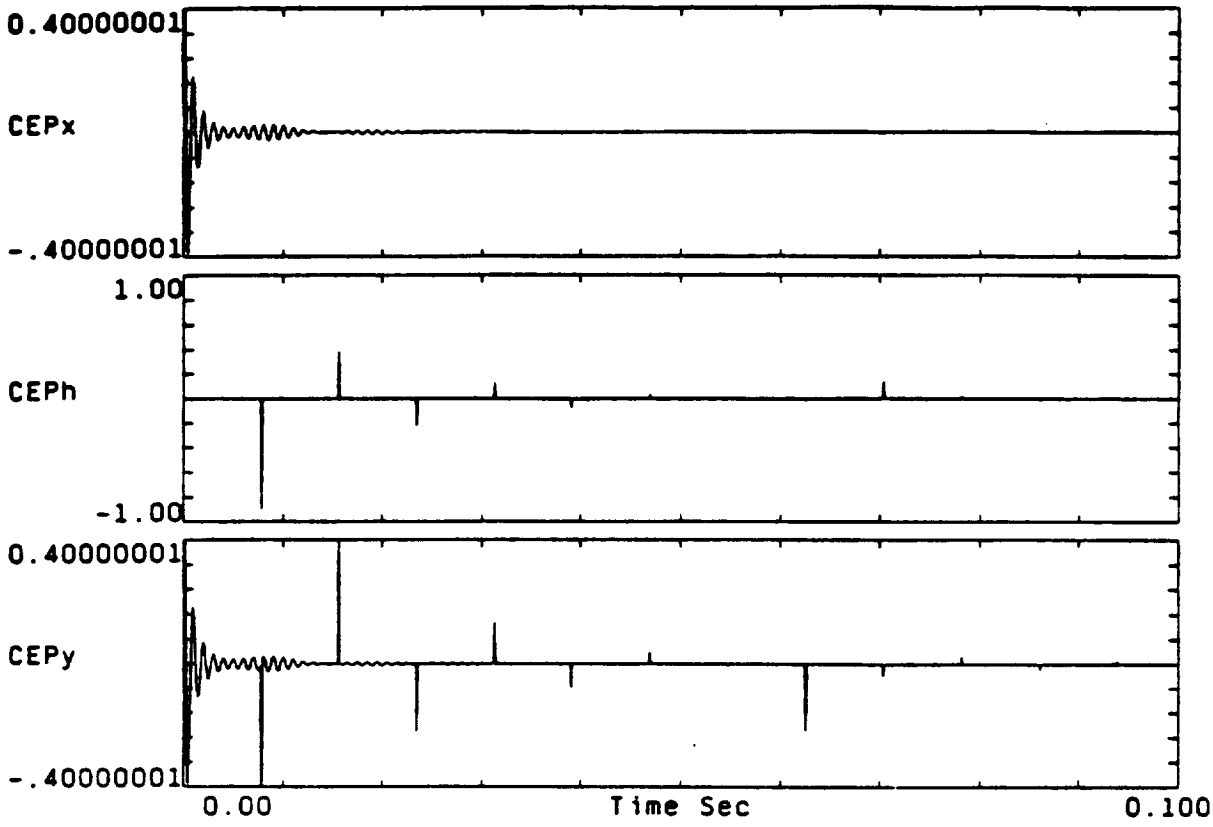

COMPLEX CEPSTRUM OF x(t), h(t), y(t)
CEPy = CEPx + CEPh

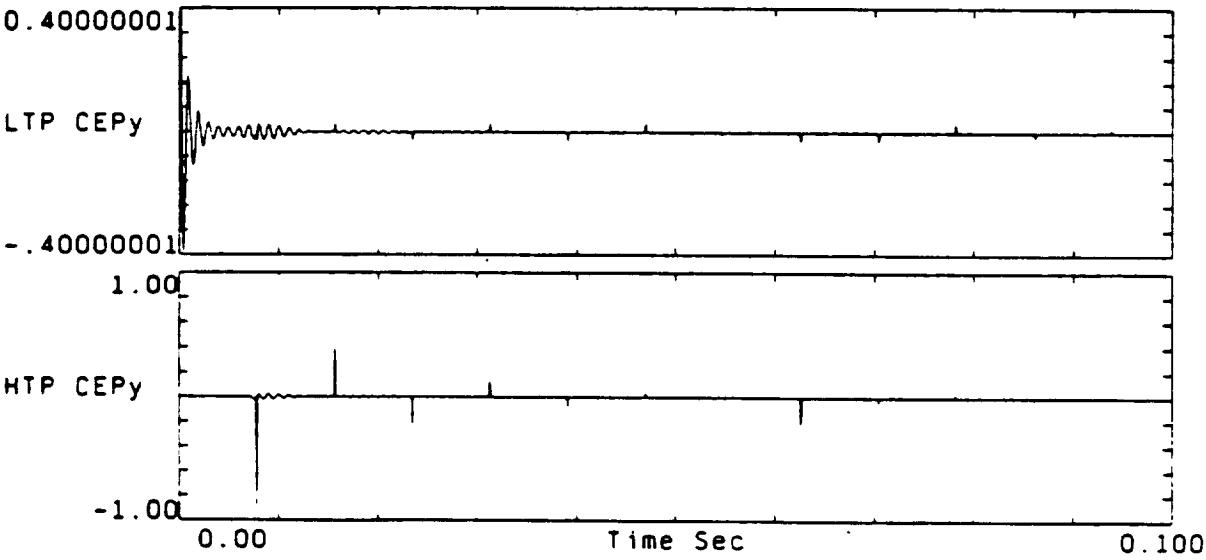

(1) LOW-TIME PASS CEPy
(2) HIGH-TIME PASS CEPy

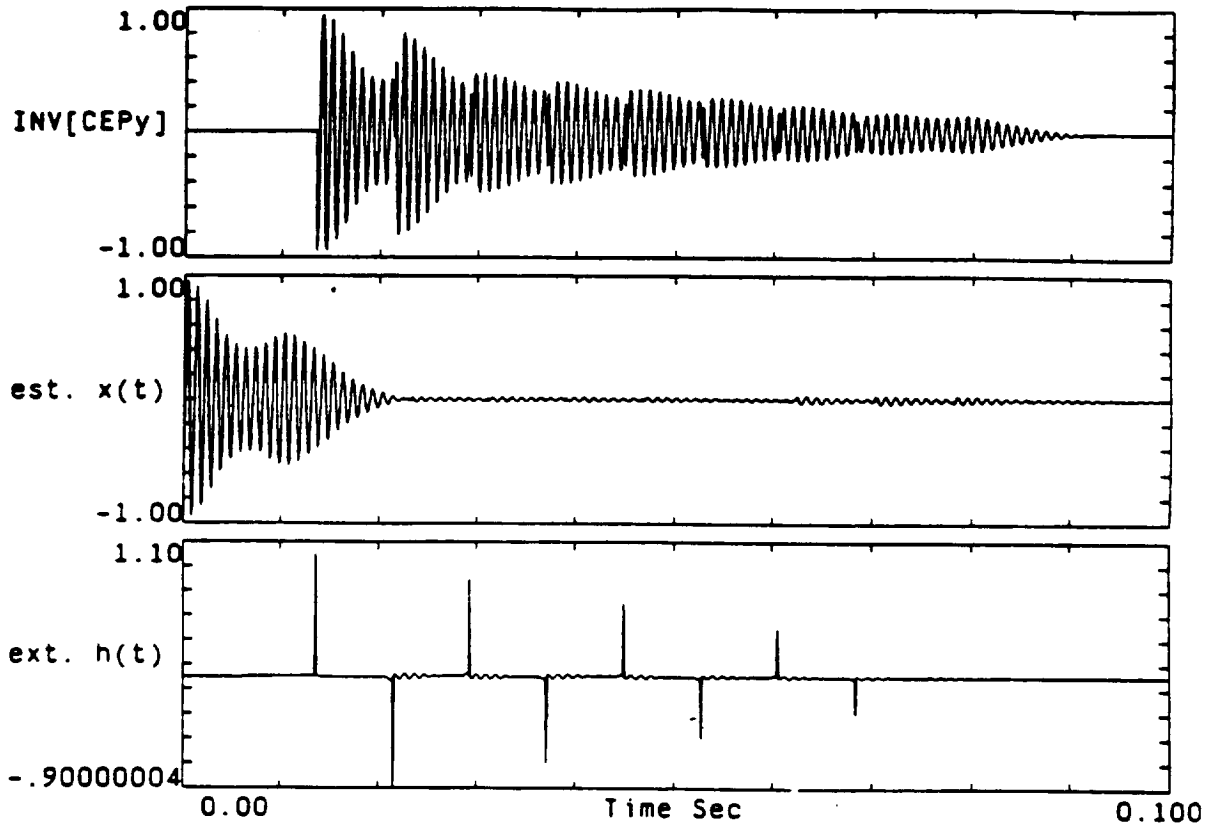

INVERSE TRANSFORM OF CEPSTRUM:
(1) CEPy (2) LOW-TIME PASS CEPy (3) HIGH-TIME PASS CEPy

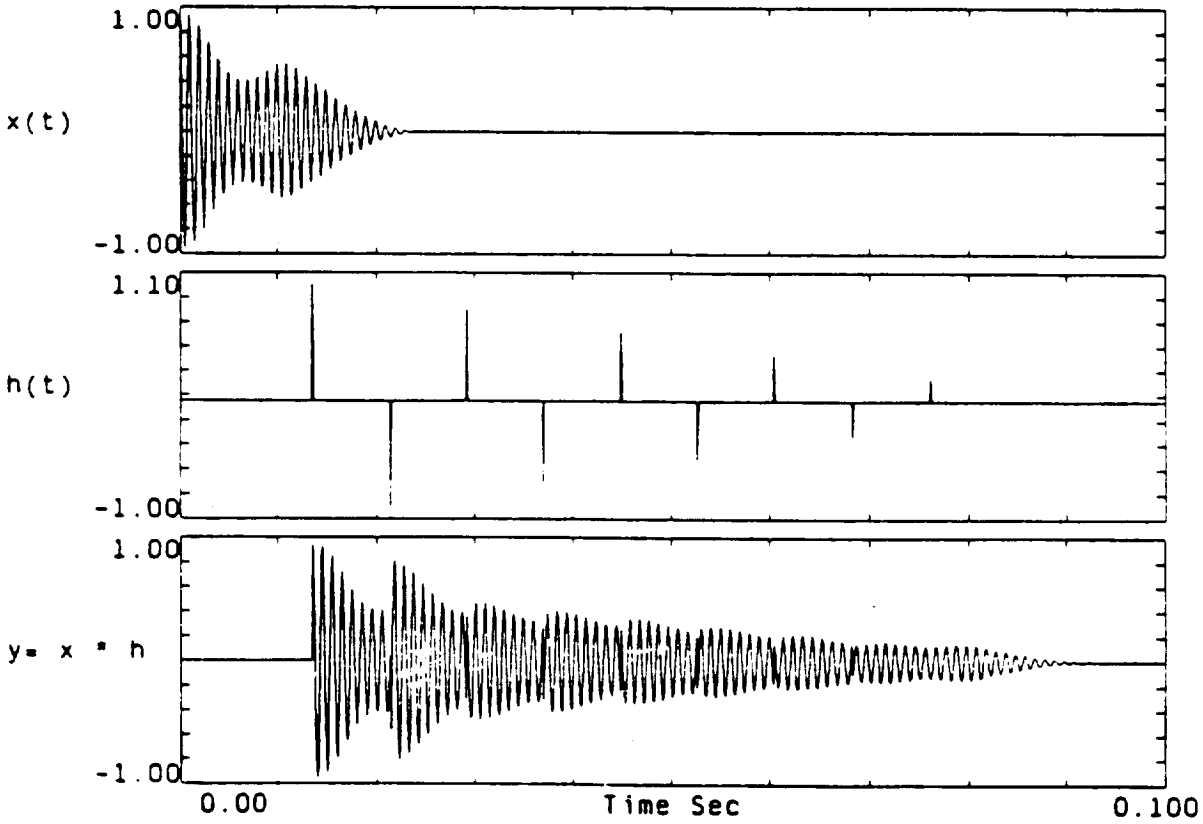

simulation for cepstrum analysis
x(t)=raw signal h(t)= I.R.F. y(t)= x(t)*h(t) with echo

ROTARY SPECTRUM ANALYSIS (C.N. Mooers)

. Linear Cross Spectrum/Coherence:

- To describe certain common or joint linear properties between two different random processes.

===> Sxx(w), Syy(w), Sxy(w), Qxy(w)

. Linear Rotary Spectrum/Coherence:

- To describe certain common or joint linear properties between two different random vectors.

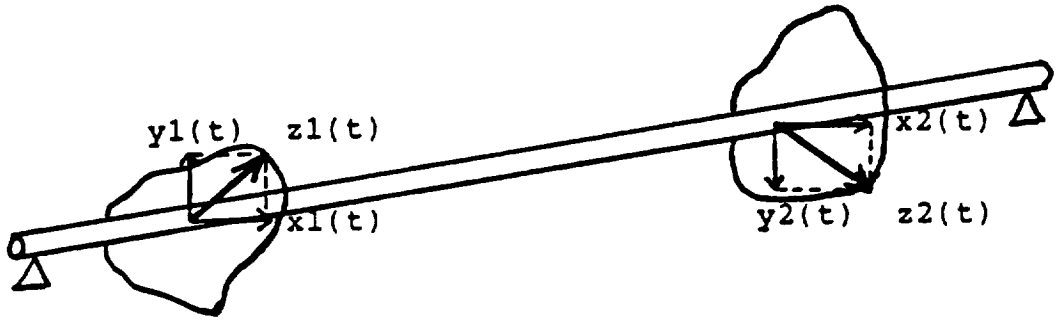

===> Complex Random Vectors $\begin{cases} z1(t) = x1(t) + j\ y1(t) \\ z2(t) = x2(t) + j\ y2(t) \end{cases}$

- At each frequency, each random vector can be decomposed into two rotational circular motions, each with its own amplitude and phase. The counterclockwise (CCW) components correspond to motions at positive frequencies, and the clockwise (CW) components correspond to motions at negative frequencies.

ROTARY AUTO-SPECTRUM

- At frequency w_o, random vector $z(t) = x(t) + j\,y(t)$ represents an elliptic motion:

$$z(t) = X\cos(w_o t + Px) + j\,Y\cos(w_o t + Py)$$

$$\Downarrow \text{ Trigonometric Identity}$$

$$z(t) = [A\cos(w_o t + Pa) + B\cos(w_o t + Pb)] + j\,[A\sin(w_o t + Pa) - B\sin(w_o t + Pb)]$$

$$\Downarrow \text{ Polar Format}$$

$$z(t) = A\,e^{+j[w_o t + Pa]} + B\,e^{-j[w_o t + Pb]}$$

C.C.W Component — C.W component

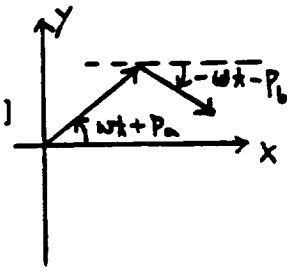

$$\Downarrow \text{ Fourier Transform}$$

$$Z(w) = [A\exp(j\,Pa)]\,\delta(w-w_o) + [B\exp(-j\,Pb)]\,\delta(w+w_o)$$

C.C.W Component at $w=+w_o$ — C.W component at $w=-w_o$

- At each frequency w, the elliptical motion is decomposed into two C.C.W. and C.W. circular motions.

{ CCW Motion: Frequency = $+w_o$ Amplitude = A Phase = Pa
{ CW Motion: Frequency = $-w_o$ Amplitude = B Phase = Pb

- Inner Auto-Spectrum $S(w) = E[\,Z(w)\,\,Z(w)^*\,]$

  ==> S(w) measures the power distribution of the C.W. and C.C.W. components at each frequency.

- Outer Auto-Spectrum $T(w) = E[\,Z(-w)\,\,Z(w)\,]$

  ==> T(w) measures the amount of correlated power between the C.W. and C.C.W. components at each frequency.

- Outer Auto-Coherence $t(w) = E[\,Z(-w)\,Z(w)\,]/[S(-w)\,S(w)]$

  ==> t(w) measures the coherence between the C.W. and C.C.W. component s at each frequency. It indicates the degree of stability of the elliptical motion.

ROTARY CROSS-SPECTRUM

- At frequency w_o, z1(t) & z2(t) represent two elliptical motions

$$\begin{cases} z1(t) = A1\, e^{+j[\, w_o t + Pa1\,]} + B1\, e^{-j[\, w_o t + Pb1\,]} \\ z2(t) = A2\, e^{+j[\, w_o t + Pa2\,]} + B2\, e^{-j[\, w_o t + Pb2\,]} \end{cases}$$

$$\begin{cases} Z1(w) = [\, A1 \exp(\, j\, Pa1)\,] \delta(w-w_o) + [\, B1 \exp(-j\, Pb1)\,] \delta(w+w_o) \\ Z2(w) = [\, A2 \exp(\, j\, Pa2)\,] \delta(w-w_o) + [\, B2 \exp(-j\, Pb2)\,] \delta(w+w_o) \end{cases}$$

- Inner Cross-Spectrum $S12(w) = E[\, Z1(w)\ \ Z2^*(w)\,]$

  ==> S12(w) measures the amount of correlated power between z1(t) and z2(t) at the same direction (both CW and CCW)

- Inner Cross-Coherence $r12(w) = S12(w)/[S11(w)\ S22(w)]$

  ==> r12(w) measures the coherence between z1(t) and z2(t) at the same direction (both CW and CCW)

z1(t)		z2(t)
CW	<====>	CW
CCW	<====>	CCW

- Outer Cross-Spectrum $T12(w) = E[\, Z1(-w)\ \ Z2(w)\,]$

  ==> T12(w) measures the amount of correlated power between z1(t) and z2(t) at the opposite direction (CW/CCW , CCW/CW)

- Outer Cross-Coherence $q12(w) = T12(w)/[S11(-w)\ S22(w)]$

  ==> q12(w) measures the coherence between z1(t) and z2(t) at the opposite direction (CW/CCW , CCW/CW)

z1(t)		z2(t)
CW	<====>	CCW
CCW	<====>	CW

SIMULATION EXAMPLE FOR ROTARY SPECTRUM

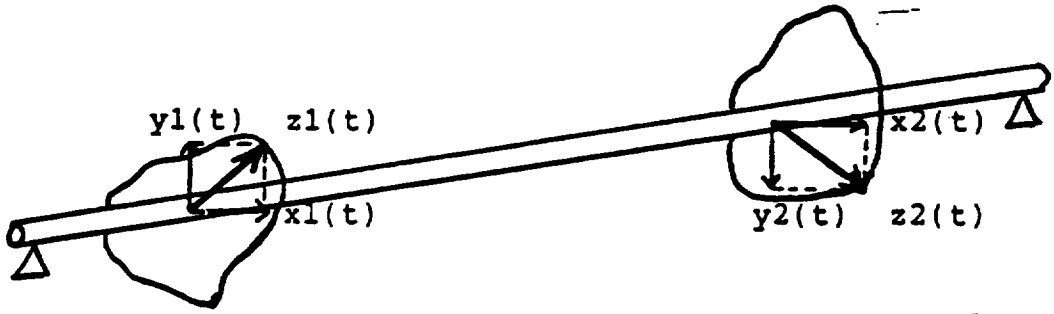

- Let z1(t) and z2(t) represent the vibration response random vectors near each end of a rotating shaft. If a bending mode of the shaft at natural frequency 1000 Hz is excited to generate a C.C.W. rotational motion. Assuming that, at this same frequency, forces from some other independent sources at each end of the shaft also generate a C.W. rotational motion.

	CORRELATED CCW MOTION	INDEPENDENT CW MOTION
$z1(t) =$	$A1\, e^{+j[\, w\, t + Pa1(t)\,]}$	$+ B1\, e^{-j[\, w\, t + Pb1(t)\,]}$
$z2(t) =$	$A2\, e^{+j[\, w\, t + Pa2(t)\,]}$	$+ B2\, e^{-j[\, w\, t + Pb2(t)\,]}$

where: $A1 = A2 = 1$ $\quad B1 = B2 = 10$ $\quad w = 1000$ Hz

$Pa2(t) = Pa1(t)$ + constant phase lag

$Pa1(t)$, $Pb1(t)$, and $Pb2(t)$ are independent random drifting phases.

==> wish to identify the correlation of the CCW motion between z1(t) and z2(t).

- Since the amplitude of the independent CW motion is 10 times larger then the amplitude of the correlated CCW motion. Therefore, the linear cross-coherence: Qx1x2(w), Qy1y2(w), Qx1y2(w), Qx2y1(w) would not be able to identify the correlation of the CCW motion between z1(t) and z2(t).

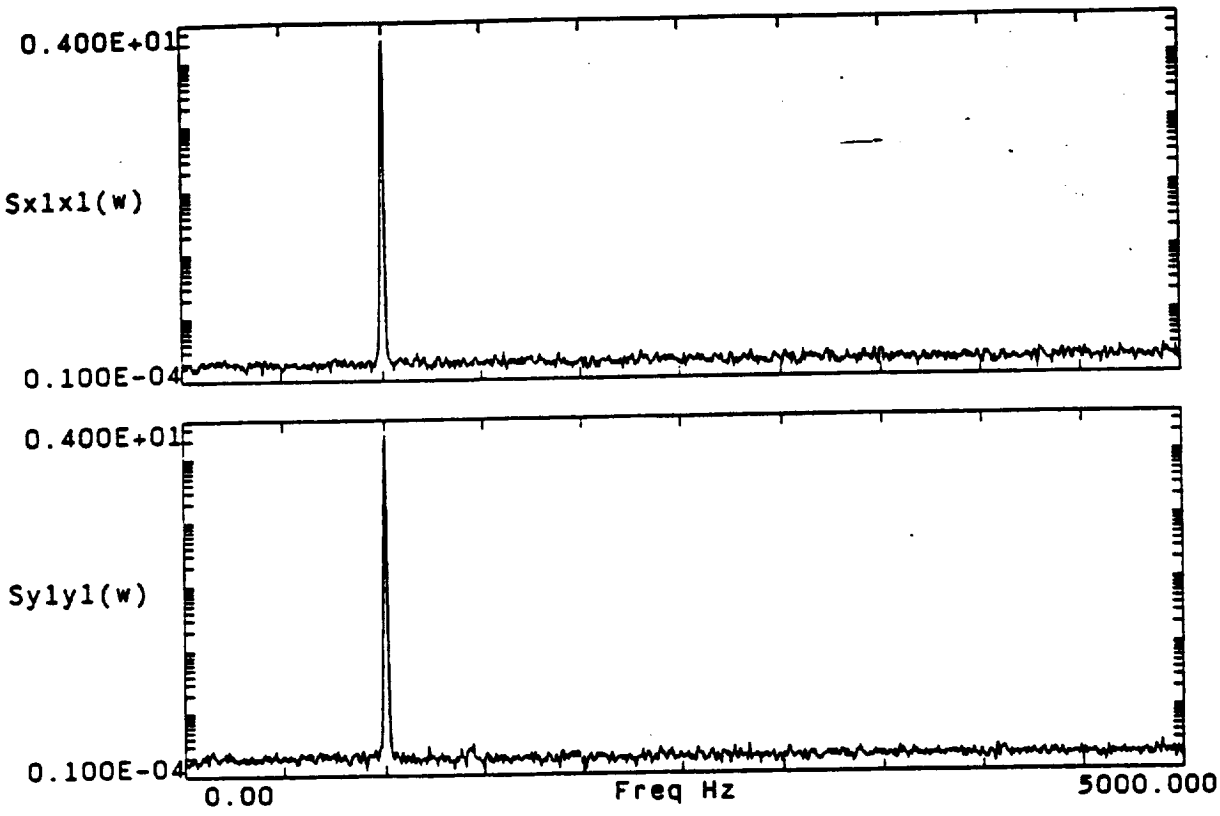

PSD of x1(t), y1(t) z1(t) = x1(t) + j y1(t)

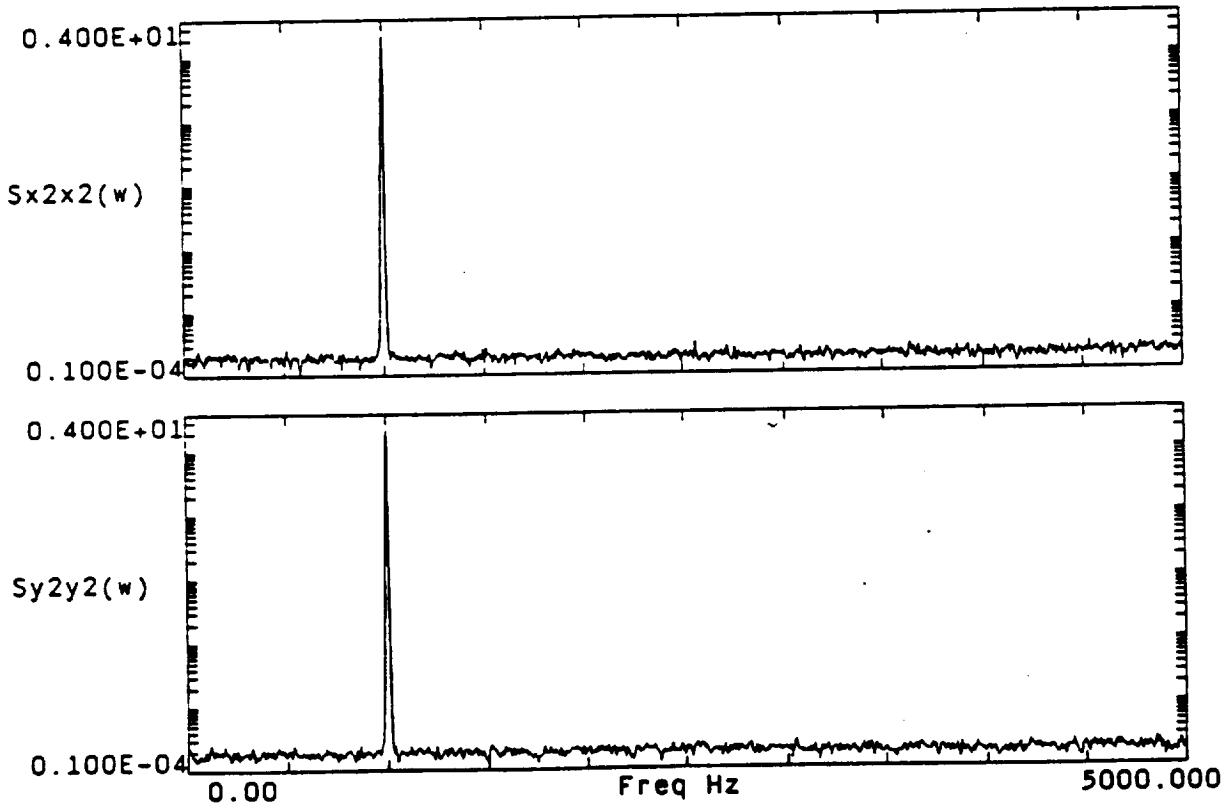

PSD of x2(t), y2(t) z2(t) = x2(t) + j y2(t)

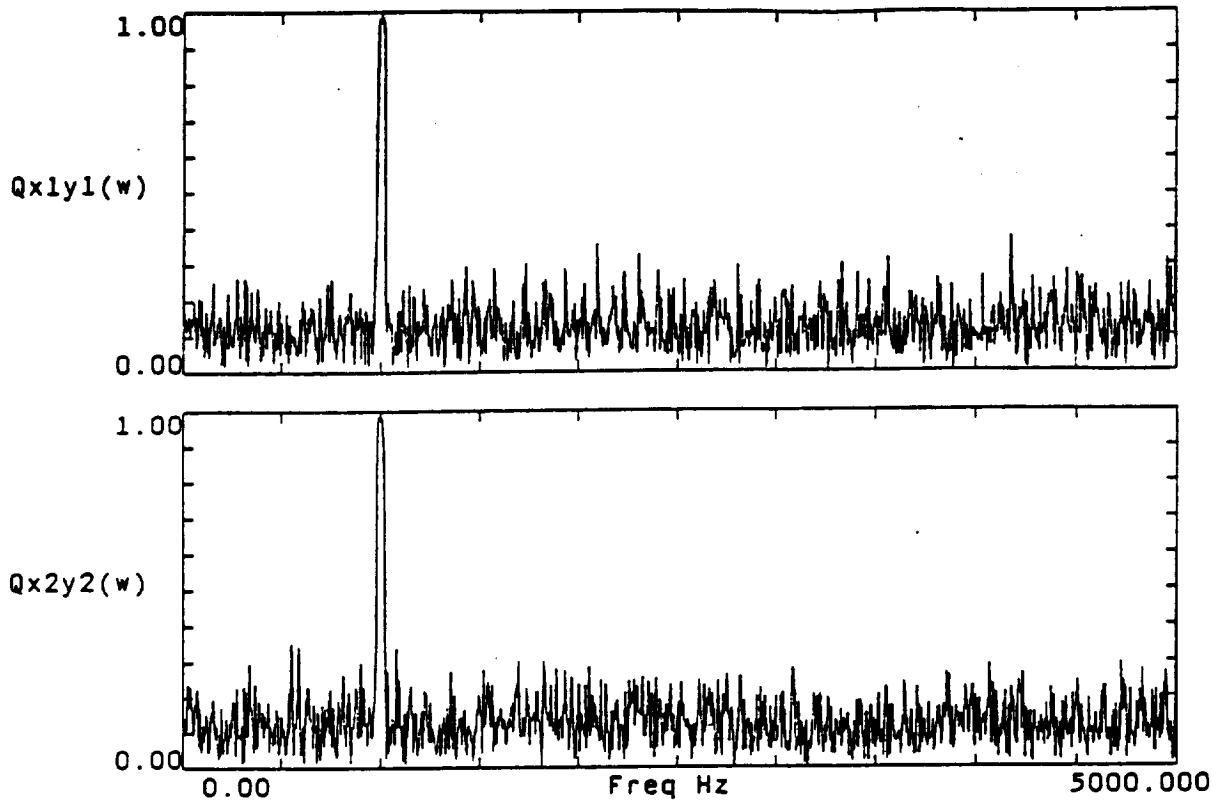

Linear Cross-Coherence for (x1,y1) (x2,y2)

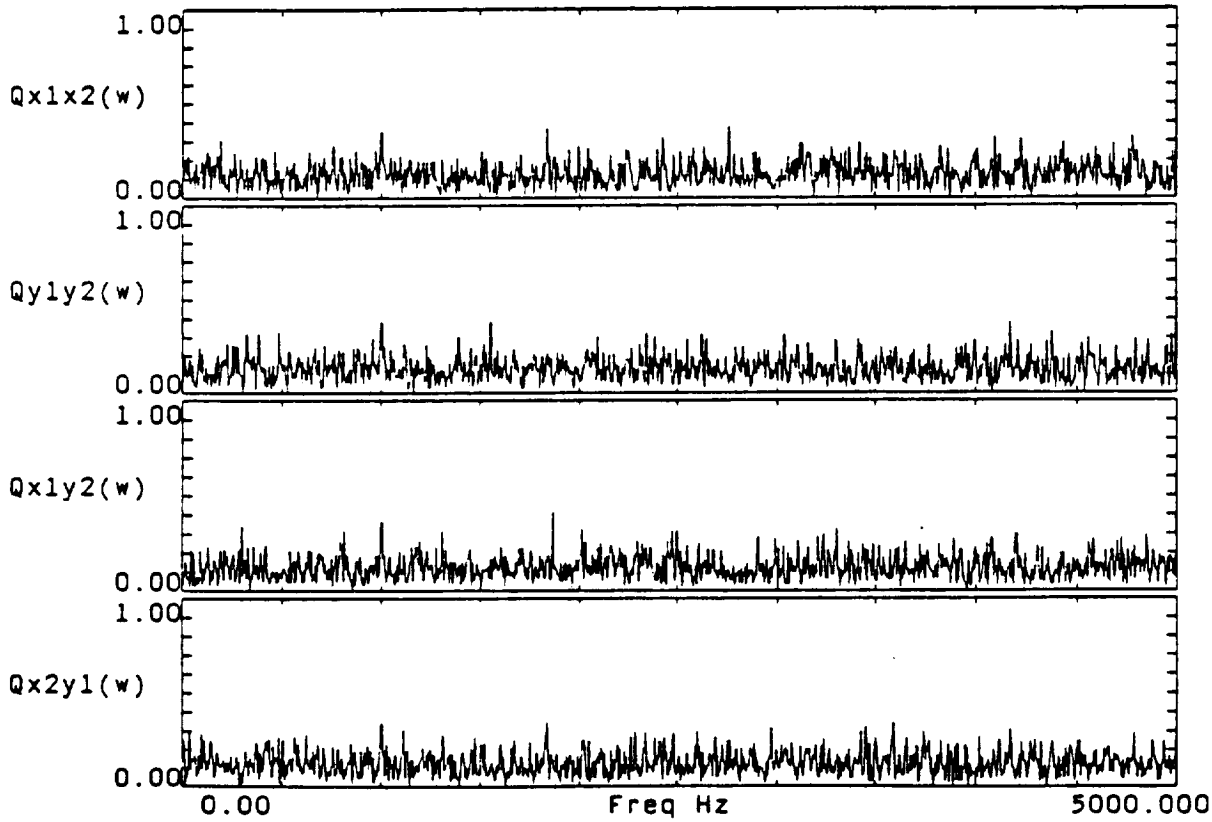

Linear Cross-Coherence for (x1,x2) (y1,y2) (x1,y2) (x2,y1)

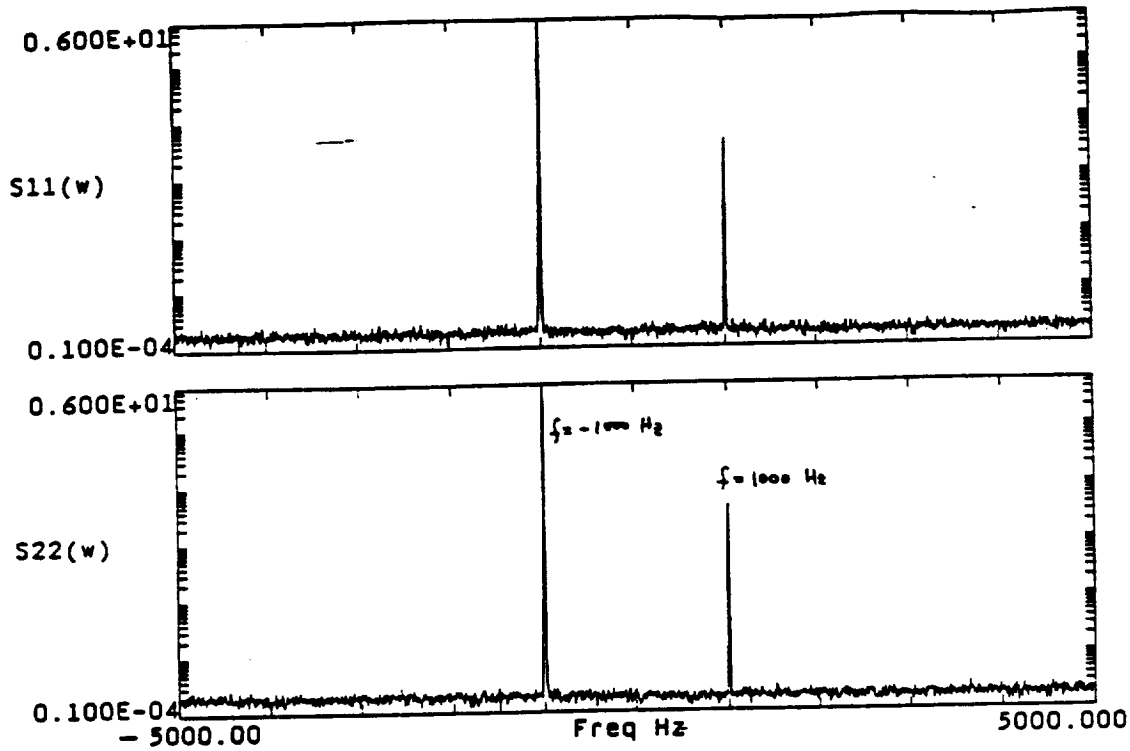

(1) S11(w) = Inner Auot-Rotary-Spectrum for Z1(t)
(2) S22(w) = Inner Auot-Rotary-Spectrum for Z2(t)

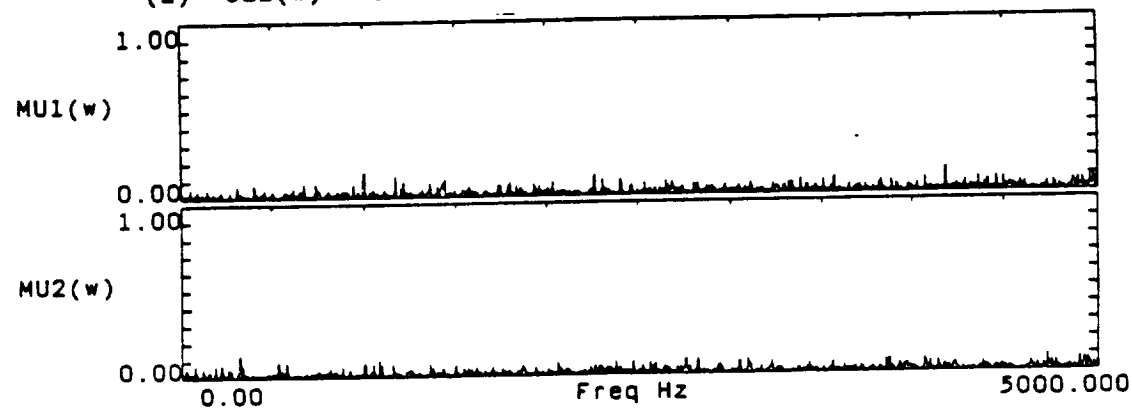

(1) MU1(w) = Stability of Ellipse for Z1(t)
(2) MU2(w) = Stability of Ellipse for Z2(t)

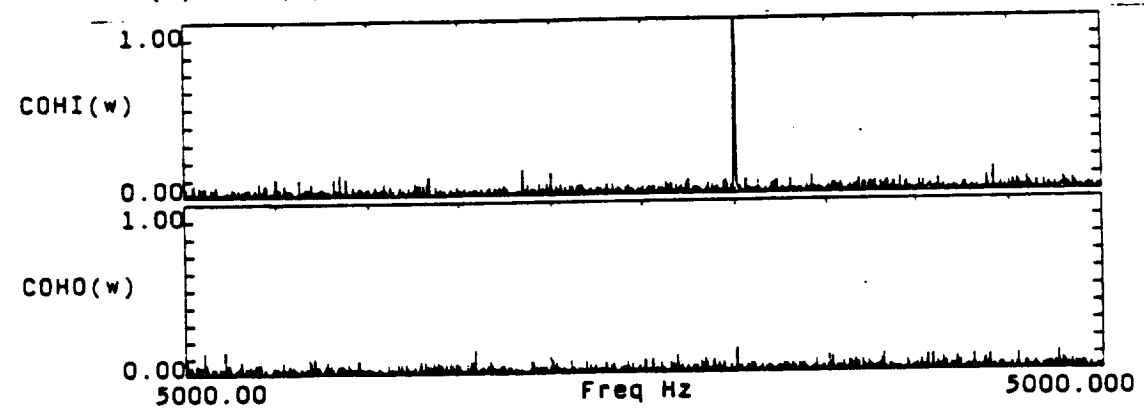

(1) COHI(W) = Inner-Cross-Coherence Between Z1(t) & Z2(t)
(2) COHO(W) = Outer-Cross-Coherence Between Z1(t) & Z2(t)

FREQUENCY WAVENUMBER SPECTRUM

. Single channel signal:

time domain <===> frequency domain

$y(t) = A \cos(wt+p)$ <===> $Y(w) = A \exp[\, jp \,]$

. Array signal:

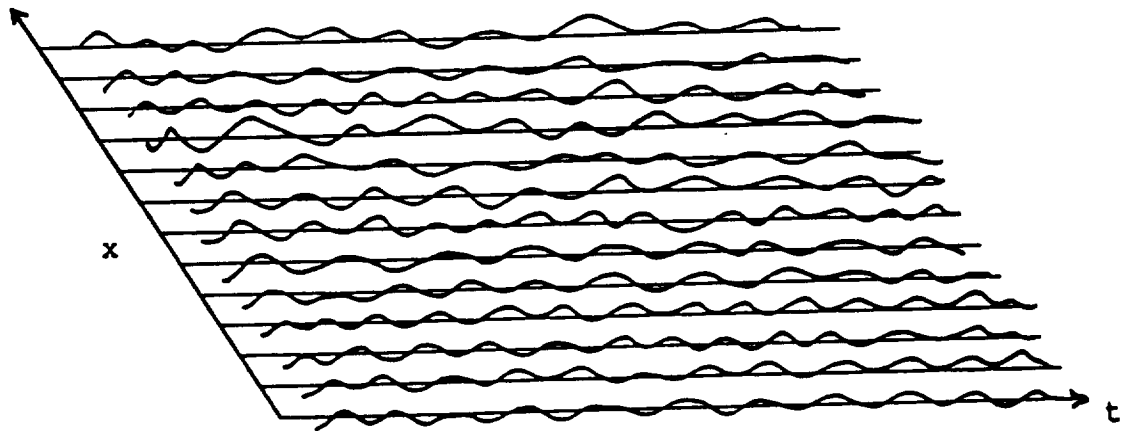

time domain <===> frequency domain

spatial domain <===> wavenumber domain

$y(t,x) = A \cos(wt+kx+p)$ <===> $Y(w,k) = A \exp[\, jp \,]$

. Conventional Methods:

- Two Dimensional FFT (Periodogram):
- Blackman/Turkey (cross-correlation) :

. Parametric Methods:

- MEM (Auto-Regressive) Model:
- LMS & MLM Adaptive array processing Algorithm:

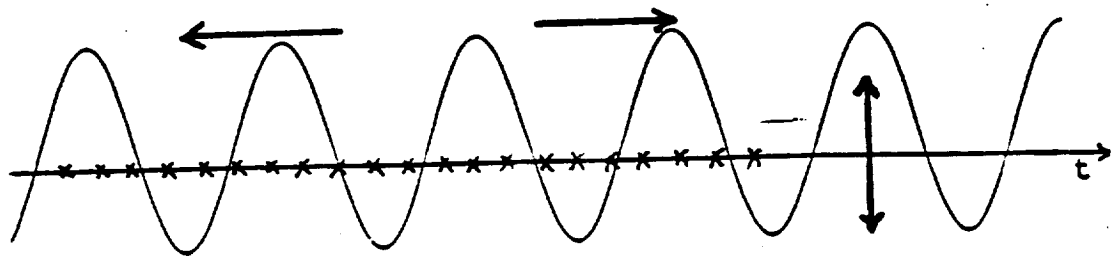

- Leftward Traveling wave:

$$y(t,x) = A \cos(\omega_o t + k_o x + p)$$

==> Positive Wavenumber

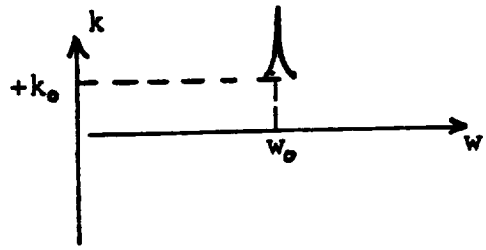

- Rightward Traveling wave:

$$y(t,x) = A \cos(\omega_o t - k_o x + p)$$

==> Negative Wavenumber

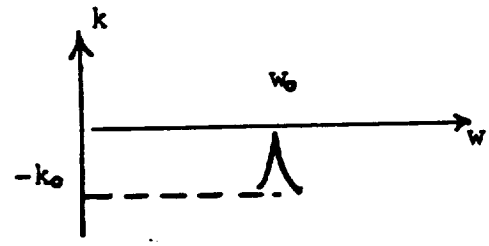

- Standing wave:

$$y(t,x) = A \cos(\omega_o t + k_o x + p) + A \cos(\omega_o t - k_o x + p)$$

$$= 2A \cos(k_o x) \cos(\omega_o t + p)$$

==> Positive & Negative Wavenumber

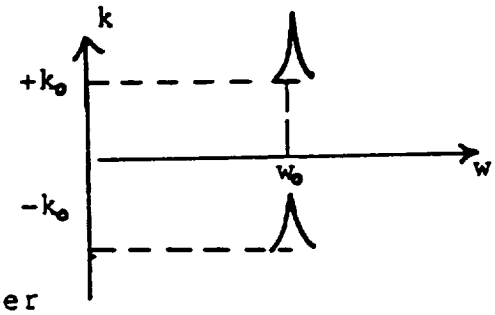

SIMULATION EXAMPLE:

$$y(t,x_j) = \sum_{w,k} A \cos(w t + k x_j + p) \qquad j=1,2,3\ldots,64$$

Freq(Hz)	100	200	300	400	500	600	700	800
Wave#	+0.25	-0.4	+0.15	.0.0	+0.15	+0.1	+0.16	-0.27
Wave#					-0.4	-0.35	+0.36	0.
Wave#								+0.12
Wave#								+0.35

{Array size = 64 sensors
{Time sample = 512 points

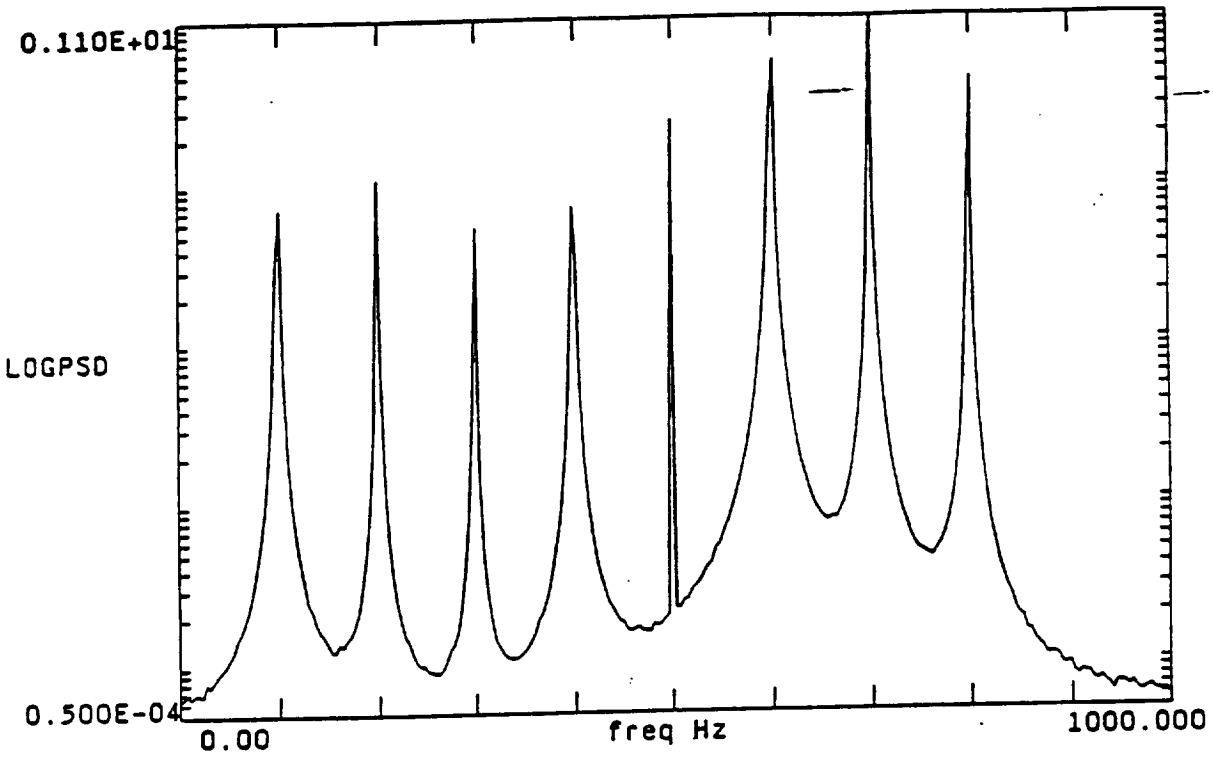

AVERAGEd PSD ACROSS 64 SENSORS

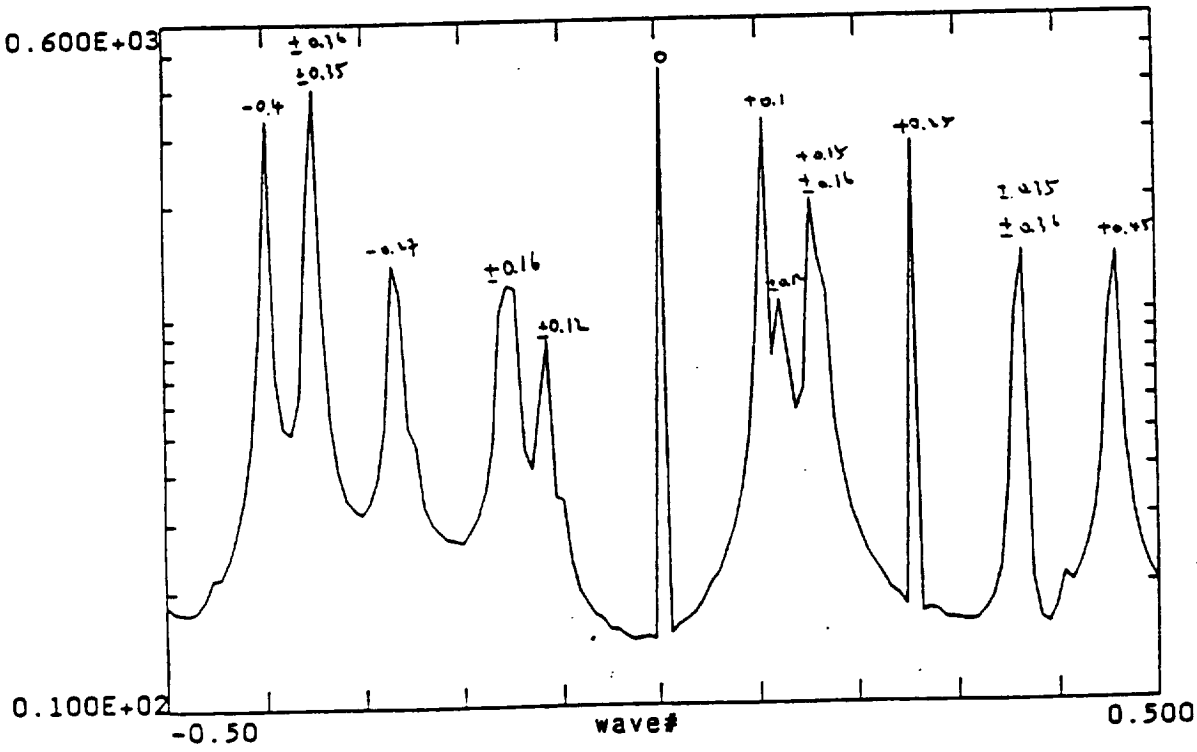

AVERAGEd WAVE#-SPECTRUM ACROSS ALL FREQUENCY

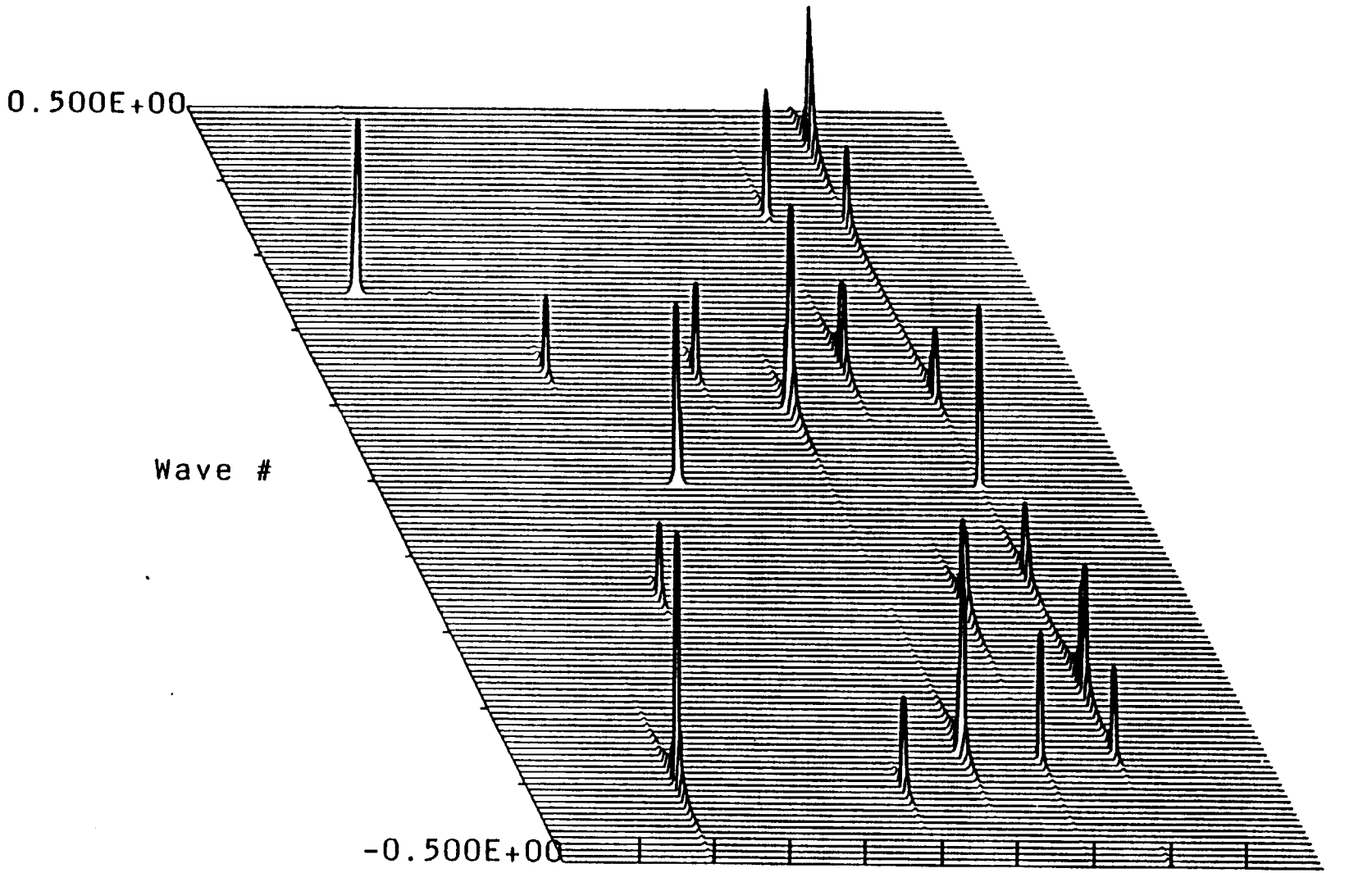

FREQ(HZ)	100.	200.	300.	400.	500.	600.	700.	800.
WAVE#	+.25	-0.4	+-0.15	0	+0.15	+0.1	+-0.16	-0.27
WAVE#					-0.4	-0.35	+-0.36	+0.45
WAVE#								0.
WAVE#								+-0.12
WAVE#								+-0.35

PHASE DOMAIN AVERAGE (PDA) COHERENCE

— Define The Degree of Discreteness of A Spectral Component Quantitatively

— Traditional Method: PDF of Bandpass Signal

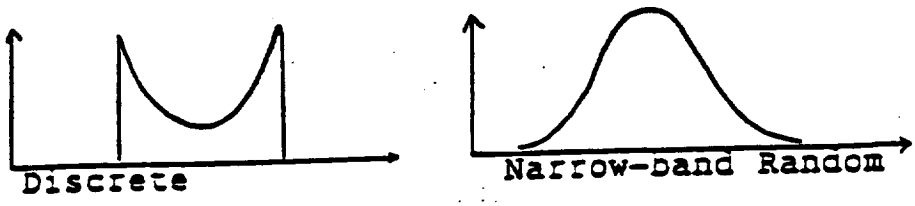

— PDA-Coherence: Quantitatively
Noise
Amplitude Variation

— PDA Track the Phase Drifting From a Reference Sine Wave

(1) Discrete

$\cos[\ \underline{Wt+p}\ ]$

(2) Discrete+Noise

$\cos[\ \underline{Wt+p}\ ]+N(T)$

(3) Narrow-Band Random

$\cos[\ \underline{W(t)t+p}\ ]$

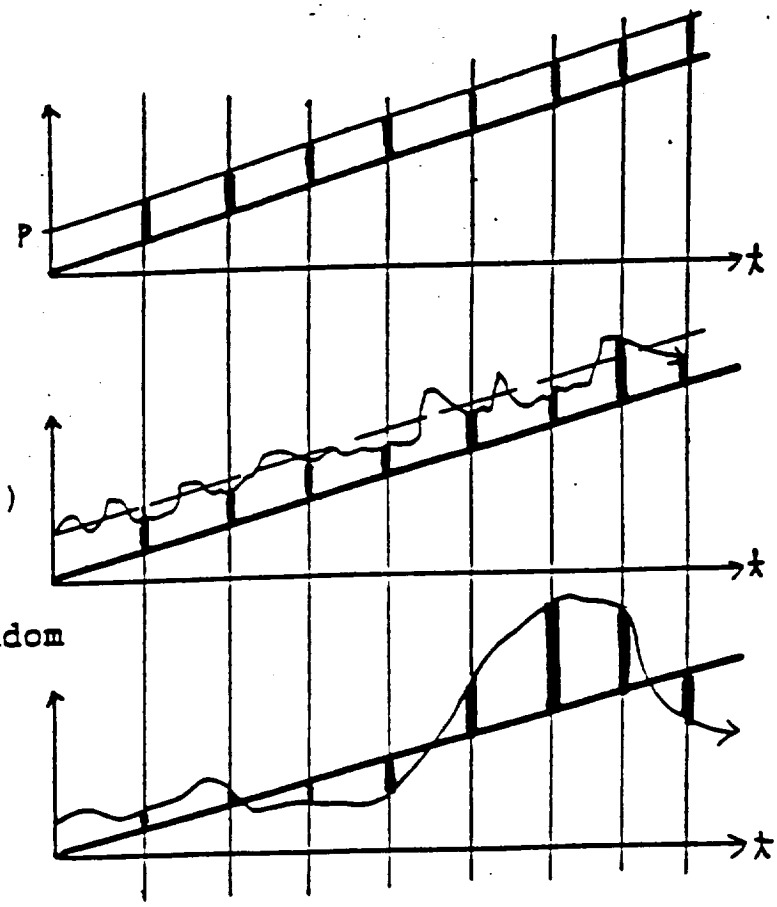

— $PDA(w) = E\ [\ P(w) - WT\ ]$

Where $P(w)$ = time Realigned Phase from $X(W)$
WT = Phase of Reference Sine Wave at time T

CHIRP-Z TRANSFORM

. Z-Transform (ZT):

$$X(z) = \sum x(n)\, z^{-n}$$

- z is a complex variable.
- X(z) is a continuous function in z-plane

. Fourier Transform (FT): evaluate ZT X(z) on the unit circle.

$$X(w) = \sum x(n) \left[e^{jw} \right]^{-n}$$

- $z = \exp(jw)$ $w=0$ to 2π ===> Unit Circle (U.C.)
- X(w) is a continuous function on the U.C. in z-plane

. Discrete Fourier Transform (DFT): evaluate FT X(w) at N equally spaced points on the U.C.

$$X(k) = \sum x(n) \left[e^{j\,2\pi k/N} \right]^{-n}$$

- $z = \exp(j\,2\pi k/N)$ $k=0,N$ ===> Frequency Interval = $2\pi/N$
- X(k) is a discrete function on the U.C. in z-plane

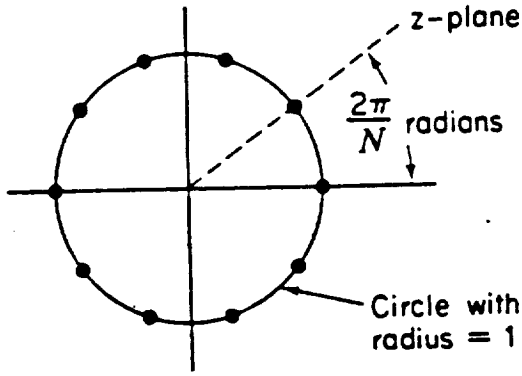

. Fast Fourier Transform (FFT): An efficient algorithm to compute DFT X(k)

. Wish to evaluate Z-Transform over a small portion on the unit circle (U.C.) with much larger # of sampling points

to evaluate Z-Transform on some other contour rather than the U.C.

====> Chirp-Z Transform (CZT)

. CZT evaluates Z-Transform over a portion on a spiral contour

$$X(k) = x(n)\left[A_0 e^{j\theta_0} W_0^{-k} e^{jk\phi_0}\right]^{-n} \qquad k=0,1,\ldots,M-1$$

A_0 and θ_0 are the starting amplitude and phase of the contour

ϕ_0 is the angular spacing sampled on the contour

W_0 controls the rate at which the contour spirals

$\begin{cases} W_0 > 1 & \Longrightarrow \text{ contour spirals inward} \\ W_0 < 1 & \Longrightarrow \text{ contour spirals outward} \end{cases}$

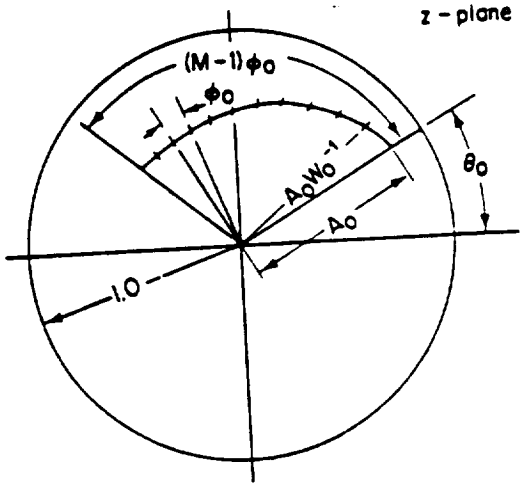

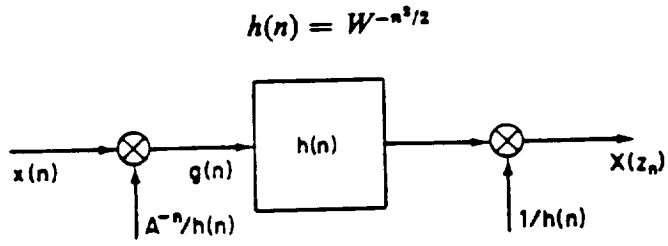

Fig. 6.32 Interpretation of Eq. (6.41) in terms of a linear system.

- Evaluation of CZT By Using FFT Algorithm

$$W = W_0 e^{-j\phi_0}$$

$$A = A_0 e^{j\theta_0}$$

CZT: $X(z_k) = \sum_{n=0}^{N-1} x(n) A^{-n} W^{nk}, \qquad k = 0, 1, \ldots, M-1$

Using the identity: $nk = \frac{1}{2}[n^2 + k^2 - (k-n)^2]$

$$X(z_k) = \sum_{n=0}^{N-1} x(n) A^{-n} W^{n^2/2} W^{k^2/2} W^{-(k-n)^2/2}$$

$$X(z_k) = W^{k^2/2} \sum_{n=0}^{N-1} x(n) A^{-n} W^{n^2/2} W^{-(k-n)^2/2}$$

$$g(n) = x(n) A^{-n} W^{n^2/2}$$

$$X(z_k) = W^{k^2/2} \sum_{n=0}^{N-1} g(n) W^{-(k-n)^2/2}, \qquad k = 0, 1, \ldots, M-1$$

⇧

Convolution between $g(n)$ and $h(n) = W^{-n^2/2}$

=====> FFT Algorithm can be used to perform the convolution

EXAMPLE FOR CHIRP-Z TRANSFORM

A synthetic speech signal was generated by exciting a five-pole system with a periodic impulse train.

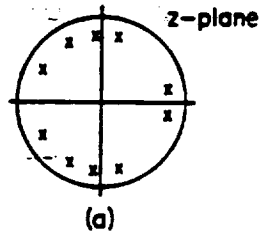

SPIRAL OUTWARD

SPIRAL OUTWARD

ON THE UNIT CIRCLE
(SAME AS FFT)

SPIRAL INWARD

SPIRAL INWARD

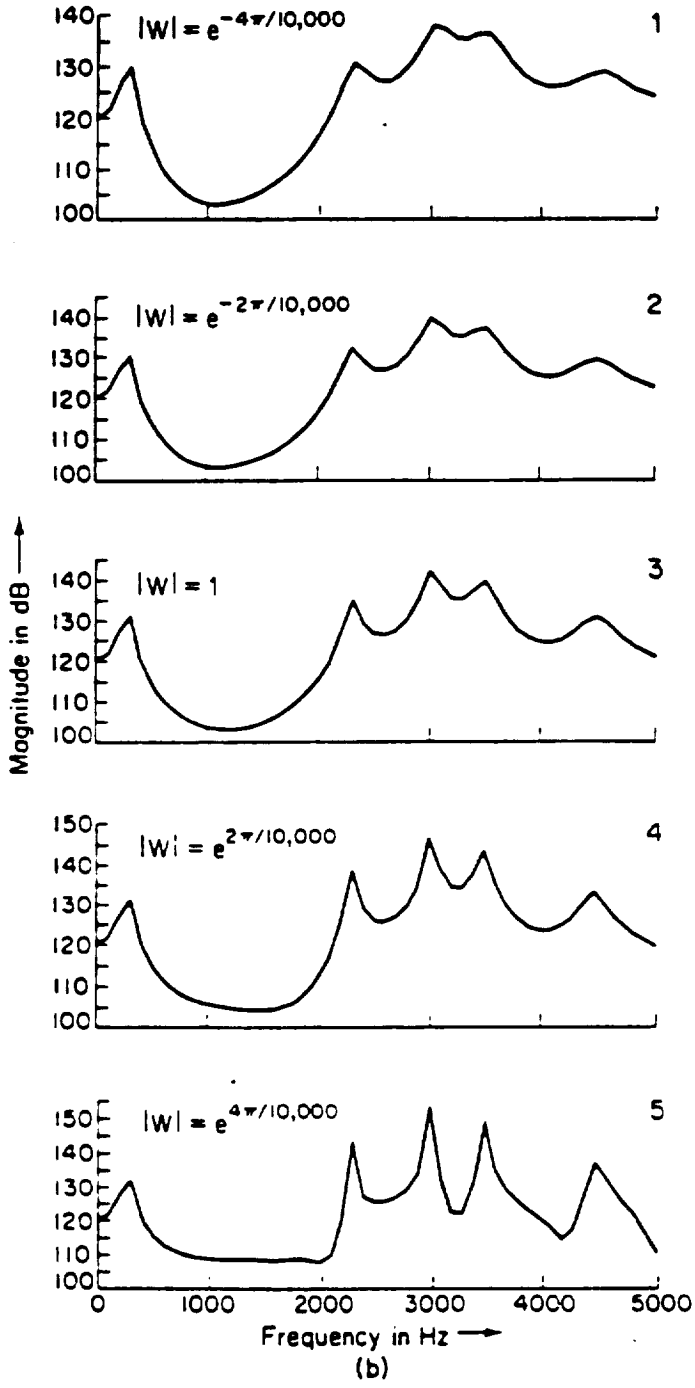

Use of the CZT algorithm. (a) z-plane pole locations for synthetic speech signal. (b) Evaluation of z-transform for several spiral contours. (After Rabiner, Schafer, and Rader [13].)

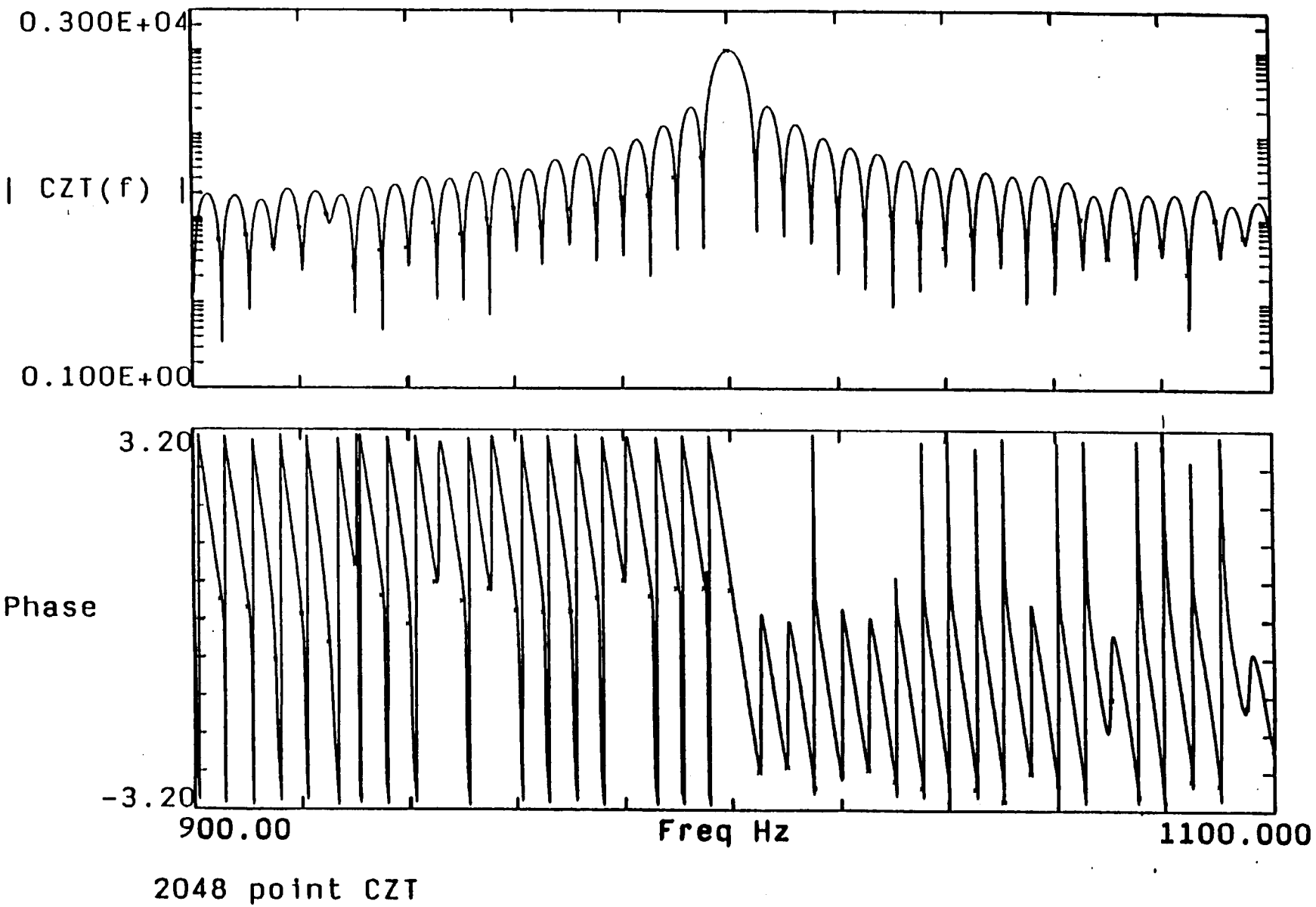
0.300E+04
| CZT(f) |
0.100E+00
3.20
Phase
-3.20
900.00
Freq Hz
1100.000
2048 point CZT

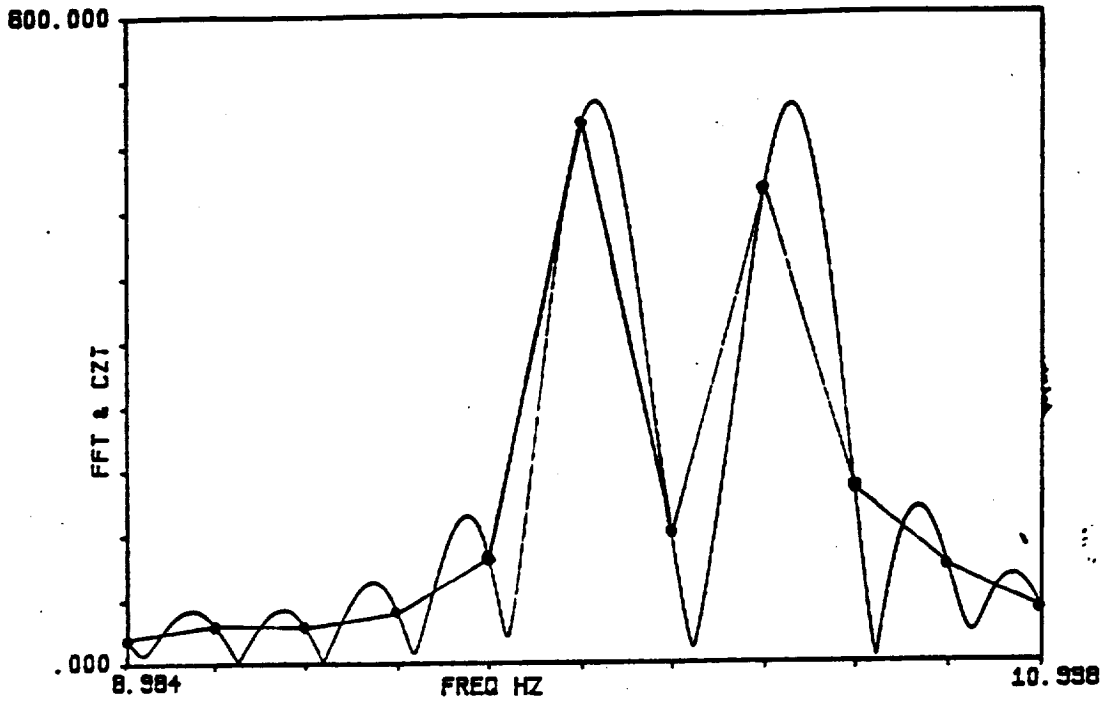

FFT & CZT OF TWO SINE WAVES AT 10.0 & 10.4 HZ FS=200 HZ BW=0.1953
ONE BLOCK DATA OF 1024 POINTS

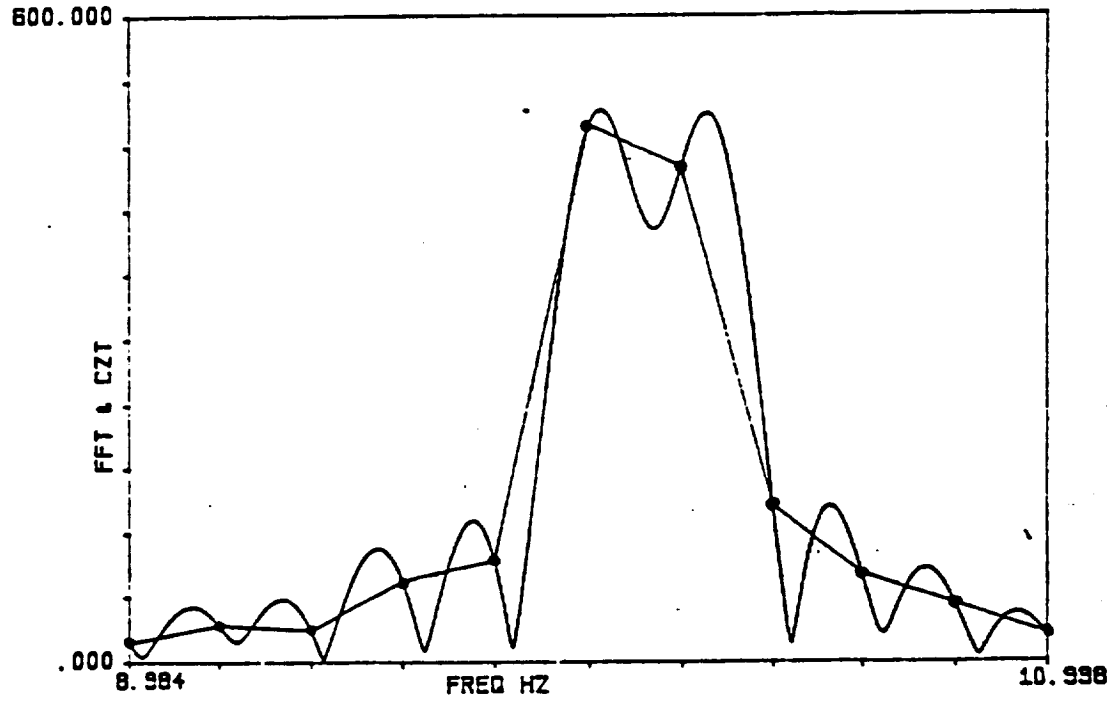

FFT & CZT OF TWO SINE WAVES F1=10.0 HZ F2=10.2 HZ BW=0.1953125
ONE BLOCK DATA OF 1024 POINTS

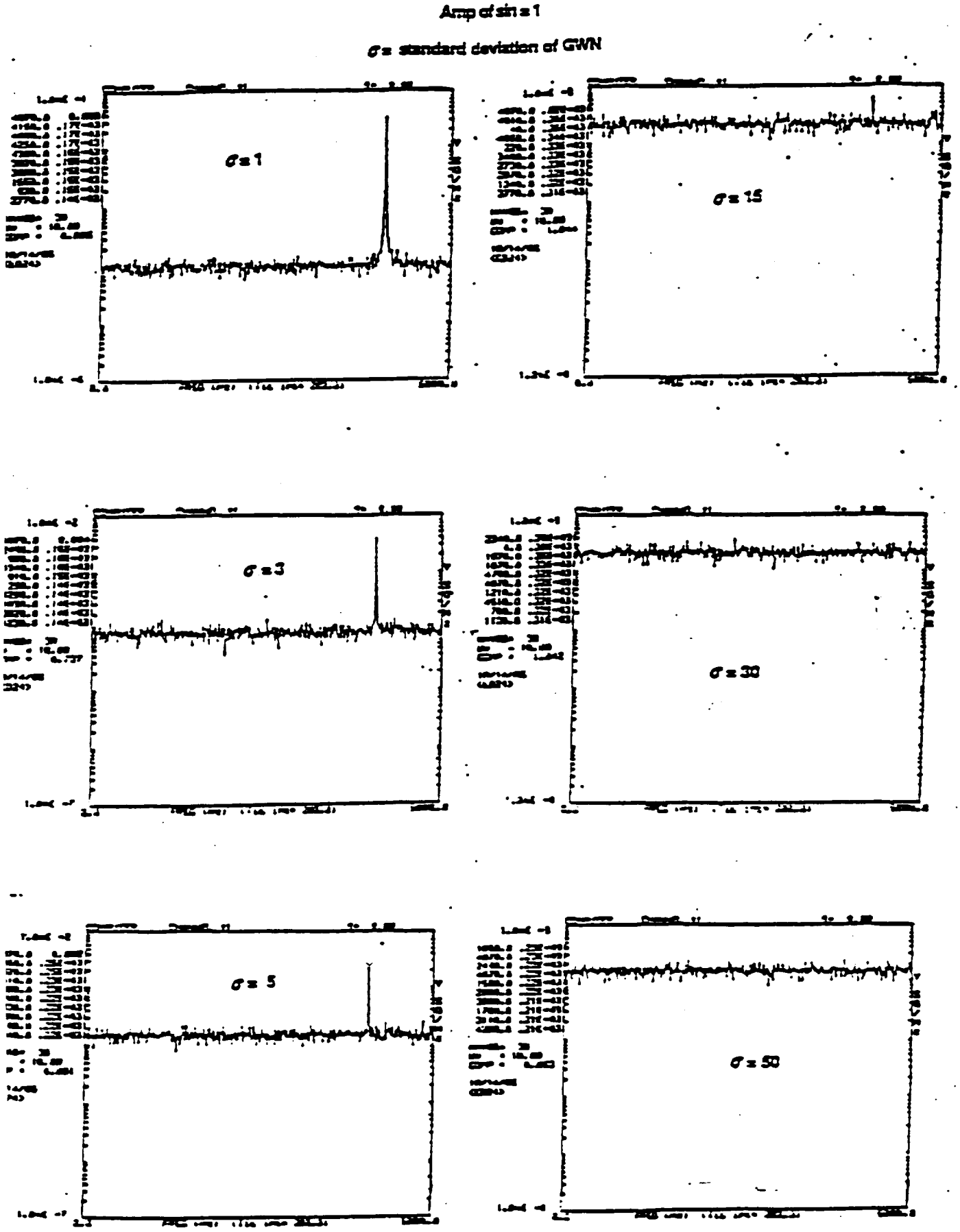

FIGURE 58. POWER SPECTRUM OF SINE WAVE PLUS NOISE FOR SELECTED SIGNAL TO NOISE RATIOS

ORIGINAL PAGE IS
OF POOR QUALITY

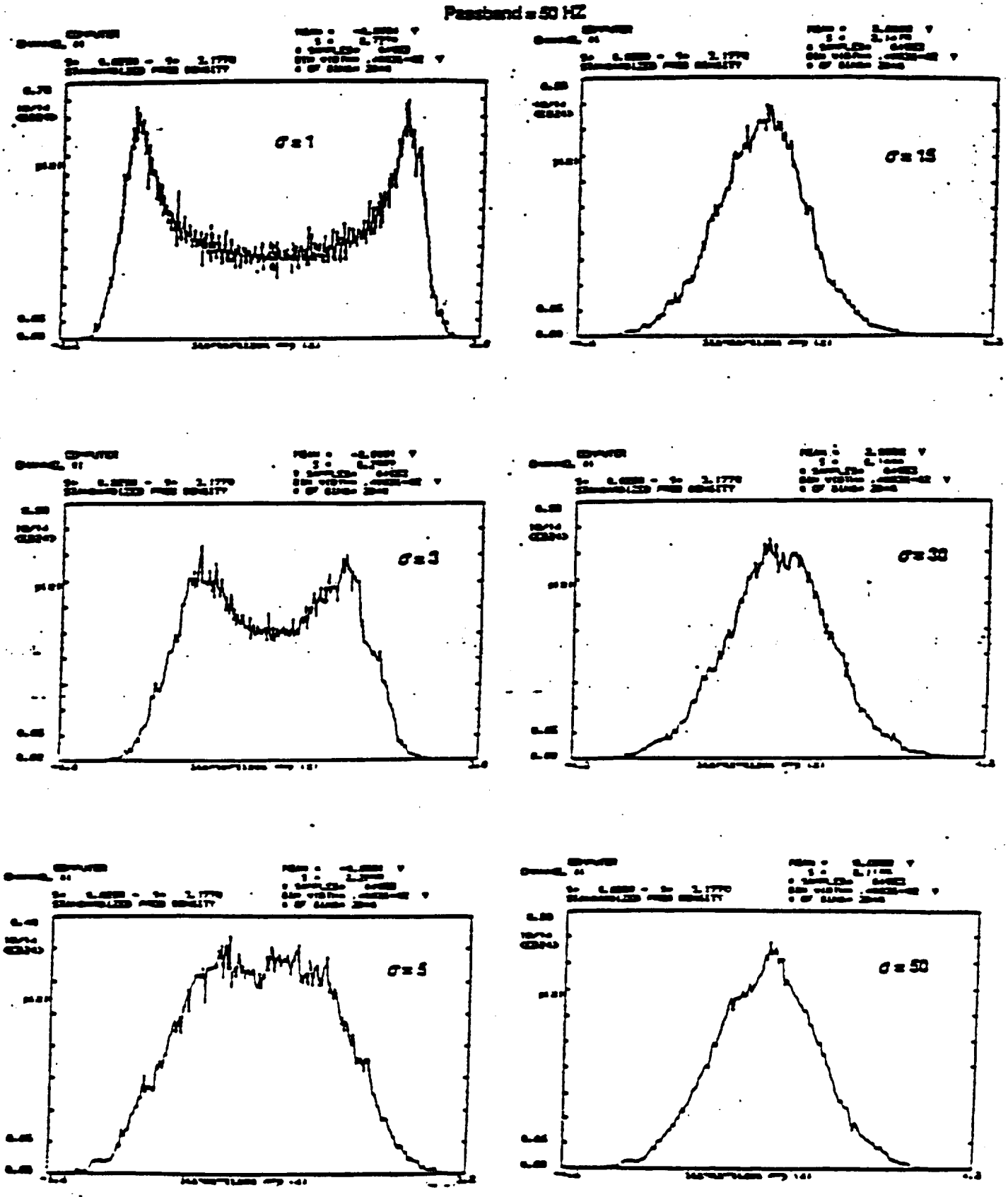

FIGURE 59. BANDPASS PROBABILITY DENSITIES FOR SINE WAVE PLUS NOISE SAMPLES

PDA–Coherence

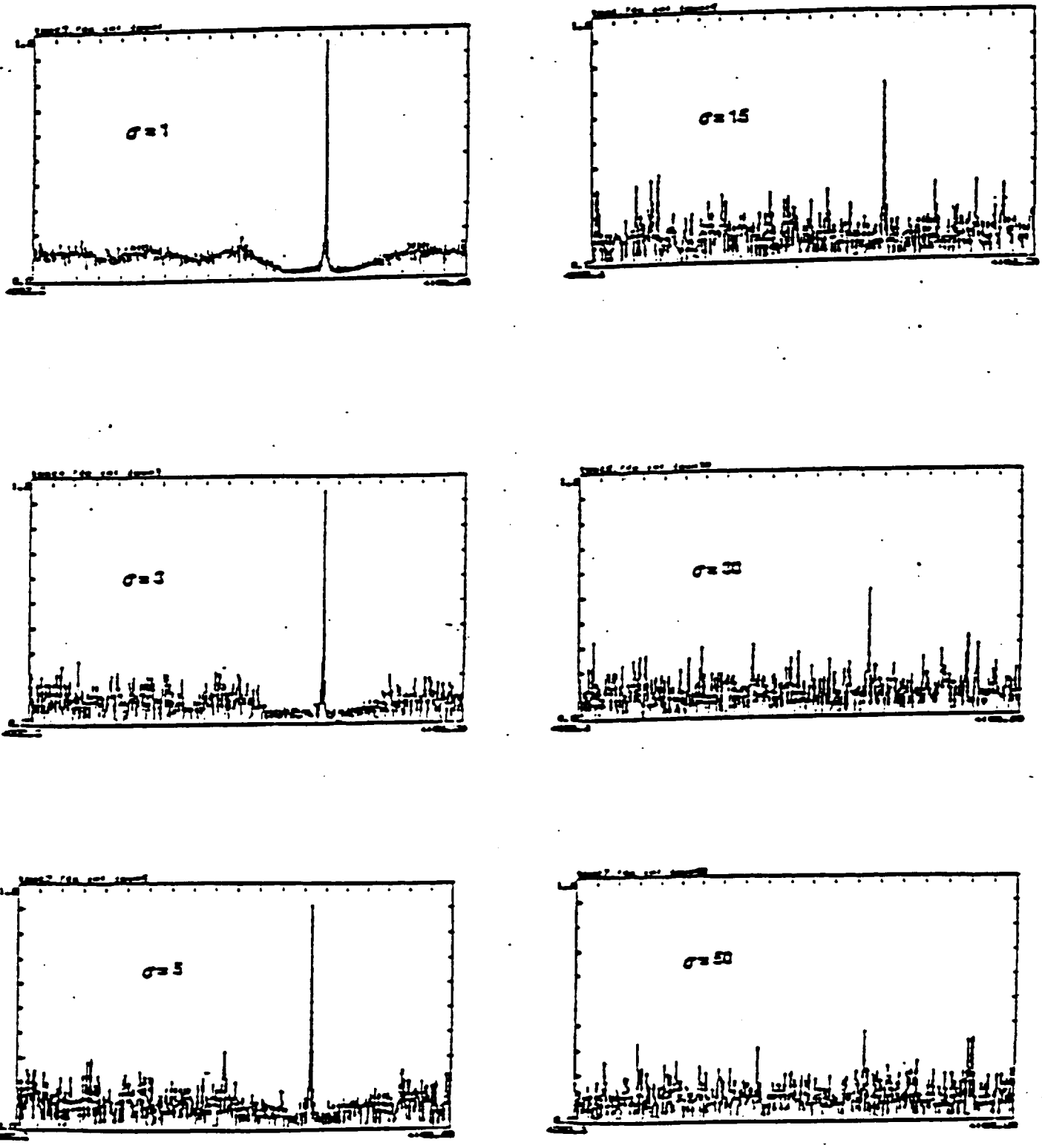

FIGURE 60. PHASE COHERENCE SPECTRA FOR SINE WAVE PLUS NOISE SAMPLES

ORIGINAL PAGE IS
OF POOR QUALITY

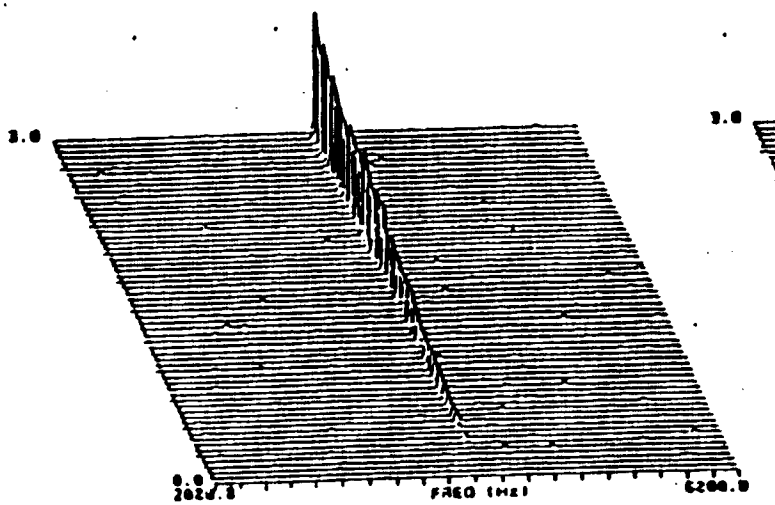

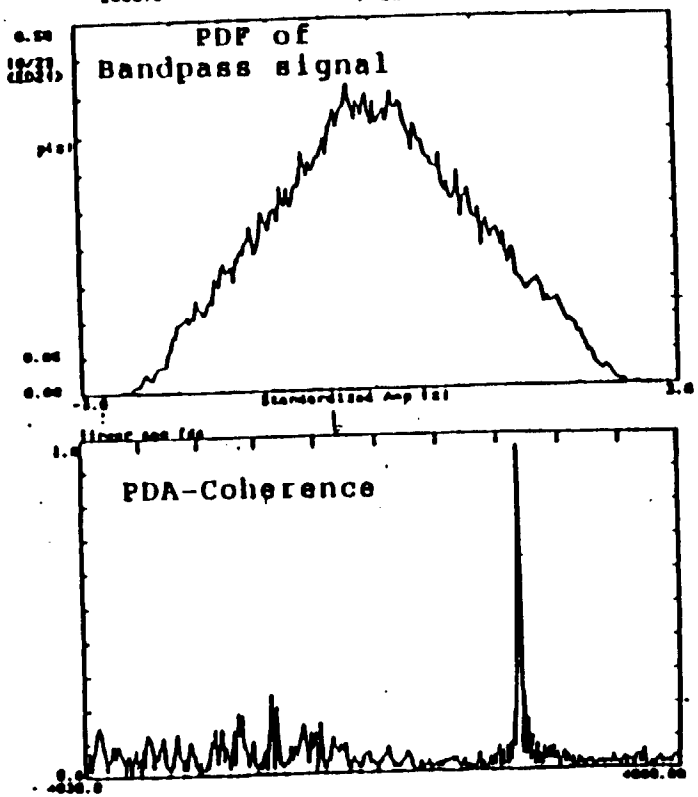

Sine Wave with Linear
Amplitude Variation

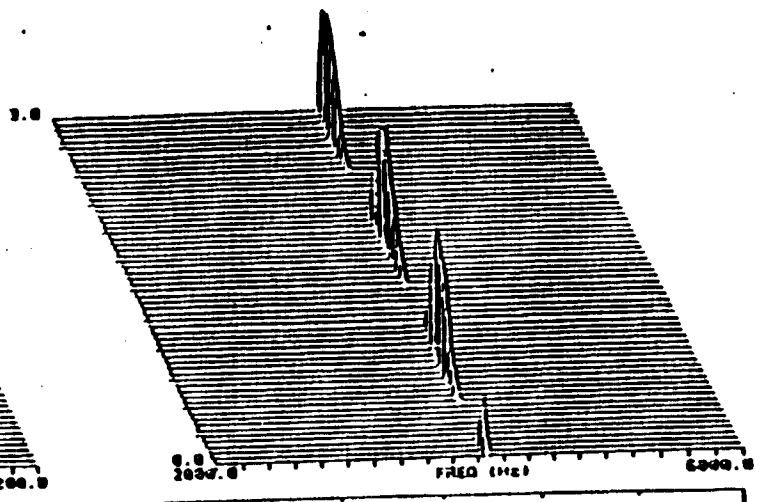

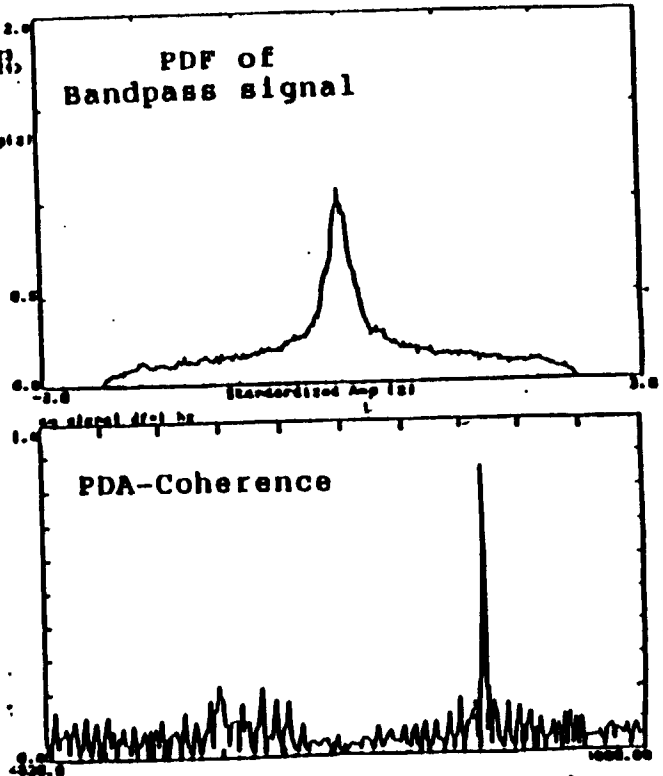

Sine Wave with Sinusoidal
Amplitude Variation

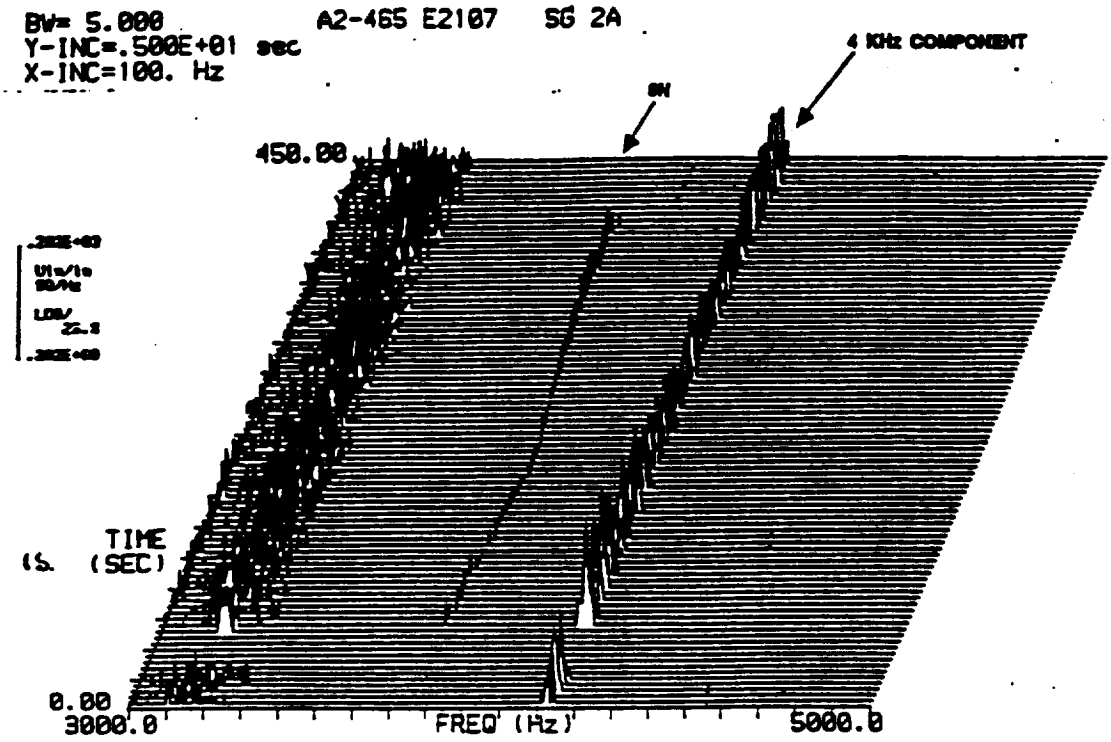

FIGURE 63. ISOPLOT OF TEST 902-465 WITH 4KHz COMPONENT PRESENTED

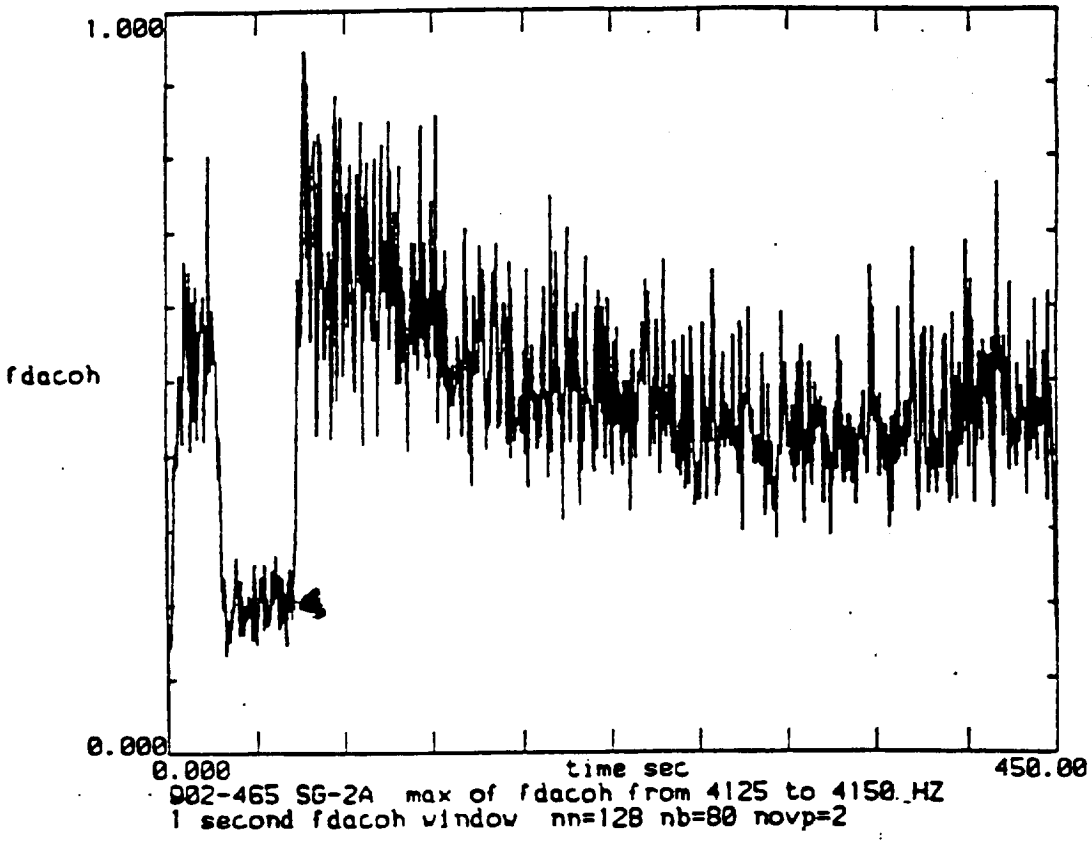

FIGURE 68. PDA TIME HISTORY SHOWING DEGREE OF DISCRETENESS OF 4 KHz AS A FUNCTION OF TIME

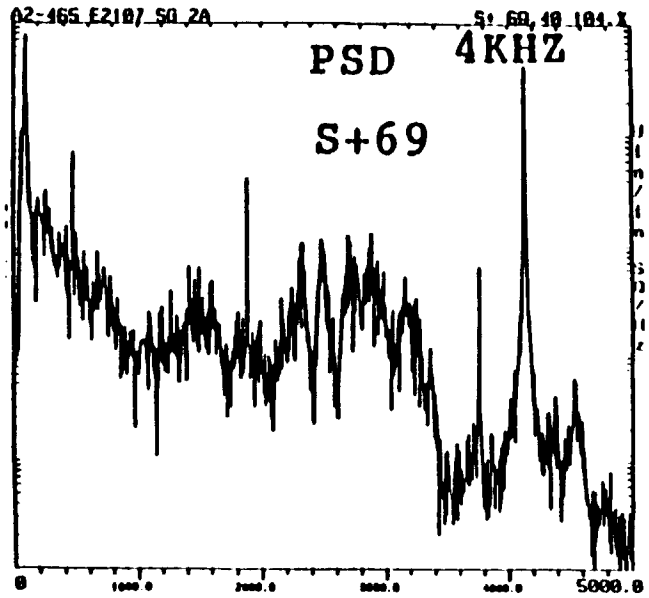
PSD 4KHZ
S+69
5000.0

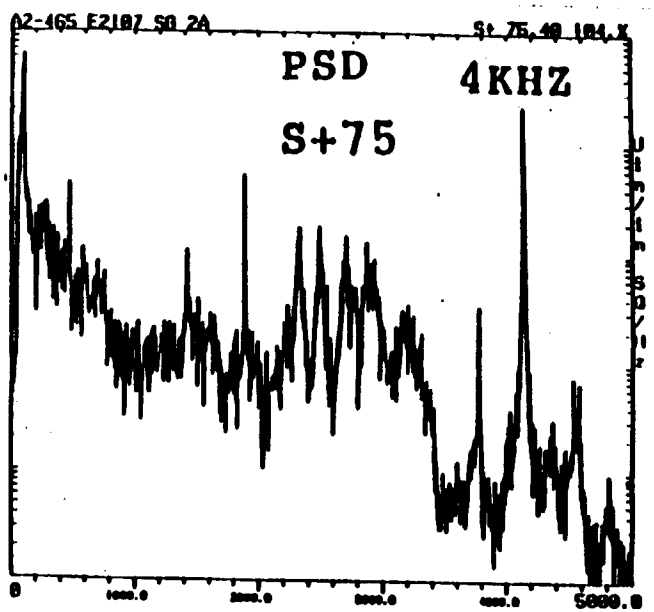
PSD 4KHZ
S+75
5000.0

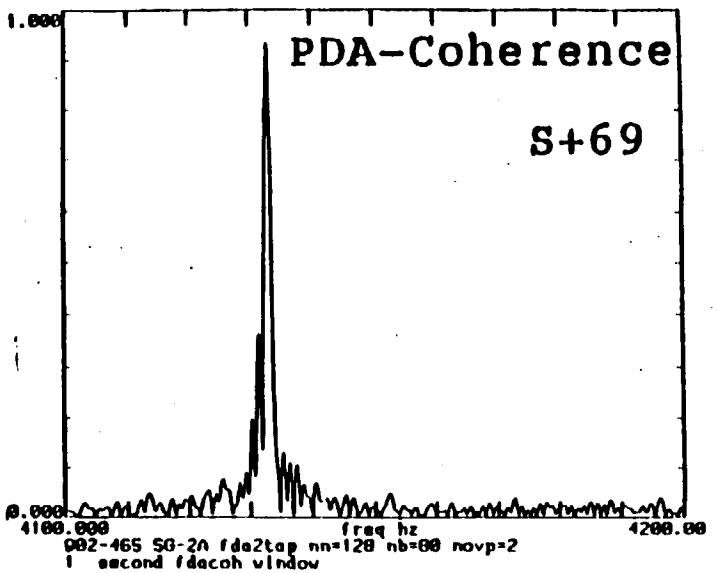
PDA-Coherence
S+69
1.000
0.000
4100.000
freq hz
4200.00
002-465 SG-2A fda2tap nn=128 nb=00 novp=2
1 second fdacoh window

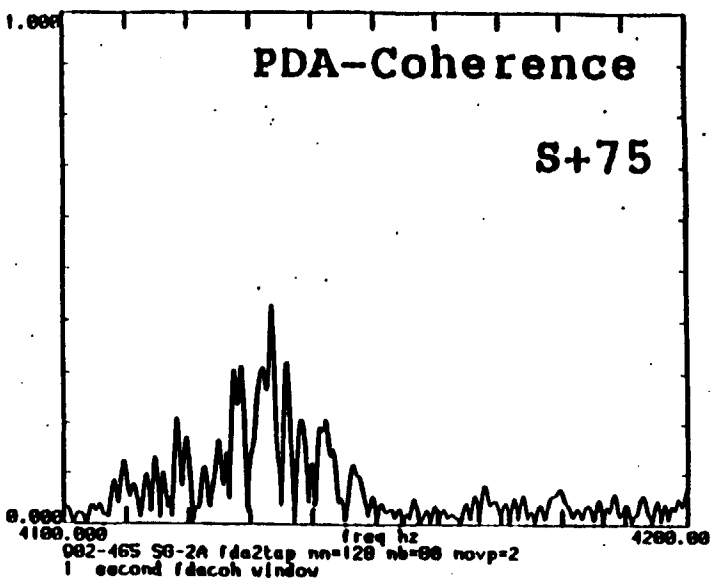
PDA-Coherence
S+75
1.000
0.000
4100.000
freq hz
4200.00
002-465 SG-2A fda2tap nn=128 nb=00 novp=2
1 second fdacoh window

A1-481 HPFP RAD186

TIME INC= .128E-01(SEC) XINC=100.(HZ)
MAX= .502E+01 LIN.

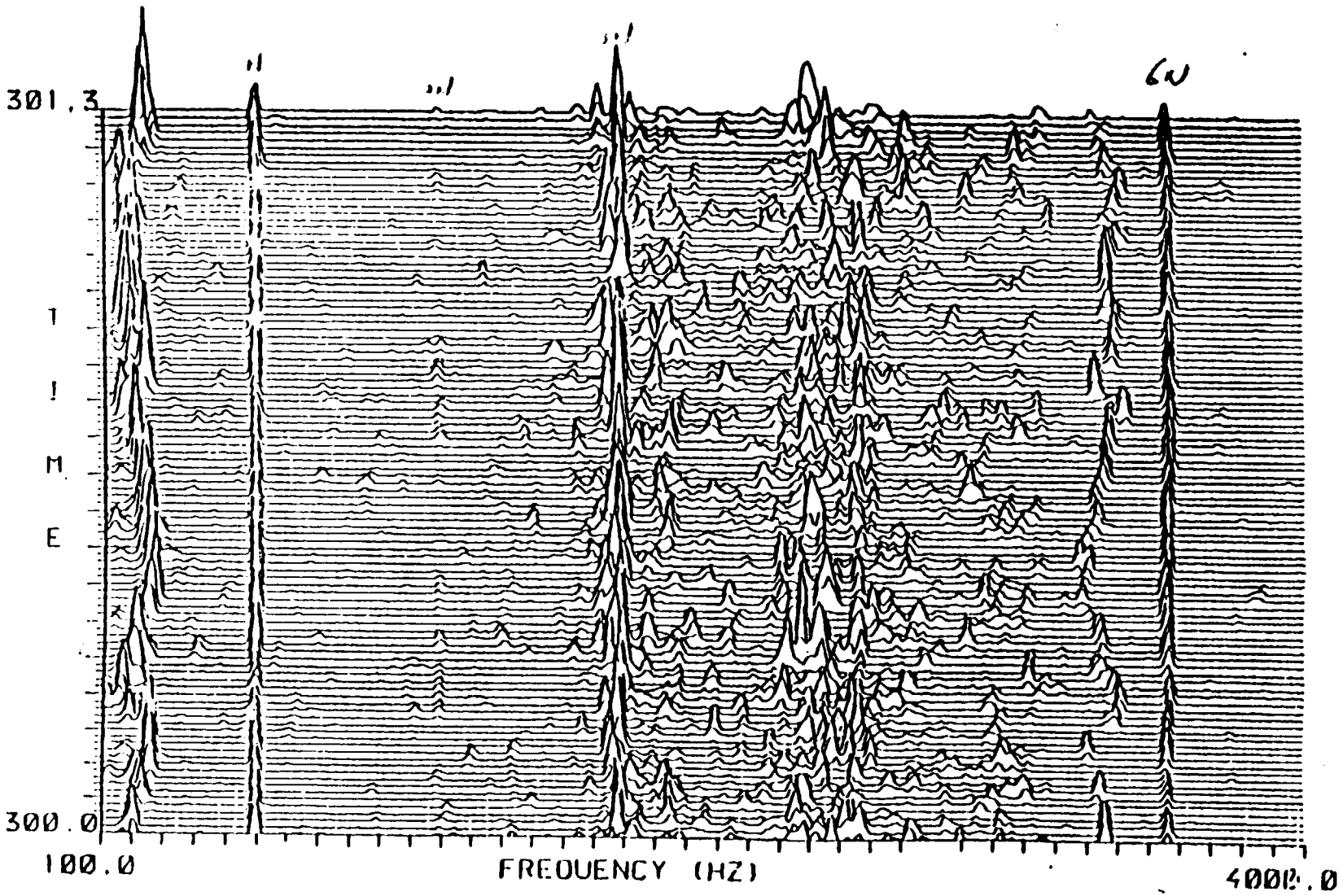

. SHRESHOLD LEVEL TOO HIGH--- Important Low Amplitude Defect Signature Will Be Ignored.

. SHRESHOLD LEVEL TOO LOW --- The Fluctuating Noise Floor Will Smear The Entire Isoplot

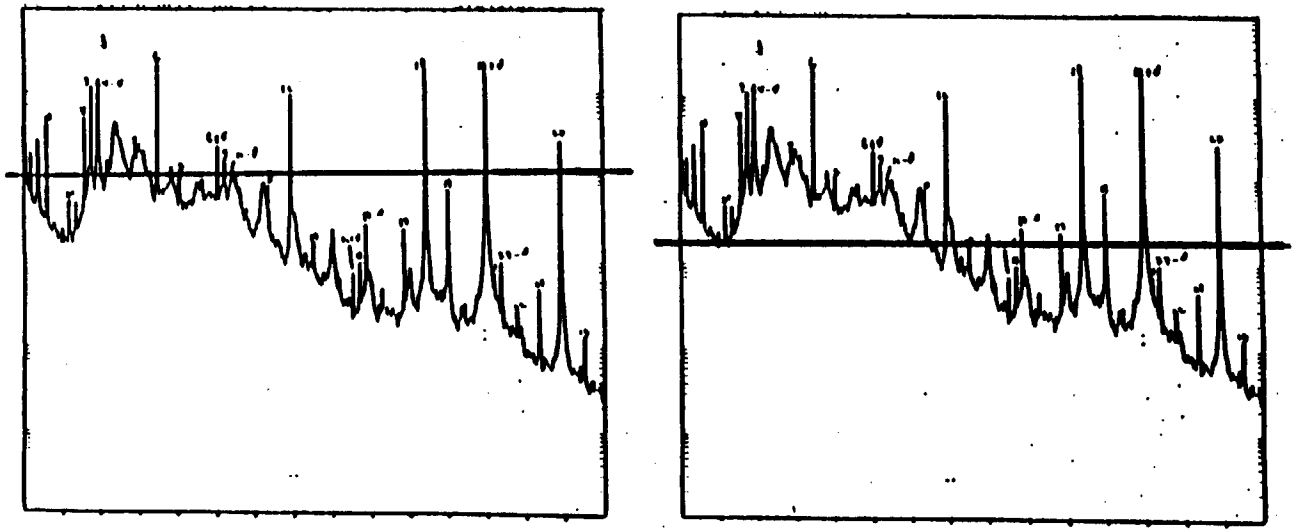

. NON-STATIONARY DATA --- Many PSD Peaks Get Compressed Too Closely Together & Cross-over Occur Among Different Spectral Components.

. SSME DATA BASE --- Compressed Signal Image Representation
Reduced Storage & Preserve Signature
Quick Access & Comparison

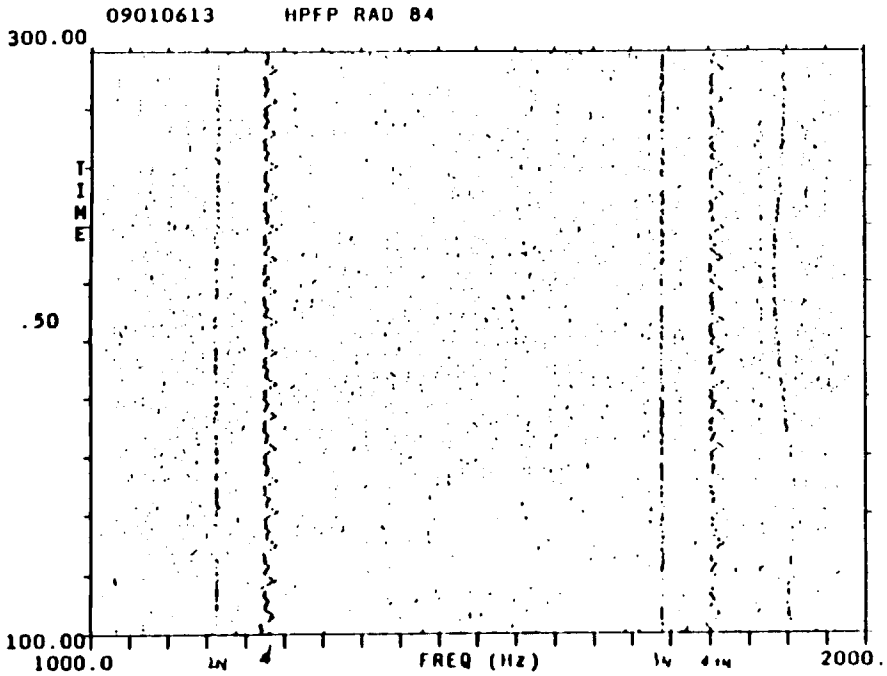
09010613 HPFP RAD 84
300.00
TIME
.50
100.00
1000.0
FREQ (Hz)
2000.

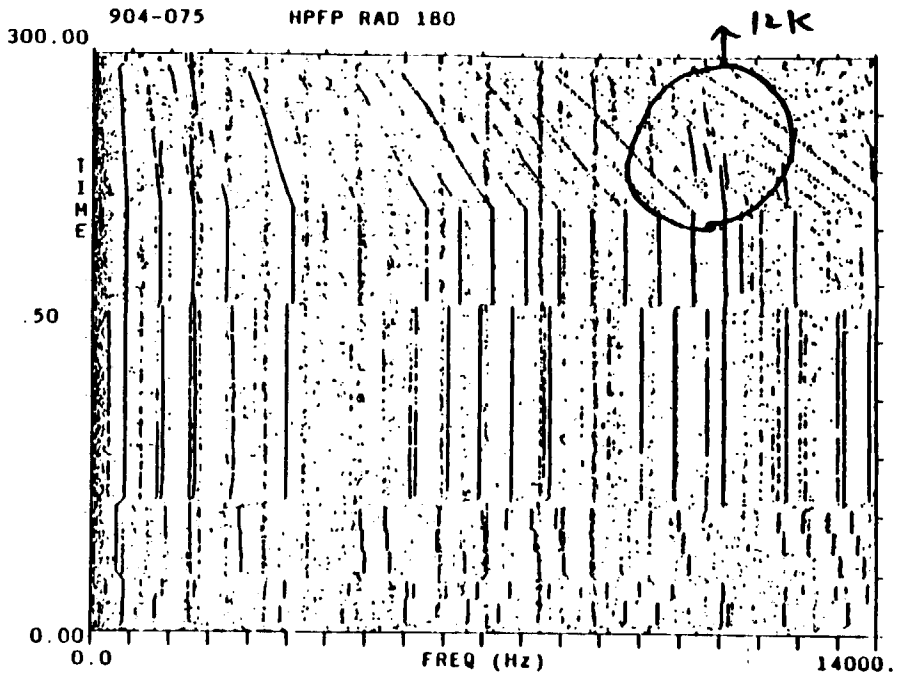
904-075 HPFP RAD 180
12K
300.00
TIME
.50
0.00
0.0
FREQ (Hz)
14000.

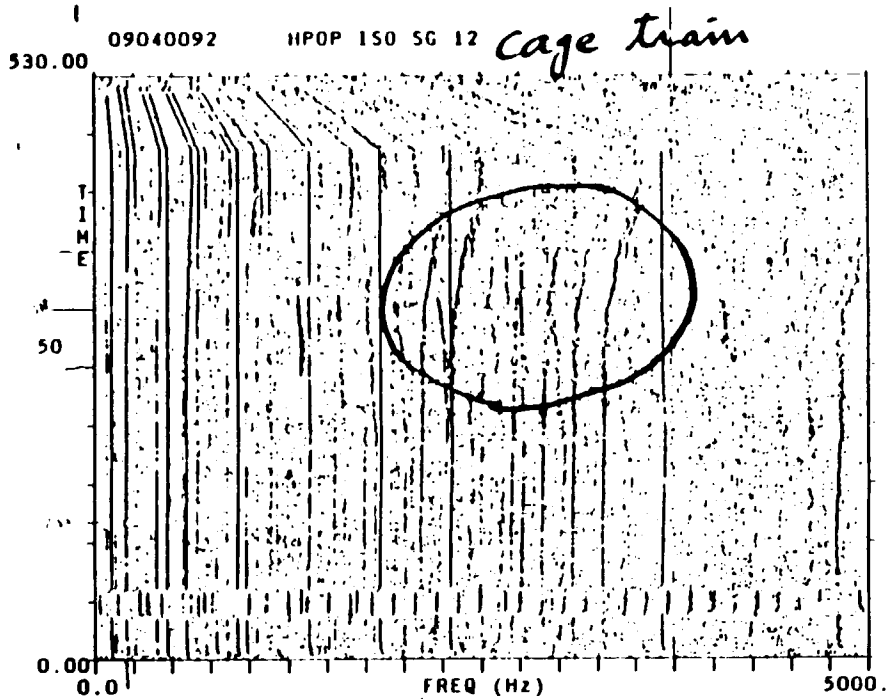
09040092 HPOP 150 SG 12
cage train
530.00
TIME
50
0.00
0.0
FREQ (Hz)
5000.

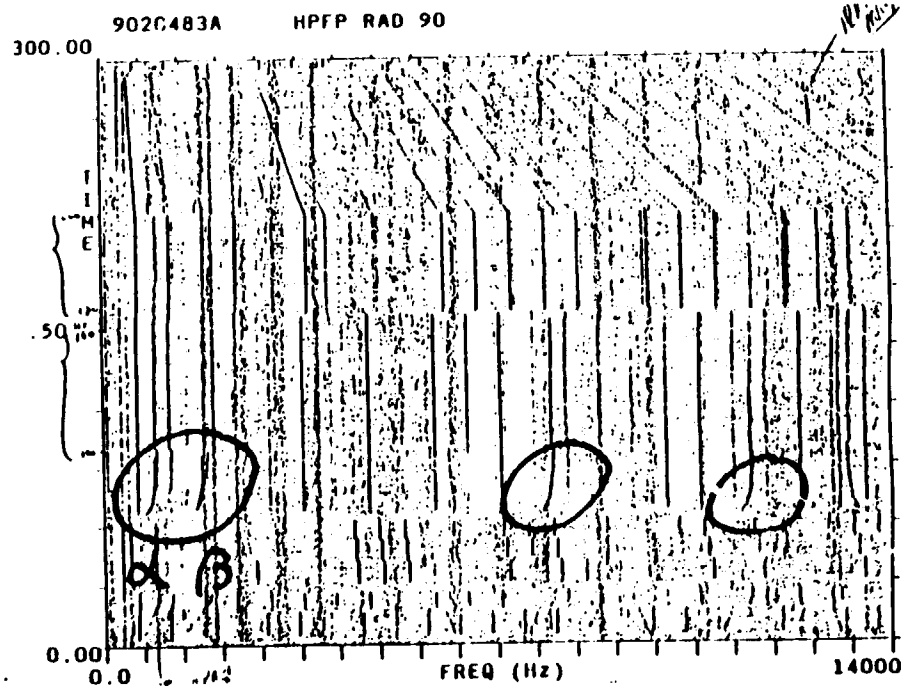
9020483A HPFP RAD 90
300.00
TIME
.50
0.00
0.0
FREQ (Hz)
14000.

COMPLEX TOPO -- COMPRESSED SSME VIBRATION DATA BASE

. For each test: Sampling Frequency = 10KHz, Time period=500 sec.
  20 Channels/Test, eg. HPFP, HPOP, LPFP, LPOP, PBP, WLD3, SPD...
  Each channel: 1250 4K data block ==> 4K FFT ==> Complex Topo
  Each FFT Peak: Amplitude, Phase, Frequency ==> Four-Byte Storage
  If store 50 peaks/FFT ==> 20*1025*50*4 = 4.1 MB
  For 600 tests: 600 * 4.1 MB = 2.46 GB of complex topo

. For Raw FFT data: 600*20*500*10240*4 = 246 GB storage
  ===> Compression Ratio = 246 GB : 2.46 GB = 100 : 1

. Identify 10 segments of stationary period, and store PSD's.
  Composite RMS time history tracking
  ===> Compression Ratio = 246 GB : 2.95 GB = 84 : 1

COMPACT DATA BASE IN A SINGLE 4-GB LASER DISC

. Provides quick and efficient recall capabilities to extract information from past test data.

. Major information is preserved with minimum storage requirement.
  - Frequency domain characteristics: Representative PSD's
  - Time-Frequency trending of different mechanical failure modes and/or any anomalous phenomena.

INFORMATION RECONSTRUCTION:

. frequency/amplitude tracking for Sync, harmonics and anomalous frequency components.

. test-to-test trend analysis

. retrieve signature characteristics

- linear cross-coherence and phase
- auto-cross bi-coherence and tri-coherence analysis
- hyper-coherence analysis
- hyper-coherence filtering: periodic waveform recovery
- orbit analysis: backward & forward rotational motion

SIGNATURE COMPARISON

. Fast recall and comparison over large amount of history tests.

. Automatic discrimination between nominal and anomalous signals.

. Pattern classification - transform various signal pattern into vectors to construct a memory matrix.

. Automated Pattern Mapping Algorithm - Associative Memory Mapping: a transformation in which a finite number of input pattern vectors is mapped into a given set of memory matrix.

IDENTIFY PROBABILITY DISTRIBUTIONS, STATISTICS OR CORRELATIONS

. Relative Phase difference between Sync and its harmonics

- Any fixed relationship? If not, what is the distribution?

. Orbit direction at different PWL

- Any fixed direction? If yes, exceptions ===> ?

. Phase of Auto-Bicoherence Bxxx(18N, 12K ; star)

- constant phase? If yes. It then represents a key signature.

. Amplitude Distribution of Sync, Harmonics, Harmonics/Sync ratio

SUMMARY

(1) High Order Cumulant Function and Cumulant Spectrum:

- Theory of General N-th Order Nonlinear Spectral Analysis

(2) Auto/Cross Bi-spectrum/Bi-coherence:

- Quadratic Correlation Among Three Waves At (W1, W2, W1+W2)

(3) Auto/Cross Tri-Spectrum/Tri-Coherence:

- Cubic Correlation Among Four Waves At (W1, W2, W3, W1+W2+W3)
- Modulation Generated Side-Band Structure At (Wc-D, Wc, Wc+D)

(4) Hyper-Coherence:

- Harmonic Identification (Wr, N*Wr)

(5) Hyper-Coherence filtering:

- Periodic Waveform Enhancement
- Orbit Plot

(6) Generalized Hyper-Coherence:

- Correlation Between Arbitrary Frequency Pair (W1, W2)
- Instantaneous Frequency

(7) MEM Spectrum Estimator:

- Prediction Auto-Correlation Function Beyond the Maximum Time Lag by Maximizing Its Entropy

(8) AR Spectrum Estimator

- Time Domain Signal Can Be Represented By An AR Model. Estimate Its AR Coefficients and PSD by Minimizing Its Prediction Error.

(9) RLS FIR Adaptive Filter & Widrow's LMS Adaptive Filter:

- Predict Background Noise In The Primary Signal From a Correlated Reference Signal.

(10) Cepstrum Analysis:

- Convert Time Domain Convolution To Frequency Domain Multiplication, To Quefrency Addition.
- Deconvolution

(11) Rotary Spectrum:

- Decompose a Random Vector Into C.W. And C.C.W. Rotational Components.
- Identify Correlation Among Different Rotational Components.

(12) Wave Number Spectrum:

- Transform Time-Spatial Array Signal Into Its Frequency-Wavenumber Domain.
- Identify Left- & Right-ward Traveling Wave or Standing Wave.

(13) Phase Domain Average (PDA):

- Identify Discreteness Of A Spectral Component By Tracing The Variation Of Phase Drifting.
- Phase Estimation Through Chirp-Z Transform.

(14) Chirp-Z Transform:

- Evaluate Z-Transform Over A Portion On A Spiral Contour.

(15) Topo:

- Transform SSME Vibration Signal into a Compressed Topo Data Base To Provide An Equivalent Image-Pattern.
- Pattern Recognition For Signal Classification.